



Deconstructable Systems for Sustainable Design of Steel and Composite Structures

Final Report to the
American Institute of Steel Construction

by

**Lizhong Wang, Lucas N. Troup, Kyle Coleman, Matthew J. Eckelman,
Jerome F. Hajjar**

*Department of Civil and Environmental Engineering
Northeastern University*

Clayton Brown, Mark D. Webster

Simpson Gumpertz and Heger, Inc.

October 2016



SIMPSON GUMPERTZ & HEGER



Engineering of Structures
and Building Enclosures

Abstract

According to the U.S. Energy Information Administration, construction and use of buildings consumed almost half of the total energy used in the United States in 2012. Design for Deconstruction (DfD) of buildings, first proposed in the 1990s, aims to minimize the environmental impacts and reduce the pollution and waste produced during construction and demolition of buildings by reclaiming the materials at the end of the service life of buildings. Contrary to the conventional material flow in buildings, which starts with the extraction or recycling of raw materials and ends with the disposal of debris in landfills, DfD attempts to close this loop by reusing the salvaged materials in future construction projects. As the most ubiquitous type of structural steel framing for commercial and residential buildings, traditional steel-concrete composite flooring system makes the most efficient use of the two materials, with steel being subjected to tension and concrete resisting compression. However, in this system the concrete slabs are poured integrally with the supporting steel framing systems, inhibiting the separation and reuse of the structural components.

The objectives of the proposed research are to develop new structural system concepts for deconstructable steel and steel-concrete composite construction to facilitate DfD coupled with the use of recycled materials in sustainably optimized construction. The proposed system not only maintains the benefits offered by composite construction but also enables disassembly and reuse of the structural components.

This report illustrates the deconstructable composite floor system utilizing clamping connectors. This floor system is anticipated to be used along with all-bolted construction for the remainder of the structure to facilitate deconstruction. A solution for connecting all the precast concrete planks in their plane using threaded rods is also presented. Diaphragm behavior is then briefly introduced, and computational results are provided to demonstrate the diaphragm response of the deconstructable composite floor system. The experimental program for investigating the performance of the system is introduced. Pushout tests are conducted to quantify the strength and ductility of the clamping connectors and evaluate the influences of the parameters. The test results along with collaborating analysis results for the pushout tests indicate that the strength of the ductile clamping connectors is comparable to that of the steel headed stud anchors. In addition, the behavior of the clamping connectors will be further validated through full-scale beam tests in which the flexural behavior of the deconstructable composite beams is investigated comprehensively. This report culminates with conclusions and recommendations for future work.

Acknowledgements

This material is based upon work supported by the National Science Foundation under Grant No. CMMI-1200820, the American Institute of Steel Construction, Northeastern University, and Simpson Gumpertz & Heger. In-kind support is provided by Benevento Companies, Capone Iron Corporation, Fastenal, Halfen, Lehigh Cement Company, Lindapter, Meadow Burke, and S&F Concrete. This support is gratefully acknowledged. The authors would like to thank Michael McNeil, Kurt Braun, Corinne Bowers, Edward Myers, Majed Alnaji, Michael Bangert-Drowns, Kara Peterman, Angelina Jay, Justin Kordas, David Padilla-Llano, and Yujie Yan for their assistance with the experiments. Any opinions, findings, and conclusions expressed in this material are those of the authors and do not necessarily reflect the views of the National Science Foundation or other sponsors.

Table of Contents

Abstract.....	2
Acknowledgements	3
Table of Contents.....	4
List of Figures.....	8
List of Tables	13
1. Introduction.....	14
1.1 Deconstructable composite prototype system	15
1.2 Research scope and organization	17
2. Literature Review.....	19
2.1 Design for Deconstruction	19
2.2 Prefabricated structural systems.....	20
2.3 Life-cycle assessment.....	21
2.4 Steel headed stud anchors	23
2.4.1 Pushout tests and beam tests	23
2.4.2 Deconstructable shear connectors	25
2.4.3 Computational analysis of steel headed stud anchors and composite beams	26
2.5 Seismic design of diaphragms.....	27
2.5.1 Seismic demand on diaphragms.....	27
2.5.2 Seismic behavior of diaphragms	28
2.5.3 Diaphragm analysis.....	28
2.5.4 Diaphragm component design	29
2.5.4.1 Composite diaphragm strength	29
2.5.4.2 Steel members.....	29
2.5.4.3 Shear connectors.....	30
2.5.5 Diaphragm seismic design methodology	30
2.5.6 Diaphragm behavior of deconstructable composite floor systems	31
2.5.6.1 Finite element model and mesh	32
2.5.6.2 Boundary conditions, load applications and contact.....	32
2.5.6.3 Material model.....	33
2.5.6.4 Analysis results	35
3. Prototype Structures.....	38
3.1 Selection and design of prototype structures.....	38
3.2 Loads.....	40
3.2.1 Gravity load	40

3.2.2	Live load reduction	41
3.2.3	Earthquake load	41
3.2.4	Wind and snow load.....	43
3.2.5	Load combinations for strength design	44
3.3	Design criteria	44
3.3.1	Gravity system	44
3.3.2	Lateral resisting system.....	45
3.3.3	Member requirements	46
3.3.4	Story drift determination.....	47
3.4	Final design	48
4.	Life Cycle Assessment.....	52
4.1	Introduction.....	52
4.2	Scope.....	54
4.3	Life cycle impact assessment	56
4.3.1	Global Climate Change (Global Warming Potential)	56
4.3.2	Human Health—Particulate (respiratory effects).....	56
4.3.3	Ecotoxicity	57
4.3.4	Photochemical Smog Formation	57
4.3.5	Fossil Fuel Depletion	57
4.4	Methodology	58
4.5	Sources of input	66
4.6	Sensitivity/Uncertainty.....	69
4.7	Results.....	70
4.8	Communication with dismantler	103
4.9	Conclusions.....	104
5.	Pushout Tests	105
5.1	Pretension tests.....	105
5.1.1	Test setup and instrumentation	105
5.1.2	Material properties	107
5.1.3	Specimen performance.....	111
5.1.4	Behavior of the bolts and channel lips	111
5.2	Pushout tests.....	115
5.2.1	Test setup and test matrix.....	115
5.2.2	Instrumentation	125
5.2.3	Loading protocol.....	132

5.2.4	Specimen performance.....	133
5.2.5	Assessment of the clamping connectors	141
5.2.6	Formation of cracks on concrete top surface	153
5.2.7	Behavior of the bolts and channel lips	156
5.2.8	Force distribution in the system.....	161
5.2.9	Response of the channel anchors and reinforcement	164
5.3	Finite element analysis	164
5.3.1	Finite element model and mesh	164
5.3.2	Boundary conditions, load applications and contact	165
5.3.3	Material model for concrete.....	166
5.3.4	Material model for steel beam, reinforcement, channels and bolts	168
5.3.5	Finite analysis results.....	169
5.4	Conclusions.....	171
6.	Beam Tests.....	173
6.1	Test setup and test matrix.....	173
6.1.1	Pretension test on fully threaded rods	176
6.2	Material properties	180
6.3	Instrumentation	185
6.4	Loading protocol.....	190
7.	Conclusions and Future Work.....	191
7.1	Conclusions from life-cycle assessment.....	191
7.2	Summary of pushout tests	192
7.3	Future work.....	194
	References	195
Appendix A.	Prototype Structure Design Summary.....	202
Appendix B.	Design of the SimaPro Model, Including Assemblies, Waste Scenarios, and Life Cycles of the Traditional and Deconstructable Buildings	210
Appendix C.	Descriptions of the Products and Processes Used in LCA, Extracted from SimaPro	230
Appendix D.	Specimen Drawings	269
D.1	Pushout test	270
D.1.1	Steel specimen shop drawings	270
D.1.2	Concrete specimen design drawings	279
D.2	Composite beam test	283
D.2.1	Steel specimen shop drawings	283
D.2.2	Concrete specimen design drawings	307
Appendix E.	Experimental Raw Data	314

E.1	Pushout test specimens.....	314
E.1.1	Pretension test.....	314
E.1.2	Pushout test.....	315
E.1.2.1	Actuator force, actuator displacement and slip.....	315
E.1.2.2	Beam strain gage.....	320
E.1.2.3	Bolt strain gage.....	322
E.1.2.4	Channel lip strain gage.....	323
E.1.2.5	Channel anchor strain gage.....	325
E.1.2.6	Reinforcement strain gage.....	326
Appendix F.	Mill Certifications.....	327
F.1	Pushout test.....	327
F.1.1	Steel frame.....	327
F.1.2	Halfen channels and bolts.....	329
F.1.3	Lindapter clamps and washers.....	333
F.1.4	Reinforcement.....	341
F.1.5	Concrete.....	343
F.2	Beam test.....	344
F.2.1	Steel frame.....	344
F.2.2	Bolted connections.....	346
F.2.3	Halfen channels and bolts.....	347
F.2.4	Lindapter clamps and washers.....	350
F.2.5	Reinforcement.....	356
F.2.6	Concrete.....	359
Appendix G.	Interpretation of Strain Gage Data.....	362
G.1	Pushout tests.....	362
G.1.1	Load distribution among the clamps.....	363
G.1.2	Bolt pretention force variation.....	366
G.1.2.1	Pretension test.....	369
G.1.2.2	Pushout test.....	370
G.1.3	Forces acting on the channel anchors.....	372
Appendix H.	Beam Test Specimen Design.....	376
H.1	Lifting points on the concrete planks.....	376
H.2	Selection of threaded rods.....	377
Appendix I.	Moment of inertia.....	382

List of Figures

Figure 1.1 Deconstructable composite beam prototype.....	16
Figure 1.2 Precast concrete plank connections	16
Figure 1.3 Precast concrete plank cross section (units: inches)	17
Figure 1.4 Typical floor plan for deconstructable composite floor system (units: feet)	17
Figure 2.1 Diaphragm components.....	27
Figure 2.2 Loading pattern for diaphragms at different levels.....	28
Figure 2.3 Finite element model for the diaphragm	32
Figure 2.4 Displacement history for the computational models	33
Figure 2.5 Material stress-strain curves	36
Figure 2.6 Load-displacement curves	37
Figure 2.7 Steel moment to concrete moment ratio.....	37
Figure 3.1 Building layout for three story buildings.....	39
Figure 4.1 Multiple reuse of components at different disposal rate.....	59
Figure 4.2 Comparison of relative environmental impacts of the 20-3-6 traditional and DfD buildings with no reuse of deconstructable components.....	74
Figure 4.3 Comparison of relative environmental impacts of the 20-3-8 traditional and DfD buildings with no reuse of deconstructable components.....	74
Figure 4.4 Comparison of relative environmental impacts of the 20-9-6 traditional and DfD buildings with no reuse of deconstructable components.....	75
Figure 4.5 Comparison of relative environmental impacts of the 20-9-8 traditional and DfD buildings with no reuse of deconstructable components.....	75
Figure 4.6 Comparison of relative environmental impacts of the 30-3-6 traditional and DfD buildings with no reuse of deconstructable components.....	76
Figure 4.7 Comparison of relative environmental impacts of the 30-3-8 traditional and DfD buildings with no reuse of deconstructable components.....	76
Figure 4.8 Comparison of relative environmental impacts of the 30-9-6 traditional and DfD buildings with no reuse of deconstructable components.....	77
Figure 4.9 Comparison of relative environmental impacts of the 30-9-8 traditional and DfD buildings with no reuse of deconstructable components.....	77
Figure 4.10 Comparison of relative environmental impacts of conventional and DfD buildings (20-3-6 w 66% reuse)	78
Figure 4.11 Comparison of relative environmental impacts of conventional and DfD buildings (20-3-6 w 75% reuse)	79
Figure 4.12 Comparison of relative environmental impacts of conventional and DfD buildings (20-3-6 w 80% reuse)	80
Figure 4.13 Comparison of relative environmental impacts of conventional and DfD buildings (20-3-8 w 66% reuse)	81
Figure 4.14 Comparison of relative environmental impacts of conventional and DfD buildings (20-3-8 w 75% reuse)	82
Figure 4.15 Comparison of relative environmental impacts of conventional and DfD buildings (20-3-8 w 80% reuse)	83
Figure 4.16 Comparison of relative environmental impacts of conventional and DfD buildings (20-9-6 w 66% reuse)	84
Figure 4.17 Comparison of relative environmental impacts of conventional and DfD buildings (20-9-6 w 66% reuse)	85
Figure 4.18 Comparison of relative environmental impacts of conventional and DfD buildings (20-9-6 w 80% reuse)	86

Figure 4.19 Comparison of relative environmental impacts of conventional and DfD buildings (20-9-9 w 66% reuse)	87
Figure 4.20 Comparison of relative environmental impacts of conventional and DfD buildings (20-9-8 w 75% reuse)	88
Figure 4.21 Comparison of relative environmental impacts of conventional and DfD buildings (20-9-8 w 80% reuse)	89
Figure 4.22 Comparison of relative environmental impacts of conventional and DfD buildings (30-3-6 w 66% reuse)	90
Figure 4.23 Comparison of relative environmental impacts of conventional and DfD buildings (30-3-6 w 75% reuse)	91
Figure 4.24 Comparison of relative environmental impacts of conventional and DfD buildings (30-3-6 w 80% reuse)	92
Figure 4.25 Comparison of relative environmental impacts of conventional and DfD buildings (30-3-8 w 66% reuse)	93
Figure 4.26 Comparison of relative environmental impacts of conventional and DfD buildings (30-3-8 w 75% reuse)	94
Figure 4.27 Comparison of relative environmental impacts of conventional and DfD buildings (30-3-8 w 80% reuse)	95
Figure 4.28 Comparison of relative environmental impacts of conventional and DfD buildings (30-9-6 w 66% reuse)	96
Figure 4.29 Comparison of relative environmental impacts of conventional and DfD buildings (30-9-6 w 75% reuse)	97
Figure 4.30 Comparison of relative environmental impacts of conventional and DfD buildings (30-9-6 w 80% reuse)	98
Figure 4.31 Comparison of relative environmental impacts of conventional and DfD buildings (30-9-8 w 66% reuse)	99
Figure 4.32 Comparison of relative environmental impacts of conventional and DfD buildings (30-9-8 w 75% reuse)	100
Figure 4.33 Comparison of relative environmental impacts of conventional and DfD buildings (30-9-8 w 80% reuse)	101
Figure 4.34 TB 30-3-8 Ecotoxicity Tree, revealing extreme impact of cold rolled sheet steel	102
Figure 5.1 Pretension test setup	106
Figure 5.2 Strain gage layout in pretension tests	107
Figure 5.3 Coupon dimensions (units: inches)	109
Figure 5.4 Bolt pretension test	113
Figure 5.5 Bolt tension variation	114
Figure 5.6 Loading frame assembly with test specimen	116
Figure 5.7 Different views of test specimen	117
Figure 5.8 Isometric view of pushout test setup	118
Figure 5.9 Shear connectors loading scenario comparison	121
Figure 5.10 Different reinforcement patterns	123
Figure 5.11 Supplementary reinforcement and surface reinforcement arrangement	124
Figure 5.12 Displacement measurements	126
Figure 5.13 Strain gages attached on the bolts, channel lips and beams	128
Figure 5.14 Strain gages attached on the reinforcement and channel anchors	131
Figure 5.15 Cyclic loading history	132
Figure 5.16 General observations in all pushout tests	134
Figure 5.17 Unique observations in each test	140
Figure 5.18 Load-slip curve of Specimen 2	141

Figure 5.19 Load-slip curve of Specimen 4	142
Figure 5.20 Load-slip curve of Specimen 7	143
Figure 5.21 Load-slip curve of Specimen 9	144
Figure 5.22 Load-slip curve of Specimen 3	146
Figure 5.23 Load-slip curve of Specimen 5	146
Figure 5.24 Load-slip curve of Specimen 6	147
Figure 5.25 Load-slip curve of Specimen 8	148
Figure 5.26 Load-slip curve of Specimen 10	149
Figure 5.27 Relationship between slip and strength reduction in the cyclic tests	152
Figure 5.28 Different black stripe patterns	153
Figure 5.29 Schematic presentation of flange underside profiles	154
Figure 5.30 Channel anchor and bolt positions	154
Figure 5.31 Illustration of the strut-and-tie model	155
Figure 5.32 Comparison of load-slip curves between specimens with different reinforcement patterns	155
Figure 5.33 Distributed area for the frictional force	156
Figure 5.34 Bolt tension vs. Slip	160
Figure 5.35 Section axial force vs slip	163
Figure 5.36 Test setup assembly and boundary conditions	166
Figure 5.37 Concrete damage variable	168
Figure 5.38 Concrete cyclic behavior	168
Figure 5.39 Load-slip curve comparison	169
Figure 5.40 Reinforcement stress contour	170
Figure 5.41 Bolt deformation	170
Figure 5.42 Channel lip deformation	170
Figure 5.43 Comparison of Concrete damage in the finite element model and test specimen	170
Figure 5.44 Bolt tension vs. slip	171
Figure 5.45 Force at clamp teeth to bolt tension ratio	171
Figure 6.1 Different views of test specimen	174
Figure 6.2 Supporting of concrete planks in the pretension test	177
Figure 6.3 Threaded rod pretension test	178
Figure 6.4 Rod tension variation	180
Figure 6.5 Mill tolerances on a W-shape cross section [(after AISC 303-10)]	181
Figure 6.6 Rod coupon dimension (units: inches)	182
Figure 6.7 Composite beam specimen instrumentation plan	190
Figure B.1 Assembly – Floor System of Traditional Building, Inputs	213
Figure B.2 Assembly – Floor system of Traditional Building, Parameters	214
Figure B.3 Assembly– Traditional Building, Inputs	215
Figure B.4 Assembly – Traditional Building, Parameters	216
Figure B.5 Assembly – DfD Components, Inputs	217
Figure B.6 Assembly – DfD Components, Parameters	218
Figure B.7 Waste Scenario – Concrete Sorting and Disposing, Inputs and Waste Treatments	219
Figure B.8 Waste Scenario – Concrete Sorting and Disposing, Parameters	220
Figure B.9 Waste Scenario – Traditional Building, Inputs and Waste Scenarios	221
Figure B.10 Waste Scenario – Reuse of Design for Deconstruction Reusable Components, Inputs and Outputs	222
Figure B.11 Waste Scenario – Reuse of Design for Deconstruction Reusable Components, Parameters	223
Figure B.12 Life Cycle – Traditional Building, Inputs and Waste Scenario	224
Figure B.13 Life Cycle – Traditional Building, Parameters	225
Figure B.14 Life Cycle – Design for Deconstruction Reusable Components (no disposal), Inputs and Waste Scenario	226

Figure B.15 Life Cycle – Design for Deconstruction Reusable Components (final use), Inputs and Waste Scenario	227
Figure B.16 Life Cycle – Design for Deconstruction Building, Inputs and Waste Scenario.....	228
Figure B.17 Life Cycle – Design for Deconstruction Building, Parameter	229
Figure C.18 Beams, columns, braces etc. and channels, represented by - steel hot rolled section, at plant - ELCD.	233
Figure C.19 Girder clamps, represented by - cast iron, at plant - US-EI 2.2	236
Figure C.20 End of life process, represented by - concrete building disposal, not reinforced, to final disposal - US-EI 2.2	239
Figure C.21 End of life process, represented by - concrete building disposal, not reinforced, to recycling - US-EI 2.2	241
Figure C.22 End of life process, represented by - concrete building disposal, not reinforced, to sorting - US-EI 2.2	243
Figure C.23 Cast in place concrete, represented by - concrete, normal, at plant - US-EI 2.2.....	245
Figure C.24 Cold formed metal deck, represented by - cold rolled sheet steel at plant - US-EI 2.2	249
Figure C.25 Deconstructable precast floor planks, including reinforcing, represented by - pre-cast concrete, minimum reinforcement, production mix, at plant - ELCD	258
Figure C.26 End of life process, represented by - recycling of steel - US-EI 2.2.....	259
Figure C.27 Steel rebar in cast in place concrete, represented by - steel rebar, blast furnace and electric arc furnace route, production mix, at plant - ELCD	261
Figure C.28 Headed studs and bolts, represented by - Steel converter unalloyed at plant - US-EI 2.2	264
Figure C.29 Transportation of materials, represented by - transport by lorry over 28t - US-EI 2.2	266
Figure C.30 Worker transportation, represented by - transport by passenger car - US-EI 2.2	268
Figure D.1 Steel Section WT5x30.....	270
Figure D.2 Steel Section WT4x15.5.....	271
Figure D.3 Stiffened W6x25 Beam Assembly	272
Figure D.4 Stability Frame for WT5x30	273
Figure D.5 Stability Frame for WT4x15.5	274
Figure D.6 Stiffened Channel C15x50	275
Figure D.7 Reaction Angle.....	276
Figure D.8 Shim between Reaction Angle and Stiffened Channel for WT4x15.5	277
Figure D.9 Shim between WT4x15.5 and Clamp Tooth	278
Figure D.10 Light Reinforcement Pattern	279
Figure D.11 Heavy Reinforcement Pattern for Two-Channel Specimens.....	280
Figure D.12 Heavy Reinforcement Pattern for Three-Channel Specimens	281
Figure D.13 Reinforcement Details.....	282
Figure D.14 Steel Section W14x38	283
Figure D.15 Steel Section W14x26	284
Figure D.16 Steel Section W18x46	285
Figure D.17 Top Spreader Beam W14x132	286
Figure D.18 Bottom Spreader Beam W8x58.....	287
Figure D.19 Brace Section W18x86.....	288
Figure D.20 Brace Section W10x49.....	289
Figure D.21 Flange Tab for Column Base.....	290
Figure D.22 Web Tab for Column Base	291
Figure D.23 Cross Beam Adapter.....	292
Figure D.24 Beam Roller Support.....	293
Figure D.25 Beam Pin Support.....	294
Figure D.26 Plate under Bottom Spreader Beam.....	295
Figure D.27 6'' Roller	296

Figure D.28 Clamp Plate for Braces.....	297
Figure D.29 Clamp Plate for Column Ends.....	298
Figure D.30 Brace Section WT4x17.5.....	299
Figure D.31 Clamp Plate for Braces.....	300
Figure D.32 Column End Shim 1.....	301
Figure D.33 Column End Shim 2.....	302
Figure D.34 Stub Beam W12x72.....	303
Figure D.35 Coupon Section W14x38.....	304
Figure D.36 Coupon Section W18x46.....	305
Figure D.37 Coupon Section W14x38.....	306
Figure D.38 One-Channel Specimen.....	307
Figure D.39 One-Channel Specimen Reinforcement.....	308
Figure D.40 Two-Channel Specimen.....	309
Figure D.41 Two-Channel Specimen Reinforcement.....	310
Figure D.42 Three-Channel Specimen.....	311
Figure D.43 Three-Channel Specimen Reinforcement.....	312
Figure D.44 Reinforcement Details.....	313
Figure E.1 Strain gage readings vs. time.....	314
Figure E.2 Actuator force, actuator displacement and slip measurements.....	319
Figure E.3 Beam strain gage readings.....	321
Figure E.4 Bolt strain gage readings.....	322
Figure E.5 Channel lip strain gage readings.....	325
Figure E.6 Channel anchor strain gage readings.....	326
Figure E.7 Reinforcement strain gage readings.....	326
Figure G.1 Strain gage locations and numbering at a section.....	364
Figure G.2 Axial force variation.....	365
Figure G.3 Stress analysis model.....	366
Figure G.4 Bolt stress strain curves.....	369
Figure G.5 Bolt material cyclic stress-strain curve.....	370
Figure G.6 Bolt axial force variation.....	371
Figure G.7 Bolt material cyclic behavior.....	371
Figure G.8 Strain transformation between different coordinates.....	372
Figure G.9 Gage orientation and new coordinate system.....	372
Figure G.10 Anchor strain and stress variation.....	375
Figure H.1 Moment diagram of a concrete plank under gravity loading (units: lb-ft).....	376
Figure H.2 Prototype structure floor plan.....	377

List of Tables

Table 2.1 Analytical model parameters	36
Table 3.1 Prototype structure matrix	40
Table 3.2 Breakdown of dead load	41
Table 3.3 Limiting width-to-thickness ratios.....	47
Table 3.4 Member sizes for the conventional composite flooring system with solid slabs	49
Table 3.5 Member sizes for the conventional composite floor system with metal deck slabs.....	50
Table 3.6 Member sizes for the deconstructable composite flooring system ^a	51
Table 4.1 Parameters for DfD building life cycle.....	61
Table 4.2 Parameters for DfD reusable components life cycle.....	63
Table 4.3 Parameters for traditional building life cycle.....	64
Table 4.4 Distribution types supported by Simapro (reproduced from PRé 2014).....	65
Table 4.5 Labor required for installation and demolition of traditional building (person-days)	67
Table 4.6 Labor required for installation and deconstruction of DfD building (person-days).....	67
Table 4.7 Traditional building inputs to SimaPro.....	68
Table 4.8 DfD building inputs to SimaPro	69
Table 4.9 Sample calculation for comparison of the 20-3-6 traditional and deconstructable buildings (with 66% reuse)	72
Table 5.1 Steel coupon testing results	109
Table 5.2 Concrete cylinder testing results (units: psi).....	111
Table 5.3 Pushout Test Matrix.....	122
Table 5.4 Clamp detachment sequence.....	140
Table 5.5 Summary of monotonic test results	145
Table 5.6 Summary of cyclic test results	150
Table 5.7 Channel true stress and true plastic strain.....	169
Table 6.1 Composite Beam Test Matrix.....	175
Table 6.2 Measured dimensions of steel beams and stubs.....	181
Table 6.3 Concrete cylinder testing results (units: psi).....	184
Table 6.4 Concrete plank pour sequence	185
Table A.1 Member sizes for the deconstructable composite floor system.....	203
Table A.2 Member sizes for the conventional composite floor system	204
Table A.3 Member sizes of lateral-force resisting systems	205
Table A.4 Member sizes of gravity columns	208
Table G.5 Bolt true stress and true plastic strain	368
Table I.1 Equivalent moment of inertia parameters.....	384

1. Introduction

According to the U.S. Energy Information Administration, buildings consumed almost half of the total energy used in the United States in 2012, while the transportation sector and the industrial sector accounted for 28% and 23%, respectively. As the leading contributor to CO₂ emission, the building sector was also responsible for 45% of all CO₂ emission (Energy Information Administration 2012). Although the embodied energy only amounts to 10-20% of the total energy of buildings (Ramesh et al. 2010), it will hold a larger proportion in the future, as technologies are developed to increase the efficiencies of the heating, ventilating and lighting systems. In addition to the depletion of nonrenewable resources and aggravating climate change, waste related to building construction and deconstruction is of major concern. Construction and demolition (C&D) waste totals nearly 160 million tons per year, including debris generated during demolition (48 percent), renovation (44 percent) and new construction (8 percent) (U.S. Environmental Protection Agency 2007). Recycling and reusing of C&D waste conserves landfill, cuts down the expenses for purchasing new materials, and reduces the environmental impacts.

Hot-rolled structural steel used in the construction of engineered steel building structures and infrastructure components currently is produced in the U.S. from nearly 100% recycled materials. A variety of sustainable concrete mixes (e.g., measured by a lowering of the required carbon footprint to manufacture the concrete) are also being developed worldwide. However, the manufacture of new building materials, even based on the use of recycled materials, still currently consumes significant energy derived from non-renewable fossil fuels. Achieving comprehensive sustainability in the built environment requires significant reduction in and eventual elimination of the use of most nonrenewable resources, both for construction materials and for energy consumption.

The need to reduce the energy consumption and material waste related to the construction industry motivates the exploration of Design for Deconstruction (DfD) of buildings. DfD of buildings, first proposed in the 1990s (Kibert 2003), aims at resolving these issues by reclaiming and repurposing the materials at the end of their service life. Contrary to the conventional linear material flow, which starts with the extraction of raw materials and ends with the disposal of debris in landfills, DfD could help close this loop by reducing the cost of recovering and reusing resources.

The benefits of deconstruction could be more rapidly realized if the building service life is much shorter. Although buildings are commonly designed for a 50-year service life, the actual life of most buildings is much less. A survey conducted by O'Conner (2004) revealed that demolition of buildings was rarely due to damage in structural systems and materials, but mainly because of

the lack of maintenance for non-structural components, changing land values and inability to meet current owners' needs.

Structural steel framing systems are particularly conducive to deconstruction at the end of the service life of a structure, so long as they have not been subjected to extensive permanent damage from an extreme hazardous event. When structural members are protected from the environment within a building envelope, as with this system, little deterioration occurs. Composite construction makes efficient use of the two materials, with concrete being subjected to compression and steel resisting tension. Steel frames are erected in place, with corrugated metal deck often laid atop the steel beams and girders, shear connectors shot onto the top flanges of the steel members, reinforcement laid in place, and a monolithic concrete floor slab cast in place. However, composite steel-concrete floor systems, by far the most ubiquitous type of structural steel framing for commercial and residential buildings, are not reusable at end-of-life. The integration of steel beams and concrete slabs via shear connectors inhibits the separation of the two materials, making impossible the deconstruction of the composite flooring systems and reuse of the structural components. Steel beams and shear studs can be recycled after being extracted from demolition debris, while concrete slabs are crushed for fill or making aggregates for new concrete. Conventional composite floor systems are therefore not the best choice for reducing the long-term environmental impacts of building materials.

The aim of this research is to establish fundamental strategies for predicting the behavior of and designing sustainable steel structures through combining sustainably optimized prefabrication strategies with DfD, achieving nearly 100% reusability for composite floor framing systems within the context of reusable bolted steel framing. This research will combine experimental testing program and finite element analysis to characterize the behavior of the new composite floor system under gravity loading and lateral loading, including seismic loading.

1.1 Deconstructable composite prototype system

A new deconstructable composite floor system is proposed in this project. This system is designed to maintain the benefits of steel-concrete composite construction, such as enhanced flexural strength and stiffness, reduced steel beam size and weight, and ease of construction, and enable sustainable design of composite floor systems in steel building structures, components disassembly and reuse of the structural components. The deconstructable composite prototype is illustrated in Figure 1.1; this concept was first introduced in Webster et al. (2007). The system consists of precast concrete planks and steel beams connected using clamping connectors. Frictional forces are generated at the steel-concrete interface to resist required shear flow and achieve composite action. Cast-in channels are embedded in concrete to provide flexibility for where the beam intersects the plank and allow for different beam width. Tongue and groove joints at the concrete plank edge ensure vertical loads transfer between adjacent planks, and offer

a level and well-matched surface. By untightening the bolts, the clamping connectors enable the precast concrete planks and the steel beams to be easily disassembled and reconfigured in future projects.

Mechanical connectors are usually used in conventional precast concrete construction to transfer in-plane diaphragm forces. In order to achieve deconstructability of the system, grouting the planks and placing a cast-in place concrete topping, which help to tie all the planks together, are eliminated. Alternatively, the precast concrete planks are connected using unbonded threaded rods before being attached to the steel beams, as shown in Figure 1.2, with a pattern of connections aligned at 4' on center and the planks staggered to help facilitate transfer of forces across the diaphragm. Friction, developed by pretensioning the rods, provides the resistance against joint sliding due to diaphragm shear and joint opening due to diaphragm flexure.

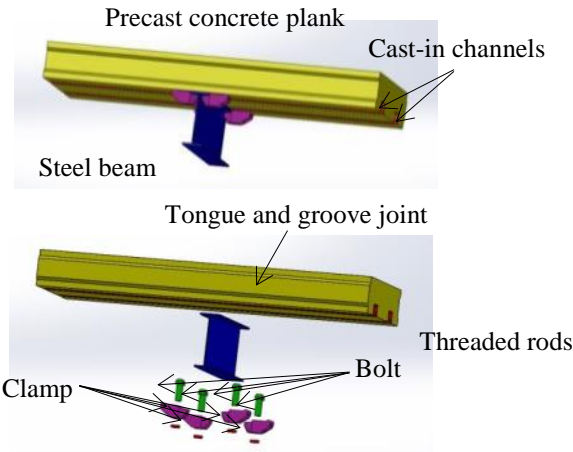


Figure 1.1 Deconstructable composite beam prototype

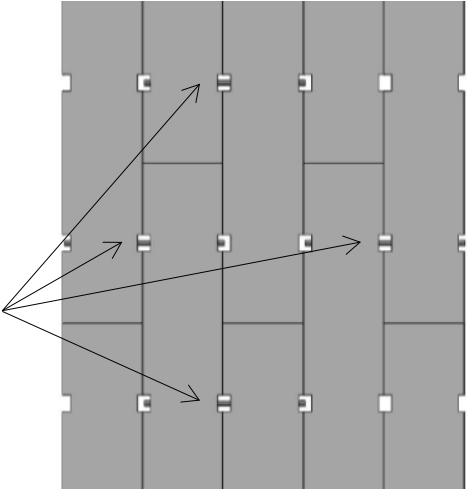


Figure 1.2 Precast concrete plank connections

Preliminary plank dimensions, presented in Figure 1.3 are 20 ft. x 2 ft. x 6 in. This size is believed to be small enough to facilitate transportation and handling, and promote reconfiguration in future structures, but large enough to have structural integrity and reduce labor for construction and deconstruction. Ideally, the planks are stocked in different sizes and concrete strengths for ready use, comparable to how steel is currently stocked at supply centers. A typical plan layout for a prototype office building using this system with a staggered plank configuration, as seen in Figure 1.2, is shown in Figure 1.4.

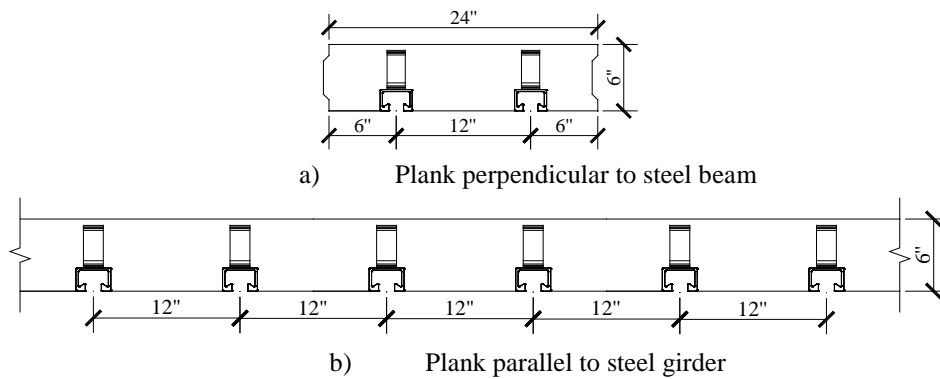
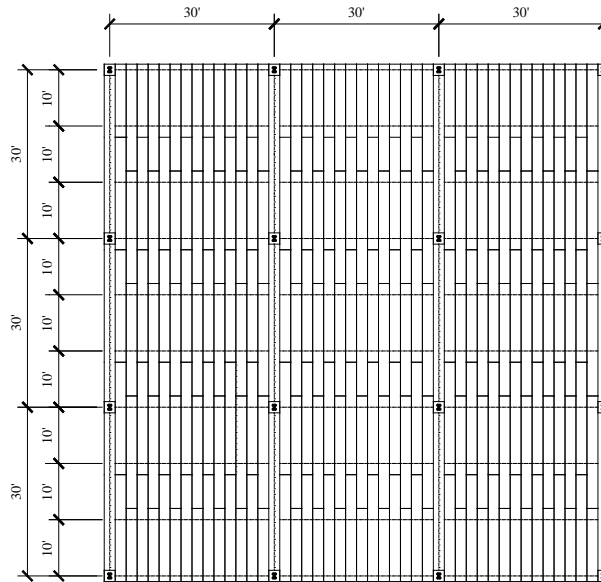


Figure 1.3 Precast concrete plank cross section (units: inches)



Notes:

1. The dashed lines show the steel framing. The beams are perpendicular to the precast concrete planks, while the girders are parallel to the planks.
2. Other precast plank patterns are also possible for the DfD system.

Figure 1.4 Typical floor plan for deconstructable composite floor system (units: feet)

1.2 Research scope and organization

This research investigates the use of Design for Deconstruction for steel building structures, including buildings having a range of gravity loading (offices, warehouses, etc.) and lateral loading that includes both wind loading and seismic loading. A review of previous research on several subjects is presented in Chapter 2, including DfD, prefabricated structural systems, steel headed stud anchors and seismic design of diaphragms. Diaphragm behavior is then briefly introduced, and computational results are provided to demonstrate the diaphragm response of the deconstructable composite floor system. Chapter 3 covers the design of several prototype structures that can be used to explore the applicability of the proposed system in an entire class

of buildings. Life cycle assessment of this system is presented in Chapter 4 to highlight the potential benefits of using deconstructable framing systems. In Chapter 5, results from pushout tests are presented to demonstrate the strength and ductility of the clamping connectors, load distribution among the steel beam and the clamps, behavior of the bolts and the channel lips, formation of cracks, responses of the channel anchors and the reinforcement, etc. Finite element models are presented that are validated by comparing the analysis predictions with the test results. To evaluate the clamping connector behavior in a realistic manner and validate the findings from pushout tests, beam tests are designed and presented in Chapter 6. This report finishes with conclusions and future work.

2. Literature Review

This section highlights the key studies and developments on the subjects related to this research, including Design for Deconstruction (DfD), prefabricated structural systems, life cycle assessment (LCA), steel headed stud anchors and seismic design of diaphragms.

2.1 Design for Deconstruction

DfD is believed to be beneficial environmentally and economically. Reuse of components is usually favored compared to recycling of materials, as less refabrication is needed. In DfD, salvaged materials from old buildings are repurposed in new projects, thus eliminating the costs of waste disposal and material manufacturing. However, the ability to reclaim materials from retired buildings depends on how the materials are integrated during building construction. The lack of practice and research on how to design with reclaimed materials also makes it difficult to implement for now.

Kibert (2003) believed that deconstruction reserved the embodied energy of the used materials and reduced the energy input required for reprocessing and remanufacturing the materials. Of the 1.9 billion metric tons of raw materials in 1996, 1.6 billion metric tonnes was related to the building sector. The huge material flow in the building sector necessitated DfD to reduce the material extraction and demolition waste. Although the design life of buildings was usually 50 to 100 years, the actual service life was unpredictable due to the degradation of the faster-cycling components, rendering buildings in disuse and disrepair. DfD, properly implemented, could mitigate these issues to facilitate material recycle and reuse.

Kilbert (2003) indicated that numerous challenges remained for DfD, such as the lack of tools for deconstructing buildings, the low disposal cost for demolition waste, the need for building codes addressing how to design with reused materials, and the inadequacy in establishing the environmental and economic benefits. Principles of DfD were suggested to address these challenges. Kilbert (2003) also indicated that the government could play a bigger role in promoting deconstruction. Increasing the disposal costs and providing tax advantages for recovered materials would encourage the owners, contractors, architects and engineers to consider and incorporate DfD into the design of new structures. This work stressed that time was a significant factor for deconstruction and should be provided in the overall project scheduling.

Durmisevic et al. (2002) argued that traditional design of buildings focused on the short-term performance, such as the optimization of functions, costs and construction schedules. Likewise, previous research on sustainable buildings concentrated on designing energy efficient buildings and using environmental-friendly materials. Because buildings are constantly changing to cater

to the needs of the owners, Durmisevic (2002) indicated they could be dynamic and flexible structures with parts that could be disassembled, replaced, recycled or reused.

The authors defined three levels of building composition: building level, system level and component level. Elements and materials were first assembled to achieve component functions. The components were then integrated to carry system functions, such as finishing, distributing and insulation. In the end, the systems were clustered to perform building functions, for example, load-bearing, enclosure, partitioning and servicing. Building composition, therefore, should be considered at each level at the beginning of the design stage to enable building disassembly. When buildings were disassembled, disassembly at the building level could offer reuse of the systems, spatial adaptation and functional adaptation of the buildings. The authors thus indicated that disassembly at the system level provided reuse of the components and functional adaptation of the systems. Disassembly at the component level enabled reuse of elements and materials as well as functional adaptation of the components. In order to design decomposable structures, the main characteristics were summarized, including modular parts dry assembled on site, independence of various systems, application of parallel instead of sequential assembly/disassembly, use of mechanical connections, etc.

Two case studies were examined by Gorgolewski (2008) to highlight the challenges inherent in DfD. Gorgolewski (2008) indicated that reuse of the components was more favorable than using recycled materials in terms of environmental impacts, but designing with reclaimed materials could add complexity to the design process. Recycled materials, which were manufactured with the used materials, had almost the same properties as the virgin materials. However, reusing deconstructed components in a new project required the establishment of their structural characteristics. Coordinating demand with supply was also important. It was common that the materials were not available at the right time, in the right amount and dimension. Unlike the traditional design approach in which the components sizes were specified before design, reused components were identified on the demolition site. The designers usually had to redesign and choose the components available. It was beneficial for the design engineers and architects to communicate and develop working relationships with the demolition and salvage contractors to obtain an inventory of available components and purchase the needed components to prevent the contractors from selling them. Gorgolewski (2008) also indicated that additional fees and costs related to identifying, testing and restoring the purchased materials were also inevitable.

2.2 Prefabricated structural systems

In prefabrication, structural components are manufactured in factories, and then transported to the construction site for assembly. Prefabrication and modularization have received increasing attention due to reduced construction time and labor cost, controlled manufacturing process,

fewer restraints by adverse weather, and standardization and customization of the products. All of these benefits are conducive to DfD.

A survey conducted by McGraw-Hill Construction (2011) indicated the following related to prefabrication and modular construction: 66% reported a decreased project schedule, with 35% reporting a decrease of four weeks or more; 65% indicated a decreased project budget, with 41% indicating a decrease of 6% or more; 77% described decreased construction waste, with 44% describing a decrease of 5% or more. All these improvements in productivity were the driving factors for contractors, engineers and architects to adopt prefabricated/modular construction. The report highlighted that a main reason for not using prefabricated/modular construction was because the architect did not design it into the project.

As an alternative to traditional bolting and welding connections between steel components, Lindapter clamping connections are designed to eliminate on-site drilling and welding, retain the integrity of the steel pieces and suit any steel beam size. The Lindapter connection can be designed for tensile, combined, frictional, compression and shear loading. More importantly, the connection can be deconstructed and reused several times (Lindapter 2013).

Sandwich plate system (SPS) is a composite material comprising two steel plates bonded with a polyurethane elastomer core. The core increases the distance between the steel plates, thus increasing the flexural strength and stiffness. In addition, the presence of the core suppresses the buckling of the steel plates. SPS delivers a high strength to weight ratio, making it an excellent alternative to both reinforced concrete and stiffened steel. SPS also promotes a sustainable built environment. SPS panels can be unbolted from the supporting steel frames and relocated to a new building. The two components of SPS panels are fully recyclable (Intelligent Engineering 2011).

A proprietary steel framing system has been developed by ConXtech (Renz 2005). ConXtech moment-resisting frames are intended for high seismic zones and eliminate the need for braced frames and shear walls. Lowering and locking connections aid both construction and deconstruction on site, enabling structural steel reuse. The moment frames employ reduced beam sections to dissipate energy during earthquakes. The absence of interior obstacles makes the structures more adaptable for future use. ConXtech utilizes robotic welding to reduce construction time and labor while increasing quality control.

2.3 Life-cycle assessment

As the building industry becomes more aware of and concerned with sustainability, guidelines and standards are improving to reflect this knowledge. Cross (2013) summarizes many of the developments in green codes, standards, and rating systems, including LEED (USGBC 2013),

ASHRAE 189.1 (ASHRAE 2011), and the International Green Construction Code (IgCC). ASHRAE 189.1 and IgCC are written in code language and are intended to provide minimum requirements of a high-performance green building. LEED is a voluntary guideline providing recommendations to improve the sustainability of a project. However, some jurisdictions require LEED for private projects. ASHRAE 189.1 and IgCC require certain levels of sustainable materials in every project, or an LCA comparing the proposed project to a baseline may be substituted. LEED version 4 has also integrated LCAs as an option to acquiring credits. As LCAs are incredibly complex, data driven tools, members of the project team may take on added responsibilities as LCAs become more popular. The members of the team will have to consider providing information about material quantities, content, and sources to validate the LCA.

Tingley et al. (2012) have developed a web-based LCA tool called Sakura to assess the environmental benefits of design for deconstruction. Tingley assumes conservatively that durable materials like steel may be reused twice within a one hundred year life span. This assumption is based on an average building life of 50 years. Knowing that buildings often have shorter lives, it is reasonable to assume DfD components may see up to three or even four reuses.

HDR and PE Americas (2010) conducted a case study LCA comparison of a building with concrete framing and a building with steel framing to investigate LCA procedures with buildings and to gain insight into the different structural framing choices. The results of the study show the steel framed building as superior in four of the five impact categories, with the concrete building only having a superior impact in energy demand. However, all of the differences in impacts fall below the 15% confidence threshold, meaning neither building type can be considered statistically superior to the other. Additionally, a survey of steel fabricators reveals a significant gap in environmental impacts, particularly energy demand, caused by the best and worst fabricators. This study shows that the impacts of concrete and steel are similar enough that other decisions will become more significant to the environmental benefit of a building. While the study focuses on the choice of fabricator, it is easy to see that fabrication as well as other impacts can be reduced by reuse of systems.

Ochsendorf et al. (2011) produced an LCA studying the emissions of several building types in Phoenix, AZ and Chicago, IL. This study seeks to advance the methodology of LCAs. The authors emphasize creating a standardized and reproducible framework for buildings LCAs, so they use DOE benchmark buildings as the subjects of their study. This study also compares a building's embodied emissions and operating emissions. Embodied emissions are the emissions resulting from the construction, maintenance, and disposal of the materials of the building. In this study, emissions are measured as CO₂ equivalent of global warming potential. Operating emissions result from lighting, heating, cooling, and all other service energies used over the life of a building. The researchers find that embodied emissions currently account for about 3% to 12% of the total emissions of a building considered over a 60 year lifespan. However, as more

energy efficient buildings are designed and built and the demand for operational energy is reduced, the proportional impacts of embodied energy will increase, as will the benefits of the reuse of materials.

A study from López et al. (2008) compared the environmental impacts of buildings with floor systems made up of hollow-core precast slabs and cast-in-place one way concrete. The subject of this case study is a 6-story building with a basement and 430 m² floors. An integral concept of the study is that hollow-core slabs can span longer distances between beams than cast-in-place slabs, while still providing the same structural performance. Thus, a building with precast floors requires fewer beams, which leads to fewer or lighter columns, and a smaller foundation, all of which means this building will be lighter than an equivalently sized building using cast-in-place floor systems. This case study concludes that the building with precast floors has a 12% lower environmental impact. The precast floors themselves cost more and have a higher impact than cast-in-place floors, but the columns and foundations, which represent a higher percentage of the structure's impact, have a lower overall impact in the building utilizing precast floor systems.

2.4 Steel headed stud anchors

Extensive research has been conducted to establish the behavior of steel headed stud anchors since their introduction after World War II. Full-scale beam tests demonstrate the realistic behavior of steel headed stud anchors; however, the shear connectors are loaded indirectly from bending of the beams and unevenly along the beam length. Because the forces acting on a stud depend on the relative stiffness of all the structural components, it is difficult to establish the behavior of the steel headed stud anchors from beam tests. As an alternative, pushout tests have been widely used to study the behavior of shear connectors. However, the pushout tests cannot represent the actual loading scenario of the shear connectors in composite beams and may lead to estimated strengths and failure modes that are inaccurate if they are not properly designed. This section summarizes several key studies related to the use of steel headed stud anchors in steel connections.

2.4.1 Pushout tests and beam tests

Ollgarrd et al. (1971) tested 48 solid slab specimens. The parameters included concrete compressive strength, concrete split tensile strength, modulus of elasticity, density, stud diameter, type of aggregate and number of connectors per slab. The test results showed that when the connectors were embedded in lightweight concrete, the strengths decreased 15% to 25% compared to the strengths of connectors in normal weight concrete. As a result of greater restraint, larger curvature was observed for the stud embedded in normal weight concrete, while the stud was seen to be nearly straight in lightweight concrete. Different crack patterns were observed for the upper and lower connectors. For the upper connectors, the crack was almost

vertical to the free end, while the crack at the lower stud propagated toward the steel beam surface at about a 45° angle. A regression analysis was employed to obtain an equation for the stud strength. An empirical expression for the load-slip relationship was also determined.

Grant et al. (1977) reported test results of 17 composite beams. The variables were the yield strength of the steel beam, the deck geometry, and the degree of shear connection. The test results of 58 beam tests conducted by other researchers were also evaluated. The parameters were weight and strength of concrete, diameter and height of shear connectors, slab reinforcements and type of loading. All tested beams were ductile, as demonstrated by the large deflections of the beams and the plastic hinges occurring near the midspan. The predominant failure mode was rib punch-through failure for the shear connectors in beams with wider slabs, while horizontal rib cracking first occurred in narrower slabs since the full development of the failure surface was truncated. A revised model for shear connector strength was provided to include the effects of rib height and embedment of the connector. Modified models for calculating effective moment of inertia and section modulus were also proposed for deflection estimation and allowable stress design of composite beams.

Strong and weak position issues in composite beams were explored through four beam tests by Easterling et al. (1993). The authors indicated that the best approach for evaluating shear connector strength was to use pushout tests to investigate the influences of the parameters and formulate design equations and then validate the equations in beam tests. The only nominal parameter was the stud positions. All the beams were ductile, but the behavior was different for strong position and weak position studs. The strong position studs exhibited higher strength than the weak position studs, which was attributed to more concrete between the studs and the metal deck. The strong position studs failed by developing concrete shear cones or shearing off in the shank, and punching through the deck rib was the limit state for the weak position studs. Test results revealed that the shear stud strength used in the AISC specification (1986) was unconservative in many cases and needed further modification.

Extensive research conducted by Rambo-Roddenberry (2002) laid the basis for the steel headed stud anchor strength expression in AISC (2010a). Twenty-four solid slab pushout test specimens were tested, and the variables were flange thickness, steel/concrete surface and normal force. The results showed (1) flange thickness did not affect the stud strength significantly; (2) sheet metal between steel beam and concrete slab reduced the frictional component of the stud strength; (3) applying normal force on the concrete slabs increased the stud strength. The equation developed by Ollgarrd et al. (1997), which was employed in the AISC specification (1993), was slightly unconservative when normal force was not applied to the specimens.

Ninety-three composite slab pushout tests were also performed. The following parameters were studied: stud diameter, concrete strength, deck height, friction at the deck/steel beam surface, and

tension in the stud shank. The main conclusions were (1) strong position studs exhibited stud shearing failure, and weak position studs exhibited rib punching through failure; (2) the limit state was rib shearing for deep deck tests; (3) 7/8'' studs had much less strength than 3/4'' studs because of limited welding abilities at the lab. The AISC strength equation for shear connectors in composite slabs was also based on the formula developed by Ollgarrd et al. (1997), but a strength reduction factor, SRF, was included to account for the presence of the metal deck. The tested shear connector strengths were significantly less than the AISC predictions. New strength prediction models were concluded from the pushout test results, which were proved to be adequate comparing to the test results elsewhere.

Three partially composite beams were designed to confirm the validity of the new equation. The main differences were the stud position and the number of studs per rib. The test results correlated well with the expected flexural strength using the AISC flexural model. Based on all composite beam test results reported, a resistance factor for composite beam flexural strength was calculated through reliability analysis.

2.4.2 Deconstructable shear connectors

Lam et al. (2013) conducted both experimental and analytical research on demountable shear connectors. The connector with a 16 mm threaded end was fabricated from the standard 19 mm diameter T. W. Nelson headed stud connector. A M16 Gr 8.8 nut was used to fasten the connector to the steel beam. Eight specimens were tested, and the parameters were the concrete compressive strength and the headed/stud collar size. Two types of failure modes were observed: fracture of the shear connectors close to the threaded end or failure by concrete crushing and splitting. For specimens failed by concrete crushing, the slabs can be easily disassembled from the steel beam and the threaded portion of the shear connectors is not damaged. By comparing the load-slip curves for welded headed studs and demountable connectors, Lam et al. (2013) found that when the concrete strength and the failure mode are similar, the demountable connectors achieve similar strength but with higher ductility than the welded connectors. A nonlinear finite element model was developed to investigate the capacity of these shear connectors embedded in a solid slab. The analytical model proved to give a good prediction of the connector capacity and load-slip behavior.

Lee et al. (2013) considered the deconstructability and sustainability of bolted shear connectors in composite beams. Precast geopolymer concrete (GPC) slabs replaced ordinary Portland concrete (OPC) slabs, as GPC was believed to mitigate the excessive CO₂ emissions associated with OPC. Four pushout tests were designed according to Eurocode 4 Specifications. Two tests were designed using M20 8.8 single nut bolts embedded in concrete slabs and the others were designed using M20 8.8 bolts through 24 mm precast holes. Three distinct stages were discovered in the load-slip curves for the pretensioned bolted shear connectors: viz. a region of

“full interaction”, a region of “zero interaction” and a region of “partial interaction”. These were delineated by the frictional force at the steel-concrete interface, by the size of the clearance hole relative to the diameter of the bolt and by the shear flow force as a result of bolts bearing against concrete. For the first two tests, only two stages were observed because the bolts were embedded in the concrete panels during the pre-casting process and therefore there was no hole clearances between the bolts and the surrounding GPC concrete.

2.4.3 Computational analysis of steel headed stud anchors and composite beams

Closed form solutions for calculating the shear connector force and slip and the beam deflection were first derived by Newmark et al. (1952). The derivation was based on the assumption of equal curvature and no separation between steel and concrete elements.

A numerical procedure was proposed by Gattesco (1999) accounting for nonlinear behavior of concrete slabs, steel beams and shear connectors. The beam was discretized into several elements with four degrees of freedom at each end: vertical displacement, rotation, horizontal displacement at the centroid of concrete and horizontal displacement at the centroid of steel section. Stiffness matrices were formed for each segment and then assembled to generate equilibrium equation for the system, which could be solved to obtain the displacements at the nodes and the internal forces.

Qureshi et al. (2010) investigated the influences of spacing and layout on the shear connector capacity parametrically. Three-dimensional nonlinear finite element models, which take into account material nonlinearity and geometric nonlinearity, were verified against the experimental test results. Three-dimensional eight-node brick and six-node wedge reduced integration elements were used for the concrete slab, shear studs and steel beam flange. The steel metal deck was modelled with four-node shell reduced integration elements, and the wire mesh was modelled by three-dimensional two-node truss elements. Surface to surface contact was defined between the top of the metal deck and the bottom of the concrete slab. Contact was also assigned between the shear studs and the surrounding concrete. The frictional coefficient was assumed to be 0.5 in both cases. The concrete damaged plasticity model, provided in Abaqus (2011), was chosen to simulate concrete cracking under tension and concrete crushing under compression. Elastic-perfectly-plastic material was utilized for the steel components. The quasi-static solution was obtained using Abaqus/Explicit by applying the loads sufficiently slowly to render the dynamic effects negligible. Subsequently, the validated models were employed to study the effects of transverse spacing and stud position on the strength of shear studs.

2.5 Seismic design of diaphragms

Diaphragms serve multiple functions in a building. Diaphragms are responsible for transferring the inertia forces within the floor systems to the seismic force-resisting systems, and also provide supports to the vertical elements to prevent buckling and reduce the additional forces associated with P-delta effects (Moehle et al. 2010). For modelling and design, diaphragms are usually simplified as deep beams consisting of the following components: diaphragm slab; tension and compression chords, collectors, and the connections to the seismic force-resisting system; see Figure 2.1.

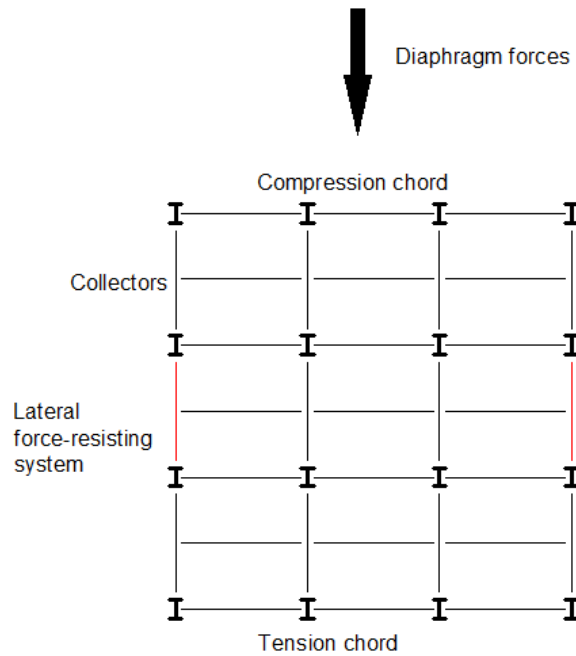


Figure 2.1 Diaphragm components

2.5.1 Seismic demand on diaphragms

Seismic demand on diaphragms is given in ASCE 7-10 Section 12.10.1.1. Design forces for vertical elements and diaphragms are different. The reason is that the maximum seismic demands on diaphragms at various levels occur at different times; therefore, using the diaphragm force to design the vertical elements would be overly conservative. Figure 2.2 presents the appropriate load patterns for evaluating the diaphragm at different levels (Sabelli et al. 2011). It should be noted that collectors are to be designed using load combinations with overstrength factors.

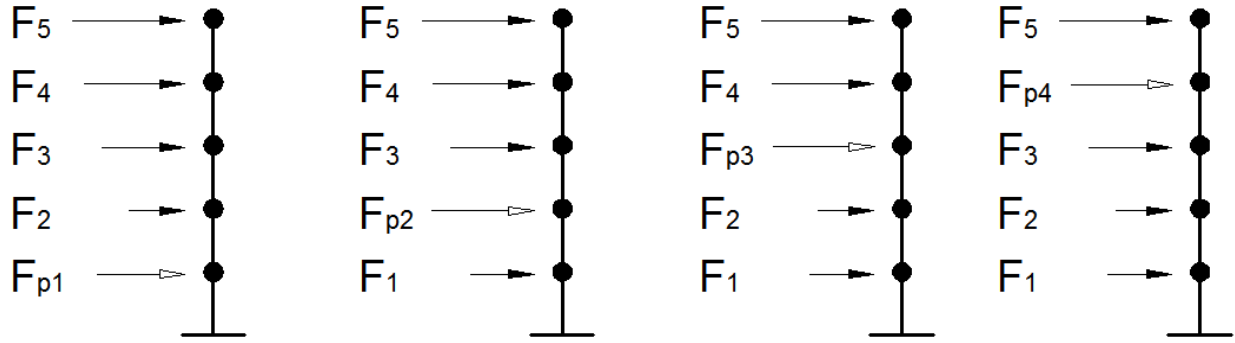


Figure 2.2 Loading pattern for diaphragms at different levels

2.5.2 Seismic behavior of diaphragms

Traditionally, diaphragms are designed to remain elastic because of their importance in maintaining building integrity. There have been few cases of observed damage in diaphragms after earthquakes (Moehle et al. 2010).

Based on the relative rigidity of the diaphragms and the seismic force-resisting systems, diaphragms can be classified as rigid, flexible and semi-rigid per ASCE 7-10 Section 12.3.1. Examples of rigid diaphragms are concrete slabs and composite slabs with span-to-depth ratio of 3 or less. For structures with rigid diaphragms, the distribution of the lateral forces depends on the relative stiffness of the vertical elements in the seismic force-resisting systems. The seismic force distribution among the vertical elements in structures with flexible diaphragms, however, depends on the tributary area supported by the vertical element. It is permitted to idealize the diaphragm as flexible if the maximum in-plane deflection of the diaphragm is more than twice the average story drift. Examples include metal deck and wood panels spanning braced frames or concrete shear walls.

2.5.3 Diaphragm analysis

Simplified models, such as an equivalent beam model, equivalent beam-on-spring model and corrected equivalent beam model, are usually adequate for modeling of diaphragms in regular buildings. Complicated models such as finite element models and strut-and-tie models are necessary for buildings with irregularities (Moehle et al. 2010). No specific provision for deciding forces in individual components is available. The required strength should be calculated in accordance with the assumed distributions, and adequate ductility is provided to ensure force redistribution. For example, when shear is uniformly distributed along the depth of the diaphragm, it is reasonable to infer that chord forces are concentrated at the diaphragm boundaries. In this case, shear ductility is required for the metal deck when the axial deformation is significant for a long collector (Sabelli et al. 2011).

2.5.4 Diaphragm component design

2.5.4.1 Composite diaphragm strength

Easterling et al. (1994) summarized the test results on composite diaphragms where strength, stiffness and limit states were reported. Parameters for the specimens were steel-deck type, steel-deck thickness, connector types, number of connectors, slab aspect ratio, edge member size, and concrete thickness. No primary or secondary reinforcements were used. All diaphragms displayed brittle behavior, but the author believed that the ductility of some specimens could be improved by adding reinforcements in the slabs. Governing limit states were identified and described. Concrete diagonal cracking or cracking parallel to and above the deck flange might occur when the concrete above the deck was thin. Deck-concrete shear transfer failure appeared in welded composite diaphragms, but this limit state was unlikely for diaphragms connected with steel headed stud anchors because shear studs restrained the relatively slip between the steel deck and the concrete slab effectively. It was also concluded that load transfer from the edge member to the composite slab took place in the edge zone, a small region along the diaphragm edge. This was shown during tests when the separation between the metal deck and the concrete slab was significant at the corners, and the interior region remained composite. Equation 2.1 was proposed to estimate the concrete shear strength. Steel Deck Institute Diaphragm Design Manual (SDI DDM03) uses a different design equation that incorporates the contributions from both the concrete slab and the deck-to-steel framing connectors.

$$V_n = 3.2t_e b \sqrt{f'_c} \quad (2.1)$$

Where

V_n = shear strength of the diaphragm

t_e = effective thickness of the composite slab including a construction from the steel deck using a transformed section approach

b = depth of the diaphragm (inches)

f'_c = concrete compressive strength (psi)

2.5.4.2 Steel members

Steel members include chords, collectors as well as members that are part of the lateral resisting system. The design procedure for all these members is not outlined in detail in design guides or specifications. Simplified design approaches are provided in the AISC 360 commentary.

Steel girders that are part of a moment frame or braced frame are often designed as non-composite sections. This is because the moments on the girders in moment frames are both positive and negative, and the axial forces in moment frame or braced frame girders could be

tension or compression depending on the direction of the external loading. Designing composite sections for the negative moment region may not be economical for using extra reinforcement in the slab. In addition, the shear connectors necessary for shear transfer in this region can only be placed in a very small length, making construction difficult.

Steel chords can be designed for combined loading of axial force due to shear transfer between the concrete slab and the steel beam as well as flexural force resulting from gravity loading and lateral loading. It is recommended in the commentary that non-composite axial strength and composite flexural strength are used in the interaction equation in Chapter H in AISC (2010a) for strength check of steel chords. A minimum 25% composite action is also suggested because the anchors will be overloaded if their number is not sufficient. Although the anchors are properly detailed for diaphragm force transfer, they are also subjected to gravity loading even if the sections are designed as bare steel.

The design of beam-to-column connections and columns needs to account for combined loads due to diaphragm behavior, for example, collector axial force that is collected through shear studs transferring the force into columns in the seismic resisting system.

2.5.4.3 Shear connectors

Typically, the flexural design of composite beams determines the detailing of shear connectors. However, while the in-plane diaphragm forces may make additional shear connectors necessary, typically they are not needed. Guidance on this issue is also provided in the AISC Commentary (AISC 2010a). The commentary states that it is not required to superimpose the horizontal shear due to bending of the beams and the horizontal shear resulting from diaphragm behavior for two reasons. First, it is recognized that reduced live load is used in load combinations with lateral loads in ASCE 7. This reduced live load decreases the demand on the shear connectors, and the “residual” strength provides certain capacity for diaphragm force transfer. Secondly, the shear flows on the shear connectors are not additive for gravity and lateral loading. Lateral loads overload the shear connectors on half of the beam and underload those on the other half, which is deemed to be acceptable since the steel headed stud anchors are ductile.

2.5.5 Diaphragm seismic design methodology

A new seismic design methodology for precast concrete diaphragms was developed by Fleischman et al. (2014). Unlike the conventional design approach for diaphragms where all the structural components are designed to be elastic or sustain minor damage during earthquakes, the new performance-based design approach utilizes prequalified precast connectors as the main energy-dissipating mechanism in the diaphragms.

Depending on the geometry of the diaphragm and the seismic design category, three seismic demand levels are defined: low, moderate and high. Three design options are also available to achieve the anticipated performance: elastic design option (EDO), basic design option (BDO) and reduced design option (RDO).

1. EDO: the diaphragm is designed to remain elastic not only for the design basis earthquake (DBE), but also for the maximum considered earthquake (MCE). The ductility requirement on the precast connectors is relatively low.
2. BDO: this approach targets elastic diaphragm under the DBE, and permits inelastic behavior in the MCE. Precast connectors with moderate ductility are required to prevent brittle failure in the MCE.
3. RDO: diaphragm yielding under the DBE is allowed for this design method. In exchange for the lower design forces, the precast connectors need to be highly ductile.

The primary improvements over the traditional design methodology are summarized as follows:

1. New equations with different coefficients were proposed for calculating the seismic demand in a precast concrete diaphragm, because the current design equations in ASCE 7-10 underestimated the required seismic forces, and could not take advantage of different design options.
2. The axial, shear and flexural strength of a precast concrete diaphragm were derived by taking into consideration the contribution from all the reinforcement at a diaphragm joint. An interaction equation could be applied to check the adequacy of reinforcement at the joint.
3. Effective flexural and shear modulus were also obtained by accounting for all the reinforcement at a joint. The effective diaphragm stiffness could be used to perform a drift check for the gravity columns and thus ensure the connections and non-structural components were detailed for this drift.

2.5.6 Diaphragm behavior of deconstructable composite floor systems

A series of preliminary analyses have been conducted to study the diaphragm behavior of the deconstructable composite floor systems. All the finite element models are developed in Abaqus/CAE and analyzed in Abaqus/Explicit. The analyses presented here employ the explicit method to solve quasi-static problems by applying cyclic loads sufficiently slowly to render the dynamic response negligible.

2.5.6.1 Finite element model and mesh

The finite element model, illustrated in Figure 2.3, represents half of a 30 ft. by 30 ft. diaphragm, which is composed of staggered precast concrete planks that are compressed together using threaded rods and then clamped to the steel beams. A similar test setup was utilized by Easterling and Porter (1994) to investigate composite diaphragms. Steel beams with size W14x30 and W12x19, acting as the chords in the diaphragm, are selected to represent potential beam sizes in a gravity system, and the shear connectors are designed accordingly. W18x40 member is chosen as the steel girder that is part of the seismic force resisting system along the perimeter. The number of connectors between the steel girder and the girder plank is varied to explore failure of the connection to the lateral force-resisting system. No reinforcement is used in the planks in these simulations.

Cast-in channels are meshed with both eight-node reduced integration brick elements (C3D8R) and six-node reduced integration triangular prism elements (C3D6R), while the steel beams and concrete planks are meshed with C3D8R only. The complex geometry of the clamps and the bolts, modelled in detail in this work, necessitates use of four-node tetrahedron elements (C3D4).

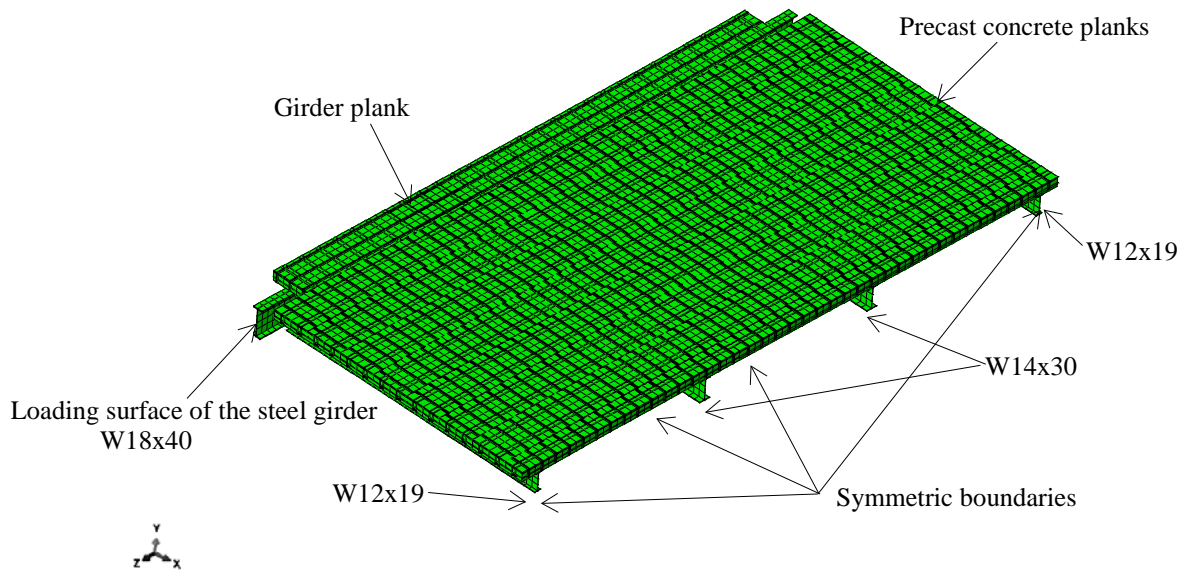


Figure 2.3 Finite element model for the diaphragm

2.5.6.2 Boundary conditions, load applications and contact

A symmetric boundary condition, as show in Figure 2.3, is defined such that nodes on these surfaces are prevented from translating in the X direction and rotating in the Y and Z directions. The ends of the steel girder are restrained from moving vertically to avoid rigid body motion of the system.

The loading history in these analyses is divided into three steps. Compression between planks is simulated by applying pressure on all the side surfaces of the diaphragm slab except for the surface where the boundary condition is defined, which is acceptable unless the response in the vicinity of the rods is studied. Bolt pretension is then obtained by assigning a thermal expansion coefficient and temperature change to the bolts, creating thermal shrinkage and generating tensile forces in the shank because of the constraints at the bolt ends. The steel girder is then subjected to cyclic loading using displacement control in the Z direction. The displacement history is provided in Figure 2.4. All the loadings are applied slowly and smoothly to minimize the dynamic effects and obtain a quasistatic solution. An optimal cyclic loading rate is found to be 0.125 mm/s.

The contact behavior between surfaces is defined in the normal direction and the tangential direction. “Hard contact”, the default normal behavior in Abaqus, puts no limit on the magnitude of the contact pressure when the contact restraint is activated once the surface clearance is zero. The contact restraint is removed when the surfaces separate, and the contact pressure becomes zero or negative. A penalty formulation, which allows a small amount of relative movement when the two surfaces are bonded, is used to characterize the behavior along the interface, and the frictional coefficient is taken as 0.3 for all the surfaces. General contact, rather than the contact pair algorithm, is selected to automatically define potential contact surfaces.

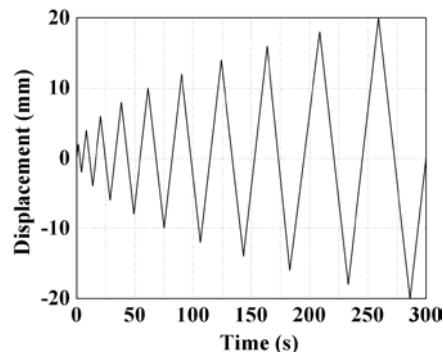


Figure 2.4 Displacement history for the computational models

2.5.6.3 Material model

- Material model for concrete

Concrete tensile cracking and compressive crushing are accounted for using the concrete damaged plasticity model provided in Abaqus. The tensile stress-strain relationship is linear elastic until the cracking stress is reached, and a softening stress-strain curve follows representing the formation of cracking. The compressive stress-strain response is linear elastic until the initial yield stress. The subsequent response is characterized by strain hardening and strain softening beyond the ultimate stress. Under cyclic loading, this concrete model can capture

opening and closing of cracks observed in tests by allowing for stiffness recovery when the load is reversed.

Because mesh sensitivity exists for concrete with little or no reinforcement, tension stiffening is defined in terms of a stress-displacement curve rather than stress-strain curve to eliminate localization issues. The compressive stress-strain curve in BS EN 1992-1-1, provided in Equation (2.2), is employed for this analysis. The elastic modulus can be calculated using Equation (2.3). The Poisson's ratio is taken as 0.2.

$$\frac{\sigma_c}{f_{cm}} = \frac{k\eta - \eta^2}{1 + (k-2)\eta} \quad (2.2)$$

$$E_{cm} = 22 \left[\frac{f_{cm}}{10} \right]^{0.33} \quad (2.3)$$

Where,

f_{cm} = mean value of concrete cylinder compressive strength (MPa)

σ_c = concrete compressive stress (MPa)

$$\eta = \frac{\varepsilon_c}{\varepsilon_{c1}}$$

ε_c = concrete compressive strain

ε_{c1} = concrete compressive strain corresponding to peak stress f_{cm}

$$\varepsilon_{c1} = 0.7f_{cm}^{0.31} \leq 2.8$$

$$k = \frac{1.05E_{cm} \times \varepsilon_{c1}}{f_{cm}}$$

The default parameters specified in Abaqus for the concrete damaged plasticity model are used to characterize the plastic behavior under general stress and stress state. The parameters include: dilation angle = 38° , eccentricity = 0.1. K_c , the ratio of the second invariant of the stress deviator on the tensile meridian to that on the compressive meridian at initial yield at a given first invariant of stress such that the maximum principal stress is negative, is equal to 0.67. The ratio of biaxial compressive yield stress to uniaxial compressive yield stress σ_{b0}/σ_{c0} is taken as 1.16.

Concrete damage variables characterize stiffness degradation when the specimen is unloaded from any point on the softening branch. The damage variables range from zero for an undamaged model to one, exhibiting complete loss of strength and stiffness. Concrete tensile damage D_c and compressive damage D_t are derived using the following expressions:

$$D_c = 1 - \sigma_c/f_c \quad (2.4)$$

$$D_t = 1 - \sigma_t/f_t \quad (2.5)$$

Mesh dependency, which means mesh refinement does not lead to a converged solution for the problems, exists for concrete with no or little reinforcement. In this case, cracking only occurs in a localized region, and no additional cracks appear in other regions with a finer mesh. In this analysis, mesh dependency is eliminated by defining a stress-displacement curve for concrete, which is based on the concrete fracture energy proposed by Hillerborg et al. (1976).

- Material model for steel beam, channels and bolts

Elastic-perfectly-plastic material is defined for the steel beam and channels. The nominal yield stress for the steel beam and channels is taken as 345 MPa. The elastic modulus is taken as 200 GPa for all of these components. The mechanical behavior is assumed to be the same in both tension and compression. A typical stress-strain curve for Grade 8.8 bolt material is provided in Kulak et al. (1987) and used for the analysis, as seen in Figure 2.5.

2.5.6.4 Analysis results

The parameters of the analytical models for the diaphragm system are listed in Table 2.1, including the compressive stress between adjacent planks and the number of shear connectors between the steel girder and the girder plank. The different compressive stresses in the table correspond to different spacing between the threaded rods. For example, when the 1 in. diameter A449 threaded rods are placed at a distance of 4 ft., an equivalent compressive stress of 1.7 MPa is assumed. Although the steel girder is designed as a bare steel section, at least twenty shear connectors are needed to ensure a minimum of 25% composite action (AISC 2010a). The spacing of the clamps is reduced from 3 ft. to 2 ft. when 28 clamps are used for the steel girder.

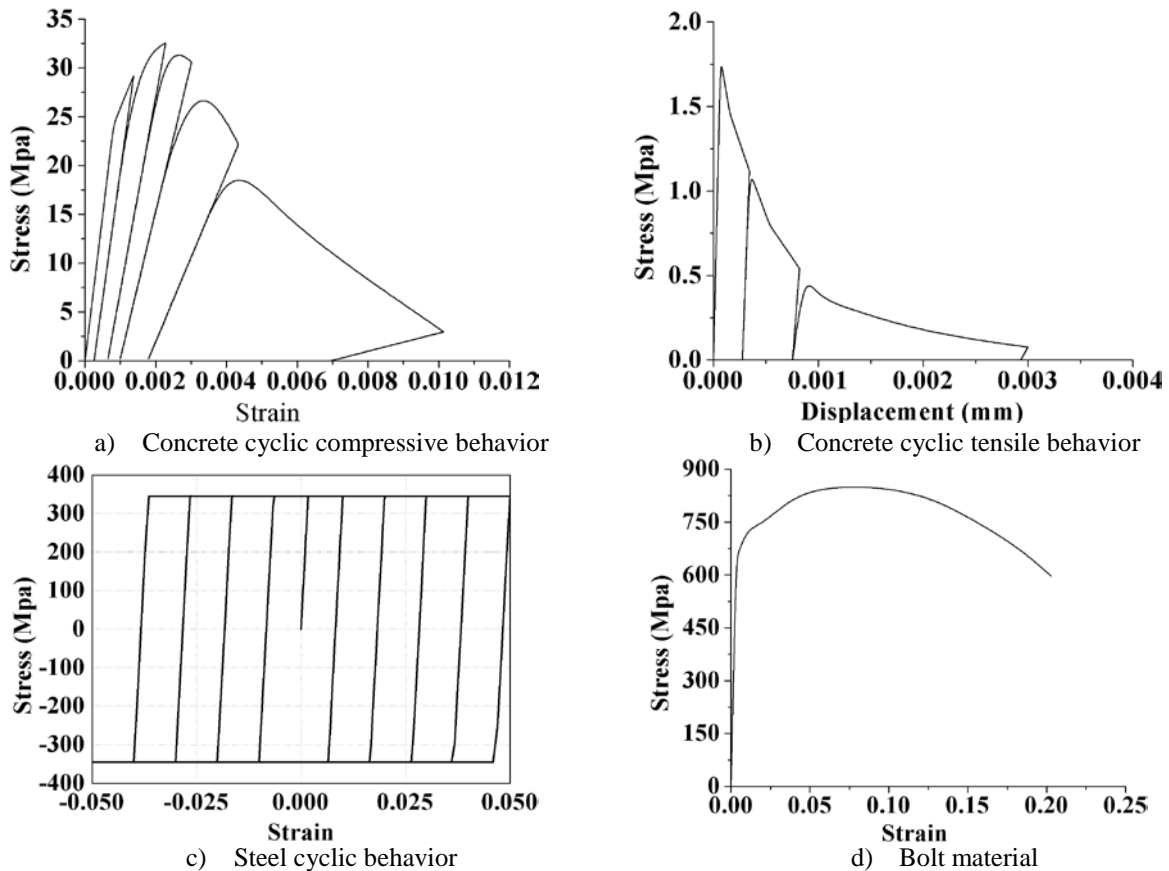


Figure 2.5 Material stress-strain curves

Table 2.1 Analytical model parameters

Model Number	Compressive stress (MPa)	Number of shear connectors
1	1.7	28
2	1.7	20
3	3.4	28
4	3.4	20
5	6.8	28
6	6.8	20

The cyclic load-displacement curves are plotted in Figure 2.6. The limit state for the first four models is joint sliding due to diaphragm shear; therefore, the compression between adjacent planks is directly related to the ultimate strength. The hysteresis loops are almost identical for Model 1 and Model 2, even though the number of shear connectors varies. Small, but slightly different, slip between the steel girder and girder plank are found for Models 3 and 4, which could explain the fact that the hysteresis curves for the two models are very much alike, but differences do exist. Because the clamping stress between the planks is doubled, the peak strength of Model 3 (Model 4) is twice that of Model 1 (Model 2). Distinct load-displacement curves are plotted for Model 5 and Model 6, as their limit state is slip of the clamps between the steel girder and the girder plank. The number of shear connectors affects the ultimate strength of

the diaphragms. After doubling the clamping stress, the strength increase of Model 3 is larger for than Model 4, which is reasonable since Model 4 has fewer clamps and slip happens earlier than Model 3. All the diaphragms demonstrate ductile behavior with no strength and stiffness degradation.

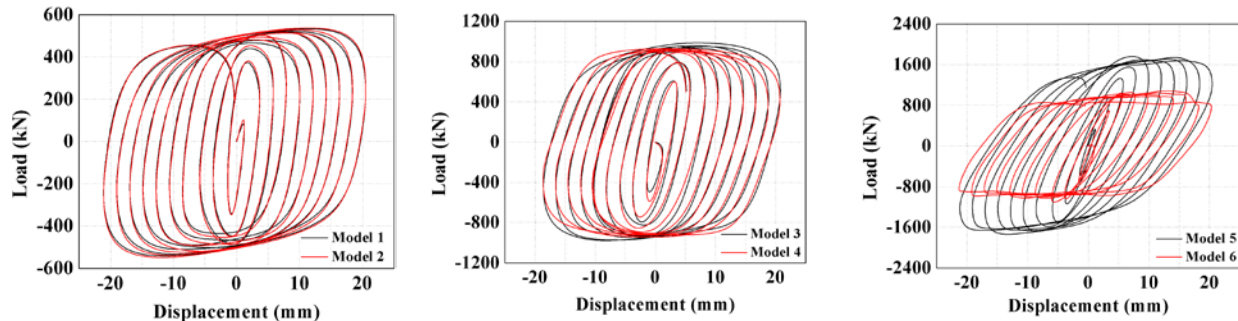


Figure 2.6 Load-displacement curves

In the diaphragm models, the moment at the symmetric boundaries is shared by the steel chords and the concrete slab in accordance with their relative stiffness. Figure 2.7 shows the ratio of the moment distributed to steel to the moment resisted by concrete for all the models during the cyclic loading process. The ratios for Models 1 and 2 are almost the same, since they have the same limit states. More force flows into concrete in Models 3 and 5 than Models 4 and 6. As the compressive stress between concrete planks increases, less force flows into steel framing. It can be concluded that the majority of the external force follows the stiffer load path and flows into the concrete slab, and the rest goes through the steel chords that are bent about their weak axis.

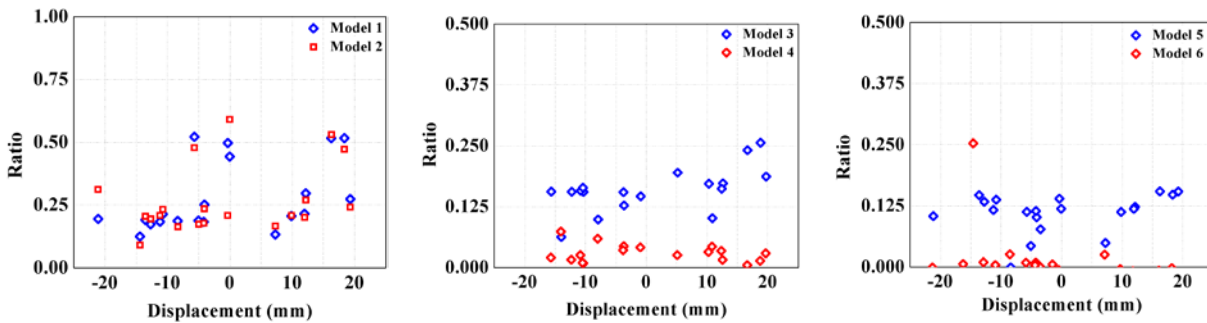


Figure 2.7 Steel moment to concrete moment ratio

While diagonal cracking may be seen in monolithic concrete diaphragms, this failure mode is uncommon in precast concrete diaphragms, since the joint between the diaphragms provides a weak link in the system. This argument is validated by minimal concrete tensile damage observed in the diaphragm models. Joint opening due to diaphragm bending, another potential limit state for a precast concrete diaphragm, did not occur for the models developed.

3. Prototype Structures

Behavior of a new structural system can be studied through the use of prototype structures. Prototype structures are developed to expand the knowledge of this system and investigate its applicability to an entire class of buildings. This section summarizes the prototype structures detailed in this research to help explore a range of design issues arising in the DfD system.

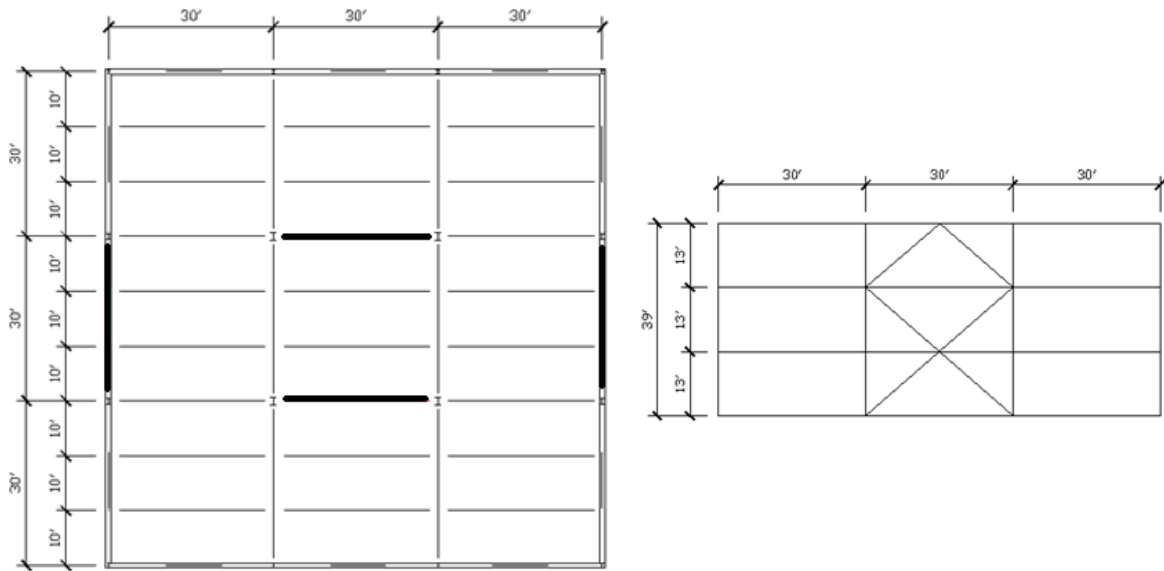
The prototype structures in this work are designed in accordance with the following codes: *Minimum Design Loads for Buildings and Other Structures* (ASCE 2010), the *AISC Specification for Structural Steel Buildings* (AISC 2010a) and the *AISC Seismic Provisions for Structural Steel Buildings* (AISC 2010b).

3.1 Selection and design of prototype structures

The prototype buildings in this work all are designed to have the same plan layout: 3 bays by 3 bays with a width of either 20 ft or 30 ft (Figure 3.1a). The buildings are 3 or 9 stories tall with a story height of 13 ft. Simple connections are assumed for beam-to-beam and beam-to-column connections within the gravity system. Concentrically braced frames are utilized to resist lateral loads, including wind loads and seismic loads. Since the buildings are assumed to be located in Los Angeles, the steel systems are detailed for seismic resistance and special concentrically braced frames (SCBF) are chosen (Figure 3.1b), with a focus on ensuring all bolted construction in the field to maximize the potential for deconstruction. The lateral loads are investigated in this system especially to highlight issues related to using deconstructable flooring systems as diaphragm systems within buildings to help transfer lateral loads to the lateral-force resistance system.

A composite floor framing system is used for all configurations, and composite beams are designed accordingly. Either headed stud anchors or girder clamps (Lindapter 2011) connect the concrete slabs with the steel beams in the conventional composite system and the deconstructable composite system, respectively. Solid slabs and composite slabs are both chosen for the prototype structures. It is assumed that the limit states of composite beams with solid slabs are more comparable to the proposed system using clamping connections, while composite beams with profiled metal deck are more widely used in current composite floor systems. Hence, composite slabs are selected as the main form of composite floor system in the life-cycle assessment conducted in Chapter 4.

Two levels of live loads are selected: high gravity, which corresponds to storage warehouse live load (250 psf) and low gravity, which corresponds to office live load and partition allowance (80 psf). In this work, it is assumed that the 3-story buildings are used as storage warehouses, while the 9-story structures are office buildings.



Thick solid lines show the locations of the braces

a) Plan view

b) Elevation view

Figure 3.1 Building layout for three story buildings

Twenty-four framing systems are designed with variations of bay width, number of stories, concrete slab thickness, and shear connection between concrete slabs and steel beams. The frames are also named in this order with “ss”, “sc”, and “gc” representing steel headed stud anchor connections in solid slabs and composite slabs and girder clamp connections, respectively. The prototype structure matrix is summarized in Table 3.1.

Table 3.1 Prototype structure matrix

Frame Number	Name	Bay width (ft.)	Number of stories	Concrete plank thickness(in.)	Connections between concrete and steel
1	20-3-6-ss	20	3	6	Studs in solid slabs
2	20-3-8-ss	20	3	8	Studs in solid slabs
3	20-9-6-ss	20	9	6	Studs in solid slabs
4	20-9-8-ss	20	9	8	Studs in solid slabs
5	30-3-6-ss	30	3	6	Studs in solid slabs
6	30-3-8-ss	30	3	8	Studs in solid slabs
7	30-9-6-ss	30	9	6	Studs in solid slabs
8	30-9-8-ss	30	9	8	Studs in solid slabs
9	20-3-6-sc	20	3	6	Studs in composite slabs
10	20-3-8-sc	20	3	8	Studs in composite slabs
11	20-9-6-sc	20	9	6	Studs in composite slabs
12	20-9-8-sc	20	9	8	Studs in composite slabs
13	30-3-6-sc	30	3	6	Studs in composite slabs
14	30-3-8-sc	30	3	8	Studs in composite slabs
15	30-9-6-sc	30	9	6	Studs in composite slabs
16	30-9-8-sc	30	9	8	Studs in composite slabs
17	20-3-6-gc	20	3	6	Girder clamps
18	20-3-8-gc	20	3	8	Girder clamps
19	20-9-6-gc	20	9	6	Girder clamps
20	20-9-8-gc	20	9	8	Girder clamps
21	30-3-6-gc	30	3	6	Girder clamps
22	30-3-8-gc	30	3	8	Girder clamps
23	30-9-6-gc	30	9	6	Girder clamps
24	30-9-8-gc	30	9	8	Girder clamps

3.2 Loads

Loading on the prototype structures includes gravity load (dead load and live load), seismic load and wind load.

3.2.1 Gravity load

The composite flooring and roofing systems are comprised of normal weight concrete slab, mechanical/electrical/plumbing, roof deck, rigid insulation, roofing (five-ply felt and gravel), ceiling system (acoustical fiber board and mechanical duct allowance) and steel framing (beams, girders and columns). Minimum design dead load for these components can be found in Table C 3-1 of ASCE (2010). The dead load on the roof and 6 in. thick floor system of the prototype structures is described in Table 3.2. The weight of exterior wall systems is transferred to the foundation directly.

Table 3.2 Breakdown of dead load

Description	Roof (psf)	Floor (psf)
Concrete slab	N/A	72.5
Mech./elec./piping	10	10
Roof deck	3	N/A
Rigid insulation	3	N/A
Roofing	6	N/A
Ceiling system	N/A	5
Steel framing	10	10
Total	32	97.5

The live load is provided in Table 4-1 of ASCE (2010). Low live load is supposed to be 70 psf (50 psf + 20 psf for partitions). However, corridor loading above first floor is given as 80 psf. Therefore, an envelope of 80 psf, rather than 70 psf, is used conservatively throughout the layout. Roof live load is assumed to be 20 psf for all configurations.

3.2.2 Live load reduction

Live load is reduced in accordance with the requirements in Section 4.7 of ASCE (2010). In the prototype structures, the beams and columns for which a value of $K_{LL}A_T$ is 400 ft² or more are designed for a reduced live load in accordance with the following formula:

$$L = L_0 \left(0.25 + \frac{15}{\sqrt{K_{LL}A_T}} \right) \quad (3.1)$$

Where

L = reduced design live load per ft² of area supported by the member

L_0 = unreduced design live load per ft² of area supported by the member

K_{LL} = live load element factor

A_T = tributary area in ft²

L is no less than $0.5L_0$ for members supporting one floor and L is no less than $0.4L_0$ for members supporting two or more floors. Live loads that exceed 100 lb/ft² are not reduced.

3.2.3 Earthquake load

Three types of analytical procedures for calculating seismic load are permitted in ASCE (2010); in this work, the equivalent lateral force method is adopted for all the buildings.

Seismic base shear

The seismic base shear, V , in a given direction is determined in accordance with the following equations:

$$V = C_s W \quad (3.2)$$

$$C_s = \frac{S_{DS}}{\left(\frac{R}{I_e}\right)} \leq \begin{cases} \frac{S_{D1}}{T \left(\frac{R}{I_e}\right)} & \text{for } T \leq T_L \\ \frac{S_{D1} T_L}{T^2 \left(\frac{R}{I_e}\right)} & \text{for } T > T_L \end{cases} \quad (3.3)$$

C_s is no less than

$$C_s = 0.044 S_{DS} I_e \geq 0.01 \quad (3.4)$$

Where

C_s = the seismic response coefficient

W = the effective seismic weight

S_{DS} = the design spectral response acceleration parameter in the short period range (Section 11.4.4 or 11.4.7 (ASCE 2010))

S_{D1} = the design spectral response acceleration parameter at a period of 1.0 s (Section 11.4.4 or 11.4.7 (ASCE 2010))

T = the fundamental period of the structure

T_L = long-period transition period (Section 11.4.5 (ASCE 2010))

R = the response modification factor (Table 12.2-1 (ASCE 2010))

I_e = the importance factor (Section 11.5.1 (ASCE 2010))

Effective seismic weight

The effective seismic weight of a structure is determined as per Section 12.7.2 in ASCE (2010).

The effective seismic weight, W , is the sum of the following:

- 100% of the dead load
- 25% of the floor live load for 3 story buildings used for storage
- 100% of the partition allowance and exterior wall systems

Period determination

The fundamental period of the structure, T , in the direction under consideration is established using the structural properties and deformational characteristics of the resisting elements in a properly substantiated analysis. As an alternative to performing an analysis to determine the fundamental period, T , the approximate building period, T_a , is used directly.

$$T_a = C_t h_n^x \quad (3.5)$$

Where

h_n = the structural height

C_t & x = coefficients based on the structural types chosen (Table 12.8.2 (ASCE 2010))

Vertical distribution of seismic forces

The lateral seismic force, F_x induced at any level is determined from the following equations:

$$F_x = C_{vx} V \quad (3.6)$$

$$C_{vx} = \frac{w_x h_x^k}{\sum_{i=1}^n w_i h_i^k} \quad (3.7)$$

Where

C_{vx} = vertical distribution factor

V = total design lateral force or shear at the base of the structure (Equation 3.2)

w_i and w_x = the portion of the total seismic weight (W) of the structure located or assigned to Level i or x

h_i and h_x = the height from base to Level i or x

k = an exponent related to the structure period

$$k = \begin{cases} 1 & T \leq 0.5 \\ 1 + 0.5(T - 0.5) & 0.5 < T < 2.5 \\ 2 & T \geq 2.5 \end{cases} \quad (3.8)$$

3.2.4 Wind and snow load

Wind loads on main wind-force resisting system (MWFRS) are determined using directional procedure in accordance with Chapter 27 of ASCE (2010). Because the prototype structures are located in Los Angeles, seismic loads, rather than wind loads, dominate the design of the lateral resisting system.

Snow loads are assumed to be zero.

3.2.5 Load combinations for strength design

Basic load combinations are provided in Section 2.3.2 in ASCE (2010).

1. $1.4D$
2. $1.2D+1.6L+0.5(L_r \text{ or } S \text{ or } R)$
3. $1.2D+1.6(L_r \text{ or } S \text{ or } R)+(L \text{ or } 0.5W)$
4. $1.2D+1.0W+L+0.5(L_r \text{ or } S \text{ or } R)$
5. $1.2D+1.0E+L+0.2S$
6. $0.9D+1.0W$
7. $0.9D+1.0E$

The load factor on L in combinations 3, 4, and 5 equals 0.5 for all occupancies in which L_0 is less than or equal to 100 psf. In other words, 0.5 is used as the load factor on L in combinations 3, 4, and 5 for office buildings, and 1.0 is used for warehouse storage.

3.3 Design criteria

The available strength for each member is computed in accordance with the AISC Specifications (AISC 2010a, 2010b). A tolerance of 5% is allowed so that small overstresses are acceptable.

3.3.1 Gravity system

Elastic analysis is required to obtain the required strength for beams, girders and columns, which comprise the gravity system. Unshored construction is assumed for all the composite floor systems. For the deconstructable composite floor systems, depending on the level of live loads, either bare steel section or composite section needs to be selected first. In the deconstructable composite floor system, it is assumed that the concrete planks and steel sections act compositely once the planks are placed on and clamped to the steel beams. Lateral-torsional buckling during construction is thus not considered as a limit state. After the most economical steel section is chosen, shear connectors are determined such that the available strength is slightly larger than the required strength.

A minimum of 50% composite action is recommended by the AISC Specification and is targeted in these designs to prevent early departure from elastic behavior in both the beams and the studs. A low amount of shear connection also requires large rotation to reach the available flexural strength of the member.

Since the method of designing composite beams using girder clamps is not available at the time of design, rigid plastic analysis developed for composite beams using shear studs is utilized.

Deflection limitation

Deflections at two phases need to be checked for the conventional composite floor systems, while the deflections of the deconstructable composite beams are only checked in the second phase.

Before the concrete hardens, dead load from the weight of the wet concrete and the steel beam and live load from the construction workers and equipment are taken by the steel beam alone. The deflection limit is $L/240$, and the steel beams can be cambered to reduce ponding effect if the limit is violated.

After the concrete hardens, all the loads are supported by the composite sections. Traditionally, the live load deflection is restricted to a maximum of $L/360$. The lower-bound moment of inertia, I_{LB} , provided in AISC Specification or transformed section properties, I_{tr} , can be used to compute live load deflection.

3.3.2 Lateral resisting system

Due to symmetry of the frames, the structure can be decomposed into two lateral-resisting frames when the lateral loads are applied in a certain direction.

The direct analysis method is selected to compute the required strength of the frames. A factor of 0.80 is applied to all stiffnesses in the structure for second-order analysis. To account for imperfections, a notional load equal to 0.002 times gravity load at each floor level is applied. An additional 0.001 times gravity load at each floor level is also used so that τ_b can be taken as unity. As an alternative to a rigorous second-order analysis, the approximate second-order analysis method (also known as the B_1 - B_2 method) in Appendix 8 of the AISC Specification (AISC 2010a) is applied.

Braced frame design

Elastic analysis is used to proportion the braces. Rectangular HSS and W shape sections are selected for the braces. A redundancy factor, ρ , is assigned to the seismic force-resisting system to account for less redundancy in the structures. The value of this factor is either 1.0 or 1.3. 1.3 is chosen for the prototype structures.

SCBFs designed in accordance with these provisions are expected to provide significant inelastic deformation capacity primarily through brace buckling and yielding of the brace in tension. Therefore, a capacity design method is used for beams, girders and columns to avoid failing prior to the braces.

The required strength of columns, beams and connections in SCBF is based on the load combinations in the applicable building code that include the amplified seismic load. In determining the amplified seismic load, the effect of horizontal forces, including overstrength, E_{mh} , is taken as the larger force determined from the following two analyses:

1. An analysis in which all braces are assumed to resist forces corresponding to their expected strength in compression or in tension
2. An analysis in which all braces in tension are assumed to resist forces corresponding to their expected strength and all braces in compression are assumed to resist their expected post-buckling strength

A vertical seismic load effect is considered in designing the beams, girders and columns that are part of the lateral resisting system:

$$E_v = 0.2S_{DS}D \quad (3.9)$$

Where

S_{DS} = design spectral response acceleration parameter at short periods (Section 11.4.4 or 11.4.7 (ASCE 2010))

D = effect of dead load

HSS braces are used when their strength is adequate; otherwise, W shape braces are used.

3.3.3 Member requirements

According to AISC (2010b), columns and braces in SCBF satisfy the requirements for highly ductile members and beams satisfy the requirements for moderately ductile members. The width-to-thickness ratios of compression members do not exceed the limiting ratios (Table 3.3.) to achieve these requirements. It is assumed that the beams are provided with sufficient lateral bracing to achieve their full plastic moment strength.

Table 3.3 Limiting width-to-thickness ratios

Member	Section requirements	b/t	h/t or h/t_w
W shape beams	Moderately ductile	$0.38 \sqrt{E/F_y}$	$0.64 \sqrt{E/F_y}$
W shape columns	Highly ductile	$0.30 \sqrt{E/F_y}$	For $C_a \leq 0.125$ $2.45 \sqrt{E/F_y} (1 - 0.93C_a)$ For $C_a > 0.125$ $0.77 \sqrt{E/F_y} (1 - 0.93C_a) \geq 1.49 \sqrt{E/F_y}$ Where $C_a = \frac{P_u}{\phi_c P_y}$ P_u = required axial strength using LRFD load combination P_y = nominal axial yield strength of a member, equal to $F_y A_g$ ϕ_c = resistance factor for compression
Rectangular HSS braces	Highly ductile	$0.55 \sqrt{E/F_y}$	$0.55 \sqrt{E/F_y}$
W shape braces	Highly ductile	$0.30 \sqrt{E/F_y}$	$1.49 \sqrt{E/F_y}$

3.3.4 Story drift determination

The deflection at level x (δ_u) used to compute the design story drift, Δ , is determined in accordance with the following equation:

$$\delta_u = \frac{C_d \delta_{xe}}{I_e} \quad (3.10)$$

Where

C_d = the deflection amplification factor (Table 12.2-1 (ASCE 2010))

δ_{xe} = the deflection at the location required by this section determined by an elastic analysis

I_e = the importance factor (Section 11.5.1(ASCE 2010))

The allowable story drift can be found in Table 12.12-1 of ASCE (2010).

P-Delta effect

P-delta effects on story shears and moments, the resulting member forces and moments, and the story drifts induced by these effects are considered where the stability coefficient (θ) as determined by the following equation is equal to or less than 0.10:

$$\theta = \frac{P_x \Delta I_e}{V_x h_{sx} C_d} \quad (3.11)$$

Where

P_x = the total vertical design load at and above Level x; where computing P_x , no individual load factor need exceed 1.0

Δ = the design story drift occurring simultaneously with V_x

I_e = the importance factor (Section 11.5.1(ASCE 2010))

V_x = the seismic shear force acting between Level x and x-1

h_{sx} = the story height below Level x

C_d = the deflection amplification factor (Table 12.2-1 (ASCE 2010))

When the stability coefficient (θ) is greater than 0.10 but less than or equal to θ_{max} , the displacements and member forces are multiplied by $1.0/(1 - \theta)$.

When θ is greater than θ_{max} , the structure is potentially unstable and is redesigned.

3.4 Final design

The following tables describe the design results for the composite flooring systems of the prototype structures. Design results of the gravity columns and members that belong to the lateral-force resisting system are given in Appendix A.

Table 3.4 Member sizes for the conventional composite flooring system with solid slabs

Name	Floor interior beam			Floor exterior beam			Floor interior girder			Floor exterior girder		
	Member size	Number of shear studs	Amount of shear connection	Member size	Number of shear studs	Amount of shear connection	Member size	Number of shear studs	Amount of shear connection	Member size	Number of shear studs	Amount of shear connection
30-3-8-ss	W18x35	48	100%	W14x22	24	79.5%	W27x84	44	69.5%	W21x44	34	100%
30-3-6-ss	W18x40	48	87.6%	W14x26	36	100%	W27x84	44	69.5%	W21x50	34	87.9%
20-3-8-ss	W12x19	30	100%	W10x15	12	58.5%	W18x35	30	62.7%	W12x19	30	100%
20-3-6-ss	W12x22	20	66.3%	W10x15	12	58.5%	W18x35	48	100%	W14x22	24	79.5%
30-9-8-ss	W16x31	24	56.6%	W12x22	18	59.8%	W21x62	52	56.5%	W16x40	34	54.8%
30-9-6-ss	W14x30	24	58.4%	W12x19	16	61.9%	W21x55	44	53.2%	W18x35	28	50.2%
20-9-8-ss	W12x19	16	61.9%	W10x15	12	58.6%	W14x30	24	58.4%	W12x19	16	61.9%
20-9-6-ss	W12x16	12	54.9%	W10x15	12	58.6%	W14x26	10	56.0%	W12x16	12	54.9%

Table 3.5 Member sizes for the conventional composite floor system with metal deck slabs

Name	Floor interior beam			Floor exterior beam			Floor interior girder			Floor exterior girder		
	Member size	Number of shear studs	Amount of shear connection	Member size	Number of shear studs	Amount of shear connection	Member size	Number of shear studs	Amount of shear connection	Member size	Number of shear studs	Amount of shear connection
30-3-8-sc	W16x40	36	52.5%	W14x22	28	74.2%	W24x68	48	51.3%	W21x44	56	92.6%
30-3-6-sc	W21x44	40	50.3%	W16x26	26	58.2%	W27x84	74	64.4%	W21x48	60	91.5%
20-3-8-sc	W14x22	20	53.0%	W10x12	14	68.0%	W18x35	34	71.0%	W12x19	24	92.6%
20-3-6-sc	W12x26	24	53.9%	W10x12	18	87.5%	W18x35	40	83.5%	W14x22	20	66.3%
30-9-8-sc	W16x31	24	45.2%	W12x19	18	55.6%	W24x55	38	50.4%	W16x26	28	78.4%
30-9-6-sc	W14x26	24	53.7%	W12x16	14	51.3%	W21x48	34	51.8%	W16x31	22	50.2%
20-9-8-sc	W10x19	18	55.1%	W10x12	12	58.3%	W16x26	18	50.4%	W10x19	14	53.6%
20-9-6-sc	W12x16	14	51.1%	W10x12	12	58.3%	W12x26	18	50.6%	W12x16	12	54.8%

Table 3.6 Member sizes for the deconstructable composite flooring system^a

Name	Floor interior beam			Floor exterior beam			Floor interior girder			Floor exterior girder		
	Member size	Number of bolts	Amount of shear connection	Member size	Number of bolts	Amount of shear connection	Member size	Number of bolts	Amount of shear connection	Member size	Number of bolts	Amount of shear connection
30-3-8-gc	W18×35	60	91.7%	W14×22	32	77.6%	W30×90	40	23.9%	W21×55	40	38.9%
30-3-6-gc	W18×40	60	80.0%	W14×26	32	65.5%	W30×99	40	21.7%	W21×55	40	38.9%
20-3-8-gc	W10×19	40	100%	W10x15	24	85.7%	W18×35	40	61.1%	W12×19	32	90.4%
20-3-6-gc	W12×22	40	97.2%	W10x15	24	85.7%	W18×40	40	53.4%	W14×26	24	49.1%
30-9-8-gc	W16x31	32	55.1%	W12x22	32	77.7%	W21x62	40	34.4%	W16x40	40	53.3%
30-9-6-gc	W14x30	32	56.9%	W12x19	32	90.4%	W21x55	40	38.9%	W18x35	40	61.1%
20-9-8-gc	W12x19	24	67.8%	W10x15	24	85.7%	W14x30	24	42.7%	W12x19	24	67.8%
20-9-6-gc	W12x16	24	80.2%	W10x15	24	85.7%	W14x26	24	49.1%	W12x16	24	80.2%

^a The final design results may change depending on the design strategies concluded from the composite beam tests .

4. Life Cycle Assessment

This chapter compares the environmental impacts of steel building structures employing Design for Deconstruction strategies to those employing traditional structural design practices. The efficacy of applying life-cycle assessment models to building comparisons is also investigated in this study.

4.1 Introduction

The construction industry has begun to assess the environmental impacts of design and material choices. One such tool employed for this purpose is life-cycle assessment (LCA), an internationally standardized method (ISO 14040, 14044:2006) that has been applied to buildings and construction projects for the past 20 years. LCA is a quantitative method that accounts for resource use, emissions, and potential environmental and health impacts over the life-cycle of a building, including extraction of raw materials, manufacturing and assembly of building assemblies, transportation, construction, building operation, maintenance, and eventual deconstruction or demolition. In this way, LCA models allow engineers, architects, and owners to examine environmental trade-offs associated with building materials, assemblies, or particular design features in a comprehensive, whole-building manner. The use of LCA can also prevent ‘burden-shifting’, where design decisions made to promote efficiency or environmental goals at one stage actually end up causing unintended consequences that obviate the original advantages.

As standardized, LCA has four steps: (1) Goal and Scope Definition, which documents the objectives and stakeholders of the study, provides basic methodological details, and defines the product system under study; (2) Life Cycle Inventory, which compiles all types of resource use (e.g., energy, water, raw materials) and emissions (e.g., carbon dioxide, wastewater) associated with the product system, along the entire building life cycle; (3) Life Cycle Inventory Assessment (LCIA), which links emissions to changes in chemical concentrations downwind and downstream, which in turn cause physical changes (such as acidification of lakes) and/or chemical exposure and adverse biological responses (such as ecotoxicity or damages to human health); and (4) Interpretation, where modeling assumptions are tested with different scenarios and uncertainty analysis, and where implications for design and decision-making are discussed. Within the ISO standard, the actual data employed, the models used for impact assessment, the categories of environmental and human health impacts included, and the processes or materials that are included/excluded can change depending on the stated scope of the study.

LCA has been applied to buildings and construction with a variety of objectives. These include choosing among specific materials, examining trade-offs between embodied energy and operational energy, identifying ‘hot-spots’ (materials or stages that dominate a category of impacts) in the building life-cycle, and evaluating new methods of construction or structural

engineering approaches (Huang et al. 2015; Singh et al. 2010). In particular, many case studies have been performed, looking at individual buildings, and collecting data from bills of materials, construction documents, and operational records or utility bills. Obviously, there are many building materials and assemblies that are commonly used. Most do not directly use energy or release emissions of some sort after they are installed in a building, but on a life-cycle basis, they require energy and release emission during their manufacturing, wherever that occurs. So, the material quantities specified in bills of materials must be linked to the energy, raw materials, and emissions associated with their production. For example, counting the carbon dioxide emissions associated with producing structural steel would need to account for fuel combustion in excavation equipment (if virgin steel), direct emissions from chemical reactions in smelters and refiners, emissions from power plants that supply electricity to mining, metallurgy, and milling operations, emissions from truck, train, or ship transport, and so on, forming a highly integrated network of industrial processes with emissions occurring at many steps. LCAs typically consider hundreds or thousands of individual substances (not just the single molecule carbon dioxide), coming from thousands of individual industrial processes. LCA practitioners studying buildings cannot directly collect information from this entire supply chain, so they link information on materials use they can collect directly (foreground data) with data sets that represent national average production (background data). This is commonly done using so-called Life Cycle Inventory (LCI) databases, which are a compilation of extensive previous studies that have investigated the supply chain or individual materials or assemblies. These individual LCI data can then be assembled to model a more complex assembly or, in this case, a building.

Performing a full LCA of a building can be a difficult task, due size and complexity of buildings, the many trades and pieces of equipment involved in construction and deconstruction/demolition, and the effort required to model or collect accurate operational energy and water use. Over time, several popular tools and software packages have been developed to provide a modeling framework or to streamline the modeling itself. General LCA software packages with built-in calculation and simulation engines include SimaPro, GaBi, and openLCA. LCI databases with records for building materials and/or assemblies include commercial databases such as ecoinvent and GaBi (both European) and public databases such as the US LCI and the LCI Data Commons (US federal efforts), and the European Life Cycle Database (ELCD). Once LCI data have been compiled, several life-cycle impact assessment (LCIA) methods have been developed that link emissions to various categories of environmental impact and health damages, by linking models together from chemical fate and transport, environmental science, ecology, exposure assessment and toxicity. Two common LCIA methods employed for buildings and construction are the US EPA Tool for the Reduction and Assessment of Chemical and Other Environmental Impacts (TRACI), and Building for Environmental and Economic Sustainability (BEES) is a web-based tool developed by the National Institute of Standards and Technology (NIST) Engineering Laboratory to measure environmental and economic performance of building products (NIST 2015). Typical impact categories considered in LCIA methods include total life-cycle energy

and water use, greenhouse gas (GHG) emissions, stratospheric ozone depletion, acidification (from acid rain) and eutrophication (nutrient pollution) of waters and soils, ecotoxicity, and health impacts from respiratory disease or cancer. LCA tools developed specifically to streamline assessments of buildings include the Athena Impact Estimator for Buildings (Athena Sustainable Materials Institute 2016), with a free version that has a proprietary LCI database for common building assemblies and design blocks, allowing for relatively quick construction of a building model, provided that standard assemblies are used. The Impact Estimator has built-in implementation of several impact categories from the TRACI model. Another tool developed by the parent company for GaBi, is a plug-in for the popular building design software Revit, and automatically links drawing objects with corresponding LCI data for those materials from GaBi. In the past, a shortcoming of LCA tools for buildings and construction is that they have offered limited material and process libraries, but in recent years, especially the commercial databases are growing quickly in size and in specificity for the building industry.

This study uses LCA to compare a series of prototype buildings with DfD composite floor systems to prototype buildings with traditional composite floors. This study makes use of the general LCA software SimaPro 8, a process-based LCA tool that offers flexibility and built-in simulation engines to allow for analysis of new structural systems and techniques (PRé 2016). This comparison includes a parametric study that varies parameters including material quantities, labor time required, transportation distances, and building loads. These parameters will be discussed in more detail when describing the models used for analysis.

4.2 Scope

The current project LCA system boundaries are cradle-to-grave, as well as post-end-of-life benefits for deconstructable and reusable materials. Only materials and processes that differ between traditional and DfD buildings are included in this study. It is assumed that, compared to current floor systems, DfD systems have insignificant impacts on maintenance and energy required to run a building and on the selection of architectural and MEP components, and so the scope excludes all operational considerations. Production of materials and transportation to the jobsite and to storage facilities are included in this study. For the construction phase, existing LCI databases libraries have limited LCIs describing construction processes. So, modeling of construction impacts is based off of engineering estimates of equipment and tool use. The environmental impacts of worker transportation to the construction site can also be modeled in SimaPro, so the primary impacts of labor required for construction and deconstruction are reflected by the total person-miles of commute to and from the jobsite. Thus, a task requiring a larger crew or more time to complete will result in higher environmental costs.

This study includes analysis of the concrete and steel that make up the floor, beams, girders, and columns. Foundations are not included in this study, since the weights of the systems compared

are similar. The quantities of concrete and steel are calculated in the parametric study conducted in Chapter 3 and shown in Appendix A.

At the end of the life of the building, materials are allocated to the appropriate landfill, recycling, or reuse scenario according to mass and material type. In a traditional building, concrete is either crushed and recycled or sent to a landfill, while all steel is assumed to be recycled. All components of the DfD building modeled in this study are allocated to reuse except for the bolts used with the clamping connectors, since they yield while pretensioning.

Much of the background data required for this LCA are already in existing LCI databases. In this study, two datasets were used: the ecoinvent 2.2 database adjusted for the US energy system (US-EI database, Earthshift, Inc.) and the European Life Cycle Database (ELCD) are used for material LCIs as well as transportation and other processes. Ideally, all information would come from a single LCI database, but no one SimaPro library is sufficiently comprehensive to satisfy the requirements of this study. See Appendix B for a comprehensive list of the products and processes used in this study from each library.

RSMeans construction cost estimating tools were used to estimate the installation times, crew sizes, and equipment required for various construction activities necessary for estimating labor rates and impacts (Reed Construction Data 2014). In this study, these estimates were made for Los Angeles where the prototype structures are located.

As the DfD plank designs vary from standard precast planks, there are assumptions that must be made in this study. Whenever possible, data derived from current comparable systems are extrapolated to describe DfD planks. For example, DfD planks are assumed to be available at the same spans as contemporary precast planks. Estimates of installation and deconstruction time required for the DfD planks are made based on times required for current precast floor systems. Until shown otherwise, DfD planks are assumed to provide structural support and fire resistance similar to current floor systems. It is assumed that DfD planks are designed and manufactured to be durable enough for two or three reuses and do not require special handling or transportation accommodations beyond that required for standard precast planks.

The LCI libraries provided by SimaPro are limited in their ability to form a consistent and comprehensive model of the impacts of installation and deconstruction labor. It is important to account for the differences in labor required for DfD and traditional buildings. To this end, data from RS Means is used to estimate the total person-days required to construct and deconstruct each element of the buildings in the model. Person-day totals are used to calculate the impact of the average commute of each laborer. However, estimating the impacts of labor and equipment used for specific tasks is outside the scope of this project.

The proprietary technologies of the DfD channels and clamps are modeled using the closest available alternative. The channels are modeled using the LCI for hot-rolled steel sections, and clamps are modelled using the LCI for cast iron. The intricacies of the production of each of these technologies cannot be modeled without information from the manufacturers. Thus, it is possible that the simplifications of this substitution over- or underestimate the actual impacts of the channels and clamps.

4.3 Life cycle impact assessment

LCIA was conducted using the EPA-developed Tool for the Reduction and Assessment of Chemical and Other Environmental Impacts, TRACI 2.1. The following impact categories are considered: Photochemical Smog Formation, Global Climate Change, Human Health—Particulate (respiratory effects), Ecotoxicity, and Fossil Fuel Depletion. SimaPro is used to model the materials and processes that make up the traditional and DfD buildings, as well as the various impact assessments via TRACI 2.1 (PRé 2016). The TRACI 2.1 User Manual describes the significance of each impact category considered.

4.3.1 Global Climate Change (Global Warming Potential)

Carbon dioxide, methane, nitrous oxide, sulfur hexafluoride, and various halocarbon emissions act as greenhouse gases in the atmosphere by absorbing infrared radiation coming from the surface of the Earth and re-radiating it back to the surface, thereby increasing surface temperatures and changing the overall energy balance of the planet. GHG emissions are measured in equivalents (CO_{2e}), which accounts for the radiative forcing or global warming effect of the various gases contributing to climate change over their atmospheric lifetimes relative to carbon dioxide. The U.S. EPA uses CO_{2e} with a time horizon of 100 years to follow the guidance of the U.N. Framework Convention on Climate Change (Bare 2012). TRACI uses the most current impact data published by the Intergovernmental Panel on Climate Change (IPCC).

4.3.2 Human Health—Particulate (respiratory effects)

Human Health—Particulate, or Respiratory Effects, are concerned with airborne particulate matter, which negatively affects human health, and may lead to respiratory illness and death. Secondary particulates are those resulting from chemical reactions in the air, most commonly induced by nitrogen oxides (NO_x) and sulfur dioxide (SO₂). Wood and fossil fuel combustion, as well as activities that produce dust, are the more common sources of particulates. The more drastic effects of airborne particulates are felt by children, the elderly, and those afflicted with asthma. Particulate matter is characterized as “fine” at diameters less than 2.5 micrometers, or

“coarse” at diameters between 2.5 and 10 micrometers. TRACI quantifies respiratory effects using equivalent quantities of fine particulate matter (PM_{2.5}) (Bare 2012).

TRACI calculates the impacts of particulates by modeling the fraction of the emitted substance that is predicted to be inhaled by a human. The quantity of substance emitted into the environment, the resulting increase in air concentration, and the breathing rate of the exposed population are used to predict the inhaled fraction of the emitted substance. Air concentration is influenced by preexisting concentration of substances, the location of released substances, and the meteorology of the location (Bare 2012).

4.3.3 Ecotoxicity

A global consensus model, known as USEtox, is used in TRACI to develop human toxicity and freshwater ecotoxicity potentials for thousands of organic and inorganic substances. The USEtox model considers chemical fate, exposure, and effects, in order to link chemical emissions with eventual toxicity endpoints. Ways in which toxicity may enter a human include inhalation, ingestion of drinking water, produce, meat, milk, and freshwater and marine fish. Units of impact are Comparative Toxicity Units for ecotoxicity (CTU_e) and human toxicity (CTU_h) (Bare 2012).

4.3.4 Photochemical Smog Formation

Chemical reactions between nitrogen oxides (NO_x) and volatile organic compounds (VOCs) in sunlight create ground level ozone (O₃), a primary component of smog, which can cause respiratory damage to humans and ecological damage to plant and animal life. Exposure to smog may cause several issues in humans, including bronchitis, asthma, and emphysema. Precursors of ozone are produced primarily by industrial facilities, motor vehicles, and electric power utilities. TRACI uses Maximum Incremental Reactivity (MIR) of all precursor emissions in order to express emissions in units of ozone equivalents (O₃e) (Bare 2012).

4.3.5 Fossil Fuel Depletion

Fossil fuel depletion quantifies fossil energy use over the life cycle, both for combustion and for use as feedstock in petrochemical-derived materials, and reflects the non-renewable character of fossil energy use as an important metric of sustainability. The units are in megajoules of surplus energy (MJ surplus).

4.4 Methodology

The building systems compared in this study are modeled in SimaPro, specifying the same materials and processes in the LCA models (linked to corresponding data in LCI databases) wherever possible for consistency. Because this is a comparative study, only elements that are different in traditional and DfD building types are modeled. This study assumes that DfD planks may be reused a maximum of three times, conservatively assuming that approximately 30 percent of reusable components will be damaged too severely during use or deconstruction to be reused in a future building.

The following is an overview of the SimaPro model. The two prototype building assemblies are titled “Traditional Building” and “DfD Building.” Each building life-cycle model is primarily composed of the appropriate floor framing material, as well as the hot-rolled steel sections used as beams, girders, columns, and diagonal bracing, and the labor and major processes required to assemble and deconstruct the building. In the interest of providing the most complete data possible, processes and materials come directly from SimaPro libraries, rather than attempting to manually describe the inputs and outputs of a process. Appendix B provides all details regarding the processes and materials used in LCA.

The disposal scenarios of these buildings are perhaps the most complicated phases of their life cycles. In the steel industry, nearly one hundred percent of structural steel is recycled or reused (Steel Construction 2012). During the material manufacturing phase, the rolled steel wide-flange sections in both traditional and deconstructable buildings are made of recycled steel. At end of life, reinforced concrete is commonly separated into its steel and concrete components, the reinforcing steel recycled, and the concrete downcycled to aggregate or relegated to landfill. The recycling rate of concrete is a variable parameter.

As DfD is a new concept, it is difficult to predict how successfully a building will be deconstructed at end of life; to account for this, it is assumed that a varying percentage of DfD components are damaged beyond reuse during deconstruction, transportation, or construction. This study considers either 20%, 25%, or 33% of DfD components have been damaged beyond reuse and that new buildings constructed using deconstructed components must incorporate an identical percentage of new components. This is similar to saying that each DfD component has been reused three, two, and one time respectively. The squares of in Figure 4.1 are a graphical representation of the total deconstructable components of a building. From left to right, each square depicts the progression of components through multiple life cycles. At the end of each building's life, a portion of the deconstructable components are disposed of, and a portion are salvaged to be used in the next building.

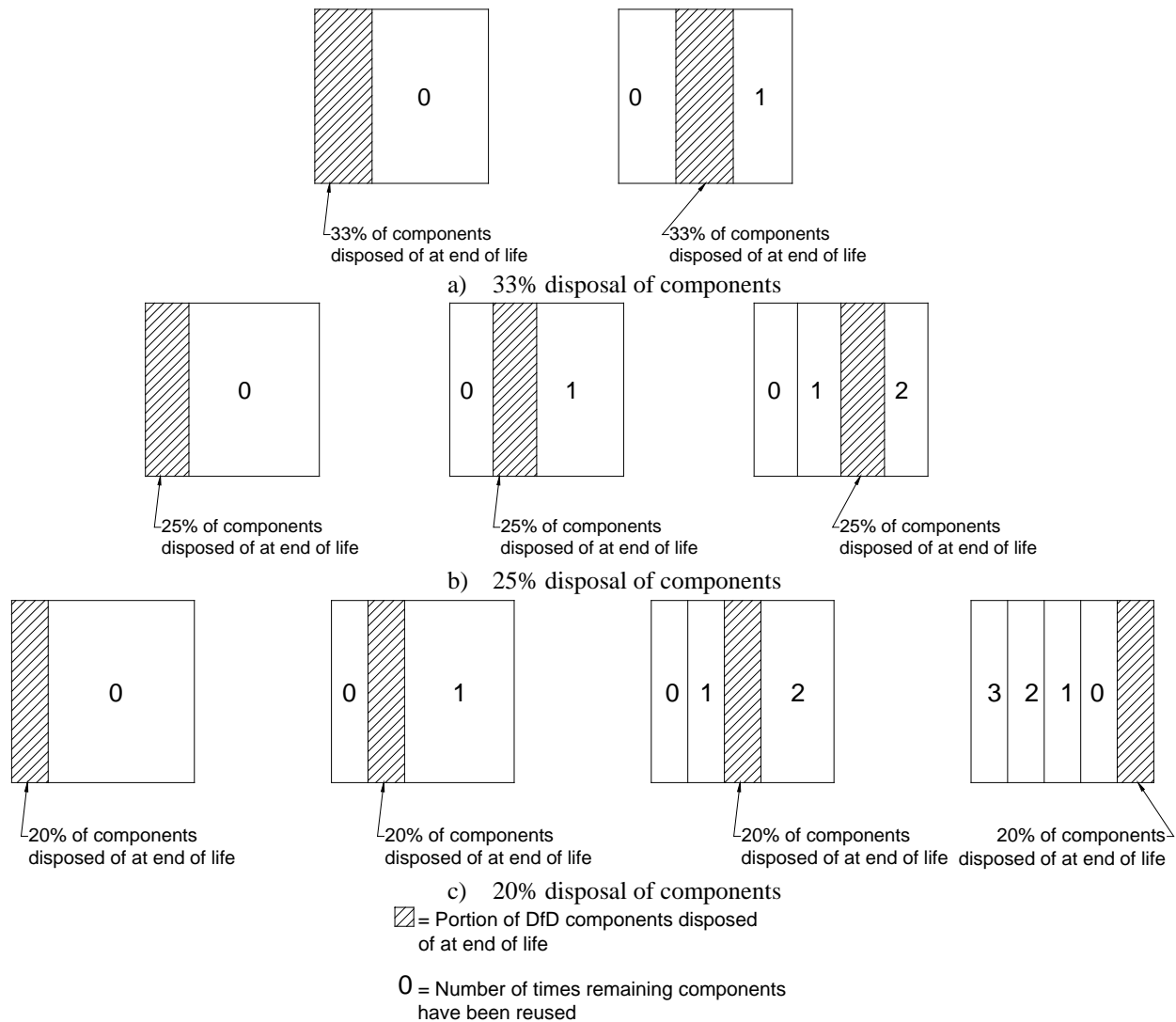


Figure 4.1 Multiple reuse of components at different disposal rate

The DfD building differs from the traditional building in that the floor framing, clamps, beams, and girders can all be reused at the end of the life of the building. Reuse is not modeled in SimaPro. As SimaPro's comparison capabilities are not geared for this application, the preferred method of describing reuse of the DfD components is to manually subtract the impacts of these DfD components from the DfD building life cycle each time they get reused by recording the manufacturing impacts of all reusable components. When modeling the life of a second DfD building, these impacts are subtracted from the DfD building LCA. After DfD components can no longer be reused, they are subjected to the same end of life conditions of a traditional building, e.g., sorting, recycling, and disposing of the concrete and recycling the steel. Thus, the life of the DfD components contains multiple cycles.

To provide a more detailed comparison of the buildings, the life cycle of each building has been broken into four stages: production, material transportation, worker transportation, and disposal. The production stage accounts for the environmental impacts associated with the creation of new materials. In this stage, DfD buildings benefit from the assumption that a percentage of deconstructable components can be reused on each new structure. The material transportation stage accounts for the impacts of transporting materials from the production facility to the site where this impact is not already accounted for in the product's life cycle inventory. For reused deconstructable components, material transportation accounts for the impacts of transportation from storage to site. Worker transportation is used to estimate labor impacts and will be described in more detail in Section 4.5. The disposal stage of the life cycle describes the impacts at the end of life of the building components.

To help capture the wide variety of building options and to investigate the impacts of certain design choices and site constraints, many aspects of this model are studied parametrically. The base variation is the building type described in Chapter 3. The parameters of this study are summarized in Table 4.1 through Table 4.3 using values from building 30-3-8-gc as an example.

Table 4.1 Parameters for DfD building life cycle

#	Parameter	Value	Units	Distribution	SD ² or 2*SDM in	Min	Max	Definition	Source(s)
1	dist_commute	6	miles	Lognormal	6			This is an approximate representation of the one way commute data given by BTS.	Bureau of Transportation Statistics - Omnibus Household Survey, October 2003
2	dist_storage	60	miles	Uniform		10	100	Storage facilities are located 10-100 miles from the center of LA.	www.calrecycle.ca.gov/FacIT and loopnet.com
3	labor_deconstruct	0.038	person-days/ton	Uniform		0.038	0.076	Approximately 0.038-0.076 person-days of labor per ton of material is required to dismantle and refurbish the DfD components.	Estimated from RS Means approximation of deconstruction time, Building Construction Cost Data 2014
4	bay_width	30	feet	Undefined				Bays in the building are 30 ft wide and long.	Wang, Hajjar, Webster, Brown, 2013
5	dist_manuf_channels	400	miles	Uniform		380	420	The channel distribution center is 400 miles from the center of LA.	www.deconusa.com
6	floor_depth	0.66667	feet	Undefined				The flooring is 8" thick.	Wang, Hajjar, Webster, Brown, 2013
7	number_of_floors	3	floors	Undefined				The building has 3 floors.	Wang, Hajjar, Webster, Brown, 2013
8	steel_bolts	6336	lbs	Undefined				6336 lbs of bolts are used in the entire building (assume bolts weigh 1 lb each).	Wang, Hajjar, Webster, Brown, 2013
9	steel_structural	233,732	lbs	Undefined				Beams, girders, columns, and braces weigh 233732 lbs.	clementsupport.com
10	clamps_bolts	25,344	lbs	Undefined				25344 lbs of clamps and bolts are used in the entire building.	Wang, Hajjar, Webster, Brown, 2013
11	dist_commute	6	miles	Lognormal	6			This is an approximate representation of the one way commute data given by BTS.	Bureau of Transportation Statistics - Omnibus Household Survey, October 2003
12	dist_manuf_clamps_bolts	340	miles	Uniform		320	360	The clamp and bolt distribution center is 340 miles from the center of LA.	clementsupport.com

Table 4.1 Parameters for DfD building life cycle (continued)

13	dist_manuf_planks	30	miles	Uniform		10	50	Precast plank manufacturing plants are 10-50 miles from the center of LA.	BlueBook (Contractors Register, Inc. 2015)
14	dist_manuf_structural_steel	55	miles	Uniform		10	100	Steel production facilities are located 10-100 miles from the center of LA.	BlueBook (Contractors Register, Inc. 2015)
15	dist_storage	55	miles	Uniform		10	100	Storage facilities are located 10-100 miles from the center of LA.	www.calrecycle.ca.gov/FacIT/ and loopnet.com
16	labor_traditional	107	person-days	Normal	21			107 person-days are required to install everything, if this were a traditional building, using RSMeans data.	RS Means, Building Construction Cost Data, 2014
17	plank_weight	2,538,151	lbs	Undefined				DfD planks (concrete, rebar, and channels) weigh 2538151 lbs.	Wang, Hajjar, Webster, Brown, 2013
18	reuse	0.66		Undefined				Percentage of building made from reused components: 0.66, 0.75, or 0.8.	Personal communication, 2014
19	structural_steel	233,732	lbs	Undefined				Beams, girders, columns, and braces weigh 233732 lbs.	Wang, Hajjar, Webster, Brown, 2013

Table 4.2 Parameters for DfD reusable components life cycle


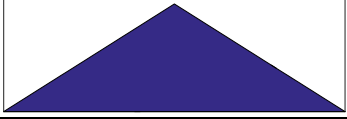
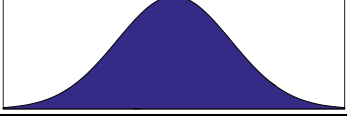
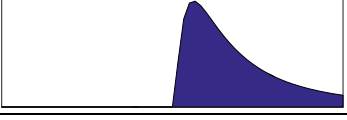
#	Parameter	Value	Units	Distribution	SD ² or 2*SDMin	Min	Max	Definition	Source(s)
1	percent_conc_recycled	50	percent	Normal	34			An average of 50 percent of concrete is recycled.	www.epa.gov/climatechange/wycd/waste/downloads/concrete-chapter10-28-10.pdf
2	bay_width	30	ft	Undefined				Bays are 30 feet wide and long.	Wang, Hajjar, Webster, Brown, 2013
3	steel_structural	233,732	lbs	Undefined				All structural steel weighs 233732 lbs.	Wang, Hajjar, Webster, Brown, 2013
4	dist_manuf_channels	400	miles	Uniform		380	420	The channel distribution center is 400 miles from the center of LA.	www.deconusa.com
5	floor_depth	0.66667	feet	Undefined				Floors are 8 inches deep.	Wang, Hajjar, Webster, Brown, 2013
6	number_of_floors	3	floors	Undefined				The building has 3 floors.	Wang, Hajjar, Webster, Brown, 2013
7	steel_bolts	6,336	lbs	Undefined				6336 lbs of bolts are used in the entire building (assume bolts weigh 1lb).	Wang, Hajjar, Webster, Brown, 2013

Table 4.3 Parameters for traditional building life cycle

#	Parameter	Value	Units	Distribution	SD ² or 2*SDMin	Min	Max	Definition	Source(s)
1	percent_conc_recycled	50	percent	Normal	48			An average of 50 percent of concrete is recycled.	http://www.epa.gov/climatechange/wycd/waste/downloads/concrete-chapter10-28-10.pdf
2	conc	1,908,563	lbs	Undefined				1908563 lbs of concrete are used in the entire building.	Wang, Hajjar, Webster, Brown, 2013
3	dist_commute	6	miles	Lognormal	6			This is an approximate representation of the one way commute data given by BTS.	Bureau of Transportation Statistics - Omnibus Household Survey, October 2003
4	dist_manuf_conc	40	miles	Uniform		5	80	Concrete manufacturing plants are 5-80 miles from the center of LA.	BlueBook (Contractors Register, Inc. 2015)
5	dist_manuf_steel	55	miles	Uniform		10	100	Steel production facilities are located 10-100 miles from the center of LA.	BlueBook (Contractors Register, Inc. 2015)
6	labor	160	person-days	Normal	32			160 person-days are required to install and demolish everything, using RSMeans data.	Estimated from RS Means approximation of deconstruction time, Building Construction Cost Data 2014
7	steel_tot	302,960	lbs	Undefined				302960 lbs of steel are used in the entire building.	Wang, Hajjar, Webster, Brown, 2013
8	steel_hot_rolled	227,792	lbs	Undefined				Beams, girders, columns, and braces weigh 227792 lbs.	Wang, Hajjar, Webster, Brown, 2013
9	bay_width	30	feet	Undefined				Bays in the building are 30 ft wide and long.	Wang, Hajjar, Webster, Brown, 2013
10	floor_depth	0.66667	feet	Undefined				The flooring is 8" thick.	Wang, Hajjar, Webster, Brown, 2013
11	number_of_floors	3	floors	Undefined				The building has 3 floors.	Wang, Hajjar, Webster, Brown, 2013
12	studs	4,968	lbs	Undefined				4968 lbs of studs are used.	Wang, Hajjar, Webster, Brown, 2013

SimaPro is capable of performing Monte Carlo simulation using different distribution types to describe the uncertainty of a given parameter. The four distribution types are range, triangle, normal, and lognormal. A range distribution implies that all values between the given minimum and maximum are equally likely to occur. A triangular distribution gives a linear distribution from the mode value to both the minimum and maximum values. It is not necessary to center the triangular distribution. A normal distribution provides a bell curve centered at the mode value with 95% of all values occurring within two standard deviations. A lognormal distribution is the most prevalent in LCA, and is the default in Simapro (PRé 2013). Lognormal is similar to normal distribution, except 95% of all values are within the limits defined by dividing and multiplying the mode value by the square of the geometric standard deviation. The distributions are illustrated in Table 4.4.

Table 4.4 Distribution types supported by Simapro (reproduced from PRé 2014)

Distribution type	Required data	Graphical presentation
Range	Min and max values	
Triangular	Min and max values and best guess	
Normal	Standard deviation and best guess	
Lognormal	Standard deviation and best guess	

The Monte Carlo approach used by Simapro relies on the distribution choices described previously. For sensitivity analysis, the variable value is selected at random from the uncertainty distribution and the results are calculated and stored. This process is then repeated with a new random variable within the distribution (PRé 2013). This process may be completed thousands of times, or until a standard error of mean has been reached. Standard error of mean describes how much the previous Monte Carlo run has changed the current mean. Thus, a lower standard error of mean indicates more reliable results. The number of runs and the threshold for the standard error of mean may be set by the user. Ten thousand calculation steps are run for every life cycle assessment scenario in this study. This ensures statistically significant results and a very low standard error of mean.

To compare results of these large sample tests, statistical analysis software, Minitab 16 (Minitab, Inc., State College PA, USA), is used to calculate the uncertainty in the difference between two

values using t-tests. T-tests are commonly used to determine if the mean of a population differs significantly from the mean of another population. The comparison is given in Equation (5.1):

$$t = \frac{\bar{x}_1 - \bar{x}_2}{\sqrt{\frac{s_1^2}{n_1} + \frac{s_2^2}{n_2}}} \quad (4.1)$$

Where \bar{x}_1 and \bar{x}_2 are the mean values of the first and second population, s_1 and s_2 are the standard deviations of the samples, and n_1 and n_2 are the sample sizes. The sample size of all populations is 10,000. Thus, t is a comparison of the difference in means of the two populations divided by the uncertainty of the populations (Devore 2009).

These calculations are summarized in Section 4.7. The P-values of all of these comparisons are zero, due to the high sample size of the populations. Because all P-values were calculated to be zero, P-values are not included in the calculation summary charts. P-value represents the probability of obtaining the sample results if the null hypothesis were true. A lower P-value means the null hypothesis is less likely to be true, and the data is considered significant. A P-value of zero indicates significant results (Devore 2009).

4.5 Sources of input

Nearly all material quantities have been calculated using values summarized in Appendix A. The naming convention for buildings in the parametric study is presented in Section 3.1. Throughout calculations and modelling, “TB” is used to abbreviate “traditional building,” and “DB” is used to abbreviate “deconstructable building.”

The weights of all rolled steel sections are found in the AISC *Specification for Structural Steel Buildings* (AISC 2010). Concrete weights are based on a density of 145 pounds per cubic foot. Two channel sizes, HTA 50/30 and HTA 72/48-Q, are used for the 6 in. and 8 in. DfD planks, respectively. The sizes and weights are found in Halfen’s *Cast-In Channels Technical Product Information* catalog (Halfen 2013). Clamps are assumed to weigh approximately four pounds each. Bolts and headed shear stud anchors are assumed to weigh one pound each. The metal deck used in traditional floor systems is 22 gage steel and is assumed to weigh 1.8 pounds per square foot (Vulcraft 2001).

Labor requirements have been estimated using RS Means data (Reed Construction Data 2014). RS Means is chosen based on its reputation as an established authority on construction cost and labor estimating. The following is a sample calculation of labor required to install the rebar in a traditional building. Installation times are used to determine labor impacts in the SimaPro model. The calculation uses material quantities from Appendix A and labor rates from RS Means.

$$26,460 \text{ lbs of rebar} \times \left(\frac{1 \text{ crew} - \text{day}}{2.9 \text{ tons of rebar}} \right) \times \left(\frac{4 \text{ rodmen}}{1 \text{ crew}} \right) \times \left(\frac{1 \text{ ton}}{2,000 \text{ lbs}} \right)$$

$$= 18.2 \text{ person} - \text{days to install the rebar}$$

The complete results of labor quantities are summarized in Table 4.5 for the traditional buildings and Table 4.6 for the DfD buildings. Labor required for deconstruction of the DfD building is calculated using the estimate that careful deconstruction will take at least half as much time as original installation and at most, an equal amount of time (Reed Construction Data 2014; Costello 2014). This range of deconstruction time is discussed in Section 4.7.

Table 4.5 Labor required for installation and demolition of traditional building (person-days)

Name	Structural steel	Rebar	Deck	Shear studs	Place concrete	Finish concrete	Demolition	Total Labor
30-3-8-ss	36	18	30	11	24	30	10	160
30-3-6-ss	37	14	30	12	17	30	10	150
20-3-8-ss	22	8	14	5	11	14	4	77
20-3-6-ss	23	6	14	5	8	14	4	73
30-9-8-ss	101	55	91	21	73	91	29	461
30-9-6-ss	98	41	91	19	51	91	29	420
20-9-8-ss	76	24	41	10	33	41	13	237
20-9-6-ss	65	18	41	9	23	41	13	209

Table 4.6 Labor required for installation and deconstruction of DfD building (person-days)

Name	Structural steel	Place concrete planks	Total construction labor	Minimum labor required for deconstruction
30-3-8-ss	39	68	107	54
30-3-6-ss	39	78	117	58
20-3-8-ss	25	30	56	28
20-3-6-ss	23	35	57	29
30-9-8-ss	104	205	309	155
30-9-6-ss	105	234	340	170
20-9-8-ss	65	91	156	78
20-9-6-ss	64	104	168	84

As the study takes place in Los Angeles, California, local facilities are used to determine manufacturing, distribution, and storage distances. Concrete mixing plants, precast concrete plants, and steel mills and fabricator locations are found using BlueBook. All can be found within the city or relatively close to it. Storage facilities for deconstructed structural components may not exist. However, current storage facilities or areas of cheap, open land approximately 10-100 miles from the city may be used (CalRecycle 2014; LoopNet, Inc. 2014). It is also

possible that current facilities like precast plants and steel service centers will develop capabilities to process and store deconstructed materials.

Clamps, channels, and bolts that lock in the channels are all specialty items, with very few options for distribution centers and manufacturing. However, a distributor for the clamps and bolts is located 340 miles from Los Angeles (Clement Support Services 2012), and the channels may be found from a distributor 400 miles from Los Angeles (Decon USA, Inc. 2013). This study excludes the transportation of these specialty items from manufacturer to distribution center because these products are assumed to have been stocked in the distribution center regardless of the demand for DfD construction.

Average commute distances of the laborers are provided by a study conducted by the Bureau of Transportation Statistics (US DoT, BTS 2003). Worker travel is modeled using personal vehicles, because the majority of commuters, 86 percent, drive a personal car to work (McKenzie, 2011). According to an EPA report, approximately 50 to 60 percent of concrete is recycled, while the remainder is landfilled (US EPA 2010).

All values required for input to SimaPro are summarized in Table 4.7 and Table 4.8.

Table 4.7 Traditional building inputs to SimaPro

Name	Weight of beam, col, gird, brace (lbs)	Concrete (lbs)	Rebar (lbs)	Deck (lbs)	Studs (lbs) (assume 1lb/stud)	Total weight of steel (lbs)	Total Labor (person-days)
30-3-8-ss	227,792	1,908,563	26,460	43,740	4,968	302,960	160
30-3-6-ss	242,414	1,321,313	19,845	43,740	5,760	311,759	150
20-3-8-ss	94,460	848,250	11,760	19,440	2,196	127,856	77
20-3-6-ss	101,966	587,250	8,820	19,440	2,484	132,710	73
30-9-8-ss	845,144	5,725,688	79,380	131,220	9,720	1,065,464	461
30-9-6-ss	779,099	3,963,938	59,535	131,220	8,964	978,818	420
20-9-8-ss	430,700	2,544,750	35,280	58,320	4,806	529,106	237
20-9-6-ss	406,590	1,761,750	26,460	58,320	4,158	495,528	209

Table 4.8 DfD building inputs to SimaPro

Name	Weight of DfD Slab				Bolts (lbs) (assume 1lb/bolt)	Clamps + bolts (lbs) (for transp)	Weight of beam, col, gird, brace (lbs)	Total Labor (person-days)	Minimum Labor required for deconstruction (person-days)
	Concrete (lbs)	Rebar (lbs)	Channels (lbs)	Tot weight for transp. (lbs)					
30-3-8-gc	2,349,000	16,232	172,919	2,538,151	6,336	25,344	233,732	107	54
30-3-6-gc	1,761,750	16,232	61,406	1,839,389	6,336	25,344	245,040	117	58
20-3-8-gc	1,044,000	7,214	76,853	1,128,067	3,528	14,112	93,166	56	28
20-3-6-gc	783,000	7,214	27,292	817,506	3,384	13,536	102,646	57	29
30-9-8-gc	7,047,000	48,697	518,756	7,614,454	12,960	51,840	876,426	309	155
30-9-6-gc	5,285,250	48,697	184,218	5,518,166	12,960	51,840	823,345	340	170
20-9-8-gc	3,132,000	21,643	230,558	3,384,202	7,128	28,512	438,242	156	78
20-9-6-gc	2,349,000	21,643	81,875	2,452,518	7,128	28,512	409,812	168	84

4.6 Sensitivity/Uncertainty

All parameters of this study have varying ranges and distributions of uncertainty. These uncertainties are accounted for using the Monte Carlo analysis feature of SimaPro. The summary of relevant uncertainty information can be found in Table 4.1 through Table 4.3. Results of the parametric study are shown in Section 4.7. These results include standard deviations resulting from the uncertainties described in this section. The design team decided against using an uncertainty distribution for steel and concrete quantities, as these uncertainties are accounted for in design equations and are consistent across all of the prototype structures.

The distribution of commutes for U.S. workers most closely resembles a lognormal distribution, with the bulk of one-way commutes between 1-15 miles. To capture this spread, labor is modeled as a lognormal distribution with a mean of 6 miles and a squared standard deviation of 6. This ensures that 95 percent of commutes fall between one and 36 miles.

All non-commute distances (storage, manufacture, distribution) are recorded using the approximate center of Los Angeles as the jobsite location. As the exact location of the building within Los Angeles has not been chosen, a uniform radius of uncertainty is added to these distances. This is meant to represent the approximate radius of the city. A uniform distribution is used because the jobsite has an equal probability of occurring anywhere within this radius.

Labor is complicated to estimate. Many factors affect construction time, including weather, site conditions, crew training and experience. It is also difficult to predict the time required to install and dismantle DfD systems. RS Means provides a best estimate to center predictions of installation time. A normal distribution is chosen with 20 percent uncertainty to describe the distribution of installation labor estimates. A normal distribution is appropriate for this, because the most likely value is the best estimate given by RS Means, and the likelihood of outliers is fairly low. Deconstruction time is assumed to range from half as much time to an equal amount of time as construction (Reed Construction Data 2014; Costello 2014).

The uncertainty of concrete recycling percentages is a normal distribution because it is conceivable, but unlikely, that all or none of the concrete may be recycled. The most likely percentage of recycled concrete is focused around the best estimate of fifty percent.

4.7 Results

This section summarizes the results of the SimaPro simulations including uncertainties described in Section 4.6. The environmental impacts of a traditional building are compared to the impacts of a DfD building with components having been reused zero, one, two and three times. The controlling assumption is that 20, 25, or 33 percent of DfD components are damaged beyond reuse during deconstruction, transportation, or construction.

A sample calculation for comparison of the 20-3-6 traditional and deconstructable buildings is provided in Table 4.9. The title of each calculation is in bold followed by a description of the calculations performed in italics.

The first calculation that must be done is to quantify the impacts of disposing of deconstructable components. For this calculation, two versions of the DfD components have been modelled in SimaPro: one in which all of the components are disposed of at the end of their life (highlighted in blue shading) and one in which all of the components are reused (i.e., not disposed of; these are highlighted in green shading). Subtracting the impacts of the reused components from the impacts of the disposed of components yields the impacts of disposing of the DfD components. The standard deviation of this subtraction is provided by T-tests performed in Minitab. The impacts resulting from the disposal of DfD components are highlighted in purple shading in the table entitled “Impacts of Disposal of DfD Components”. A similar calculation is performed for the traditional building in the table titled “Impacts of Disposal of Traditional Building (TB).”

Below the disposal calculations, the life cycle stages of the traditional building and DfD building are compiled in separate tables. Each stage is calculated separately in SimaPro, except for the disposal/end of life stage.

Figure 4.2-Figure 4.9 provide a comparison of the relative environmental impacts when comparing the conventional building to the “baseline” DfD building. This is a hypothetical scenario in which all deconstructable components of the DfD building have been constructed from scratch. To show each impact category in the same graph, results have been normalized to the maximum impact of each category. In all eight of the building types, the traditional building has lower fossil fuel depletion, global warming potential, and smog effects. This is due to the fact that the DfD building uses a solid concrete plank, rather than the corrugated metal deck of the traditional building. This corrugation allows the traditional building to use 20-25 percent less concrete than the DfD building, which in turn reduces the weight of the steel structure required to resist the loads of the building.

Figure 4.10-Figure 4.33 present comparisons of the traditional/conventional and DfD buildings by each environmental impact category and broken out into life cycle stages of production, material transportation, worker transportation, and disposal. Uncertainty values have been calculated, but the data is presented without uncertainty bars because the trends of the graphs are easier to view as presented.

For each of the prototype buildings, comparisons are shown for 66%, 75%, and 80% reuse of deconstructable components. In all instances, the deconstructable building has lower environmental impacts than the traditional building. Production accounts for the majority of the impacts of each environmental category. Disposal of both the conventional and deconstructable buildings generates considerable respiratory impacts, and material transportation contributes the greatest relative impact to fossil fuel depletion and smog. Worker transportation has a negligible impact on all environmental categories due to the relatively small role that worker transportation plays in the total life cycle of a building.

In general, the DfD buildings with 8 in. floors have relatively higher impacts than the DfD buildings with 6 in. floors. This is due to the relatively larger weight of concrete required by the 8 in. DfD planks compared to the 6 in. floors. The traditional building has relatively high levels of ecotoxicity, compared to the DfD building. This is due to the cold rolled sheet steel used for the deck of the traditional building, which contributes to ecotoxicity far more significantly than other components. This trend can be seen in Figure 4.34, which depicts an example tree of ecotoxicity impacts for TB 30-3-8. In this instance, 95.2% of ecotoxicity impacts are attributed to cold rolled sheet steel.

Table 4.9 Sample calculation for comparison of the 20-3-6 traditional and deconstructable buildings (with 66% reuse)

		Impacts of Disposal of DfD Components							
		(Final Use)		(No Disposal)		DfD Disposal Impacts			
Impact category	Units	Mean ₁	SD ₁	Mean ₂	SD ₂	Mean _{DfD}	SD _{DfD}	95% Conf. Int.	
		SimaPro		SimaPro		Mean ₁ - Mean ₂	$\sqrt{((SD_1^2 + SD_2^2)/n)}$	Mean - $t_{\alpha/2} * SD$	Mean + $t_{\alpha/2} * SD$
Ecotoxicity	CTUe	163000	75600	153000	68600	10000	1021	7999	12001
Fossil fuel depletion	MJ surplus	69900	2220	61200	1150	8700	25.0	8651	8749
Global warming	kg CO2 eq	130000	1610	121000	1100	9000	19.5	8962	9038
Respiratory effects	kg PM2.5 eq	64.20	6.02	34.30	2.39	29.90	0.06	29.77	30.03
Smog	kg O3 eq	7530	346	5570	115	1960	3.65	1953	1967

		Impacts of Disposal of Traditional Building (TB)							
		Traditional Bldg (TB)		TB No Disposal		DfD Disposal Impacts			
Impact category	Units	Mean _{TB}	SD _{TB}	Mean ₂	SD ₂	Mean _{DfD}	SD _{DfD}	95% Conf. Int.	
		SimaPro		SimaPro		Mean ₁ - Mean ₂	$\sqrt{((SD_1^2 + SD_2^2)/n)}$	Mean - $t_{\alpha/2} * SD$	Mean + $t_{\alpha/2} * SD$
Ecotoxicity	CTUe	891000	516000	881923	507462	9077	7237	7740	10414
Fossil fuel depletion	MJ surplus	63600	3440	58957	3396	4643	48.34	4578	4708
Global warming	kg CO2 eq	125000	6000	119227	5957	5773	84.55	5738	5809
Respiratory effects	kg PM2.5 eq	49.30	4.49	27.19	1.67	22.11	0.05	22.06	22.16
Smog	kg O3 eq	6520	460	5075	364.3	1445	5.87	1438	1452

		Life Cycle Stages of Traditional Building (TB)									
		Production		Material Transportation		Worker Transportation		End of Life		Total	
Impact category	Units	Mean _{TBP}	SD _{TBP}	Mean _{TBM}	SD _{TBM}	Mean _{TBW}	SD _{TBW}	Mean _{TBE}	SD _{TBE}	Mean _{totTB}	
		SimaPro		SimaPro		SimaPro		Mean ₁ - Mean ₂	$\sqrt{((SD_1^2 + SD_2^2)/n)}$	Mean _{DBP} + Mean _{DBM} + Mean _{DBW} + Mean _{DBE}	$\sqrt{((SD_{DBP}^2 + SD_{DBM}^2 + SD_{DBW}^2 + SD_{DBE}^2)/n)}$
Ecotoxicity	CTUe	876348	500181	2757	1403	242.4	157.7	9077	7237	888424	5002
Fossil fuel depletion	MJ surplus	51414	2437	6929	1985	534.4	162.2	4643	48.34	63520	31.48
Global warming	kg CO2 eq	115504	5674	3267	930	297.8	86.06	5773	84.55	124842	57.51
Respiratory effects	kg PM2.5 eq	25.47	1.44	1.56	0.56	0.10	0.03	22.11	0.05	49.24	0.02
Smog	kg O3 eq	4436	279.7	610.5	222.3	18.14	5.83	1445	5.87	6510	3.57

Table 4.9 Sample calculation for comparison of the 20-3-6 traditional and deconstructable buildings (with 66% reuse) (continued)

		Life Cycle Stages of DfD Building (DB)									
		Production		Material Transportation		Worker Transportation		End of Life		<i>Total</i>	
Impact category	Units	Mean _{DBP}	SD _{DBP}	Mean _{DBM}	SD _{DBM}	Mean _{DBW}	SD _{DBW}	Mean _{DBE}	SD _{DBE}	Mean _{totDB}	SD _{totDB}
		SimaPro		SimaPro		SimaPro		$Mean_1 - Mean_2$	$\sqrt{((SD_1 + SD_2^2)/n)}$	$Mean_{DBP} + Mean_{DBM} + Mean_{DBW} + Mean_{DBE}$	$\sqrt{((SD_{DBP}^2 + SD_{DBM}^2 + SD_{DBW}^2 + SD_{DBE}^2)/n)}$
Ecotoxicity	CTUe	153619	68025	4487	5036	193.1	239.6	10000	1021	168299	682.2
Fossil fuel depletion	MJ surplus	59711	998.0	11084	3155	414.1	125.6	8700	25.0	79909	33.11
Global warming	kg CO2 eq	120175	1032	5230	1490	231.0	66.89	9000	19.5	134636	18.14
Respiratory effects	kg PM2.5 eq	33.68	2.32	2.49	0.90	0.07	0.02	29.90	0.06	66.15	0.02
Smog	kg O3 eq	5350	80.51	979	357.5	14.07	4.56	1960	3.65	8303	3.67

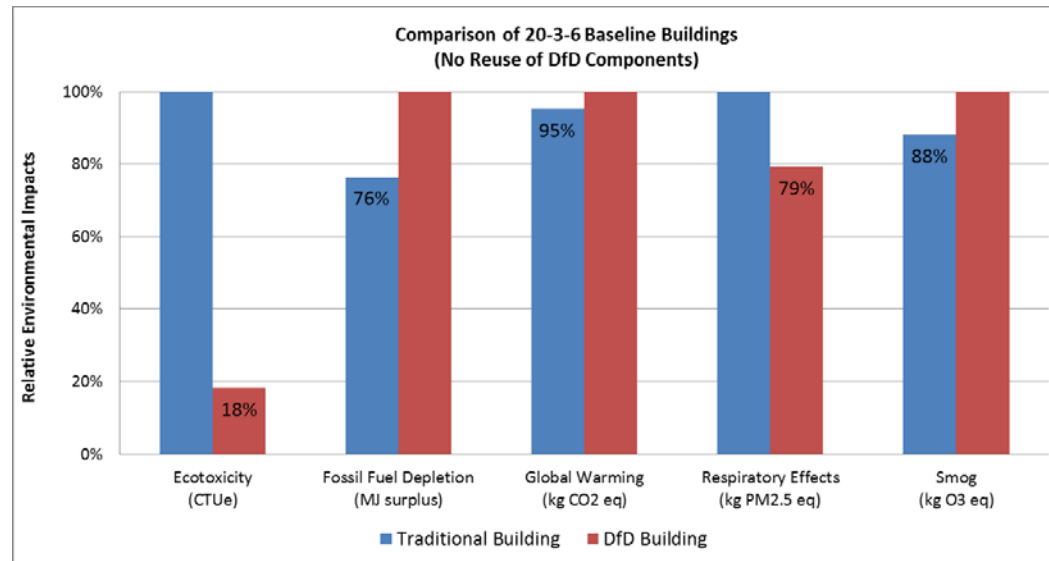


Figure 4.2 Comparison of relative environmental impacts of the 20-3-6 traditional and DfD buildings with no reuse of deconstructable components

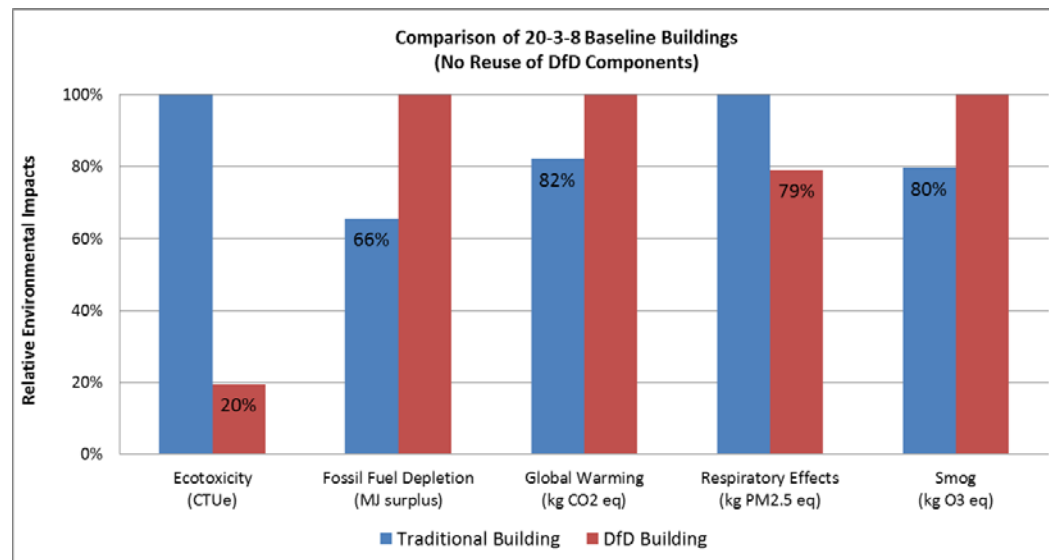


Figure 4.3 Comparison of relative environmental impacts of the 20-3-8 traditional and DfD buildings with no reuse of deconstructable components

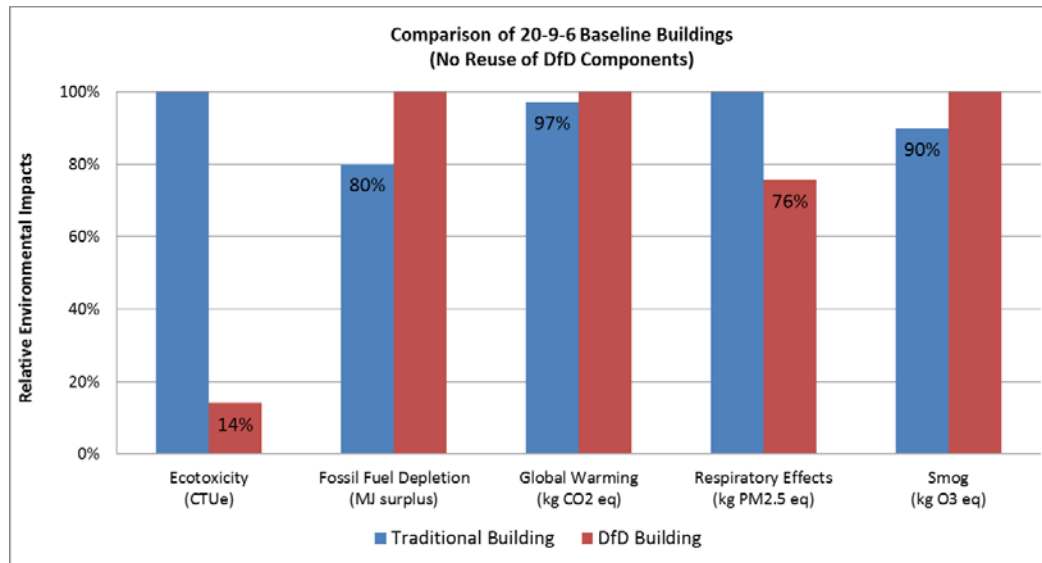


Figure 4.4 Comparison of relative environmental impacts of the 20-9-6 traditional and DfD buildings with no reuse of deconstructable components

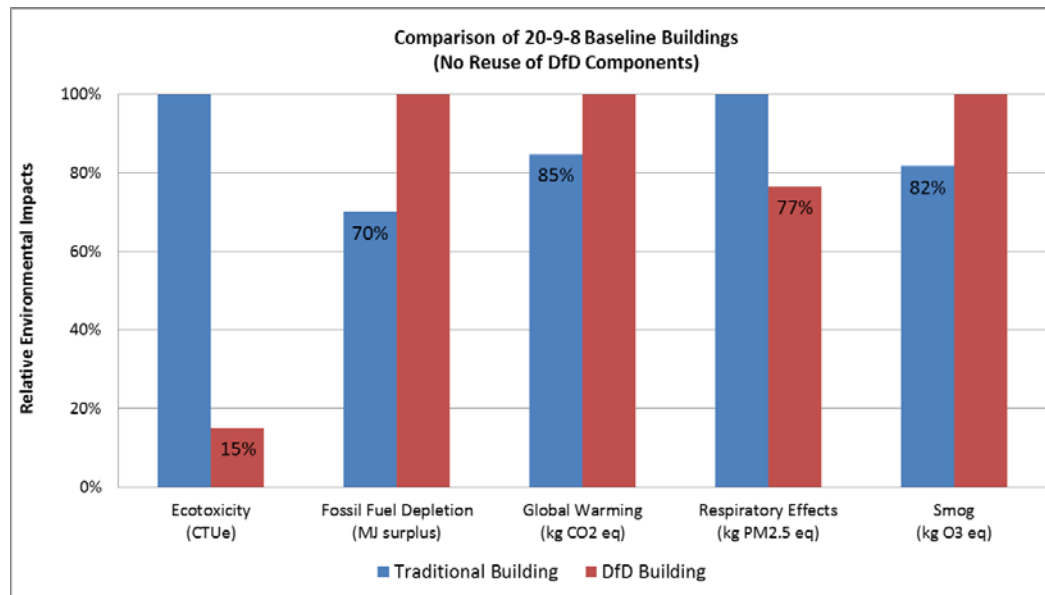


Figure 4.5 Comparison of relative environmental impacts of the 20-9-8 traditional and DfD buildings with no reuse of deconstructable components

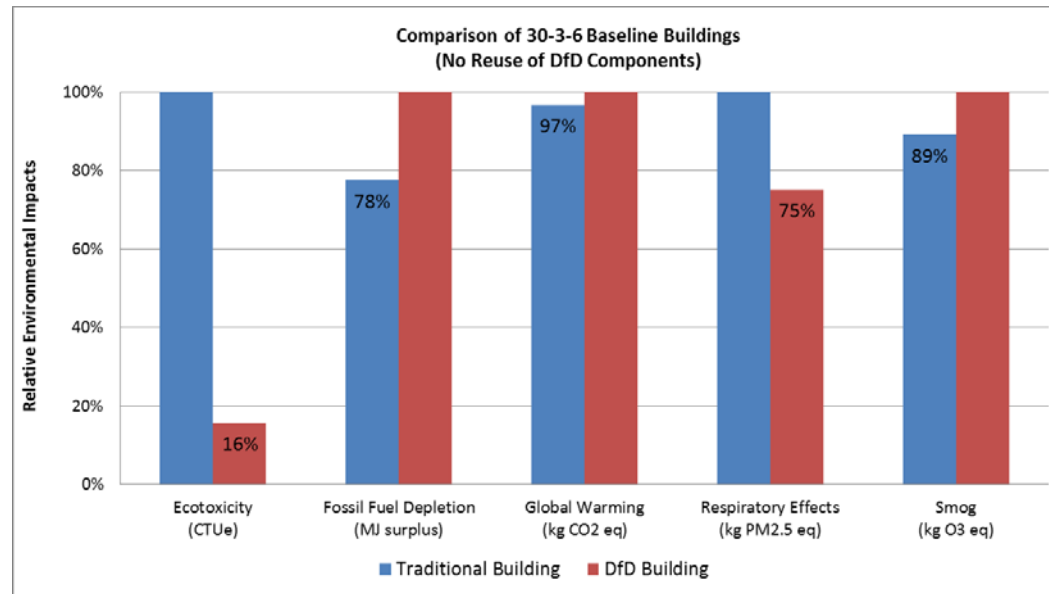


Figure 4.6 Comparison of relative environmental impacts of the 30-3-6 traditional and DfD buildings with no reuse of deconstructable components

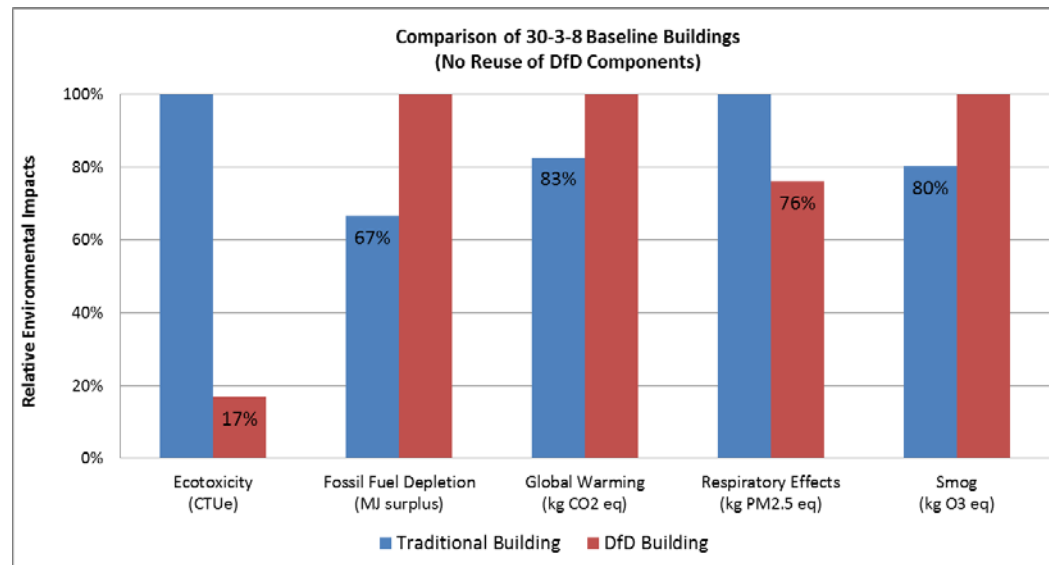


Figure 4.7 Comparison of relative environmental impacts of the 30-3-8 traditional and DfD buildings with no reuse of deconstructable components

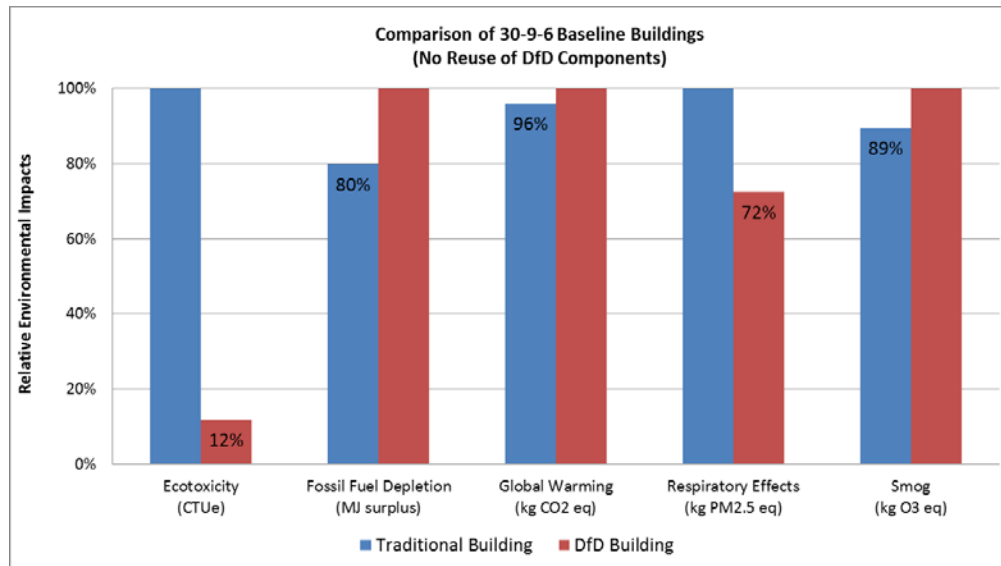


Figure 4.8 Comparison of relative environmental impacts of the 30-9-6 traditional and Dfd buildings with no reuse of deconstructable components

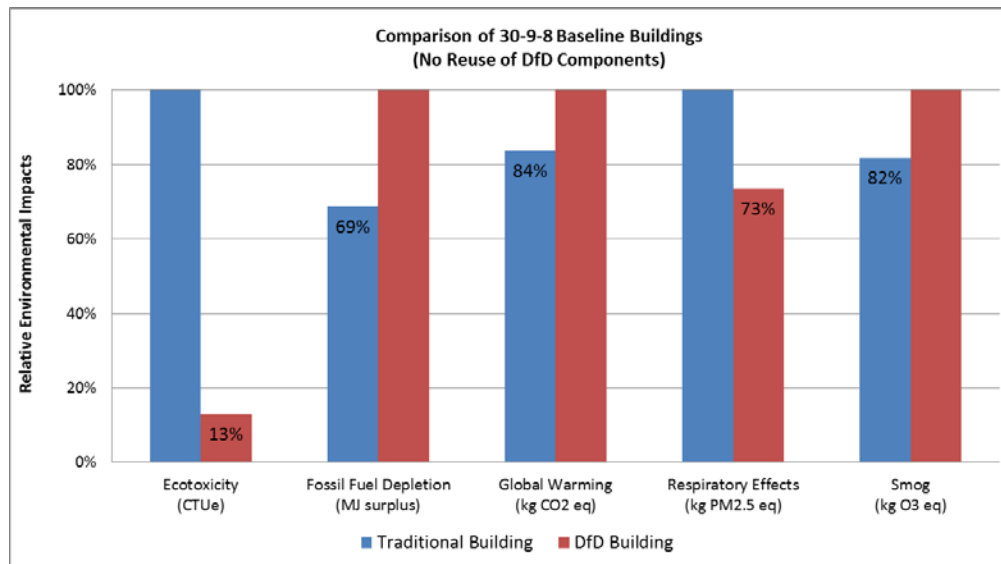


Figure 4.9 Comparison of relative environmental impacts of the 30-9-8 traditional and Dfd buildings with no reuse of deconstructable components

20-3-6 building configuration with 66% reuse of deconstructable components

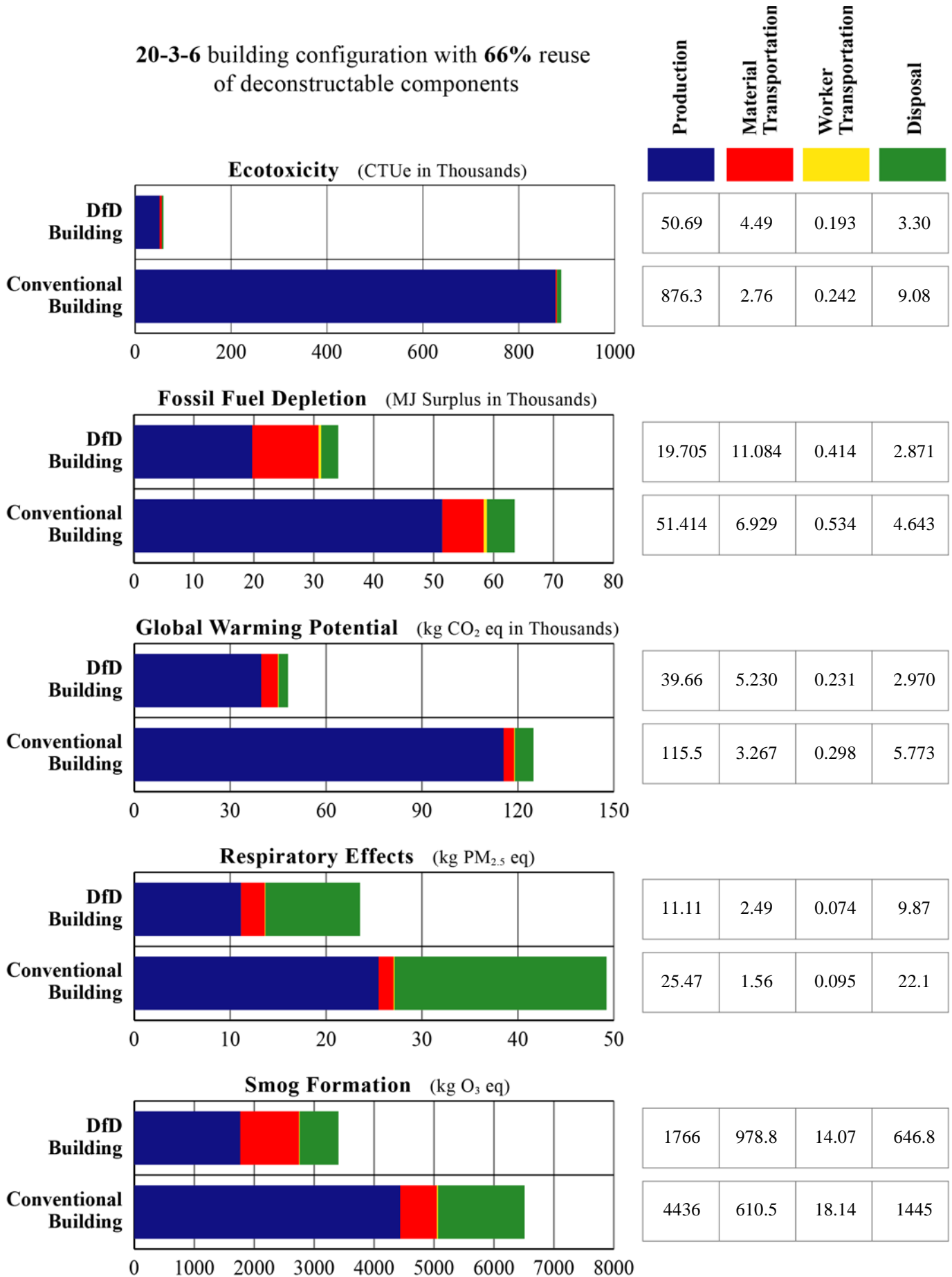


Figure 4.10 Comparison of relative environmental impacts of conventional and DfD buildings (20-3-6 w 66% reuse)

20-3-6 building configuration with 75% reuse of deconstructable components

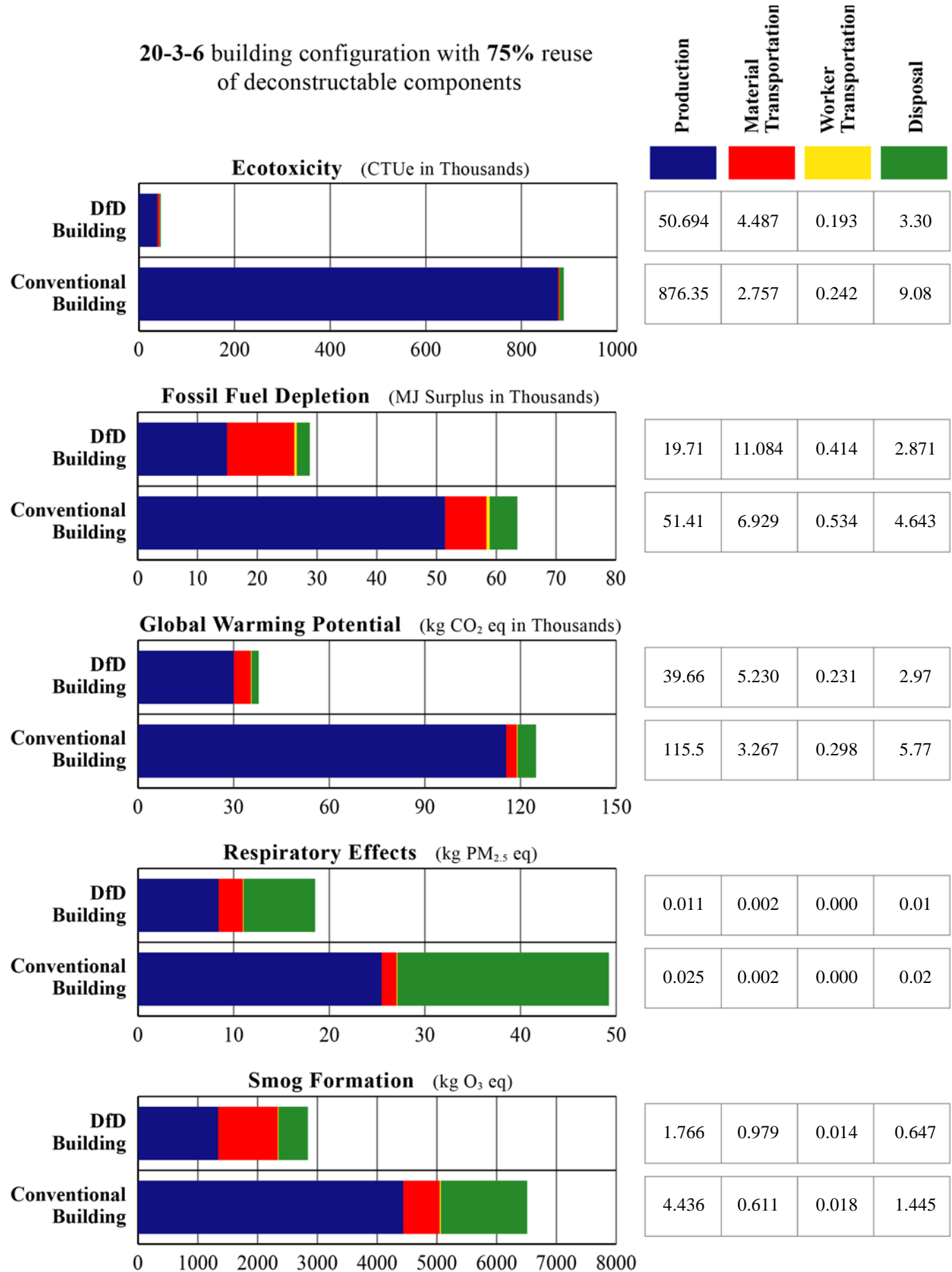


Figure 4.11 Comparison of relative environmental impacts of conventional and DfD buildings (20-3-6 w 75% reuse)

20-3-6 building configuration with 80% reuse of deconstructable components

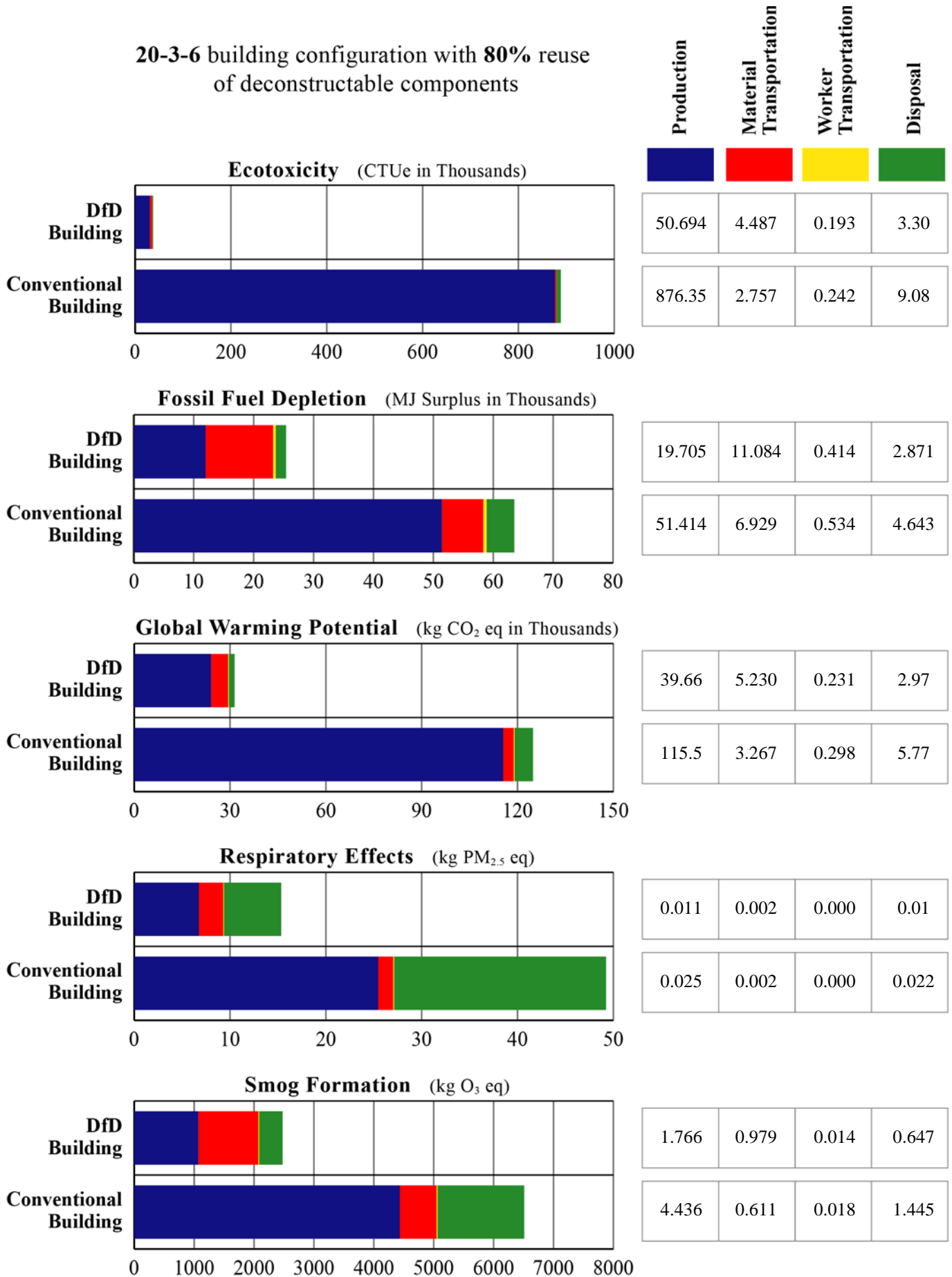


Figure 4.12 Comparison of relative environmental impacts of conventional and DfD buildings (20-3-6 w 80% reuse)

20-3-8 building configuration with 66% reuse of deconstructable components

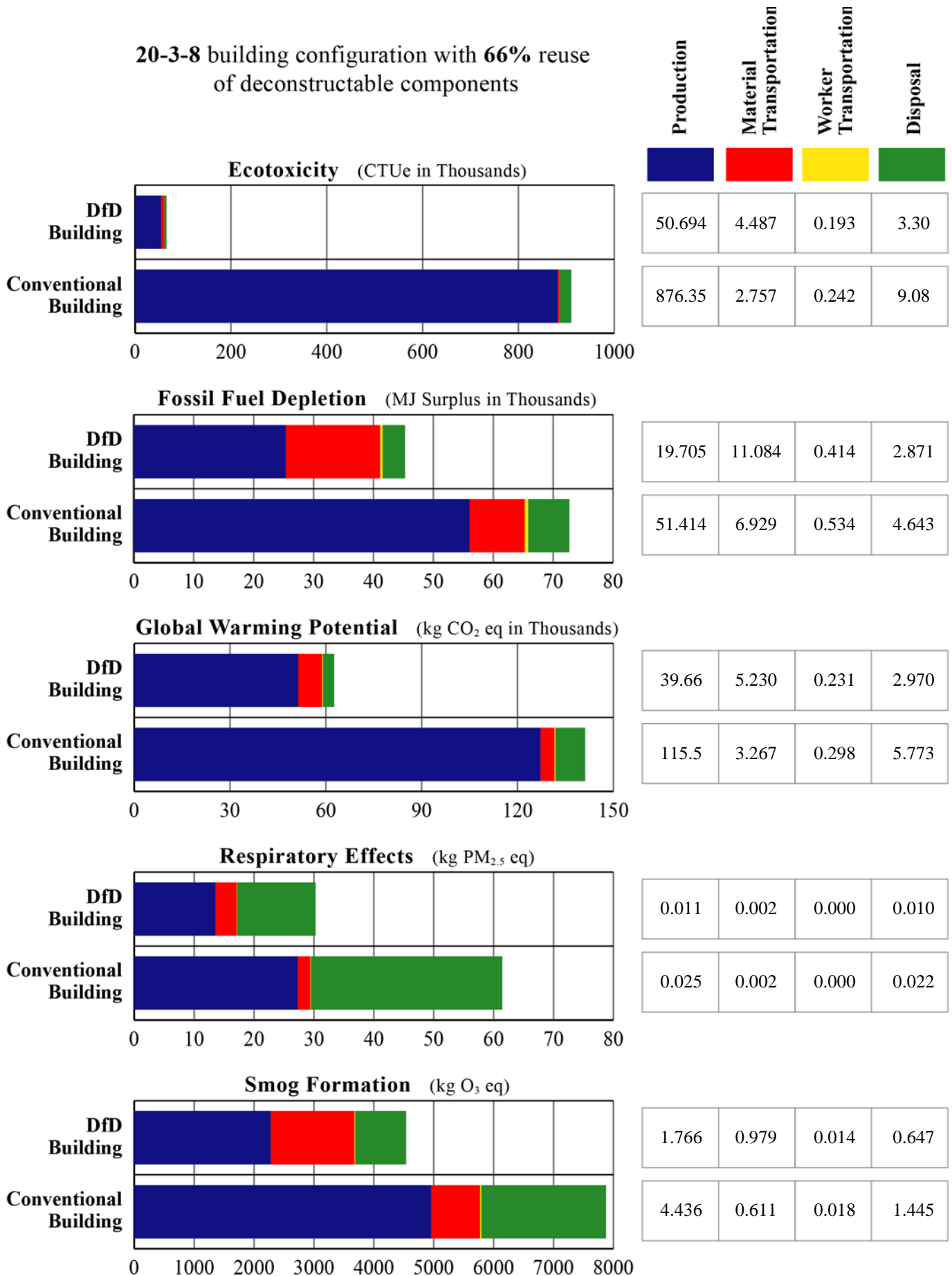


Figure 4.13 Comparison of relative environmental impacts of conventional and DfD buildings (20-3-8 w 66% reuse)

20-3-8 building configuration with 75% reuse of deconstructable components

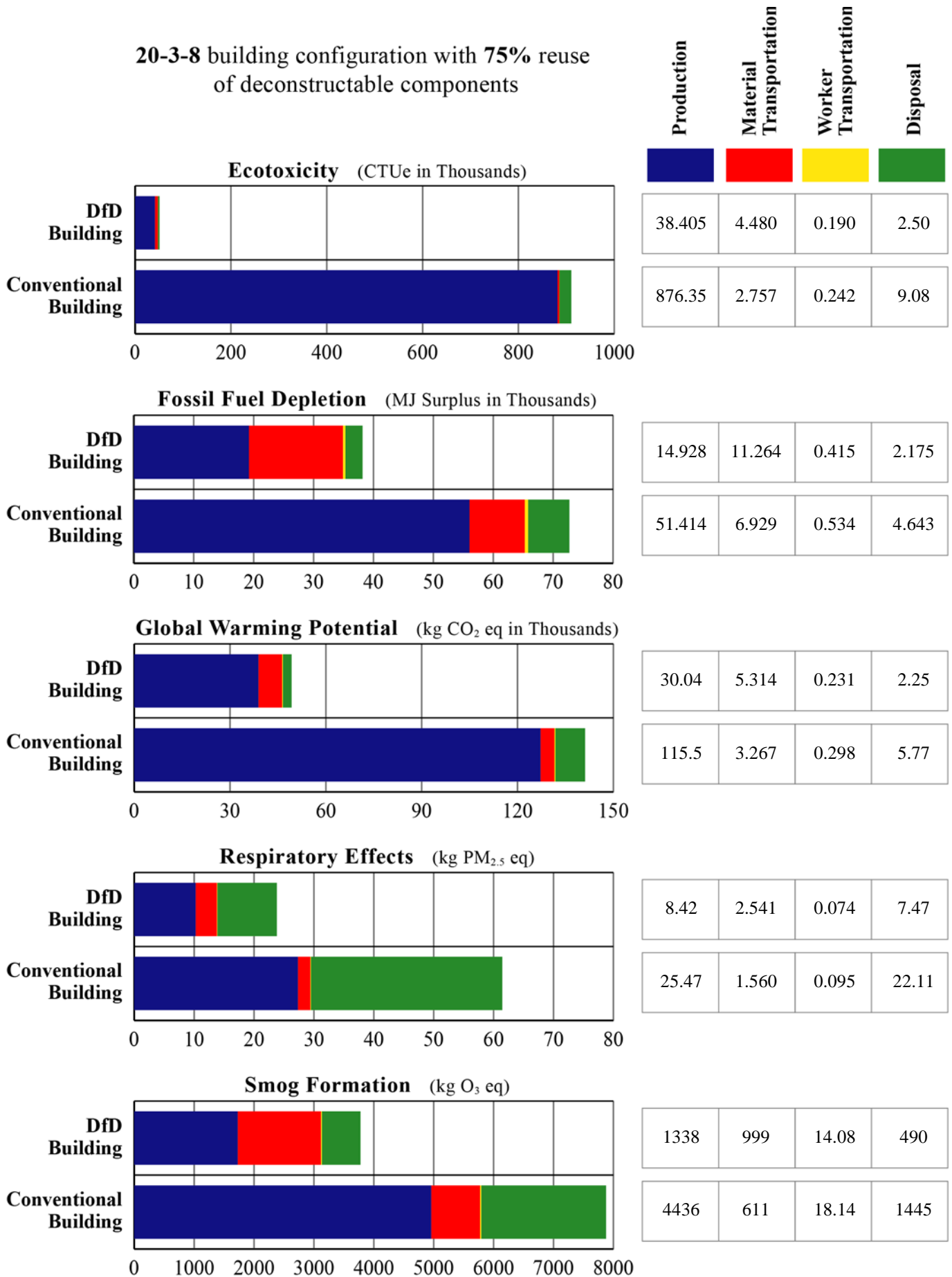


Figure 4.14 Comparison of relative environmental impacts of conventional and DfD buildings (20-3-8 w 75% reuse)

20-3-8 building configuration with 80% reuse of deconstructable components

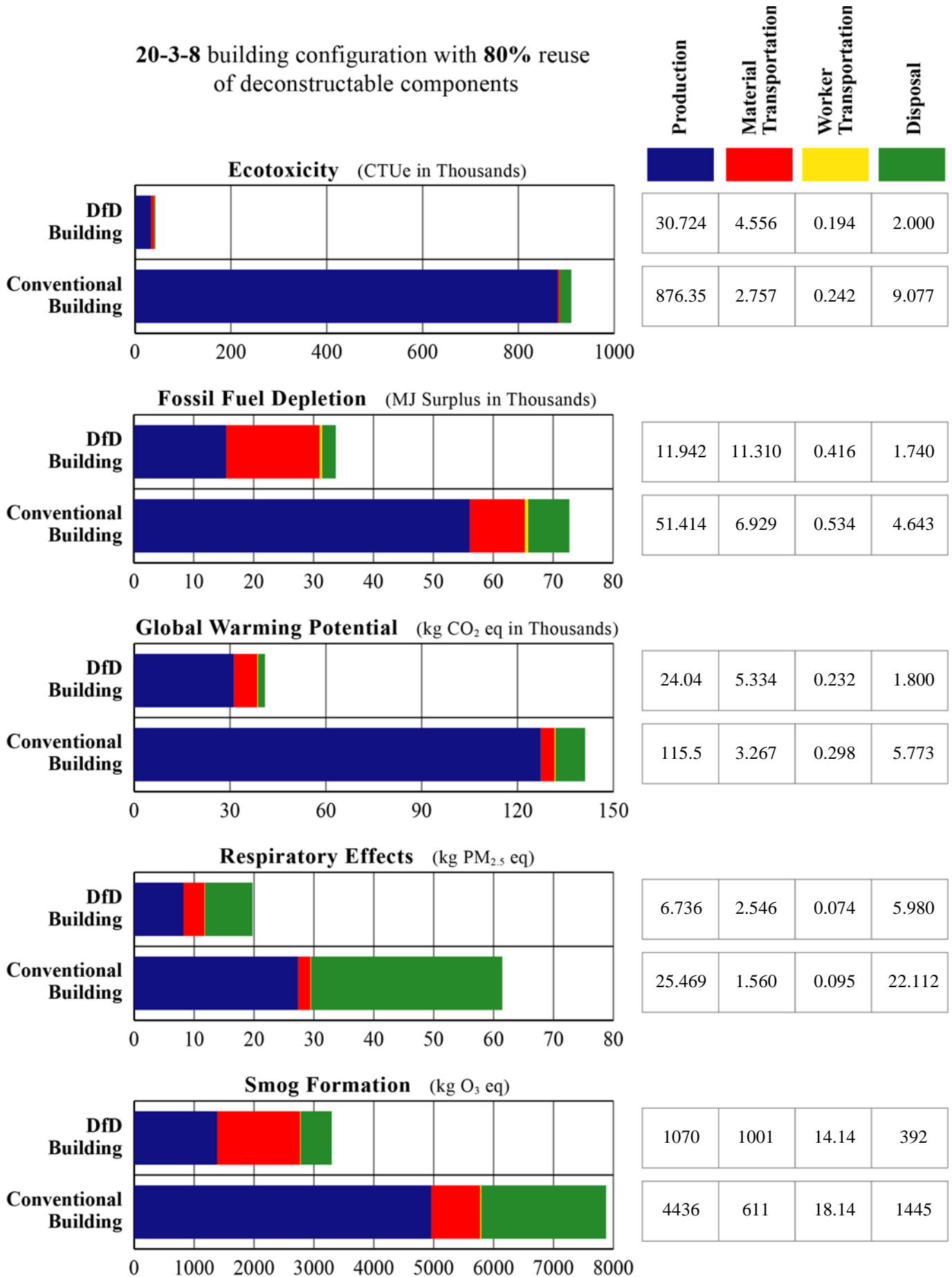


Figure 4.15 Comparison of relative environmental impacts of conventional and DfD buildings (20-3-8 w 80% reuse)

20-9-6 building configuration with 66% reuse of deconstructable components

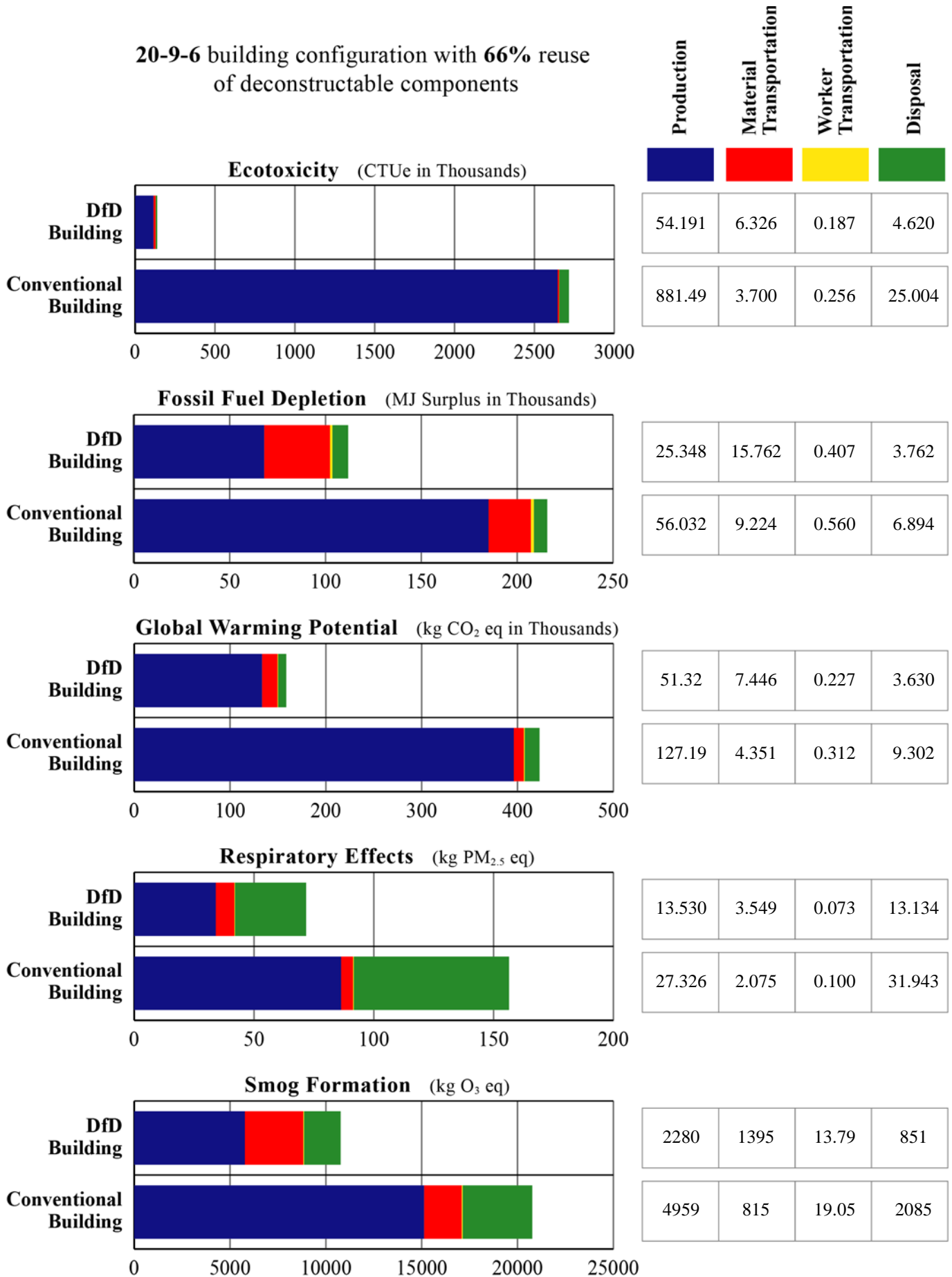


Figure 4.16 Comparison of relative environmental impacts of conventional and DfD buildings (20-9-6 w 66% reuse)

20-9-6 building configuration with 75% reuse of deconstructable components

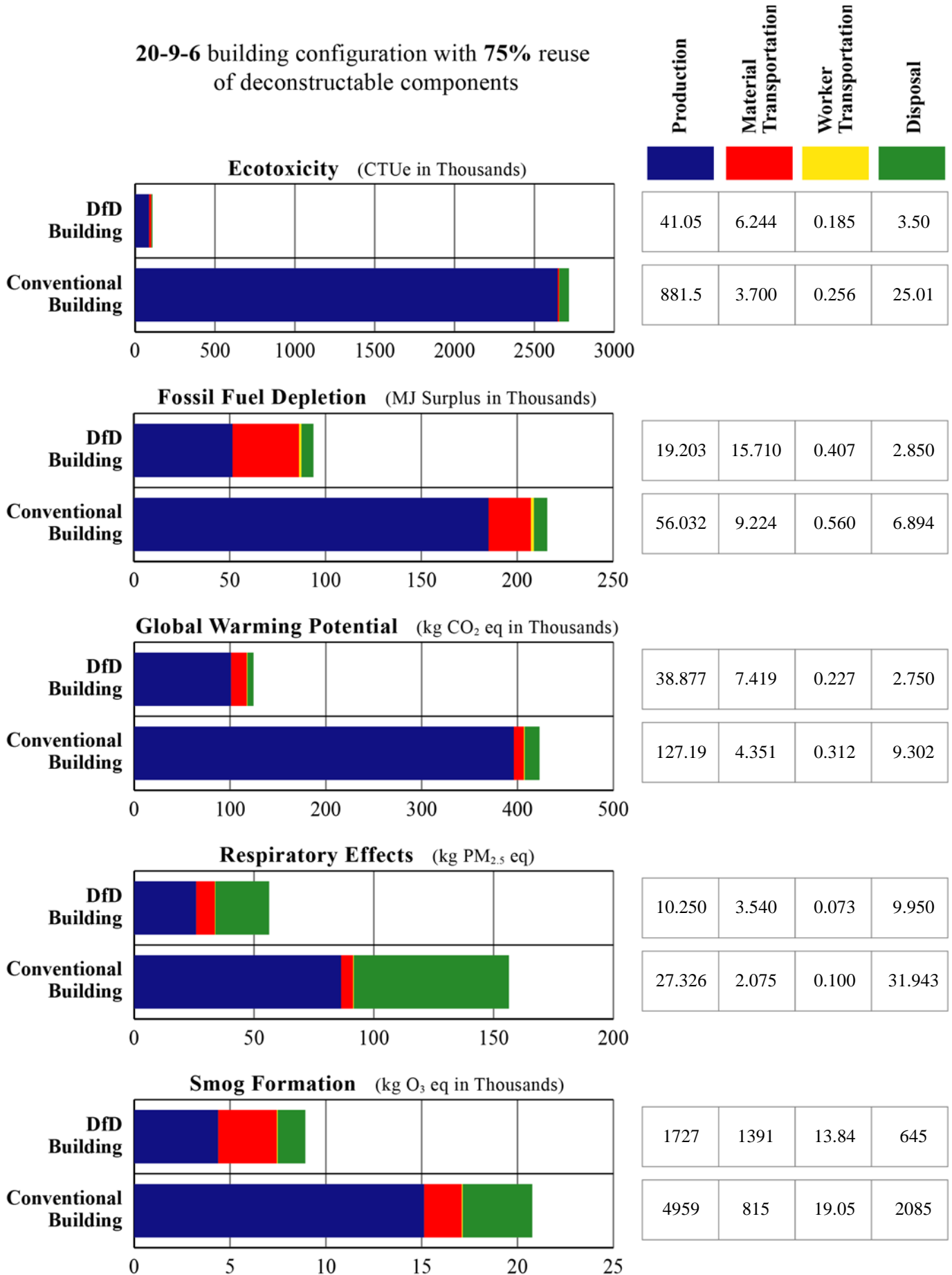


Figure 4.17 Comparison of relative environmental impacts of conventional and DfD buildings (20-9-6 w 66% reuse)

20-9-6 building configuration with 80% reuse of deconstructable components

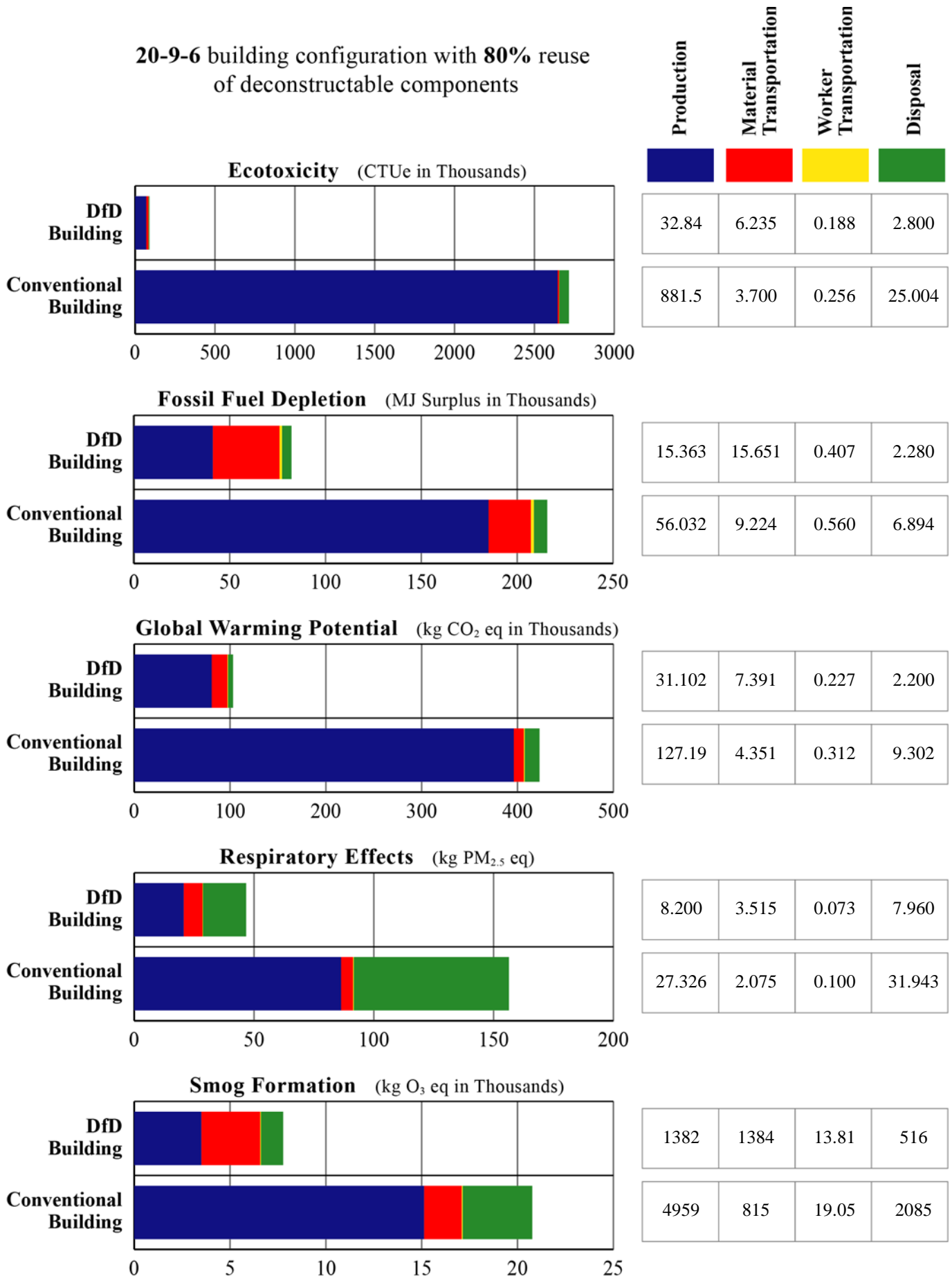


Figure 4.18 Comparison of relative environmental impacts of conventional and DfD buildings (20-9-6 w 80% reuse)

20-9-8 building configuration with 66% reuse of deconstructable components

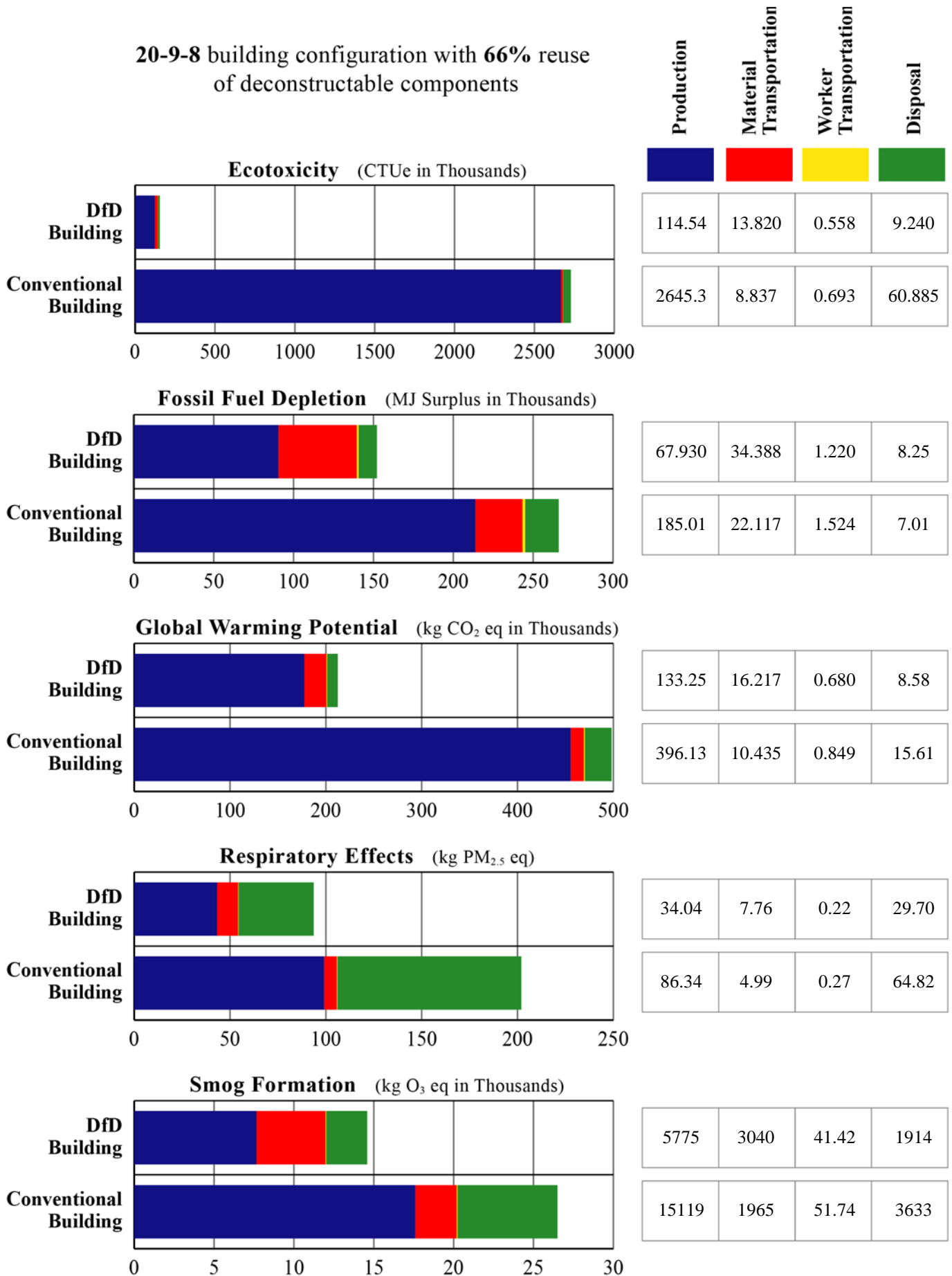


Figure 4.19 Comparison of relative environmental impacts of conventional and DfD buildings (20-9-9 w 66% reuse)

20-9-8 building configuration with 75% reuse of deconstructable components

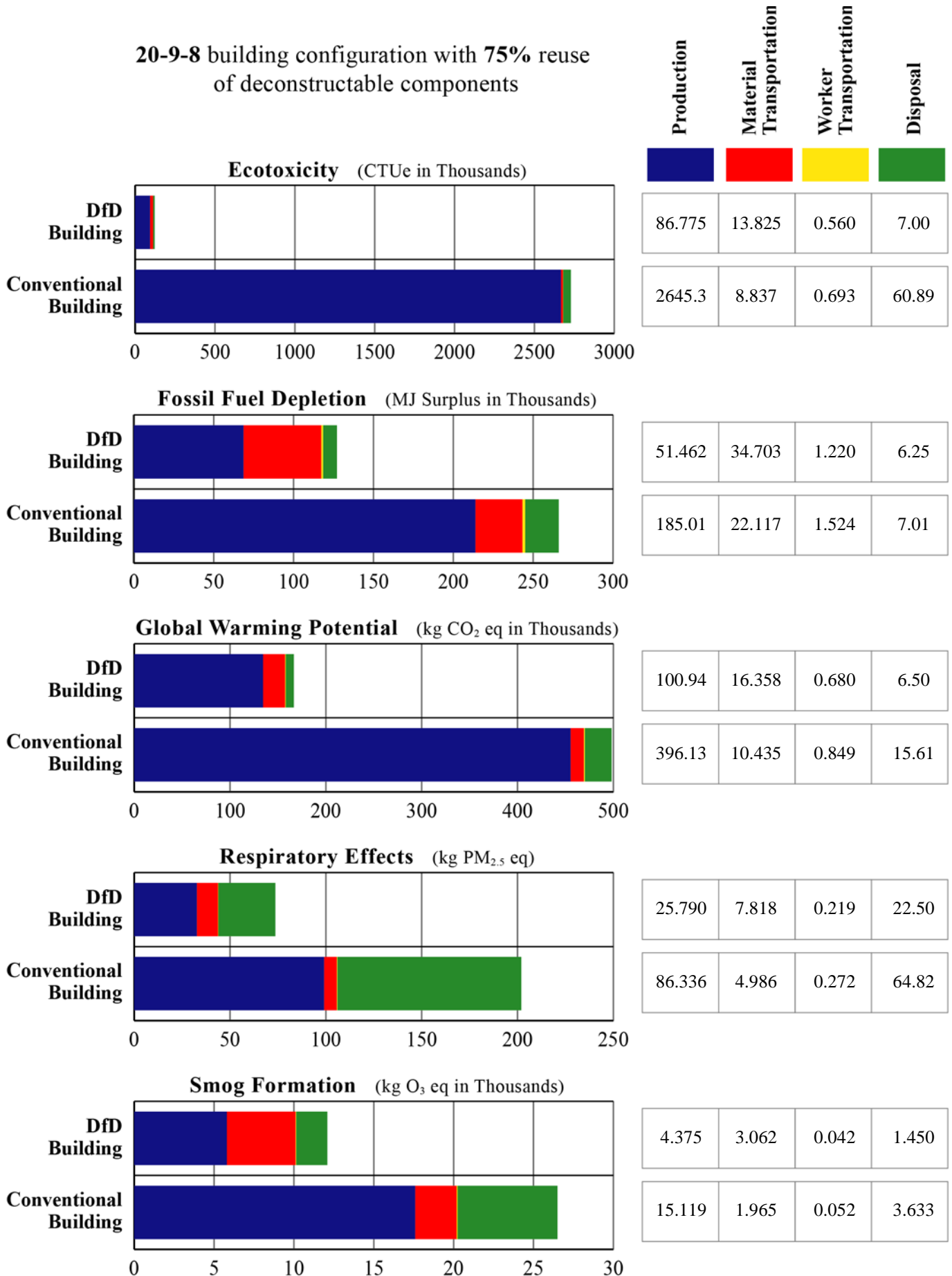


Figure 4.20 Comparison of relative environmental impacts of conventional and DfD buildings (20-9-8 w 75% reuse)

20-9-8 building configuration with 80% reuse of deconstructable components

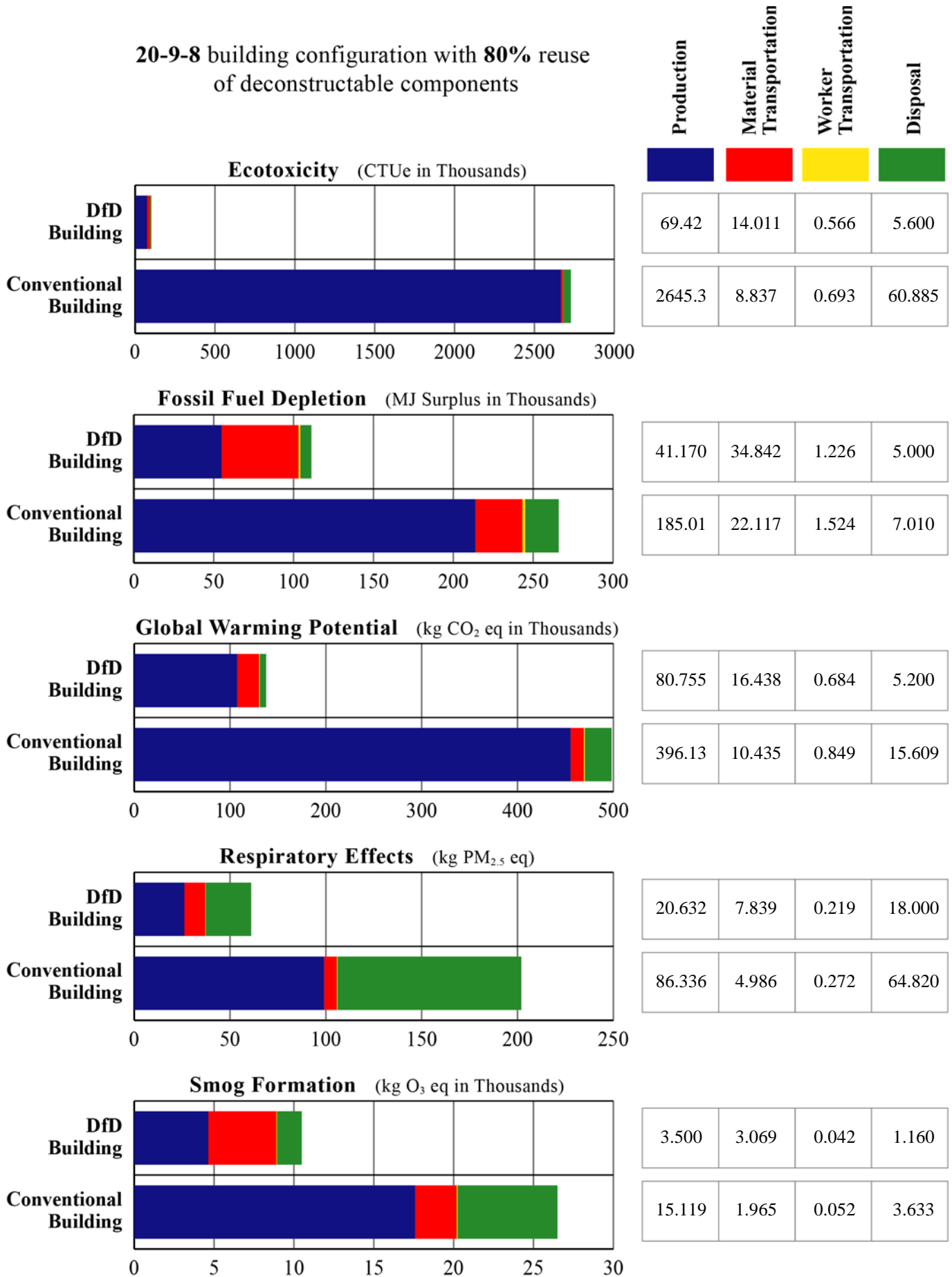


Figure 4.21 Comparison of relative environmental impacts of conventional and DfD buildings (20-9-8 w 80% reuse)

30-3-6 building configuration with 66% reuse of deconstructable components

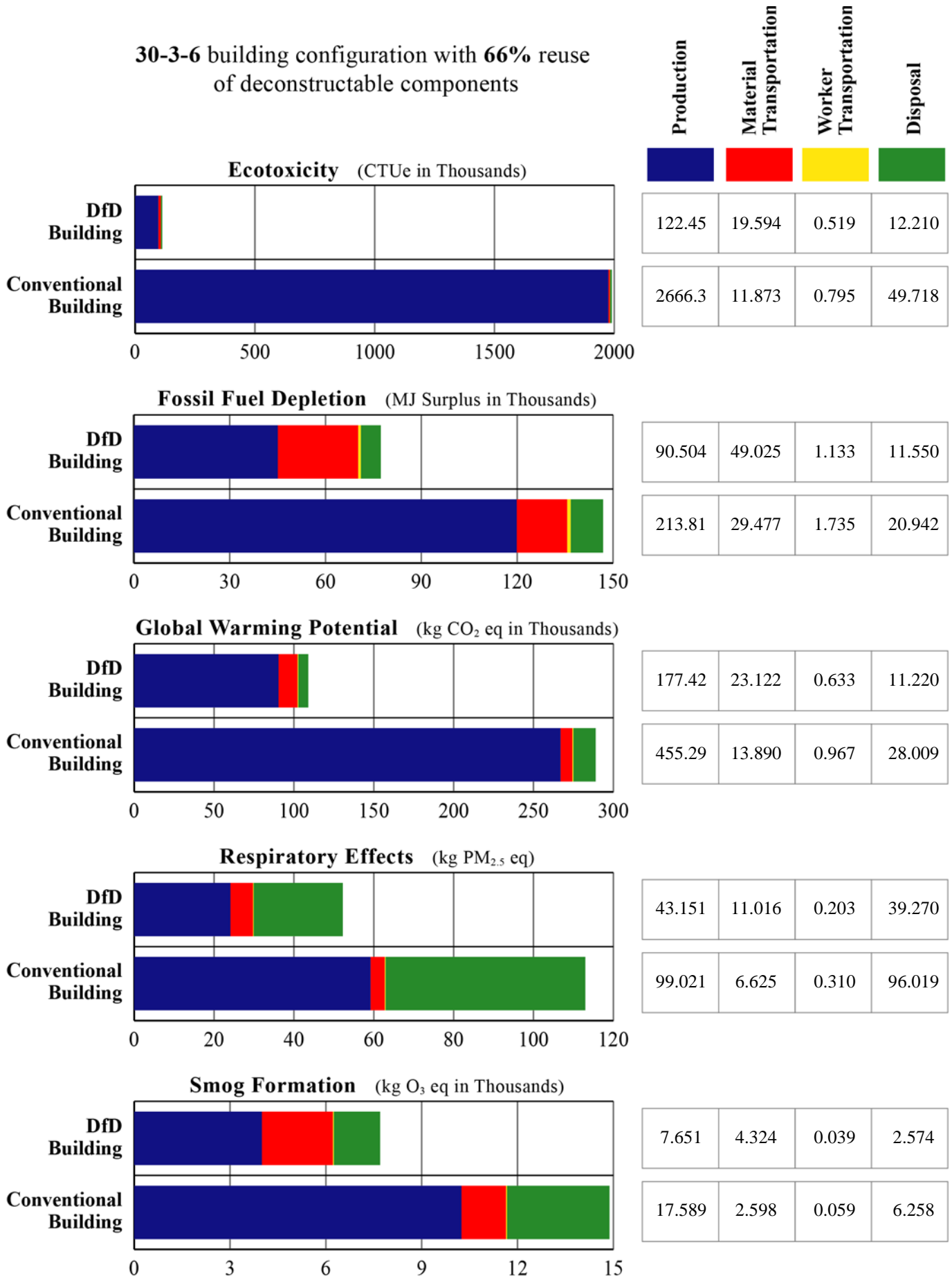


Figure 4.22 Comparison of relative environmental impacts of conventional and DfD buildings (30-3-6 w 66% reuse)

30-3-6 building configuration with 75% reuse of deconstructable components

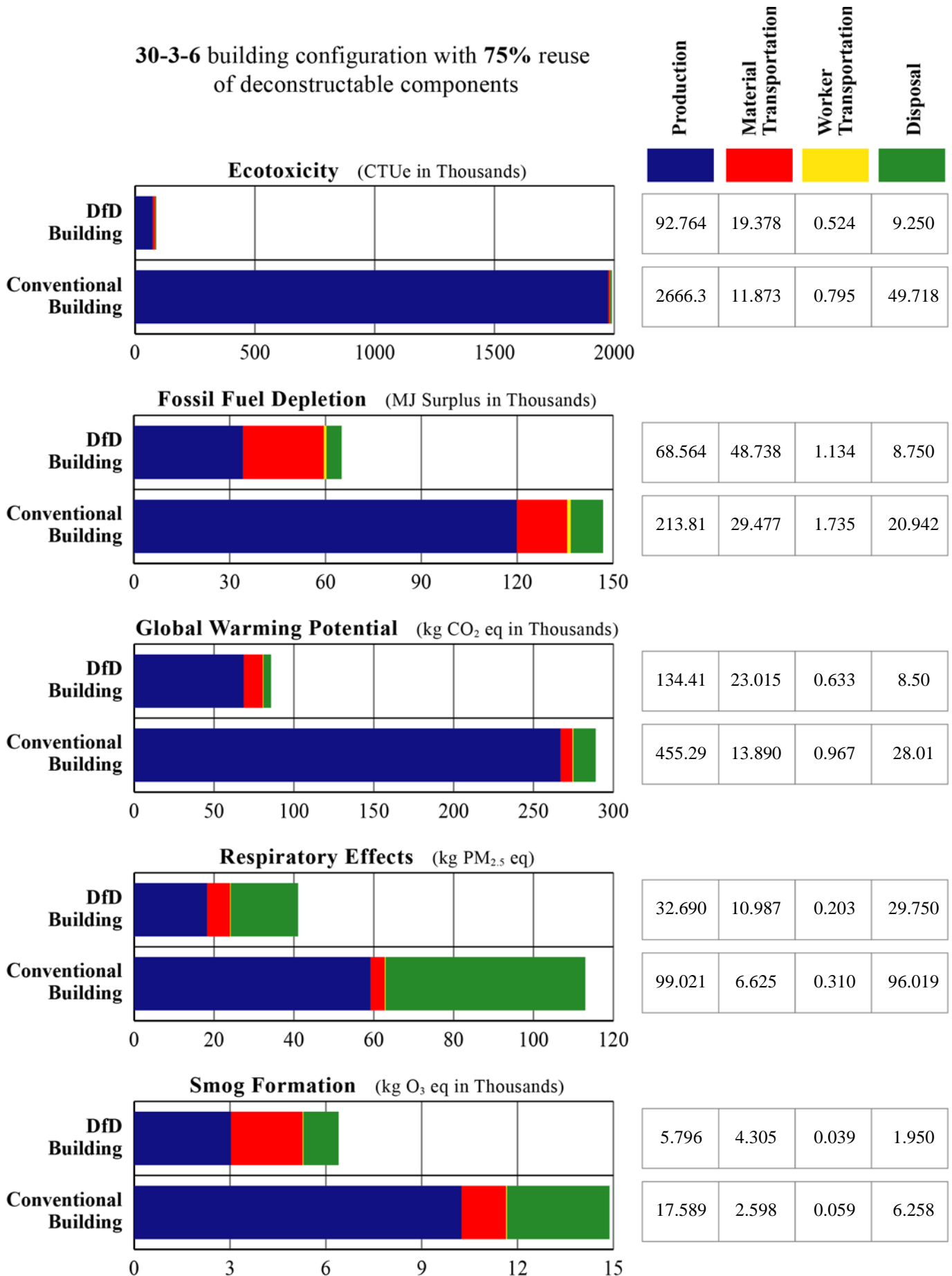


Figure 4.23 Comparison of relative environmental impacts of conventional and DfD buildings (30-3-6 w 75% reuse)

30-3-6 building configuration with 80% reuse of deconstructable components

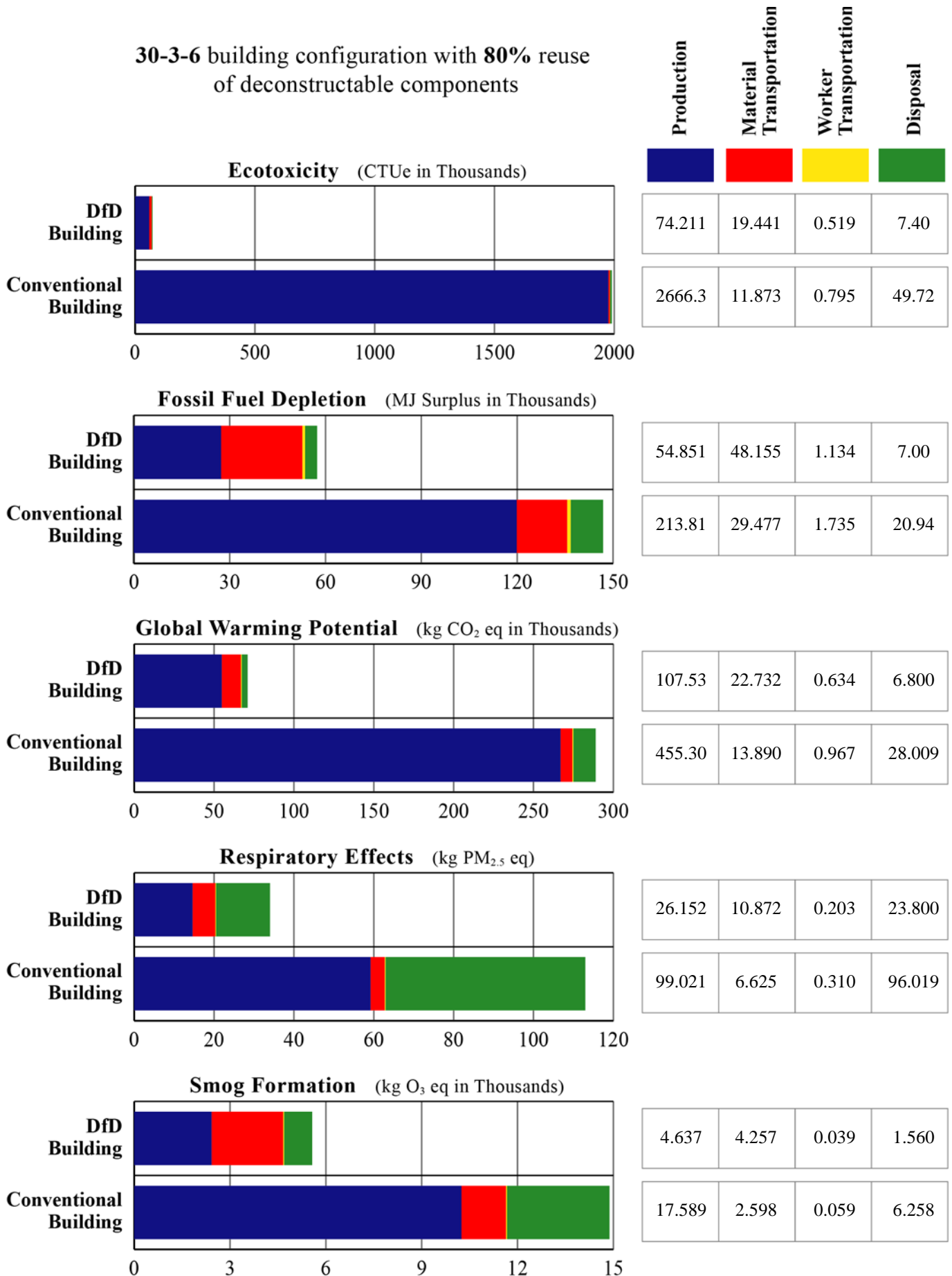


Figure 4.24 Comparison of relative environmental impacts of conventional and DfD buildings (30-3-6 w 80% reuse)

30-3-8 building configuration with 66% reuse of deconstructable components

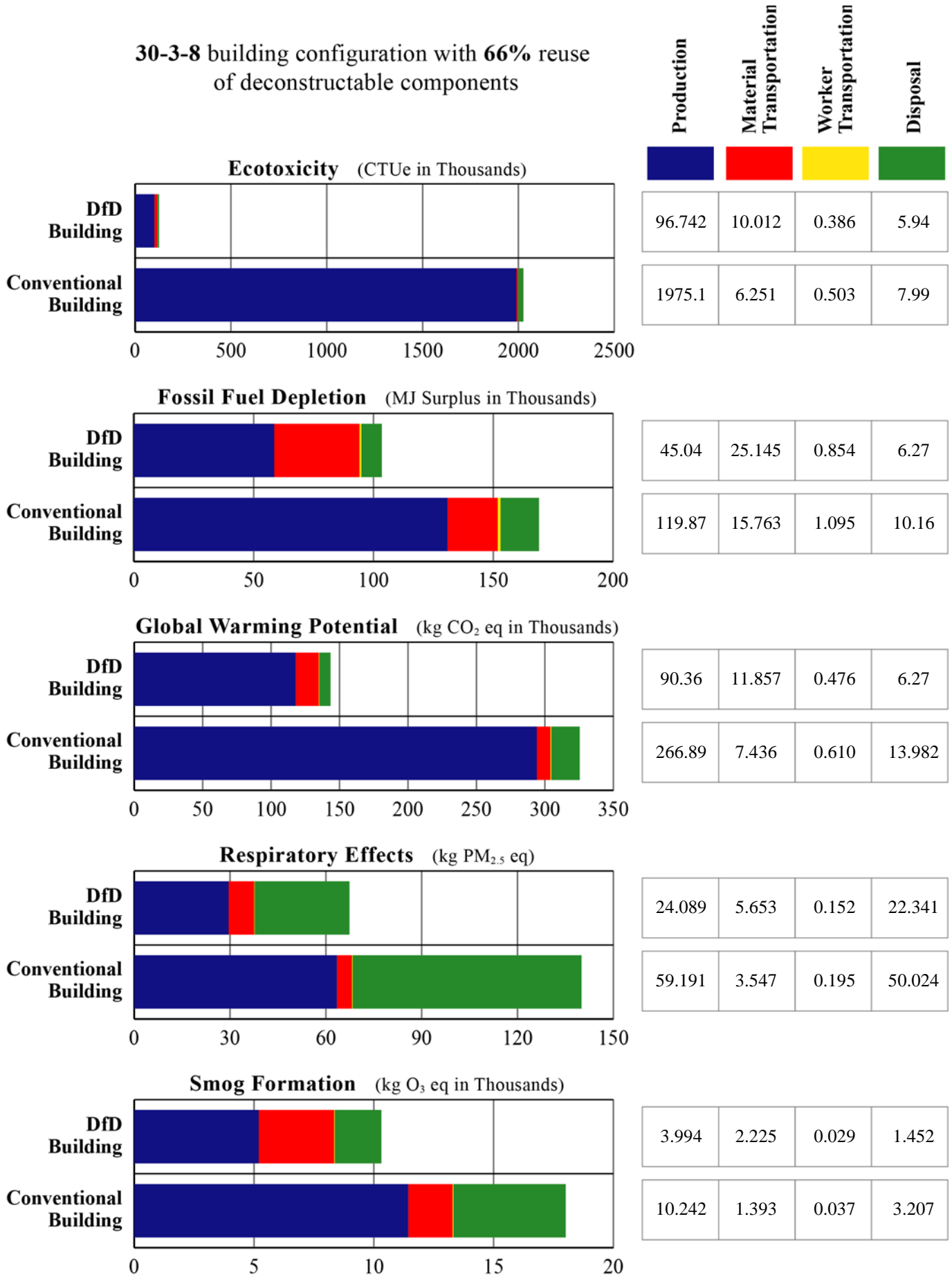


Figure 4.25 Comparison of relative environmental impacts of conventional and DfD buildings (30-3-8 w 66% reuse)

30-3-8 building configuration with 75% reuse of deconstructable components

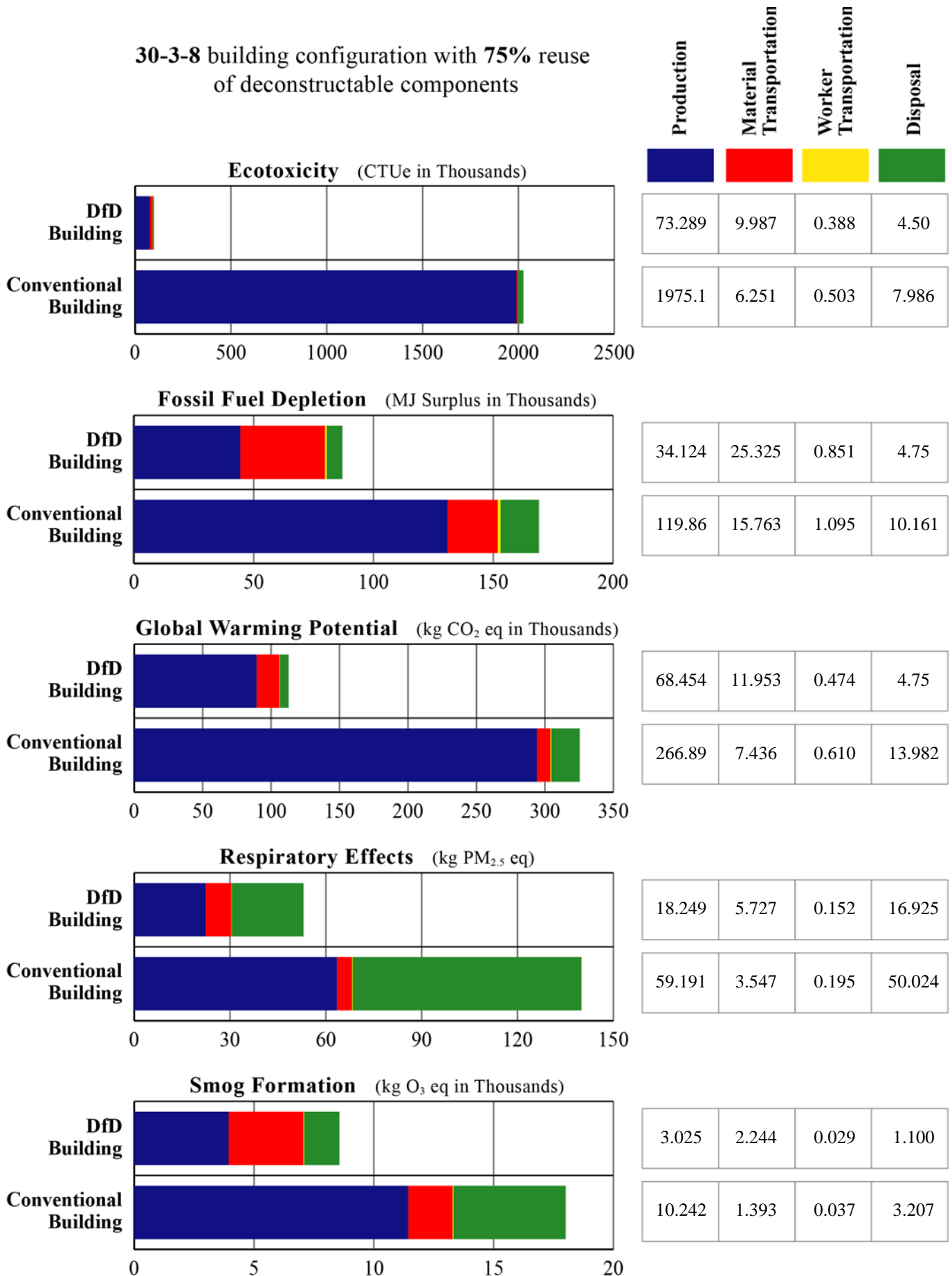


Figure 4.26 Comparison of relative environmental impacts of conventional and DfD buildings (30-3-8 w 75% reuse)

30-3-8 building configuration with 80% reuse of deconstructable components

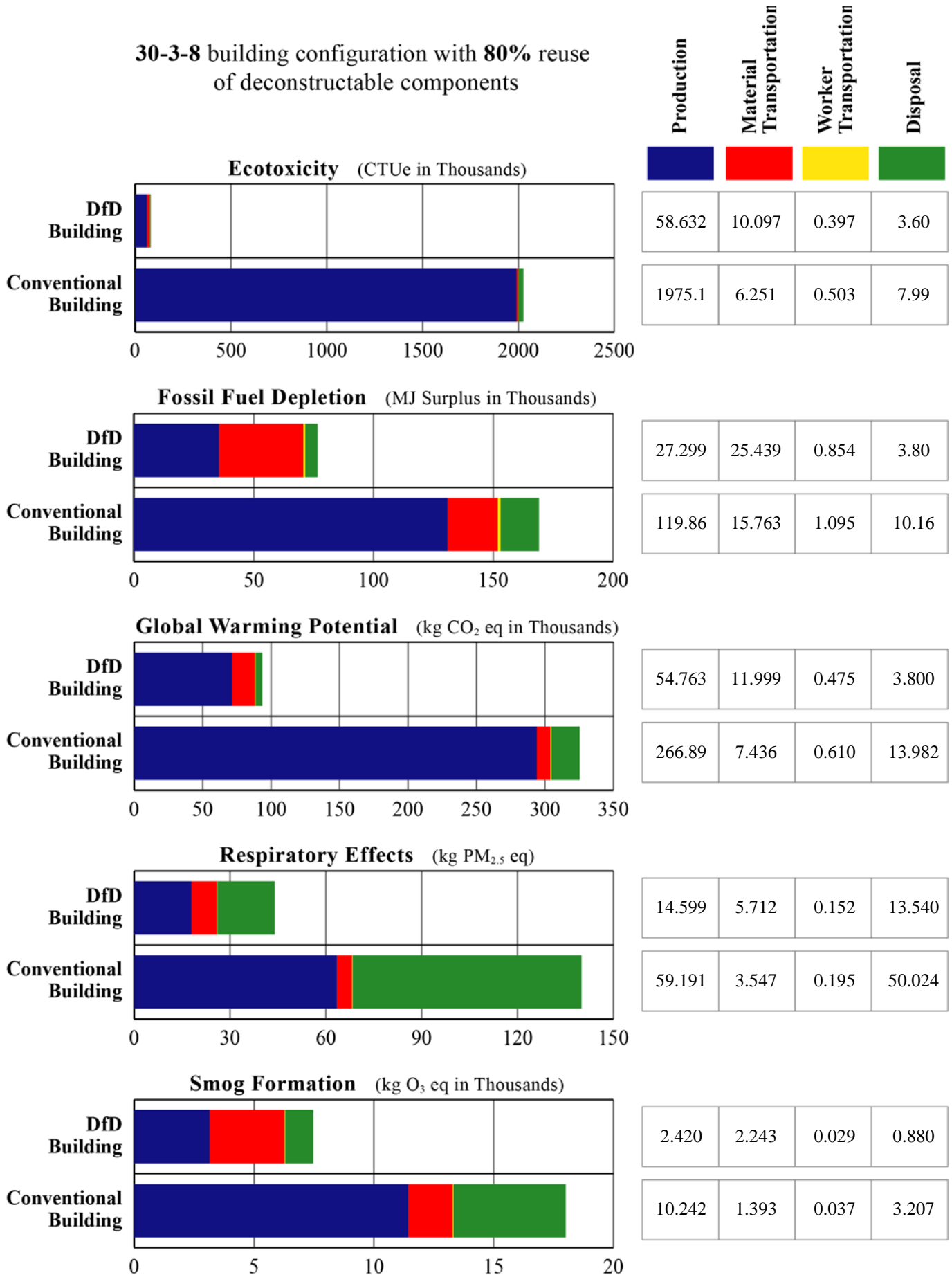


Figure 4.27 Comparison of relative environmental impacts of conventional and DfD buildings (30-3-8 w 80% reuse)

30-9-6 building configuration with 66% reuse of deconstructable components

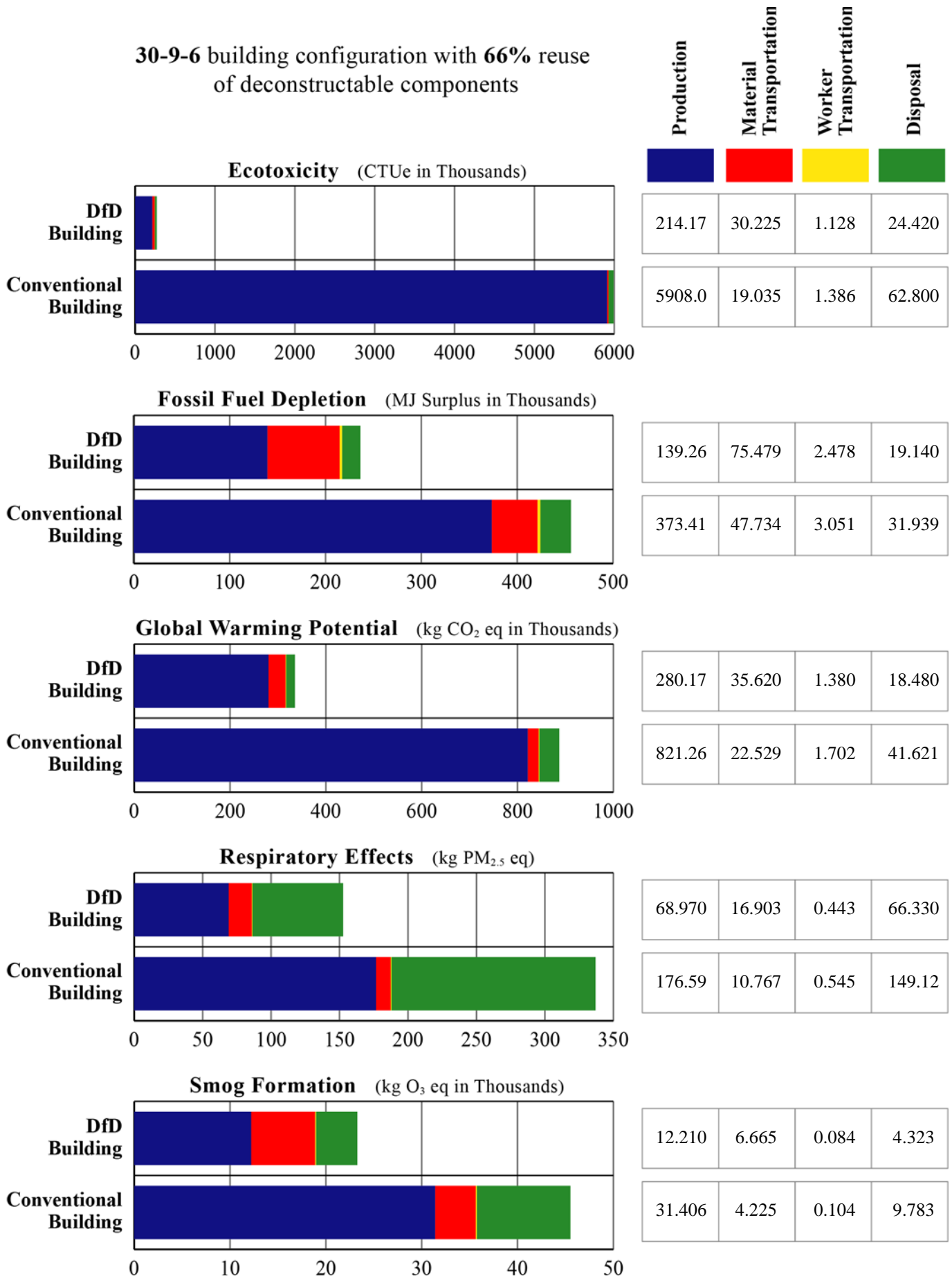


Figure 4.28 Comparison of relative environmental impacts of conventional and DfD buildings (30-9-6 w 66% reuse)

30-9-6 building configuration with 75% reuse of deconstructable components

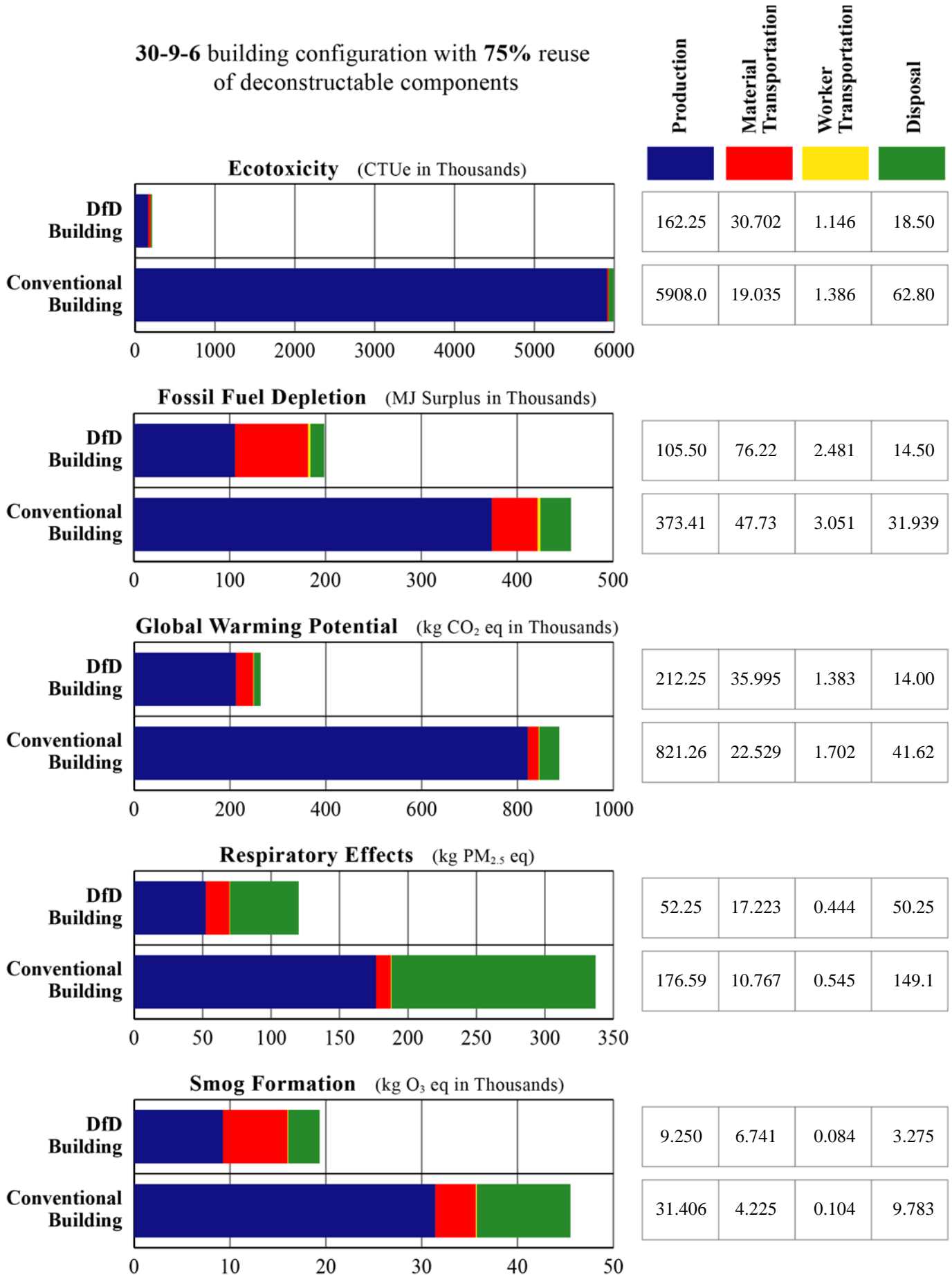


Figure 4.29 Comparison of relative environmental impacts of conventional and DfD buildings (30-9-6 w 75% reuse)

30-9-6 building configuration with 80% reuse of deconstructable components

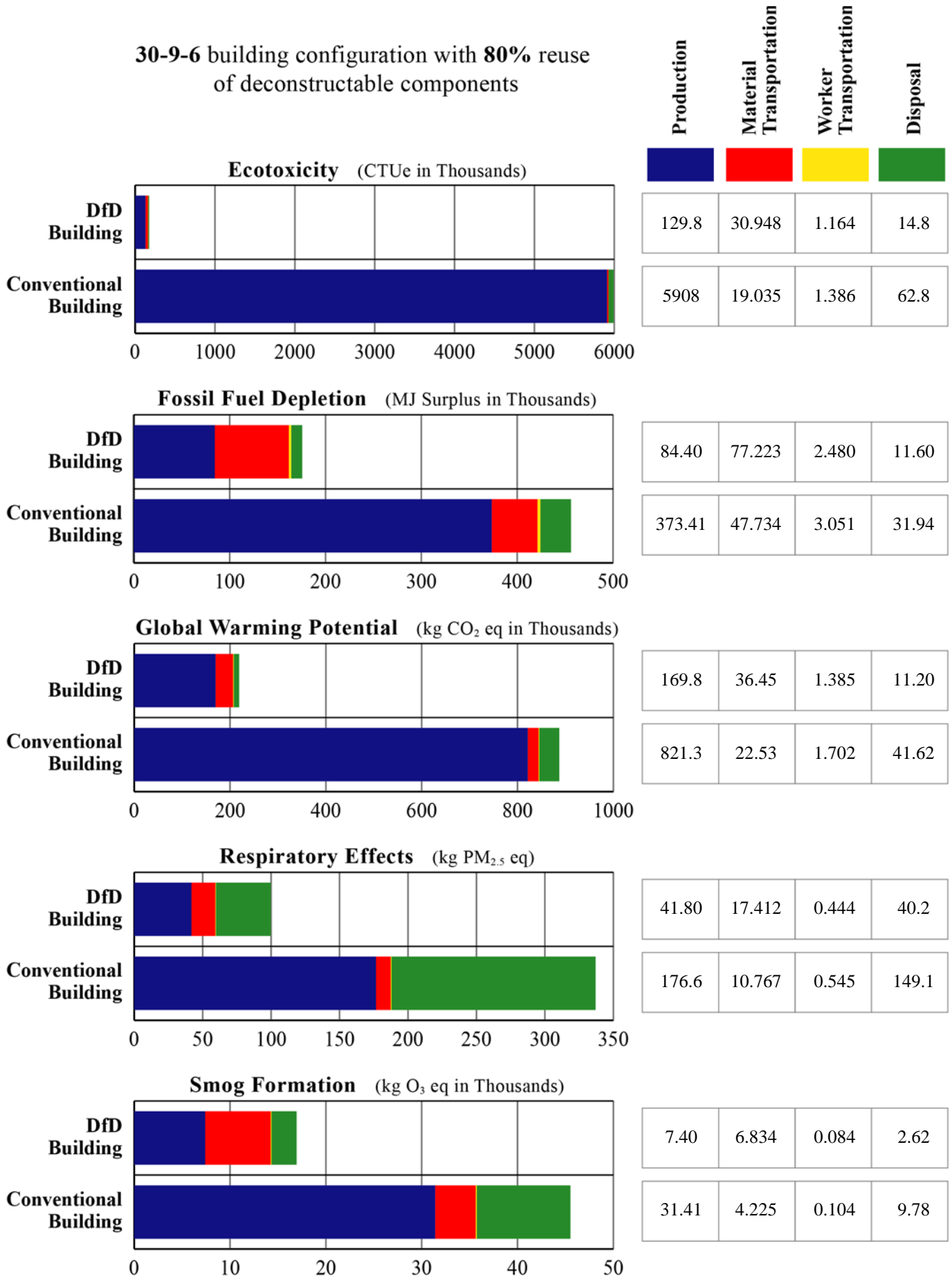


Figure 4.30 Comparison of relative environmental impacts of conventional and DfD buildings (30-9-6 w 80% reuse)

30-9-8 building configuration with 66% reuse of deconstructable components

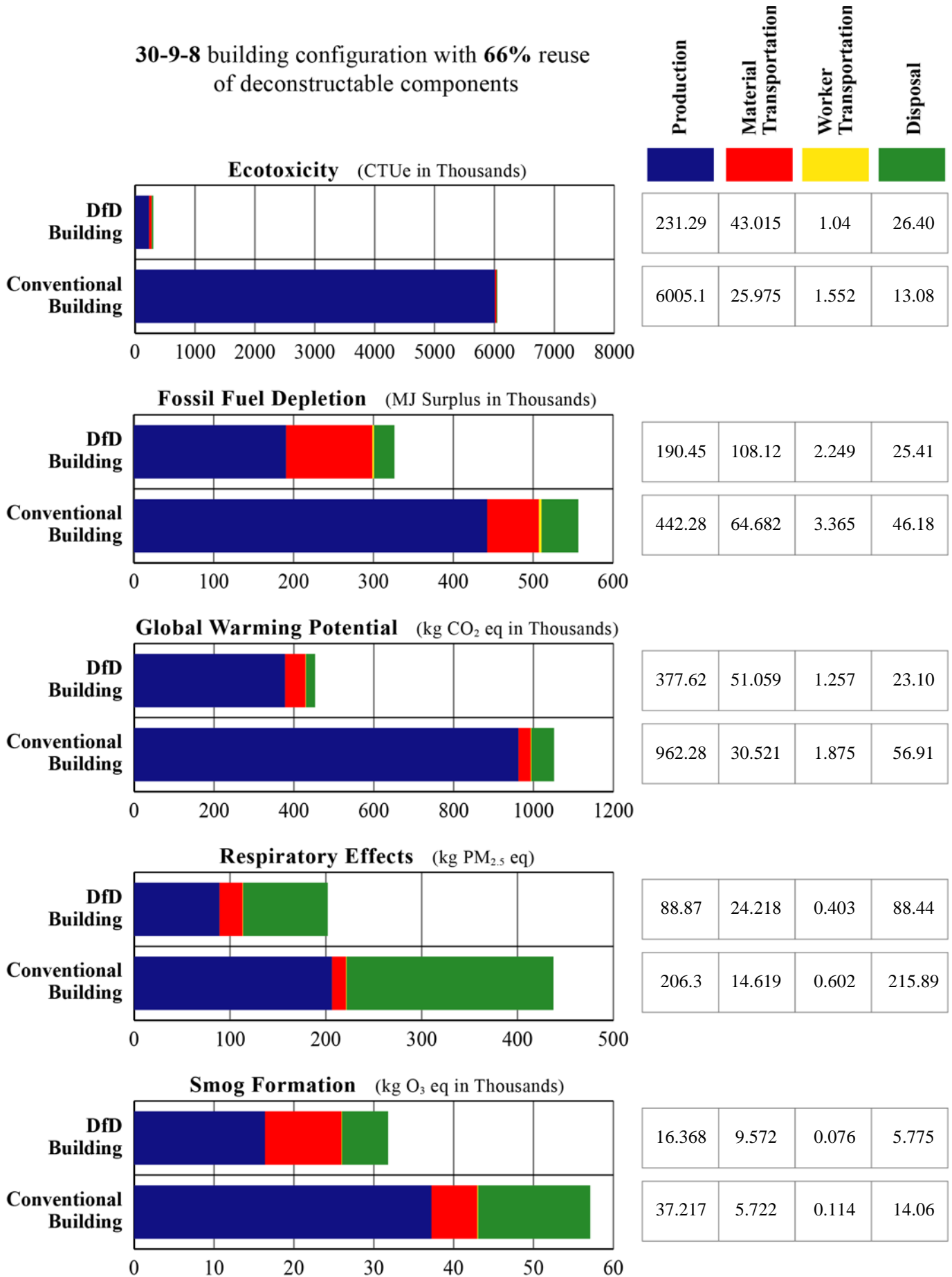


Figure 4.31 Comparison of relative environmental impacts of conventional and DfD buildings (30-9-8 w 66% reuse)

30-9-8 building configuration with 75% reuse of deconstructable components

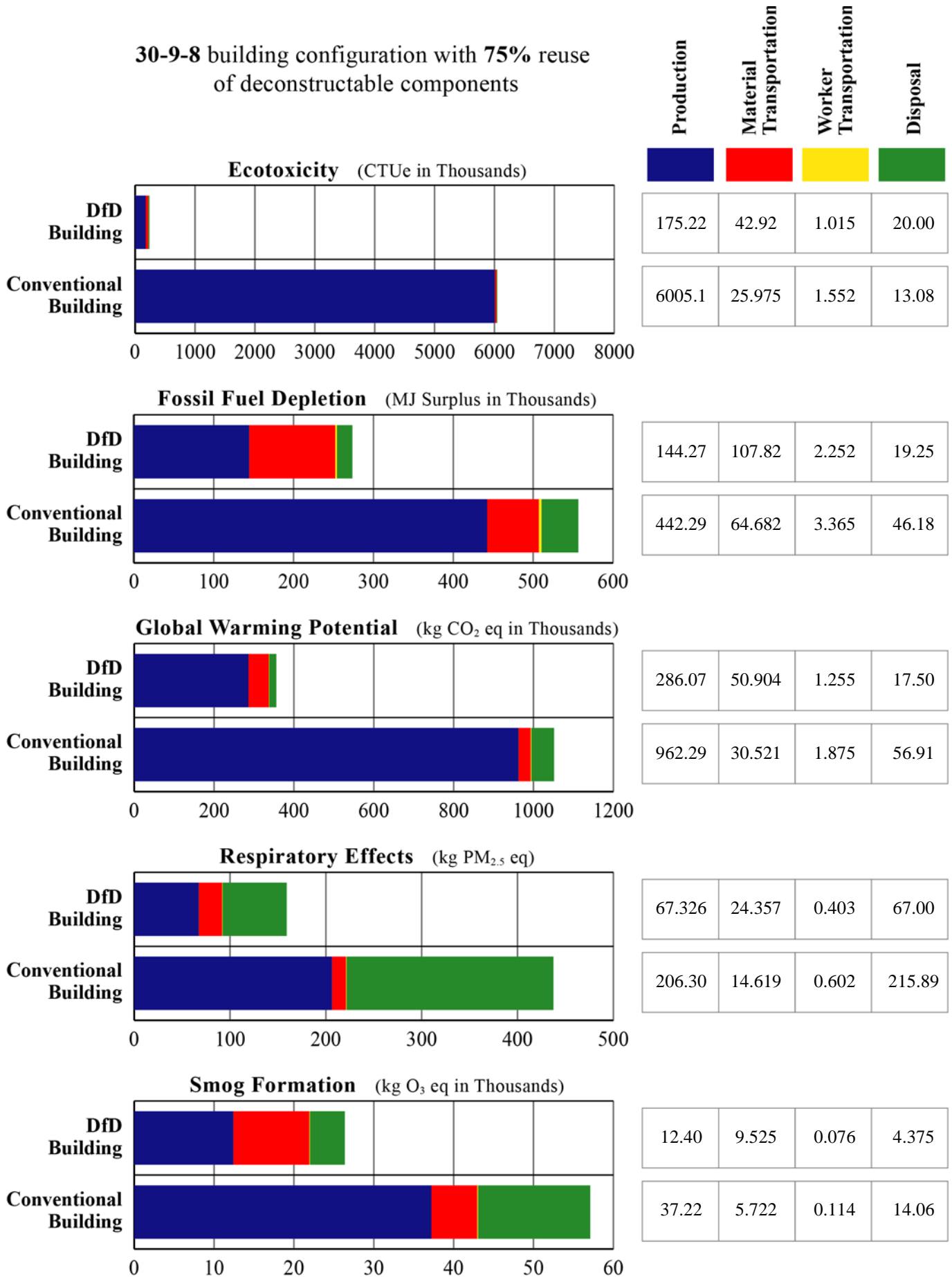


Figure 4.32 Comparison of relative environmental impacts of conventional and DfD buildings (30-9-8 w 75% reuse)

30-9-8 building configuration with 80% reuse of deconstructable components

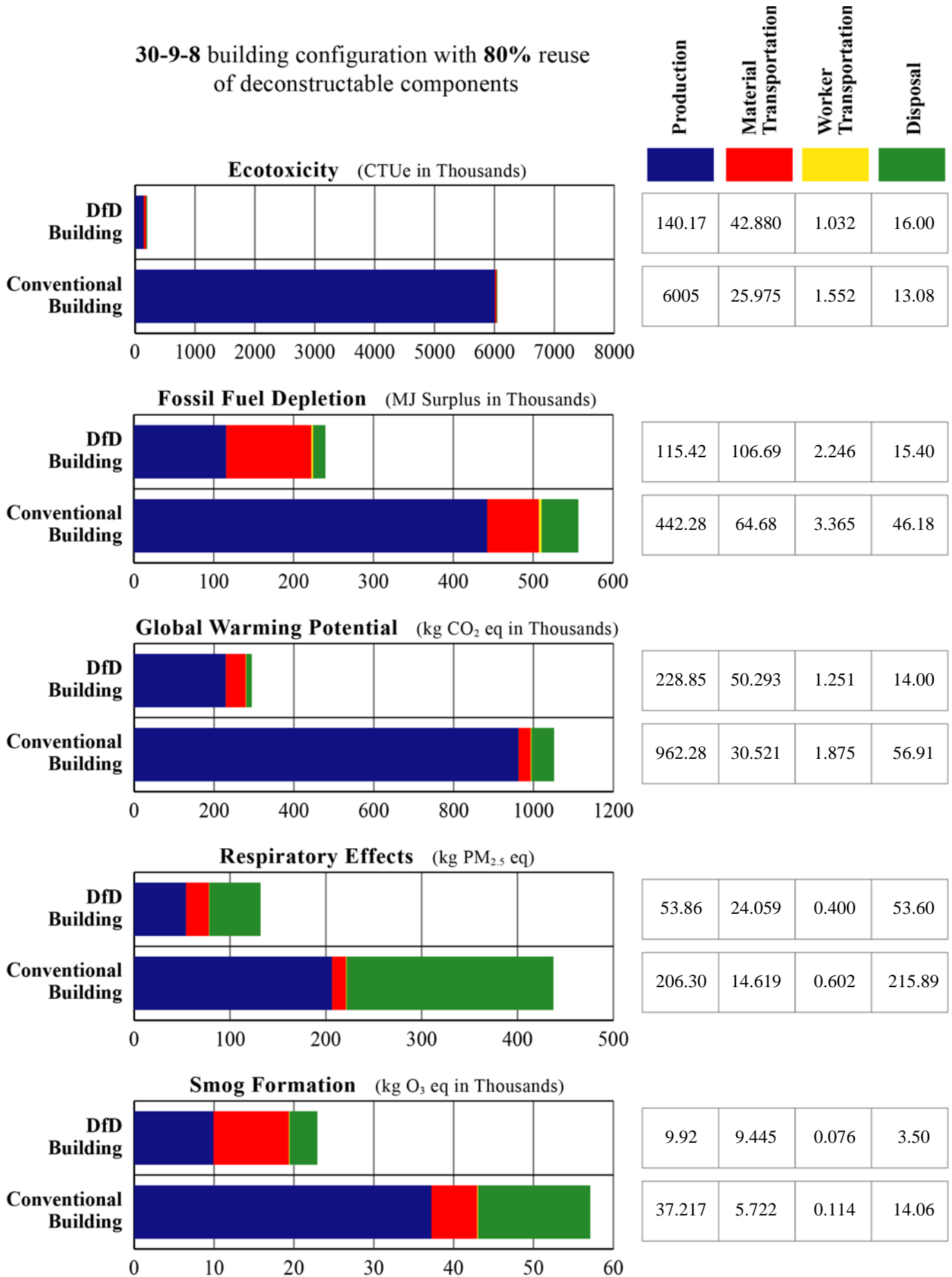


Figure 4.33 Comparison of relative environmental impacts of conventional and DfD buildings (30-9-8 w 80% reuse)

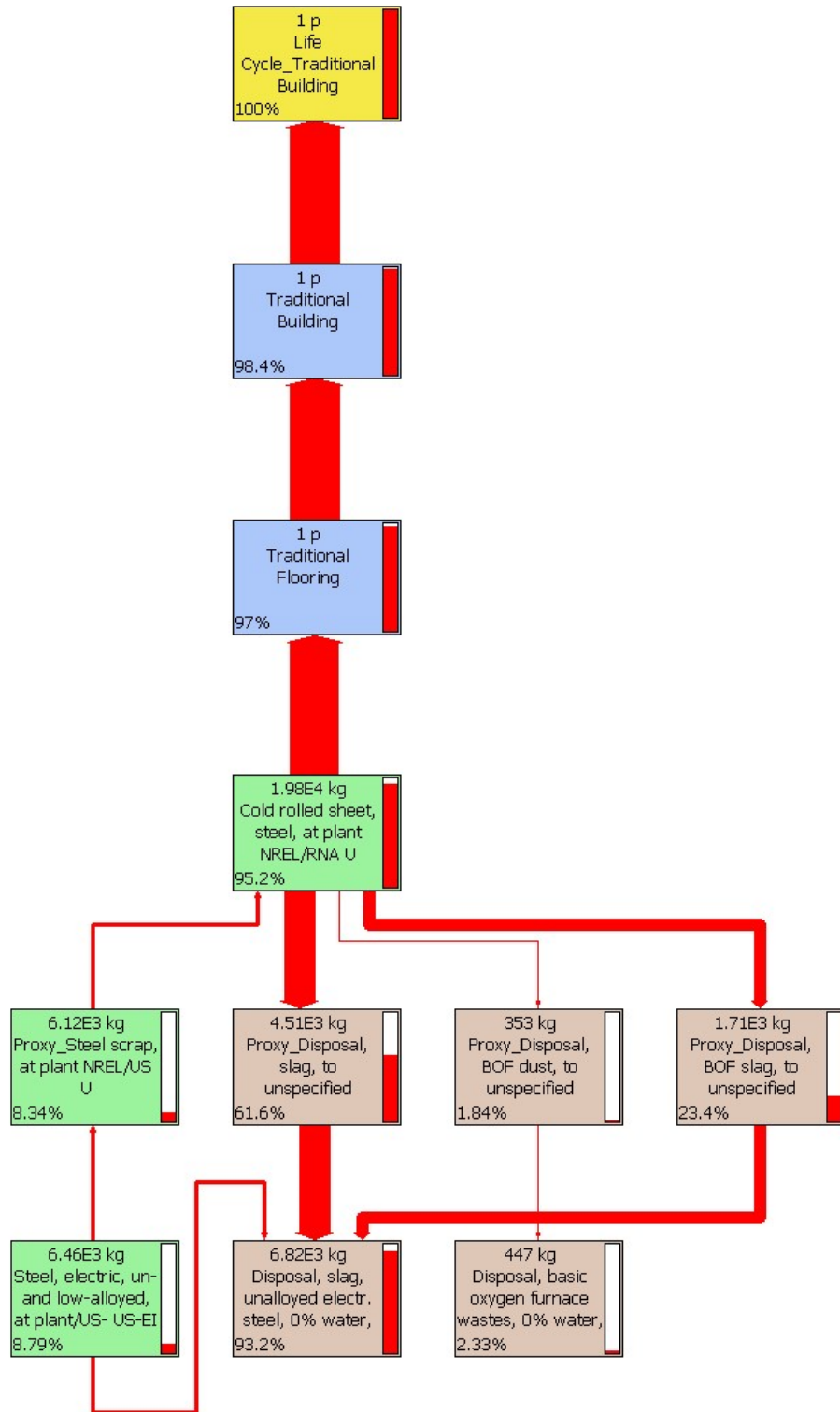


Figure 4.34 TB 30-3-8 Ecotoxicity Tree, revealing extreme impact of cold rolled sheet steel

4.8 Communication with dismantler

In parallel with comparing the environmental impacts of the traditional buildings with the DfD buildings, this research also included extensive discussions with a demolition contractor, including observing a building undergoing dismantling to ascertain the challenges for dismantling current steel structures and the flow of the disassembled materials. Main conclusions are summarized below:

- An extensive environmental survey (checking for asbestos, lead paint, PCBs, etc.) is necessary before dismantling to ensure that there is nothing harmful for the health of the workers and also to determine which materials may be reused or recycled depending on whether there are harmful materials involved (such as painted bricks, or asbestos in caulk attached to steel framing, etc.). Usually a dismantler will isolate several samples of each material for testing. After the environmental survey is completed, they cut and cap utilities. The dismantler will first remove partition walls, suspended ceiling systems and mechanical systems, and then remove the structural system. Typically, the dismantler will also determine which materials can be reused, recycled, or sent to a landfill. After locating buyers and identifying the value of each of the materials, the dismantler decides whether reusing, recycling, or sending the materials to a landfill is most cost-effective.
- Bricks or concrete blocks are often crushed and used as aggregates. The dismantler also tries to salvage bricks or blocks where possible, as reclaimed bricks have enough value if the mortar is easily removable, and if any paint can be removed safely. Mortar is typically removed manually. Monolithic concrete is typically recycled (down-cycled to aggregate) or disposed of in a landfill. Steel members and joists are in some cases salvaged for reuse (e.g. by removing bolts) or more typically recycled (in which case they often torch, saw, or tear with machines during dismantling). Aluminum, copper, and metals are generally recycled. There is no determination made for whether the steel was ever overloaded during its life in the building.
- Materials that go to landfill only account for 10% of all the materials for this specific demolition project.
- Use of robotics will enhance options for deconstruction.
- It is more expensive to sort items if a soft demolition of finish materials cannot be conducted prior to the major structural demolition.

- The values of steel scrap varies, with top quality being for beams, plate, and other structural steel, followed by bar joists, then sheet metal/light iron, which is voluminous, and must be shredded.
- The dismantlers may use strong magnets and eddy currents to separate ferrous and nonferrous metals from mixed debris, like reinforced concrete rubble.
- The architectural finishes are mostly mixed and crushed and sent off site to a sorting facility.

4.9 Conclusions

The environmental impacts of Design for Deconstruction buildings compare favorably to traditional buildings under the constraints of this study, assuming reuse occurs in the future. In all environmental impact categories the DfD buildings have lower impacts if deconstructable components are reused at least once. Using the 30-3-6 prototype as an example:

- The initial environmental impacts of the DfD alternative are greater than the traditional alternative in the fossil fuel depletion, global warming, and smog production impact categories, and less in the ecotoxicity and human respiratory health categories.
- All life-cycle environmental impacts of the DfD alternative are less than the traditional alternatives when accounting for the reuse potential of the deconstructable components.
 - Assuming 67 percent reuse, the impact reductions range from about 94% for ecotoxicity to about 47% for fossil fuel depletion.
 - Assuming 80 percent reuse, the impact reductions range from about 96% for ecotoxicity to about 61% for fossil fuel depletion.
- For most impact categories examined, the production phase impacts are the largest contributor to full life-cycle impacts. End-of-life impacts are most significant for the human respiratory health category.
- Transportation impacts are most significant for the fossil fuel depletion and smog production categories, though generally much less than the production impacts.
- Worker transport contributes little to life-cycle environmental impacts.

The durability of DfD components will be a deciding factor in their sustainability, as well as the ability to make the initial systems efficient by minimizing the amount of materials used compared to traditional buildings. This study considers the impacts resulting from the assumption that 80, 75, and 67 percent of deconstructable components are reused at the end of each service life. To prove environmental superiority, it is necessary to estimate with accuracy the rates at which deconstructable components can be salvaged and reused.

5. Pushout Tests

The pushout experimental program includes two series of tests. In the pretension tests, the number of turns of the nut is first determined to ensure adequate and reliable axial forces generated in the bolts. Pushout tests are then performed to study the strength and ductility of the clamping connectors and explore the influences of the testing parameters. This research focuses on hot-rolled channels HTA-CE 72/48 with shortened anchors, HS 72/48 Grade 8.8 M24 and M20 bolts and Type AFW clamps with short tails (Halfen 2011; Lindapter 2011).

5.1 Pretension tests

Bolts can be pretensioned by either the turn-of-nut method or using a calibrated wrench. The turn-of-nut method is based on displacement control; therefore, the pretension depends on the material properties of the bolts. For regular bolts, the nut rotation needed to develop the minimum bolt pretension from a snug-tight position can be found in Table 8.2 in the RCSC specification (RCSC 2009), provided the joint is compacted and the bolt head (or nut) is held when the nut (or bolt head) is turned. The calibrated wrench method is a torque control method which is affected by various factors, such as the finish and tolerance on the bolt and nut threads, the uniformity, degree and condition of lubrication, the friction between the nut and the washer and between the nut and the bolt threads, etc. Equations and tables that correlate torque to tension cannot be used without verification. Calibration should be performed at least daily, and each time when the joint assembly is changed, the surface conditions of the bolts, nuts, and washers are different or major changes are made for the wrench (RCSC 2009). The turn-of-nut method is preferred in the field due to its ease and consistency, and thus selected as the method for pretensioning the Halfen bolts.

Unlike regular bolts, the Halfen bolts are inserted in cast-in channels which can deform significantly when the bolts are pretensioned. As a result, more turns of the nut than in standard bolted connections are needed to enable the bolts to deform into the inelastic range and meet minimum pretension requirements in the AISC specifications (2010a). Three M24 and M20 bolts are tested under torqued tension until fracture to develop the relationship between the number of turns of the nut and the bolt axial force.

5.1.1 Test setup and instrumentation

A 6 in. by 2 ft. by 4 ft. heavily reinforced concrete slab is placed on a flat surface with the channels facing up, and the steel beam is then attached to the slab with the clamps. WT5x30 and WT4x15.5 are chosen for testing M24 and M20 bolts, respectively. The reinforcement configuration and the selection of these two sections are further discussed in Section 5.2.1.

While torque is applied to a bolt, the other three bolts are at snug-tight positions to ensure the beam does not move, see Figure 5.1. No additional restraint is needed, as the system is self-reacting when the nut is being turned. Before testing, moly coating is used to lubricate the bolt and nut threads and the washers. The tested bolt is first turned to a hand-tight position, and then to a snug-tight position using a spud wrench. The nut and the clamp are marked to facilitate recording their relative rotation when a hydraulic wrench is used to rotate the nut from the snug-tight position until fracture. The nut is turned at an increment about 15 degrees, and the total rotation is recorded at each turn.

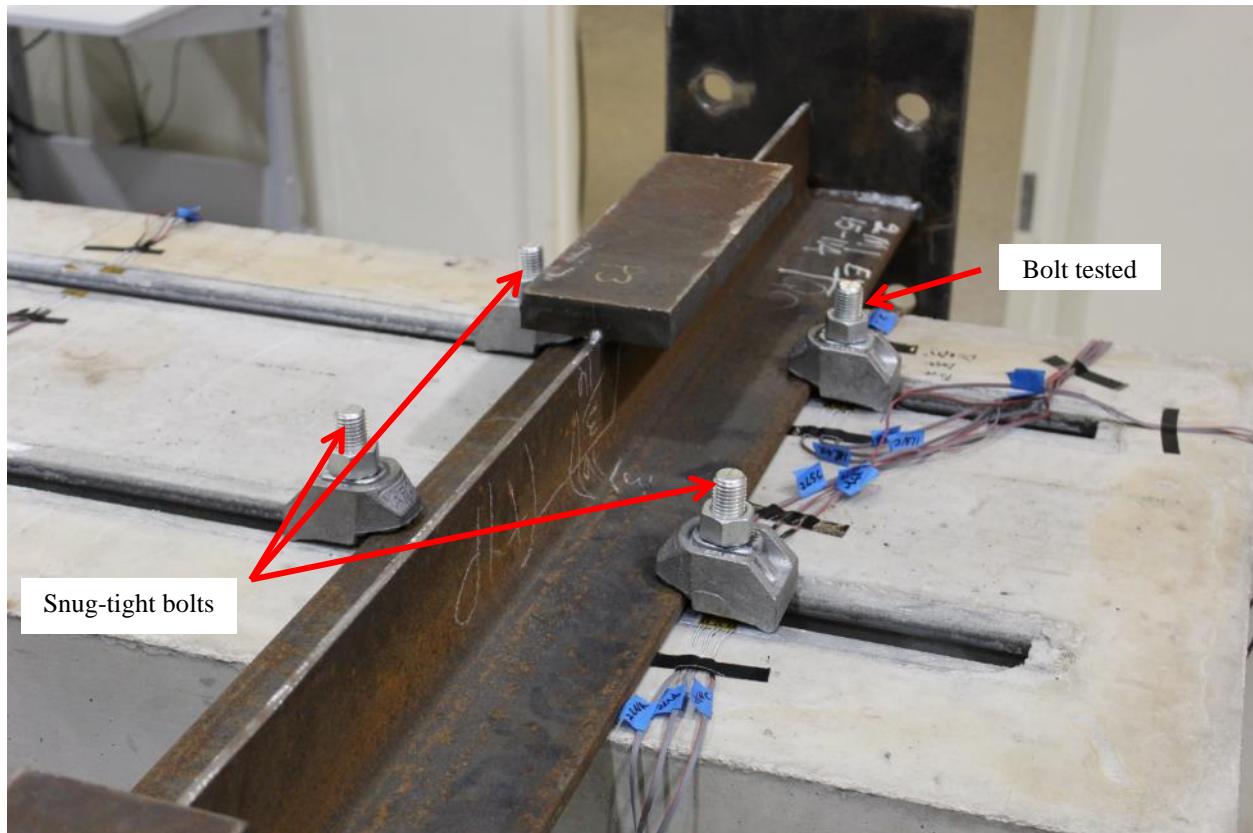
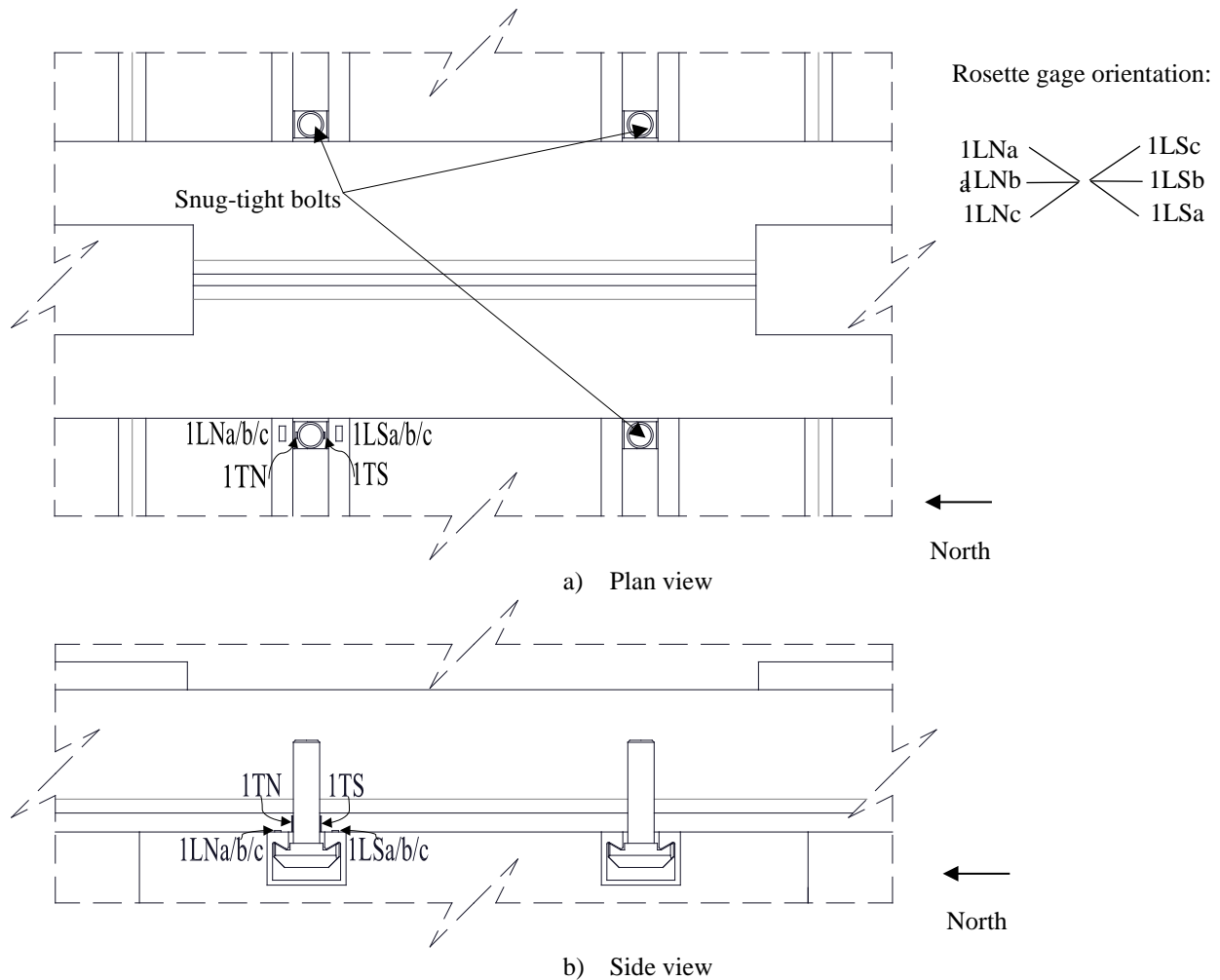


Figure 5.1 Pretension test setup

The configuration of the clamping connection enables the strain gages to be attached to the bolt shanks after the threads are removed locally. The strain gage locations are shown in Figure 5.2. Since the reduced section is prone to fracture prematurely, removing the threads may alter the ultimate failure modes, and the total rotation prior to fracture could also be underestimated. Channel lips are instrumented with rosette strain gages to study their behavior.



Note: 1TN and 1TS are uniaxial strain gages attached on the bolt shank; 1LNa/b/c and 1LSa/b/c are rosette strain gages attached on the channel lips.

Figure 5.2 Strain gage layout in pretension tests

5.1.2 Material properties

This section covers the ancillary testing for both the pretension tests and the pushout tests. In these tests, all materials of the same size are from the same heat.

Mill certifications for all the steel components are attached in Appendix F, including steel frame, regular bolts, cast-in channels, T bolts, reinforcement, clamps, and washers. Material testing is conducted to measure and compare the material properties of certain components to those documented in the mill certifications.

In addition to bolts subjected to direct tension and shear, round coupon specimens are machined from the T bolts and tested to obtain the stress-strain curves of the bolt materials, which is crucial for deciding the nut rotation from a snug-tight condition to reach the minimum pretension and

tracking the variation of bolt pretension during pushout tests and beam tests based on the strain gage measurements. Dogbone-shaped coupons are machined for the other steel parts. ASTM Standard A370-14 and ASTM Standard E8/E8M-13a dictate the dimensions of these coupons. All the tested reinforcement specimens are bars with full sections. The compressive strength and splitting tensile strength of cylindrical concrete specimens are determined according to ASTM Standard C496/C496M-11 and ASTM Standard C39/C39M-14a. Testing details and results are provided in the following sections.

Steel properties

Two coupons are machined for the bolts from each diameter. Although the bolt coupons all have the same diameter for the reduced section, the other dimensions are slightly different between the two types because the shank lengths are 6 in. and 4 in. for the M24 and M20 bolts, respectively. The dimensions have to be adjusted to ensure that the grip length is adequate, and the minimum length and radius required by the ASTM standard are satisfied. Among the six coupons cut for the channel section, three are from the flange, and the other three are from the web. These coupons are away from the edges and the flange-to-web joint of the section to avoid residual stresses. Dimensions of all the coupons are depicted in Figure 5.3. Three bars are tested for each type of reinforcement.

According to ASTM Standard E8/E8M-13a, the gage length for the bolt coupons should be 2 in.; however, the limited height between the loading heads of the testing machine prevents the 2 in. extensometer from being used. Hence, the 1 in. extensometer is chosen to measure the strain of the coupons. The gauge length for the cast-in channel coupons is 2 in., while the reinforcement specimens use a gage length of 8 in.

The loading process is based on Technical Memorandum of Structural Stability Research Council (SSRC), which summarizes the methods for determining the static yield stress. In this process, several pauses are needed to establish the yield stress at zero strain rate, i.e., the static yield stress. For the coupons with a gage length of 2 in., the loading rate starts at 0.025 in. /min, and increases to 0.125 in. /min after the first interruption. These rates are adjusted to 0.10 in. /min and 0.50 in. /min for the specimens with a gage length of 8 in.

Tension testing of the steel coupons is performed with the 100 kip capacity MTS hydraulic testing machine in the Laboratory for Structural Testing of Resilient and Sustainable Systems (STReSS LAB) at Northeastern University. For the coupons exhibiting a plateau region in the stress-strain curve, the material properties reported are: elastic modulus E_s , strain hardening modulus E_{sh} , static yield stress F_{ys} , dynamic yield stress F_{yd} , ultimate tensile stress F_u , and strain at the initiation of strain hardening ϵ_{sh} . The static yield stress is taken as the average of the three low values at the interruptions. When a plateau region is not seen in the stress-strain

curve, the material properties documented include: elastic modulus E_s , static yield stress F_{ys} , dynamic yield stress F_{yd} , and ultimate tensile stress F_u . A line is plotted through the low points of the pauses, and the static yield stress is determined by the 0.2% offset intercept. In Table 5.1, because the testing is paused at large strains for coupon 1 of M24 bolts, its dynamic yield stress is lower than the static yield stress. Hence, the pauses are moved earlier for the other coupons to avoid this problem. All the bolt coupons fail outside of the 1 in. gage length. After testing the M24 bolt coupons, the M20 bolt coupons are purposely marked to distinguish the two ends, and both coupons fracture close to the bolt head end. Fracture of all the other coupons occurs within the gage length.

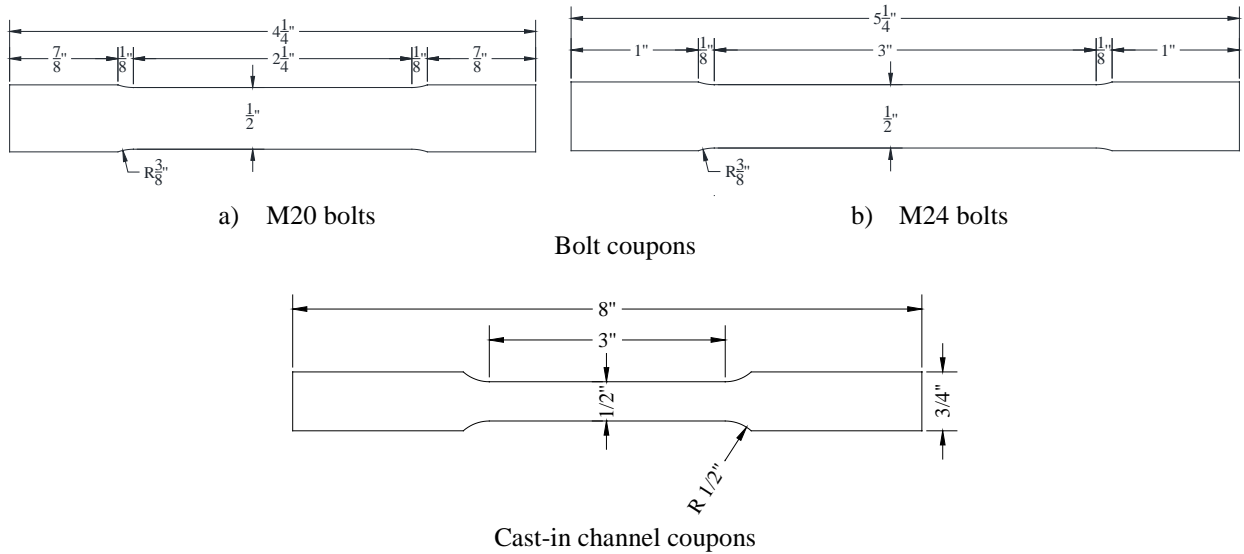


Figure 5.3 Coupon dimensions (units: inches)

Table 5.1 Steel coupon testing results

Type		E_s (ksi)	E_{sh} (ksi)	F_{ys} (ksi)	F_{yd} (ksi)	F_u (ksi)	ϵ_{sh} ($\mu\epsilon$)
Cast-in channel	Flange 1	27900	130	63.5	67.5	72.3	26000
	Flange 2	27400	120	65.1	68.3	73.5	24700
	Flange 3	28700	80	62.5	65.9	70.7	29500
	Web 1	26500	100	56.7	60.2	65.0	37000
	Web 2	28500	40	58.5	63.2	67.4	39000
	Web 3	28500	80	58.5	62.6	67.5	34000
No.4 longitudinal reinforcement	1	24100	600	62.0	65.9	89.8	15200
	2	27200	600	63.9	68.0	91.7	15300
	3	25100	510	62.8	66.9	90.4	15500
No.3 longitudinal reinforcement	1	29000	520	61.2	65.0	91.8	14500
	2	28800	510	61.3	64.2	90.8	14400
	3	27400	580	61.2	65.2	91.7	15100
No.3 transverse reinforcement	1	29500	-	67.5	73.0	102.0	-
	2	29200	-	65.2	70.5	99.7	-
	3	26900	-	64.7	70.4	101.7	-
M24 bolt	1	31800	-	122.4	121.6	138.2	-
	2	30200	-	110.1	117.7	134.6	-
M20 bolt	1	29800	-	107.9	116.6	133.0	-
	2	31900	-	108.9	117.1	132.5	-

Concrete properties

A green concrete mix was designed to decrease the embodied energy of concrete. In the mix, a certain amount of cement was substituted with fly ash or slag to reduce the environmental impacts as well as maintain high performance. Type III cement, an accelerating admixture, was added to the mix to help concrete obtain high early strength since fly ash or slag slows strength gain. Nonetheless, the concrete suppliers prefer using their own formulas. Considering material strength is more important than sustainability in terms of structural testing, a ready-mix concrete formula provided by the concrete supplier is still used.

The initially measured slump in the concrete plant is 3.0''; however, the desired slump is from 6.0'' to 8.0''. Hence, 6.0 gallons of water is added before the pour to adjust slump and increase workability, which, in the meanwhile, increases the water/cement ratio and decreases the concrete strength.

Thirty-three cylinders are divided into three groups, with each group consisting of eleven 6 in. by 12 in. cylinders. Along with concrete cylinder Group A, specimens 1 through 3 are first poured and vibrated. Specimens 4 through 6 and concrete cylinder Group B are then poured and vibrated. Three slump tests are conducted consecutively afterwards, and the measured slumps are 6.25'', 5.25'' and 4.50'', respectively. Cylinder Group C is cast between specimen 8 and specimen 9. These three groups of cylinders represent concrete at different stages (i.e., beginning, middle and end) during the pour.

Concrete specimens are left to air-dry for a couple of hours until they start to harden. After about 8 hours, specimens are sprayed and covered with wet burlaps. A plastic sheet is put over the burlaps to prevent loss of moisture. Forms for the specimens and cylinders are stripped on the next day to simulate the scenario that forms are usually stripped within 24 hours to facilitate reuse in the precast concrete industry. Half of the cylinders in each group are placed close to the specimens and cured in the same manner as the specimens, while the other cylinders are put into a water bath to mimic moisture-cured conditions. All specimens are cured till 28 days. Table 5.2 provides the curing condition, the testing date and the purpose of the testing for the cylinders.

Table 5.2 Concrete cylinder testing results (units: psi)

Curing Condition	Test type	Testing date	Cylinder A	Cylinder B	Cylinder C	Average
Moist-cured	Compressive strength (psi)	3 days	2,802	3,117	2,796	2,905
		7 days	3,835	3,810	3,393	3,679
		21 days	4,450	4,309	4,200	4,320
		28 days	4,079	4,373	4,158	4,203
	Splitting tensile strength (psi)	28 days	373	356	419	383
Same as the specimen	Compressive strength (psi)	3 days	2,832	3,148	2,669	2,883
		7 days	3,715	3,661	3,252	3,542
		28 days	4,651	4,659	4,122	4,477
		Test day for specimen 1-3	6,319	6,232	6,543	6,365
		Test day for specimen 4-6	6,587	6,347	6,403	6,446
		Test day for specimen 7-10	5,933	5,883	5,833	5,883

5.1.3 Specimen performance

M24 Bolts

After certain rotations, concrete flakes are observed due to the deformed channel lips bearing against concrete, but no concrete crushing is seen when the flakes are cleared after the tests. When the clamp connections are disassembled after the tests, plastic deformation of the lips, as well as dents on the beam flanges under the clamp teeth, is found. The failure modes, nonetheless, are different for the three bolts. Fracture occurs at the head of the first bolt, with the north head fracturing at 4.29 turns and the south head fracturing at 5.83 turns. Twist of the shank is insignificant during the test. For Bolt 2 and 3, the shanks are twisted off at 5.44 and 4.79 turns respectively, and 90° twists of the shanks are observed when the fracture is approached. Cracking at the bolt head is also detected for the second bolt after the test. See Figure 5.4 (a).

M20 Bolts

Minor inelastic deformation is observed in the channel lips because the pretension force is much less than that generated in the M24 bolts. All three bolts fracture due to twisting of the shanks under the applied torque. Bolt 1 and 2 both fracture at 5.16 turns, while bolt 3 fractures at 5.33 turns. See Figure 5.4 (b).

5.1.4 Behavior of the bolts and channel lips

The uniaxial strain gage readings in the pretension tests are plotted in Figure E.1. After each turn the readings drop and then stabilize because the tests are paused to record the nut rotation and the general behavior of the specimens.

In the M24 bolt testing, the readings of both gages increase until an abrupt drop is noticed in one of the gages. The reading from the other gage also falls subsequently. After the drop, the readings level off until the end of the tests when the death of the gage is signified by another dramatic change in the reading. In the third bolt test, the north gage dies prematurely, but the sudden drop also happens for the south gage. As a result of the torsional deformation in the shank, debonding of strain gages, which is discovered after testing, occurs during testing and cause the readings to level off. During the M20 bolt tests, only one strain gage exhibits the same strain drop as happens in the M24 tests, while the other measurements continue increasing until the maximum gage elongation is reached.

A number of mechanical models were developed that specify how steel behaves under cyclic loading, ranging from simple ones, such as the elastic-perfectly-plastic model and Prager model (Prager 1949) to complex ones, such as Shen steel model (Shen et al. 1995) and Chaboche model (Chaboche et al. 1986). Most models use the Von Mises yield function to determine the yield condition and the associated flow rule to prescribe the direction of the plastic flow, but they differ in terms of strain hardening rules that stipulates the post-yielding material behavior.

Since bolts are not supposed to be the main energy dissipating component in a structural system, the cyclic behavior of the bolt material under shear or tension has not been studied. However, the uniaxial stress-strain curve of the bolt material is obtained from tensile coupon testing, and details of the testing are discussed in Section 5.1.2.

In this report, since the bolt coupons are not loaded in compression, the test data is insufficient to calibrate the isotropic hardening rule. Therefore, the Chaboche model without isotropic hardening, which is incorporated in ABAQUS (2011), is employed to calculate the stress variation based on the strain history. This model is believed to be capable of interpreting the bolt behavior, because the axial stress in the bolt cannot be compressive no matter how the strain varies in the pretension tests and the pushout tests, and material yielding in the compressive direction is not of a concern. Appendix G.1.2 contains the details regarding how to implement the material model in ABAQUS to track the bolt axial stress variation under torqued tension. It should be pointed out that once the bolt material is yielded, the axial stress or force could be overestimated by the current model that neglects the shear stress due to torsion.

In Figure 5.5, bolt tension variation, which is calculated using the average axial strain measurement, is depicted until the dramatic strain drop happens or the strain gage reading starts to level off, because they do not indicate actual behavior of the bolt, and the recorded data is meaningless. The cyclic stress-strain relationship of the bolt material during the test is plotted in Appendix G.1.2.1.



(1) During testing



(2) After testing

Concrete flakes and channel lip deformation



(3) Cracking in the bolt head



From right to left: Bolt1, Bolt2, and Bolt 3

(4) Fracture of bolts

(a) M24 bolts



(1) Channel lip deformation



From right to left: Bolt1, Bolt2, and Bolt 3

(2) Fracture of bolts

(b) M20 bolts

Figure 5.4 Bolt pretension test

The plots in Figure 5.5 indicate that the bolt tension increase becomes less for the same amount of nut rotation, indicating that the bolts have yielded, and any variation in the strain or elongation in the bolt leads to a small change in the pretension force. Because the pretension force for the M20 bolts is smaller than that in the M24 bolts, less nut rotation is anticipated to obtain the minimum pretension force. One and a half turn is eventually selected for pretensioning the M20 bolts. The factor of safety against twist-off in the shank or fracture in the head is at least 2 and 3 for the M24 and M20 bolts, respectively.

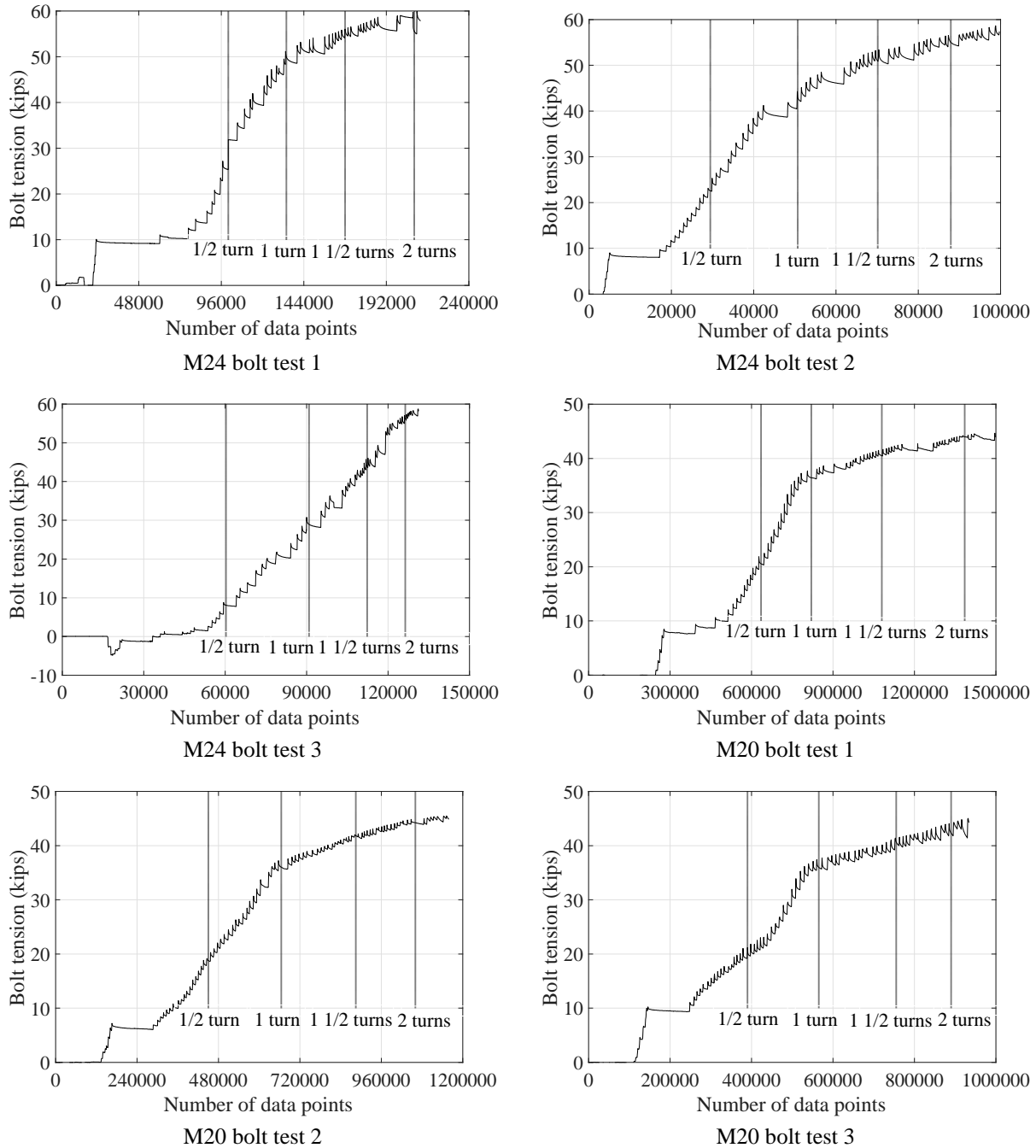


Figure 5.5 Bolt tension variation

5.2 Pushout tests

After the number of turns of the nut is determined based on the pretension test, shear tests are conducted on the concrete specimens. Although the concrete specimen that is used for the pretension test may not be intact, a shakedown test is performed on that specimen to verify the adequacy of the data acquisition system, the control system, the test frame, etc.

5.2.1 Test setup and test matrix

The strength of steel headed stud anchors in both solid slabs and composite slabs is well studied and established in the relevant design provisions. Shear connectors in composite beams should be strong to transfer shear forces between concrete slabs and steel beams; otherwise, the two materials would behave individually, and no composite action exists. Although the ductility requirements on shear connectors are not explicitly mentioned in the AISC specification (AISC 2010a), they are as important as the strength requirements. Shear connectors will undergo large deformation in composite beams with low amount of composite action, resulting in possible fracture in the connector shank and loss of load-carrying capacity. Therefore, the strength and ductility of shear connectors should be treated equally.

Numerous pushout test setups have been developed in the past to study the behavior of steel headed stud anchors, see Gattesco et al. (1996), Anderson et al. (2000), Saari et al. (2004) and Lam et al. (2005). The behavior of shear studs can vary considerably depending on the test setup. An extensive discussion on the influences of various parameters is reported by Ernst (2006). These parameters include width of specimen, number of connectors in one slab, the reinforcing of the specimen, recess in concrete slabs, specimen preparation, horizontal restraint, normal forces, stress regime in concrete, etc. Eurocode 4 (CEN 2004) specified a standard test specimen for shear studs embedded in solid slabs, and it is permitted to modify the standard test specimen to conform to the beam to which the pushout test is related. However, no comment is provided on how to modify the test when metal deck is employed. Generally, it is believed that pushout tests yield conservative strength estimation for shear connectors due to the following reasons: (1) normal force existing in a composite floor system will induce compression between concrete slabs and steel beams, suppressing concrete crushing and fracture of steel anchors; (2) compressive stress due to shear connectors bearing against concrete is distributed over a smaller width in pushout tests; (3) the smaller width also makes possible longitudinal splitting of concrete slabs.

The pushout test setup utilizing a self-reacting frame is illustrated in Figure 5.6. This test setup can be used for both monotonic and cyclic loading tests. The test specimen consists of a precast concrete plank attached to a WT section using clamping connectors. The size of the precast concrete plank is 4 ft. × 2 ft. × 6 in. Since the applied load is anticipated to flow mainly through the beam flange, WT sections are chosen over W sections. Selection of the steel sections is

limited by both clamp sizes and flange or web local buckling. WT5x30 and WT4x15.5 represent beams with different potential flange thicknesses, with the larger WT tested with M24 clamps and the smaller WT matching with M20 clamps. WT4x15.5 can also be used with M24 clamps, requiring shims between the clamps and the WT flange since the flange is relatively thin. The stem of the WT at the end of the member that attaches to the actuator is coped to ensure that the actuator load is applied only to the flange to reduce eccentricity of the force application in the WT. A stiffened C15x50 connects the test specimen to the self-reacting frame. L8x4x1 is chosen as the reaction angle to react against the concrete plank and provide bearing stiffness and compressive stress distribution within the concrete comparable to those in a composite beam. The whole test setup is restrained vertically by stiffened W6x25 assembly, as separation of the concrete slab and the steel beam is rarely seen in composite beams. Plates welded on the WT stems distribute the reaction generated due to the overturning of the specimen and provide support against web local buckling. Stability frames are designed to ensure that the WT section moves only along its axial direction. Detailed dimensions of the test setup are given in Figure 5.7.

All connections are designed as slip-critical to reduce as much slip as possible. Since the reuse of A325 bolts is allowed, they are selected for connections where tightening and untightening bolts are frequent due to switching new concrete specimens and steel beams. A490 bolts, however, are used for connections that remain intact during the testing. Teflon sheeting is attached at the interface between the WT section and the stability frames, since the frictional force is undesirable. An isometric view of the test setup is given in Figure 5.8.

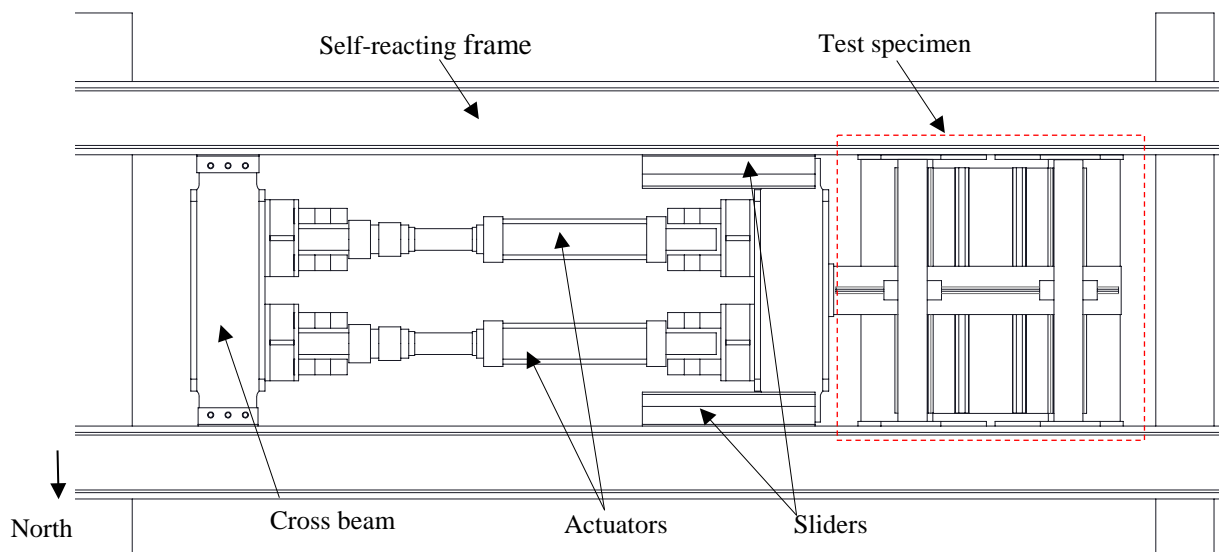


Figure 5.6 Loading frame assembly with test specimen

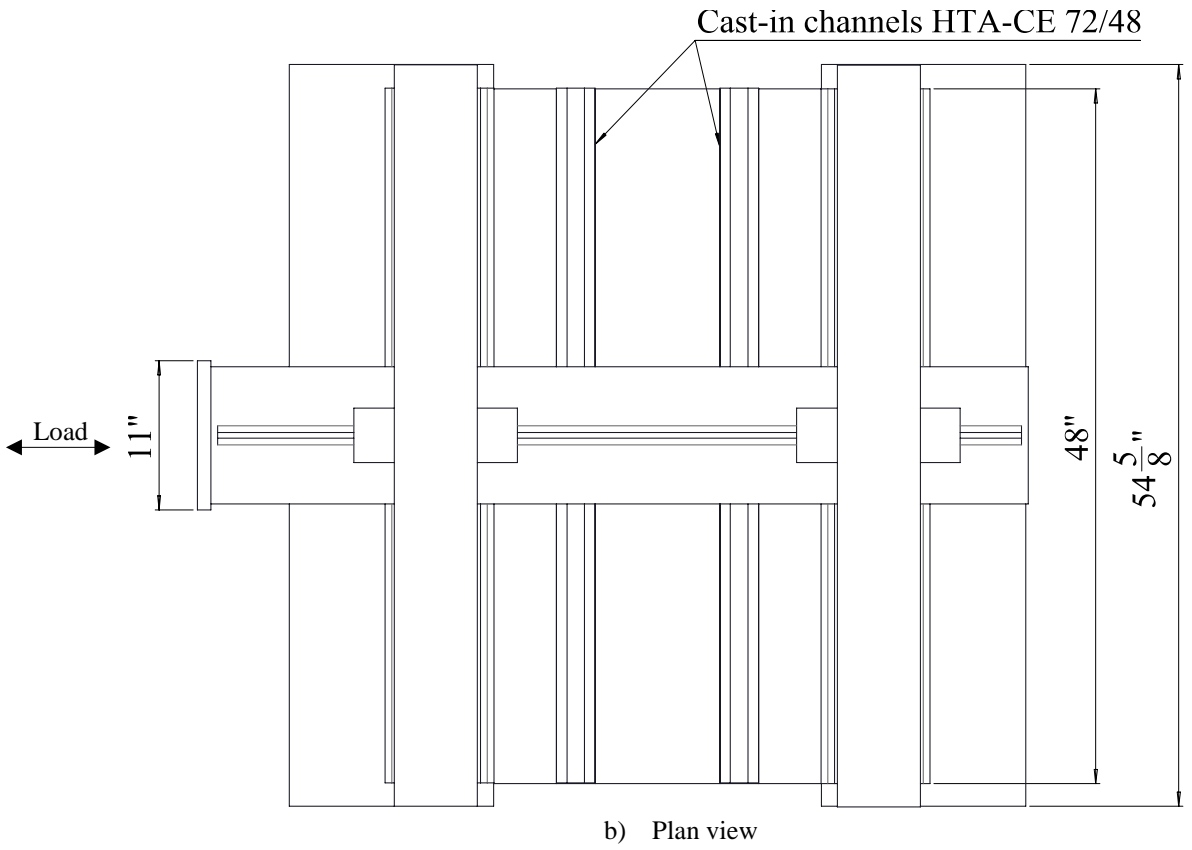
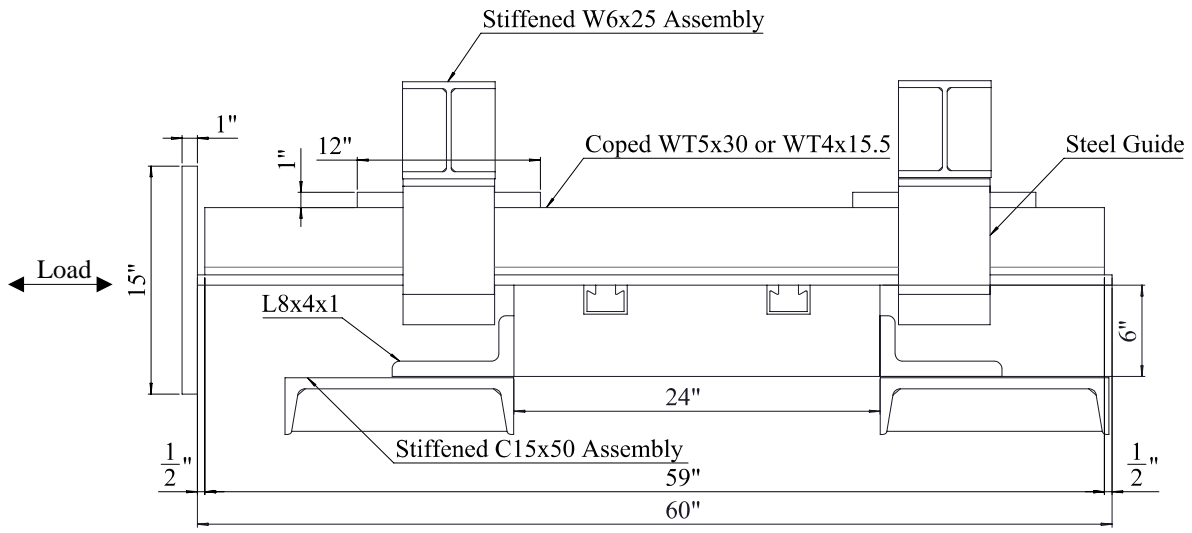


Figure 5.7 Different views of test specimen

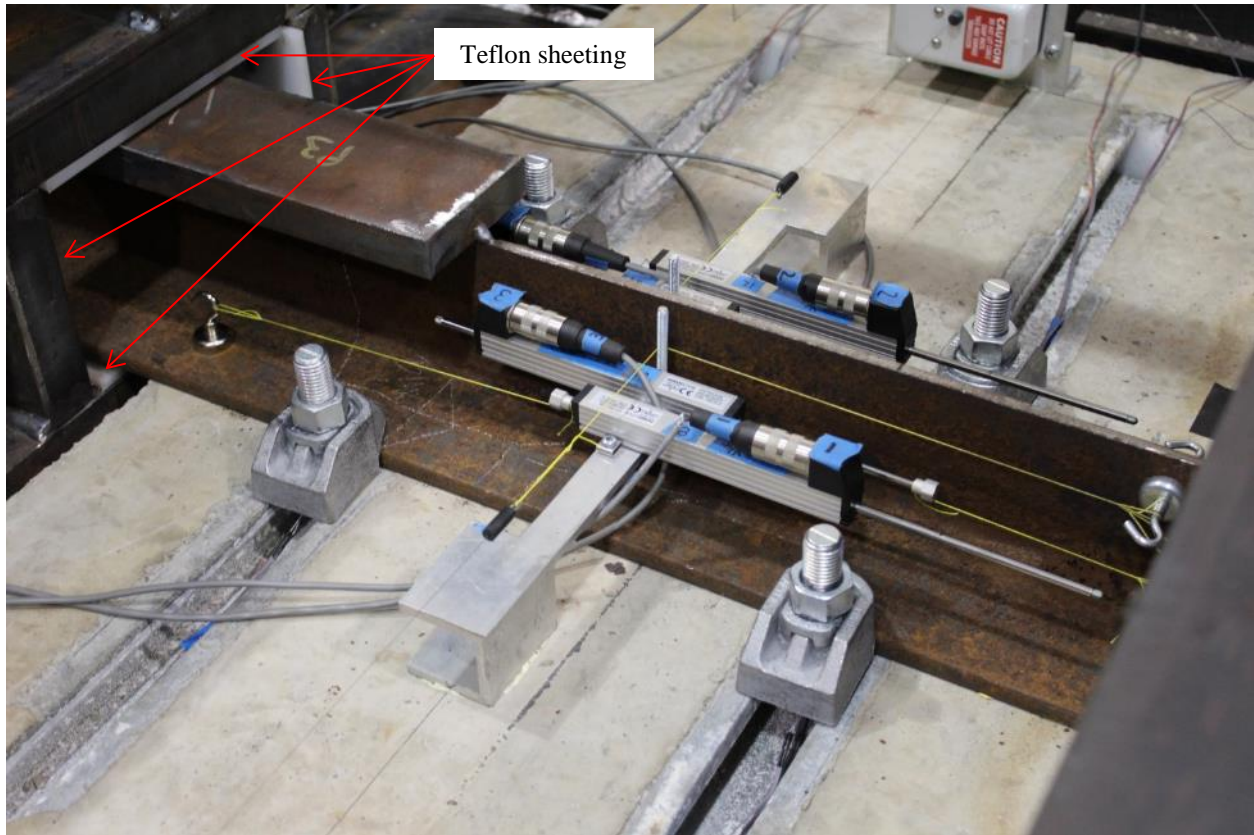


Figure 5.8 Isometric view of pushout test setup

Although pushout tests cannot replicate the actual loading scenario of shear connectors in composite beams, they should be designed properly to imitate the forces induced in the shear connector and eliminate limit states that never happen in composite beams. A comparison of the forces acting on the shear connectors in a composite beam and in the pushout test setup is illustrated in Figure 5.9.

When the actuator force is not large enough to engage the steel guides, the behavior of the system can be interpreted using Equations (5.1) through (5.3). The shear connectors are still under pure shear.

Concrete free body diagram:

$$F_{shear} = F_{reac} \quad (5.1)$$

$$F_{shear} \times H = F_{fric} \times W \quad (5.2)$$

Steel beam free body diagram:

$$F_{shear} = F_{act} \quad (5.3)$$

Where

F_{shear} = shear force acting on the shear connectors

F_{reac} = horizontal reaction force from the angle

F_{fric} = friction generated at the concrete and reaction angle interface

F_{act} = horizontal actuator force exerted on the steel beam

H = distance between F_{shear} and F_{reac}

W = width of the concrete plank, which is equal to 24 in.

Equations (5.4) through (5.8) present the behavior of the system when the actuator force is large enough to cause the steel beam to bear against the steel guides.

Concrete free body diagram:

$$F_{shear} = F_{reac} \quad (5.4)$$

$$F_{shear}H = F_{fric}W + F_{norm}D_1 \quad (5.5)$$

Steel beam free body diagram:

$$F_{act} = F_{shear} + f_1 + f_2 \quad (5.6)$$

$$f_1 = f_2 = \mu P_{reac} \quad (5.7)$$

$$F_{norm}D_1 + f_1h_1 = P_{reac} D_2 + f_2h_2 \quad (5.8)$$

Where

F_{norm} = idealized normal forces induced at the steel-concrete interface

P_{reac} = vertical reaction force from the steel guides

f_1, f_2 = friction generated at the steel beam and steel guides interfaces

D_1 = distance between F_{norm} , which is equal to 12 in.

D_2 = distance between P_{reac} , which is equal to 32.75 in.

h_1 = distance between f_1 and F_{act} , which is equal to half flange thickness.

h_2 = distance between f_2 and F_{act} , which is equal to section depth minus half flange thickness.

μ = frictional coefficient between Teflon sheets and steel beam

It can be concluded that the normal forces at the steel-concrete interface now become uneven, with the normal forces increasing on one side and decreasing on the other side, which is similar to the loading scenario in a composite beam.

Combining Equations (5.1) through (5.8) results in the following:

$$F_{shear} = \frac{(D_2 + \mu h_2 - \mu h_1)F_{act} + 2\mu W F_{fric}}{D_2 + \mu h_2 + 2\mu H - \mu h_1} \quad (5.9)$$

Conservatively assuming that $\mu = 0.2$, $F_{fric} = 0$, and $H = 6 \text{ in.}$,

For Section WT5x30:

$$F_{shear} = \frac{32.75 + 0.2 \times (5.11 - 0.34) - 0.2 \times 0.34}{32.75 + 0.2 \times (5.11 - 0.34) + 2 \times 0.2 \times 6 - 0.2 \times 0.34} F_{act} = 0.933 F_{act}$$

For Section WT4x15.5:

$$F_{shear} = \frac{32.75 + 0.2 \times (4 - 0.22) - 0.2 \times 0.22}{32.75 + 0.2 \times (4 - 0.22) + 2 \times 0.2 \times 6 - 0.2 \times 0.22} F_{act} = 0.933 F_{act}$$

The above calculation indicates that the majority of the actuator force is taken by the shear connectors after the steel guides are involved, and the friction generated at the WT and steel guides interfaces is negligible.

Parameters for the pushout tests include bolt diameter, number of channels, reinforcement configuration, loading protocol, and usage of shims, see Table 5.3. The naming convention of the specimens is explained using Test 4-M24-2C-RH-LM-S, with 4 describing the cast sequence during the concrete pour, M24 describing M24 bolts, 2C describing two channels embedded in the concrete plank, RH describing heavy reinforcement pattern, LM describing monotonic loading, and S describing shims. Two-channel planks are assumed to be standard in this research; nonetheless, long span beams with heavy gravity loading may necessitate three-channel planks to obtain larger flexural strengths than the two-channel planks. Loading on a shear connector is usually unidirectional under gravity loading, but the load could change sign when the composite floor system is under seismic loading and shear connectors are employed to connect collector beams with composite diaphragms. Typically, cyclic loading decreases the ultimate strength of the steel headed stud anchors (in design, a 25% reduction in shear strength is typical; see AISC 2010b). Its influence on the clamping connectors is also investigated in the pushout tests. Shims are common in the bolted steel connection to make up differences in plate thicknesses. Likewise, 5 in. x 2 in. x 1/8 in. shims are inserted between thin steel flanges and clamp teeth. For the specimens, the number of turns of the nut applied to the bolts after a snug-tight position is shown in the last column of the table.

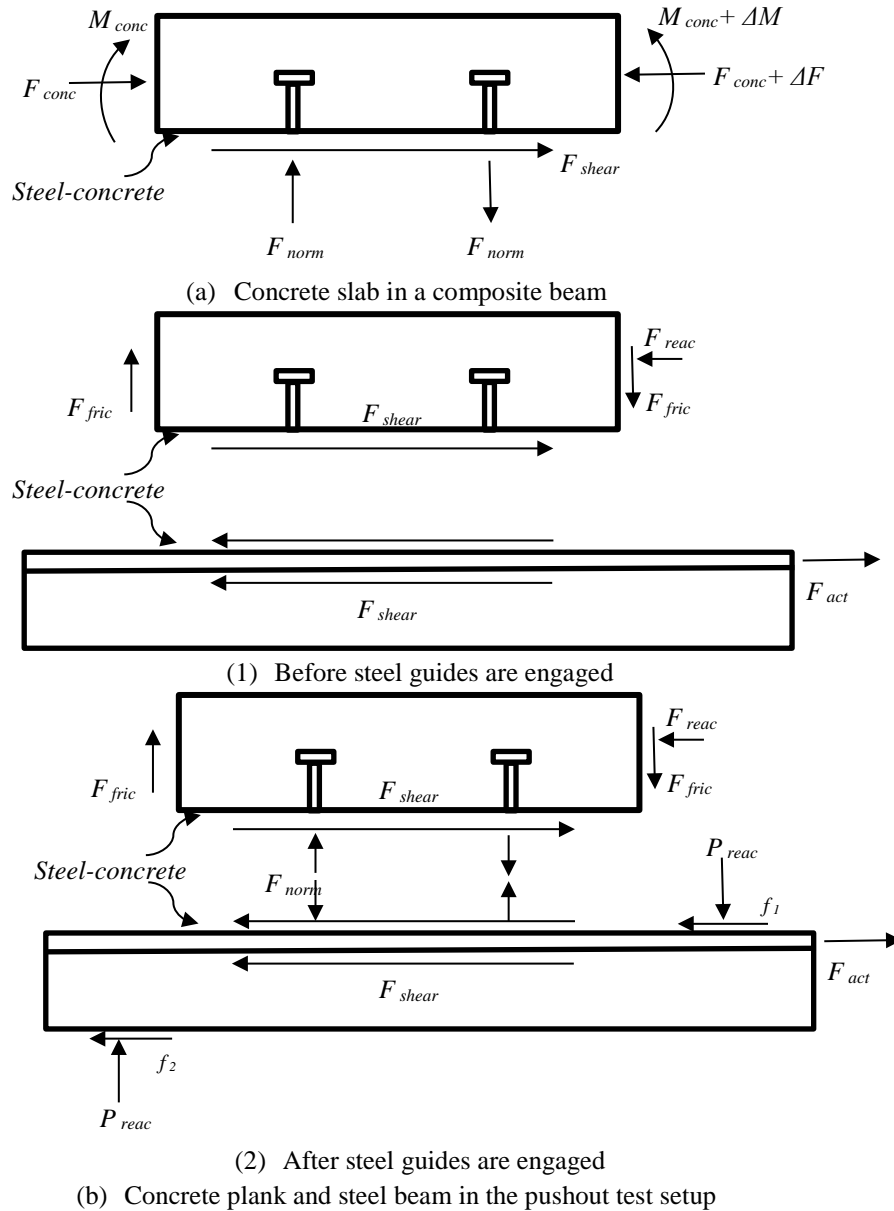


Figure 5.9 Shear connectors loading scenario comparison

Initially, three full turns is utilized for the M24 bolts in Tests 2-M24-2C-RH-LM and 4-M24-2C-RH-LM-S, see Table 5.3. However, one bolt head fractures during Test 4. Subsequently, it is decided that two full turns be used for the remaining tests. Table 5.5 indicates that three full turns does not yield higher pretension force than two full turns, which is demonstrated by the negligible difference of the slip load and the peak strength per clamp between Test 2-M24-2C-RH-LM and Test 7-M24-3C-RH-LM.

Table 5.3 Pushout Test Matrix

Name	Test parameters										Number of turns
	Bolt diameter		Number of channels		Reinforcement configuration		Loading		Shim		
	M24	M20	2	3	Light	Heavy	Monotonic	Cyclic	Yes	No	
1-pretension test	✓	✓	N/A			✓	Apply torque until bolt fracture			✓	
2-M24-2C-RH-LM	✓		✓			✓	✓			✓	3 turns
3-M24-2C-RL-LC	✓		✓		✓			✓		✓	2 turns
4-M24-2C-RH-LM-S	✓		✓			✓	✓		✓		3 turns
5-M24-2C-RH-LC	✓		✓			✓		✓		✓	2 turns
6-M24-2C-RH-LC-S	✓		✓			✓		✓	✓		2 turns
7-M24-3C-RH-LM	✓			✓		✓	✓			✓	2 turns
8-M24-3C-RH-LC	✓			✓		✓		✓		✓	2 turns
9-M20-2C-RH-LM		✓	✓			✓	✓			✓	1.5 turns
10-M20-2C-RH-LC		✓	✓			✓		✓		✓	1.5 turns

Two reinforcement patterns are designed for the pushout test specimens, see Figure 5.10 and specimen drawings in Appendix D.1.2. The heavy reinforcement pattern includes supplementary reinforcement that bridges all potential concrete failure planes to restrain the opening and propagation of the cracks. The red lines in Figure 5.11 (a) and (b) indicate possible concrete failure cones. Because those reinforcement are not designed to take the entire load, they are considered as supplementary reinforcement, not anchor reinforcement. Considering the splitting forces, surface reinforcement is also added to resist the force arising from the strut-and-tie model (CEN 2009). The light reinforcement pattern, which only retains the bars designed for gravity loading and eliminates some of the shear reinforcement, is used for specimens where premature concrete failure is anticipated to explore this limit state. All the reinforcement conforms to the detailing requirements in ACI 318-11, see Figure A.13. The hooks for the transverse bars are regarded as standard hooks, and the bend diameter and the end extension are $6D_b$ and $12D_b$, respectively. The transverse bars are rotated to fit into the thickness of the planks. The waveform bars are considered as stirrups, and the bend diameter and the end extension are $4D_b$ and $6D_b$, respectively. ACI Section 12.13.2.1 stipulates that the ends of waveform bars can be anchored using a standard hook around longitudinal reinforcement. However, straight anchorage is not

allowed because it is difficult to hold the stirrup in the right position when pouring concrete and the development of the stirrup is ineffective. A706 reinforcement with a minimum yield stress of 60,000 psi is selected. No.4 bars are used as longitudinal reinforcement, and No.3 bars are chosen as the transverse and waveform reinforcement. The spacing of the channel anchors is 9.65 in. (245 mm), which is equal to the distance between the transverse reinforcement in the light reinforcement pattern. In the heavy reinforcement pattern, the reinforcement spacing decreases close to the clamping connectors to provide extra protection against concrete breakout. Reinforcement drawings are provided in Appendix D.1.2

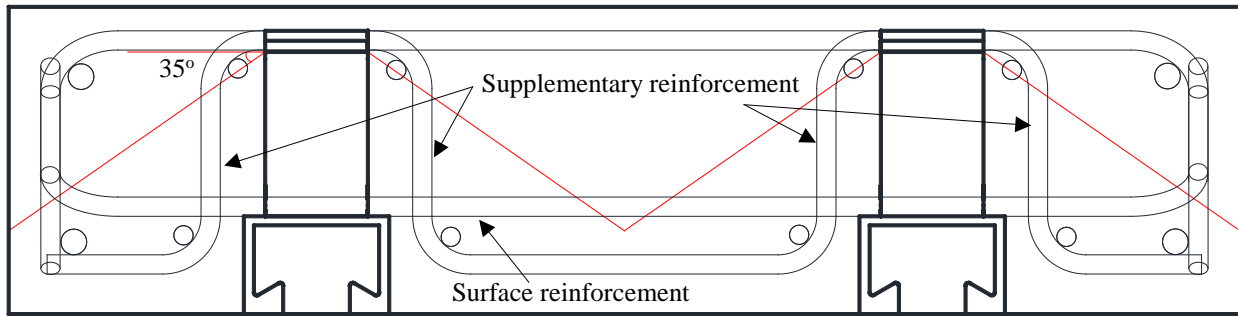


(a) Light reinforcement pattern

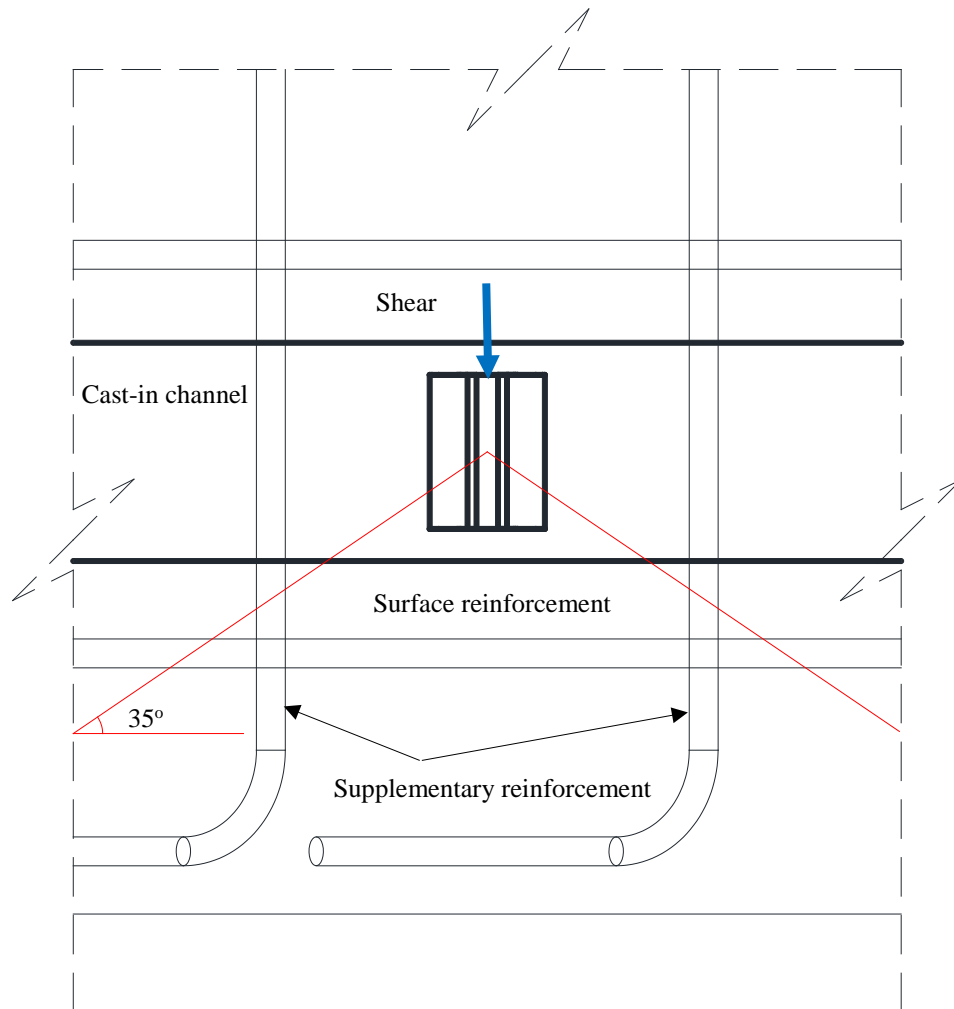


(b) Heavy reinforcement pattern

Figure 5.10 Different reinforcement patterns



a) Anchor tensile force



b) Anchor shear force

Figure 5.11 Supplementary reinforcement and surface reinforcement arrangement

5.2.2 Instrumentation

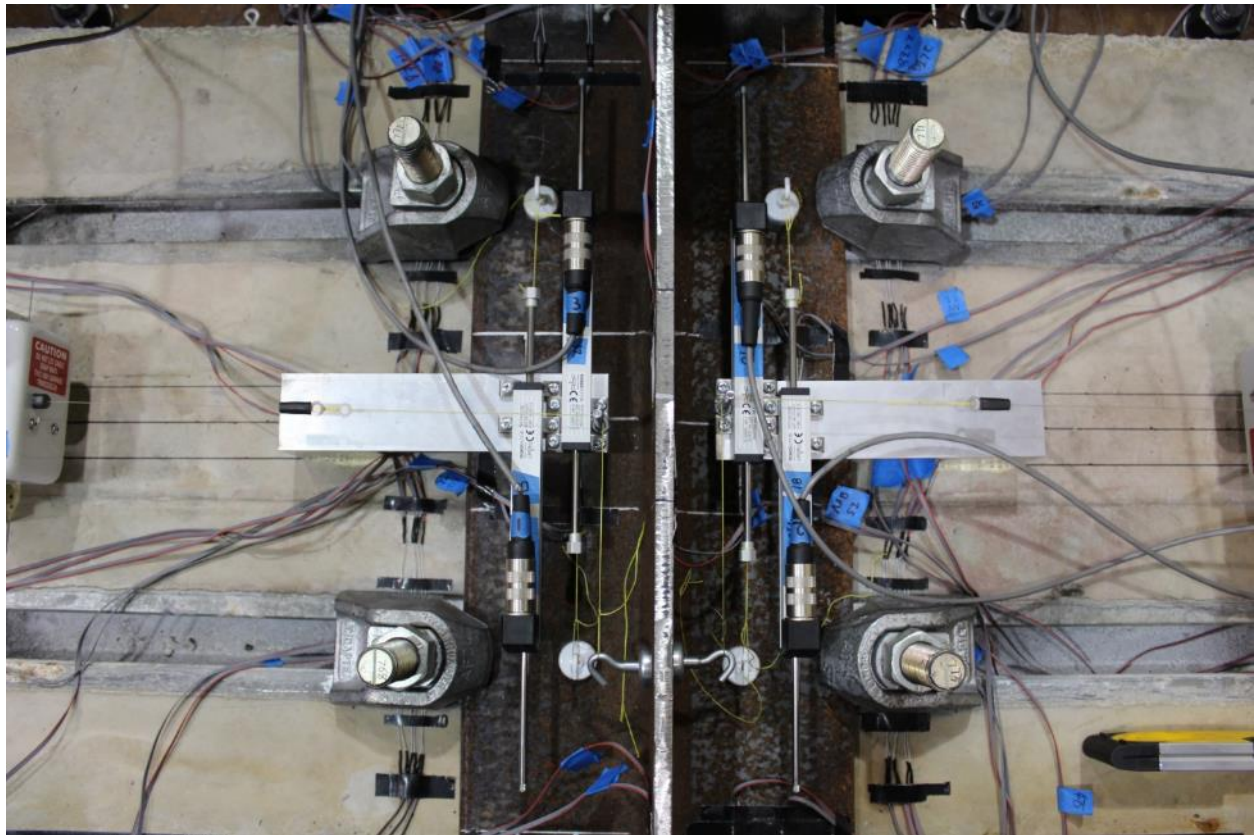
Displacement measurements

Four linear potentiometers with a stroke length of 4 in. are placed to record the relative displacement between the steel beam and the concrete slab, i.e., slip of the clamps. Two string pots are also utilized which are capable of measuring up to 15 in. displacement. During testing, the pauses needed for adjusting loading rates are based on the readings from the linear potentiometers since they have a better resolution for small slips than the string pots. After the linear potentiometers reach their capacity and are disabled, the string pots become the only sensors for slip measurements.

In addition, relative deflection of the cantilever legs of the reaction angles with respect to the channels C15x50 are measured with four linear potentiometers with a stroke length of 1 in., see Figure 5.12. Dial gages are installed to monitor the vertical deflection of the steel guides which are designed to be sufficiently stiff to restrain the overturning of the system. The horizontal deflection of the steel guides reflects the out-of-plane movement of the beam. The load and displacement measurements are recorded for all the specimens with the data acquisition system.

Strain measurements

Strains are measured only for Specimens 3-M24-2C-RL-LC, 5-M24-2C-RH-LC, 8-M24-3C-RH-LC and 10-M20-2C-RH-LC. Specimen 3-M24-2C-RL-LC is chosen because premature concrete failure is anticipated only in this specimen. Using shims for steel beams with thin flanges is not considered to be common. Hence, Specimen 5-M24-2C-RH-LC is preferred to Specimen 6-M24-2C-RH-LC-S. Compared to Specimen 7-M24-3C-RH-LM, Specimen 8-M24-3C-RH-LC is under cyclic loading, and more data is available for interpreting the behavior. Between the two specimens using M20 bolts, Specimen 10-M20-2C-RH-LC is chosen over Specimen 9-M20-2C-RH-LM. In Tests 6-M24-2C-RH-LC-S and 9-M20-2C-RH-LM, the bolts are instrumented to track the changes of pretension forces.



Slip measurements



North string pot



Dial gages



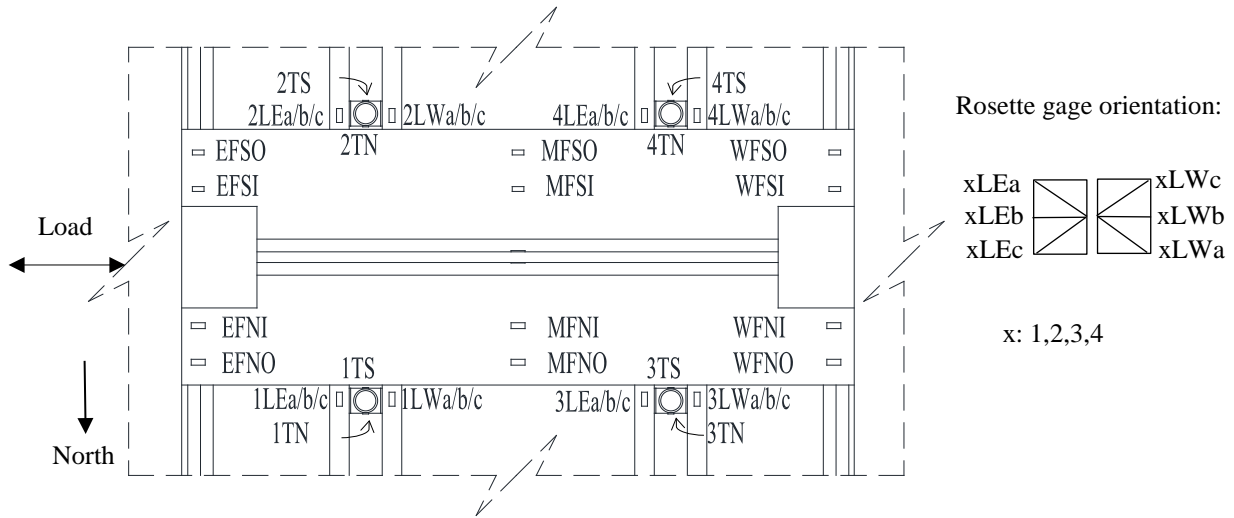
linear potentiometer
at northwestern corner

Figure 5.12 Displacement measurements

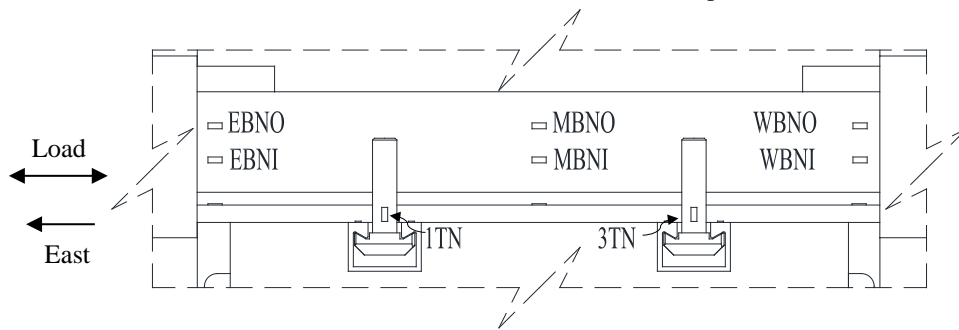
The force distribution among these clamps is calculated based on the axial strain measurements at certain sections of the WT beams. These sections are far from the clamps since the clamping forces acting on the flanges could render the stress vary along the flange thickness. The gaged locations are the third points of the webs and the flanges. Meanwhile, uniaxial strain gages are attached on the bolt shanks to study the variation of the bolt pretension. Bolt gages in the pushout tests are placed at right angles to those used in the pretension tests to avoid being crushed when the bolts bear against the clamps under shear. Channel lips are instrumented with rosette strain gages to demonstrate their three-dimensional behavior. The layout of the strain gages on the beams, channel lips and bolts is depicted in Figure 5.13.

The rosette strain gages are identified with the convention below: the first number describes the number of the gaged channel lip; the second letter indicates the member (i.e., channel lips); the third letter demonstrates the channel lip location using cardinal directions; the last letter implies one of the legs in the gage. The uniaxial strain gages attached on the bolt shanks employ a very similar method, with the first number describing the number of the gaged bolt, the second letter indicating the member (i.e., bolts), and the third letter demonstrating the gage location using cardinal directions.

The following nomenclature is employed for the uniaxial strain gages on the beams: the first letter indicates the instrumented section using cardinal directions; the second letter represents the gaged member; the third letter implies the gage location using cardinal directions; the last letter shows whether the gage is close to or further way from the flange and web joint.



a) Plan view of two-channel test specimen instrumentation



b) Side view of two-channel specimen instrumentation

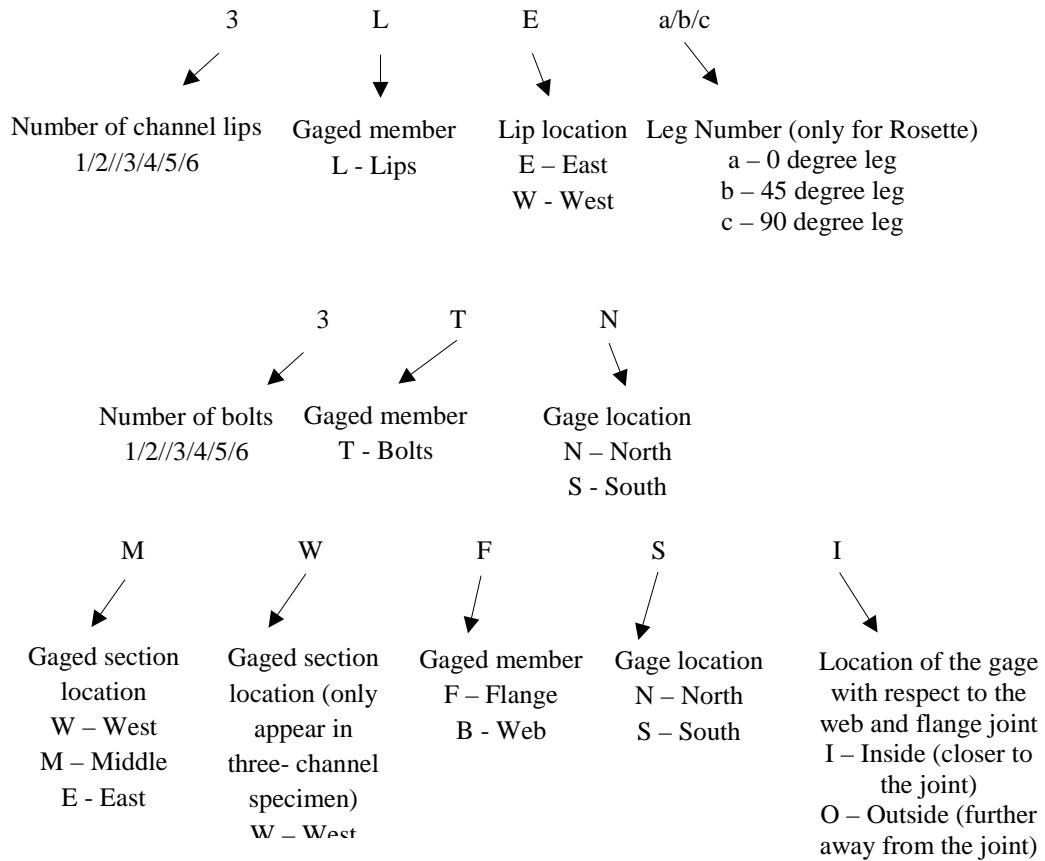
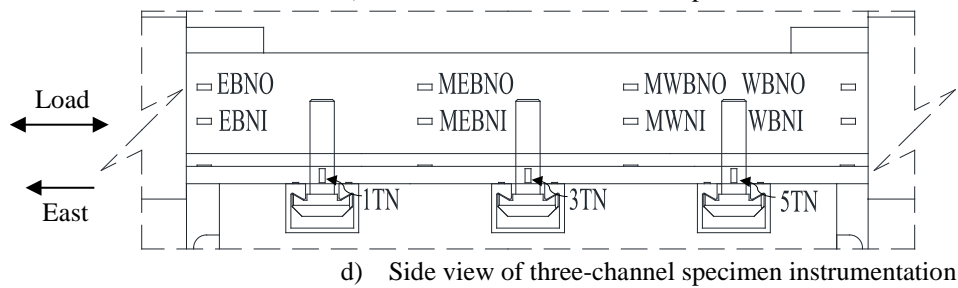
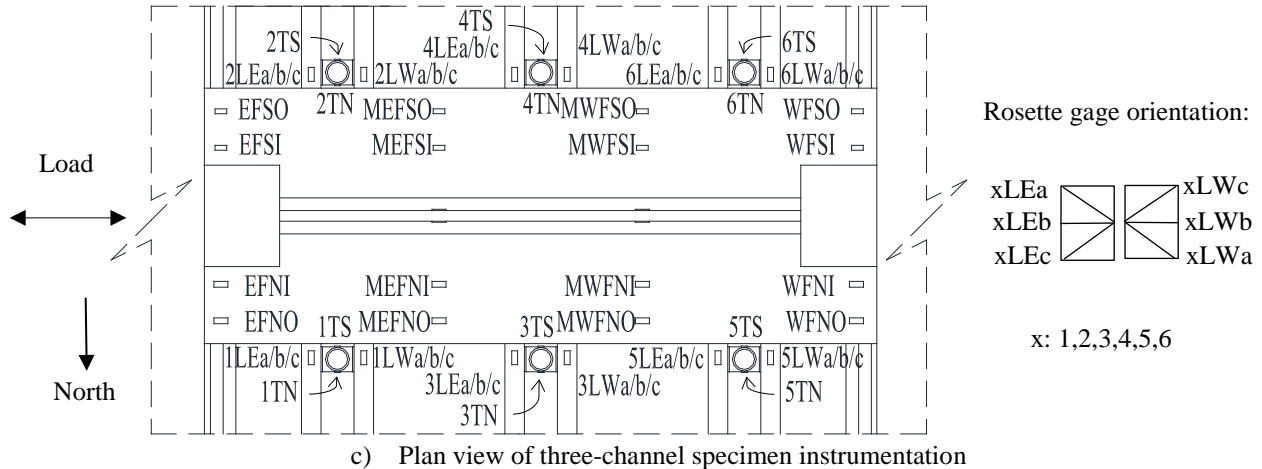
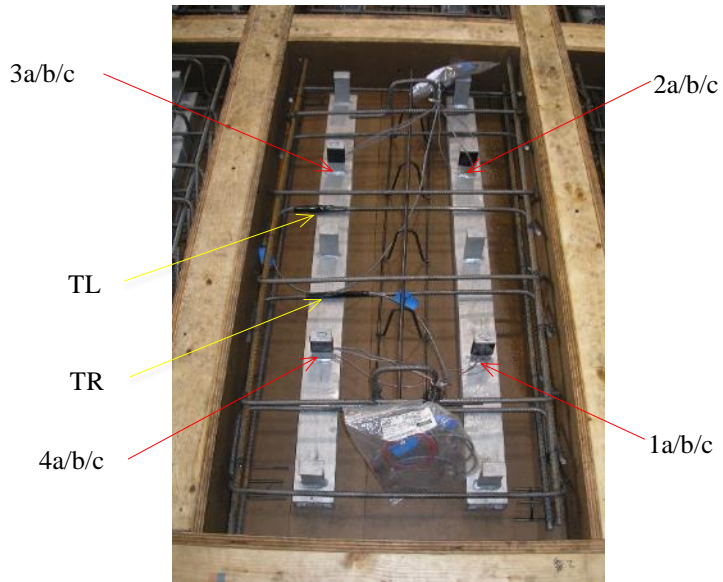


Figure 5.13 Strain gages attached on the bolts, channel lips and beams

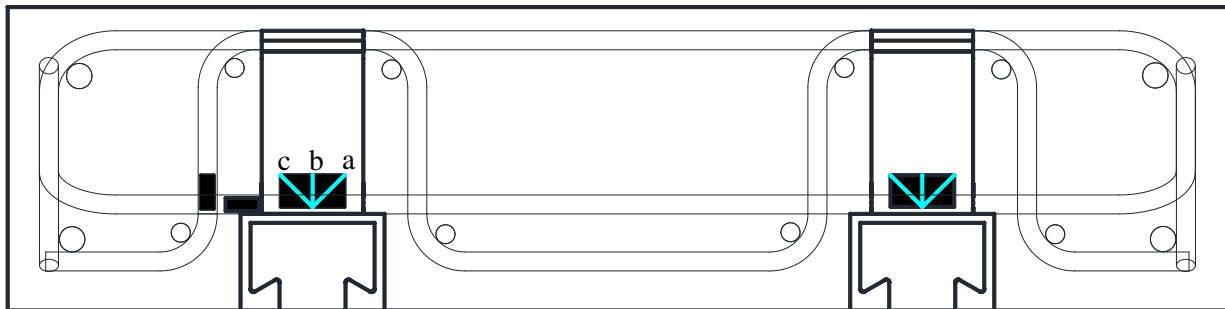
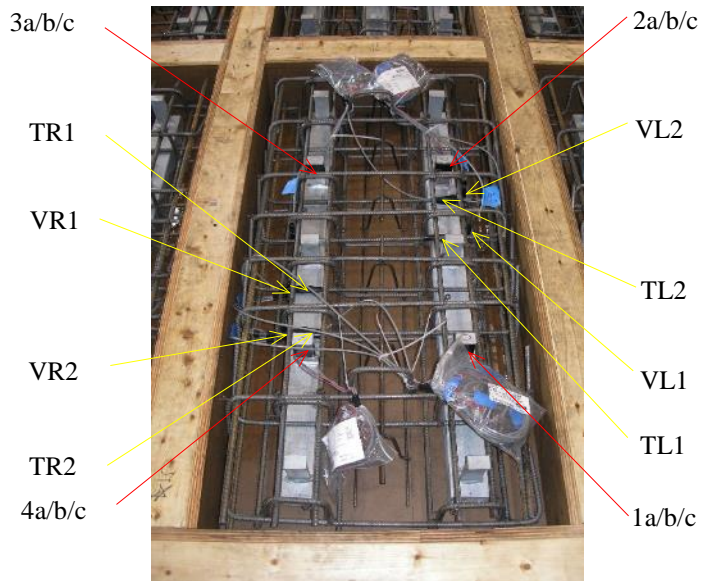
The following strain gages are placed inside the concrete specimen before pouring concrete. rosette strain gages are attached to the channel anchors to measure the strain variations in three directions (0-45-90), and these measurements can be used to estimate the axial force and shear force acting on the anchors. On each channel, two strain gages are installed on the same side of the two selected anchors, which are deemed to take large forces and have small resistance against concrete failure. All the strain gages are placed along the anchor centerline and as close to the welds as possible. The gages are capable of measuring 50,000 microstrains in the positive direction (tensile strain) and the negative direction (compressive strain).

Uniaxial strain gages are utilized to monitor the axial strain variations in the transverse and vertical reinforcement. Since the specimen with the light reinforcement cage is under monotonic loading, instrumentations are on the same side of the selected transverse reinforcement. For the heavy reinforcement cages, some transverse and vertical reinforcement are instrumented on one side, while strain gages are attached on the other side of other reinforcement, because cyclic loading is applied to these specimens. Using preliminary finite element analysis results, the bar gages are placed at the maximum tensile stress locations.

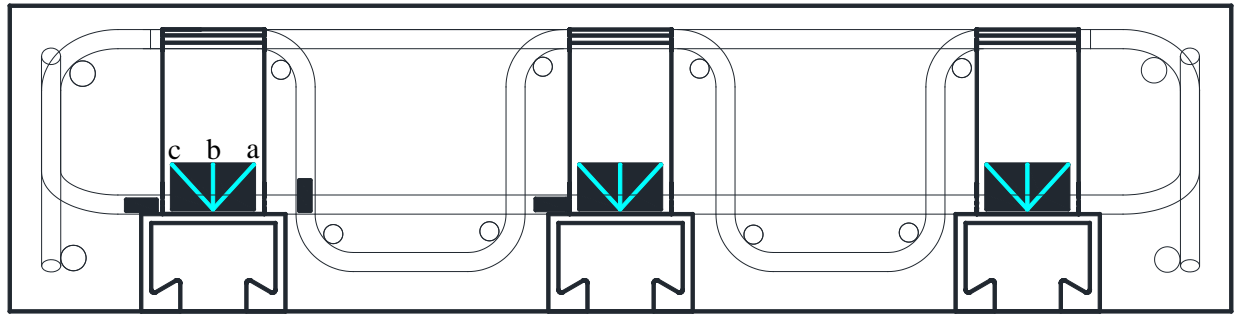
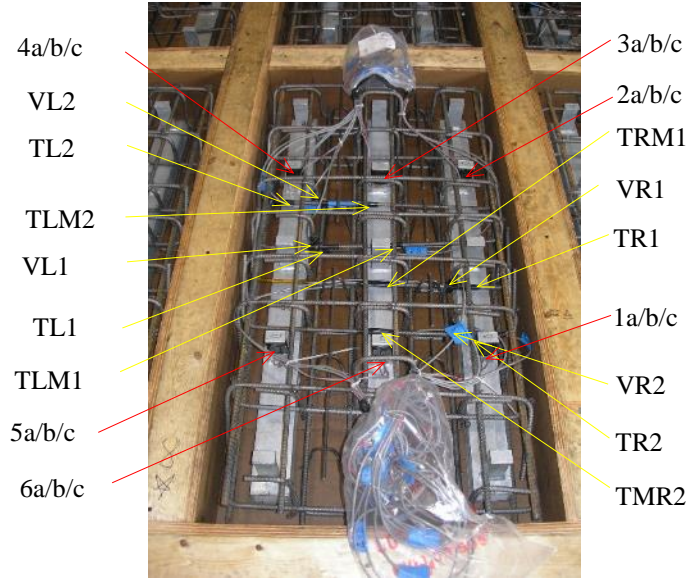
The rosette strain gages are named in the following manner: the first number implies the anchor being instrumented; the second letter defines the measuring grid in the rosette gage. The nomenclature for the uniaxial strain gages adopts another approach, and the first letter represents the type of reinforcement; the second letter indicates the location of the gage with respect to the centerline of the specimen; the last number implies whether the gage is closer to or further away from the centerline. Reinforcement cages and instrumentations before pouring concrete are shown in Figure 5.14.



a) Light reinforcement pattern with two channels



b) Heavy reinforcement pattern with two channels



c) Heavy reinforcement pattern with three channels

3

a/b/c

Location of the gage: the numbering is in a counter-clockwise direction; the 1st gage is at the lower right corner
1/2/3/4/5/6

Leg Number (only for Rosette)
a – 0 degree leg
b – 45 degree leg
c – 90 degree leg

T L M 2

Reinforcement type
T - Transverse
V - Vertical

Location of the reinforcement with respect to the specimen centerline
L- Left
R- Right

Gage at the middle of the transverse reinforcement
t
M/Not
Applicable

Location of the reinforcement with respect to the specimen centerline
1 - closer to the centerline
2 - further away from the centerline

Figure 5.14 Strain gages attached on the reinforcement and channel anchors

5.2.3 Loading protocol

All the pushout specimens are displacement-controlled. In the first monotonic test, i.e., Test 2-M24-2C-RH-LM, the actuator displacement rate was chosen to be 0.0025 in. per minute before the slip reaches 0.02 in. However, the actual slip rate is much smaller at the beginning of the test. Therefore, for the remaining monotonic tests, a rate of 0.0075 in. per minute movement of the actuators was first adopted until slips between concrete and steel are detected, which means gaps are closed and contact is established between the components. Subsequently, the variation of the actuator displacement starts to match the change of the slips. The actuator displacement rate is switched to 0.0025 in. per minute until a slip of 0.02 in. is attained. The subsequent loading rates are the same as those used in the cyclic tests at the same slip, see Figure 5.15. In the monotonic tests, the specimens are loaded in the east direction or the tensile direction. Since the monotonic load-slip curves show gradual changes in response, the load corresponding to a slip of 0.02 in. is defined as the slip load, in accordance with the RCSC Specification (RCSC 2009).

The cyclic loading history is depicted in Figure 5.15. The AISC loading protocol for beam-to-column moment connections is used as a guide for establishing a cyclic loading history for the clamped connections. Because the slips are too small to discern, 37.5%, 50% and 75% of the slip load, which is obtained from the corresponding monotonic test, are respectively used as the targets for the first three levels. Slip is then used as the target for the other cycles. During each loading cycle, the specimen is first loaded in the east direction or the tensile direction, then unloaded, then loaded in the west direction or the compressive direction and then unloaded. In the first cyclic test, i.e., Test 5-M24-2C-RH-LC, the actuator displacement rate is 0.0075 in. per minute for the first load level. However, this rate is found to be slow, and this test is then completed using the above protocol.

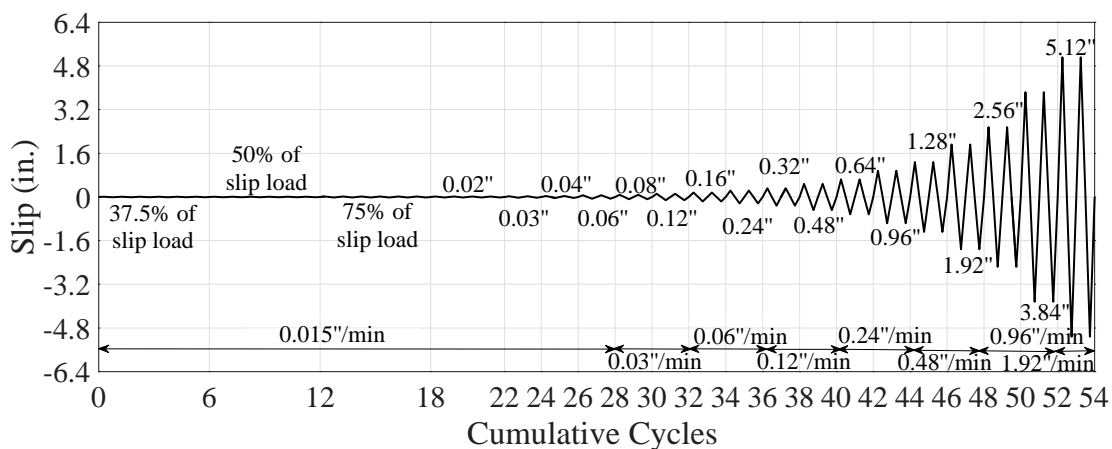


Figure 5.15 Cyclic loading history

5.2.4 Specimen performance

Similar behavior of the specimen occurs in all the tests, as shown in Figure 5.16. No movement or damage is detected when the relative movement between concrete and steel is small. As the slip increases, rotation of the clamps becomes noticeable. Noises are occasionally heard when the steel beam is being pushed, and they become louder and more frequent as the test proceeds. The Teflon sheet attached to the top of the west guide is torn off in several tests. After disassembling the test specimens, it can be found that the channel lips deform inelastically in the M24 bolt tests, while the lip deformation is imperceptible in the M20 bolt tests. Concrete cracking is discovered in almost all the specimens, but most cracks are narrow and localized. Cracks, similar to those discovered in the pretension tests, also appear at the heads of some bolts with three full turns from a snug-tight condition, probably indicating that the rotation is excessive. Abrasion on the steel flanges and concrete surfaces occurs in each test.

Monotonic specimens

Test 2-M24-2C-RH-LM

When the slip is approaching 2.56 in., the rotation of Clamp 3 becomes significant which almost causes that clamp to be disengaged, see Figure 5.17. As the specimen is further loaded to the next level (5.12 in. slip), the south string pot is found to be malfunctioning due to some configuration problems. Due to safety concern for the test rig, the test is terminated when the slip is about 10 in.

Test 4-M24-2C-RH-LM-S

Linear potentiometer 4 in this test does not work properly before 0.08 in. slip, but it starts to function successfully thereafter. The hook for linear potentiometer 2 falls off during the test, as indicated in the slip plot.

When the beam is loaded to a slip of 1.28 in., a loud sound is heard, which is later found to be bolt head fracture in one of the four bolts after disassembling the test setup. Along with frequent noises caused by slips, oscillation in the loading starts to appear and becomes significant. In order to eliminate dynamic effects, the loading rate is slowed down from 0.96 to 0.12 in. per minute in the last step; however, oscillation still exists. Rotation and slip of the shims are discovered during the test. The test is terminated prematurely at a slip of 5.12 in. because the Teflon sheet attached to the west guide is severely torn off.



Rotation of clamps



Abrasion on the steel flanges



M24 bolt test



M20 bolt test

Channel lip deformation



Cracks in the middle of a slab



Cracks in the vicinity of the bolts

Abrasion and cracks on the concrete surface

Figure 5.16 General observations in all pushout tests

Test 7-M24-3C-RH-LM

Linear potentiometers 1 and 2 first detect slip of the clamps, but the remaining linear potentiometers and string pots do not start to read slip until sensors 1 and 2 display a slip of 0.04 in. and 0.08 in., respectively. During the test, concrete cracks emerge behind Clamps 1 and 3, and the cracks become wider as the slip increases. Behind the rear clamps, i.e., Clamps 5 and 6, much deeper and wider cracks are discovered underneath the steel beam after dismantling the

specimen, and the cracking pattern is similar to that found in other tests. A unique observation in this test is that the lip of the rear channel is significantly bent due to the frictional force. Rotation is found for the clamps on the north side, but the south clamps remain still. As the test continues, the south clamps start to rotate, but the rotation is always less than the north clamps. Similar to test 4, due to the frictional force induced by the steel beam bearing against the west guide, the Teflon sheet is torn off, and the test is terminated prematurely at 5.12 in. slip.

Test 9-M20-2C-RH-LM

Cracks appear behind all four clamps when the slip is 0.02 in., and they become wider as the beam moves. Rotation of clamps is noticeable at a slip of 0.16 in., which occurs much earlier than the M24 bolt tests. Because of their relatively small sizes, the M20 clamps cannot hold their positions as stably as the M24 clamps. Clamp 3 is first disengaged, followed by Clamps 1 and 4. Only Clamp 2 maintains its position during the whole test. Due to safety concern for the test rig, the test is terminated when the slip is about 10 in.

Cyclic specimens

Test 3-M24-2C-RL-LC

This is the only specimen designed with the light reinforcement pattern, and significant concrete failure is anticipated. The slip load, which is necessary to define the first three load magnitudes in the cyclic loading protocols, adopts that obtained from Test 2-M24-2C-RH-LM, since no corresponding monotonic specimen exists for Specimen 3. Starting at a slip of 0.02 in., diagonal concrete cracking adjacent to Clamp 2 and 4 is discovered. The cracks open when the beam is loaded in the compressive or west direction, and close when the beam is loaded in the tensile or east direction. Clamp 1 is almost disengaged at the end of the test, while the others seem to maintain their positions well. The test is terminated when the maximum slip that can be measured is reached.

Test 5-M24-2C-RH-LC

This specimen behaves in a similar manner as Test 3-M24-2C-RL-LC. Wearing off of the flange is observed as the beam moves further. It is noted that Clamp 2 and 4 occasionally rotate in opposite directions because the rotation of the clamps does not synchronize with the displacement of the beam, especially at larger slips. At a slip of 1.92 in., Clamp 3 and 4 start to lose contact, and Clamp 4 is completely disengaged in the very last cycle (5.12 in. slip). The test is terminated when the maximum slip that can be measured is reached.

Test 6-M24-2C-RH-LC-S

Since one bolt head fractures in Test 4-M24-2C-RH-LM-S, the corresponding monotonic test, bolts are instrumented in Test 6. The strains in Bolt 4 reach about 0.04 after one and two-thirds turns, and pretensioning of this bolt is stopped due to concern of bolt fracture. The strains are reasonable for the other bolts after two full turns. During the test, the specimen rotates because of the eccentricity between the actuator force and the reaction from the reaction angle. The specimen jerks when it is unloaded from 42.4 kips (75% of the slip load) to approximately 10 kips in compression. The reason is that the rotated specimen cannot return to a level position smoothly. Hence, the sliders shown in Figure 5.6 are reinforced to minimize the vertical movement of the cross beam, which connects the actuators and the test specimen, as well as the overturning of the system during loading.

When the specimen is loaded to a slip of 0.48 in., a loud noise is heard, followed by considerable load drop and continuous noise from slip. The strength regains shortly, and the load starts to oscillate. The subsequent loud noises are always accompanied by sudden changes in the slip measurements. This phenomenon occurs in every following cycle. Shims detach from the clamps one after another at large slips. The sequence and the slip levels are: Shim 1 at 1.92 in.; Shim 3 at 2.56 in.; Shim 4 at 3.84 in.; Shim 2 at 3.84 in. Accordingly, the test is terminated.

Test 8-M24-3C-RH-LC

When the slip is 0.03 in., cracks are found at Clamps 1 and 2, but the crack at Clamp 1 shown in Figure 5.17 is unusual and not seen in the other tests. At 0.06 in. slip, another crack is seen in the neighborhood of Clamp 6. The test is terminated when the maximum slip that can be measured is reached.

Test 10-M20-2C-RH-LC

It is believed that the loss of contact between the clamp teeth and the steel beam flange and between the clamp tail and the channel lips leads to the undesirable strength degradation at large slips in the corresponding monotonic test. Hence, it is decided that steel blocks be inserted into the channels to improve the clamp performance under cyclic loading by supporting the clamp tails. Those blocks are finely machined such that they fit inside the channels perfectly. One and a half turns are utilized for pretensioning the M20 bolts.

Hairline cracks first emerge in the concrete specimen at 27.38 kips (75% of slip load), and as the slip increases, existing cracks become wider and additional cracks appear. The clamps begin to rotate when the slip is 0.16 in. As a result of large rotation, the corner of Clamp 4 falls into the gap between the channel lips at a slip of 0.96 in. However, the majority of the tail still bears

against the block inside the channels, which may defer the decrease of the loading. As the test proceeds, all clamps start to lose contact, and all four clamps are disengaged ultimately, and the concrete slab is no longer clamped to the steel beam.



Clamp tail disengaged

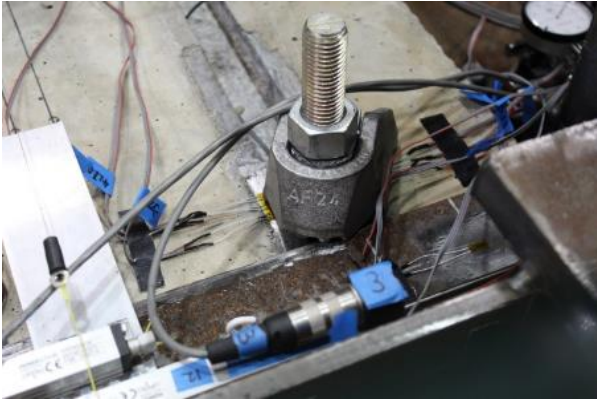


Crack in the bolt head

Test 2-M24-2C-RH-LM



Concrete crack adjacent to Clamp 2

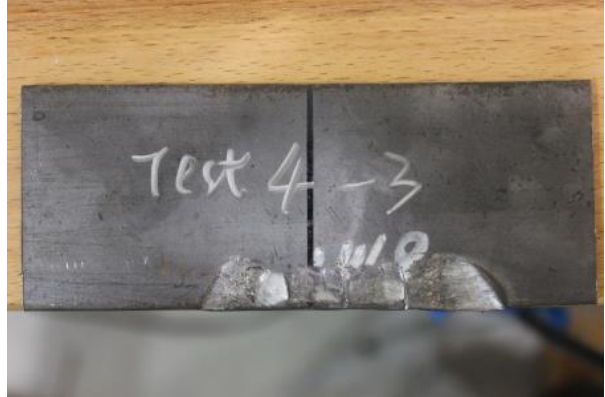


Clamp 1 almost disengaged

Test 3-M24-2C-RL-LC



Rotation and slip of shim under Clamp 1



Shim crushed

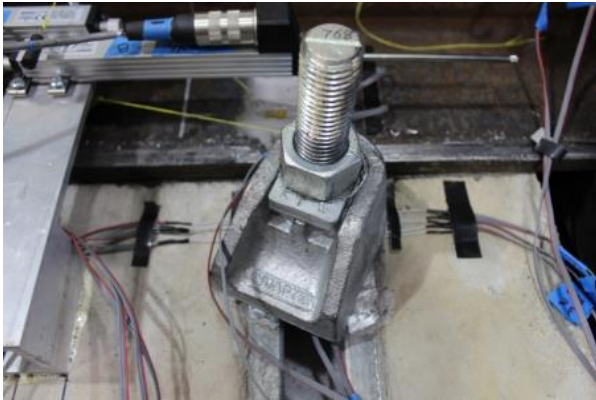


Head fracture in Bolt 4



Teflon torn off

Test 4-M24-2C-RH-LM-S



Large rotation at Clamp 3



Complete disengagement of Clamp 4

Test 5-M24-2C-RH-LC



Shim fully separated from Clamp 1



Scraped shim

Test 6-M24-2C-RH-LC-S



Concrete crack adjacent to Clamp 1

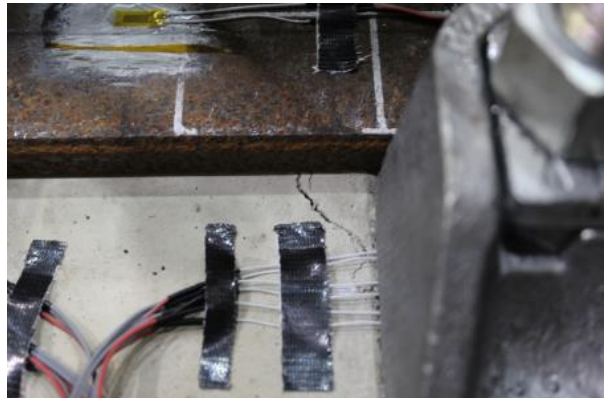


Concrete crack and bent channel lips adjacent to rear clamps

Test 7-M24-3C-RH-LM



Unusual concrete crack adjacent to Clamp 1



Concrete crack adjacent to Clamp 2

Test 8-M24-3C-RH-LC



Concrete crack adjacent to clamp 1



Complete disengagement of Clamp 3

Test 9-M20-2C-RH-LM



Clamps 1 and 3 rotating in opposite directions



Complete detachment of clamps with beam

Test 10-M20-2C-RH-LC

Figure 5.17 Unique observations in each test

Table 5.4 summarizes the clamp detachment sequence in each test. For example, all the clamps separate from the beam in Test 9-M20-2C-RH-LM, except for Clamp 2. Clamp 3 first detaches from the beam, then followed by Clamp 1 and Clamp 4. This table indicates that clamps are less likely to detach from beams in the monotonic tests than in the cyclic tests. The M20 clamps and the usage of shims increase the possibility of detachment.

Table 5.4 Clamp detachment sequence

Test \ Clamp	1	2	3	4	5	6
2	X	X	X	X	N/A	N/A
3	1	X	X	X	N/A	N/A
4	X	X	X	X	N/A	N/A
5	X	X	X	1	N/A	N/A
6	1	4	2	3	N/A	N/A
7	X	X	X	X	N/A	N/A
8	X	X	X	X	X	X
9	2	X	1	3	N/A	N/A
10	2	4	3	1	N/A	N/A

Note: (1) X: clamps still contact beams; (2) N/A: not applicable.

5.2.5 Assessment of the clamping connectors

Monotonic specimens

Test 2-M24-2C-RH-LM

The load-slip curve is shown in Figure 5.18 using the slip measurement from the north string pot. The system starts to deviate from being elastic when the force and slip are approximately 53 kips and 0.003 in. Defined at 0.02 in. slip, the slip load is about 60.8 kips. The peak load, which occurs at a slip of 1.12 in., is around 88.5 kips. When the slip is approximately 2.15 in., the load starts to drop gradually, which could be caused by the loss of pretension force in Clamp 3 because of the large rotation.

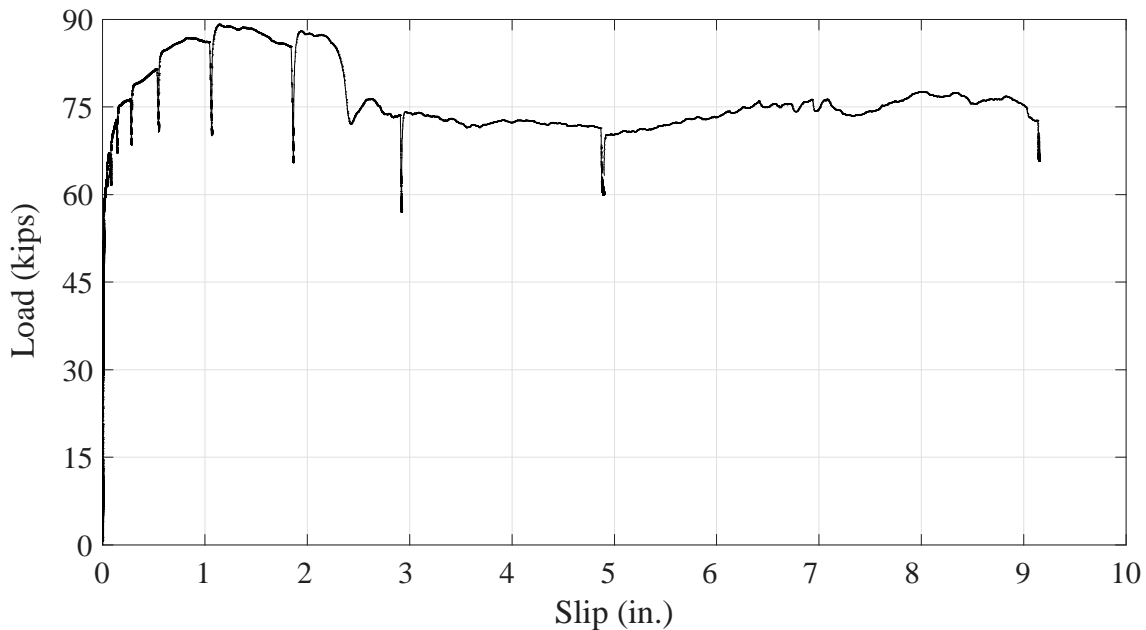


Figure 5.18 Load-slip curve of Specimen 2

Test 4-M24-2C-RH-LM-S

The load-slip curve is shown in Figure 5.19 using the average slip measurement from the string pots. The slip load is about 56.5 kips. Occurring at a slip of 0.55 in., the peak load is around 87.9 kips. Fracture of the bolt head is signified by the dramatic load drop. Shortly strength regains to 66 kips, only 75% of the peak load. This ratio may indicate that the pretension is released in the fractured bolt. Subsequently, the load begins to oscillate, which could be caused by a stick-slip mechanism, exasperated by the shims. The alternation happens along with a change of the friction force for the difference between the static frictional coefficient and the kinetic frictional coefficient. This phenomenon was also observed in prior research by Grigorian and Popov (1994).

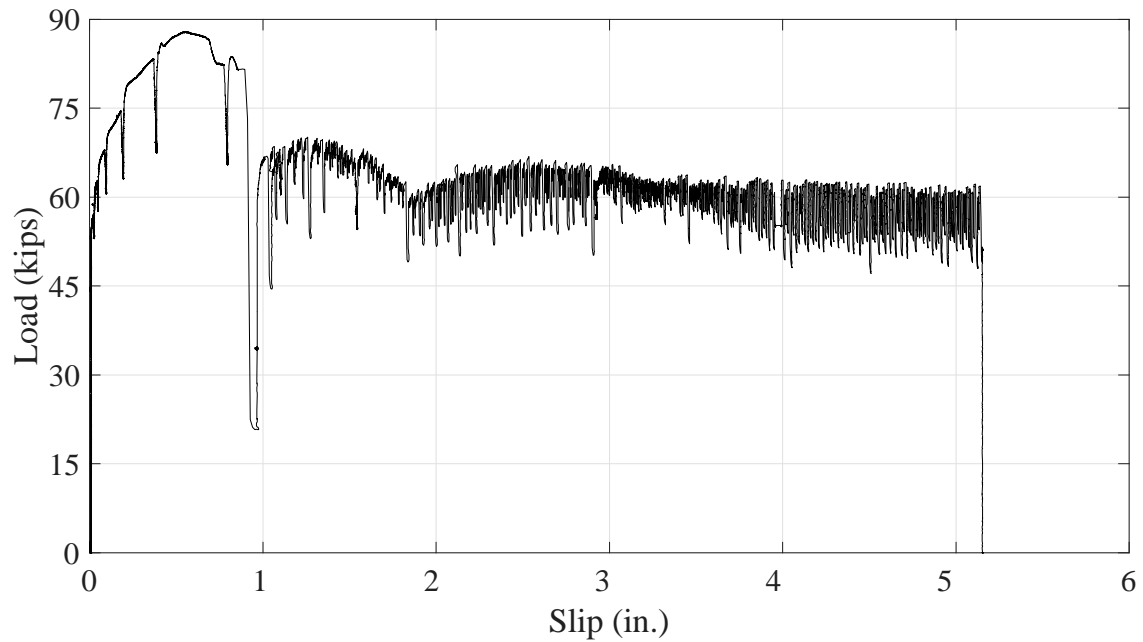


Figure 5.19 Load-slip curve of Specimen 4

Test 7-M24-3C-RH-LM

The load-slip curve is shown in Figure 5.20 using the average slip measurement from the string pots. Based on this curve, the slip load defined at 0.02 in. slip is about 113.2 kips. However, the slip load is only 87.0 kips when the readout from linear potentiometer 1 and 2 is 0.02 in. The peak load, which occurs at a slip of 0.30 in., is 130.1 kips. The system can still retain about 80% of the peak load even at a slip of 5 in.

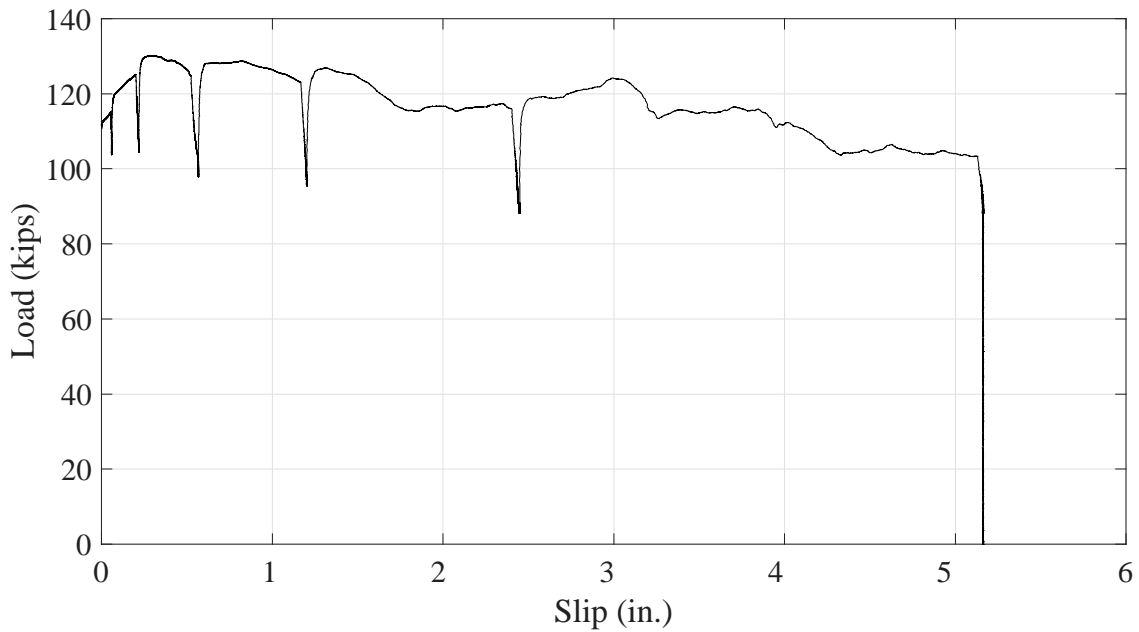


Figure 5.20 Load-slip curve of Specimen 7

Test 9-M20-2C-RH-LM

The load-slip curve is shown in Figure 5.21 using the average slip measurement from the string pots. The slip load defined at 0.02 in. slip is about 36.5 kips. The peak load, which occurs at a slip of 0.54 in., is around 55.3 kips. Unlike the M24 bolts which retain most of their strength at large slips, the load starts to drop after 0.68 in. slip until the end of the test. The reason is the loss of pretension as a result of the disengagement of the clamps.

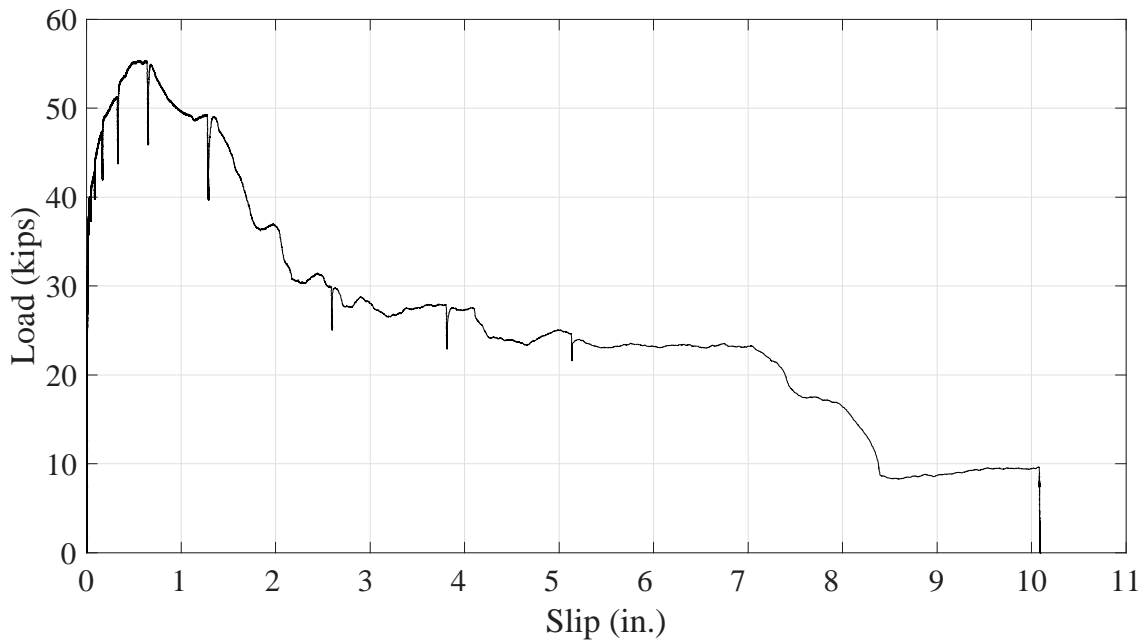


Figure 5.21 Load-slip curve of Specimen 9

The monotonic test results are summarized in Table 5.5. For each test, the slip load and peak load are both normalized relative to Test 2-M24-2C-RH-LM. The usage of shims does not reduce the slip load or the peak load. However, the selected steel shims do not exhibit desirable behavior at large slips due to a stick-slip mechanism. The slip strength and peak strength of Test 7-M24-3C-RH-LM in which three channels are used are approximately 50% higher than those of Test 2-M24-2C-RH-LM, which uses two channels, implying that the shear force can be distributed among the clamps. Although severe cracks are seen in Test 7-M24-3C-RH-LM, they do not reduce the specimen strength. In Test 9-M20-2C-RH-LM, M20 bolts are tested, and the strength is about 60% of the standard M24 bolt specimen (i.e., Test 2-M24-2C-RH-LM). Nevertheless, the $\frac{3}{4}$ in. bolts cannot maintain their strength as well as the M24 bolts, as is indicated by the load decrease at larger slips.

Table 5.5 Summary of monotonic test results

Monotonic test	Slip load (kips)		Peak load (kips)			Peak load/Slip load	Load at 5 in. slip (kips)	
	Absolute	Normalized	Absolute	Normalized	slip (in.)		Absolute	Percentage of peak load
2-M24-2C-RH-LM	60.8	1.00	88.5	1.00	1.12	1.46	68.9	78%
4-M24-2C-RH-LM-S	56.5	0.93	87.9	0.99	0.55	1.56	55.1	63%
7-M24-3C-RH-LM	87.0	1.43	130.1	1.47	0.30	1.50	104.0	80%
9-M20-2C-RH-LM	36.5	0.60	55.3	0.62	0.54	1.52	24.9	45%

Cyclic specimens

The following sign convention is defined for the slip and the load measurements: the load is positive when the beam is under compression; the slip is positive when the beam moves west.

Test 3-M24-2C-RL-LC

The load-slip curve is shown in Figure 5.22 using the average slip measurement from the string pots. The plateau load at the second cycle of each slip level decreases compared to that of the first cycle, particularly at larger slips. As more and more cycles are completed, the teeth of the clamps and the steel flanges begin to wear down, reducing the frictional force. At each cycle, the load first stabilizes, and then increases considerably because the clamp teeth engage new positions on the beam flanges.

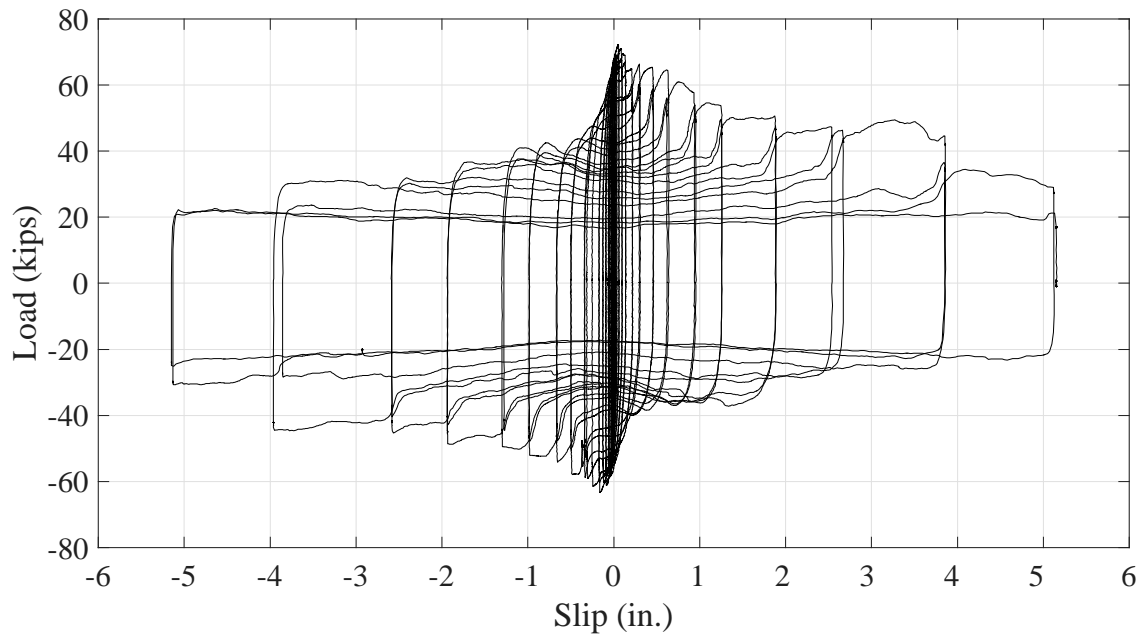


Figure 5.22 Load-slip curve of Specimen 3

Test 5-M24-2C-RH-LC

The load-slip curve is shown in Figure 5.23 using the average slip measurement from the string pots. The load-slip plot of this specimen is very similar to that of Specimen 3-M24-2C-RL-LC.

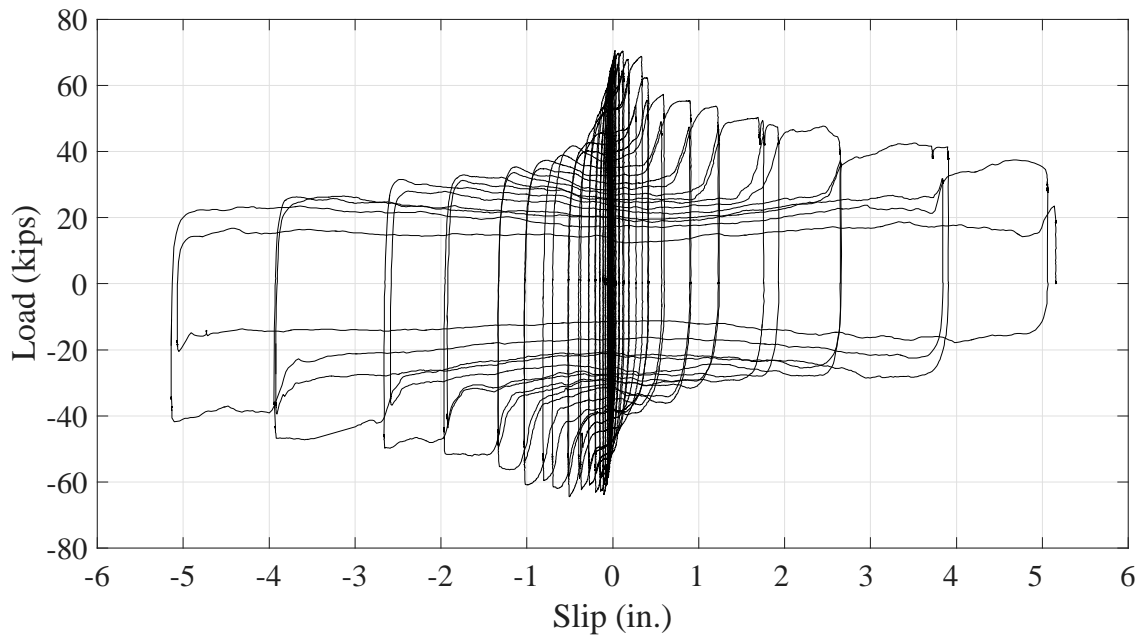


Figure 5.23 Load-slip curve of Specimen 5

Test 6-M24-2C-RH-LC-S

The load-slip curve is shown in Figure 5.24 using the average slip measurement from the string pots. The readouts from the string pots are asymmetric, and the plot is shifted towards the negative slip direction. On the whole, this curve has a similar shape as the other cyclic specimens, but distinct differences can be seen. As indicated by the sudden load drop and slip measurement change in the load-slip plot, a stick-slip phenomenon persists, similar to what occurs in the corresponding monotonic test, Test 4-M24-2C-RH-LM-S, and load oscillation usually ensues. The load reduces dramatically once the shims start to separate from the clamps consecutively, and ultimately the capacity approaches zero after all the shims are detached.

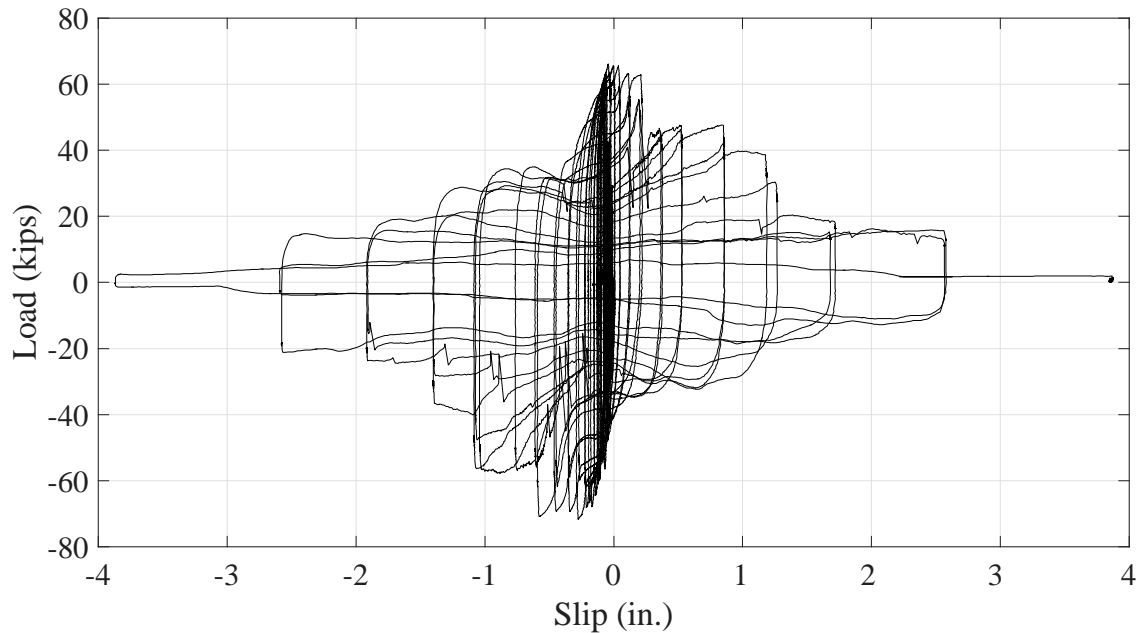


Figure 5.24 Load-slip curve of Specimen 6

Test 8-M24-3C-RH-LC

The load-slip curve is shown in Figure 5.25 using the average slip measurement from the string pots. Except for the strength, the load-slip curve of this specimen is very similar to those of Specimens 3-M24-2C-RL-LC and 5-M24-2C-RH-LC.

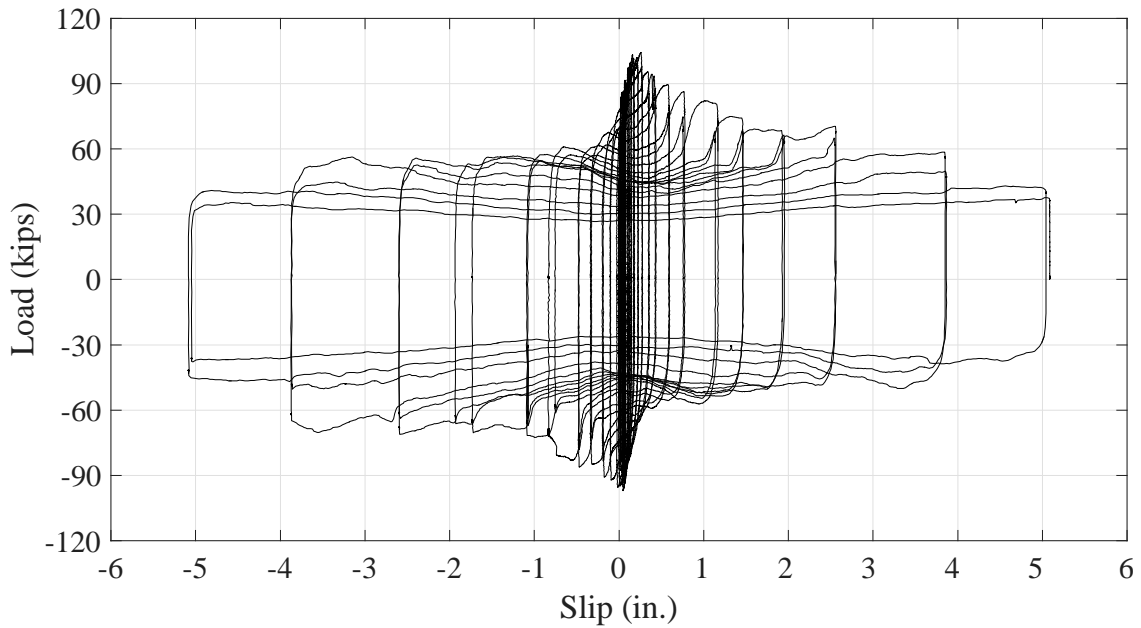


Figure 5.25 Load-slip curve of Specimen 8

Test 10-M20-2C-RH-LC

The load-slip curve is shown in Figure 5.26 using the average slip measurement from the string pots. In this test, the decrease of peak load and plateau load at each cycle is more than that in the M24 bolt testing. Compared to the corresponding monotonic test, Test 9-M20-2C-RH-LM, the strength of the cyclic test shows considerable reduction at much larger slips. After all the clamps lose contact with the steel beam, the strength of the system approaches zero at 5.12 in. slip.

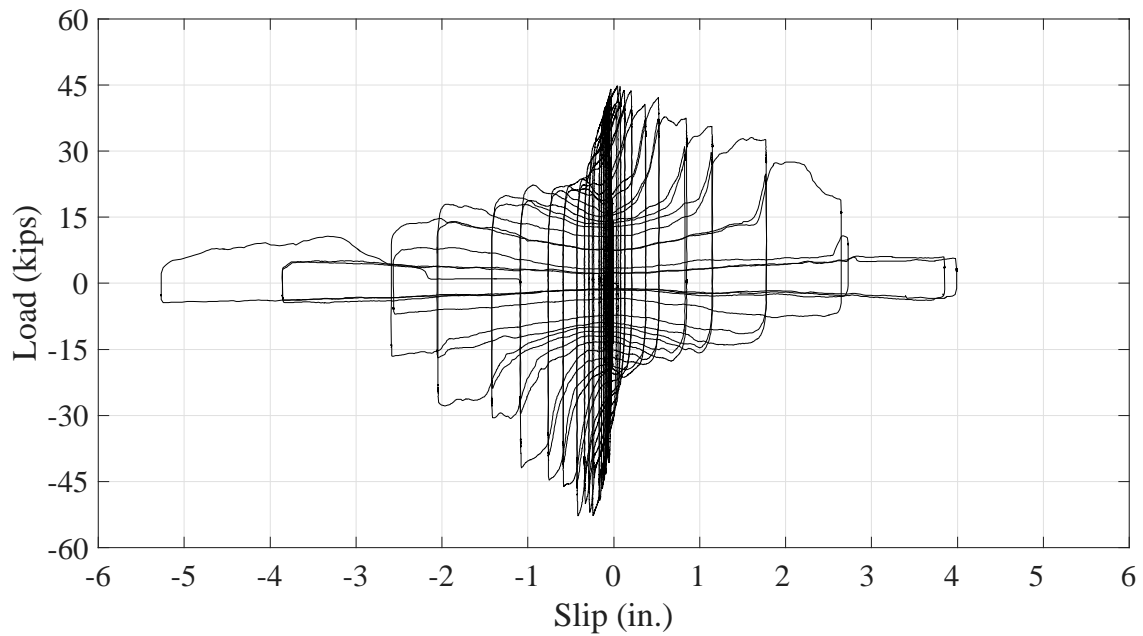


Figure 5.26 Load-slip curve of Specimen 10

The cyclic test results are summarized in Table 5.6. For each test, the peak load and the plateau load at a certain slip level in a certain direction are normalized with the peak load in that direction. Figure 5.27 depicts the strength reduction variation with slip. At a certain slip level, the strength generally degrades less in the first cycle than the second cycle. The peak load decreases roughly linearly, while the plateau load declines approximately exponentially.

Table 5.6 Summary of cyclic test results

Cyclic test	Slip (in.)	Peak load (kips)								Plateau load (kips)							
		Positive slip				Negative slip				Positive load				Negative load			
		Cycle 1	Cycle 2	Ratio 1	Ratio 2	Cycle 1	Cycle 2	Ratio 1	Ratio 2	Cycle 1	Cycle 2	Ratio 1	Ratio 2	Cycle 1	Cycle 2	Ratio 1	Ratio 2
3-M24-2C-RL-LC	0.08	72.2	69.6	1.00	0.96	-58.4	-61.2	0.92	0.97	65.3	63.3	0.90	0.88	-53.0	-53.8	0.84	0.85
	0.12	70.9	68.2	0.98	0.94	-60.2	-58.5	0.95	0.92	64.3	62.5	0.89	0.87	-54.2	-54.3	0.86	0.86
	0.16	69.4	66.9	0.96	0.93	-63.3	-60.2	1.00	0.95	64.0	61.5	0.89	0.85	-57.7	-55.8	0.91	0.88
	0.24	64.9	60.0	0.90	0.83	-61.4	-59.1	0.97	0.93	60.6	55.2	0.84	0.76	-54.6	-52.5	0.86	0.83
	0.32	66.3	59.8	0.92	0.83	-58.7	-52.6	0.93	0.83	55.0	50.7	0.76	0.70	-48.1	-45.0	0.76	0.71
	0.48	65.3	58.5	0.90	0.81	-57.9	-50.0	0.91	0.79	46.9	42.4	0.65	0.59	-40.9	-37.7	0.65	0.60
	0.64	64.5	55.6	0.89	0.77	-54.0	-47.8	0.85	0.76	41.7	39.3	0.58	0.54	-35.9	-34.3	0.57	0.54
	0.96	60.9	53.6	0.84	0.74	-52.4	-47.9	0.83	0.76	36.9	34.7	0.51	0.48	-32.7	-31.5	0.52	0.50
	1.28	54.5	49.3	0.75	0.68	-50.2	-44.2	0.79	0.70	35.0	33.1	0.48	0.46	-30.9	-31.4	0.49	0.50
	1.92	50.6	47.4	0.70	0.66	-48.7	-42.5	0.77	0.67	32.2	31.2	0.45	0.43	-30.5	-28.8	0.48	0.45
	2.56	47.5	46.1	0.66	0.64	-45.1	-39.6	0.71	0.63	27.9	25.8	0.39	0.36	-28.1	-26.2	0.44	0.41
	3.84	49.4	35.9	0.68	0.50	-44.7	-28.8	0.71	0.45	23.6	19.7	0.33	0.27	-23.2	-19.6	0.37	0.31
	5.12	34.4	21.3	0.48	0.30	-30.8	-24.9	0.49	0.39	18.4	16.8	0.25	0.23	-17.8	-17.5	0.28	0.28
	5-M24-2C-RH-LC	0.08	70.6	68.7	1.00	0.97	-63.6	-60.8	0.99	0.94	62.7	61.5	0.89	0.87	-52.8	-54.1	0.82
0.12		69.7	66.3	0.99	0.94	-62.5	-58.7	0.97	0.91	62.0	59.2	0.88	0.84	-54.2	-53.5	0.84	0.83
0.16		70.4	64.4	1.00	0.91	-63.0	-57.3	0.98	0.89	60.3	56.6	0.85	0.80	-54.6	-52.1	0.85	0.81
0.24		67.9	62.8	0.96	0.89	-60.9	-57.2	0.95	0.89	55.2	52.7	0.78	0.75	-50.7	-48.4	0.79	0.75
0.32		68.8	54.1	0.97	0.77	-62.3	-58.9	0.97	0.91	52.9	45.2	0.75	0.64	-47.4	-44.1	0.74	0.68
0.48		62.3	55.6	0.88	0.79	-64.4	-58.2	1.00	0.90	42.3	39.1	0.60	0.55	-41.1	-38.3	0.64	0.59
0.64		57.2	48.6	0.81	0.69	-62.0	-59.5	0.96	0.92	37.2	35.1	0.53	0.50	-38.0	-36.4	0.59	0.57
0.96		55.4	47.3	0.78	0.67	-60.9	-53.6	0.95	0.83	32.6	30.1	0.46	0.43	-33.3	-31.3	0.52	0.49
1.28		53.7	46.8	0.76	0.66	-56.3	-49.0	0.87	0.76	28.4	26.9	0.40	0.38	-30.1	-29.3	0.47	0.45
1.92		50.4	48.2	0.71	0.68	-52.2	-43.1	0.81	0.67	25.7	25.3	0.36	0.36	-28.7	-27.8	0.45	0.43
2.56		47.6	36.7	0.67	0.52	-49.7	-36.4	0.77	0.57	23.7	22.6	0.34	0.32	-26.5	-23.5	0.41	0.36
3.84		42.6	31.6	0.60	0.45	-47.2	-38.8	0.73	0.60	20.0	20.5	0.28	0.29	-21.1	-18.7	0.33	0.29
5.12		37.4	23.1	0.53	0.33	-41.9	-19.8	0.65	0.31	17.5	13.2	0.25	0.19	-14.0	-11.4	0.22	0.18

Table 5.7 Summary of cyclic test results (continued)

Cyclic test	Slip (in.)	Peak load (kips)								Plateau load (kips)							
		Positive slip				Negative slip				Positive slip				Negative slip			
		Cycle 1	Cycle 2	Ratio 1	Ratio 2	Cycle 1	Cycle 2	Ratio 1	Ratio 2	Cycle 1	Cycle 2	Ratio 1	Ratio 2	Cycle 1	Cycle 2	Ratio 1	Ratio 2
6-M24-2C-RH-LC-S	0.12	65.4	61.3	0.99	0.93	-68.2	-62.0	0.95	0.86	56.7	54.9	0.86	0.83	-59.6	-54.9	0.83	0.76
	0.16	65.5	59.2	1.00	0.90	-71.8	-60.0	1.00	0.84	56.5	53.4	0.86	0.81	-57.0	-53.8	0.79	0.75
	0.24	63.0	54.6	0.96	0.83	-69.4	-59.1	0.97	0.82	50.8	44.4	0.77	0.67	-51.8	-46.7	0.72	0.65
	0.32	62.6	55.0	0.95	0.84	-69.5	-61.8	0.97	0.86	41.7	35.9	0.63	0.55	-46.0	-38.5	0.64	0.54
	0.48	55.0	43.9	0.84	0.67	-71.1	-54.8	0.99	0.76	33.1	32.6	0.50	0.50	-33.9	-33.5	0.47	0.47
	0.64	47.7	45.8	0.72	0.70	-56.6	-57.9	0.79	0.81	31.3	27.4	0.48	0.42	-34.6	-32.9	0.48	0.46
	0.96	47.6	41.9	0.72	0.64	-56.5	-47.8	0.79	0.67	24.3	23.8	0.37	0.36	-28.4	-25.6	0.40	0.36
	1.28	39.6	30.3	0.60	0.46	-40.1	-29.8	0.56	0.42	21.4	18.2	0.33	0.28	-23.8	-20.5	0.33	0.29
	1.92	20.2	15.0	0.31	0.23	-24.7	-20.1	0.34	0.28	13.2	11.3	0.20	0.17	-16.9	-14.5	0.24	0.20
	2.56	15.9	15.7	0.24	0.24	-21.4	-5.4	0.30	0.08	11.1	9.8	0.17	0.15	-9.2	-5.2	0.13	0.07
3.84	6.7		0.10		-5.8		0.08		5.9		0.09		-5.2		0.07		
8-M24-3C-RH-LC	0.16	104.0	97.4	1.00	0.94	-95.6	-84.4	0.92	0.81	92.8	85.4	0.96	0.88	-79.6	-78.0	0.82	0.80
	0.24	95.4	85.2	0.92	0.82	-92.4	-81.0	0.89	0.78	82.4	75.2	0.85	0.78	-69.8	-70.8	0.72	0.73
	0.32	94.2	87.4	0.91	0.84	-91.2	-96.4	0.88	0.93	75.4	68.8	0.78	0.71	-65.2	-61.8	0.67	0.64
	0.48	89.4	76.4	0.86	0.73	-85.2	-72.8	0.82	0.70	64.2	59.6	0.66	0.61	-59.4	-57.4	0.61	0.59
	0.64	86.2	73.4	0.83	0.71	-86.4	-77.4	0.83	0.74	55.6	52.8	0.57	0.54	-53.2	-51.6	0.55	0.53
	0.96	81.8	67.8	0.79	0.65	-83.4	-61.0	0.80	0.59	49.0	47.0	0.51	0.48	-46.6	-45.8	0.48	0.47
	1.28	74.8	67.8	0.72	0.65	-72.8	-66.4	0.70	0.64	44.4	45.2	0.46	0.47	-44.8	-44.4	0.46	0.46
	1.92	68.8	66.0	0.66	0.63	-70.4	-66.8	0.68	0.64	45.2	45.2	0.47	0.47	-44.6	-44.2	0.46	0.46
	2.56	70.2	63.6	0.68	0.61	-70.8	-63.8	0.68	0.61	43.0	41.2	0.44	0.42	-43.6	-41.2	0.45	0.42
	3.84	58.2	49.2	0.56	0.47	-70.4	-50.4	0.68	0.48	38.2	33.4	0.39	0.34	-36.0	-31.8	0.37	0.33
5.12	42.6	37.4	0.41	0.36	-47.2	-37.8	0.45	0.36	30.0	26.8	0.31	0.28	-28.6	-26.4	0.29	0.27	
10-M20-2C-RH-LC	0.12	44.9	44.9	1.00	1.00	-52.5	-44.0	1.00	0.84	39.9	35.0	0.89	0.78	-41.0	-36.0	0.78	0.69
	0.16	44.6	41.3	0.99	0.92	-51.8	-46.4	0.99	0.88	36.1	33.1	0.80	0.74	-35.2	-32.9	0.67	0.63
	0.24	43.9	40.5	0.98	0.90	-49.9	-44.8	0.95	0.85	32.5	29.1	0.72	0.65	-30.4	-28.0	0.58	0.53
	0.32	43.8	39.7	0.98	0.88	-52.7	-44.8	1.00	0.85	28.0	22.9	0.62	0.51	-27.0	-22.8	0.51	0.43
	0.48	40.6	37.2	0.90	0.83	-46.0	-40.3	0.88	0.77	21.0	19.0	0.47	0.42	-20.1	-19.8	0.38	0.38
	0.64	42.3	37.4	0.94	0.83	-44.5	-38.9	0.85	0.74	18.1	16.1	0.40	0.36	-18.5	-17.0	0.35	0.32
	0.96	37.9	30.7	0.84	0.68	-41.7	-29.3	0.79	0.56	15.4	14.2	0.34	0.32	-15.3	-13.2	0.29	0.25
	1.28	35.7	29.8	0.80	0.66	-30.6	-23.6	0.58	0.45	13.6	12.9	0.30	0.29	-11.9	-10.9	0.23	0.21
	1.92	33.2	24.2	0.74	0.54	-27.7	-16.7	0.53	0.32	10.8	7.9	0.24	0.18	-9.8	-8.8	0.19	0.17
	2.56	27.7	11.0	0.62	0.24	-16.5	-6.8	0.31	0.13	7.8	3.5	0.17	0.08	-7.1	-3.4	0.14	0.06
3.84	6.3	6.1	0.14	0.14	-4.3	-3.7	0.08	0.07	2.4	2.6	0.05	0.06	-1.3	-1.2	0.02	0.02	

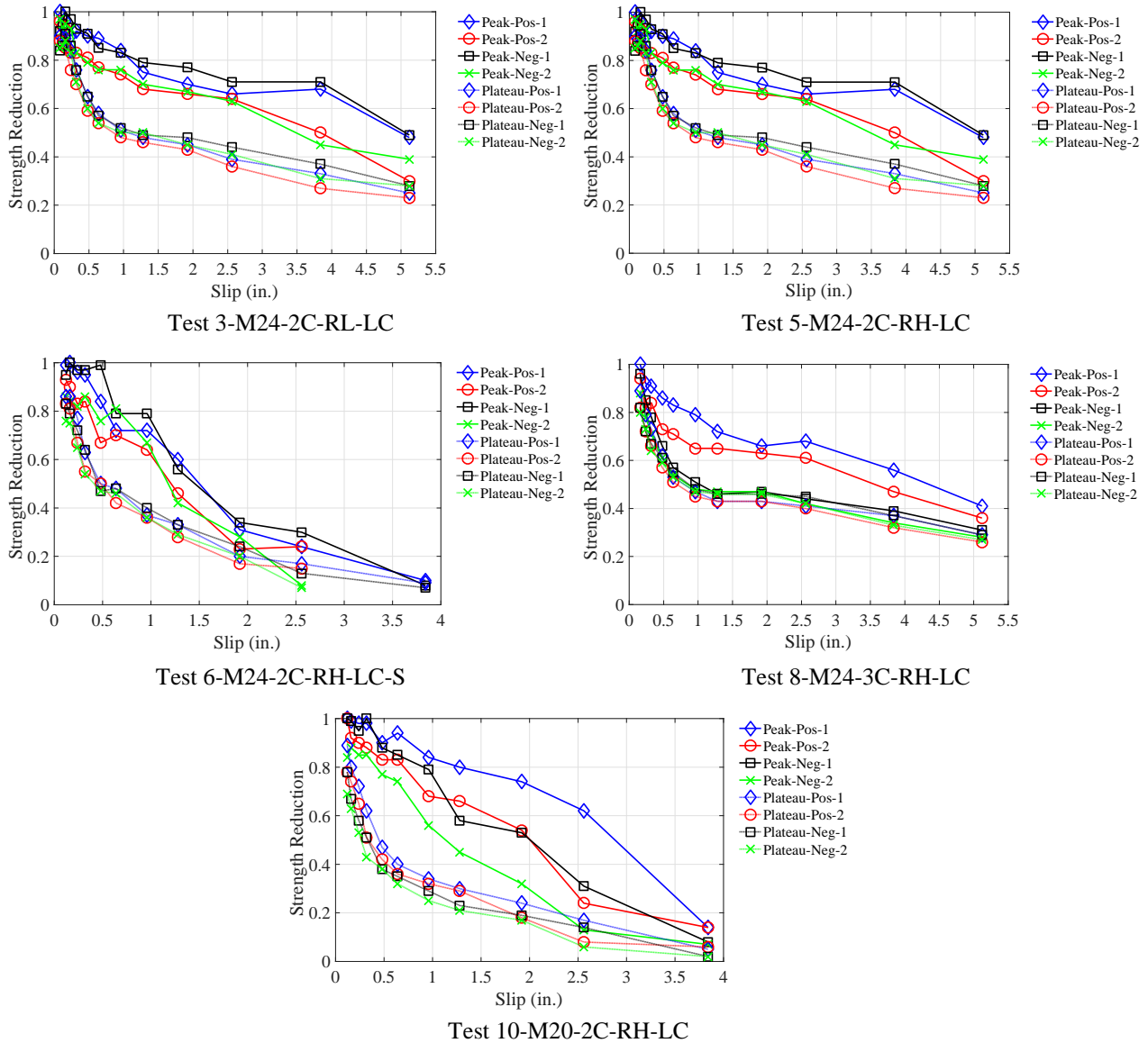


Figure 5.27 Relationship between slip and strength reduction in the cyclic tests

Based on the results from statistical analysis of load and slip characteristics of 16 pushout tests, Oehlers and Coughlan (1986) recommended Equation (5.10) to estimate the mean ultimate slip of shear studs.

$$S_{ult} = (0.48 - 0.0042f_c)d_{sh} \quad (5.10)$$

Where

S_{ult} = ultimate slip capacity (mm)

f_c = compressive cylinder strength of concrete (Mpa)

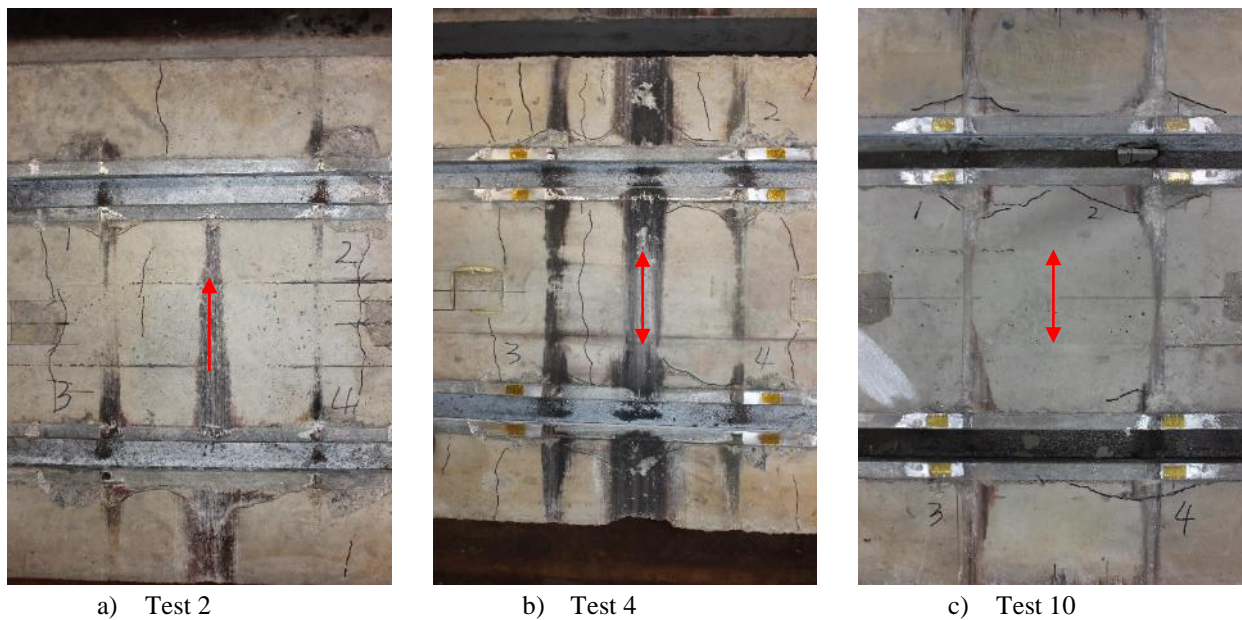
d_{sh} = diameter of the shank of a shear stud connector (mm)

Using the above equation, the ultimate slip is 0.27 in. for a 3/4" diameter shear stud embedded in 4 ksi concrete. This slip capacity is much smaller than that of the clamping connectors. In a composite beam with low composite action, the deformation demand on the shear connectors at the ends of the beams is high, and thus the beam has limited ductility after the nominal strength is reached.

5.2.6 Formation of cracks on concrete top surface

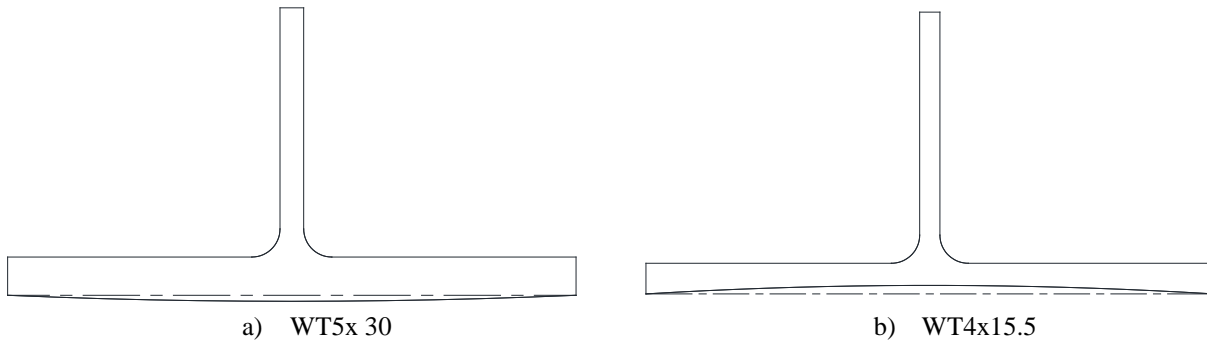
In a concrete specimen, the cracks observed during testing mostly initiate around the bolts before or close to the peak strength, and those cracks are localized in the vicinity of the bolts. After disassembling the test setup, cracks, mainly located in the middle of the plank, are found beneath the steel beam. See Figure 5.16. Most of the cracks are less than 1/16 in. wide, and the widest crack has a width of 1/2 in. in the three-channel monotonic test (i.e., Test 7-M24-3C-RH-LM).

As shown in Figure 5.28, two black stripes are always found on the concrete specimen surface, signifying the contact between the concrete plank and the edges of the steel beam flange. Hence, the frictional forces are mainly flowing along the edges of the flange. Another stripe is also seen in the middle of the plank in the tests using the larger steel section. A preliminary inspection has revealed that the flanges of the WT5x30 and WT4x15.5 sections have outlines schematically shown in Figure 5.29. The profiles of the flanges explain why the additional stripe appears in the tests where WT5x30 is used.



Note: Arrows in the figures show the loading direction.

Figure 5.28 Different black stripe patterns



Note: dashed lines are the theoretical profiles of the flange; solid lines are the actual profiles of the flange.

Figure 5.29 Schematic presentation of flange underside profiles

Concrete pry-out failure under shear cannot be the main cause of the cracks, in that the locations of the cracks do not always match the positions of the channel anchors, especially for the cracks in the vicinity of the bolts, i.e., no anchors are located below those cracks. See Figure 5.30. The peak strengths of the tests using shims (i.e., Tests 4-M24-2C-RH-LM-S and 6-M24-2C-RH-LC-S) are close to those of the tests without shims (i.e., Tests 2-M24-2C-RH-LM and 5-M24-2C-RH-LC); therefore, the shear force the middle channel anchor is subjected to should be almost identical for both types of tests. Nonetheless, no crack forms in the middle of the plank in Tests 4-M24-2C-RH-LM-S and 6-M24-2C-RH-LC-S. In addition, Eurocode 2 (CEN 2009) states that the majority of the shear force acting on the anchor channels is transferred to concrete directly through channel bearing. Only a small fraction flows into the anchors via bending of the anchor.

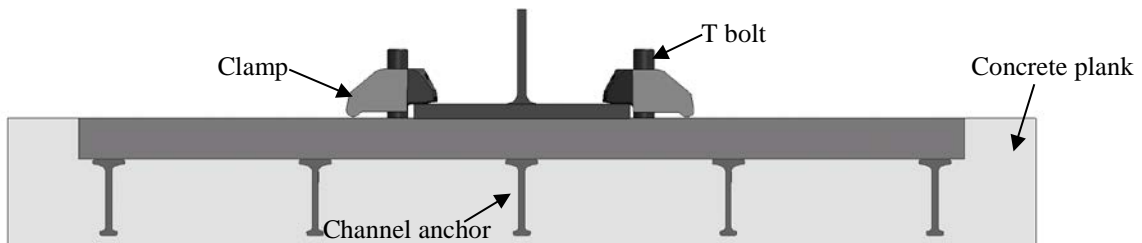


Figure 5.30 Channel anchor and bolt positions

A strut-and-tie model is utilized to explain the cracks discovered in the three-channel monotonic test, see Figure 5.31. In this model, the struts are parallel to the orientation of initial cracking, and the channel acts as the tie. The frictional force is applied on the surface of the concrete specimen. The cracks in the neighborhood of the bolts can also be interpreted with this model.

The comparison presented in Figure 5.32 does not demonstrate significant disparities between the load-slip curves of the two specimens with different reinforcement configurations, indicating that the elimination of the additional reinforcement does not induce premature concrete failure mode and strength reduction. Moreover, the wide cracks do not affect the load-slip curve and the behavior of Specimen 7. Concrete cracking is thus not regarded as a limit state in the pushout tests.

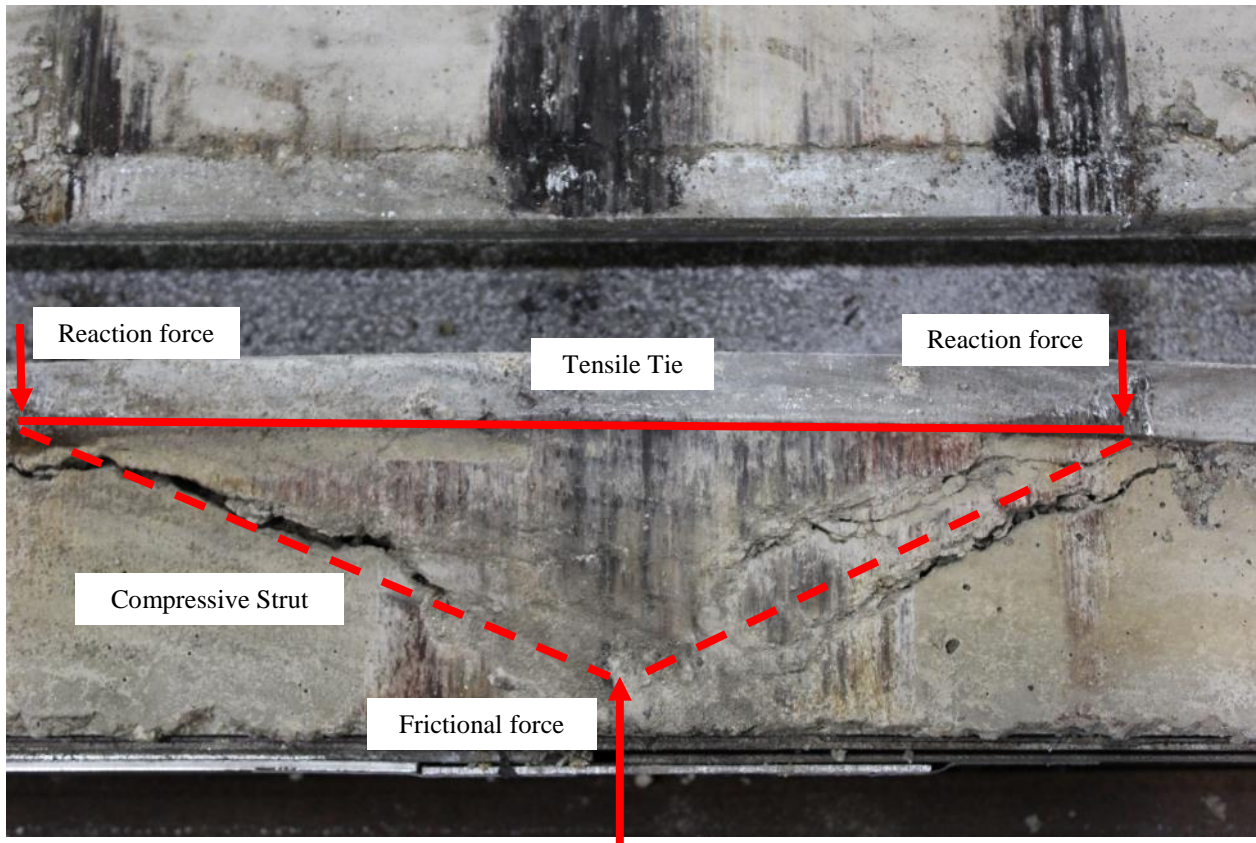


Figure 5.31 Illustration of the strut-and-tie model

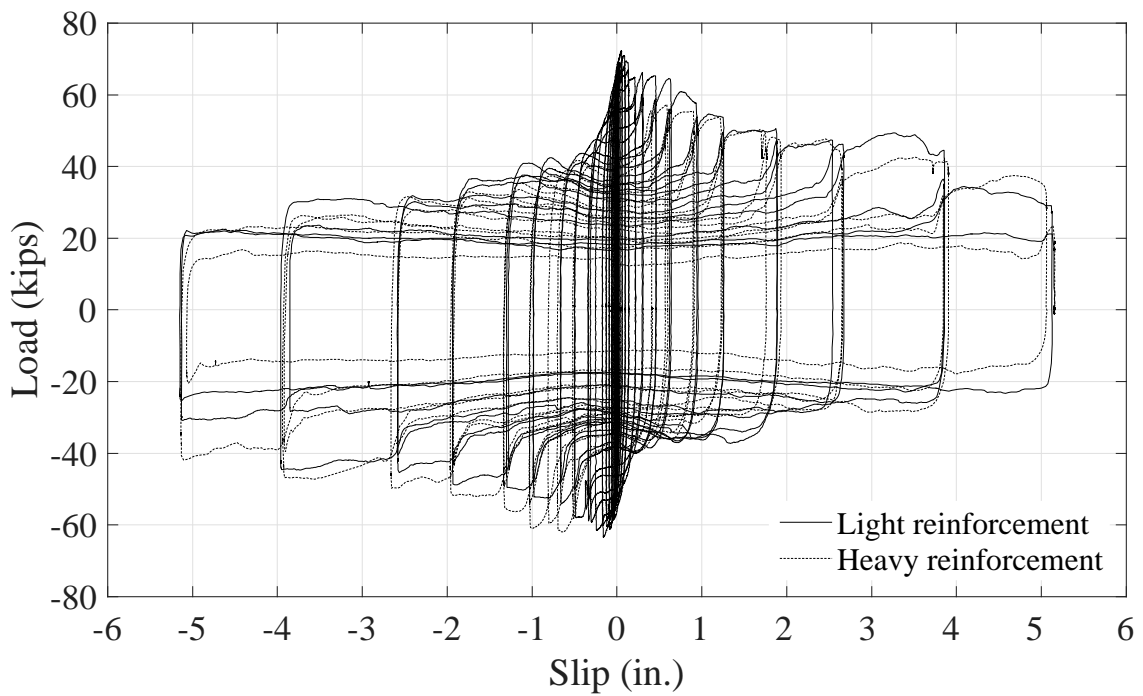


Figure 5.32 Comparison of load-slip curves between specimens with different reinforcement patterns

As shown in Figure 5.9., the normal force between the concrete plank and the steel beam becomes uneven after the steel guides are involved. Consequently, the friction is not uniformly spread across the concrete surface. As the beam is loaded in the west (or east) direction, more friction is generated at the east (or west) side of concrete. This speculation can be verified by the tapered stripe in Figure 5.28 (a), because the stripe is wider at the end where the friction is larger and narrower at the end where the friction is smaller. Likewise, in Figure 5.28 (b), as a result of the unevenly distributed friction on the concrete surface, the stripe is light in the middle and dark at both ends.

In the three-channel specimen, the outside channel is closer to the concrete edge, and therefore the frictional force is distributed over a smaller area, see Figure 5.33, increasing the tensile stresses in concrete and leading to wider and deeper cracks.

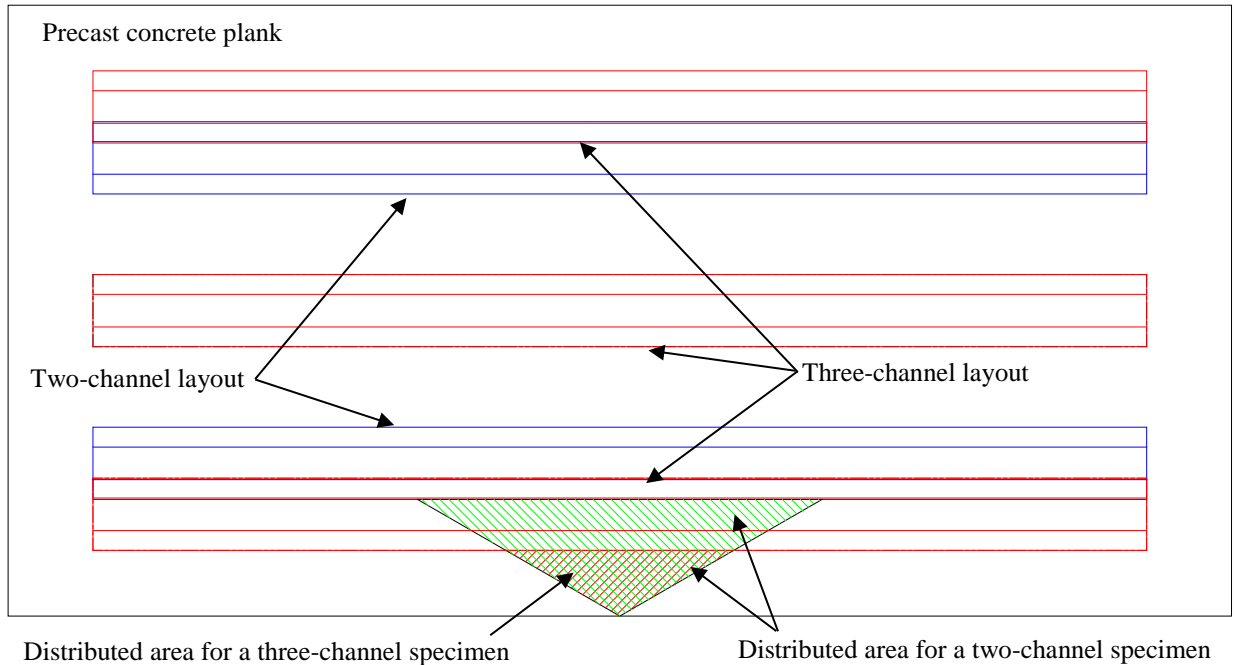


Figure 5.33 Distributed area for the frictional force

5.2.7 Behavior of the bolts and channel lips

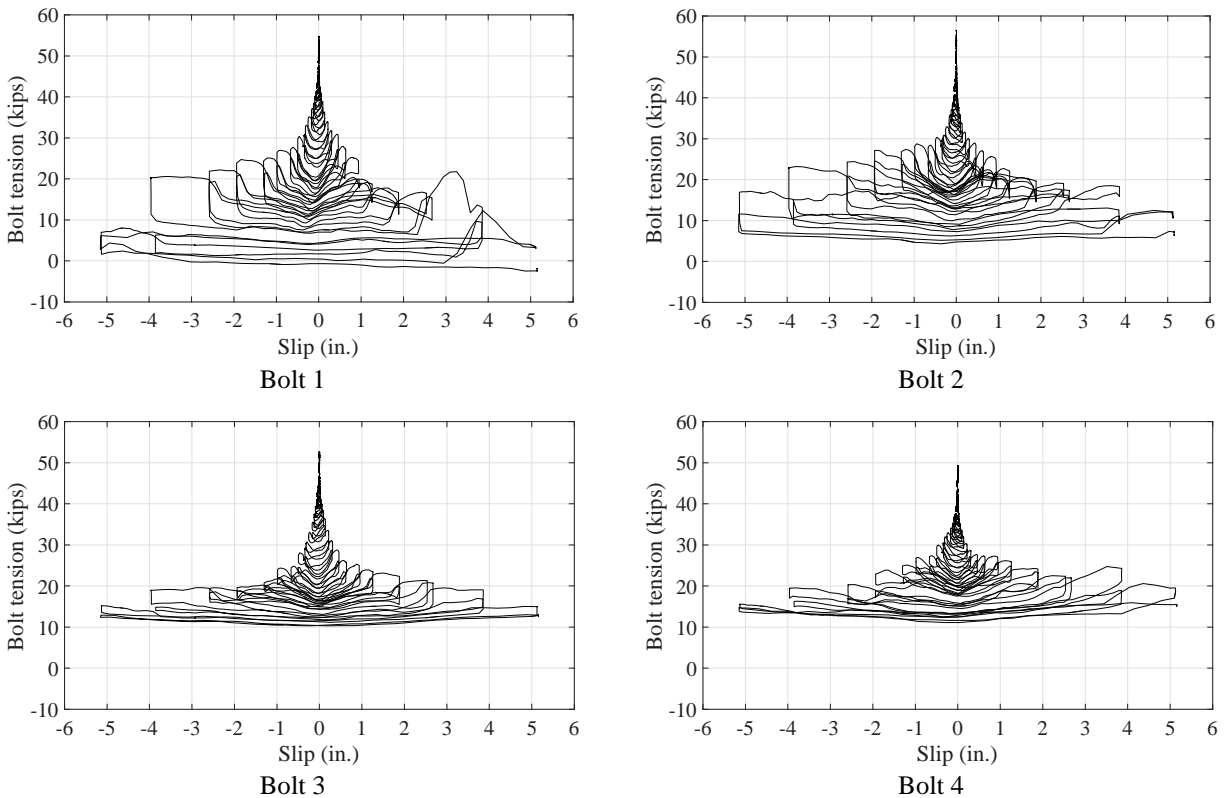
In order to estimate the bolt tension variation, bolt axial strains are measured. The model described in Appendix G.1.2 is utilized to convert the strain readings to stress values. As mentioned in Section 5.1.4, once the bolt material is yielded, the axial stress or force could be overestimated by the current model that neglects the shear stresses due to torsion and shear.

Figure 5.34 illustrates the relationship between bolt load and slip. Calculated with the average axial strain measurements, bolt tension variations throughout the tests are plotted in Appendix

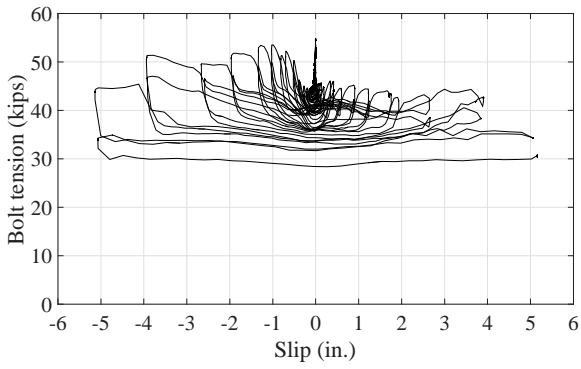
G.1.2.2. The cyclic stress-strain curves of the bolt material during the tests are also given. During the cyclic tests, bolt tensions appear to gradually decrease. Initially, the loss of pretension could be attributed to the increasing shear force. Von Mises yield criterion is presumed when converting axial strain measurements to axial stresses. In order to not breach this criterion, the axial stress may decline as the shear stress increases. After a couple of cycles, the bolt tension may be released, because the damage to the clamp teeth and beam flange removes materials, reducing the clamping force and shear resistance at the contact surface. In the monotonic test, bolt tensions maintain, and then decrease as the slip increases. These figures tend to correlate with Table 5.4 in that the bolt tension appears to be lower for the clamps which detach from the beams earlier.

As shown in Figure 5.34, the bolt axial force may be negative at larger slips, which is unrealistic since the bolt is not likely to be under compression. This could be due to the shifting of the zero signals of the strain gages at very high strains.

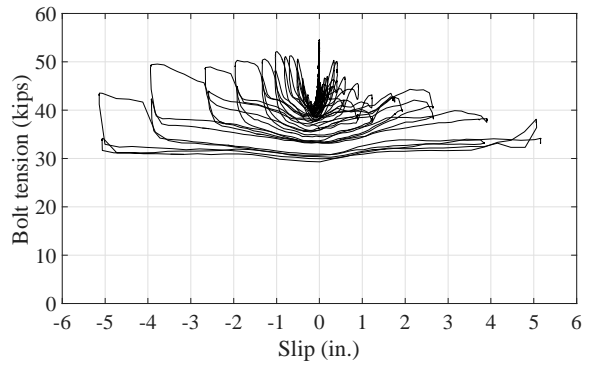
The strains measured by the rosette strain gages attached on the channel lips are shown in Appendix E.



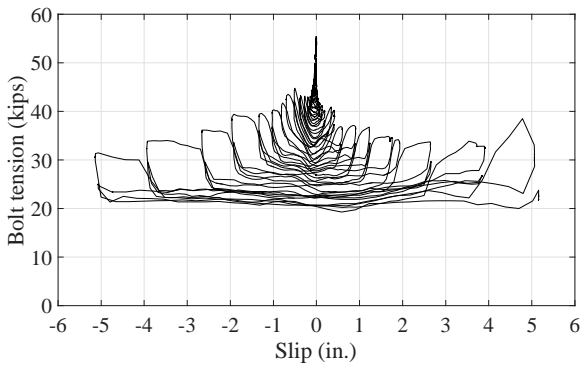
Test 3-M24-2C-RL-LC



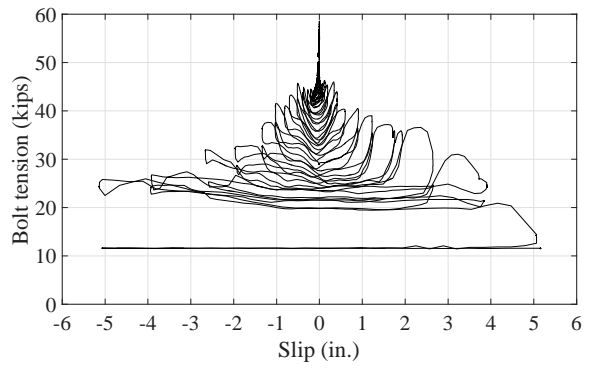
Bolt 1



Bolt 2

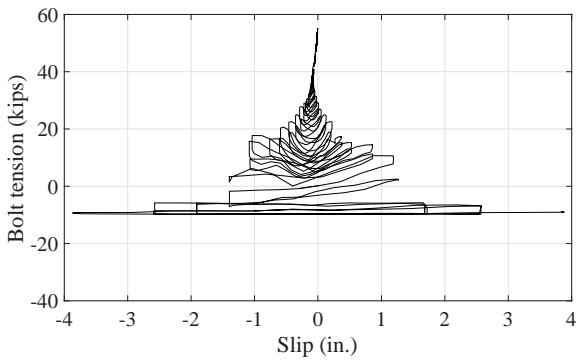


Bolt 3

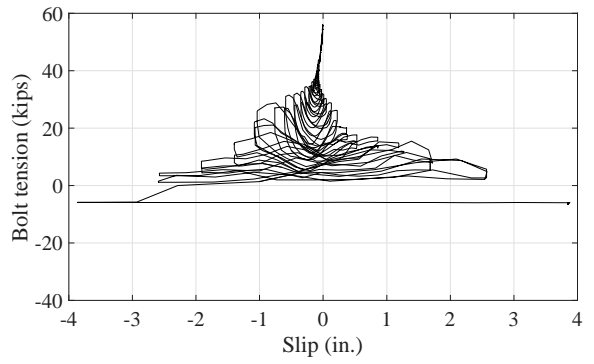


Bolt 4

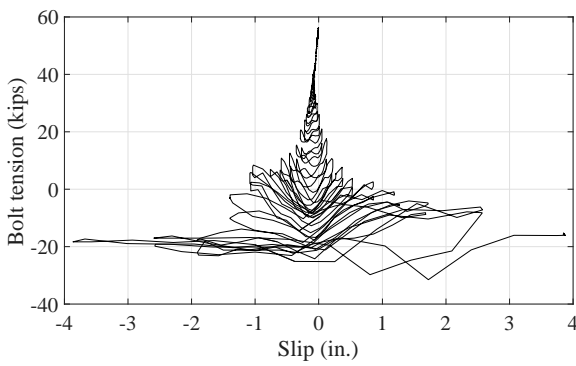
Test 5-M24-2C-RH-LC



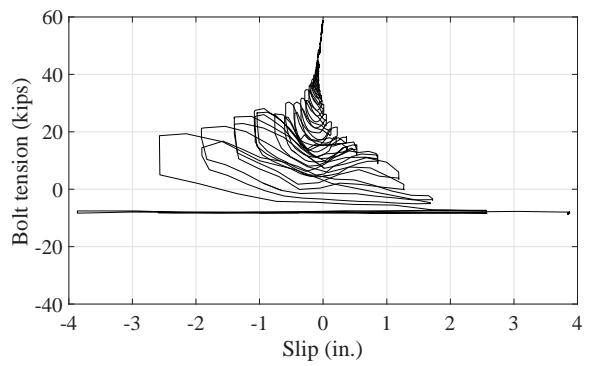
Bolt 1



Bolt 2

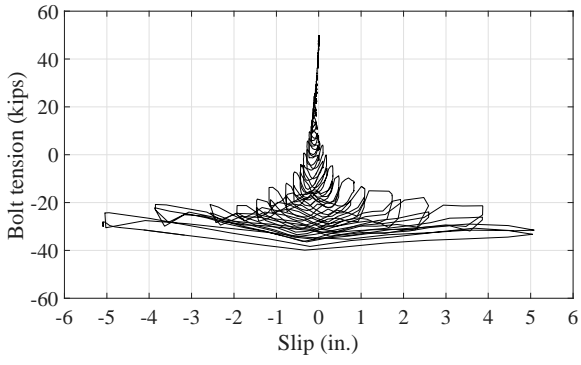


Bolt 3

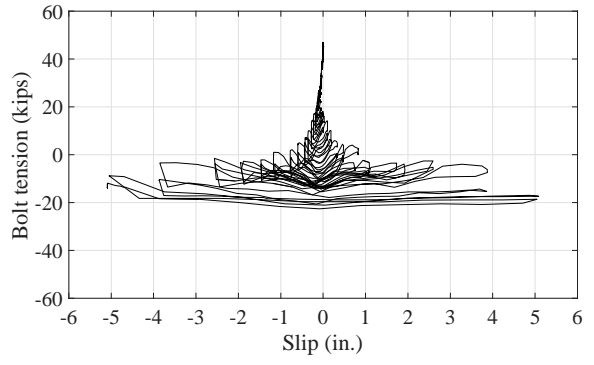


Bolt 4

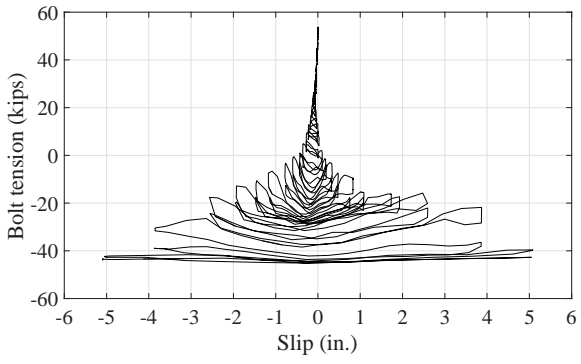
Test 6-M24-2C-RH-LC-S



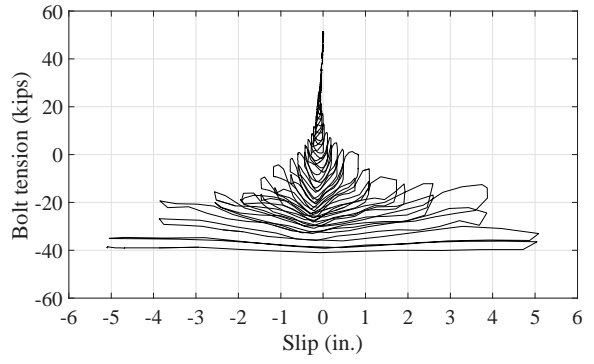
Bolt 1



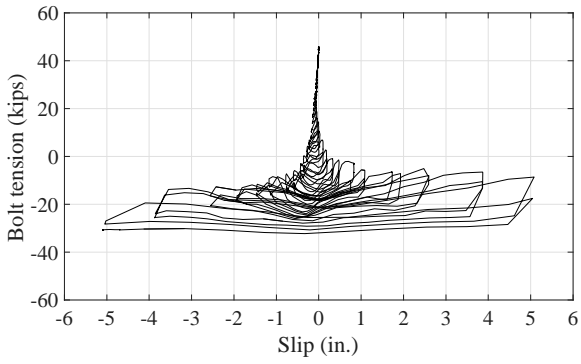
Bolt 2



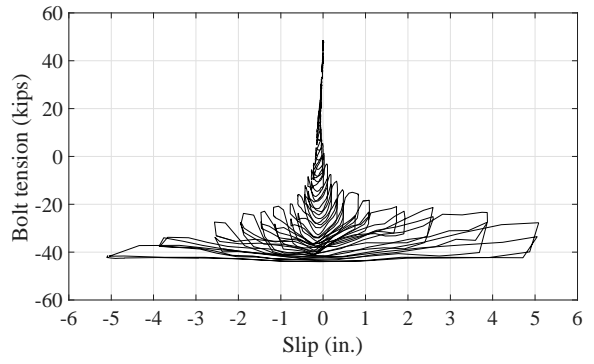
Bolt 3



Bolt 4

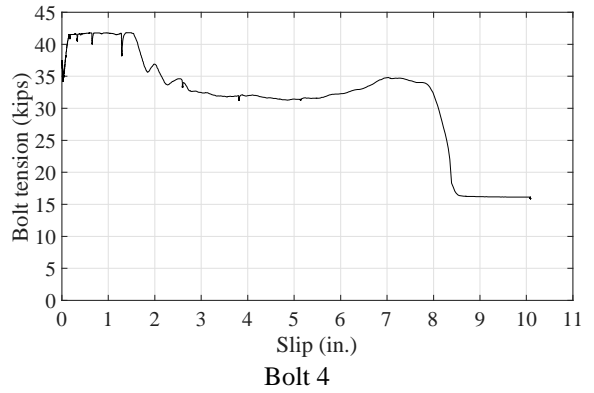
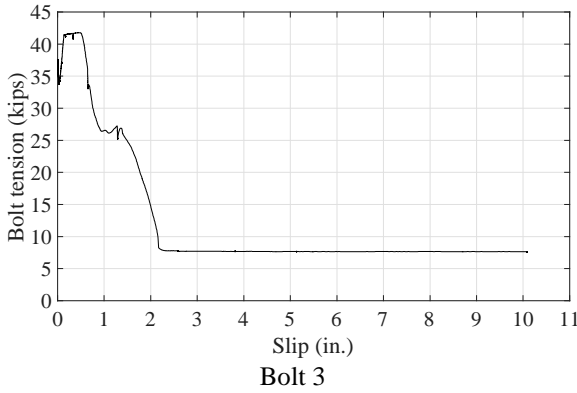
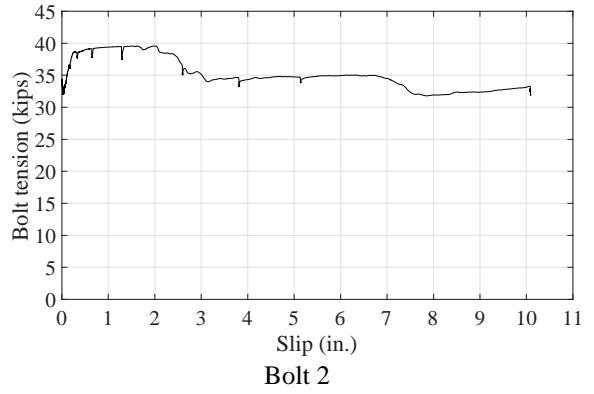
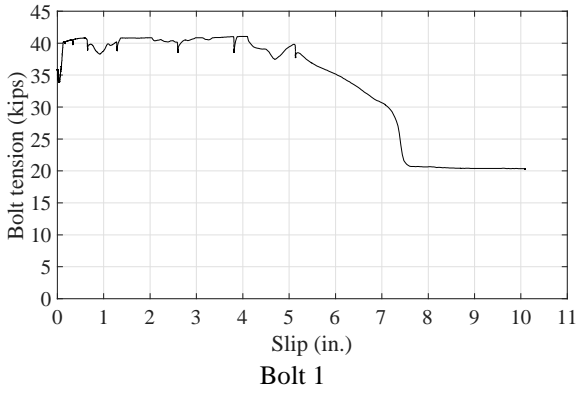


Bolt 5

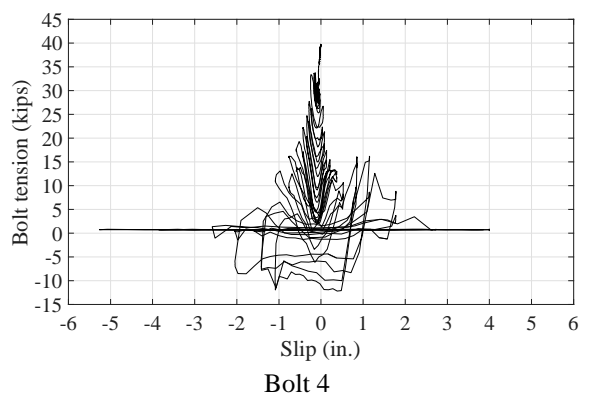
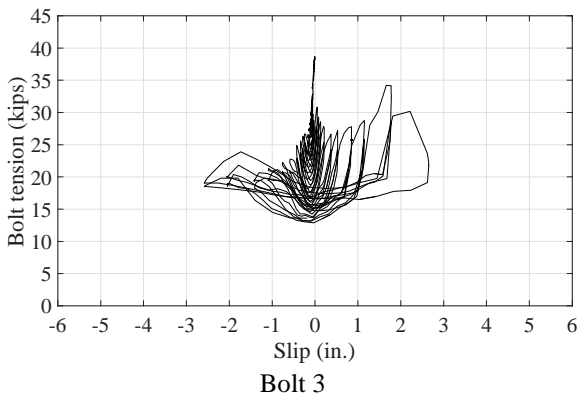
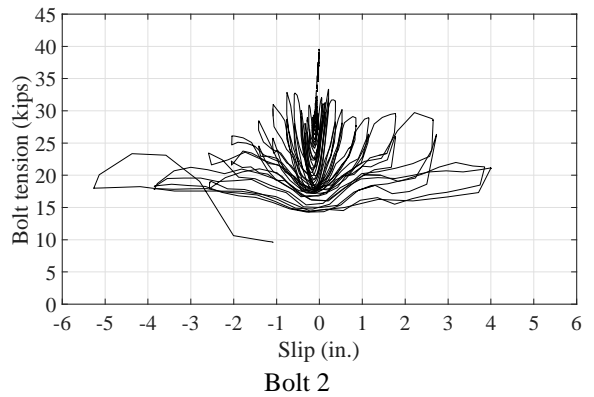
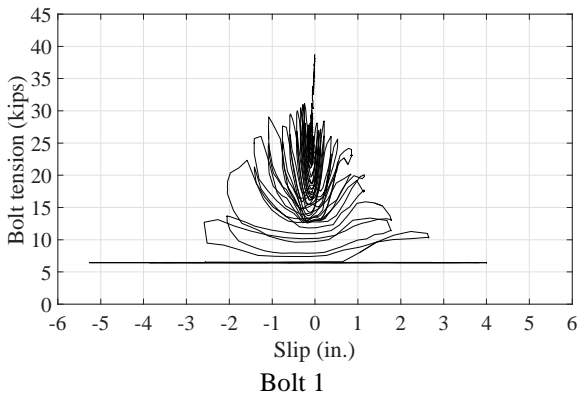


Bolt 6

Test 8-M24-3C-RH-LC



Test 9-M20-2C-RH-LM



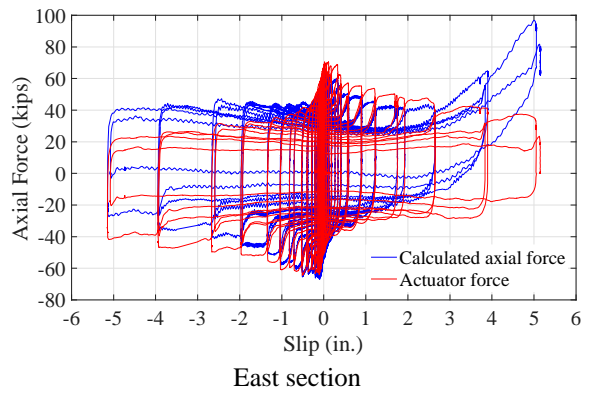
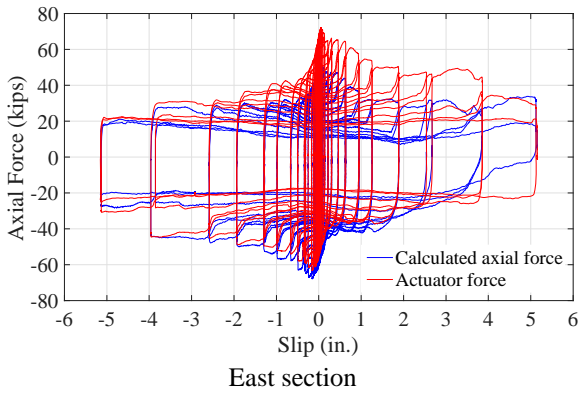
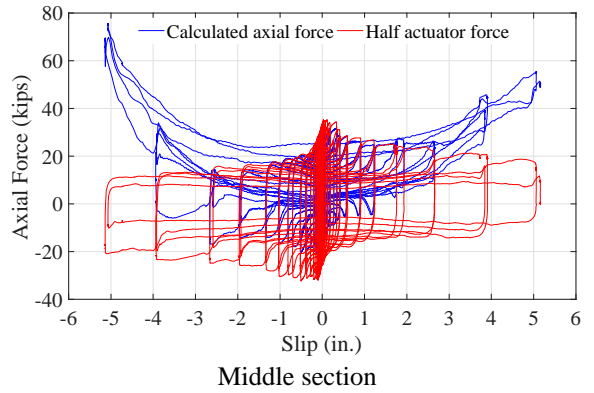
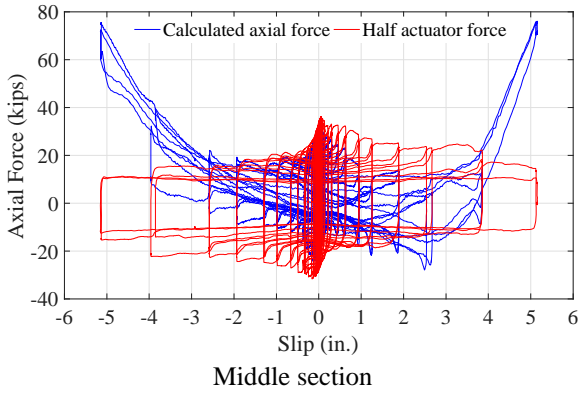
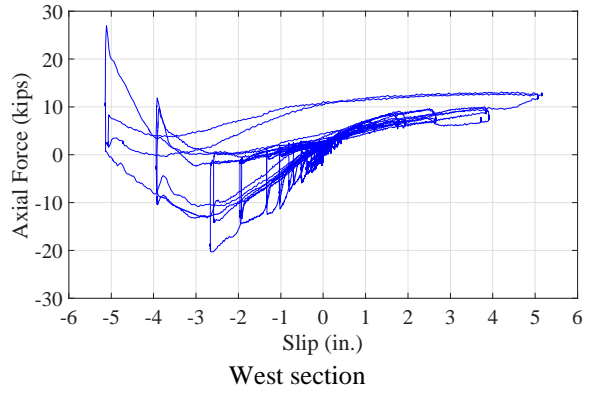
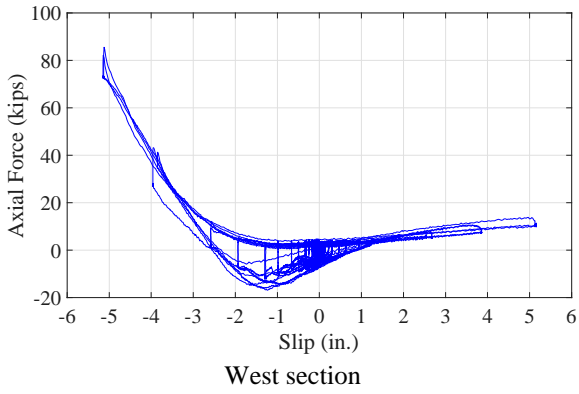
Test 10-M20-2C-RH-LC

Figure 5.34 Bolt tension vs. Slip

5.2.8 Force distribution in the system

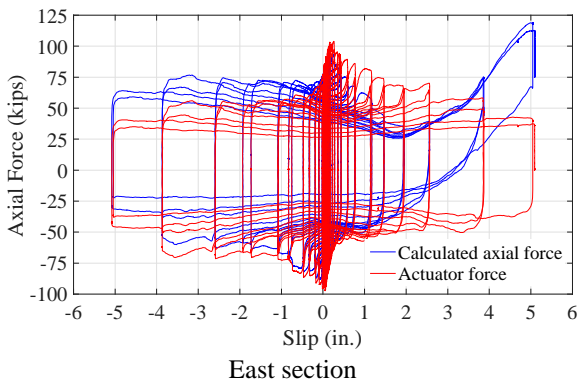
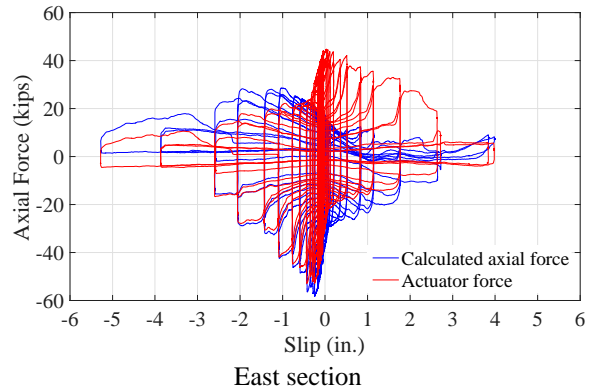
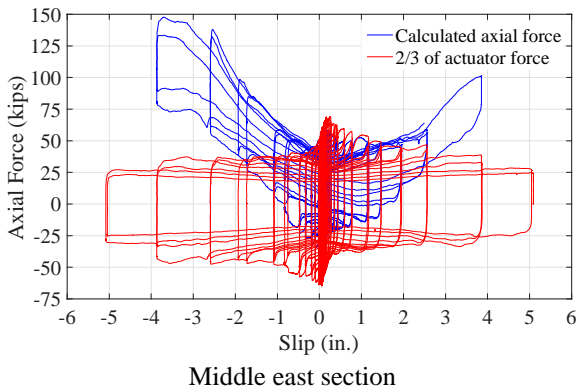
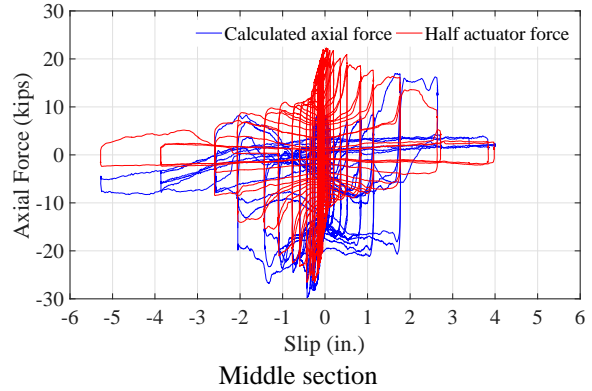
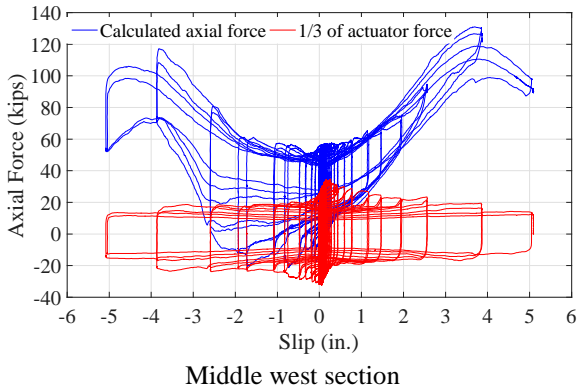
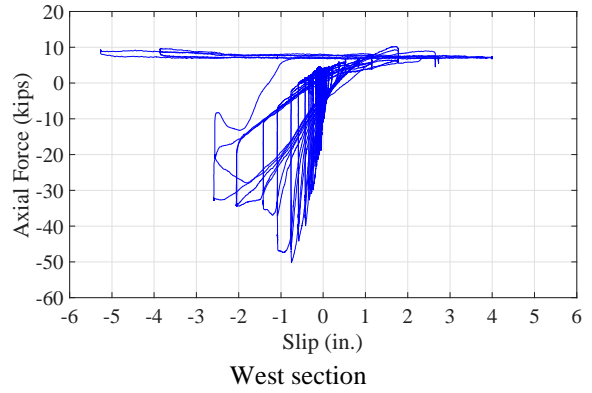
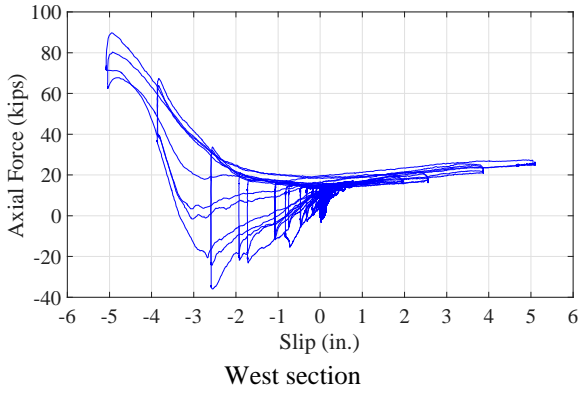
As discussed in Section 5.2.4, the clamping connectors are considered ductile. Hence, it is predicted that the applied shear is distributed among the connectors. This prediction is validated with the strain gages on the WT sections. Strain measurements at different sections of the beams are shown in Appendix E.1.2.2. It is seen that the strains are all smaller than the yield strain of the steel beam, indicating that the instrumented locations are elastic during testing.

Figure 5.35 compares the axial force calculated with the strain gage readings to the theoretical value provided that the shear force is evenly distributed among the clamps. It should be pointed out that the calculated axial forces are not negligible at the instrumented sections after pretensioning the bolts, which is contrary to the belief that these forces are trivial before shear is applied. Hence, the axial forces are offset such that the axial force-slip plots start from the origin. Common features are distinguished from the plots. As the beam moves west, the axial force at the west section does not vary much, coinciding with the fact that the west end is free. With the beam loaded east, the axial force at the east section matches the applied actuator forces. When the strain gages approach the clamps, compressive strains are measured at numerous spots on the selected sections, and compressive axial forces are thus obtained.



a) Test 3-M24-2C-RL-LC

b) Test 5-M24-2C-RH-LC



c) Test 8-M24-3C-RH-LC

d) Test 10-M20-2C-RH-LC

Note: positive value represents compressive force; negative value represents tensile force.

Figure 5.35 Section axial force vs slip

5.2.9 Response of the channel anchors and reinforcement

Rosette strain gages are attached to the channel anchors to estimate the tensile force and the in-plane shear force which the anchors have to be designed for. The out-of-plane forces acting on the anchors are assumed to be negligible, and the anchors are in a two-dimensional plane stress state. The tensile stress and the shear stress can be recovered from the strain gage data using the procedures provided in Appendix G.1.3. In addition, the Von Mises stress is calculated to ascertain whether the anchor behaves elastically because this process is no longer applicable when the material yields.

It is noted that shear stress is generated in an anchor during bolt pretension. The reason could be that asymmetry occurs occasionally, with one side of the bolt head and the channel lips taking more force than the other side. This argument could be supported by the discrepancy between the axial strain measurements from the gages attached on the same bolt. The fluctuation of the shear stress could be attributed to the varying cyclic shear force applied to the beam.

Uniaxial strain gages are attached on the reinforcement to figure out whether the reinforcement functions to control the crack propagation in the specimen. The measurements from existing gages indicate that the tensile stresses in the reinforcement are low, as shown in Figure E.7 in Appendix E.

5.3 Finite element analysis

Finite element models are developed in ABAQUS/CAE and analyzed using a central difference algorithm within ABAQUS/Explicit, which is effective for simulations containing material failure and contact. This procedure can be used for quasi-static problems if the loads are applied sufficiently slowly. Unlike the implicit method which iterates to solve a nonlinear problem, the explicit method solves the problem by advancing the kinematic state incrementally (ABAQUS 2011). Hence, the implicit method could be computationally expensive when the model has a large number of degrees of freedom (DOF), and convergence may be an issue, particularly for a problem containing contact.

5.3.1 Finite element model and mesh

Cast-in channels are meshed with both eight-node reduced integration brick elements (C3D8R) and six-node reduced integration triangular prism elements (C3D6R). Steel beams and concrete planks are meshed with C3D8R only. Due to the complex geometry of the clamps and the bolts, four-node tetrahedron elements (C3D4) are employed. Reinforcement is modelled using two-node three-dimensional truss elements (T3D2).

As a result of shear locking, the displacement is usually underpredicted in an analysis when the load mainly produces bending in the model, and fully integration linear solid elements are used for the mesh. Shear locking can be eliminated by using reduced integration elements which have fewer integration points than the full integration elements and are computationally more efficient. The reduced integration elements lose the resistance to certain type of deformation; and therefore ABAQUS automatically adds a small amount of artificial “hourglass stiffness” to avoid the propagation of the spurious modes. In this analysis, enhanced hourglass stiffness is used to avoid excessive element distortion.

5.3.2 Boundary conditions, load applications and contact

The boundary conditions for the model are shown in Figure 5.36. A symmetric boundary condition is defined such that nodes on these surfaces are prevented from translating in the Z direction and rotating in the X and Y directions.

The loading process can be divided into two steps. Pretension is first applied by assigning a thermal expansion coefficient and temperature change to the bolts, creating thermal shrinkage and generating tensile forces in the bolt shank because of the constraints at the bolt ends. The steel beam flange is then loaded in the X direction using displacement control. In order to obtain a quasi-static solution, it is essential to apply the loading slowly and smoothly to minimize dynamic effects. An optimal loading rate is found to be 0.003125 in. /s.

A tie constraint is defined for a surface pair where the surfaces are attached using slip-critical connections, making all the active degrees of freedom equal for the surface pair. The interaction between the concrete plank and the reinforcement is simulated using an embedded constraint. Only the translational degrees of freedom of the embedded reinforcement are constrained to those of the corresponding points in the plank. The contact behavior between surfaces is defined in the normal direction and the tangential direction. “Hard contact”, the default normal behavior in ABAQUS, puts no limit on the magnitude of the contact pressure when the contact restraint is activated once the surface clearance is zero. The contact restraint is removed when the surfaces separate, and the contact pressure becomes zero or negative. A penalty formulation is used to characterize the behavior along the interface. In this formulation, no limit is placed on the shear stress, and an elastic slip is used that generates a small amount of relative movement between the surfaces when they are still sticking. The frictional coefficient is taken as 0.4 for all the surfaces, except for the contact between the steel beam and the Teflon sheets where the frictional coefficient is 0.1. General contact, rather than the contact pair algorithm, is selected to automatically select potential contact surfaces.

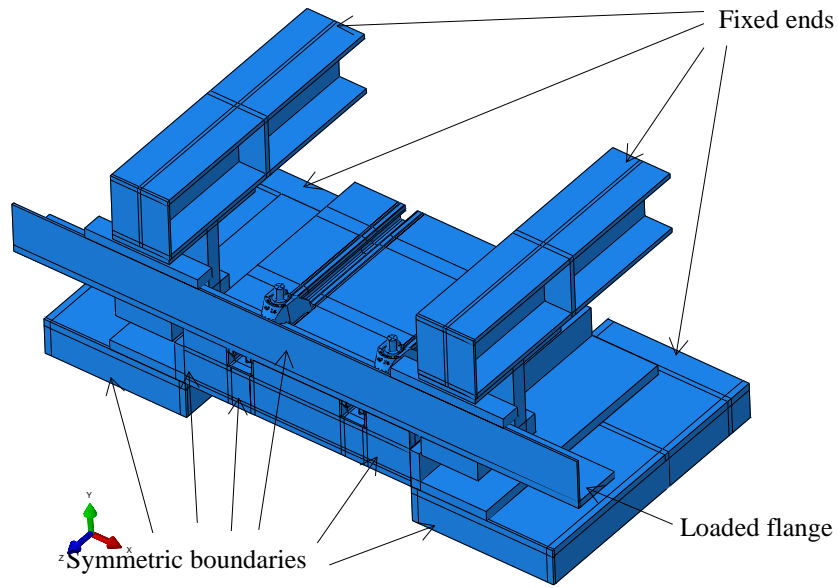


Figure 5.36 Test setup assembly and boundary conditions

5.3.3 Material model for concrete

A concrete damaged plasticity model is used to model the concrete plank. The concrete model assumes the nonassociated flow rule, and the plastic potential function and the yield function are different. The Drucker-Prager hyperbolic function is used to define the direction of the plastic flow, while the yield function is based on the model proposed by Lubliner et al. (1989) and modified by Lee and Fenves (1998). The compressive stress-strain curve proposed by Popovics (1973) is employed for this analysis, see Equation (5.11). The elastic modulus can be calculated using Equation (5.12). The Poisson's ratio is taken as 0.15.

$$f_c = f'_c \frac{\varepsilon_c}{\varepsilon'_c} \frac{n}{n - 1 + \left(\frac{\varepsilon_c}{\varepsilon'_c}\right)^n} \quad (5.11)$$

$$E_c = 57,000 \sqrt{f'_c} \quad (5.12)$$

Where,

f_c = concrete compressive stress

f'_c = concrete peak compressive stress

ε_c = concrete compressive strain

ε'_c = concrete compressive strain at peak stress

n = normalized modulus of elasticity = $0.4 \times 10^{-3} f'_c + 1$

The default parameters specified in ABAQUS for the concrete damaged plasticity model are used to characterize the plastic behavior under general stress and stress state. The parameters include: dilation angle = 38° , signifying the volumetric change of concrete under inelastic stress states, eccentricity = 0.1, implying the dilation angle does not vary much as the confining pressure stresses change. K_c , the ratio of the second invariant of the stress deviator on the tensile meridian to that on the compressive meridian at initial yield at a given first invariant of stress such that the maximum principal stress is negative, is equal to 0.67. The ratio of biaxial compressive yield stress to uniaxial compressive yield stress σ_{bo}/σ_{co} is taken as 1.16.

Mesh dependency, which means mesh refinement does not lead to a converged solution for the problems, exists for concrete with no or little reinforcement. As the mesh size becomes smaller, the structure can withstand more loading. Concrete also exhibits size effect, in the sense that the cracking stress depends on the specimen size (Bazant 1984). A stress-displacement curve, based on the concept of concrete fracture energy and proposed by Hillerborg et al. (1976), is defined for concrete to eliminate mesh dependency. Fracture energy is the energy needed to open a unit area of crack furnace. It is a material constant which is independent of the specimen size. The Hillerborg model assumes two regions along the crack length. In the real crack zone, the cracking process is completed and the concrete tensile stresses vanish. In the microcracked zone, however, the stress is equal to the concrete tensile strength at the crack tip and decreases as the crack width increases. Different stress-displacement curves are available for modeling tension stiffening, for instance, the linear relationship (Hillerborg et al. 1997), the bilinear relationship (CEB-FIP 1993), and the exponential relationship (Cornelissen et al. 1986). In this analysis, the exponential relationship obtained by fitting experimental results is selected to describe the post-failure tensile behavior. The mathematical model is given in Equation (5.13) and (5.14).

$$\frac{\sigma_t}{f_t} = f(w) - \frac{w}{w_0} f(w_0) \quad (5.13)$$

$$f(w) = \left(1 + \left(\frac{c_1 w}{w_0}\right)^3\right) e^{-\frac{c_2 w}{w_0}} \quad (5.14)$$

Where

w = crack opening displacement

w_0 = crack opening displacement at which the stress can no longer be transferred; equal to $160 \mu m$

c_1, c_2 = material parameters; equal to 3 and 6.93, respectively

Concrete damage variables characterize stiffness degradation when the specimen is unloaded from any point on the softening branch. The damage variables range from zero for an undamaged model to one, exhibiting complete loss of strength and stiffness. Concrete compressive damage D_c and tensile damage D_t are derived using the following expressions:

$$D_c = 1 - \sigma_c/f_c \quad (5.15)$$

$$D_t = 1 - \sigma_t/f_t \quad (5.16)$$

The damage evolution of concrete under compression and tension are shown in Figure 5.37 respectively. Since the concrete behavior in tension is defined with a stress-displacement relationship, the damage variable is also defined as a function of displacement. Considering the degraded unloading stiffness due to damage, the concrete compressive and tensile responses under cyclic loading are plotted in Figure 5.38.

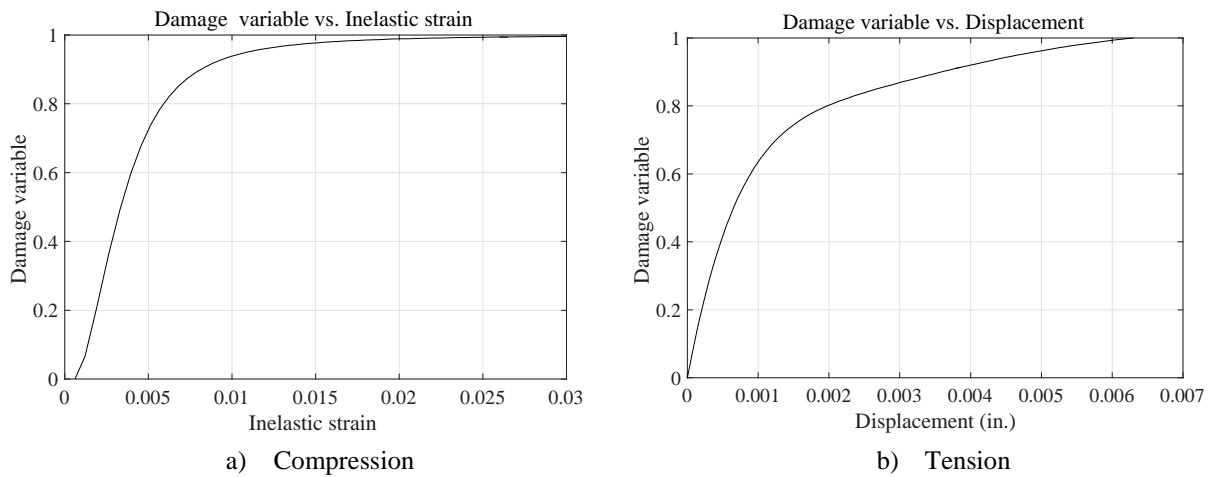


Figure 5.37 Concrete damage variable

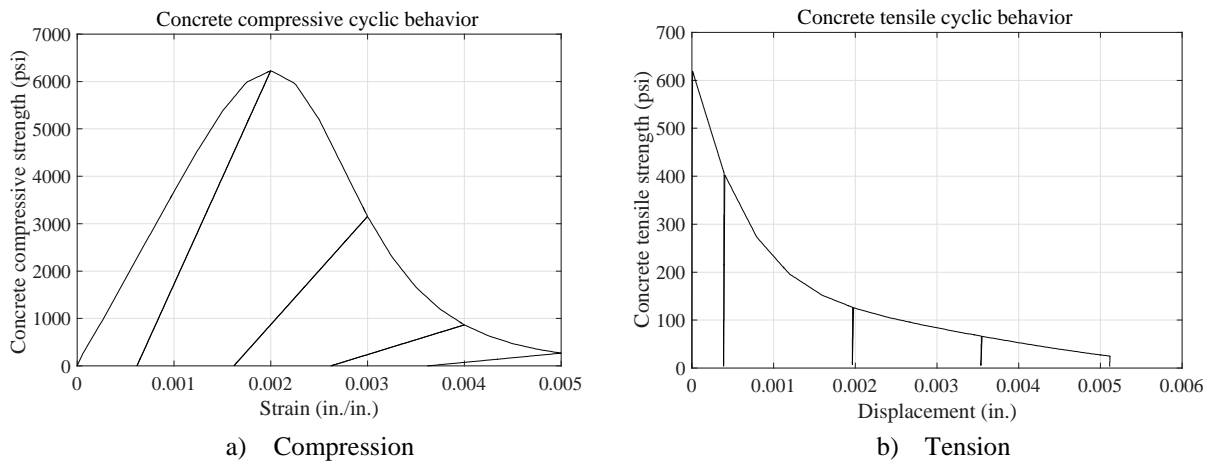


Figure 5.38 Concrete cyclic behavior

5.3.4 Material model for steel beam, reinforcement, channels and bolts

The steel beam, reinforcement, channels and bolts are simulated using the metal model which uses Von Mises yield function and associated flow rule.

Except for localized regions that may yield under the clamping force, the steel section remains elastic during the test. Elastic-perfectly-plastic material is defined for the steel beam and reinforcement. The yield stress for the steel beam and reinforcement is taken as 50 ksi and 60 ksi, respectively. The elastic modulus is taken as 29000 ksi. The mechanical behavior is assumed to be the same in both tension and compression. A bilinear relationship is assumed for the channel. All the material properties employ those obtained from coupon testing, as listed in Table 5.7. The bolt stress-strain curve used for the analysis is given in Figure G.4.

Table 5.8 Channel true stress and true plastic strain

True stress (ksi)	True plastic strain
65.3	0.000
71.8	0.029

5.3.5 Finite analysis results

The experimental result and finite element result are plotted in Figure 5.39 for Test 2-M24-2C-RH-LM. As shown in the plot, the peak strength of the finite element model is slightly larger than that of the test specimen; however, the slip at which the peak occurs is different. The reason is attributed to the friction simulation in Abaqus, which automatically chooses the penalty stiffness to ensure the elastic slip is a very small fraction of the characteristic element length.

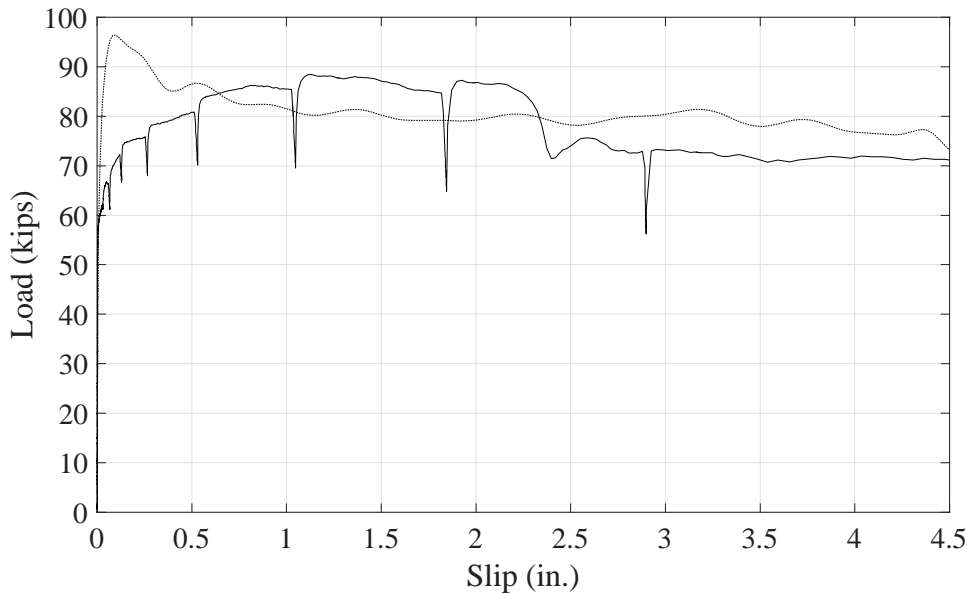


Figure 5.39 Load-slip curve comparison

The stress contour for the reinforcement is shown in Figure 5.40. The maximum stress is 13.6 ksi (94 MPa) and the strain is 469 microstrains, which is similar to the measured strains depicted in Figure E.7 in the cyclic specimens. The comparisons between the finite element model and the test in Figure 5.41 through Figure 5.43 indicate the validity of the analytical model and results.

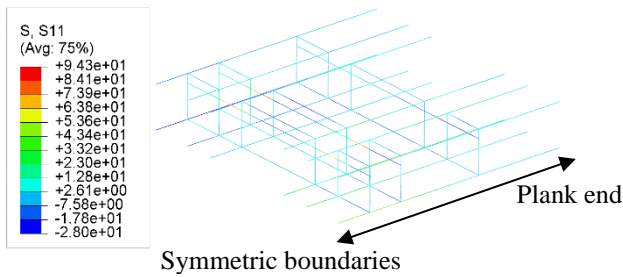
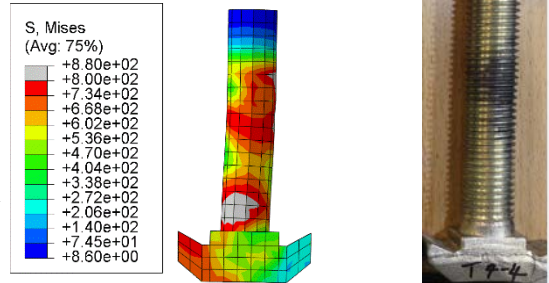
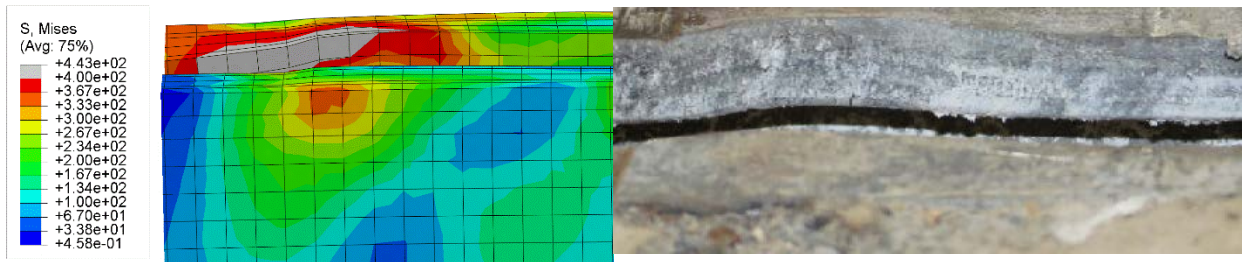


Figure 5.40 Reinforcement stress contour



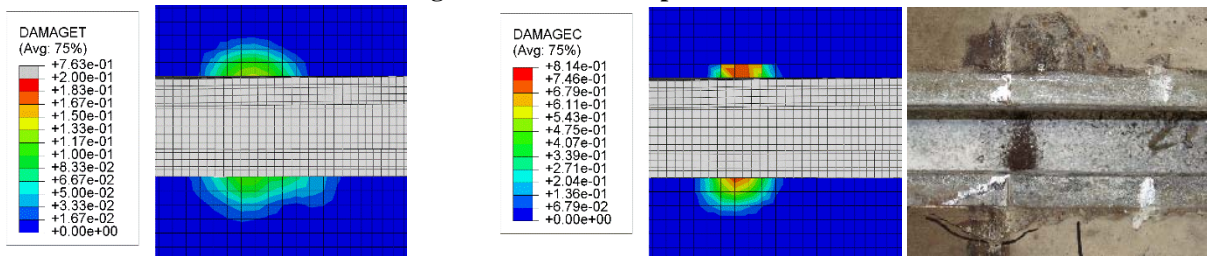
a) Finite element model b) Test

Figure 5.41 Bolt deformation



a) Finite element model b) Test

Figure 5.42 Channel lip deformation



a) Finite element model b) Test

Figure 5.43 Comparison of Concrete damage in the finite element model and test specimen

Using the analytical results, the relationship between bolt tension and slip is provided in Figure 5.44. As slip increases, bolt tension first decreases and then levels off. When a bolt is pretensioned, the bolt force is distributed among the clamp teeth and clamp tail. Only the force transferred to the clamp teeth contributes to the shear resistance of the system. Figure 5.45 shows the ratio of the force at the clamp teeth to the total bolt tension, which varies from 0.65 to 0.8.

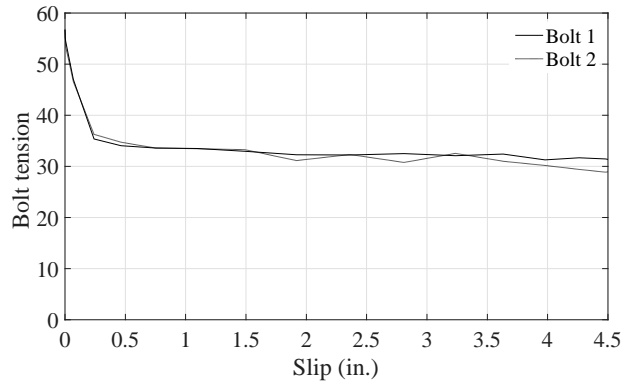


Figure 5.44 Bolt tension vs. slip

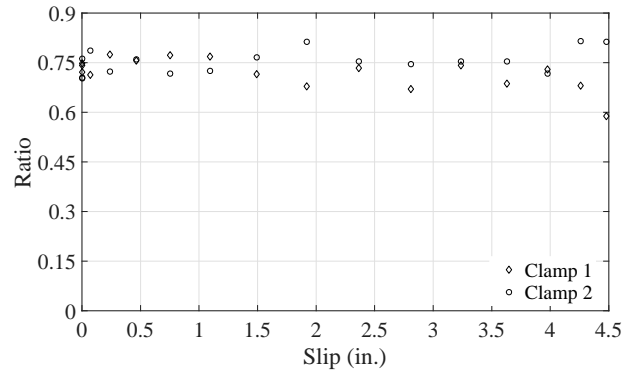


Figure 5.45 Force at clamp teeth to bolt tension ratio

5.4 Conclusions

Based on the test and analysis results presented in this chapter, the following conclusions can be reached:

- (1) Except for one bolt that fractures at the bolt heads, most bolts in the pretension tests ultimately fracture due to excessive torsional deformation. Two turns and 1.5 turns after a snug-tight condition are selected for pretensioning the M24 and M20 bolts, respectively. It is also noted that in the M24 bolt tests, moderate plastic deformation occurs in the channel lips, while the inelastic deformation of the channel lips is minor when the M20 bolts are pretensioned.
- (2) The load-slip curves indicate that the deconstructable clamping connectors using M24 bolts are ductile. Compared to shear studs which fracture at a much smaller slip, the M24 clamping connectors can retain almost 80% of the peak strength even at 5 in. slip under monotonic loading.
- (3) Shims are used for specimens using M24 clamps and thin flange sections, and undesirable load oscillation is observed due to a stick-slip mechanism, although the strength is not affected. Usage of the selected shims between the clamp and the flange may not be recommended in this application.
- (4) Compared to the monotonic specimens, the peak strengths of the cyclic specimens are lower, but stabilized in a manner that may be addressed in design provisions. This is comparable to the decrease in strength seen in headed shear connectors when subjected to cyclic loading.
- (5) After going through a couple of cycles, the strengths of the cyclic specimens begin to degrade, which could be attributed to the reduction of bolt pretension force and the

lowering of frictional coefficient as a result of the abrasion between the clamp teeth and steel flange and between the concrete plank and steel beam.

- (6) Considerable load drop is seen after 0.68 in. slip in the load-slip curve of the monotonic specimen using M20 bolts. Large rotation and complete disengagement of some clamps are noted. With the steel blocks inserted into the channels to support the clamp tails, the cyclically loaded specimen performs better than the corresponding monotonic specimen even though all the clamps ultimately lose contact with the beam flanges.
- (7) In terms of strength and state of cracks, the specimen with light reinforcement does not perform worse than the specimen with heavy reinforcement. This implies that the additional reinforcement are not engaged which are designed to bridge potential cracking planes due to channel anchor forces, which is further proved by the low stresses in the reinforcement.
- (8) A strut-and-tie model is used to explain the formation of cracks which are induced by the friction acting on the concrete surface, rather than concrete pryout failure. Since the frictional force distributes in a non-uniform manner, the damage concentrates on one side of the concrete plank when it is loaded monotonically.
- (9) Bolt axial strain measurements throughout the cyclic tests indicate that bolt tension gradually decreases. When the slip is small, the tension decrease is attributed to the shear force acting on the bolt, while the bolt tension releases as the slip increases. The bolt tension vs. slip plots appear to correlate with the clamp detachment sequence.
- (10) The shear force applied to a steel beam is distributed among the clamps, demonstrating the potential of using clamps as shear connectors in composite beams. Unfortunately, the strain gage measurements are “contaminated” when the gages are close to the clamps, and the calculated axial forces of the instrumented sections cannot represent the actual axial forces.
- (11) In order to simulate the pushout test specimen, a finite element model is developed which takes into account material nonlinearly, geometric nonlinearly and contact between different components. The finite element model predicts the peak strength, but the slip at which the peak strength occurs in the test is achieved more gradually than the computational simulation.

6. Beam Tests

Full-scale beam tests are essential in evaluating realistic behavior of the shear connectors. As discussed in Section 2.3, deducing the ultimate strength of shear connectors from beam test results is problematic. Hence, beam tests are usually used as confirmatory tests where the proposed design strength equations or load-slip curves obtained from pushout tests are validated. In prior research, various configurations have been used for composite beam tests. For example, most composite beams are loaded on the concrete slabs, but the loading is applied directly to the top flange of the steel beam through a concrete pocket in the tests conducted by Ernst et al. (2006). Alternatively, the loading could be applied across the whole concrete slab (Grant et al., 1977; Ranzi et al., 2009) or only the region above the steel flange (Easterling et al., 1993). Ductile behavior was observed for almost all the composite beams with steel headed stud anchors connecting concrete and steel, and the predicted ultimate flexural strengths based on the rigid plastic assumption match the test results very well (Ranzi et al., 2009).

At the time of the writing of this report, the beam tests are not yet completed. The test setup is outlined in this report to reflect the scope of the research. Future publications will incorporate the results of the beam tests and associated conclusions and design recommendations for this structural system.

6.1 Test setup and test matrix

The full-scale composite beam test setup is provided in Figure 6.1. The test specimens consist of 30-foot W-shape beams, each with fifteen 2-ft.-wide planks attached using clamping connectors. The composite beam span is 30 ft., but the total beam length is 32 ft. due to the 1 ft. extension of the steel beam at each end to facilitate out-of-plane support and accommodate the deflection of the beam. The planks are 8 ft. long, which provides a sufficient composite slab width to prevent concrete premature failure in a narrow slab (Grant et al. 1977). The actuator force is spread using the spreader beams to simulate uniform loading on concrete slabs. Stiffeners are welded on the spreader beams to increase their torsional resistance and eliminate instability during testing. The bolted connection between the top spreader beams and the bottom spreader beams not only enhances the stability of the spreader system but also facilitates test setup assembly. Braces at both sides of the slab are engaged if the slab torques or displaces laterally due to uneven loading. Potential twisting of the steel beam is inhibited by the guides at the ends of the section. A pin support and a roller support are used to simulate the actual boundary conditions of a simple beam. Teflon sheeting is attached to surfaces where frictional forces are undesirable, such as the interface between the steel beam and the end guides. Figure 6.1 shows the components in a composite beam specimen. Shop drawings for the composite beam test setup can be found in Appendix D.

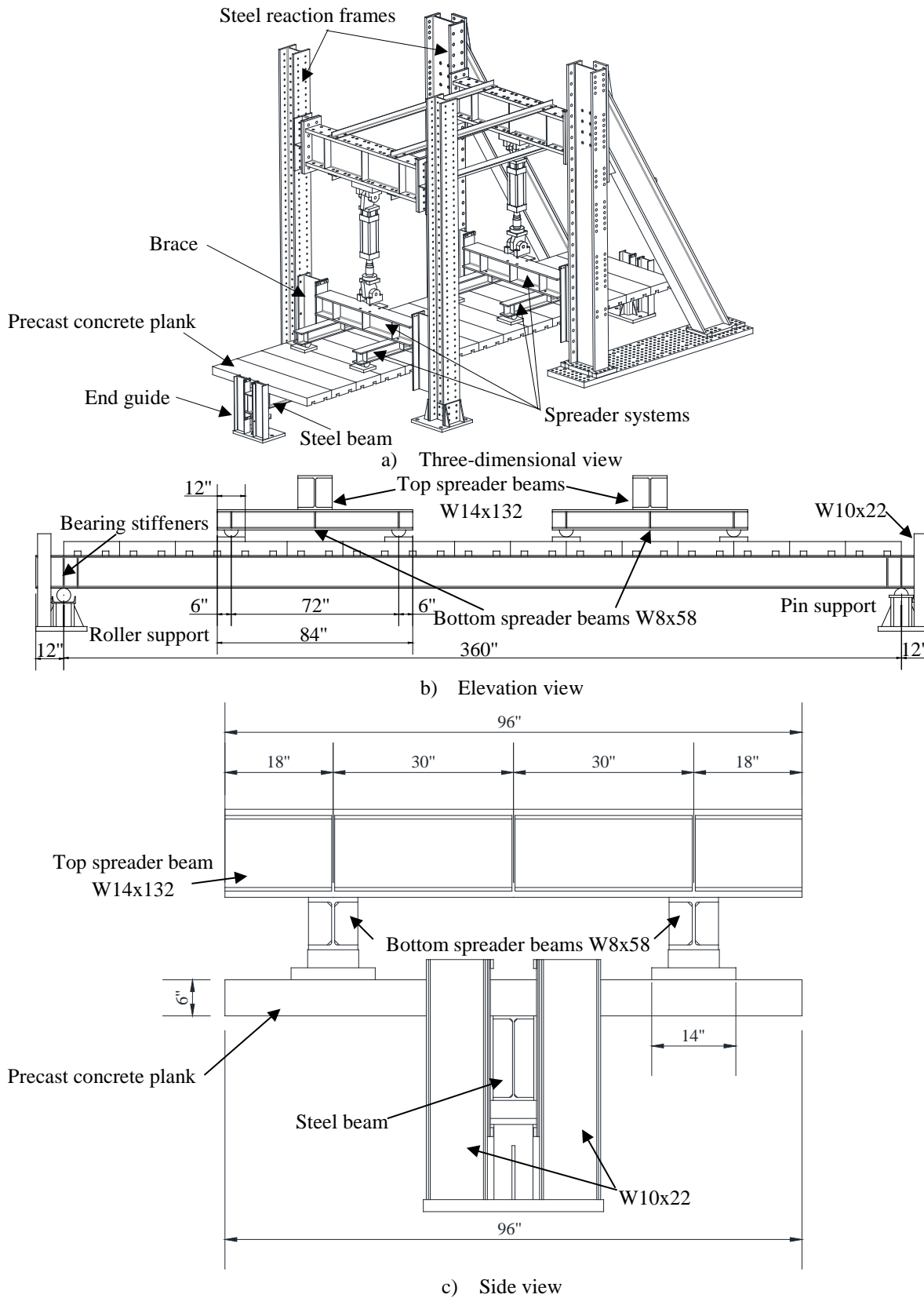


Figure 6.1 Different views of test specimen

Generally, only partially composite beams with relatively low composite action (<50%) are tested, since the shear connector behavior governs the strength and stiffness of the beams. However, fully composite beams are also designed and tested in this research to verify the design methodology and obtain a comprehensive understanding of the deconstructable composite floor system under gravity loading. A total of four specimens are designed and tested to document the progression of damage in composite beams, see Table 6.1.

The naming convention of the specimens is explained using Test 2-M24-1C-RL, with 2 describing the test sequence of the beam, M24 describing M24 bolts, 1C describing one channel embedded in each of the concrete planks, RL describing light reinforcement pattern. The parameters include bolt diameter, number of channels per plank, steel beam section, and reinforcement configuration. The amount of composite action is also varied such that composite beams with a wide range of composite action can be investigated. All the planks are connected to the beam flanges using clamps in the current design. In the future, it might be instrumental in studying the effect of not attaching certain planks to the beams. In Table 6.1, the degree of shear connection is calculated using both nominal steel strength and tested steel strength. The first type of composite action is usually referred to in design practice, while the other type is more important when exploring the behavior of a composite beam.

Table 6.1 Composite Beam Test Matrix

Composite beam #	Bolt size	# of channels per plank	Steel beam section	Reinforcement configuration	Number of bolts (clamps)	Percentage of composite action	
						Nominal	Actual
1-M24-2C-RH	M24	2	W14x38	Heavy	60	118.5%	
2-M24-1C-RL	M24	1	W14x38	Light	30	55.3%	
3-M20-3C-RL	M20	3	W14x26	Light	90	158.2%	
4-M20-1C-RL	M20	1	W14x26	Light	30	50.3%	

To simplify specimen construction, tongue and groove joints in the planks shown in Figure 1.1 are eliminated. These connections can assist load transfer between planks, but they are not believed to enhance the beam strength. The in-plane connections between the planks may not be necessary for supporting gravity loading, but they are required to ensure the integrity of the structural system under seismic loading. Therefore, Grade A36, 5/8 in. threaded rods are chosen for connecting adjacent planks in the beam test. The calculations in Appendix H. justify the selection of these rods. Spaced at a distance of 24 in., 3 in. by 2 ½ in. cutouts are needed for the threaded rod connections. Schedule 40, 3/4 in. inside diameter PVC pipes are reserved in the planks as the ducts for the threaded rods.

Two reinforcement patterns are designed for the specimens. The bars that comprise the light reinforcement configuration are designed for all the tests. Planks in Test 1 use the heavy reinforcement configuration in which additional waveform bars are utilized to bridge potential cracking planes induced by channel anchor forces. Because the load is spread across the slab width, the longitudinal reinforcement is designed to resist negative bending of the planks. Two types of U bars are placed around the cutouts. The longer type reinforces the cutout corners that are vulnerable to handling, while the shorter type restrains the propagation of potential bursting cracks caused by post-tensioning forces of the rods (ACI 2011). All the reinforcement meets the detailing requirements in ACI 318-11, see Figure G.44. The U bars and the waveform reinforcement are regarded as stirrups, and the bend diameter and the end extension are $4D_b$ and $6D_b$, respectively. The transverse loops have standard hooks, and the bend diameter and the end extension are $6D_b$ and $12D_b$, respectively. Legs of the transverse loops are spliced with a splice length of 8.5 in. The longitudinal reinforcement uses No.4 bars, and No.3 bars are chosen for the other reinforcement. The reinforcement selections enable testing of the two extremes: a fully composite beam in which concrete breakout failures are less likely, but heavily reinforced; a partially composite beam in which concrete breakout failures are more likely, but lightly reinforced. Since the lightly reinforced specimen does not fail prematurely in the pushout test, this pattern is used for three out of the four beam tests.

Concrete panels are lifted at the outer fifth points of both ends using the embedded lifting lugs inserts reduce the maximum tensile stress induced by self-weight when stripping off the formwork and pulling planks from the formwork. Calculations are included in Appendix H. to show that concrete is intact during handling.

6.1.1 Pretension test on fully threaded rods

Fully threaded rods that connect adjacent planks are pretensioned, which is essential to generate frictional forces and avoid relative sliding between adjacent planks under diaphragm forces. To reduce the tension variation in the rods, they are loaded into the inelastic range. For such long rods, the RCSC specification (RCSC 2009) requires testing that mimics the actual application to determine the nut rotation.

Because the behavior of the threaded rods during the beam test is unclear, only the rods needed for the first beam test are ordered. The length of the rods is 45 in., but they are not long enough when a load cell is placed at one end to monitor the tension variation. Hence, additional rods are requested which are 46.5 in. long, but from a heat that is different from the 45 in. long rods. During the pretension test, since the percentage of length difference is small ($\approx 3.3\%$) and the material properties are similar, the nut rotation determined for the 46.5 in. long rods is believed to be valid for the shorter rods.

Due to alignment issues, all the PVCs embedded in the concrete planks are removed before the pretension testing. Since the composite beams are shored during construction by supporting the ends of the concrete planks to avoid lateral-torsional buckling, the planks are also propped in the pretension test in a similar manner, as shown in Figure 6.2. The pretension test setup is shown in Figure 6.3a. Plank 1 is clamped to the steel beam and not allowed to move during the test. As the rods are twisted, plank 2, which seats on the beam freely, starts to move towards and bear against plank 1.

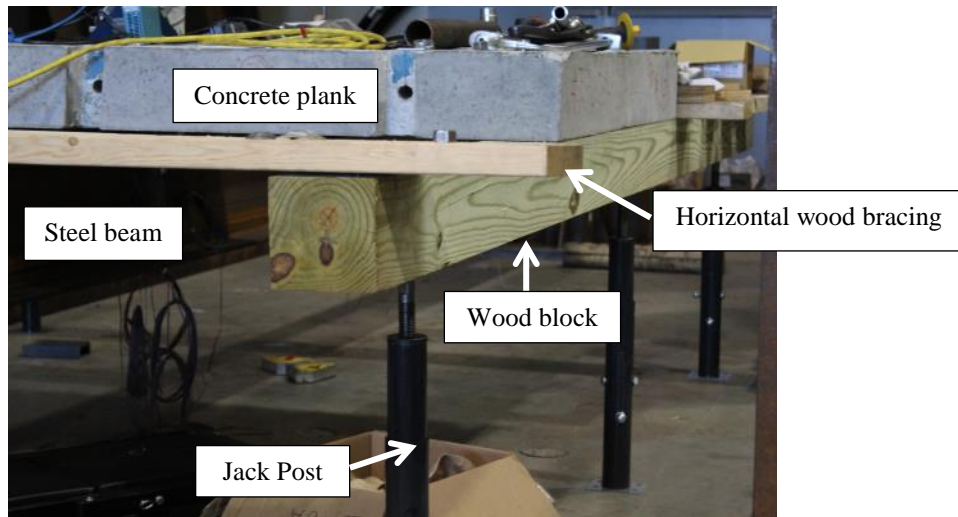
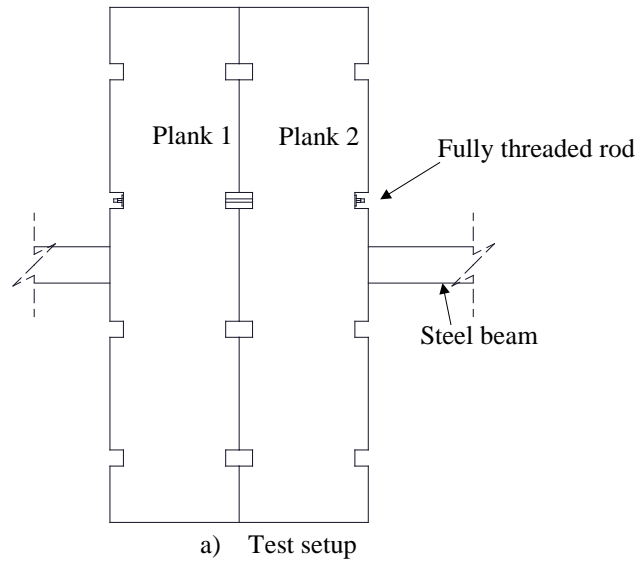
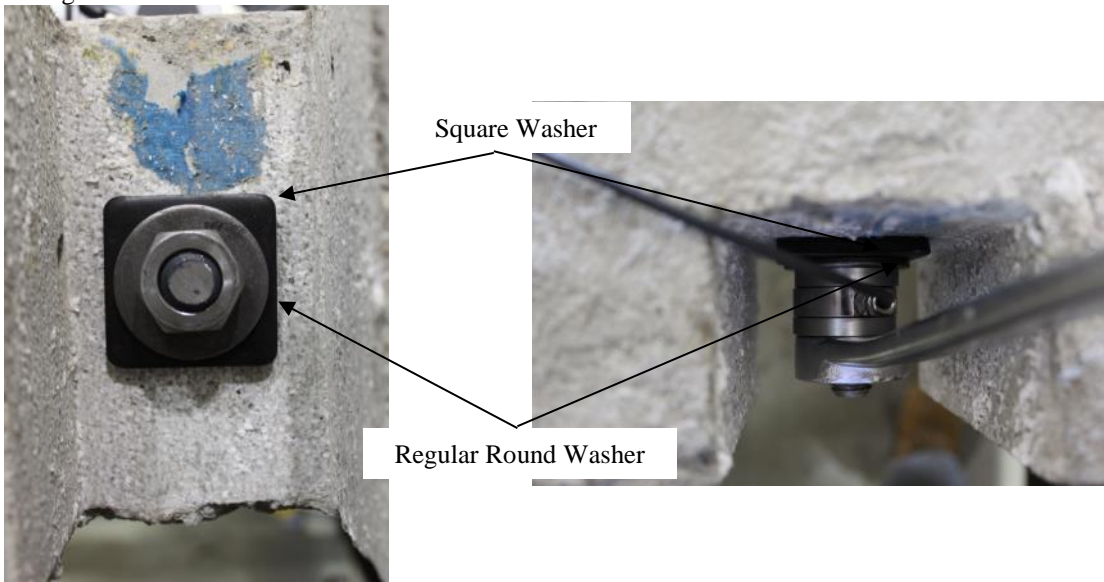


Figure 6.2 Supporting of concrete planks in the pretension test

A load cell is placed on one side of the rod to monitor the tension variation, while the nut on the other side is turned. On the load side, a square washer, having a case hardness of at least 40 HRC, is placed adjacent to the concrete plank to distribute the compressive load on the concrete. The 1/4 in. thick square washer has a dimension of 2 in. by 2 in., with a 5/8 in. diameter hole at the center. A regular thin round washer is between the nut and the square washer to ensure the deformation of the washers is minimized, and the hole in the concrete is intact after testing. On the other side, the load cell is between the square washer and the nut. Along with the load cell, two washers with a hardness of at least 43 HRC are also supplied which are employed as force introduction components for the load cells. See Figure 6.3b and Figure 6.3c. Before testing, the washers and nut threads on the load side are lubricated using moly coating. The snug-tight condition is first achieved with the full effort of a worker using a torque wrench with a 12 in. lever arm. A multiplier is then used with the torque wrench to reduce the effort to turn the nut. As the worker turns the nut, the rod tension is recorded.



Before testing:



After testing:

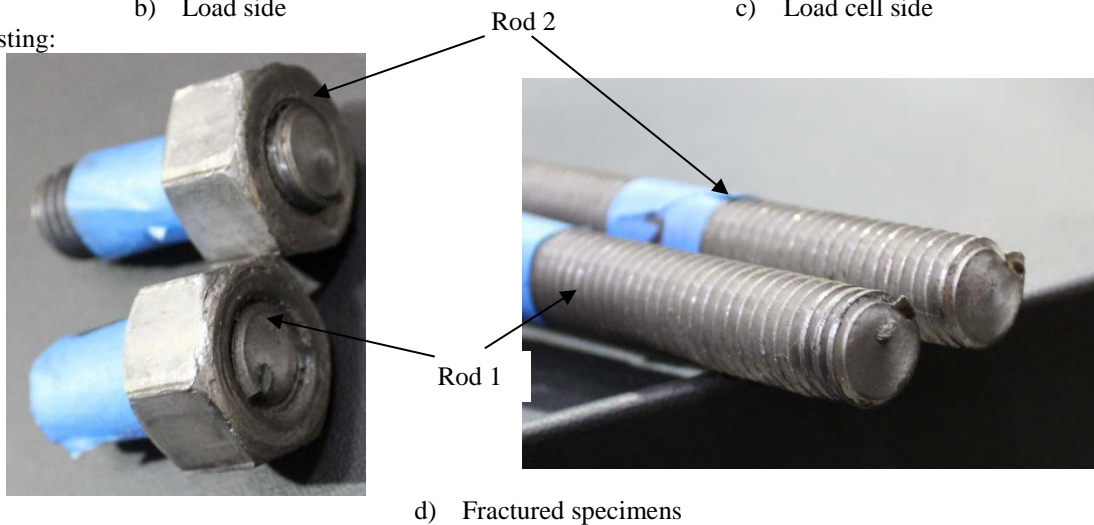


Figure 6.3 Threaded rod pretension test

Two rods are tested, and both fracture as a result of torqued tension, see Figure 6.3 (d). When testing Rod 1, ping is first heard at the 8th complete turn after the snug-tight position. Starting from the 12th complete turn, the ping noise becomes frequent. As the rod is elongated, it is harder to achieve the engagement between the nut threads and the rod threads. When new rod threads are engaged, an abrupt force change is seen from the display, and a ping sound is also heard. At the 17th complete turn, the ratchet of the wrench stops clicking, and it becomes very difficult to turn the nut. Rod 1 fractures after 22 complete turns. For Rod 2, the first ping is heard at the 8th complete turn, and the ping noise becomes frequent after the 16th turn. At the 18th turn, a squeak is heard. Starting from the 20th turn, it is very hard to turn the nut. A loud noise is heard at the 23rd turn, and turning the nut is slightly easier. The rod ultimately fractures after 25 complete turns. Because there is no deformation of the square washers, the holes are intact after both testing.

The rod tension variation is plotted in Figure 6.4. Each dashed line indicates a complete nut rotation (360 degrees). The force decrease is caused by excessive torsional deformation, which releases the tensile strain in the rod. Based on these plots, it is decided that 1 turn is adequate to ensure yielding of the rods, and the safety factor is at least 22 before the rods are twisted off.

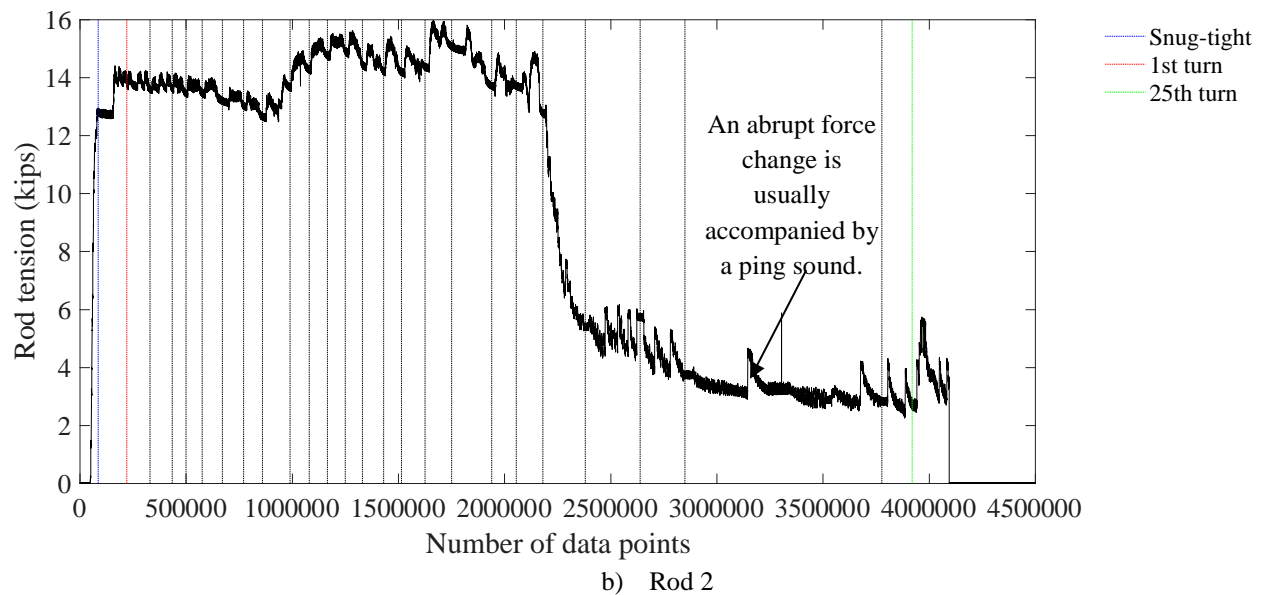
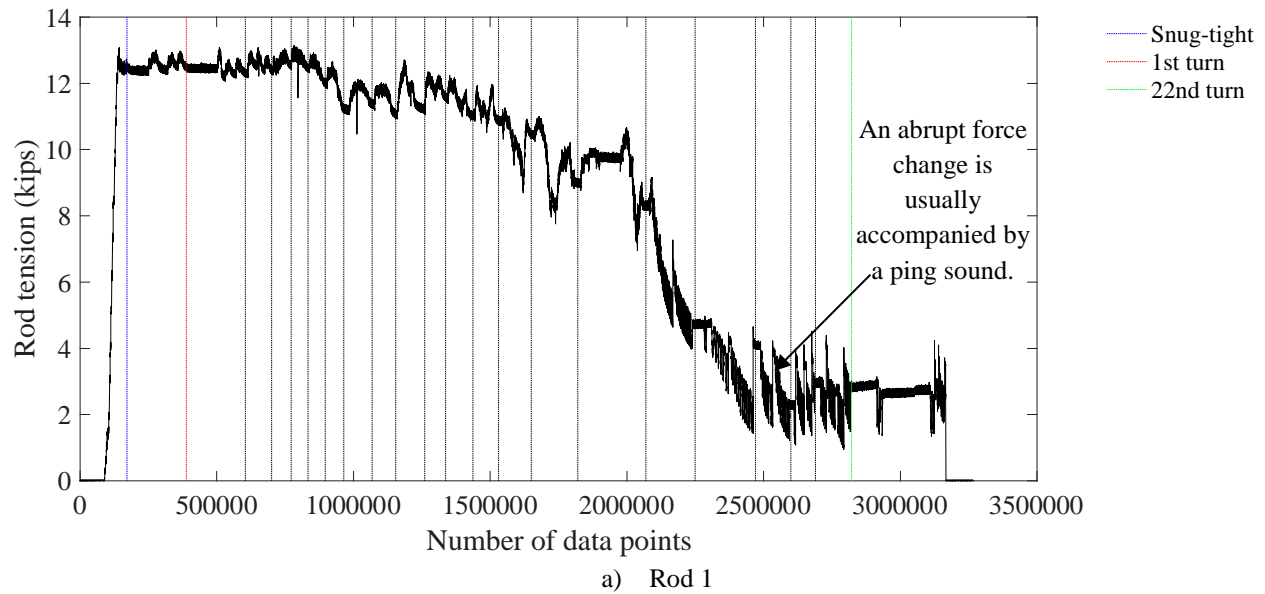


Figure 6.4 Rod tension variation

6.2 Material properties

Steel properties

When the steel beams are delivered, the flange width of a W14x26 beam is noticeably narrower than that of the other W14x26 beam. The major dimensions of all the beams are thus measured, see Table 6.2. Beams 1 through 4 correspond to the steel sections used in Tests 1-M24-2C-RH through 4-M20-2C-RL. Steel stubs where the coupons are cut are designated as Beams 5 and 6.

After comparing the measured dimensions to the tolerances given in Figure 6.5, the flange widths of Beams 4 and 6 are found to be larger than the maximum allowable width, which is equal to 5.28 in. Except for the marking on Beam 4, which is too blurry to discern, those on steel Beams 1, 2 and 3 indicate the sizes are as requested. No markings are found on Beams 5 and 6 since they are too short. Yet, the measured dimensions of Beams 4 and 6 are closest to the nominal dimensions of a W14x26 section.

Because all the W14x38 sections have similar dimensions, they are assumed to be from the same heat, and coupons cut from Beam 6 are representative. Nonetheless, it is not certain whether Beam 3 is from the same heat as Beam 4 and 6. Thus, the material properties of Beam 3 are obtained by testing coupons cut from low stress regions of the beam.

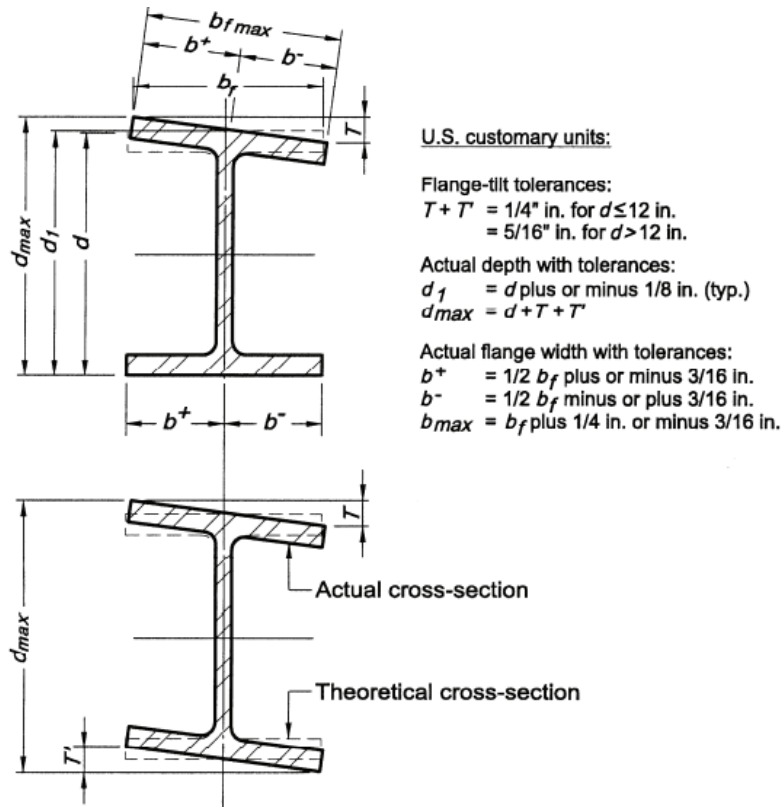


Figure 6.5 Mill tolerances on a W-shape cross section [(after AISC 303-10)]

Table 6.2 Measured dimensions of steel beams and stubs

Beam #	Section	Length (ft)	d (in.)	t_w (in.)	b_f (in.)	t_f (in.)
1	W14x38	32.0	14-1/8	0.310	6-3/4	0.527
2	W14x38	32.0	14-1/4	0.349	6-3/4	0.460
3	W14x26	32.0	14	0.419	4-7/8	0.270
4	W14x26	32.0	13-7/8	0.378	5-3/8	0.270
5	W14x38	3.5	14-1/4	0.323	6-3/4	0.531
6	W14x26	3.5	13-7/8	0.358	5-1/2	0.282

Tension testing is conducted to document material properties. Refer to Section 5.1.2 for the dimensions and procurement of steel coupons from the channels, reinforcement and bolts. In addition, coupons are cut from the steel beams and fully threaded rods, and the dimensions are given in Figure 6.6. The testing procedures described in Section 5.1.2 are utilized.

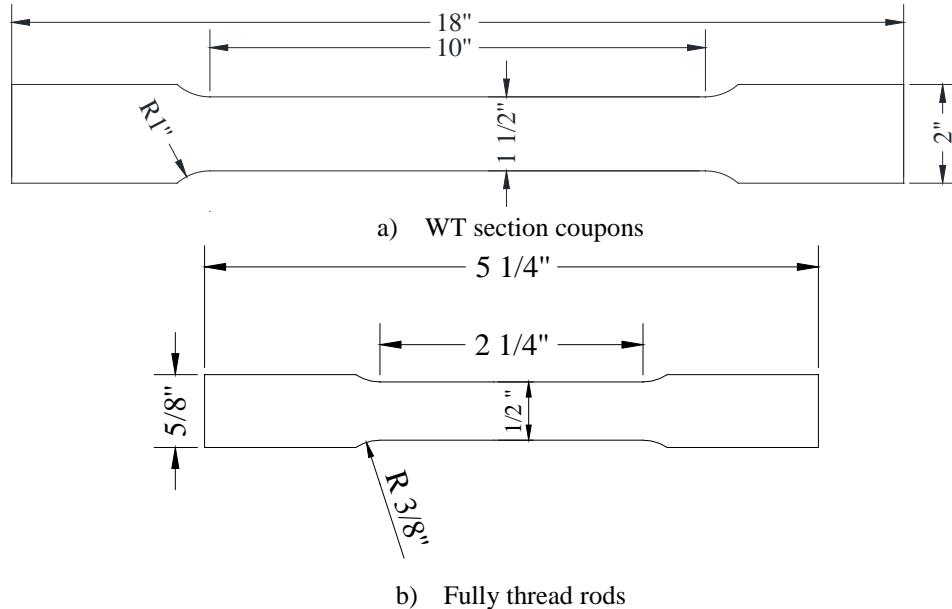


Figure 6.6 Rod coupon dimension (units: inches)

Concrete properties

The precast concrete planks are completed in three pours, with 20 planks cast in each pour. Planks from each of the first three tests are from the same pour. Test 4-M20-1C-RL, however, has planks from all three pours, which mimics the situation where planks of different strength reclaimed from different projects are reused in a new project.

The batch sheets and the delivery tickets for all the pours are included in Section 2.6 in Appendix F. It should be noted that the mix designs are not the same among the pours.

For each pour, thirty-nine cylinders are cast and divided into three groups, with each group consisting of thirteen 6 in. by 12 in. cylinders. These three groups of cylinders represent concrete at different stages (i.e., beginning, middle and end) during the pour.

An overview is given for each pour.

- Pour 1: An initial slump of 5.0 in. was measured before pouring the specimens and cylinders. Specimens 1 through 5 were first poured and vibrated. While Cylinder group A was cast and vibrated, another slump test was conducted, and the measured slump was 6 in. Specimens 6 through 10 were poured and vibrated, followed by Cylinder group B.

Two slump tests were conducted consecutively, and the measured slumps were both 3.0 in. Because the slump decreased substantially, two gallons of water was added to the truck mixer after pouring Slab 10. Specimens 11 through 15 were then poured and vibrated. The concrete for Cylinder group C was sampled before pouring the remaining planks, except for Cylinders 2C, 4C, 7C and 11C, half volume of which was cast using concrete concurrent with the remaining planks. Meanwhile, another test showed the slump was 4.25 in. The last 5 specimens, which were all single-channel slabs, were poured. After the pour ended, the measured slump was 3 in.

- Pour 2: An initial slump of 6.0 in. was measured before pouring the specimens and cylinders. Specimens 1 through 5 were first poured and vibrated. While Cylinder group A was cast and vibrated, another slump test was conducted, and the measured slump was 5-3/8 in. Specimens 6 through 10 were poured and vibrated, followed by Cylinder group B and a slump test that displayed a slump of 4.5 in. Five gallons of water was added to the truck mixer after casting the cylinders. Specimens 11 through 15 were then poured and vibrated. The concrete for Cylinder group C was sampled before pouring the remaining 5 planks; another test showed the slump is 5 in. After the pour ended, the measured slump was 3 in.
- Pour 3: When the concrete truck mixer arrived, the slump was estimated to be 3.5 in., and 10 gallons of water was thus added to increase workability of the concrete. An initial slump of 4.5 in. was measured after water was added. Specimens 1 through 5 were first poured and vibrated. While Cylinder group A was cast and vibrated, another slump test was conducted, and the measured slump was 3.75 in. Specimens 6 through 10 were poured and vibrated, followed by Cylinder group B and a slump test that showed a slump of 1.5 in. Due to the low slump, per ASTM Standard C31/C31M-12, the vibration of most cylinders in group B was prolonged to 8s. 7B, 8B, 10B, and 11B were vibrated for 10 seconds. In addition, the outside of the cylinder forms was usually tapped 12 times for each layer, but it was increased to 20 times each layer as a result of the poor workability of the concrete. After adding 15 gallons of water to the remaining concrete, specimens 11 through 15 were then poured and vibrated. The concrete for Cylinder group C was sampled before pouring the last 5 planks; another test showed the slump was 5.75 in. After the pour ended, the measured slump was 3-7/8 in. It was noticed that the 15 gallons of water, which were added before pouring specimens 11 through 15, might be excessive, as was indicated by the lower concrete strength shown in Table 6.3.

When the concrete specimens start to harden, the specimens are sprayed and covered with wet burlaps. A plastic sheet is put over the burlaps to prevent loss of moisture. Except for the plywood underneath the concrete planks, all the other forms for the specimens and cylinders are stripped on the next day. Some of the cylinders in each group are placed close to the specimens

and cured in the same manner as the specimens, while the other cylinders are put into a water bath to mimic moisture-cured conditions. All the specimens are left in place for 7 days, and then moved into the lab. Curing of specimens continues till 28 days. Table 6.3 includes the concrete compressive or tensile strength under different curing conditions at various testing dates.

Table 6.3 Concrete cylinder testing results (units: psi)

Pour #	Curing Condition	Test type	Testing date	Cylinder A	Cylinder B	Cylinder C	Average
1	Moist-cured	Compressive test	3 days	3,625	3,380	3,360	3,455
			7 days	4,160	4,210	3,850	4,073
			21 days	4,870	5,210	5,195	5,092
			28 days	5,131	5,521	5,493	5,382
	Same as the specimen	Splitting tensile strength	28 days	481	493	438	470
		Compressive test	3 days	4,115	3,895	3,545	3,852
			7 days	4,560	4,390	4,175	4,375
			21 days	5,135	5,315	5,080	5,177
			28 days	5,450	5,761	5,513	5,575
Splitting tensile strength	Test day for specimen 1	10A	10B	10C			
	Test day for specimen 4	12A	12B	12C			
2	Moist-cured	Compressive test	3 days	3,382	3,273	3,164	3,273
			7 days	4,117	4,262	4,247	4,209
			21 days	5,318	5,532	5,516	5,456
			28 days	5,667	6,245	5,918	5,943
	Same as the specimen	Splitting tensile strength	28 days	449	477	436	454
		Compressive test	3 days	3,713	3,750	3,377	3,613
			7 days	4,597	4,590	4,590	4,592
			21 days	5,886	6,034	5,941	5,953
			28 days	5,734	6,076	5,545	5,785
Splitting tensile strength	Test day for specimen 2	10A	10B	10C			
	Test day for specimen 4	12A	12B	12C			
3	Moist-cured	Compressive test	3 days	3,404	3,421	2,464	3,096
			7 days	3,733	3,974	3,243	3,650
			21 days	4,931	4,571	3,936	4,479
			28 days	5,225	5,340	4,193	4,919
	Same as the specimen	Splitting tensile strength	28 days	459	481	358	433
		Compressive test	3 days	3,331	3,510	2,597	3,146
			7 days	4,534	4,629	3,525	4,228
			21 days	5,779	5,805	4,511	5,365
			28 days	5,674	5,929	4,932	5,511
Splitting tensile strength	Test day for specimen 3	10A	10B	10C			
	Test day for specimen 4	12A	12B	12C			
Splitting tensile strength	Test day for specimen 3	11A	11B	11C			
	Test day for specimen 4	13A	13B	13C			

Planks in a composite beam are numbered, with the very east plank numbered as 1 and the very west plank numbered as 15, see Figure 6.7. The correspondence between the plank numbering and the plank pour sequence is given in Table 6.4.

Table 6.4 Concrete plank pour sequence

Test #	Plank #	Pour sequence	Pour #
1	1	4	1
	2	2	
	3	11	
	4	1	
	5	5	
	6	12	
	7	9	
	8	3	
	9	14	
	10	15	
	11	7	
	12	10	
	13	8	
	14	13	
	15	6	

6.3 Instrumentation

Displacement measurements

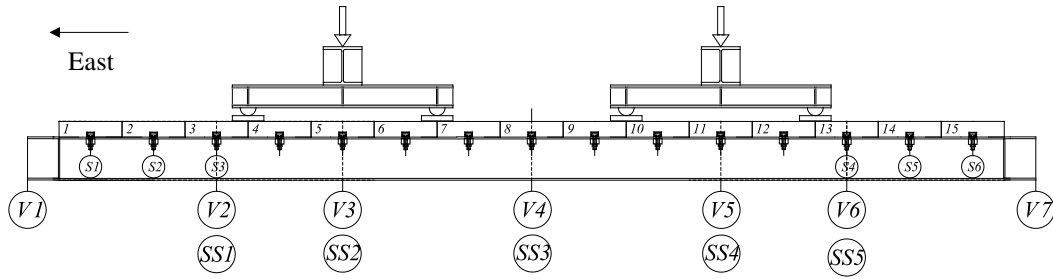
The composite beam deflection, which could be utilized to estimate the elastic stiffness of the beam specimen, is measured at different locations along the beam length. Those locations are named as V1 through V7 in Figure 6.7. The ductility of the composite beam specimens can also be computed based on the load-displacement curves. Slips between the steel beams and the concrete planks are measured at locations from S1 through S6. The slip is measured at the ends of the beam, since the slip is increasing from zero at the center to maximum at the end of the beam. The end slip provides deformation demand for the deconstructable connectors in the tested beams.

Strain measurements

Several cross sections along the length of each beam are instrumented. As shown in Figure 6.7, at Section SS3 eight strain gages are attached on the steel cross section: two at the bottom of the top flange; four at the third points of the web; two at the bottom of the bottom flange. Sections SS2 and SS4 are instrumented with six strain gages. Since Sections SS1 and SS5 are expected to be elastic during the test, only the flange strains are measured. All the strain gages are placed at locations where the residual stress is minimal, except for those attached at the mid-height of the web at Sections SS2 and SS4. In order to evaluate the effective width of the deconstructable

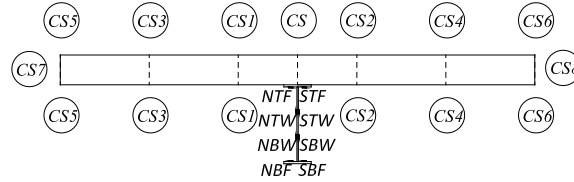
composite beams, the strain variation along the width of the slab at the mid-section is measured. At other sections, the strains are measured along the height of the slab. Because concrete is an inhomogeneous material, it is commonly recommended to choose strain gages with longer measuring grids to avoid localized strains. In this test, the concrete strains are calculated by tracking the length change of an 8 in. gage length with linear potentiometers. For the mid-section where the bending moment is maximum, linear potentiometers with a stroke length of 1 in. are selected, while linear potentiometers with a stroke length of 0.5 in. are utilized at other sections. The recorded concrete and steel strain profiles can be used to calculate the locations of the neutral axes in concrete and steel.

According to the pushout test results, different reinforcement patterns and the number of channels in a plank do not affect the strains of the channel lips and the channel anchors. It is decided to instrument the channel lips in Test 2-M24-1C-RL and Test 4-M20-1C-RL to investigate their behavior under different amount of pretension. In each test, only the channel lips of two end planks (Planks 1 and 15 in Figure 6.7) and one middle plank (Plank 8 in Figure 6.7) are gaged. The two end planks are at regions where the shear is maximum, and the moment is zero, while the moment is maximum, and the shear is zero at the middle plank. In Test 2-M24-1C-RL, strain gages are also attached to the middle two channel anchors in these three planks, since the anchor axial and shear forces are anticipated to be the largest among all the tests. Considered as the most important component, bolts at the very end and middle of all the beams are instrumented to track the bolt tension variation during the test. In Test 1-M24-2C-RH and Test 4-M20-1C-RL, transverse and longitudinal reinforcement are gaged. The strain in the transverse reinforcement can be compared to the calculated concrete strain, and the longitudinal reinforcement strains are used to calculate the negative bending moment in the overhanging slab along the length of the beams.



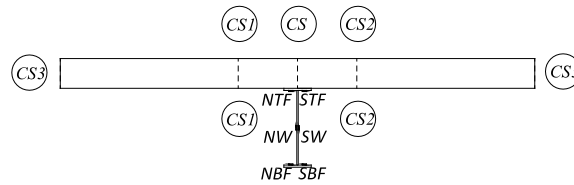
SS3 section

←
North



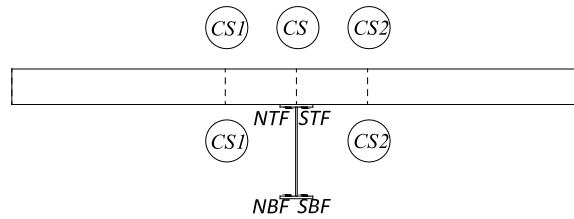
SS2 and SS4 sections

←
North

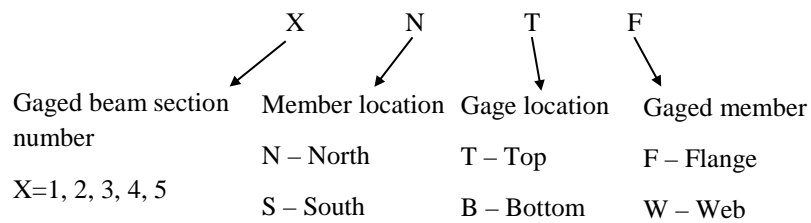


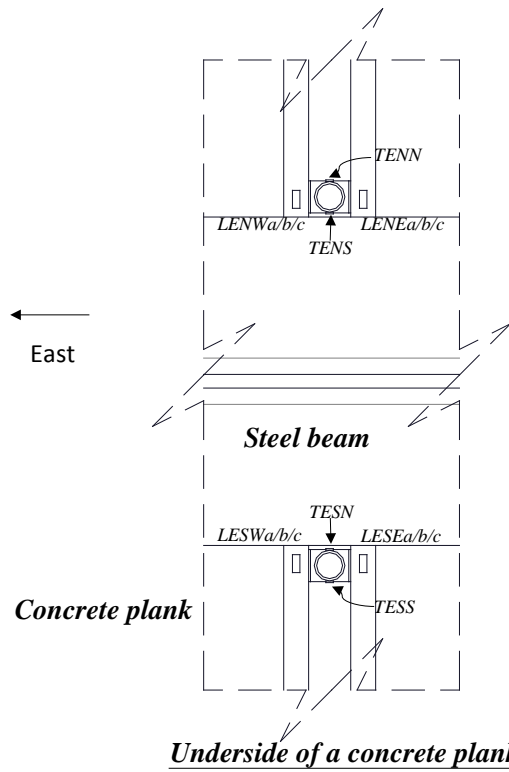
SS1 and SS5 sections

←
North

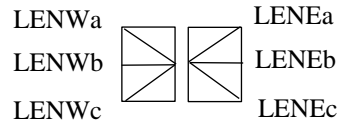


S1-S6 : slip of clamps
 V1-V7: vertical deflection
 SS1-SS5: strain gaged sections
 CS: concrete strain measured with linear potentiometers



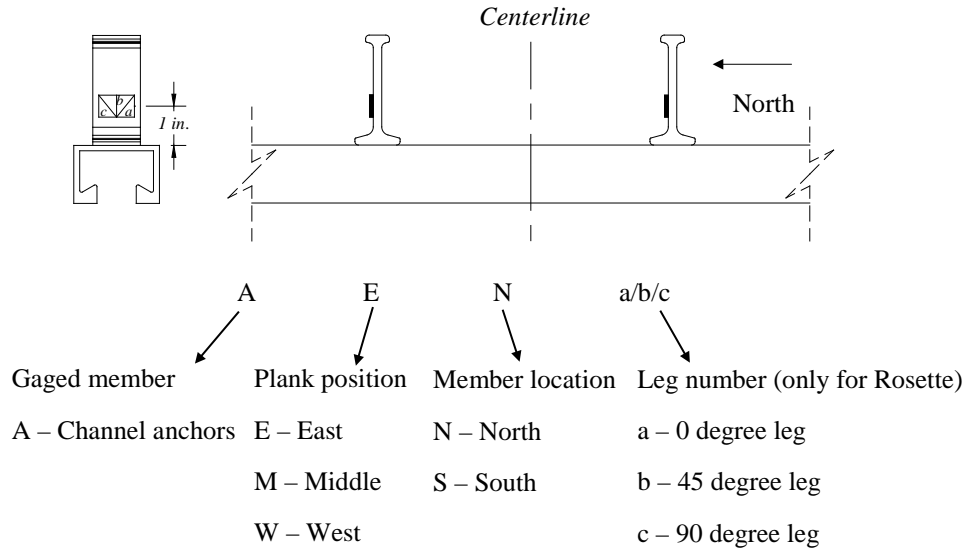


Rosette gage orientation:

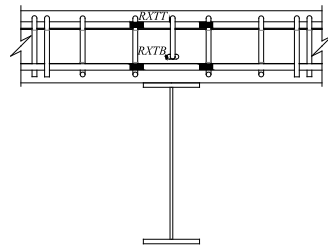


	L	E	NW	a/b/c
Gaged member	Plank position	Gage location	Leg number (only for Rosette)	
L – Channel lips	E – East	NW – Northwest	a – 0 degree leg	
	M – Middle	NE – Northeast	b – 45 degree leg	
	W – West	SW – Southwest	c – 90 degree leg	
		SE – Southeast		

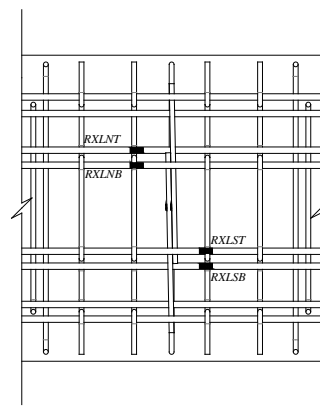
	T	E	N	N
Gaged member	Plank position	Bolt location	Gage location	
T - Bolts	E – East	N – North	N – North	
	M – Middle	S – South	N – South	
	W – West			



Composite beam 1:

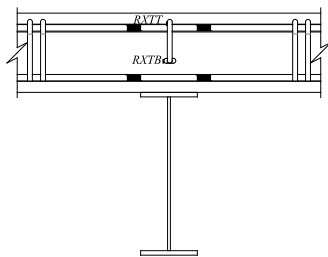


Elevation view

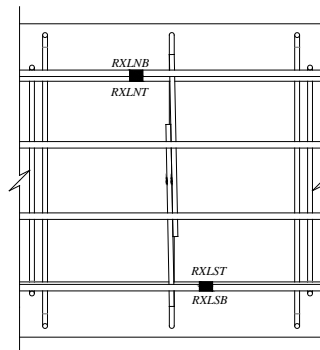


Plan view

Composite beam 4:

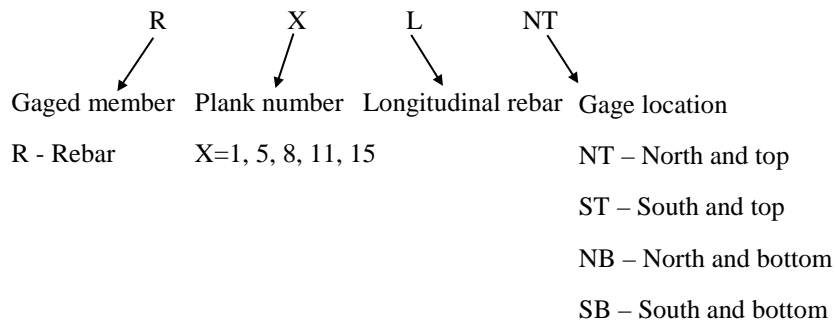


Elevation view



Plan view

Longitudinal reinforcement:



Transverse reinforcement:

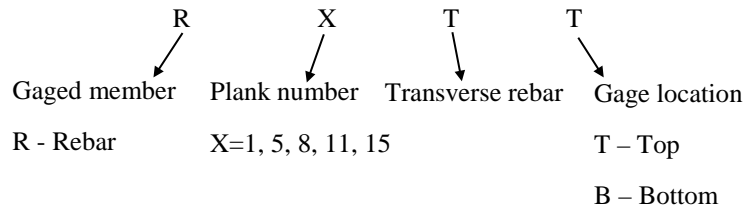


Figure 6.7 Composite beam specimen instrumentation plan

6.4 Loading protocol

The testing protocol for the composite beam specimens includes loading at an increment of approximately 10 percent of the estimated ultimate strength using force control until the force vs. midspan deflection curve becomes nonlinear. The specimen is unloaded, and then reloaded three times using the same force increment, which is intended to mimic serviceability conditions under which the loading may vary significantly. Subsequently, displacement control will be used to complete the tests by loading the beam well past its peak strength to investigate the softening behavior of the system.

7. Conclusions and Future Work

A deconstructable composite floor system is proposed which consists of precast concrete planks and steel beams connected using clamping connectors. This system maintains the benefits of composite construction, such as enhanced flexural strength and stiffness, reduced steel beam size and weight, and ease of construction. In the conventional composite floor systems, steel beams are commonly recycled, and concrete slabs are sent to landfill or downcycled for aggregate; however, sustainable design of composite beams and floors is achieved in the new system by enabling deconstruction of buildings and reuse of the structural components and reducing the energy consumption and material waste.

The work in this report includes comparing the environmental impacts of buildings employing Design for Deconstruction strategies to those employing traditional structural practices and conducting pushout tests to quantify the strength and ductility of the deconstructable clamping connectors.

7.1 Conclusions from life-cycle assessment

A life cycle assessment (LCA) model is implemented to compare the environmental impacts of a series of prototype buildings using DfD composite floor systems to prototype buildings using traditional, cast-in-place floors. Five impact categories are considered: Photochemical Smog Formation, Global Climate Change, Human Health—Particulate (respiratory effects), Ecotoxicity, and Fossil Fuel Depletion.

The processes and materials in the software libraries are used for both the conventional and deconstructable structures to provide the most complete data possible. For the buildings employing DfD strategies, the reduced environmental impacts resulting from reusing the DfD components is accounted for by manually subtracting the impacts of manufacturing, transporting, and disposing of a percentage of these DfD components from the DfD building life cycle each time the components are reused. To provide a more detailed comparison of the buildings, the life cycle of each building has been broken into four stages: material production, material transportation, worker transportation, and material disposal.

The following conclusions are obtained based on the comparison:

- (1) The environmental impacts of Design for Deconstruction buildings compare favorably to traditional buildings under the constraints of this study, assuming reuse occurs in the future. In all environmental impact categories the DfD buildings have lower impacts if deconstructable components are reused at least once.

- (2) The initial environmental impacts of the DfD alternative are greater than the traditional alternative in the fossil fuel depletion, global warming, and smog production impact categories, and less in the ecotoxicity and human respiratory health categories.
- (3) For most impact categories examined, the production phase impacts are the largest contributor to full life-cycle impacts. End-of-life impacts are most significant for the human respiratory health category. Transportation impacts are most significant for the fossil fuel depletion and smog production categories, though generally much less than the production impacts. Worker transport contributes little to life-cycle environmental impacts.
- (4) The traditional building has relatively high levels of ecotoxicity, compared to the DfD building. This is due to the cold rolled sheet steel used for the deck of the traditional building, which contributes to ecotoxicity far more significantly than other components and is absent from the floor construction of the DfD building.

7.2 Summary of pushout tests

The pushout test program includes two series of tests. In the pretension tests, the number of turns of the nut is first determined to ensure adequate and reliable axial forces generated in the bolts. Pushout tests are then performed to study the strength and ductility of the clamping connectors and explore the influences of the testing parameters.

The clamping system uses T-bolts inserted into cast-in channels. Because the cast-in channels can deform significantly when the bolts are pretensioned, more turns of the nut than in standard bolted connections are needed to enable the bolts to deform into the inelastic range and meet minimum pretension requirements in the AISC specification (2010a). Three M24 and M20 bolts are tested under torqued tension until fracture to develop the relationship between the number of turns and the bolt axial force. Except for one bolt that fractures at the bolt heads, most bolts in the pretension tests ultimately fracture due to excessive torsional deformation. Two turns and 1.5 turns after a snug-tight condition are selected for pretensioning the M24 and M20 bolts, respectively. It is also noted that in the M24 bolt tests, moderate plastic deformation occurs in the channel lips, while the inelastic deformation of the channel lips is minor when the M20 bolts are pretensioned.

After the number of turns of the nut for the M24 and M20 bolts is selected, all the pushout specimens are tested using a self-reacting frame. The specimens consist of 4 ft. × 2 ft. × 6 in. precast concrete planks attached to WT5x30 or WT4x15.5 sections using clamping connectors. WT5x30 and WT4x15.5 sections represent typical floor beams with different flange thicknesses, with the larger WT tested with M24 clamps and the smaller WT tested with M20 clamps. The

WT4x15.5 sections are also used with M24 clamps, requiring shims between the clamps and the WT flange since the flange is relatively thin. Parameters for the pushout tests include bolt diameter, number of channels, reinforcement configuration, loading protocol, and usage of shims. In the lightly reinforced specimens, the reinforcement is designed only for gravity loading. Additional supplementary reinforcement is placed around the channel anchors to prevent anchor-related failures in the heavily reinforced specimens. The pushout tests are all displacement-controlled. The AISC loading protocol for beam-to-column moment connections is used as a guide for establishing a cyclic loading history for the clamped connections.

Based on the pushout test results and the analysis results, the following conclusions can be reached:

- (1) The load-slip curves indicate that the deconstructable clamping connectors using M24 bolts are ductile. Compared to shear studs which fracture at a much smaller slip, the M24 clamping connectors can retain almost 80% of the peak strength even at 5 in. slip under monotonic loading.
- (2) Shims are used for specimens using M24 clamps and thin flange sections, and undesirable load oscillation is observed due to a stick-slip mechanism, although the strength is not affected. Usage of the selected shims between the clamp and the flange may not be recommended in this application.
- (3) Compared to the monotonic specimens, the peak strengths of the cyclic specimens are lower, but stabilized in a manner that may be addressed in design provisions. This is comparable to the decrease in strength seen in headed shear connectors when subjected to cyclic loading.
- (4) After going through a couple of cycles, the strengths of the cyclic specimens begin to degrade, which could be attributed to the reduction of bolt pretension force and the lowering of frictional coefficients as a result of the abrasion between the clamp teeth and steel flange and between the concrete plank and steel beam.
- (5) Considerable load drop is seen after 0.68 in. slip in the load-slip curve of the monotonic specimen using M20 bolts. Large rotation and complete disengagement of some clamps are noted. With the steel blocks inserted into the channels to support the clamp tails, the cyclically loaded specimen performs better than the corresponding monotonic specimen even though all the clamps ultimately lose contact with the beam flanges.
- (6) In terms of strength and state of cracks, the specimen with light reinforcement does not perform worse than the specimen with heavy reinforcement. This implies that the

additional reinforcement are not engaged which are designed to bridge potential cracking planes due to channel anchor forces, which is further proved by the low stresses in the reinforcement.

- (7) A strut-and-tie model is used to explain the formation of cracks which are induced by the friction acting on the concrete surface, rather than concrete pryout failure. Since the frictional force distributes in a non-uniform manner, the damage concentrates on one side of the concrete plank when it is loaded monotonically.
- (8) Bolt axial strain measurements throughout the cyclic tests indicate that bolt tension gradually decreases. When the slip is small, the tension decrease is due to the shear force acting on the bolt, while the bolt tension releases as the slip increases. The bolt tension vs. slip plots appear to correlate with the clamp detachment sequence.
- (9) The shear force applied to a steel beam is distributed among the clamps, demonstrating the potential of using clamps as shear connectors in composite beams. Unfortunately, the strain gage measurements are “contaminated” when the gages are close to the clamps, and the calculated axial forces of the instrumented sections cannot represent the actual axial forces.
- (10) In order to simulate the pushout test specimen, a finite element model is developed which takes into account material nonlinearly, geometric nonlinearly and contact between different components. The finite element model predicts the peak strength, but the slip at which the peak strength occurs in the test is achieved more gradually than the computational simulation.

7.3 Future work

Composite beam tests will be conducted, and the following will be investigated and documented: the load-deflection curves; the progression of damage; the limit states; the elastic stiffness and ultimate strength; the maximum slip of the clamping connectors during the test; the variation of the plastic neutral axis locations; effective width.

Design recommendations will be provided for the DfD system, particularly the clamping connectors and composite beams. Construction and deconstruction sequences will also be recommended, including recommendations for achieving serviceability criteria and consideration of safety issues during the deconstruction process

References

- ABAQUS 6.11 (2011). *Abaqus User Manual*, Dassault Systèmes Simulia Corp., Providence, Rhode Island.
- ACI (2011). *Building code requirements for structural concrete (ACI 318-11) and commentary*. American Concrete Institute, Farmington Hills, Michigan.
- AISC (2010). *Code of Standard Practice for Steel Buildings and Bridges (AISC 303-10)*, American Institute of Steel Construction, Chicago, Illinois.
- AISC (2010a). *Specification for Structural Steel Buildings*, American Institute of Steel Construction, Chicago, Illinois.
- AISC (2010b). *Seismic Provisions for Structural Steel Buildings*, American Institute of Steel Construction, Chicago, Illinois.
- Anderson, N. S., & Meinheit, D. F. (2005). "Pryout capacity of cast-in headed stud anchors". *PCI journal*, Vol. 50, No. 2, pp. 90-112.
- ASCE (2010). *Minimum Design Loads for Buildings and Other Structures*, American Society of Civil Engineers, Reston, Virginia.
- ASHRAE (2011). *Standard for the Design of High-Performance Green Buildings*. American Society of Heating, Refrigerating and Air-Conditioning Engineers, Atlanta, Georgia.
- ASTM (2011). *Standard Test Methods for Splitting Tensile Strength of Cylindrical Concrete Specimens (C496/C496M-11)*, American Society for Testing and Materials, Philadelphia, Pennsylvania.
- ASTM (2012). *Standard Practice for Making and Curing Concrete Test Specimens in the Field (C31/C31M-12)*, American Society for Testing and Materials, Philadelphia, Pennsylvania.
- ASTM (2013). *Standard Test Methods for Tension Testing of Metallic Materials (E8/E8M-13a)*, American Society for Testing and Materials, Philadelphia, Pennsylvania.
- ASTM (2014). *Standard Test Method for Compressive Strength of Cylindrical Concrete Specimens (C39/C39M-14a)*, American Society for Testing and Materials, Philadelphia, Pennsylvania.
- ASTM (2014). *Standard Test Methods and Definitions for Mechanical Testing of Steel Products (A370-14)*, American Society for Testing and Materials, Philadelphia, Pennsylvania.
- Athena Sustainable Materials Institute (2016). *Athena Sustainable Materials Institute*. <http://www.athenasmi.org> (accessed December 2015).

- Bazant, Z. P. (1984). "Size effect in blunt fracture: concrete, rock, metal," *Journal of Engineering Mechanics*, Vol. 110, No. 4, pp. 518-535.
- Bare, J., Young, D., Hopton, M. (2012). *Tool for the Reduction and Assessment of Chemical and other Environmental Impacts (TRACI) User's Manual*. United States Environmental Protection Agency, Cincinnati, Ohio.
- Bowers, R. C., Clinton, W. C., & Zisman, W. A. (1953). *Frictional behavior of polyethylene, polytetrafluoroethylene, and halogenated derivatives* (No. NRL-4167). Naval Research Lab.
- California Department of Resources Recycling and Recovery (CalRecycle) (2104). <http://www.calrecycle.ca.gov>. (accessed March, 2014).
- CEN (2004). *Eurocode 4: Design of Composite Steel and Concrete Structures, EN1994-1-1*, European Committee for Standardization, Brussels, Belgium.
- CEN (2009). *Eurocode 2: Design of fastenings for use in concrete - Part 4-3: Anchor channels, EN1992-4-3*, European Committee for Standardization, Brussels, Belgium.
- Chaboche, J. L. (1986). "Time-independent constitutive theories for cyclic plasticity," *International Journal of plasticity*, Vol. 2, No. 2, pp. 149-188.
- Clement Support Services (2012). *Clement Support Services*. <http://clementsupport.com> (accessed March 2014).
- Construction, M. H. (2011). Prefabrication and modularization: Increasing productivity in the construction industry. *Smart Market Report*.
- Cornelissen, H. A. W., Hordijk, D. A., & Reinhardt, H. W. (1986). "Experimental determination of crack softening characteristics of normalweight and lightweight concrete," *HERON*, Vol. 31, No. 2, pp. 45-56.
- Contractors Register, Inc. (2015). *The Blue Book Building & Construction Network*. www.thebluebook.com (accessed December 2015).
- Costello, D. (2014). Personal communication.
- Cross, J. (2013). "Navigating the ever-expanding landscape of green codes, standards and rating systems," *Modern Steel Construction*, Vol. 53, No. 2, pp. 20-25.
- Decon USA Inc. (2013). *Decon USA*. <http://deconusa.com> (accessed March 2014).

- Devore, J. (2009). *Probability and Statistics for Engineering and the Sciences, Seventh Edition*. Brooks/Cole, Cengage Learning, Belmont, California.
- Durmisevic, E., & Brouwer, J. (2002). "Design aspects of decomposable building structures," *Design for Deconstruction and Material Reuse. Proceedings of the CIB Task Group 39-Deconstruction Meeting, OMER S. DENIZ*.
- Easterling, W. S., Gibbings, D. R., & Murray, T. M. (1993). "Strength of shear studs in steel deck on composite beams and joists," *Engineering Journal*, Vol. 30, No. 2, pp. 44-55.
- Easterling, W. S., & Porter, M. L. (1994). "Steel-Deck-Reinforced Concrete Diaphragms. I," *Journal of Structural Engineering*, Vol. 120, No. 2, pp.560-576.
- Energy Information Administration (2012) *Annual Energy Review*. U.S. Energy Information Administration, Washington, D.C.
- Ernst, S. (2006). "Factors Affecting the Behavior of the Shear Connection of Steel-Concrete Composite Beams," Ph.D. Dissertation, School of Engineering, University of Western Sydney, Sydney, Australia.
- GaBi (2015). *GaBi Software*. <http://www.gabi-software.com/america/index> (accessed December 2015).
- Gattesco, N. (1999). "Analytical modeling of nonlinear behavior of composite beams with deformable connection," *Journal of Constructional Steel Research*, Vol. 52, No. 2, pp. 195-218.
- Gattesco, N., & Giuriani, E. (1996). "Experimental study on stud shear connectors subjected to cyclic loading," *Journal of Constructional Steel Research*, Vol. 38, No. 1, pp.1-21.
- Gorgolewski, M. (2008). "Designing with reused building components: some challenges," *Building Research & Information*, Vol. 36, No. 2, pp. 175-188.
- Grant, J. A., Fisher, J. W., and Slutter, R. G. (1977). "Composite beams with formed steel deck," *Engineering Journal*, Vol. 14, No. 1, pp. 24-43.
- Grigorian, C. E., & Popov, E. P. (1994). "Energy Dissipation with Slotted Bolted Connections". Report UCB/EERC-94/02. Earthquake Engineering Research Center, College of Engineering, University of California at Berkeley, Berkeley, California.
- Halfen (2011). *Halfen Anchoring Systems*, Halfen, Converse, Texas.
- Halfen (2103). *Halfen Cast-In Channels: Technical Product Information*. Halfen, Langenfeld, Germany.

- HDR and PE Americas (2010). *Task 2.0 - Plan and Implement a Comparative Study to Contrast the Difference Between Building Products*. American Institute of Steel Construction (AISC), Chicago, Illinois.
- Hillerborg, A., Modeer, M., and Petersson, P. E. (1976). "Analysis of Crack Formation and Crack Growth in Concrete by Means of Fracture Mechanics and Finite Elements," *Cement and Concrete Research*, Vol. 6, No. 6, pp. 773-782.
- Huang, B., Xing, K., and Pullen, S. (2015), "Energy and carbon performance evaluation for buildings and urban precincts: review and a new modelling concept," *Journal of Cleaner Production*.
- IgCC Public Comment Hearing Committee. (2010). *International green construction code*. International Code Council, INC., USA.
- Intelligent Engineering (2011). *SPS floors, Intelligent Engineering*, Ottawa, Ontario, Canada.
- International Organization for Standardization (ISO) (2006). *Environmental management - Life cycle assessment - Requirements and guidelines*. ISO, Geneva, Switzerland.
- Kibert, C. J. (2003). "Deconstruction: the start of a sustainable materials strategy for the built environment," *Industry and environment*, Vol. 26, No. 2-3, pp. 84-88.
- Kulak, G. L., Fisher, J. W., & Struik, J. H. (1987). *A Guide to Design Criteria for Bolted and Riveted Joints*, Wiley, NY.
- Lam, D. (2000). "New test for shear connectors in composite construction," *Composite Construction in Steel and Concrete IV*, American Society of Civil Engineers, May 2002, Alberta, Canada, pp. 404-414.
- Lam, D., Dai, X., & Saveri, E. (2013). "Behavior of Demountable Shear Connectors in Steel-Concrete Composite Beams," *Composite Construction in Steel and Concrete VII*, American Society of Civil Engineers, July 2013, Queensland, Australia, pp. 618-631.
- Lee, J., & Fenves, G. L. (1998). "Plastic-damage model for cyclic loading of concrete structures," *Journal of engineering mechanics*, Vol. 124, No. 8, pp. 892-900.
- Lee, S. S. M., & Bradford, M. A. (2013). Sustainable composite beam behavior with deconstructable bolted shear connectors. *Composite Construction in Steel and Concrete VII*, American Society of Civil Engineers, July 2013, Queensland, Australia, pp. 445-455.
- Leon, R.T. and Alsamsam, I. (1993). Performance and serviceability of composite floors. Structural Engineering in Natural Hazards Mitigation, *Proceedings of the ASCE Structures Congress*, ASCE, pp.1479-1484.
- Lindapter (2011). *Steelwork Fixings Catalogue*, Lindapter, Bradford, U.K.

- LoopNet, Inc. (2014). <http://www.loopnet.com>. (accessed March 2014).
- López-Mesa, B., Pitarch, A., Tomas, A., Gallego, T. (2008). "Comparison of environmental impacts of building structures with in situ cast floors and with precast concrete floors," *Building and Environment*, Vol. 44, No. 2009, pp. 699-712.
- Lubliner, J., Oliver, J., Oller, S., & Onate, E. (1989). "A plastic-damage model for concrete," *International Journal of solids and structures*, Vol. 25, No. 3, pp. 299-326.
- Luttrell, L. D. (2004). *Steel deck institute diaphragm design manual*. Steel Deck Institute.
- MC90, CEB-FIP. (1993). Code 1990. London: Thomas Telford; 1993.
- McKenzie, B, Rapino, M. (2011). *Commuting in the United States: 2009*, American Community Survey Reports, ACS-15. U.S. Census Bureau, Washington, DC.
- Moehle, Jack P., Hooper, John D., Kelly, Dominic J., and Meyer, Thomas R. (2010). "Seismic design of cast-in-place concrete diaphragms, chords, and collectors: a guide for practicing engineers," *NEHRP Seismic Design Technical Brief No. 3*, produced by the NEHRP Consultants Joint Venture, a partnership of the Applied Technology Council and the Consortium of Universities for Research in Earthquake Engineering, for the National Institute of Standards and Technology, Gaithersburg, MD, NIST GCR 10-917-4.
- Newmark, N. M., Siess, C. P., & Viest, I. (1951). "Tests and analysis of composite beams with incomplete interaction," *Proc. Soc. Exp. Stress Anal*, Vol. 9, No. 1, pp. 75-92.
- National Institute of Standards and Technology (2015). *BEES Online*. <https://www.nist.gov/services-resources/software/bees> (accessed December 2015).
- O'Connor, J. (2004). "Survey on actual service lives for North American buildings," *Woodframe housing durability and disaster issues conference, Las Vegas*.
- Ochsendorf, J. et al. (2011). *Methods, Impacts, and Opportunities in the Concrete Building Life Cycle*. Massachusetts Institute of Technology, Cambridge, MA.
- Ollgaard, J. G., Slutter, R. G., & Fisher, J. W. (1971). "Shear strength of stud connectors in lightweight and normal-weight concrete," *AISC Engineering Journal*, Vol. 8, No. 2, pp. 55-64.
- PCI (2010). *PCI Design Handbook: Precast and Prestressed Concrete, 7th edition*. Precast/Prestressed Concrete Institute, Chicago, Illinois.
- Prager, W. (1949). "Recent developments in the mathematical theory of plasticity," *Journal of Applied Physics*, Vol. 20, No. 3, pp. 235-241.

- PRé (2013). *Introduction to LCA with SimaPro*. PRé Consultants, Amersfoort, The Netherlands.
- PRé (2016). *SimaPro 8*. PRé Consultants, Amersfoort, The Netherlands.
- Popovics, S. (1973). "A numerical approach to the complete stress-strain curve of concrete," *Cement and concrete research*, Vol. 3, No. 5, pp. 583-599.
- Qureshi, J., Lam, D., & Ye, J. (2011). "Effect of shear connector spacing and layout on the shear connector capacity in composite beams," *Journal of constructional steel research*, Vol. 67, No. 4, pp. 706-719.
- Rambo-Roddenberry, M. D. (2002). "Behavior and strength of welded stud shear connectors." Doctoral dissertation, Virginia Polytechnic Institute and State University.
- Ramesh, T., Prakash, R., and Shukla, K. K. (2010). "Life cycle energy analysis of buildings: An overview," *Energy and Buildings*, Vol. 42, No. 10, pp. 1592-1600.
- Ranzi, G., Bradford, M. A., Ansourian, P., Filonov, A., Rasmussen, K. J. R., Hogan, T. J., & Uy, B. (2009). "Full-scale tests on composite steel–concrete beams with steel trapezoidal decking," *Journal of Constructional Steel Research*, Vol. 65, No. 7, pp. 1490-1506.
- Reed Construction Data (2014). *RS Means Building Construction Cost Data*. Reed Construction Data, Kingston, MA.
- RCSC (2009). *Specification for Structural Joints Using High-Strength Bolts*, Research Council on Structural Connections, Chicago, Illinois.
- Renz, B. (2005). Innovative Connections. *Modern Steel Construction*, American Institute of Steel Construction, Chicago, Illinois, August.
- Sabelli, Rafael, Sabol, Thomas A., and Easterling, Samuel W. (2011). "Seismic design of composite steel deck and concrete-filled diaphragms: A guide for practicing engineers," *NEHRP Seismic Design Technical Brief No. 5*, produced by the NEHRP Consultants Joint Venture, a partnership of the Applied Technology Council and the Consortium of Universities for Research in Earthquake Engineering, for the National Institute of Standards and Technology, Gaithersburg, MD, NIST GCR 11-917-10..
- Saari, W. K., Hajjar, J. F., Schultz, A. E., and Shield, C. K. (2004). "Behavior of shear studs in steel frames with reinforced concrete infill walls," *Journal of Constructional Steel Research*, Vol. 60, No. 10, pp. 1453-1480.
- Shen, C., P. Mamaghani, I. H., Mizuno, E., and Usami, T. (1995). "Cyclic behavior of structural steels. II: Theory," *Journal of Engineering Mechanics*, Vol. 121, No. 11, pp. 1165-1172.
- Singh, A., Berghorn, G., Joshi, S., and Syal, M. (2010), "Review of life-cycle assessment applications in building construction," *Journal of Architectural Engineering*, Vol.17, No.1, pp. 15-23

- Steel Construction (2012). *Recycling and Reuse*.
http://www.steelconstruction.info/Recycling_and_reuse (accessed January 2014).
- Tingley, D., Davison, B. (2012). "Developing an LCA methodology to account for the environmental benefits of design for deconstruction," *Building and Environment*, Vol. 57, No. 2012, pp. 387-395.
- U.S. Department of Transportation, Bureau of Transportation Statistics (US DoT, BTS). (2003). *Omnistats*. US Department of Transportation, Washington, D.C.
- U.S. Environmental Protection Agency (2008). *Municipal Solid Waste in the United States: 2007 Facts and Figures*. EPA 530-R-08-010, Washington, D.C., November.
- U.S. Environmental Protection Agency (EPA). (2014). *US EPA*.
<http://www.epa.gov/climatechange/wycd/waste/downloads/concrete-chapter10-28-10.pdf>.
- USGBC (2013). *LEED v4 Reference Guide for Building Design and Construction*. United States Green Building Council, Washington, D.C.
- Vulcraft (2001). *Steel and Joist Girders, Steel Roof and Floor Deck, Composite & Non Composite Floor Joists*. Vulcraft, Florence, South Carolina.
- Webster, M., Kestner, D., Parker, J., Johnson, M. (2007) "Deconstructable and Reusable Composite Slab," Winners in the Building Category: Component – Professional Unbuilt, Lifecycle Building Challenge <<http://www.lifecyclebuilding.org/2007.php>>

Appendix A. Prototype Structure Design Summary

This appendix summarizes the design of the lateral-force resistance systems of the steel prototype buildings.

Table A.1 summarizes the size and weight of the beams and girders of the 8 prototype buildings using deconstructable floor systems. The required number of clamps per beam and girder is also given. Table A.2 summarizes the required number of shear studs per beam and girder and the size and weight of the beams and girders of the 8 prototype buildings using traditional composite floor systems.

The columns and lateral resistance systems are designed to be the same for both traditional and deconstructable floor systems, which could be somewhat inefficient for the composite slab because its weight is smaller than the other two types of floors. However, to enable more consistent comparisons, the lateral system is taken to be the same across each system. Thus, Table A.1 and Table A.2 may be used for both systems. Table A.3 summarizes the sizes and weights of the beams, girders, braces, and columns that make up the lateral resistance systems for both traditional and deconstructable buildings. Gravity columns are those not involved in the lateral system. Table A.4 summarizes the size and weights of gravity columns for both building types.

Table A.1 Member sizes for the deconstructable composite floor system

Name	Floor interior beam			Floor exterior beam			Floor interior girder			Floor exterior girder		
	Member size	Number of bolts	Weight (lbs)	Member size	Number of bolts	Weight (lbs)	Member size	Number of bolts	Weight (lbs)	Member size	Number of bolts	Weight (lbs)
30-3-8-gc	W18x35	60	69,300	W14x22	32	11,880	W30x90	40	48,600	W21x55	40	19,800
30-3-6-gc	W18x40	60	79,200	W14x26	32	14,040	W30x99	40	53,460	W21x55	40	19,800
20-3-8-gc	W10x19	40	14,820	W10x15	24	5,400	W18x35	40	12,600	W12x19	32	4,560
20-3-6-gc	W12x22	40	17,160	W10x15	24	5,400	W18x40	40	14,400	W14x26	24	6,240
30-9-8-gc	W16x31	32	184,140	W12x22	32	35,640	W21x62	40	100,440	W16x40	40	43,200
30-9-6-gc	W14x30	32	178,200	W12x19	32	30,780	W21x55	40	89,100	W18x35	40	37,800
20-9-8-gc	W12x19	24	44,460	W10x15	24	16,200	W14x30	24	32,400	W12x19	24	13,680
20-9-6-gc	W12x16	24	37,440	W10x15	24	16,200	W14x26	24	28,080	W12x16	24	11,520

Table A.2 Member sizes for the conventional composite floor system

Name	Floor interior beam			Floor exterior beam			Floor interior girder			Floor exterior girder		
	Member size	Number of Shear Studs	Weight (lbs)	Member size	Number of Shear Studs	Weight (lbs)	Member size	Number of Shear Studs	Weight (lbs)	Member size	Number of Shear Studs	Weight (lbs)
30-3-8-sc	W16x40	36	79,200	W14x22	28	11,880	W24x68	48	36,720	W21x44	56	15,840
30-3-6-sc	W21x44	40	87,120	W16x26	26	14,040	W27x84	74	45,434	W21x48	60	17,280
20-3-8-sc	W14x22	20	17,160	W10x12	14	4,320	W18x35	34	12,634	W12x19	24	4,560
20-3-6-sc	W12x26	24	20,280	W10x12	18	4,320	W18x35	40	12,640	W14x22	20	5,280
30-9-8-sc	W16x31	24	184,140	W12x19	18	30,780	W24x55	38	89,138	W16x26	28	28,080
30-9-6-sc	W14x26	24	154,440	W12x16	14	25,920	W21x48	34	77,794	W16x31	22	33,480
20-9-8-sc	W10x19	18	44,460	W10x12	12	12,960	W16x26	18	28,098	W10x19	14	13,680
20-9-6-sc	W12x16	14	37,440	W10x12	12	12,960	W12x26	18	28,098	W12x16	12	11,520

Table A.3 Member sizes of lateral-force resisting systems

Name	Floor Level	Seismic Design (Beams)						Seismic Design (Girders)					
		Braces		Beams		Columns		Braces		Girders		Columns	
		Member size	Weight (lbs)	Member Size	Weight (lbs)	Member Size	Weight (lbs)	Member size	Weight (lbs)	Member Size	Weight (lbs)	Member Size	Weight (lbs)
30-3-8	Roof	HSS4X4X5/16	1,177	W30X108	4,320	W8X40	2,080	HSS4X4X5/16	1,177	W30X108	4,320	W8X40	2,080
	3	HSS7X7X1/2	2,759	W30X99	3,960	W12X96	4,992	HSS7X7X1/2	2,759	W30X99	3,960	W10X77	4,004
	2	HSS8X8X5/8	3,892	W33X130	7,800	W14X132	6,864	HSS8X8X5/8	3,892	W36X135	8,100	W12X96	4,992
30-3-6	Roof	HSS4X4X5/16	1,177	W30X108	4,320	W8X40	2,080	HSS4X4X5/16	1,177	W30X108	4,320	W8X40	2,080
	3	HSS7X7X1/2	2,759	W30X99	3,960	W12X96	4,992	HSS7X7X1/2	2,759	W30X99	3,960	W10X77	4,004
	2	HSS8X8X5/8	3,892	W33X130	5,200	W14X132	6,864	HSS8X8X5/8	3,892	W36X135	5,400	W12X96	4,992
20-3-8	Roof	HSS3-1/2X3-1/2X1/4	690	W24X76	3,040	W8X40	2,080	HSS3-1/2X3-1/2X1/4	690	W24X76	3,040	W8X40	2,080
	3	HSS5-1/2X5-1/2X3/8	1,636	W21X50	2,000	W10X68	3,536	HSS5-1/2X5-1/2X3/8	1,636	W24X68	2,720	W8X67	3,484
	2	HSS6X6X1/2	2,312	W24X84	3,360	W10X77	4,004	HSS6X6X1/2	2,312	W30X99	3,960	W10X68	3,536
20-3-6	Roof	HSS3-1/2X3-1/2X1/4	690	W24X76	3,040	W8X40	2,080	HSS3-1/2X3-1/2X1/4	690	W24X76	3,040	W8X40	2,080
	3	HSS5-1/2X5-1/2X3/8	1,636	W21X50	2,000	W10X68	3,536	HSS5-1/2X5-1/2X3/8	1,636	W24X68	2,720	W8X67	3,484
	2	HSS6X6X1/2	2,312	W24X84	5,040	W10X77	4,004	HSS6X6X1/2	2,312	W30X99	5,940	W10X68	3,536
30-9-8	Roof	HSS4-1/2X4-1/2X5/16	1,347	W30X116	4,640	W8X40	2,080	HSS4-1/2X4-1/2X5/16	1,347	W30X116	4,640	W8X40	2,080
	9	HSS7X7X5/8	3,333	W24X76	3,040	W12X96	4,992	HSS7X7X5/8	3,333	W27X94	3,760	W10X88	4,576
	8	HSS9X9X5/8	4,449	W30X116	4,640	W12X106	5,512	HSS9X9X5/8	4,449	W30X116	4,640	W12X96	4,992
	7	W10X88	5,773	W30X124	4,960	W14X283	14,716	W10X88	5,773	W30X124	4,960	W14X233	12,116
	6	W12X96	6,298	W24X68	2,720	W14X283	14,716	W12X96	6,298	W24X76	3,040	W14X233	12,116
	5	W12X96	6,298	W30X124	4,960	W14X455	23,660	W12X96	6,298	W30X124	4,960	W14X426	22,152
	4	W12X106	6,954	W27X84	3,360	W14X455	23,660	W12X106	6,954	W30X99	3,960	W14X426	22,152
	3	W12X106	6,954	W30X124	4,960	W14X665	34,580	W12X106	6,954	W30X124	4,960	W14X605	31,460
	2	W12X106	6,954	W18X40	2,400	W14X665	34,580	W12X106	6,954	W21X44	2,640	W14X605	31,460

Table A.3 Member sizes of lateral-force resisting systems (continued)

Name	Floor Level	Seismic Design (Beams)						Seismic Design (Girders)					
		Braces		Beams		Columns		Braces		Girders		Columns	
		Member size	Weight (lbs)	Member Size	Weight (lbs)	Member Size	Weight (lbs)	Member size	Weight (lbs)	Member Size	Weight (lbs)	Member Size	Weight (lbs)
30-9-6	Roof	HSS4-1/2X4-1/2X5/16	1,347	W30X116	4,640	W8X40	2,080	HSS4-1/2X4-1/2X5/16	1,347	W30X116	4,640	W8X40	2,080
	9	HSS7X7X5/8	3,333	W24X76	3,040	W12X96	4,992	HSS7X7X5/8	3,333	W24X76	3,040	W10X88	4,576
	8	HSS9X9X5/8	4,449	W30X116	4,640	W12X106	5,512	HSS9X9X5/8	4,449	W30X116	4,640	W10X88	4,576
	7	W10X77	5,052	W30X124	4,960	W14X257	13,364	W10X77	5,052	W30X124	4,960	W14X233	12,116
	6	W10X88	5,773	W30X99	3,960	W14X257	13,364	W10X88	5,773	W30X99	3,960	W14X233	12,116
	5	W12X96	6,298	W30X124	4,960	W14X455	23,660	W12X96	6,298	W30X124	4,960	W14X398	20,696
	4	W12X96	6,298	W18X35	1,400	W14X455	23,660	W12X96	6,298	W21X44	1,760	W14X398	20,696
	3	W12X96	6,298	W30X124	4,960	W14X665	34,580	W12X96	6,298	W30X124	4,960	W14X550	28,600
2	W12X96	6,298	W18X35	1,400	W14X665	34,580	W12X96	6,298	W18X40	1,600	W14X550	28,600	
20-9-8	Roof	HSS3-1/2X3-1/2X1/4	690	W24X76	3,040	W8X40	2,080	HSS3-1/2X3-1/2X1/4	690	W24X76	3,040	W8X40	2,080
	9	HSS6X6X1/2	2,312	W16X40	1,600	W8X67	3,484	HSS6X6X1/2	2,312	W21X50	2,000	W8X67	3,484
	8	HSS7X7X1/2	2,759	W21X55	2,200	W10X68	3,536	HSS7X7X1/2	2,759	W24X62	2,480	W8X67	3,484
	7	HSS7X7X5/8	3,333	W18X55	2,200	W14X159	8,268	HSS7X7X5/8	3,333	W21X62	2,480	W14X145	7,540
	6	HSS8X8X5/8	3,892	W21X62	2,480	W14X159	8,268	HSS8X8X5/8	3,892	W24X68	2,720	W14X145	7,540
	5	HSS8X8X5/8	3,892	W21X68	2,720	W14X283	14,716	HSS8X8X5/8	3,892	W24X76	3,040	W14X283	14,716
	4	HSS9X9X5/8	4,449	W21X55	2,200	W14X283	14,716	HSS9X9X5/8	4,449	W24X68	2,720	W14X283	14,716
	3	HSS9X9X5/8	4,449	W21X62	2,480	W14X426	22,152	HSS9X9X5/8	4,449	W24X76	3,040	W14X426	22,152
2	HSS9X9X5/8	4,449	W14X22	880	W14X426	22,152	HSS9X9X5/8	4,449	W18X35	1,400	W14X426	22,152	

Table A.3 Member sizes of lateral-force resisting systems (continued)

Name	Floor Level	Seismic Design (Beams)						Seismic Design (Girders)					
		Braces		Beams		Columns		Braces		Girders		Columns	
		Member size	Weight (lbs)	Member Size	Weight (lbs)	Member Size	Weight (lbs)	Member size	Weight (lbs)	Member Size	Weight (lbs)	Member Size	Weight (lbs)
20-9-6	Roof	HSS3-1/2X3-1/2X1/4	690	W24X76	3,040	W8X40	2,080	HSS3-1/2X3-1/2X1/4	690	W24X76	3,040	W8X40	2,080
	9	HSS5-1/2X5-1/2X3/8	1,636	W16X40	1,600	W8X67	3,484	HSS5-1/2X5-1/2X3/8	1,636	W18X46	1,840	W8X58	3,016
	8	HSS7X7X1/2	2,759	W30X99	3,960	W8X67	3,484	HSS7X7X1/2	2,759	W30X99	3,960	W8X58	3,016
	7	HSS7X7X1/2	2,759	W18X55	2,200	W14X159	8,268	HSS7X7X1/2	2,759	W21X62	2,480	W14X145	7,540
	6	HSS7X7X5/8	3,333	W24X62	2,480	W14X159	8,268	HSS7X7X5/8	3,333	W24X68	2,720	W14X145	7,540
	5	HSS7X7X5/8	3,333	W18X55	2,200	W14X283	14,716	HSS7X7X5/8	3,333	W21X62	2,480	W14X283	14,716
	4	HSS8X8X5/8	3,892	W21X55	2,200	W14X283	14,716	HSS8X8X5/8	3,892	W24X62	2,480	W14X283	14,716
	3	HSS8X8X5/8	3,892	W18X55	2,200	W14X398	20,696	HSS8X8X5/8	3,892	W21X62	2,480	W14X398	20,696
2	HSS8X8X5/8	3,892	W12X19	760	W14X398	20,696	HSS8X8X5/8	3,892	W16X31	1,240	W14X398	20,696	

Table A.4 Member sizes of gravity columns

Name	Floor Level	Edge Column		Corner Column	
		Member size	Weight (lbs)	Member size	Weight (lbs)
30-3-8	Roof	W8X31	1,612	W8X31	1,612
	3	W8X35	1,820	W8X31	1,612
	2	W12X53	2,756	W8X31	1,612
30-3-6	Roof	W8X31	1,612	W8X31	1,612
	3	W10X33	1,716	W8X31	1,612
	2	W10X49	2,548	W8X31	1,612
20-3-8	Roof	W8X31	1,612	W8X31	1,612
	3	W8X31	1,612	W8X31	1,612
	2	W8X31	1,612	W8X31	1,612
20-3-6	Roof	W8X31	1,612	W8X31	1,612
	3	W8X31	1,612	W8X31	1,612
	2	W8X31	1,612	W8X31	1,612
30-9-8	Roof	W8X31	1,612	W8X31	1,612
	9	W8X31	1,612	W8X31	1,612
	8	W8X31	1,612	W8X31	1,612
	7	W8X40	2,080	W8X31	1,612
	6	W10X49	2,548	W8X31	1,612
	5	W12X58	3,016	W10X39	2,028
	4	W12X65	3,380	W10X45	2,340
	3	W12X72	3,744	W10X49	2,548
30-9-6-gc	Roof	W8X31	1,612	W8X31	1,612
	9	W8X31	1,612	W8X31	1,612
	8	W8X31	1,612	W8X31	1,612
	7	W8X35	1,820	W8X31	1,612
	6	W8X48	2,496	W8X31	1,612
	5	W10X49	2,548	W8X35	1,820
	4	W12X58	3,016	W8X40	2,080
	3	W12X65	3,380	W8X48	2,496
	2	W12X72	3,744	W10X49	2,548

Table A.4 Member sizes of gravity columns (continued)

Name	Floor Level	Edge Column		Corner Column	
		Member size	Weight (lbs)	Member size	Weight (lbs)
20-9-8	Roof	W8X31	1,612	W8X31	1,612
	9	W8X31	1,612	W8X31	1,612
	8	W8X31	1,612	W8X31	1,612
	7	W8X31	1,612	W8X31	1,612
	6	W8X31	1,612	W8X31	1,612
	5	W8X31	1,612	W8X31	1,612
	4	W10X39	2,028	W8X31	1,612
	3	W10X45	2,340	W8X31	1,612
	2	W10X49	2,548	W8X31	1,612
20-9-6	Roof	W8X31	1,612	W8X31	1,612
	9	W8X31	1,612	W8X31	1,612
	8	W8X31	1,612	W8X31	1,612
	7	W8X31	1,612	W8X31	1,612
	6	W8X31	1,612	W8X31	1,612
	5	W8X31	1,612	W8X31	1,612
	4	W8X35	1,820	W8X31	1,612
	3	W8X40	2,080	W8X31	1,612
	2	W10X45	2,340	W8X31	1,612

Appendix B. Design of the SimaPro Model, Including Assemblies, Waste Scenarios, and Life Cycles of the Traditional and Deconstructable Buildings

To aid in the reproducibility of the LCA study, screenshots of all assemblies, waste scenarios, and life cycles that make up the SimaPro models of the traditional building, traditional floor framing, deconstructable components, and deconstructable building are attached below (PRÉ 2014). Inputs and outputs are included, and where parameters are used, these are also shown. Parameters have been summarized in Table 4.1-Table 4.3. As an example, values shown are for the 30-3-8 buildings, which have 30 ft. by 30 ft. bays, three floors, and 8 in. thick floors.

The first step in creating the life cycles of a building in SimaPro is to define the “assemblies” that make up the building. An assembly is a collection of materials and processes that can be grouped together as a functional unit. Subassemblies may also make up an assembly. Figure B.1 shows the materials that make up the floor system of a traditional building. The appropriate steels for rebar, headed stud anchors, and the cold formed deck are included, along with the concrete that will be cast in place.

Figure B.2 shows the various parameters that can be adjusted to affect the quantities of steel and concrete required for floor system of the traditional building. Deck weight and the density of concrete are the only listed parameters that remain constant. Below the list of input parameters is a list of calculated parameters. Calculated parameters are dependent upon the input parameters. For example, the inputs of number of floors, bay width, and deck weight are used to calculate the total weight of cold formed steel required for the deck.

Figure B.3 describes the inputs to the assembly of the traditional building. The traditional floor system is a sub-assembly to the traditional building. The additional required materials are the rolled steel that make up the columns, beams, girders, and braces. Figure B.4 shows the lone parameter required to describe the traditional building. As all other material quantities are described in the sub-assembly of the traditional floor system, the only input required is the rolled steel required for the columns, beams, girders, and braces.

Figure B.5 and Figure B.6 show the inputs and parameters of the deconstructable components. Channels must be transported from their manufacturing or distribution centers to the locations where precast planks will be manufactured. The transportation of other materials, like the beams and clamps, is captured in the life cycle stage of analysis, because those components are assembled on site.

Figure B.7 and Figure B.8 describe the waste scenario of sorting and disposing of concrete. This scenario takes all concrete and sends it to sorting as shown under the “Inputs from the technosphere” line in Figure B.7. After the concrete has been sorted, it is either sent to landfill or recycled as shown under the “Materials and/or waste types separated from waste stream” line in Figure B.7. Both concrete and cement waste types are considered. The percentage of material that is designated to landfill or recycle is defined by a normal distribution centered about a fifty percent recycling rate as shown in Figure B.8.

Figure B.9 shows the waste scenario for disposing of the materials in a traditional fashion, i.e., without reusing them. Concrete and cement are sorted and either disposed of or sent to landfill, as described previously, and steel is recycled.

Figure B.10 and Figure B.11 show the custom end of life scenario that accounts for the impacts of reusing Design for Deconstruction components. Figure B.10 shows the two major transportations considered, the transportation of materials by truck to storage and the transportation of laborers to deconstruct the components. Figure B.11 shows the parameters that affect these transportation requirements: the distance from the jobsite to storage, the commute distance of laborers, and the time required to deconstruct the building. All values shown are the required values per ton of material reused.

Figure B.12 and Figure B.13 describe the life cycle of the traditional building. Figure B.12 shows that the assembly considered is the “Traditional Building” assembly described in Figure B.3 and Figure B.4. The processes involved are the transportation of materials to site and the transportation of laborers. The waste scenario is the traditional disposal scenario described in Figure B.9. The relevant parameters, shown in Figure B.13, are the quantities of steel and concrete, the distances to manufacturers, and the commute distances and total labor days required.

To calculate the reuse and disposal impacts of deconstructable components, two life cycles have been created for the DfD components. The first life cycle, shown in Figure B.14, models the impacts of DfD components when they are reused and not disposed of. This life cycle uses a “dummy” waste scenario at the end of life of the components. The dummy wastes scenario is an empty scenario that does not impose any environmental impacts. The second life cycle, shown in Figure B.15, models the impacts of DfD components when they are disposed of at the end of their useful life or when they have been damaged in deconstruction. In this life cycle, traditional disposal conditions, as described in Figure B.9, are applied to the DfD components.


Figure B.16 and Figure B.17 describe the life cycle of the Design for Deconstruction building. The assembly considered is the “DfD Components” assembly described in Figure B.5 and Figure B.6. Transportation of materials and workers are the processes that also contribute to the

environmental impacts of the DfD building. The waste scenario described in Figure B.10 and Figure B.11 is applied to the DfD building. The parameters shown in Figure B.17 are the distances from manufacturers and distribution centers to the jobsite, material quantities for transportation calculations, and labor requirements.

C:\Users\Public\Documents\SimaPro\Database\USEL_2013_Library; Design for Deconstruction - [Edit assembly 'Traditional Floor System']

File Edit Calculate Tools Window Help

Input/output Parameters

Name: Traditional Floor System Image:  Comment: Values for entire traditional building

Status: None

Materials/Assemblies	Amount	Unit	Distribution SD ² or 2*SDMin	Max	Comment
Steel rebar, blast furnace and electric arc furnace route, production mix, at plant GLO S	rebar = 2.65E4	lb			rebar
Steel, converter, unalloyed, at plant/US- US-EI U	studs = 4.97E3	lb			studs
Cold rolled sheet, steel, at plant NREL/RNA U	deck = 4.37E4	lb			deck
Concrete, normal, at plant (2380 kg/m3)/US* US-EI U	concrete = 1.91E6	lb			concrete
(Insert line here)					

Processes	Amount	Unit	Distribution SD ² or 2*SDMin	Max	Comment
(Insert line here)					

NEU 8.0.2 PhD

Figure B.1 Assembly – Floor System of Traditional Building, Inputs

C:\Users\Public\Documents\SimaPro\Database\USEI_2013_Library; Design for Deconstruction - [Edit assembly 'Traditional Floor

File Edit Calculate Tools Window Help

Input/output Parameters

Input parameters						
Name	Value	Distribution	SD^2 or 2*SDMin	Max	Hide	Comment
bay_width	30	Undefined			<input type="checkbox"/>	ft
deck_weight	1.8	Undefined			<input checked="" type="checkbox"/>	lb/ft2
density_conc	145	Undefined			<input checked="" type="checkbox"/>	lb/ft3
floor_depth	0.6666667	Undefined			<input type="checkbox"/>	ft
number_of_floors	3	Undefined			<input type="checkbox"/>	
studs	4968	Undefined			<input type="checkbox"/>	lb
(Insert line here)						
Calculated parameters						
Name	Expression					Comment
concrete	$density_conc * number_of_floors * (floor_depth - 0.125) * 9 * bay_width^2 = 1.91E6$					lb
deck	$number_of_floors * deck_weight * 9 * bay_width^2 = 4.37E4$					lb
rebar	$iff(floor_depth = .5, .82, 1.09) * number_of_floors * 9 * bay_width^2 = 2.65E4$					lb
(Insert line here)						

No	Error	Additional info


NEU

Figure B.2 Assembly – Floor system of Traditional Building, Parameters

C:\Users\Public\Documents\SimaPro\Database\USEI_2013_Library; Design for Deconstruction - [Edit assembly 'Traditional Building']

File Edit Calculate Tools Window Help

Input/output Parameters

Name: Traditional Building Image:  Comment:

Status:

Materials/Assemblies	Amount	Unit	Distribution	SD ² or 2*SDMin	Max	Comment
Steel hot rolled section, blast furnace and electric arc furnace route, production mix, at plant GLO S	steel_hot_rolled = 2.28E5	lb				beams, girders, braces, and columns
Traditional Flooring	1	p	Undefined			

(Insert line here)

Processes	Amount	Unit	Distribution	SD ² or 2*SDMin	Max	Comment
(Insert line here)						

NEU 8.0.2 PhD

Figure B.3 Assembly– Traditional Building, Inputs

C:\Users\Public\Documents\Simapro\Database\USEI_2013_Library; Design for Deconstruction - [Edit assembly 'Traditional B

File Edit Calculate Tools Window Help

Input/output Parameters

Input parameters

Name	Value	Distribution	SD ² or 2*SDMin	Max	Hide	Comment
steel_hot_rolled	227792	Undefined			<input type="checkbox"/>	lbs
(Insert line here)						

Calculated parameters

Name	Expression	Comment
(Insert line here)		

No	Error	Additional info

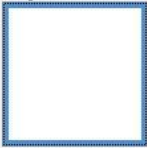
NEU

Figure B.4 Assembly – Traditional Building, Parameters

C:\Users\Public\Documents\SimaPro\Database\USEI_2013_Library; Design for Deconstruction - [Edit assembly 'Dfd Components']

File Edit Calculate Tools Window Help

Input/output Parameters

Name: Dfd Components
 Image: 
 Comment: Components of the Dfd building that can be reused

Status: None

Materials/Assemblies	Amount	Unit	Distribution	SD ² or 2*SDMin	Max	Comment
Cast iron, at plant/US- US-EI U	clamps = 1.9E4	lb				clamps
Pre-cast concrete, min. reinf., prod. mix, concrete type C20/25, w/o consideration of casings RER S	concrete+rebar = 2.37E6	lb				conc. & reinforcement
Steel hot rolled section, blast furnace and electric arc furnace route, production mix, at plant GLO S	steel_structural = 2.34E5	lb				structural steel
Steel hot rolled section, blast furnace and electric arc furnace route, production mix, at plant GLO S	channels = 1.73E5	lb				channels
Steel, converter, unalloyed, at plant/US- US-EI U	steel_bolts = 6.34E3	lb				bolts
(Insert line here)						
Processes	Amount	Unit	Distribution	SD ² or 2*SDMin	Max	Comment
Transport, lorry >28t, fleet average/US* US-EI U	transp_channels = 3.46E4	tmi*				tmi transported from channel manuf plant to precast manuf plant
(Insert line here)						

NEU 8.0.2 PhD

Figure B.5 Assembly – Dfd Components, Inputs

C:\Users\Public\Documents\SimaPro\Database\USEI_2013_Library; Design for Deconstruction - [Edit assembly 'DfD Components']

File Edit Calculate Tools Window Help

Input/output Parameters

Input parameters						
Name	Value	Distribution	SD^2 or 2*SDMin	Max	Hide	Comment
bay_width	30	Undefined			<input type="checkbox"/>	ft
density_conc	145	Undefined			<input checked="" type="checkbox"/>	lb/ft ³
dist_manuf_channels	400	Uniform	360	420	<input type="checkbox"/>	miles from channel manuf plant to precast manuf plant
floor_depth	0.6666667	Undefined			<input type="checkbox"/>	ft
number_of_floors	3	Undefined			<input type="checkbox"/>	number of floors
steel_bolts	6336	Undefined			<input type="checkbox"/>	lb bolts
steel_structural	233732	Undefined			<input type="checkbox"/>	lb structural steel
(Insert line here)						
Calculated parameters						
Name	Expression	Comment				
concrete	$\text{number_of_floors} * \text{density_conc} * \text{floor_depth} * 9 * \text{bay_width}^2 = 2.35\text{E}6$	lb concrete				
clamps	$\text{steel_bolts} * 3 = 1.9\text{E}4$	lb clamps				
channels	$\text{iff}(\text{floor_depth} = .5, 2.527, 7.116) * \text{number_of_floors} * 9 * \text{bay_width}^2 = 1.73\text{E}5$	lb channels				
transp_channels	$\text{channels} * \text{dist_manuf_channels} / 2000 = 3.46\text{E}4$	tmi transported from channel manuf plant to precast manuf plant				
rebar	$0.668 * \text{number_of_floors} * 9 * \text{bay_width}^2 = 1.62\text{E}4$	lb rebar				
(Insert line here)						

No	Error	Additional info

NEU

Figure B.6 Assembly – DfD Components, Parameters

C:\Users\Public\Documents\Simapro\Database\USEI_2013_Library; Design for Deconstruction - [Edit waste scenario process 'Concrete Sorting and Disposing']

File Edit Calculate Tools Window Help

Documentation Input/output Parameters System description

Products

Waste specification

Name	Amount	Unit	Category	Comment
Concrete Sorting and Disposing	1	ton	Others	

Inputs

Known inputs from technosphere (materials/fuels)

Name	Amount	Unit	Distribution	SD^2 or 2*SDMin	Max
(Insert line here)					

Known inputs from technosphere (electricity/heat)

Name	Amount	Unit	Distribution	SD^2 or 2*SDMin
Disposal, building, concrete, not reinforced, to sorting plant/CH U (COPY)	1	ton	Undefined	
(Insert line here)				

Outputs

Materials and/or waste types separated from waste stream

Waste scenario/treatment	Material / Waste type	Percentage
Disposal, building, concrete, not reinforced, to recycling/US* US-EI U	Concrete	percent_conc_recycled = 50%
Disposal, building, concrete, not reinforced, to recycling/US* US-EI U	Cement	percent_conc_recycled = 50%
Disposal, building, concrete, not reinforced, to final disposal/US* US-EI U	Concrete	100-percent_conc_recycled = 50%
Disposal, building, concrete, not reinforced, to final disposal/US* US-EI U	Cement	100-percent_conc_recycled = 50%
(Insert line here)		

Waste streams remaining after separation

Waste scenario/treatment	Percentage	Comment
DummyWasteTreatment	100 %	
(Insert line here)		

NEU

Figure B.7 Waste Scenario – Concrete Sorting and Disposing, Inputs and Waste Treatments

C:\Users\Public\Documents\Simapro\Database\USEI_2013_Library; Design for Deconstruction - [Edit waste scenario]

File Edit Calculate Tools Window Help

Documentation | Input/output | Parameters | System description |

Input parameters

Name	Value	Distribution	SD ² or 2*SDMin	Max	Hide	Comment
percent_conc_recycled	50	Normal	34		<input type="checkbox"/>	percent
(Insert line here)						

Calculated parameters

Name	Expression	Comment
(Insert line here)		

No	Error	/	Additional info

NEU

Figure B.8 Waste Scenario – Concrete Sorting and Disposing, Parameters

C:\Users\Public\Documents\SimaPro\Database\USEI_2013_Library; Design for Deconstruction - [Edit waste scenario process 'Traditional Building - Disposal']

File Edit Calculate Tools Window Help

Documentation Input/output Parameters System description

Products

Waste specification

Name	Amount	Unit	Category	Comment
Traditional Building - Disposal	1	ton	Waste USA	

Inputs

Known inputs from technosphere (materials/fuels)

Name	Amount	Unit	Distribution	SD ² or 2*SDMin	Max	Comment
(Insert line here)						

Known inputs from technosphere (electricity/heat)

Name	Amount	Unit	Distribution	SD ² or 2*SDMin	Max	Comment
(Insert line here)						

Outputs

Materials and/or waste types separated from waste stream

Waste scenario/treatment	Material / Waste type	Percentage	Comment
Concrete Sorting and Disposing	Concrete	100 %	Custom scenario to sort concrete, then split it to recycling and landfill
Concrete Sorting and Disposing	Cement	100 %	
Recycling steel and iron/US- US-EI U	Steel	100 %	
(Insert line here)			

Waste streams remaining after separation

Waste scenario/treatment	Percentage	Comment
Disposal, building, reinforced concrete, to final disposal/US* US-EI U	100 %	
(Insert line here)		

NEU

8.0.2 PhD

Figure B.9 Waste Scenario – Traditional Building, Inputs and Waste Scenarios

C:\Users\Public\Documents\SimaPro\Database\USEI_2013_Library; Design for Deconstruction - [Edit waste scenario process 'Reuse of DfD Building components']

File Edit Calculate Tools Window Help

Documentation Input/output Parameters System description

Products

Waste specification

Name	Amount	Unit	Category	Comment
Reuse of DfD Building components	1	ton*	Recycling	Aside from transport and laborer commutes, this is an empty process, because I will be manually recreating reuse scenarios with Excel. Assume all items are stored in the same location.

Inputs

Known inputs from technosphere (materials/fuels)

Name	Amount	Unit	Distribution	SD^2 or 2*SDMin	Max	Comment
(Insert line here)						

Known inputs from technosphere (electricity/heat)

Name	Amount	Unit	Distribution	SD^2 or 2*SDMin	Max	Comment
Transport, lorry >28t, fleet average/US* US-EI U	dist_storage = 60	tmi*				transport items to storage
Transport, passenger car, petrol, fleet average/US* US-EI U	commute = 0.456	pmi				commute of laborers
(Insert line here)						

Outputs

Materials and/or waste types separated from waste stream

Waste scenario/treatment	Material / Waste type	Percentage	Comment
DummyWasteTreatment	All waste types	100 %	I am using this empty process, because I will be manually recreating reuse scenarios with Excel.
(Insert line here)			

Waste streams remaining after separation

Waste scenario/treatment	Percentage	Comment
DummyWasteTreatment	100 %	
(Insert line here)		

NEU

8.0.2 PhD

Figure B.10 Waste Scenario – Reuse of Design for Deconstruction Reusable Components, Inputs and Outputs

C:\Users\Public\Documents\SimaPro\Database\USEI_2013_Library; Design for Deconstruction - [Edit waste scenario process 'Reuse of DfD Building compon

File Edit Calculate Tools Window Help

Documentation | Input/output | Parameters | System description |

Input parameters

Name	Value	Distribution	SD ² or 2*SDMin	Max	Hide	Comment
dist_storage	60	Uniform		10	<input type="checkbox"/>	miles
dist_commute	6	Lognormal	6		<input type="checkbox"/>	miles one way
labor_deconstruct	0.038	Uniform		0.038	<input type="checkbox"/>	additional person-days (PER TON) to deconstruct building
(Insert line here)						

Calculated parameters

Name	Expression	Comment
commute	dist_commute*2*labor_deconstruct = 0.456	
(Insert line here)		

No	Error	Additional info

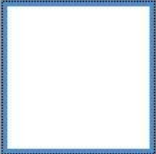
NEU

Figure B.11 Waste Scenario – Reuse of Design for Deconstruction Reusable Components, Parameters

C:\Users\Public\Documents\SimaPro\Database\USEL_2013_Library; Design for Deconstruction - [Edit life cycle 'Life Cycle_Traditional Building']

File Edit Calculate Tools Window Help

Input/output Parameters

Name: Life Cycle_Traditional Building Image:  Comment:

Status: None

Assembly	Amount	Unit	Distribution	SD ² or 2*SDMin	Max	Comment
Traditional Building	1	p	Undefined			

Processes	Amount	Unit	Distribution	SD ² or 2*SDMin	Max	Comment
Transport, passenger car, petrol, fleet average/US- US-EI U	commute = 1.92E3	pmi				commute of laborers
Transport, lorry >28t, fleet average/US* US-EI U	steel_transp = 8.33E3	tmi*				transporting steel from manf.
Transport, lorry >28t, fleet average/US* US-EI U	conc_transp = 3.82E4	tmi*				transporting concrete from manf.
(Insert line here)						

Waste/Disposal scenario: Traditional Building - Disposal Comment:

Additional life cycles	Number	Distribution	SD ² or 2*SDMin	Max	Comment
(Insert line here)					

NEU 8.0.2 PhD

Figure B.12 Life Cycle – Traditional Building, Inputs and Waste Scenario

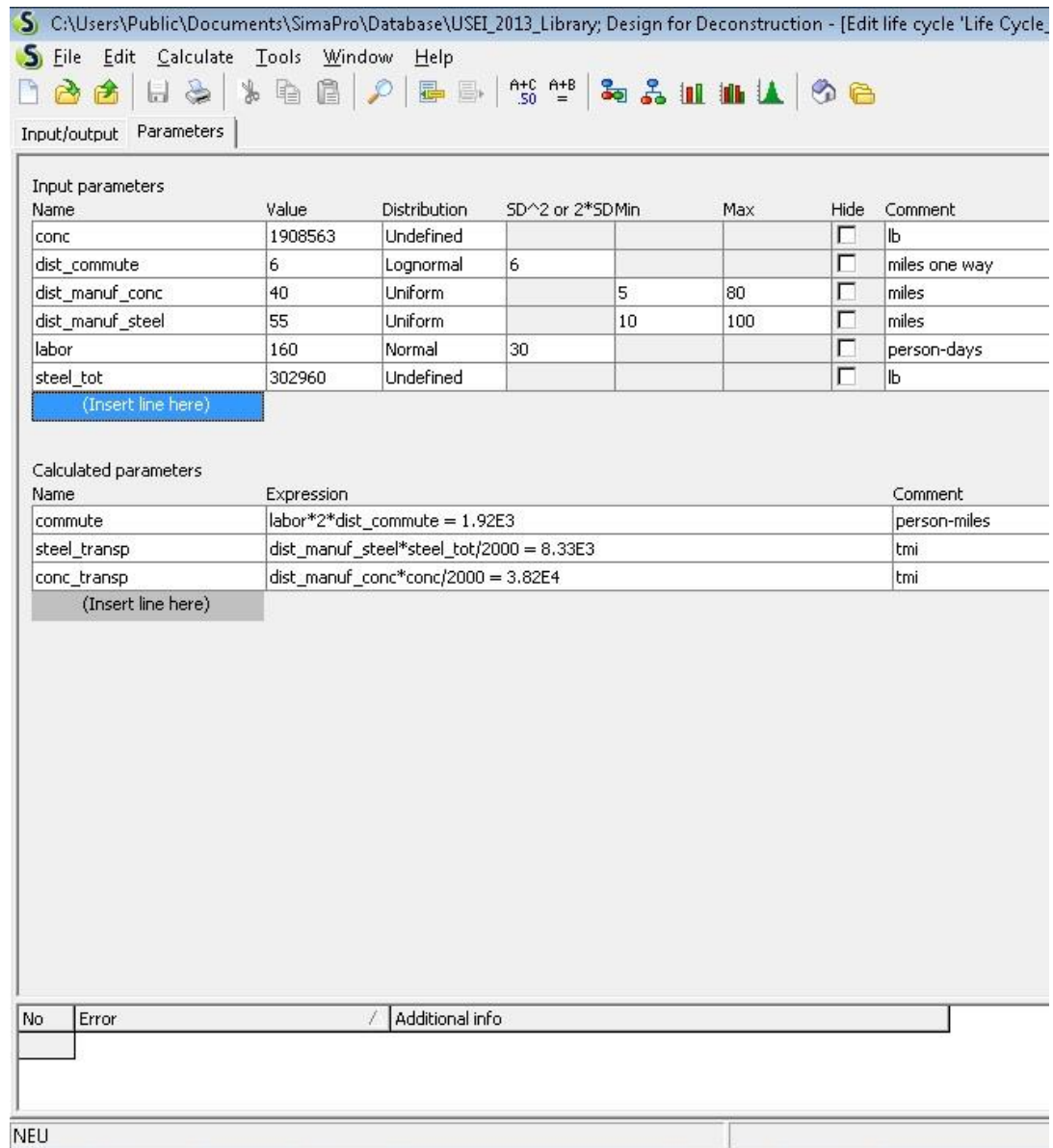
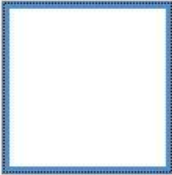


Figure B.13 Life Cycle – Traditional Building, Parameters

C:\Users\Public\Documents\SimaPro\Database\USEI_2013_Library; Design for Deconstruction - [Edit life cycle 'Life Cycle_DfD Components (no disposal)']

File Edit Calculate Tools Window Help

Input/output Parameters

Name: Life Cycle_DfD Components (no disposal) Image:  Comment: Life cycle assessment of reusable components WITHOUT disposal. This is used to calculate the impacts of disposal of reusable components.

Status: None

Assembly	Amount	Unit	Distribution	SD ² or 2*SDMin	Max	Comment
DfD Components	1	p	Undefined			

Processes

(Insert line here)	Amount	Unit	Distribution	SD ² or 2*SDMin	Max	Comment
(Insert line here)						

Waste/Disposal scenario: DummyWasteScenario Comment:

Additional life cycles

(Insert line here)	Number	Distribution	SD ² or 2*SDMin	Max	Comment
(Insert line here)					

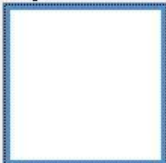
NEU 8.0.2 PhD

Figure B.14 Life Cycle – Design for Deconstruction Reusable Components (no disposal), Inputs and Waste Scenario

C:\Users\Public\Documents\SimaPro\Database\USEI_2013_Library; Design for Deconstruction - [Edit life cycle 'Life Cycle_DfD Components (final use)']

File Edit Calculate Tools Window Help

Input/output Parameters

Name: Life Cycle_DfD Components (final use) Image:  Comment: Life cycle assessment of reusable components WITH disposal. This is used to calculate the impacts of disposal of reusable components.

Status: None

Assembly	Amount	Unit	Distribution	SD ² or 2*SDMin	Max	Comment
DfD Components	1	p	Undefined			

Processes

Processes	Amount	Unit	Distribution	SD ² or 2*SDMin	Max	Comment
(Insert line here)						

Waste/Disposal scenario

Traditional Building - Disposal

Additional life cycles

Additional life cycles	Number	Distribution	SD ² or 2*SDMin	Max	Comment
(Insert line here)					

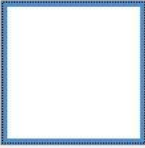
NEU 8.0.2 PhD

Figure B.15 Life Cycle – Design for Deconstruction Reusable Components (final use), Inputs and Waste Scenario

C:\Users\Public\Documents\SimaPro\Database\USEI_2013_Library; Design for Deconstruction - [Edit life cycle 'Life Cycle_DFD Building']

File Edit Calculate Tools Window Help

Input/output Parameters

Name: Life Cycle_DFD Building
 Image: 
 Comment:

Status:

Assembly	Amount	Unit	Distribution	SD^2 or 2*SDMin	Max	Comment
DFD Components	1	p	Undefined			

Processes	Amount	Unit	Distribution	SD^2 or 2*SDMin	Max	Comment
Transport, lorry >28t, fleet average/US* US-EI U	$(1-reuse)*transp_clamps_bolts_manuf+reuse*transp_clamps_bolts_storage =$	tmi*				transporting bolts and clamps from manuf and storage
Transport, lorry >28t, fleet average/US* US-EI U	$(1-reuse)*transp_planks_manuf+reuse*transp_planks_storage = 3.81E4$	tmi*				transporting planks from manuf and storage
Transport, lorry >28t, fleet average/US* US-EI U	$(1-reuse)*transp_steel_manuf+reuse*transp_steel_storage = 6.43E3$	tmi*				transporting structural steel from manuf and storage
Transport, passenger car, petrol, fleet average/US- US-EI U	commute = 1.28E3	pmi				commute of laborers
(Insert line here)						

Waste/Disposal scenario:
 Comment:

Additional life cycles	Number	Distribution	SD^2 or 2*SDMin	Max	Comment
(Insert line here)					

NEU 8.0.2 PhD

Figure B.16 Life Cycle – Design for Deconstruction Building, Inputs and Waste Scenario

C:\Users\Public\Documents\SimaPro\Database\USEI_2013_Library; Design for Deconstruction - [Edit life cycle 'Life Cycle_DfD Building']

File Edit Calculate Tools Window Help

Input/output Parameters

Input parameters

Name	Value	Distribution	SD^2 or 2*SDMin	Max	Hide	Comment
clamps_bolts	25344	Undefined			<input type="checkbox"/>	lb clamps and bolts (assumed to be manuf at same facility)
dist_commute	6	Lognormal	6		<input type="checkbox"/>	miles one way
dist_manuf_clamps_bolts	340	Uniform		320 360	<input type="checkbox"/>	miles between clamps and bolts distribution center and jobsite
dist_manuf_planks	30	Uniform		10 50	<input type="checkbox"/>	miles from precast manufacturing plant or precast storage location to jobsite
dist_manuf_structural_steel	55	Uniform		10 100	<input type="checkbox"/>	miles from steel plant to jobsite
dist_storage	55	Uniform		10 100	<input type="checkbox"/>	miles to storage from jobsite
labor_traditional	107	Normal	21		<input type="checkbox"/>	person-days to install everything
plank_weight	2538151	Undefined			<input type="checkbox"/>	lb conc+rebar+channel. Weight is for transportation calculations
reuse	0	Undefined			<input type="checkbox"/>	0 if new building. 0.7 if second life cycle
structural_steel	233732	Undefined			<input type="checkbox"/>	lb structural steel
(Insert line here)						

Calculated parameters

Name	Expression	Comment
commute	labor_traditional*2*dist_commute = 1.28E3	person miles
transp_clamps_bolts_manuf	dist_manuf_clamps_bolts*clamps_bolts/2000 = 4.31E3	tmi
transp_clamps_bolts_storage	dist_storage*clamps_bolts/2000 = 697	tmi
transp_planks_manuf	dist_manuf_planks*plank_weight/2000 = 3.81E4	tmi
transp_planks_storage	dist_storage*plank_weight/2000 = 6.98E4	tmi
transp_steel_manuf	dist_manuf_structural_steel*structural_steel/2000 = 6.43E3	tmi
transp_steel_storage	dist_storage*structural_steel/2000 = 6.43E3	tmi
(Insert line here)		

No	Error	Additional info

NEU 8.0.2 f

Figure B.17 Life Cycle – Design for Deconstruction Building, Parameter

Appendix C. Descriptions of the Products and Processes Used in LCA, Extracted from SimaPro

The figures below are the descriptions of each of the products and processes used in LCA. The information displayed is extracted from the libraries in SimaPro's databases. Some materials are represented by the closest available inventory in the SimaPro database. For example, the proprietary girder clamps are modelled using the cast iron inventory.

SimaPro 8.0.2	process	Date:	3/1/2015	Time:	4:38 PM				
Project	Design for Deconstruction								
Process									
Category type	material								
Process identifier	ELCDDATA13292600080								
Type	System								
Process name	Steel hot rolled section, blast furnace and electric arc furnace route, product								
Status	Finished								
Time period	Unspecified								
Geography	Unspecified								
Technology	Unspecified								
Representativeness	Unspecified								
Multiple output allocation	Unspecified								
Substitution allocation	Unspecified								
Cut off rules	Unspecified								
Capital goods	Unspecified								
Boundary with nature	Unspecified								
Infrastructure	No								
Date	4/9/2010								
Record	Conversion from ELCD to SimaPro was done by GreenDeltaTC, Germany, www.greendeltaTC.com.								
Generator	worldsteel								
Literature references	ELCD database 2.0								
Collection method									
Data treatment	Extrapolation: Relevant upstream data (of the DEAM database) was adapted according to the worldsteel boundary conditions, e.g. for iron ore, coke, zinc etc.								
Verification	Use advice for data set: The data set includes the burden and credit associated with the recycling of steel scrap during steel production, manufacturing and End-of-Life. For this, the current global average recycling rate is estimated to be 80 %. For specific steel data set requests contact the European Confederation of Iron and Steel Industries, Eurofer (European data): www.eurofer.org; the World Steel Association, worldsteel (Global data): www.worldsteel.org and APEAL (Steel packaging data): www.apeal.org.; Technical purpose of product or process: A steel section rolled in a hot rolling mill. Steel section includes I-beams, H-beams, wide-flange beams, and sheet piling. It can be found on the market for direct use. This product is used in construction, multi-story buildings, industrial buildings, bridge trusses, vertical highway supports, and riverbank reinforcement.; Technology description including background system: Raw material extraction and processing, e.g. coal, iron ore, etc., and recycling of steel scrap, Coke making, Sinter, Blast Furnace, Basic Oxygen Furnace, Hot strip mill. DEAM database also used. Electric Arc Furnace Route and section rolling. Steel product manufacturing route can be found in Appendices 1 and 2 of the worldsteel LCA Methodology Report. The worldsteel Recycling Methodology describes the implementation of the method in detail, incorporating a burden for using steel scrap in the steel making process and a credit for the end of life recycling of steel scrap. Steelmaking processes shown in flow diagram. Inputs included in the LCI relate to all raw material inputs, including steel scrap, energy, water, and transport.								
Comment									
Allocation rules									
System description	ELCD 2.0								
Products									
Steel hot rolled section, blast furnace and electric arc furnace route, pr		1 kg		100 Steel		Metals\Ferro			
Avoided products									

Resources			
Calcite, in ground	in ground	0.093534 kg	Undefined
Energy, from oil	in ground	1.796965 MJ	Undefined
Dolomite, in ground	in ground	0.024528 kg	Undefined
Energy, from coal	in ground	7.408719 MJ	Undefined
Metamorphous rock, graphite containing, in ground	in ground	0.205436 kg	Undefined
Iron, 46% in ore, 25% in crude ore, in ground	in ground	0.308154 kg	Undefined
Energy, from gas, natural	in ground	2.481119 MJ	Undefined
Water, unspecified natural origin/kg	in water	3.485375 kg	Undefined
Zinc, in ground	in ground	-0.00422 kg	Undefined
Materials/fuels			
Electricity/heat			
Emissions to air			
Dioxin, 2,3,7,8 Tetrachlorodibenzo-p-		3.99E-12 kg	Undefined
Cadmium		6.53E-08 kg	Undefined
Carbon dioxide, land transformation		1.099687 kg	Undefined
Carbon monoxide, fossil		0.013262 kg	Undefined
Chromium		8.83E-07 kg	Undefined
Hydrogen chloride		3.93E-05 kg	Undefined
Hydrogen sulfide		3.25E-05 kg	Undefined
Lead		2.4E-06 kg	Undefined
Mercury		1.1E-07 kg	Undefined
Methane		0.00072 kg	Undefined
Nitrogen oxides		0.001687 kg	Undefined
Dinitrogen monoxide		4.81E-05 kg	Undefined
NM VOC, non-methane volatile organic compounds, unspecified origin		0.000131 kg	Undefined
Particulates, > 2.5 um, and < 10um		0.000614 kg	Undefined
Sulfur dioxide		0.002049 kg	Undefined
Zinc		1.35E-05 kg	Undefined
Emissions to water			
Ammonia	groundwater	0.000163 kg	Undefined
Cadmium	groundwater	3.81E-09 kg	Undefined
COD, Chemical Oxygen Demand	groundwater	3.91E-05 kg	Undefined
Chromium	groundwater	4.35E-08 kg	Undefined
Iron	groundwater	0.000117 kg	Undefined
Lead	groundwater	1.96E-07 kg	Undefined
Nickel	groundwater	5.3E-08 kg	Undefined
Nitrogen	groundwater	1.65E-05 kg	Undefined
Particulates, > 10 um	groundwater	6.78E-05 kg	Undefined
Phosphate	groundwater	1.55E-05 kg	Undefined
Zinc	groundwater	3.06E-07 kg	Undefined
Emissions to soil			
Final waste flows			
Waste, unspecified		0.449876 kg	Undefined
Non material emissions			
Social issues			

SimaPro 8.0.2	process	Date:	3/1/2015	Time:	4:39 PM															
Project	Design for Deconstruction																			
Process																				
Category type	material																			
Process identifier	Standard09424500305																			
Type	Unit process																			
Process name	cast iron, at plant/kg/RER																			
Status																				
Time period	Unspecified																			
Geography	Unspecified																			
Technology	Unspecified																			
Representativeness	Unspecified																			
Multiple output allocation	Unspecified																			
Substitution allocation	Unspecified																			
Cut off rules	Unspecified																			
Capital goods	Unspecified																			
Boundary with nature	Unspecified																			
Infrastructure	No																			
Date	8/13/2007																			
Record	Data entry by: Hans-Jörg Althaus Telephone: 0041 44 823 44 94;E-mail: empa@ecoinvent.org;Company: EMPA;Country: CH																			
Generator	Generator/publisher: Hans-Jörg Althaus Telephone: 0041 44 823 44 94;E-mail: empa@ecoinvent.org;Company: EMPA;Country: CH																			
Literature references	Life Cycle Inventories of Metals/2009/Classen M. Data has been published entirely in Copyright: true																			
Collection method	Sampling procedure: Internet search																			
Data treatment	Extrapolations: see technology Uncertainty adjustments: none																			
Verification	Proof reading validation: passed Validator: Roland Hischer Telephone: 0041 71 274 78 47;E-mail: empa@ecoinvent.org;Company: EMPA;Country: CH																			
Comment	Translated name: Gusseisen, ab Werk Included processes: Transports of metal and other input materials to electric arc furnace, melting and refining process and casting. Remark: 35% scrap and 65% pig iron assumed as iron input;Geography: Data relate to plants in the EU Technology: Electric arc furnace for melting. Energy consumption and emissions from EAF steel making Version: 2.2 Synonyms: grey iron, white iron, Grauguss Energy values: Undefined Production volume: unknown Local category: Metalle Local subcategory: Gewinnung Source file: 01069.XML																			
Allocation rules																				
System description	US-EI																			

Disposal, building, concrete, not reinforced, to final disposal/US* U			1 kg	All waste ty Constructii SWITZERLAND				
Avoided products								
Resources								
Materials/fuels								
Diesel, burned in building machine/GLO US-EI U			0.0437 MJ	Lognormal	1.7			energy for demolition. Uncertainty from range in (DAFSTB 1996)
Transport, lorry 20-28t, fleet average/US* US-EI U			0.015 tkm	Lognormal	1			transport to disposal facilities. Uncertainty calculated from uncertainty in transported masses and the uncertainty in generic transportation distances
Electricity/heat								
Emissions to air								
Particulates, < 2.5 um	high. pop.		1.66E-05 kg	Lognormal	3.1			emission from dismantling and handling. (2,3,3,3,1,5) & basic uncertainty of 3;from one extrapolated PM10 emission factor and generic PM fractions from measurements
Particulates, > 2.5 um, and < 10um	high. pop.		6.34E-05 kg	Lognormal	2.1			emission from dismantling and handling. (2,3,3,3,1,5) & basic uncertainty of 2;from one extrapolated PM10 emission factor and generic PM fractions from measurements
Particulates, > 10 um	high. pop.		8.35E-05 kg	Lognormal	1.6			emission from dismantling and handling. (2,3,3,3,1,5) & basic uncertainty of 1.5;from one extrapolated PM10 emission factor and generic PM fractions from measurements
Emissions to water								
Emissions to soil								
Final waste flows								
Non material emissions								
Social issues								
Economic issues								
Waste to treatment								
Disposal, inert waste, 5% water, to inert material landfill/US* US-EI			1 kg	Lognormal	1			disposed masses. Uncertainty calculated from uncertainty of waste composition
Input parameters								
Calculated parameters								

Figure C.20 End of life process, represented by - concrete building disposal, not reinforced, to final disposal - US-EI 2.2

Allocation rules	Source file: 02149.XML				
System description	Ecoinvent				
Products					
Disposal, building, concrete, not reinforced, to so	1 kg	100	not defined	Others	SWITZERLAND
Avoided products					
Resources					
Materials/fuels					
Diesel, burned in building machine/GLO U	0.0437 MJ	Lognormal	1.7	energy for demolition. Uncertainty from range in (DAFSTB 1996)	
Excavation, hydraulic digger/RER U	0.000505 m3	Lognormal	1.2	handling in sorting plant. Uncertainty from range in literature	
Electricity, low voltage, at grid/CH U	0.0037 kWh	Lognormal	1.2	demand in sorting plant. Uncertainty from range in literature	
Transport, lorry 20-28t, fleet average/CH U	0.0218 tkm	Lognormal	1.1	transport to disposal facilities. Uncertainty calculated from uncertainty in transported masses and the uncertainty in generic transportation distances	
Electricity/heat					
Sorting plant for construction waste/CH/I U	1E-10 p	Lognormal	1	Uncertainty heeded in exchanges, 1kg = 1kg	
Emissions to air					
Particulates, < 2.5 um	high. pop.	1.66E-05 kg	Lognormal	3.1	emission from dismantling and handling. (2,3,3,3,1,5) & basic uncertainty of 3; from one extrapolated PM10 emission factor and generic PM fractions from measurements
Particulates, > 2.5 um, and < 10um	high. pop.	6.34E-05 kg	Lognormal	2.1	emission from dismantling and handling. (2,3,3,3,1,5) & basic uncertainty of 2; from one extrapolated PM10 emission factor and generic PM fractions from measurements
Particulates, > 10 um	high. pop.	8.35E-05 kg	Lognormal	1.6	emission from dismantling and handling. (2,3,3,3,1,5) & basic uncertainty of 1.5; from one extrapolated PM10 emission factor and generic PM fractions from measurements
Heat, waste	high. pop.	0.0133 MJ	Lognormal	1.2	emission in sorting plant. Uncertainty from range in literature
Emissions to water					
Emissions to soil					
Final waste flows					
Non material emissions					
Social issues					
Economic issues					
Waste to treatment					
Disposal, inert material, 0% water, to sanitary land	0.4 kg	Lognormal	1.5	disposed masses. Uncertainty calculated from uncertainty in transfer coefficients and uncertainty of waste fractions	
Input parameters					
Calculated parameters					

Figure C.22 End of life process, represented by - concrete building disposal, not reinforced, to sorting - US-EI 2.2

Products										
Cold rolled sheet, steel, at plant NREL/RNA U		1 kg		100 Steel	Metals\Fer					
Avoided products										
Resources										
Coal, 26.4 MJ per kg, in ground	in ground	0.17508 kg		Undefined						
Coal, 26.4 MJ per kg, in ground	in ground	0.621409 kg		Undefined					Value changed from	
Energy, from hydro power	in water	0.24912 MJ		Undefined					0.6615 to correct for	
Gas, natural, 46.8 MJ per kg, in ground	in ground	0.08357 kg		Undefined					changed energy	
Iron ore	in ground	1.336 kg		Undefined					content of used coal	
Limestone	in ground	0.21142 kg		Undefined						
Oil, crude, 42 MJ per kg, in ground	in ground	0.071222 kg		Undefined						
Oxygen, in air	in air	0.095477 kg		Undefined						
Uranium, 2291 GJ per kg, in ground	in ground	6.92E-07 kg		Undefined						
Wood and wood waste, 9.5 MJ per kg	biotic	0.000178 kg		Undefined						
Materials/fuels										
Proxy_Steel scrap, at plant NREL/US U		0.30826 kg		Undefined						
Electricity/heat										
Emissions to air										
Acrolein		5.98E-09 kg		Undefined						
Aldehydes, unspecified		5.36E-06 kg		Undefined						
Ammonia		1.89E-06 kg		Undefined						
Antimony		3E-09 kg		Undefined						
Arsenic		2.14E-08 kg		Undefined						
Benzene		8.51E-09 kg		Undefined						
Beryllium		2.49E-09 kg		Undefined						
Cadmium		5.56E-09 kg		Undefined						
Carbon dioxide, biogenic		0.000232 kg		Undefined						
Carbon dioxide, fossil		2.58 kg		Undefined						
Carbon monoxide		0.000514 kg		Undefined						
Carbon monoxide, fossil		0.025799 kg		Undefined						
Chlorine		1.46E-08 kg		Undefined						
Chromium		3.44E-08 kg		Undefined						
Cobalt		8.53E-09 kg		Undefined						
Dinitrogen monoxide		3.73E-06 kg		Undefined						
Dioxin, 2,3,7,8 Tetrachlorodibenzo-p-		3.26E-14 kg		Undefined						
Ethene, tetrachloro-		5.69E-09 kg		Undefined						
Ethene, trichloro-		5.64E-09 kg		Undefined						
Formaldehyde		2.09E-06 kg		Undefined						
Hydrogen chloride		3.02E-05 kg		Undefined						
Hydrogen fluoride		4.17E-06 kg		Undefined						
Kerosene		1.53E-07 kg		Undefined						
Lead		2.09E-08 kg		Undefined						
Manganese		6.77E-08 kg		Undefined						
Mercury		1.16E-08 kg		Undefined						
Metals, unspecified		9.33E-08 kg		Undefined						
Methane		0.001449 kg		Undefined						
Methane, dichloro-, HCC-30		2.54E-08 kg		Undefined						
Methane, tetrachloro-, CFC-10		9.44E-09 kg		Undefined						
N-Nitrodimethylamine		1.26E-09 kg		Undefined						

	Permanent data set URL: http://lca.jrc.ec.europa.eu/lcaifohub/datasets/elcd/processes/898618b0-3306-11dd-bd11-0800200c9a66_02.00.000.xml								
Allocation rules									
System description	ELCD 2.0								
Products									
Pre-cast concrete, min. reinf., prod. mix, concrete type		1 kg	100	Cement	Construction	Concrete			
Avoided products									
Resources									
Air	in air	0.096872	kg	Undefined					
Barite, 15% in crude ore, in ground	in ground	2.05E-17	kg	Undefined					
Barite, 15% in crude ore, in ground	in ground	1.93E-05	kg	Undefined					
Basalt, in ground	in ground	1.22E-06	kg	Undefined					
Aluminium, 24% in bauxite, 11% in crude ore, in ground	in ground	0.000393	kg	Undefined					
Clay, bentonite, in ground	in ground	0.000262	kg	Undefined					
Biomass, feedstock	biotic	3.86E-12	MJ	Undefined					
Energy, from coal, brown	in ground	0.122594	MJ	Undefined					
Calcite, in ground	in ground	0.226798	kg	Undefined					
Calcium chloride	in ground	2.1E-15	kg	Undefined					
Carbon dioxide, in air	in air	0.000369	kg	Undefined					
Chromium, in ground	in ground	1.35E-06	kg	Undefined					
Clay, unspecified, in ground	in ground	0.006926	kg	Undefined					
Colemanite, in ground	in ground	3.35E-08	kg	Undefined					
Copper, in ground	in ground	7.23E-08	kg	Undefined					
Energy, from oil	in ground	0.172269	MJ	Undefined					
Dolomite, in ground	in ground	6.15E-10	kg	Undefined					
Fluorspar, 92%, in ground	in ground	2.87E-09	kg	Undefined					
Gold, in ground	in ground	6.08E-13	kg	Undefined					
Water, well, in ground	in water	0.00014	m3	Undefined					
Gypsum, in ground	in ground	0.004795	kg	Undefined					
Energy, from coal	in ground	0.209065	MJ	Undefined					
Metamorphous rock, graphite containing, in ground	in ground	0.178583	kg	Undefined					
Iron, 46% in ore, 25% in crude ore, in ground	in ground	0.001053	kg	Undefined					
Kaolinite, 24% in crude ore, in ground	in ground	2.63E-08	kg	Undefined					
Lead, in ground	in ground	2E-07	kg	Undefined					
Magnesite, 60% in crude ore, in ground	in ground	3.04E-08	kg	Undefined					
Magnesium chloride	in ground	2.09E-05	kg	Undefined					
Manganese, in ground	in ground	4.25E-05	kg	Undefined					
Molybdenum, in ground	in ground	8.1E-11	kg	Undefined					
Natural aggregate	in ground	0.8268	kg	Undefined					
Energy, from gas, natural	in ground	0.052647	MJ	Undefined					
Nickel, in ground	in ground	5.34E-06	kg	Undefined					
Nitrogen, in air	in air	-7E-10	kg	Undefined					
Olivine, in ground	in ground	1.1E-18	kg	Undefined					
Oxygen, in air	in air	-0.0002	kg	Undefined					
Palladium, in ground	in ground	4.39E-15	kg	Undefined					
Energy, from peat	in ground	5.66E-07	MJ	Undefined					
Phosphorus, in ground	in ground	1.45E-09	kg	Undefined					
Platinum, in ground	in ground	5.27E-14	kg	Undefined					
Potassium chloride	in ground	3.19E-08	kg	Undefined					
Energy, geothermal, converted	in ground	8.66E-06	MJ	Undefined					

Zinc	ocean	1.36E-08	kg	Undefined															
Zinc	groundwater	2.45E-09	kg	Undefined															
Emissions to soil																			
Aluminium		8.71E-10	kg	Undefined															
Ammonia		3.94E-07	kg	Undefined															
Arsenic		3.09E-13	kg	Undefined															
Bromide		1.17E-10	kg	Undefined															
Cadmium		3.35E-12	kg	Undefined															
Calcium		2.77E-09	kg	Undefined															
Chloride		1.37E-07	kg	Undefined															
Chromium		7.7E-10	kg	Undefined															
Chromium, ion		2.77E-11	kg	Undefined															
Cobalt		1.37E-11	kg	Undefined															
Copper		3.55E-11	kg	Undefined															
Decane		2.05E-08	kg	Undefined															
Fluoride		3.9E-09	kg	Undefined															
Iron		1.12E-09	kg	Undefined															
Lead		4.17E-11	kg	Undefined															
Magnesium		3.84E-10	kg	Undefined															
Manganese		1.66E-10	kg	Undefined															
Mercury		2.92E-13	kg	Undefined															
Nickel		2.55E-10	kg	Undefined															
Phosphate		2.26E-07	kg	Undefined															
Potassium		9.96E-08	kg	Undefined															
Sodium		2.42E-10	kg	Undefined															
Strontium		2.49E-07	kg	Undefined															
Sulfate		1.26E-08	kg	Undefined															
Sulfide		7.56E-08	kg	Undefined															
Zinc		1.97E-10	kg	Undefined															
Final waste flows																			
Calcium fluoride waste		1.75E-08	kg	Undefined															
Construction waste		5.6E-05	kg	Undefined															
Waste, nuclear, unspecified/kg		5.22E-08	kg	Undefined															
Waste, nuclear, unspecified/kg		6.2E-08	kg	Undefined															
Mineral waste, from mining		0.054106	kg	Undefined															
Mineral waste, from mining		0.196667	kg	Undefined															
Waste, nuclear, unspecified/kg		1.04E-10	kg	Undefined															
Radioactive tailings		3.07E-05	kg	Undefined															
Slags		8.05E-06	kg	Undefined															
Slag (uranium conversion)		1.16E-07	kg	Undefined															
Rejects		0.148788	kg	Undefined															
Waste returned to mine		2.42E-05	kg	Undefined															
Waste, nuclear, unspecified/kg		1.04E-07	kg	Undefined															
Waste, nuclear, unspecified/kg		1.2E-07	kg	Undefined															
Non material emissions																			
Social issues																			
Economic issues																			
Waste to treatment																			

Figure C.25 Deconstructable precast floor planks, including reinforcing, represented by - pre-cast concrete, minimum reinforcement, production mix, at plant - ELCD

SimaPro 8.0.2	process	Date:	3/1/2015	Time:	4:27 PM										
Project	Design for Deconstruction														
Process															
Category type	waste treatment														
Process identifier	Standard09424503282														
Type	Unit process														
Process name	Recycling of steel														
Status															
Time period	Unspecified														
Geography	Unspecified														
Technology	Unspecified														
Representativeness	Unspecified														
Waste treatment allocation	Unspecified														
Cut off rules	Unspecified														
Capital goods	Unspecified														
Boundary with nature	Unspecified														
Infrastructure	No														
Date	12/10/2007														
Record	PRé consultants. SH														
Generator															
Literature references															
Collection method															
Data treatment															
Verification															
Comment	This is an empty process because of the cut-off at recycling. The recycling benefit and costs are allocated to the production of the recycled steel. To include this benefit and cost the following data should be included: Pig iron should be used as avoided product and scrap iron should be used as input from technosphere.														
Allocation rules															
System description															
Waste treatment															
Recycling steel and iron/US- US-EI U						1 kg			Ferro met: Recycling						
Avoided products															
Resources															
Materials/fuels															
Electricity/heat															
Emissions to air															
Emissions to water															
Emissions to soil															
Final waste flows															
Non material emissions															

Figure C.26 End of life process, represented by - recycling of steel - US-EI 2.2

SimaPro 8.0.2	process	Date:	3/1/2015	Time:	4:28 PM															
Project	Design for Deconstruction																			
Process																				
Category type	material																			
Process identifier	ELCDDATA13292600026																			
Type	System																			
Process name	Steel rebar, blast furnace and electric arc furnace route, production mix, at pl																			
Status	Finished																			
Time period	Unspecified																			
Geography	Unspecified																			
Technology	Unspecified																			
Representativeness	Unspecified																			
Multiple output allocation	Unspecified																			
Substitution allocation	Unspecified																			
Cut off rules	Unspecified																			
Capital goods	Unspecified																			
Boundary with nature	Unspecified																			
Infrastructure	No																			
Date	4/9/2010																			
Record	Conversion from ELCD to SimaPro was done by GreenDeltaTC, Germany, www.greendeltaTC.com.																			
Generator	worldsteel																			
Literature references	ELCD database 2.0																			
Collection method																				
Data treatment	Extrapolation: Relevant upstream data (of the DEAM database) was adapted according to the worldsteel boundary conditions, e.g. for iron ore, coke, zinc etc.																			
Verification																				
Comment	Use advice for data set: The data set includes the burden and credit associated with the recycling of steel scrap during steel production, manufacturing and End-of-Life. For this, the current global average recycling rate is estimated to be 80 %. For specific steel data set requests contact the European Confederation of Iron and Steel Industries, Eurofer (European data): www.eurofer.org; the World Steel Association, worldsteel (Global data): www.worldsteel.org and APEAL (Steel packaging data): www.apeal.org.; Technical purpose of product or process: A steel reinforcing bar (rebar) is rolled in a hot rolling mill. It can be found on the market for direct use or is further processed into finished products by the manufacturers. This product is used to strengthen concrete in highway and building construction. It is also used as a primary product for the wire rod process.; Technology description including background system: Raw material extraction and processing, e.g. coal, iron ore, etc., and recycling of steel scrap, Coke making, Sinter, Blast Furnace, Basic Oxygen Furnace, Hot strip mill. DEAM database also used. Electric Arc Furnace Route and section rolling. Steel product manufacturing route can be found in Appendices 1 and 2 of the worldsteel LCA Methodology Report. The worldsteel Recycling Methodology describes the implementation of the method in detail, incorporating a burden for using steel scrap in the steel making process and a credit for the end of life recycling of steel scrap. Steelmaking processes shown in flow diagram. Inputs included in the LCI relate to all raw material inputs, including steel scrap, energy, water, and transport.																			
Allocation rules																				
System description	ELCD 2.0																			
Products																				
Steel rebar, blast furnace and electric arc furna		1 kg		100 Steel		Metals\Ferro														
Avoided products																				
Resources																				
Calcite, in ground	in ground		0.07598 kg	Undefined																

SimaPro 8.0.2	process	Date:	3/1/2015	Time:	4:34 PM															
Project	Design for Deconstruction																			
Process																				
Category type	material																			
Process identifier	Standard09424503562																			
Type	Unit process																			
Process name	steel, converter, unalloyed, at plant/kg/RER																			
Status																				
Time period	Unspecified																			
Geography	Unspecified																			
Technology	Unspecified																			
Representativeness	Unspecified																			
Multiple output allocation	Unspecified																			
Substitution allocation	Unspecified																			
Cut off rules	Unspecified																			
Capital goods	Unspecified																			
Boundary with nature	Unspecified																			
Infrastructure	No																			
Date	8/13/2007																			
Record	Data entry by: Hans-Jörg Althaus Telephone: 0041 44 823 44 94;E-mail: empa@ecoinvent.org;Company: EMPA;Country: CH																			
Generator	Generator/publisher: Hans-Jörg Althaus Telephone: 0041 44 823 44 94;E-mail: empa@ecoinvent.org;Company: EMPA;Country: CH																			
Literature references	Life Cycle Inventories of Metals/2009/Classen M. Data has been published entirely in Copyright: true																			
Collection method	Sampling procedure: based on literature																			
Data treatment	Extrapolations: none Uncertainty adjustments: none																			
Verification	Proof reading validation: passed Validator: Roland Hirschier Telephone: 0041 71 274 78 47;E-mail: empa@ecoinvent.org;Company: EMPA;Country: CH																			
Comment	Translated name: Blasstahl, unlegiert, ab Werk Included processes: Transports of hot metal and other input materials to converter, steel making process and casting.																			
	Remark: This process produces primary steel. Scrap is only used for cooling the liquid steel.;Geography: Data relate to plants in the EU Technology: EU technology mix (mainly LD converter) Version: 2.2 Energy values: Undefined Production volume: unknown Local category: Metalle Local subcategory: Gewinnung Source file: 01151.XML																			
Allocation rules																				
System description	US-EI																			

Products						
Steel, converter, unalloyed, at plant/US- US-EI U	1 kg	100	Steel	Metals\Fer Europe		
Avoided products						
Resources						
Water, unspecified natural origin/m3	in water	0.0027 m3	Lognormal	1.1094	(2,3,2,3,1,3,12)	
Materials/fuels						
Blast oxygen furnace converter/RER/I US-EI U	1.3333E-11 p		Lognormal	3.2254	(5,nA,nA,nA,nA,9)	
Dolomite, at plant/US- US-EI U	0.00275 kg		Lognormal	1.1094	(2,3,2,3,1,3,4)	
Electricity, medium voltage, production UCTE*, at grid/UCTE US-	0.021944 kWh		Lognormal	1.1094	(2,3,2,3,1,3,2)	
Ferronickel, 25% Ni, at plant/GLO US-EI U	0.006 kg		Lognormal	1.1094	(2,3,2,3,1,3,3)	
Hard coal coke, at plant/US- US-EI U	0.00025 MJ		Lognormal	1.1094	(2,3,2,3,1,3,11)	
Iron ore, 65% Fe, at beneficiation/GLO US-EI U	0.022 kg		Lognormal	1.1094	(2,3,2,3,1,3,3)	
Iron scrap, at plant/US- US-EI U	0.2125 kg		Lognormal	1.1094	(2,3,2,3,1,3,3)	
Natural gas, high pressure, at consumer/US- US-EI U	0.0375 MJ		Lognormal	1.1094	(2,3,2,3,1,3,11)	
Oxygen, liquid, at plant/US- US-EI U	0.07145 kg		Lognormal	1.1094	(2,3,2,3,1,3,4)	
Pig iron, at plant/GLO US-EI U	0.9 kg		Lognormal	1.1094	(2,3,2,3,1,3,3)	
Quicklime, in pieces, loose, at plant/US* US-EI U	0.0425 kg		Lognormal	1.1094	(2,3,2,3,1,3,4)	
Transport, barge/US- US-EI U	0.00066 tkm		Lognormal	2.0074	(2,nA,1,3,1,3,5)	
Transport, freight, rail/US- US-EI U	0.1438 tkm		Lognormal	2.095	(4,5,nA,nA,nA,nA,5)	
Transport, lorry >16t, fleet average/US- US-EI U	0.022275 tkm		Lognormal	2.095	(4,5,nA,nA,nA,nA,5)	
Transport, transoceanic freight ship/OCE US-EI U	0.0594 tkm		Lognormal	2.0069	(2,nA,1,1,1,3,5)	
Electricity/heat						
Emissions to air						
Carbon dioxide, fossil	0.0756 kg		Lognormal	1.1094	(2,3,2,3,1,3,14)	
Carbon monoxide, fossil	0.00473 kg		Lognormal	5.0131	(2,3,2,3,1,3,17)	
Chromium	1.85E-07 kg		Lognormal	5.0131	(2,3,2,3,1,3,22)	
Copper	2.5E-08 kg		Lognormal	5.0131	(2,3,2,3,1,3,22)	
Dioxin, 2,3,7,8 Tetrachlorodibenzo-p-	3.05E-14 kg		Lognormal	3.0115	(2,3,2,3,1,3,21)	
Heat, waste	0.11675 MJ		Lognormal	1.0834	(1,3,2,3,1,2,13)	
Lead	5.15E-07 kg		Lognormal	5.0131	(2,3,2,3,1,3,22)	
Manganese	6.05E-07 kg		Lognormal	5.0131	(2,3,2,3,1,3,22)	
Nitrogen oxides	1.25E-05 kg		Lognormal	1.5154	(2,3,2,3,1,3,16)	
PAH, polycyclic aromatic hydrocarbons	1.2E-10 kg		Lognormal	3.0115	(2,3,2,3,1,3,21)	
Particulates, < 2.5 um	4.75E-05 kg		Lognormal	3.0115	(2,3,2,3,1,3,27)	
Emissions to water						
Emissions to soil						
Final waste flows						
Non material emissions						
Social issues						
Economic issues						
Waste to treatment						
Disposal, basic oxygen furnace wastes, 0% water, to residual ma	0.032077 kg		Lognormal	1.1094	(2,3,2,3,1,3,6)	
Disposal, dust, unalloyed EAF steel, 15.4% water, to residual ma	0.0010625 kg		Lognormal	1.1094	(2,3,2,3,1,3,6)	
Disposal, inert waste, 5% water, to inert material landfill/US* US-I	0.0029 kg		Lognormal	1.1094	(2,3,2,3,1,3,6)	

Figure C.28 Headed studs and bolts, represented by - Steel converter unalloyed at plant - US-EI 2.2

SimaPro 8.0.2	process	Date:	3/1/2015	Time:	4:11 PM															
Project	Design for Deconstruction																			
Process																				
Category type	transport																			
Process identifier	Standard09424503726																			
Type	Unit process																			
Process name	transport, lorry >28t, fleet average/tkm/CH																			
Status																				
Time period	Unspecified																			
Geography	Unspecified																			
Technology	Unspecified																			
Representativeness	Unspecified																			
Multiple output allocation	Unspecified																			
Substitution allocation	Unspecified																			
Cut off rules	Unspecified																			
Capital goods	Unspecified																			
Boundary with nature	Unspecified																			
Infrastructure	No																			
Date	9/13/2007																			
Record	Data entry by: Michael Spielmann Telephone: 0041 56 310 4706;E-mail: psi@ecoinvent.org;Company: PSI;Country: CH																			
Generator	Generator/publisher: Michael Spielmann Telephone: 0041 56 310 4706;E-mail: psi@ecoinvent.org;Company: PSI;Country: CH																			
Literature references	Life Cycle Inventories of Transport Services/2007/Spielmann M. Data as such not published elsewhere Copyright: true																			
Collection method	Sampling procedure: Literature data.																			
Data treatment	Extrapolations: none Uncertainty adjustments: none																			
Verification	Proof reading validation: passed Validator: Thomas Kägi Telephone: 0041 44 377 72 95;E-mail: art@ecoinvent.org;Company: ART;Country: CH																			
Comment	Translated name: Transport, Lkw >28t, Flottendurchschnitt Included processes: operation of vehicle;production, maintenance and disposal of vehicles;construction and maintenance and disposal of road. Remark: Inventory refers to the entire transport life cycle. For road infrastructure, expenditures and environmental interventions due to construction, renewal and disposal of roads have been allocated based on the Gross tonne kilometre performance. Expenditures due to operation of the road infrastructure, as well as land use have been allocated based on the yearly vehicle kilometre performance. For the attribution of vehicle share to the transport performance a vehicle life time performance of 2.39E05 pkm/vehicle has been assumed.;Geography: The data for vehicle operation and road infrastructure reflect Swiss conditions. Data for vehicle manufacturing and maintenance represents generic European data. Data for the vehicle disposal reflect the Swiss situation.																			
	Technology: Petrol, various emission treatment standards																			
	Version: 2.2																			
	Energy values: Undefined																			
	Percent representativeness: 100.0																			
	Production volume: not known																			
	Local category: Transportsysteme																			
	Local subcategory: Strasse																			
	Source file: 01944.XML																			

Allocation rules									
System description	US-EI								
Products									
Transport, lorry >28t, fleet average/US* US-EI U		1 tkm		100 not defined	Road	SWITZERLAND			
Avoided products									
Resources									
Materials/fuels									
Operation, lorry >28t, fleet average/US* US-EI U		0.10204 km	Lognormal	2.0131					(3,1,1,1,1,na);own calculations
Lorry 40t/RER/I US-EI U		1.8896E-07 p	Lognormal	3.0125					(3,1,1,2,1,na);own calculations
Maintenance, lorry 40t/CH/I US-EI U		1.8896E-07 p	Lognormal	3.0125					(3,1,1,2,1,na);own calculations
Road/US*/I US-EI U		0.0015338 my	Lognormal	3.0124					(3,1,1,1,1,na);own calculations
Operation, maintenance, road/US*/I US-EI U		0.00011642 my	Lognormal	3.0124					(3,1,1,1,1,na);own calculations
Electricity/heat									
Emissions to air									
Emissions to water									
Emissions to soil									
Final waste flows									
Non material emissions									
Social issues									
Economic issues									
Waste to treatment									
Disposal, lorry 40t/CH/I US-EI U		1.8896E-07 p	Lognormal	3.0125					(3,1,1,2,1,na);own calculations
Disposal, road/US*/I US-EI U		0.0015338 my	Lognormal	3.0124					(3,1,1,1,1,na);own calculations
Input parameters									
Calculated parameters									

Figure C.29 Transportation of materials, represented by - transport by lorry over 28t - US-EI 2.2

SimaPro 8.0.2	process	Date:	3/1/2015	Time:	4:06 PM				
Project	Design for Deconstruction								
Process									
Category type	transport								
Process identifier	Standard09424503777								
Type	Unit process								
Process name	transport, passenger car, petrol, fleet average/personkm/RER								
Status									
Time period	Unspecified								
Geography	Unspecified								
Technology	Unspecified								
Representativeness	Unspecified								
Multiple output allocation	Unspecified								
Substitution allocation	Unspecified								
Cut off rules	Unspecified								
Capital goods	Unspecified								
Boundary with nature	Unspecified								
Infrastructure	No								
Date	9/13/2007								
Record	Data entry by: Michael Spielmann Telephone: 0041 56 310 4706;E-mail: psi@ecoinvent.org;Company: PSI;Country: CH								
Generator	Generator/publisher: Michael Spielmann Telephone: 0041 56 310 4706;E-mail: psi@ecoinvent.org;Company: PSI;Country: CH								
Literature references	Life Cycle Inventories of Transport Services/2007/Spielmann M. Data as such not published elsewhere Copyright: true								
Collection method	Sampling procedure: Literature data.								
Data treatment	Extrapolations: none Uncertainty adjustments: none								
Verification	Proof reading validation: passed Validator: Thomas Kägi Telephone: 0041 44 377 72 95;E-mail: art@ecoinvent.org;Company: ART;Country: CH								
Comment	Translated name: Transport, Pkw, Benzin, Flottendurchschnitt Included processes: operation of vehicle;production, maintenance and disposal of vehicles;construction and maintenance and disposal of road. Remark: Inventory refers to the entire transport life cycle. For road infrastructure, expenditures and environmental interventions due to construction, renewal and disposal of roads have been allocated based on the Gross tonne kilometre performance. Expenditures due to operation of the road infrastructure, as well as land use have been allocated based on the yearly vehicle kilometre performance. For the attribution of vehicle share to the transport performance a vehicle life time performance of 2.39E05 pkm/vehicle has been assumed.;Geography: The data for vehicle operation and road infrastructure reflect Swiss conditions. Data for vehicle manufacturing and maintenance represents generic European data. Data for the vehicle disposal reflect the Swiss situation.								
	Technology: Petrol, various emission treatment standards Version: 2.2 Energy values: Undefined Percent representativeness: 100.0 Production volume: not known Local category: Transportsysteme Local subcategory: Strasse Source file: 10818.XML								
Allocation rules									
System description	US-EI								

Appendix D. Specimen Drawings

This appendix contains drawings of all the specimens in both pushout tests and beam tests, including shop drawings for the steel specimens, design drawings for the concrete specimens, details of the reinforcement, etc.

D.1 Pushout test

D.1.1 Steel specimen shop drawings

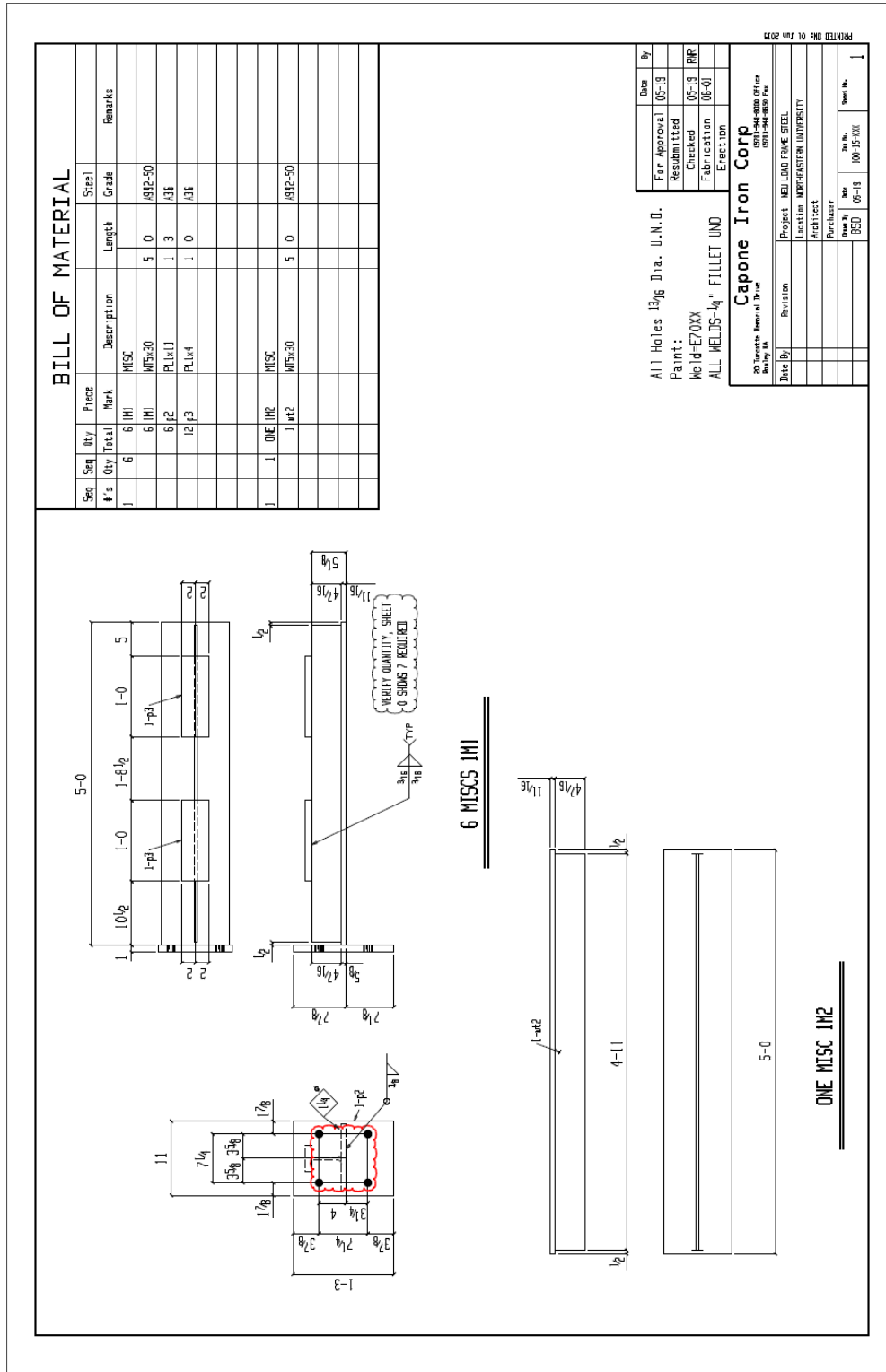


Figure D.1 Steel Section WT5x30

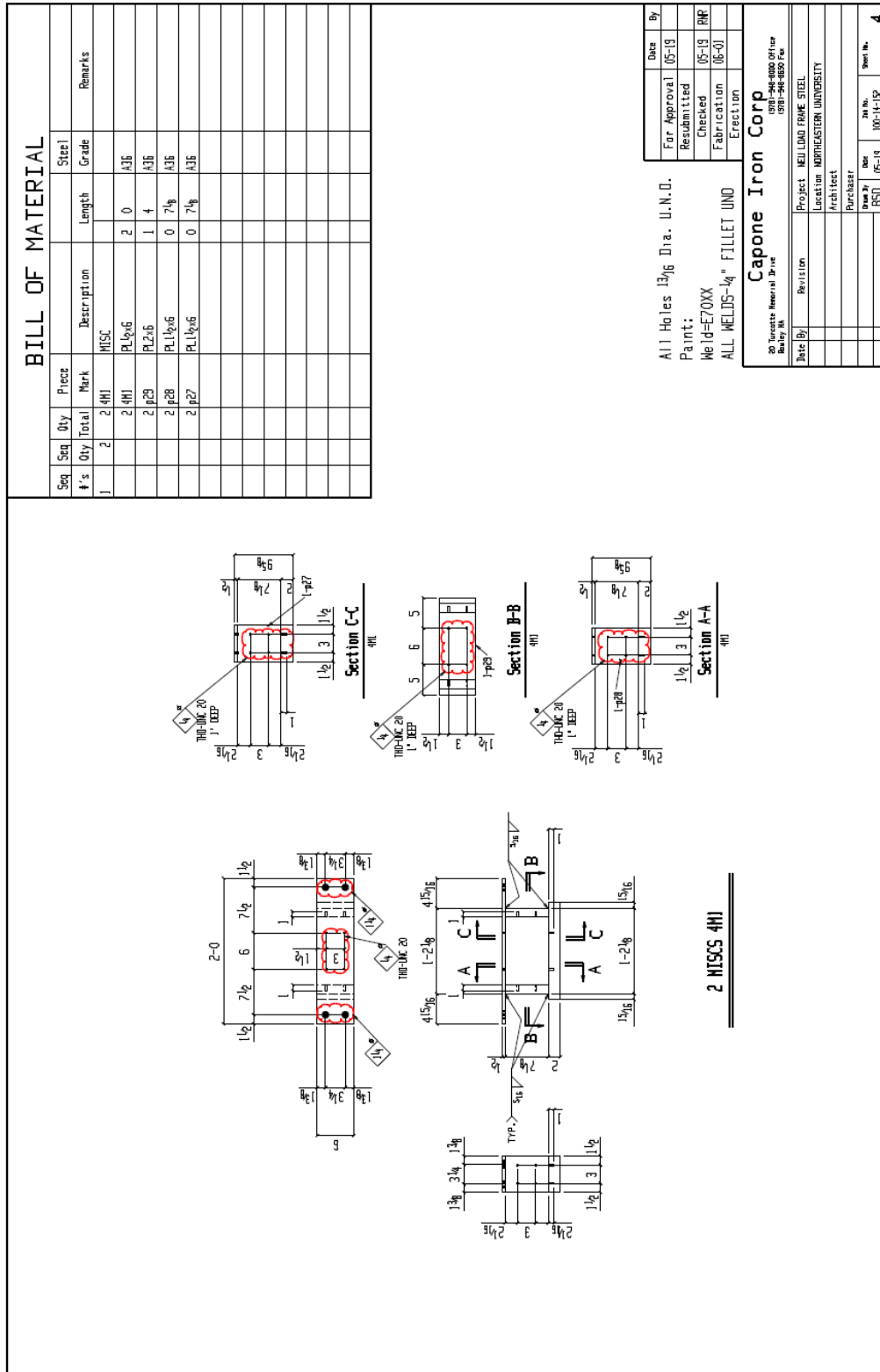


Figure D.4 Stability Frame for WT5x30

D.1.2 Concrete specimen design drawings

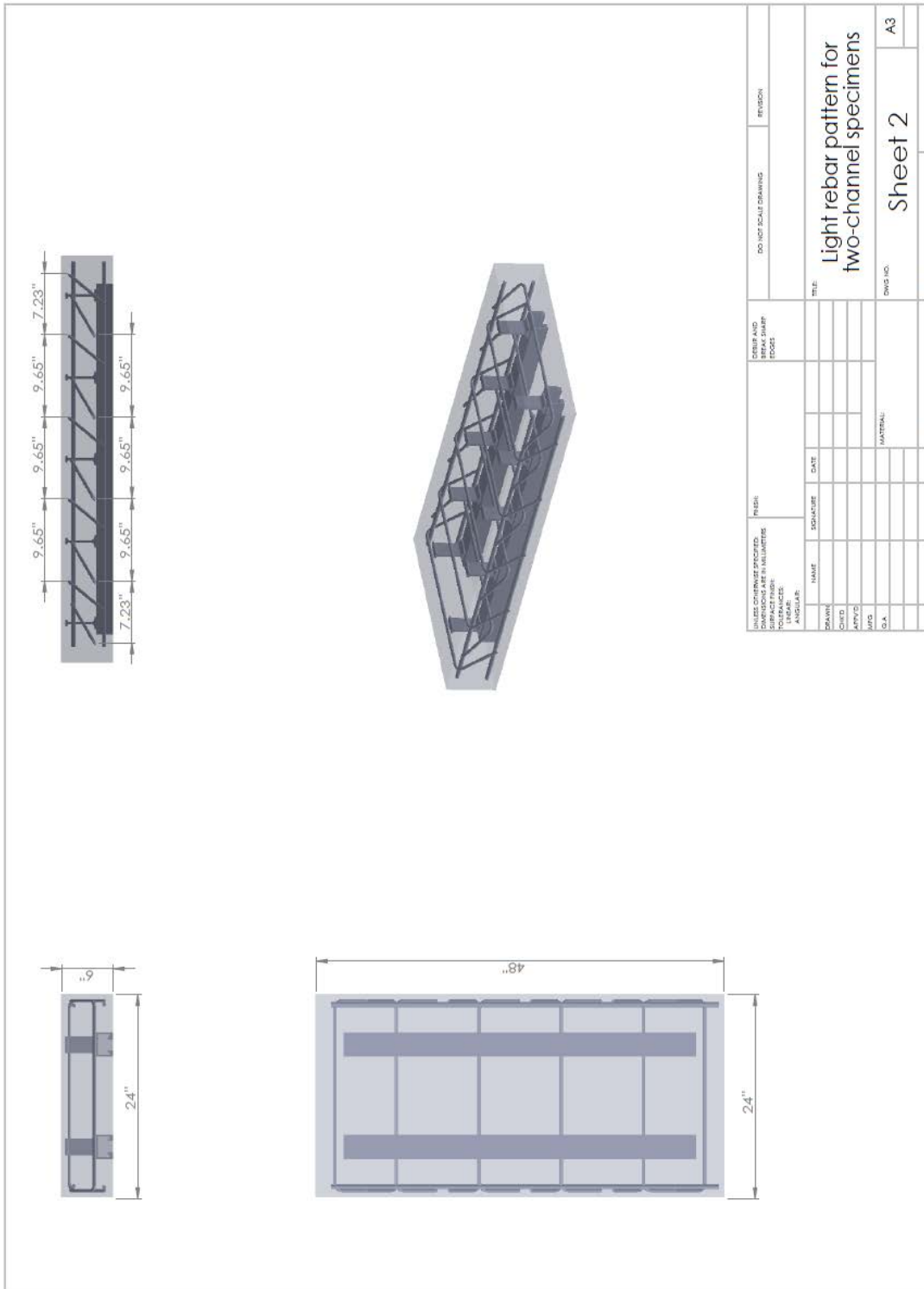
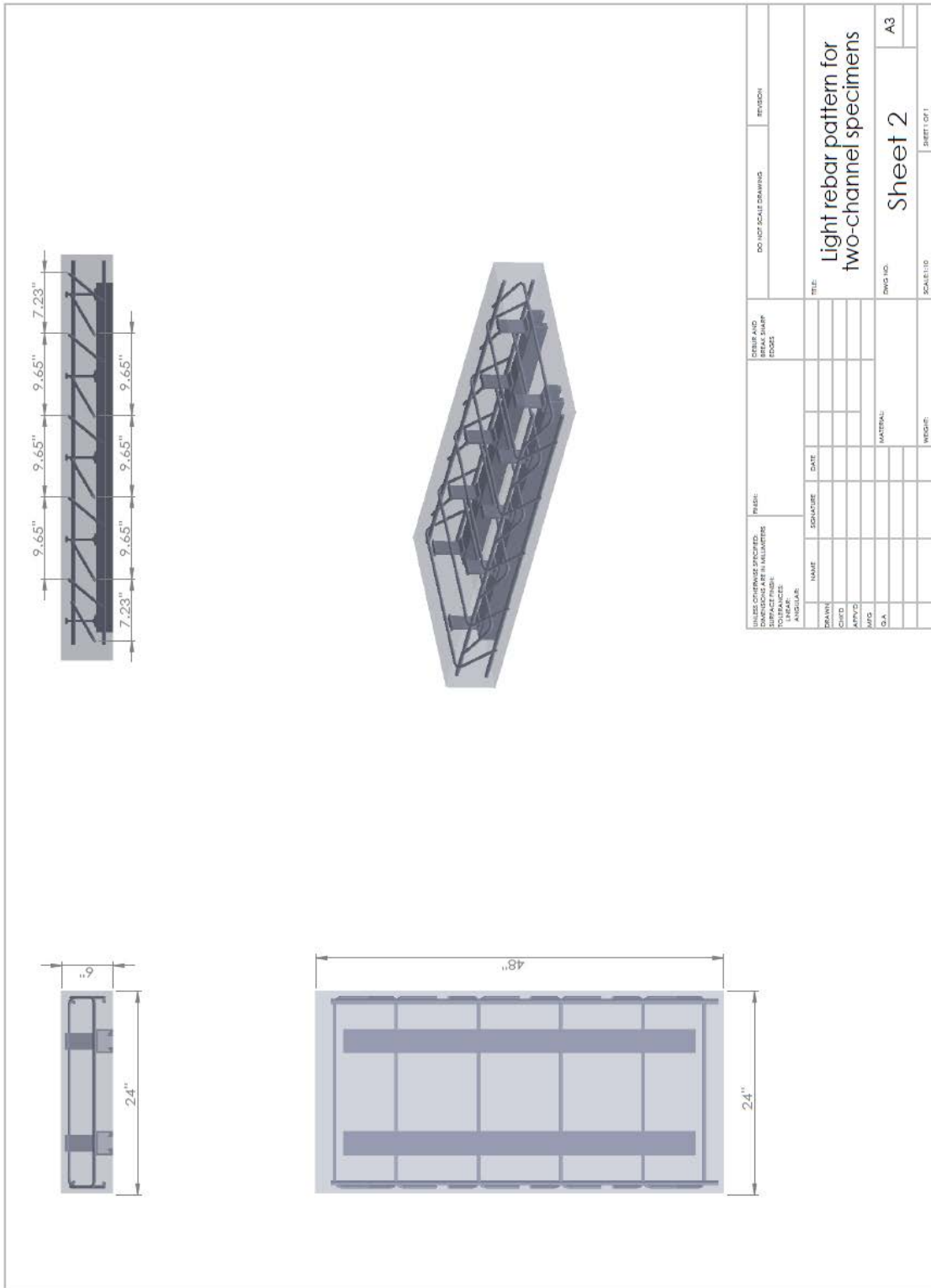


Figure D.10 Light Reinforcement Pattern



UNLESS OTHERWISE SPECIFIED, DIMENSIONS ARE IN INCHES.		DESIGN AND DRAWING CODES		DO NOT SCALE DRAWING		REVISION	
SURFACE FINISH:		DRAWING NO.		TITLE:		SHEET NO.	
TOLERANCES:		DATE:		Light rebar pattern for		A3	
ANGULAR:		MATERIAL:		two-channel specimens		Sheet 2	
DESIGNER:	NAME:	SIGNATURE:	DATE:	SCALE:	SHEET TOTAL		
DRAWN:	NAME:	SIGNATURE:	DATE:	WEIGHT:			
CHECK:	NAME:	SIGNATURE:	DATE:				
APPROVE:	NAME:	SIGNATURE:	DATE:				
DATE:	NAME:	SIGNATURE:	DATE:				
DATE:	NAME:	SIGNATURE:	DATE:				

Figure D.11 Heavy Reinforcement Pattern for Two-Channel Specimens

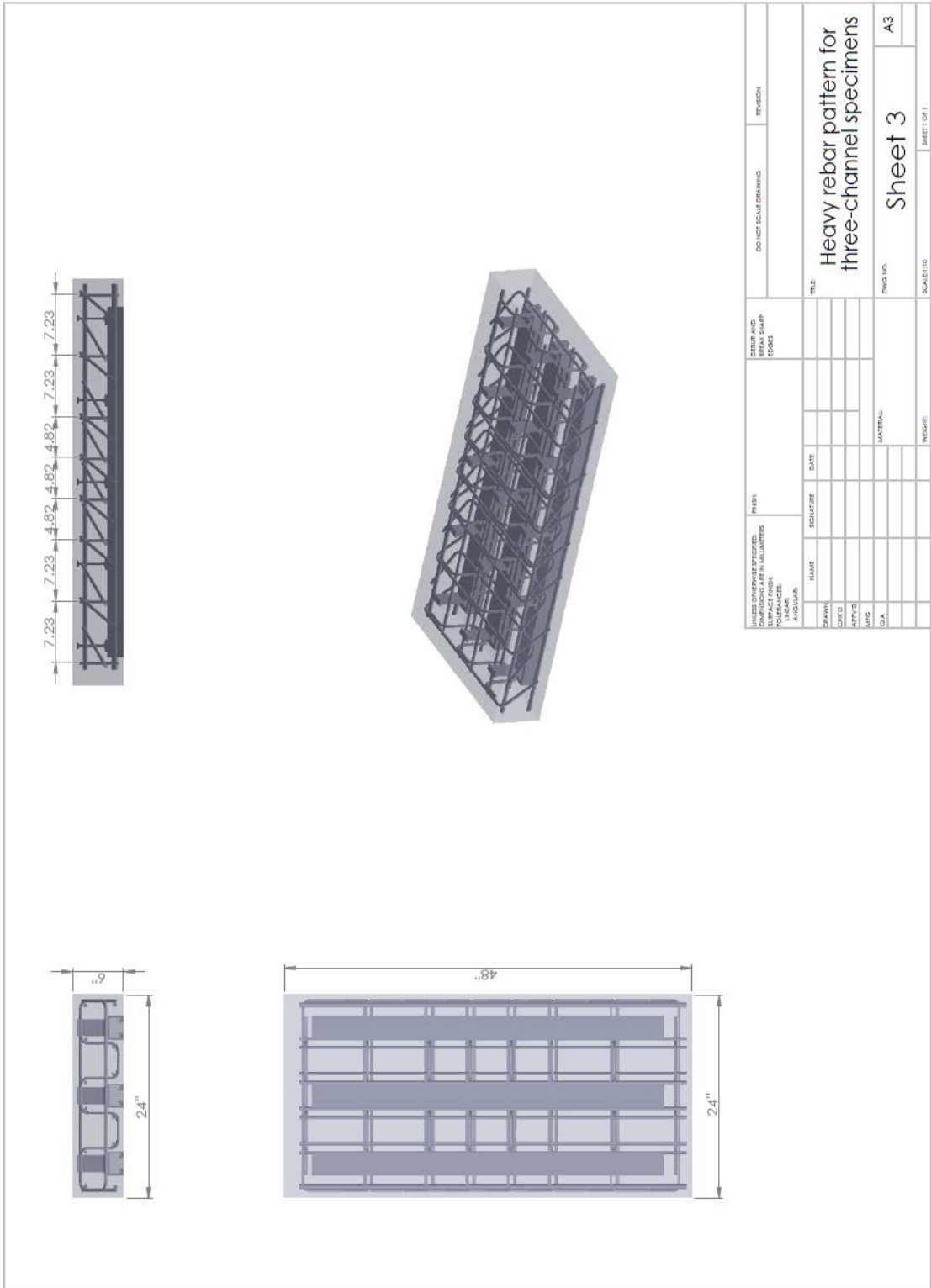


Figure D.12 Heavy Reinforcement Pattern for Three-Channel Specimens

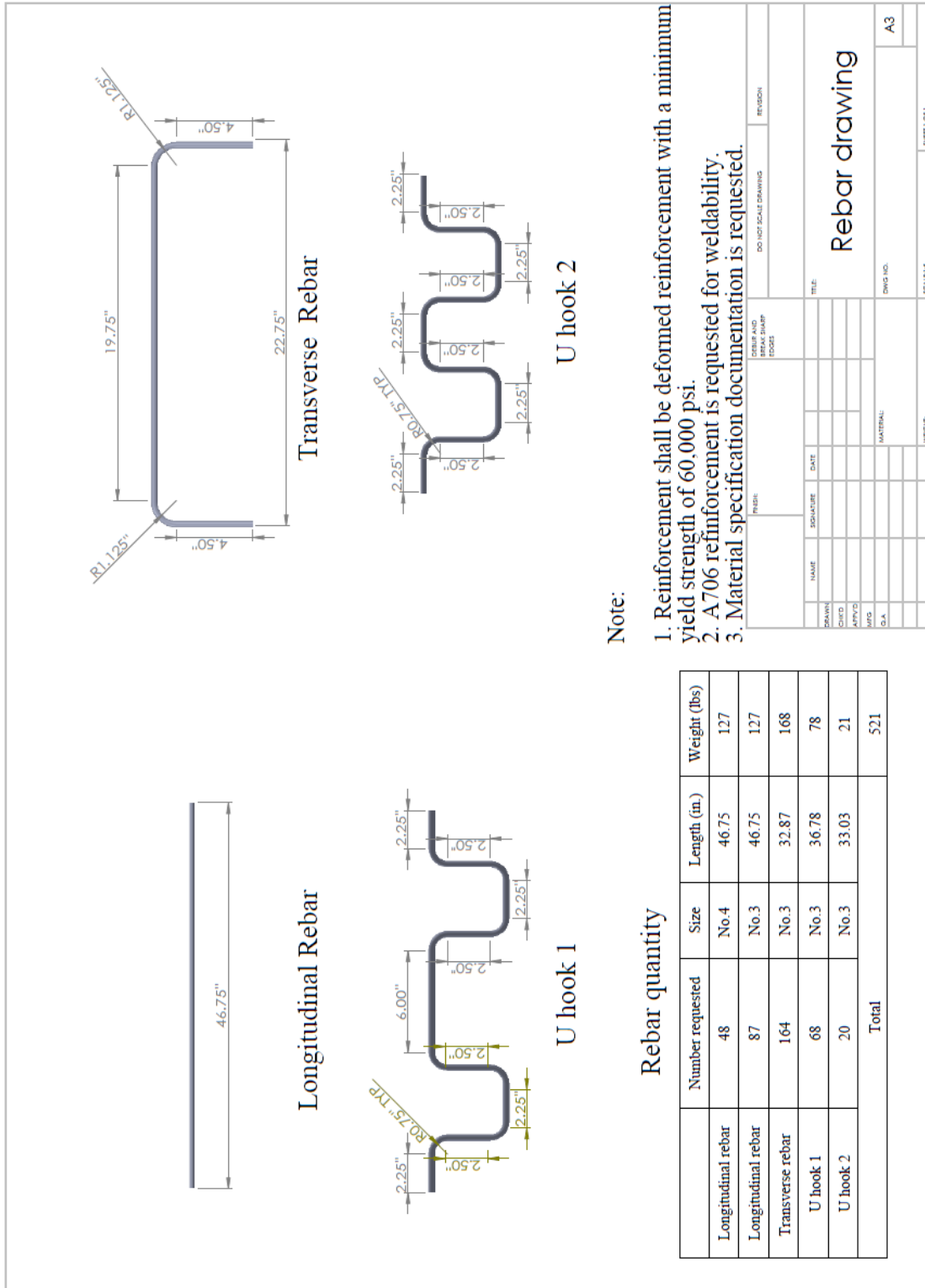


Figure D.13 Reinforcement Details

D.2 Composite beam test

D.2.1 Steel specimen shop drawings

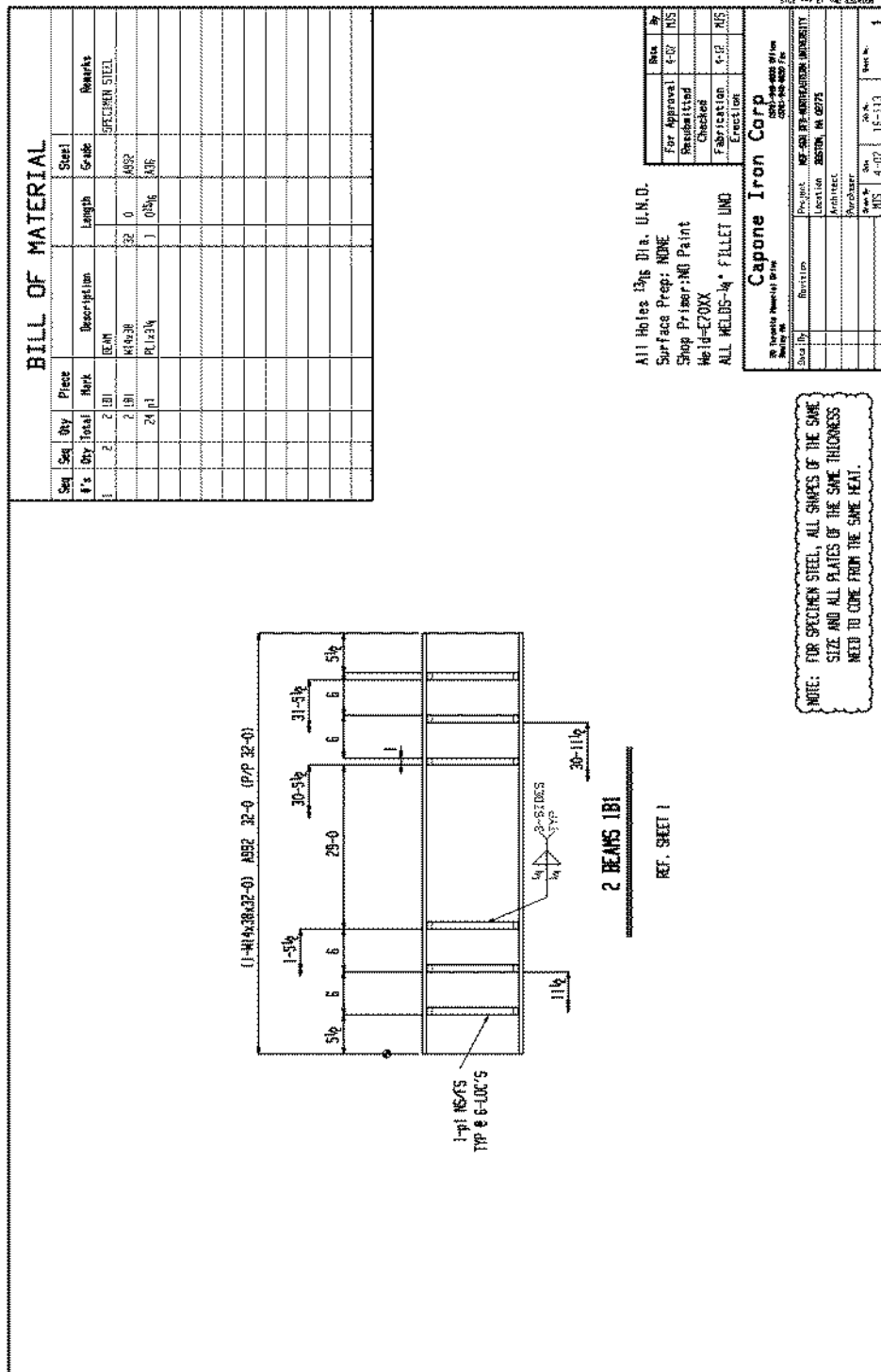


Figure D.14 Steel Section W14x38

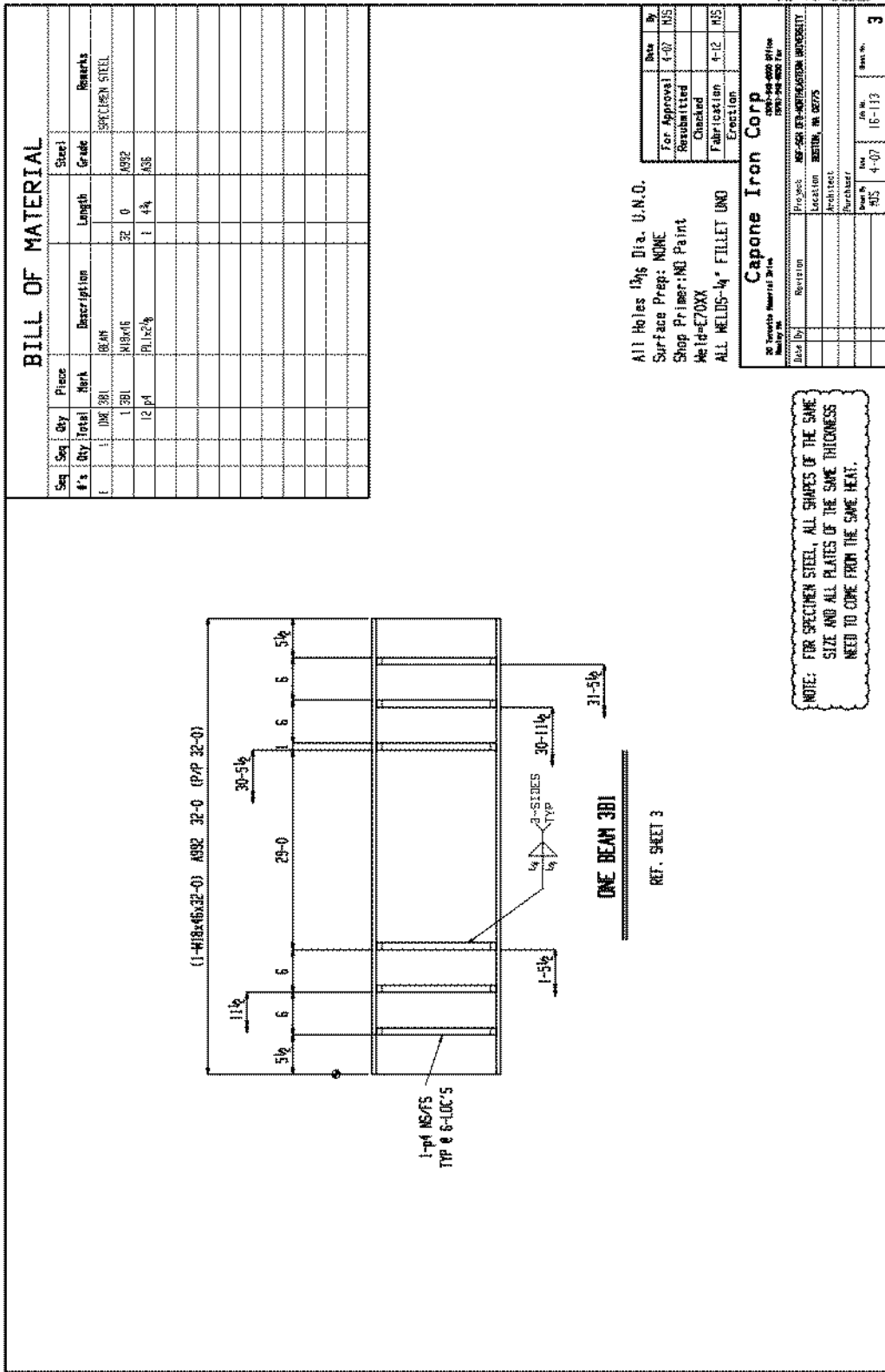


Figure D.16 Steel Section W18x46

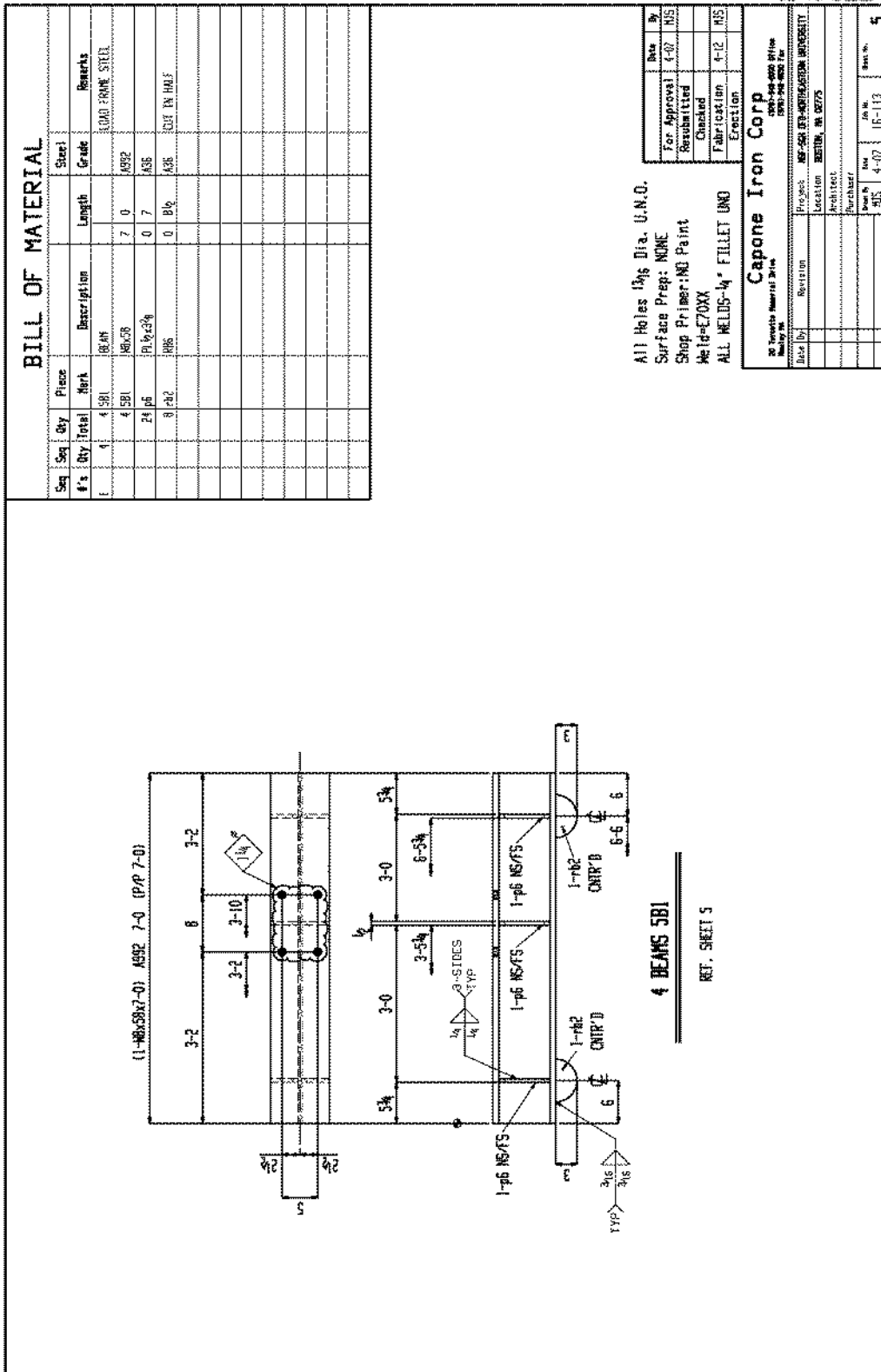


Figure D.18 Bottom Spreader Beam W8x58

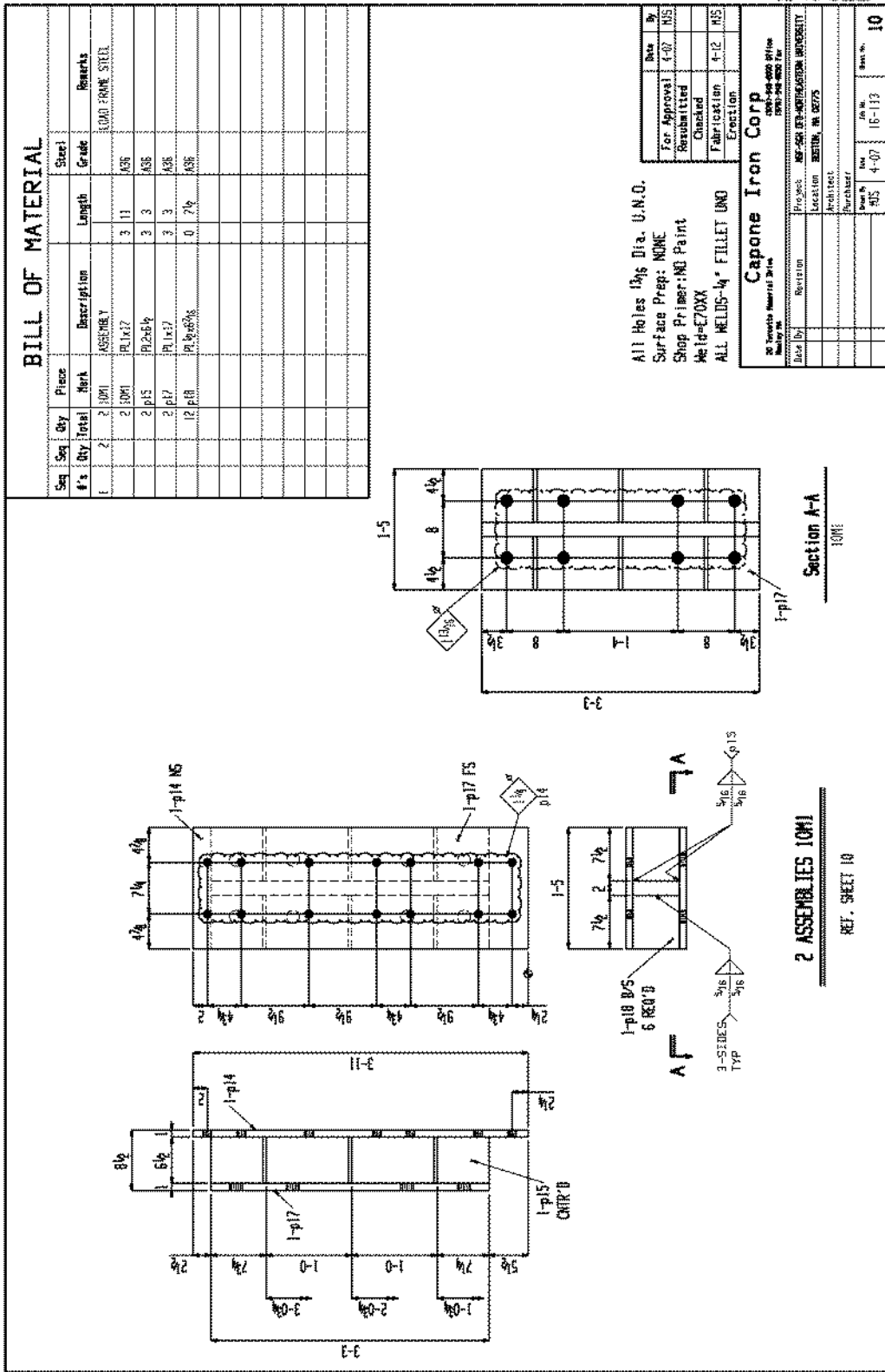


Figure D.23 Cross Beam Adapter

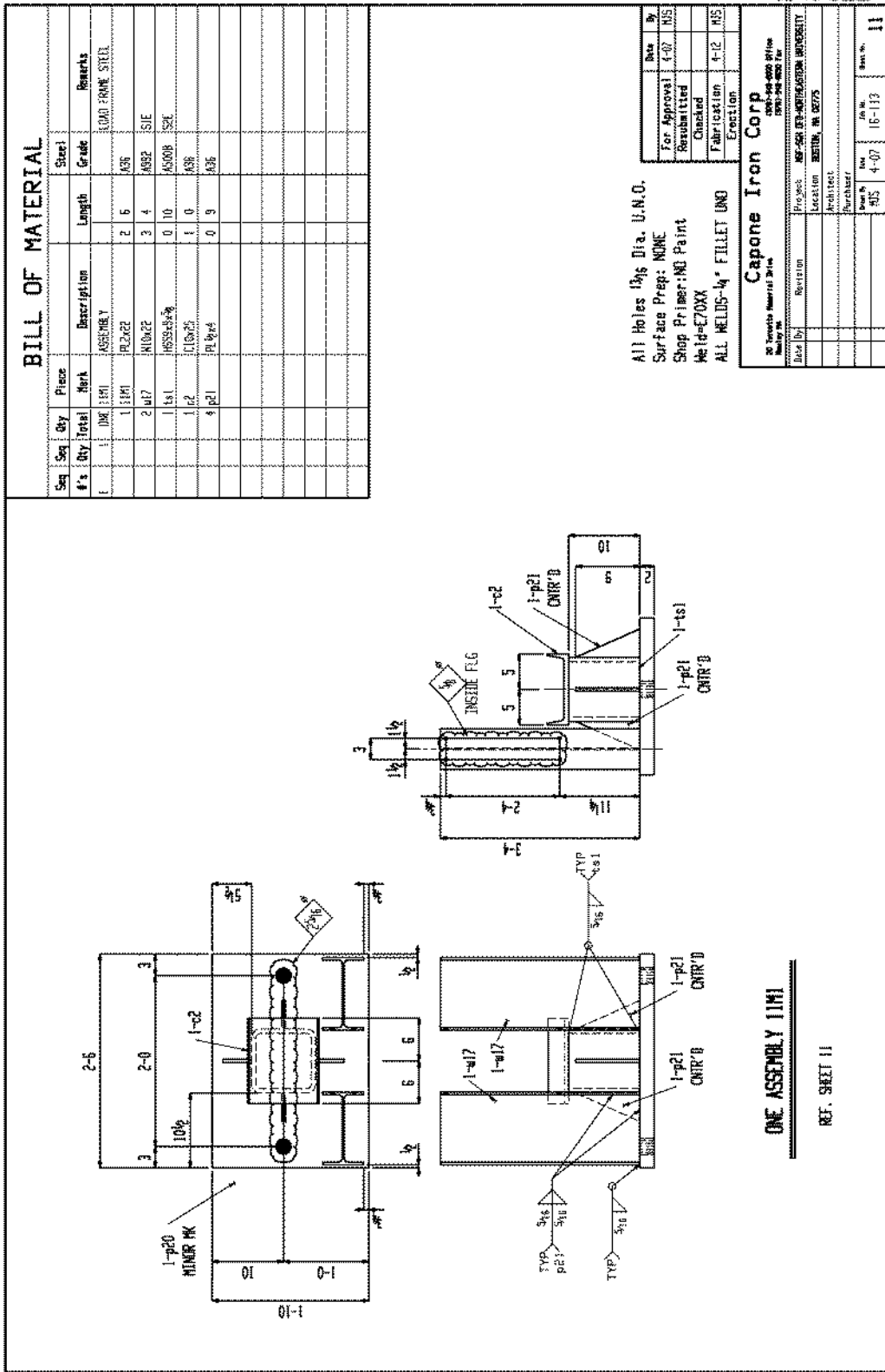


Figure D.24 Beam Roller Support

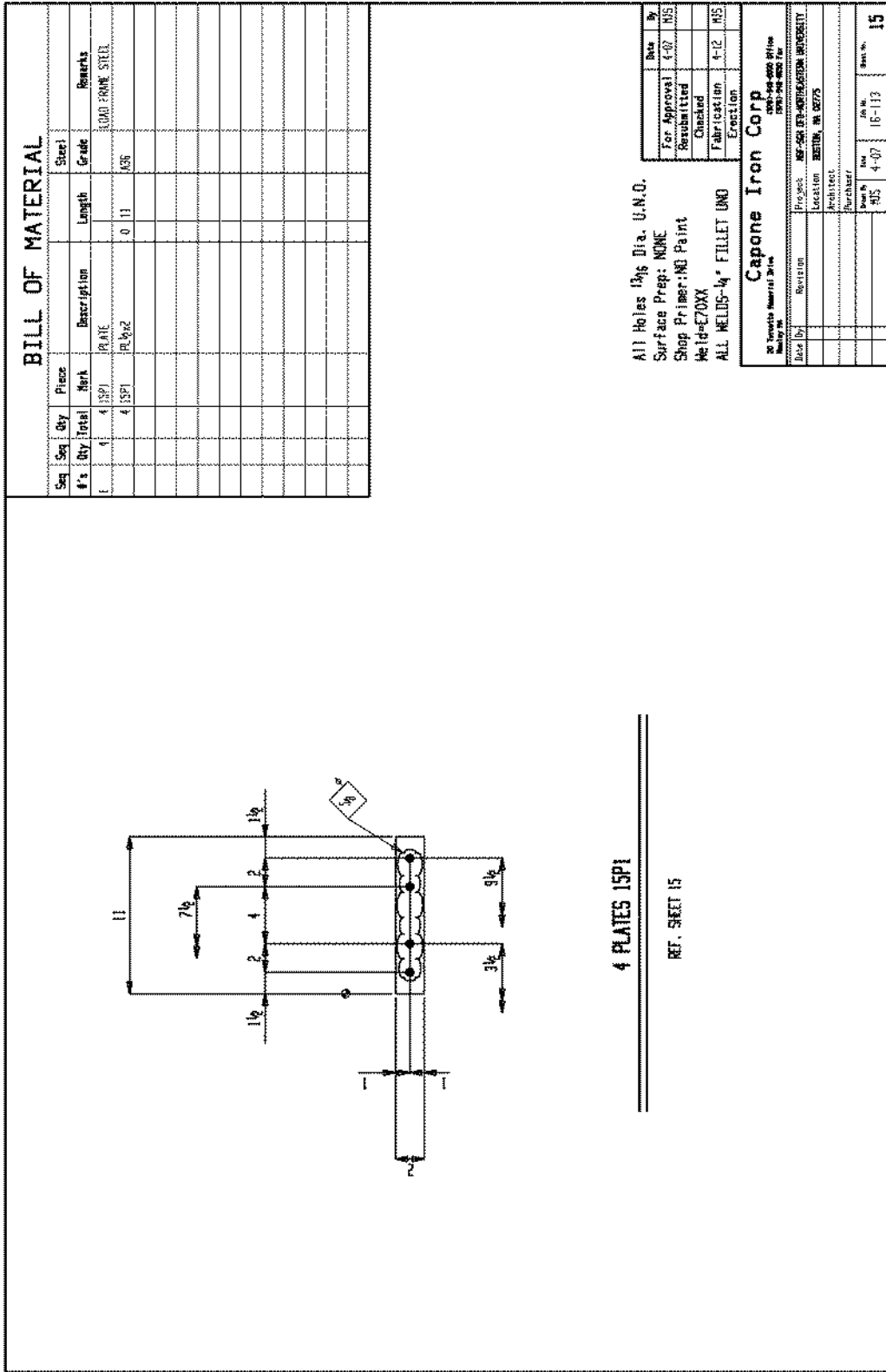


Figure D.28 Clamp Plate for Braces

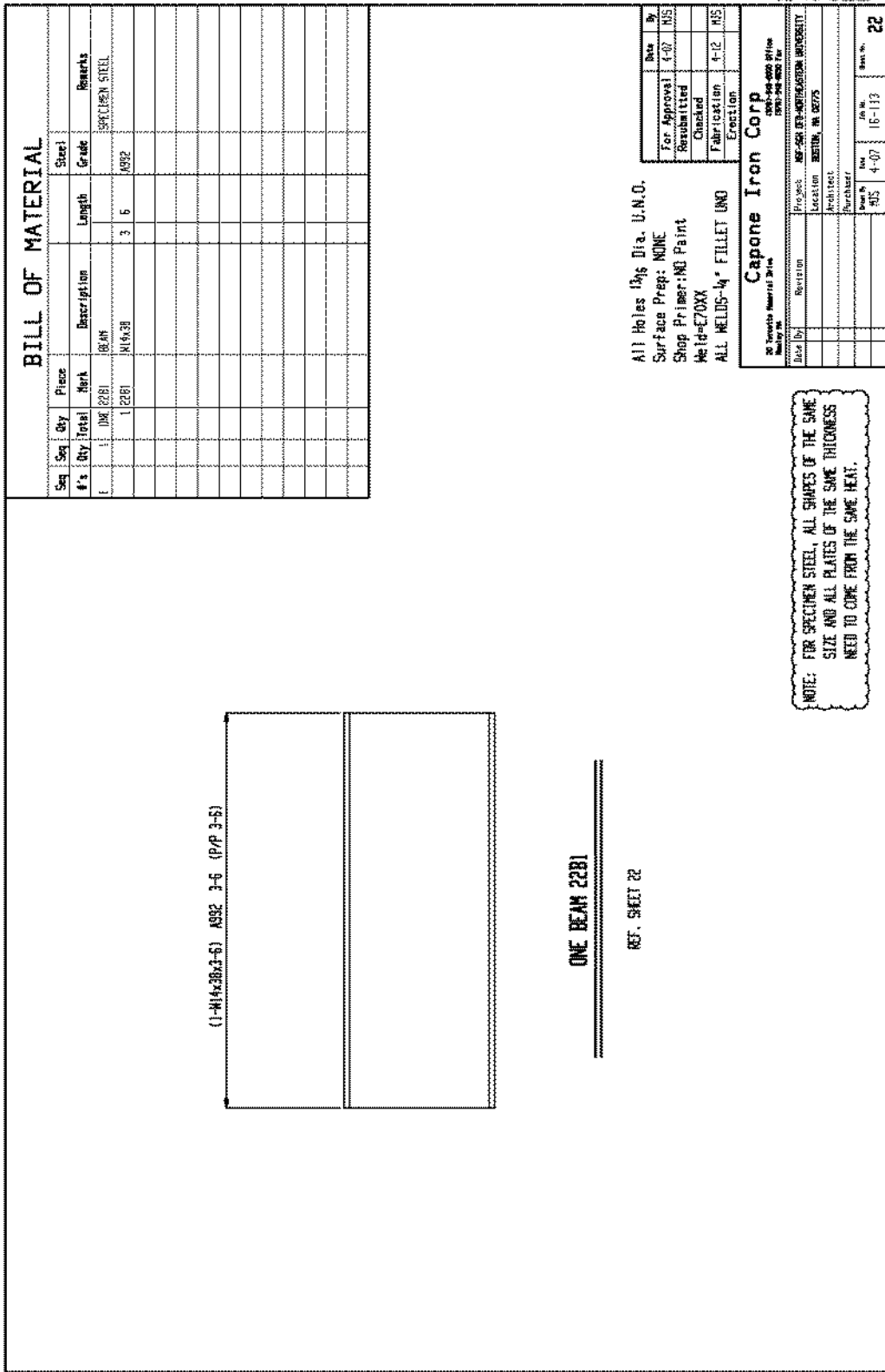


Figure D.35 Coupon Section W14x38

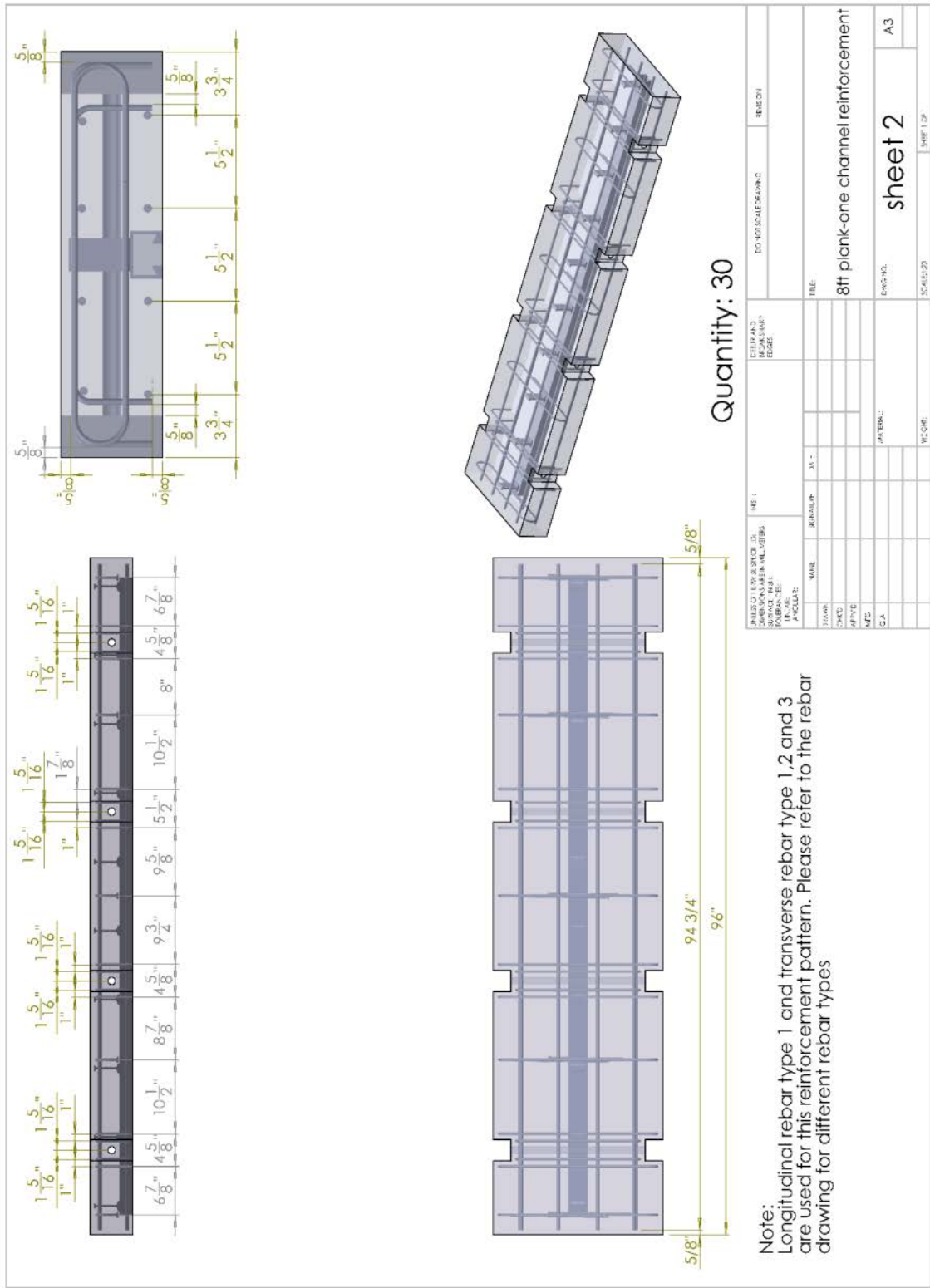


Figure D.39 One-Channel Specimen Reinforcement

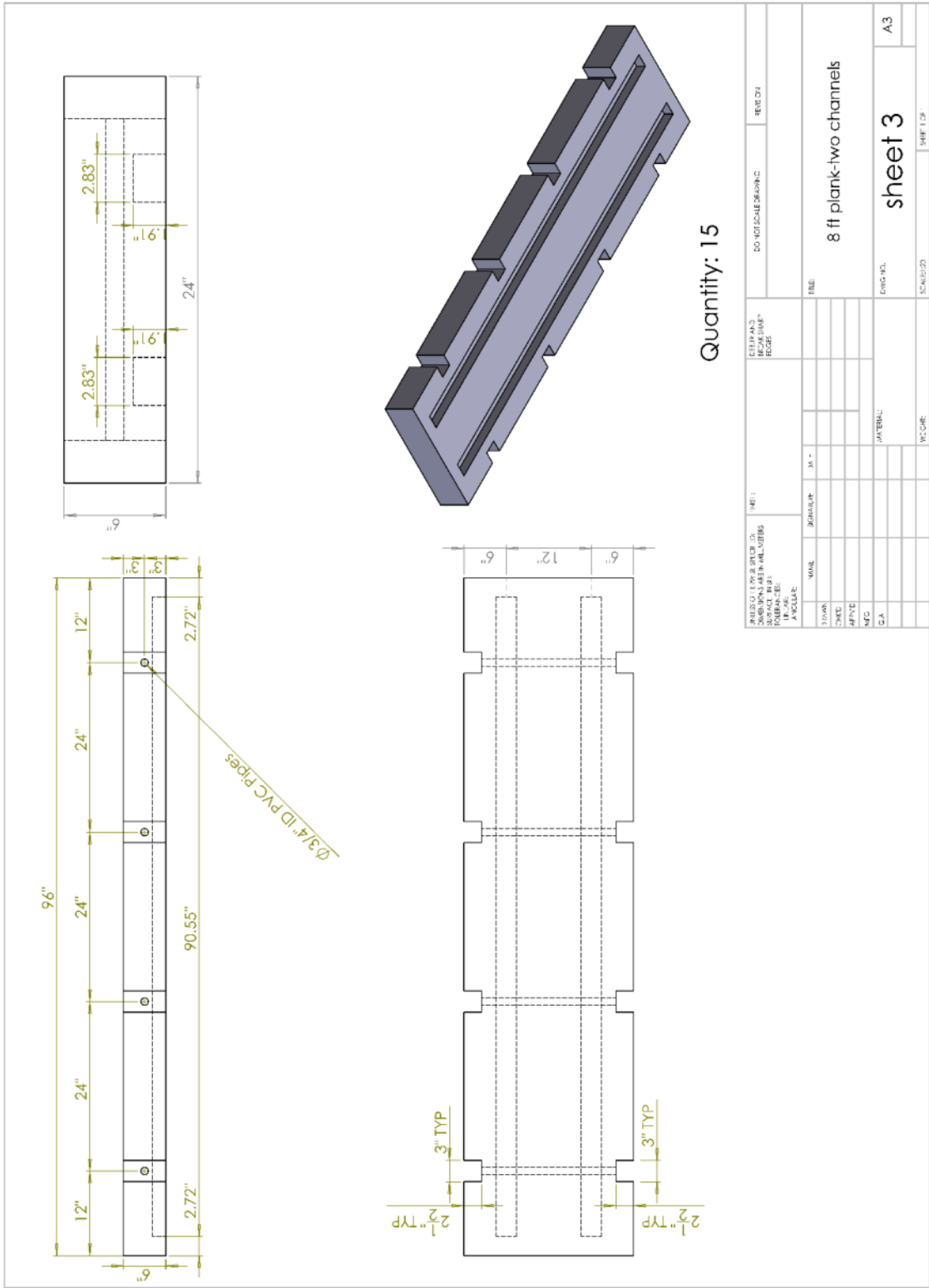


Figure D.40 Two-Channel Specimen

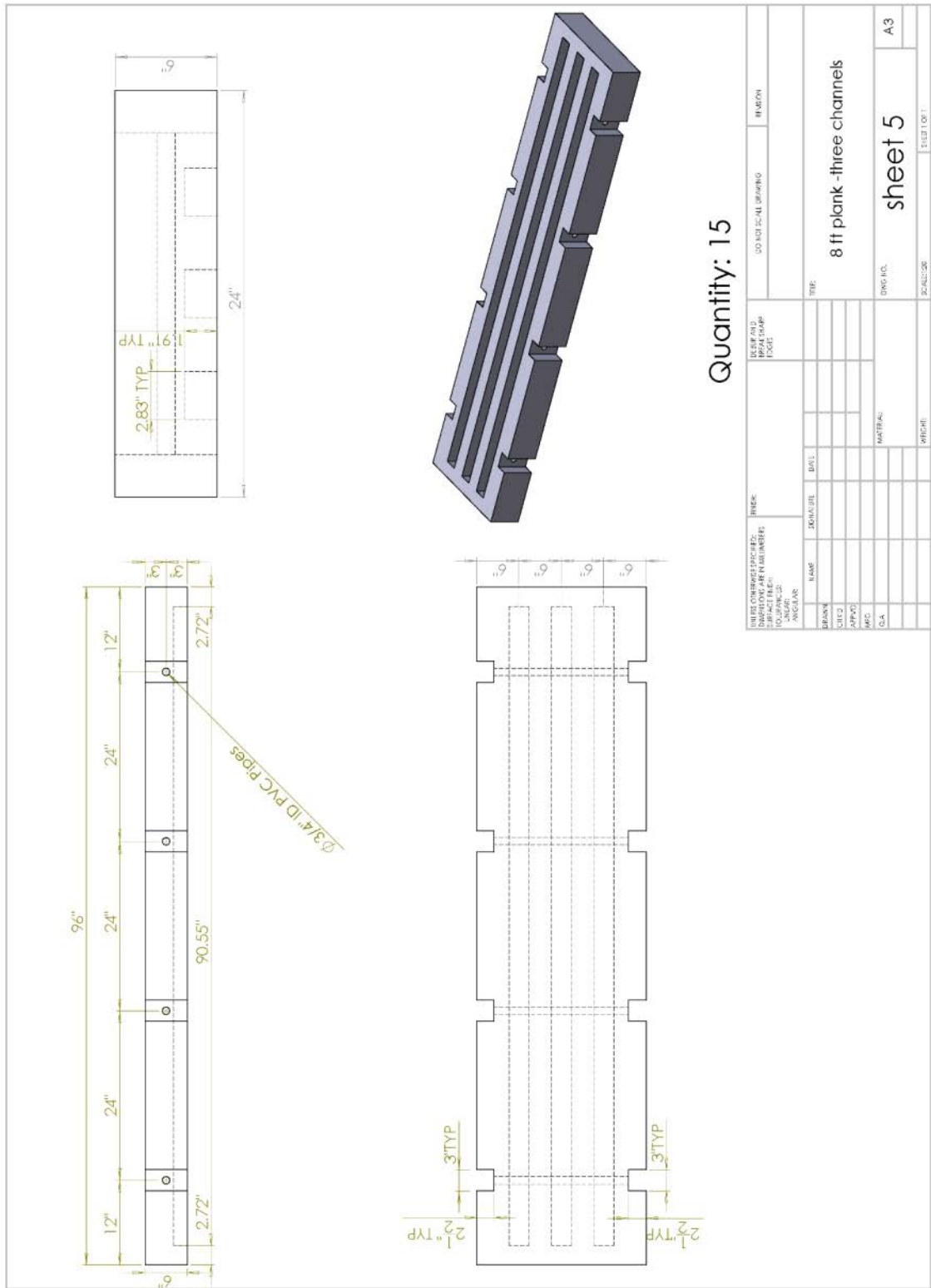


Figure D.42 Three-Channel Specimen

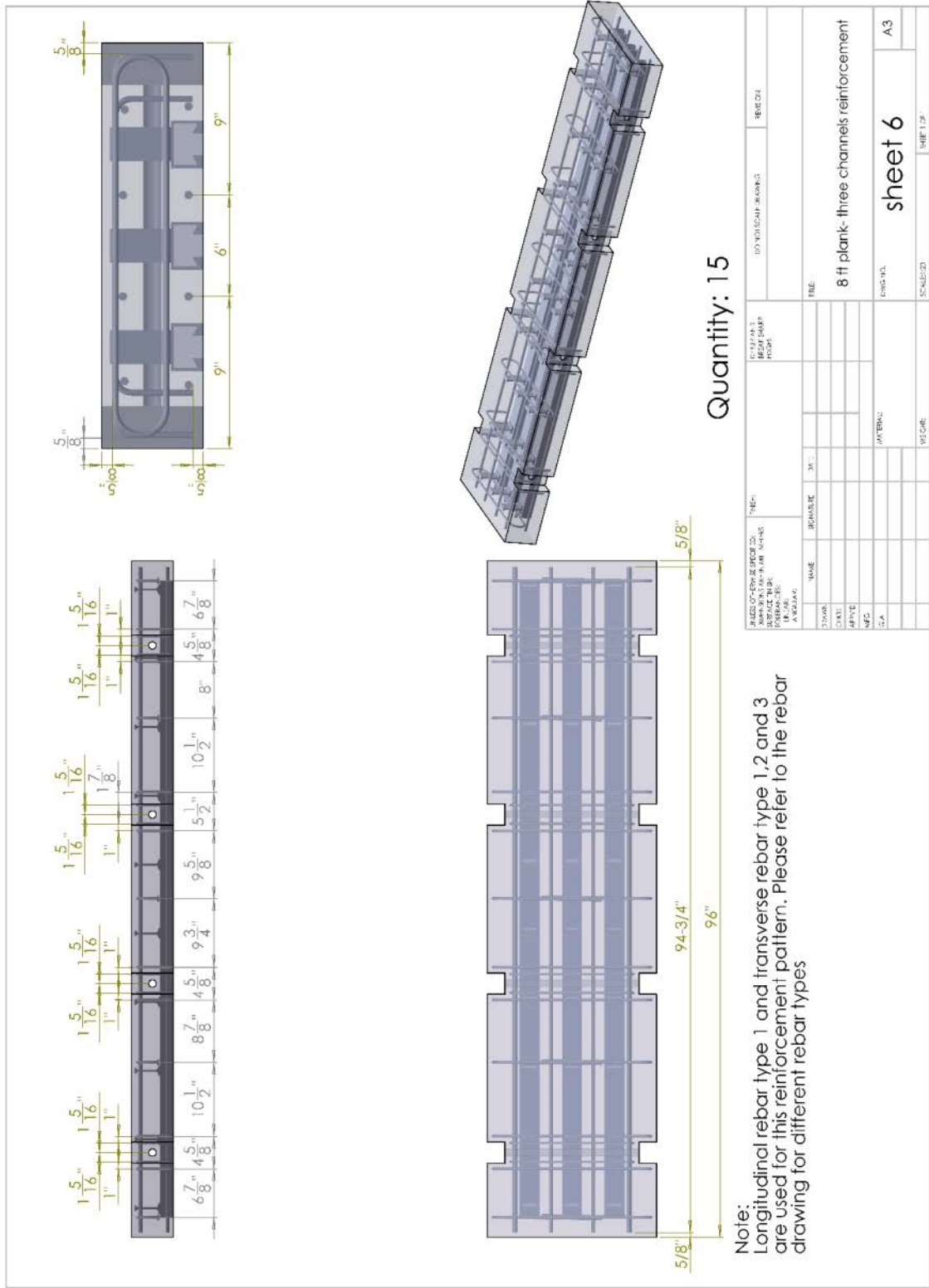
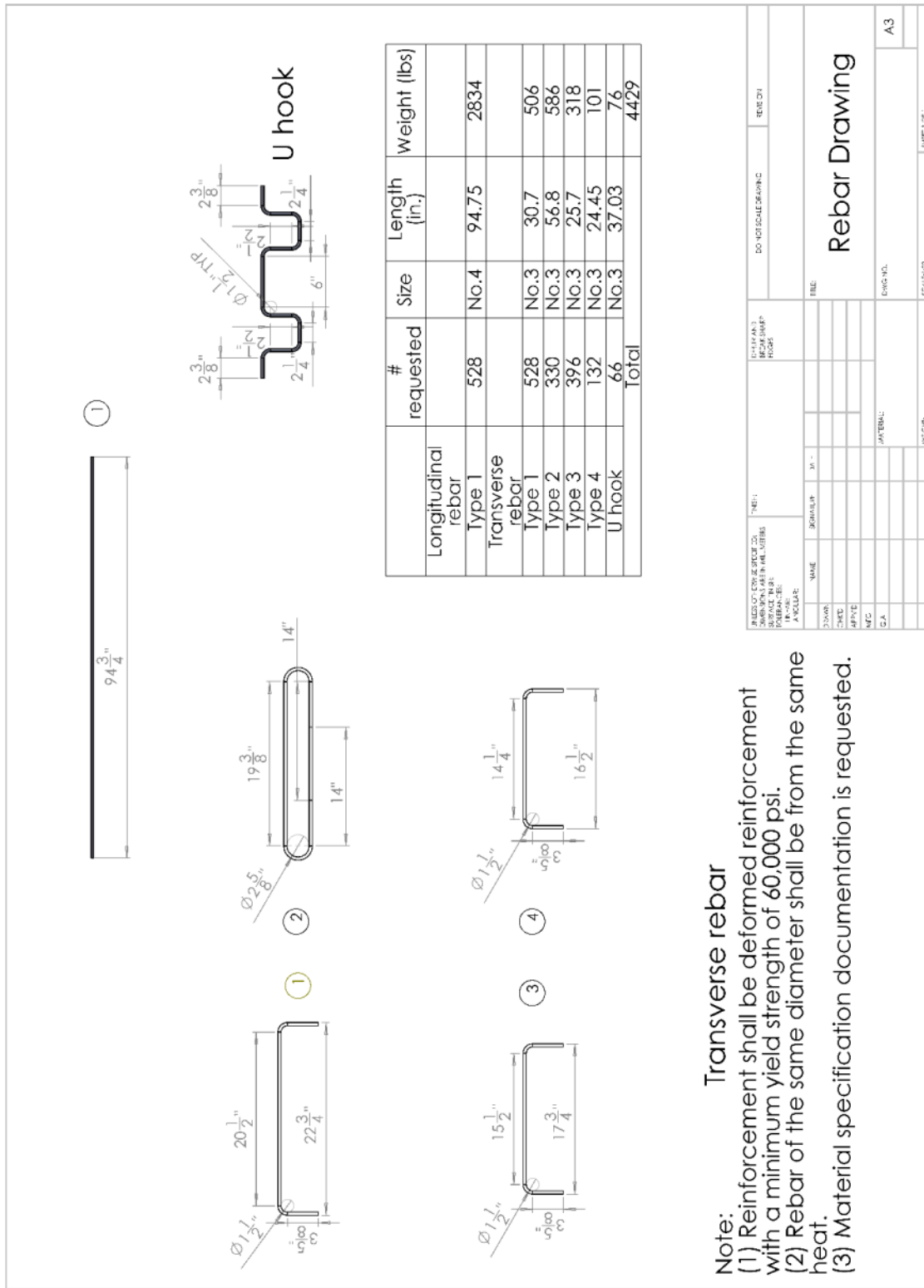


Figure D.43 Three-Channel Specimen Reinforcement



Note:
 (1) Reinforcement shall be deformed reinforcement with a minimum yield strength of 60,000 psi.
 (2) Rebar of the same diameter shall be from the same heat.
 (3) Material specification documentation is requested.

PROJECT: _____ SHEET: _____
 DRAWN BY: _____ CHECKED BY: _____
 DATE: _____
 SCALE: _____
 MATERIAL: _____
 WEIGHT: _____
 SHEET 1 OF 3

Figure D.44 Reinforcement Details

Appendix E. Experimental Raw Data

This appendix contains all the raw data from the experimental programs. All the data is recorded with engineering units.

E.1 Pushout test specimens

E.1.1 Pretension test

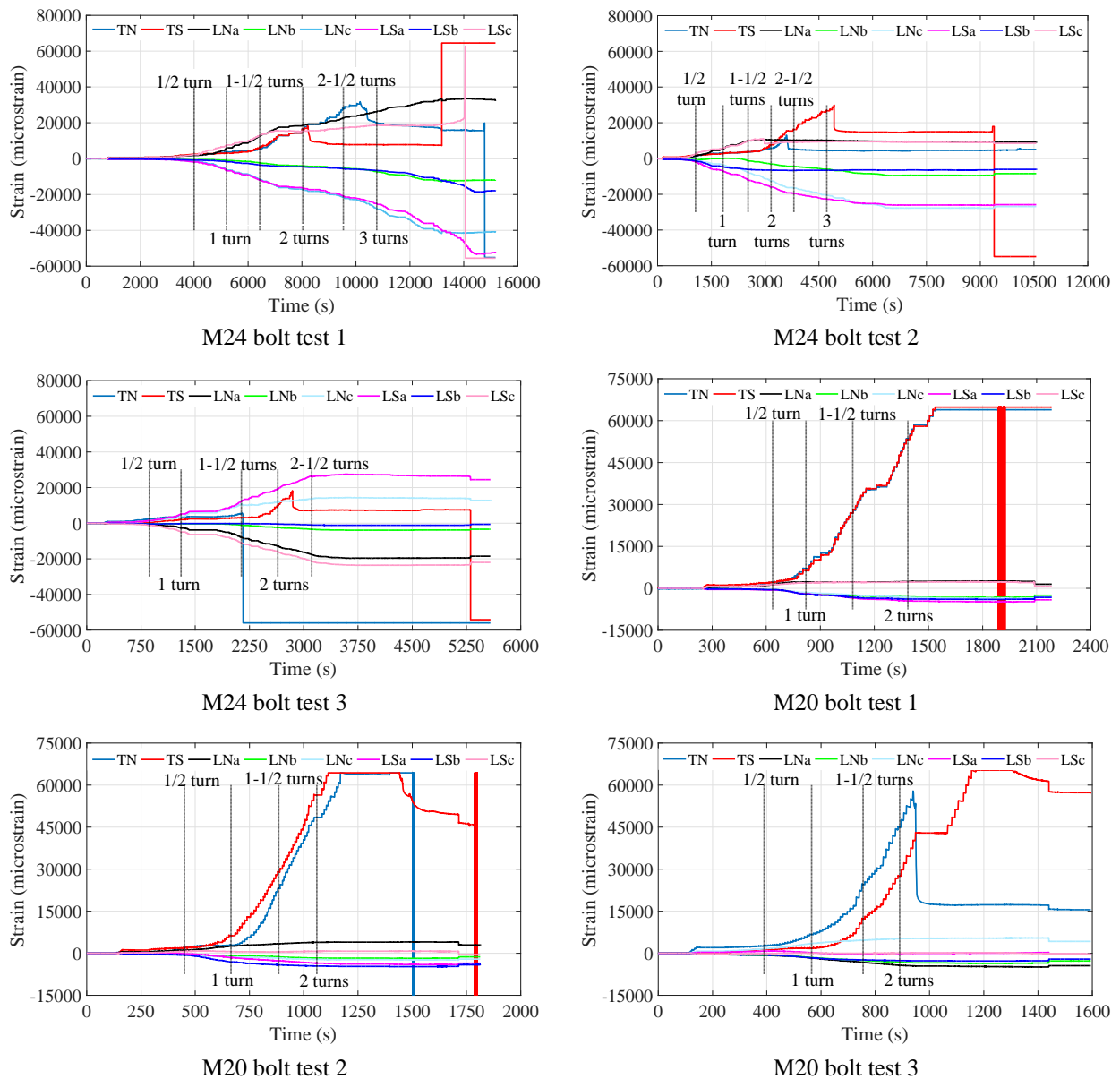
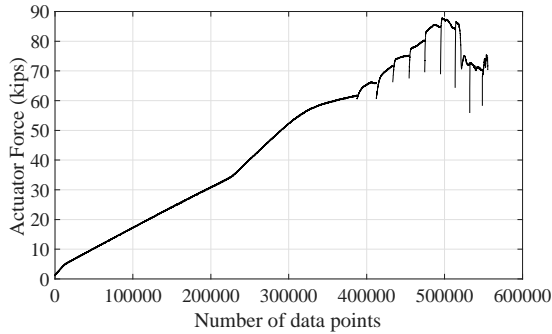


Figure E.1 Strain gage readings vs. time

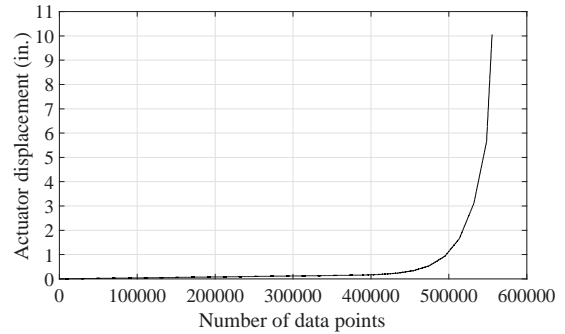
E.1.2 Pushout test

E.1.2.1 Actuator force, actuator displacement and slip

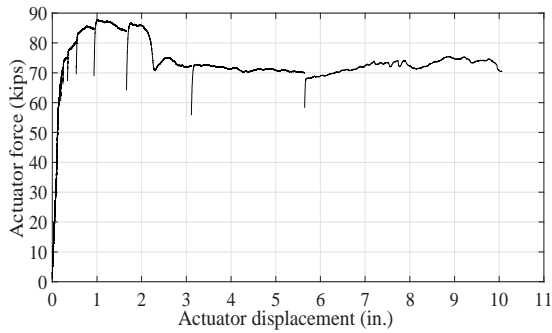
Two 110 kips actuators are used in the pushout tests. The plots titled “Actuator Force Variation” show the summation of the actuator forces, while the average of the actuator displacements is given in the figures titled “Actuator Displacement Variation”



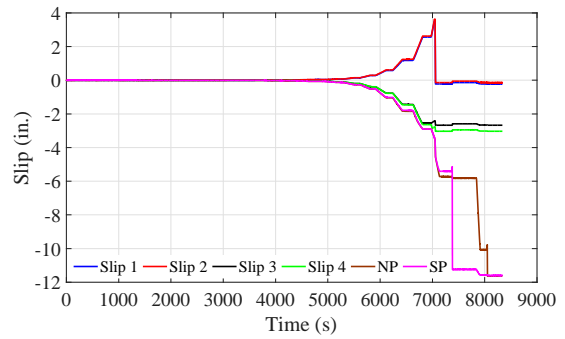
Actuator force variation



Actuator displacement variation

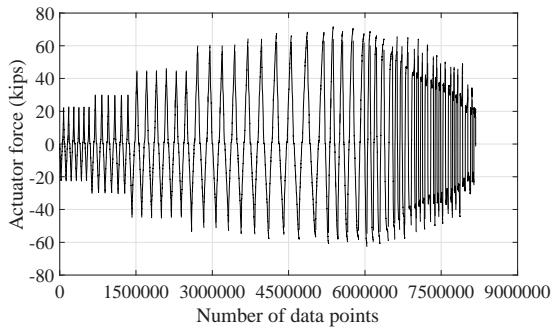


Actuator force vs. Actuator displacement

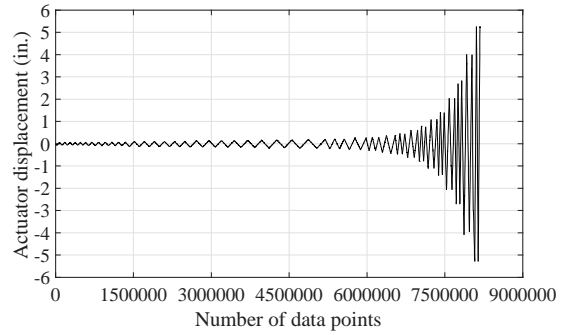


Slip vs. Time

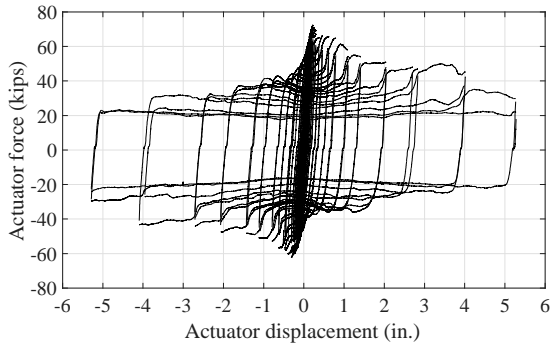
Test 2-M24-2C-RH-LM



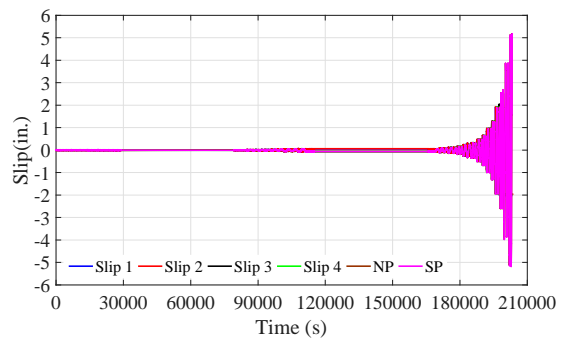
Actuator force variation



Actuator displacement variation

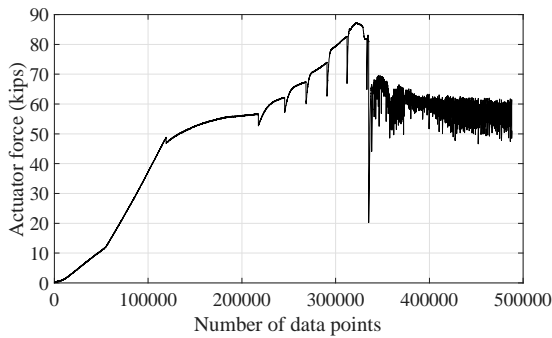


Actuator force vs. Actuator displacement

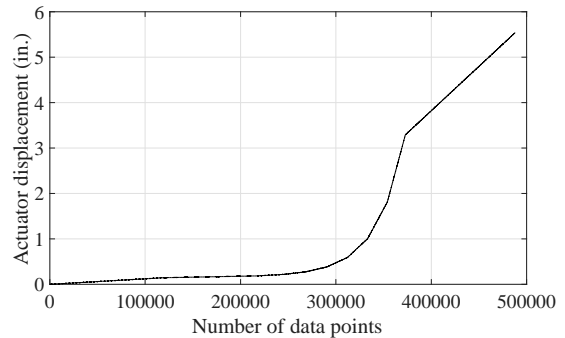


Slip vs. Time

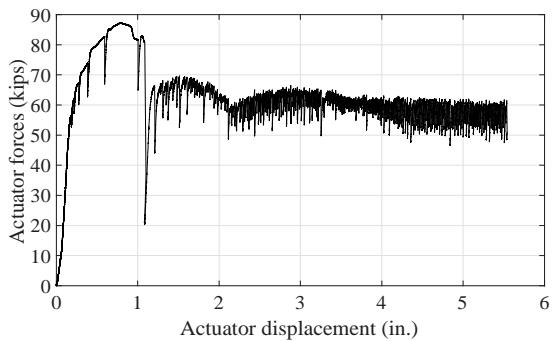
Test 3-M24-2C-RL-LC



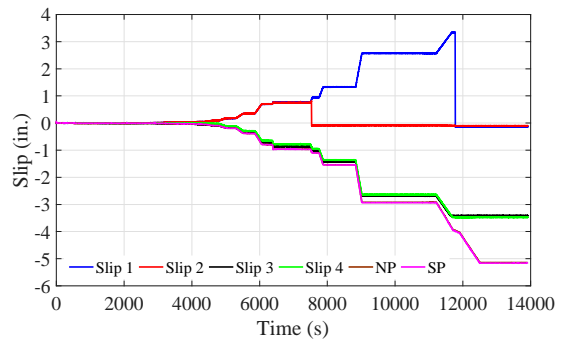
Actuator force variation



Actuator displacement variation

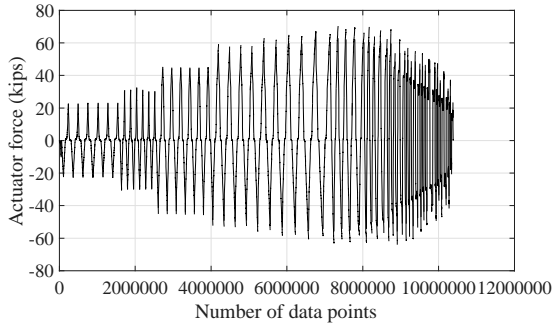


Actuator force vs. Actuator displacement

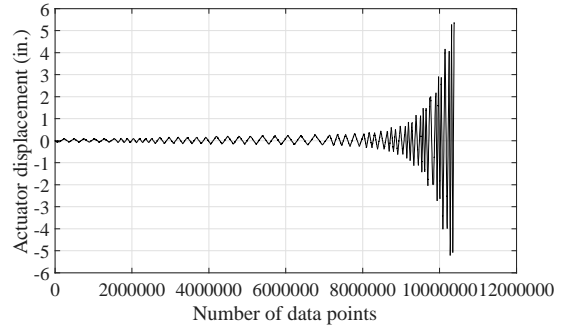


Slip vs. Time

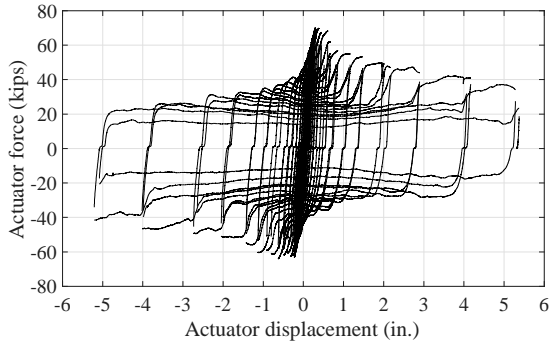
Test 4-M24-2C-RH-LM-S



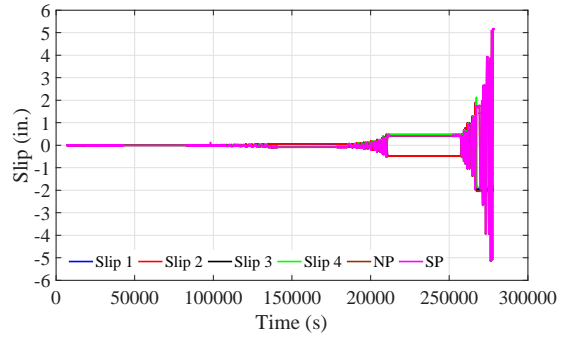
Actuator force variation



Actuator displacement variation

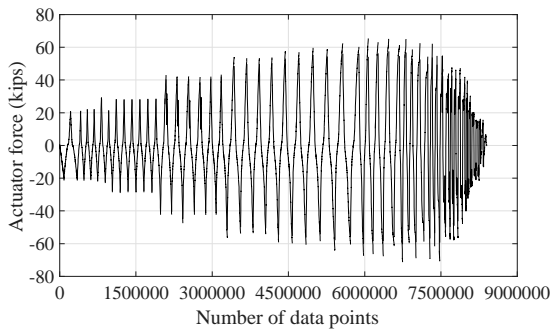


Actuator force vs. Actuator displacement

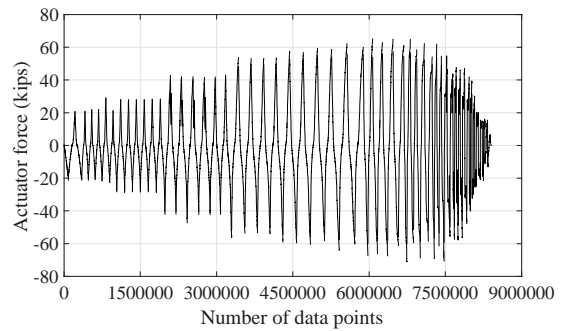


Slip vs. Time

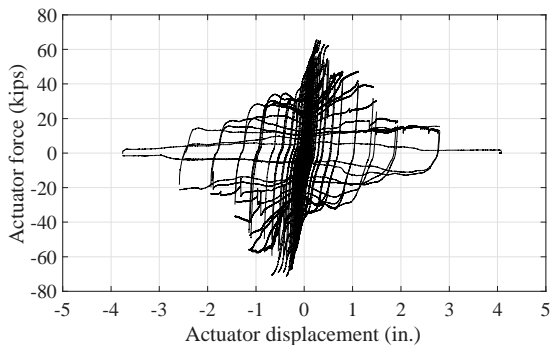
Test 5-M24-2C-RH-LC



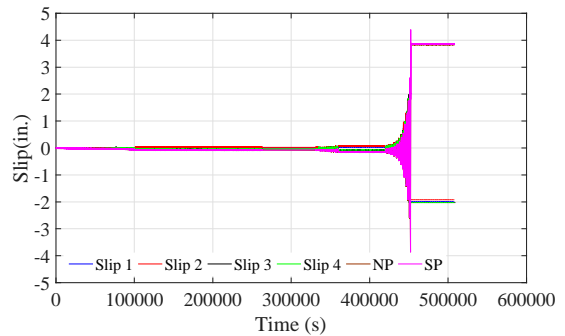
Actuator force variation



Actuator displacement variation

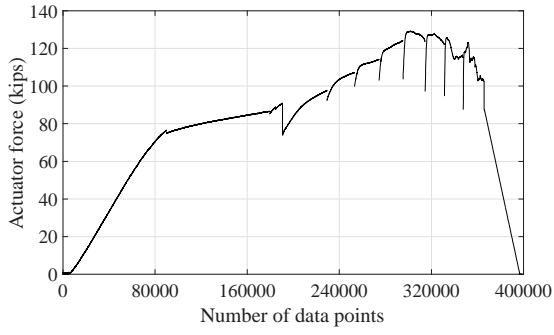


Actuator force vs. Actuator displacement

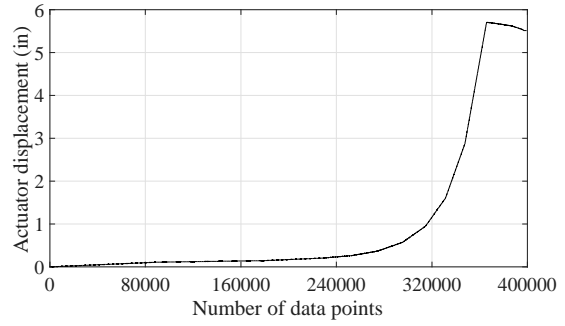


Slip vs. Time

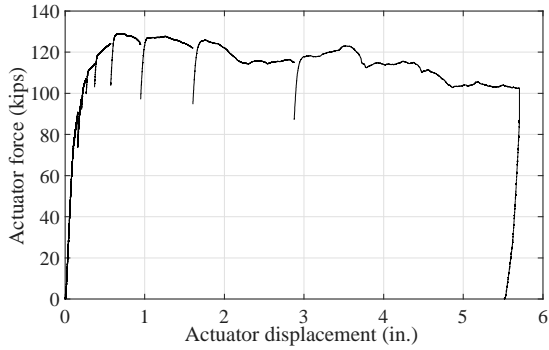
Test 6-M24-2C-RH-LC-S



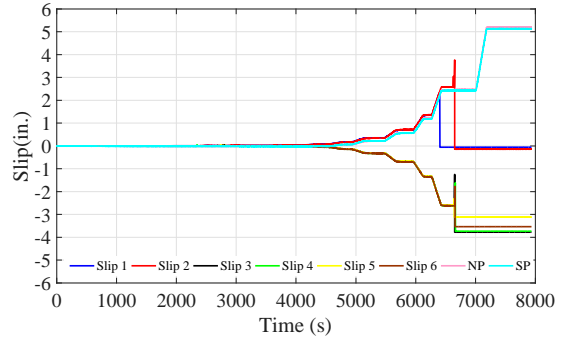
Actuator force variation



Actuator displacement variation

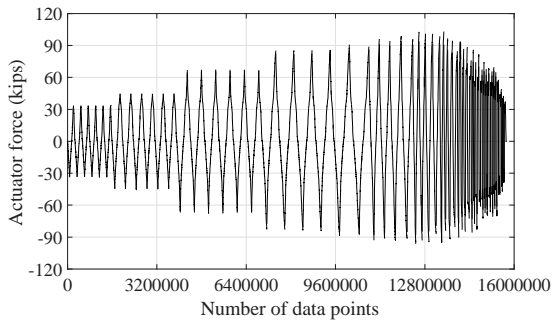


Actuator Force vs. Actuator Displacement

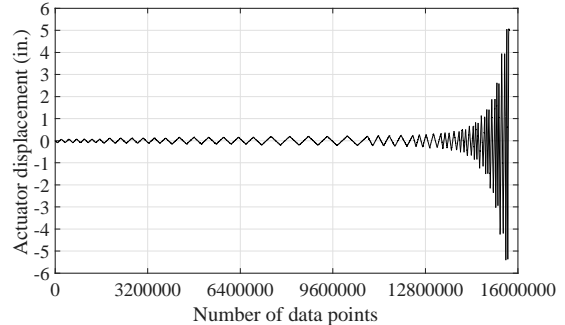


Slip vs. Time

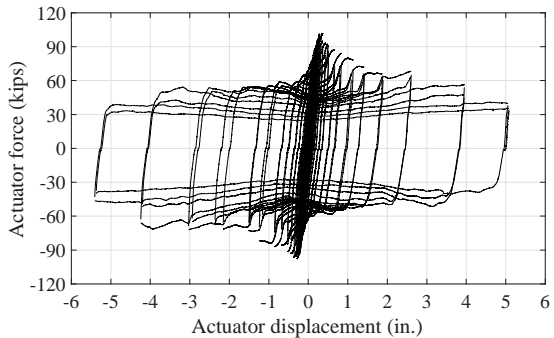
Test 7-M24-3C-RH-LM



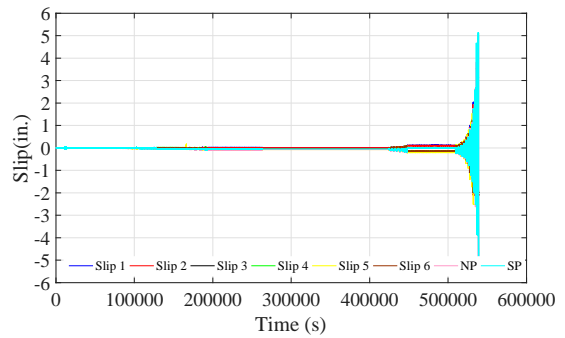
Actuator force variation



Actuator displacement variation

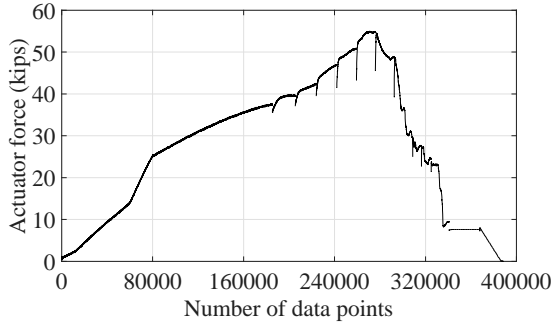


Actuator force vs. Actuator displacement

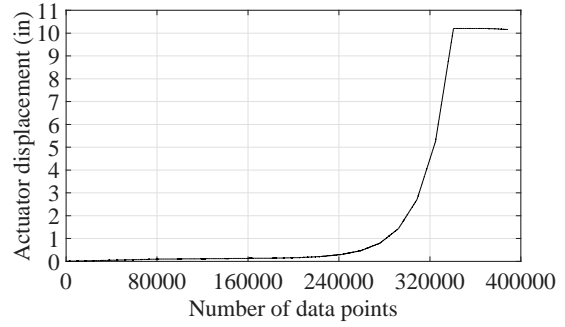


Slip vs. Time

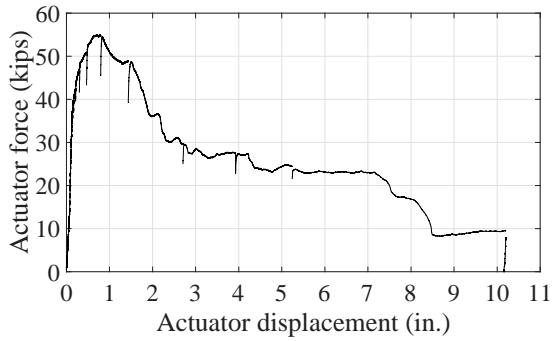
Test 8-M24-3C-RH-LC



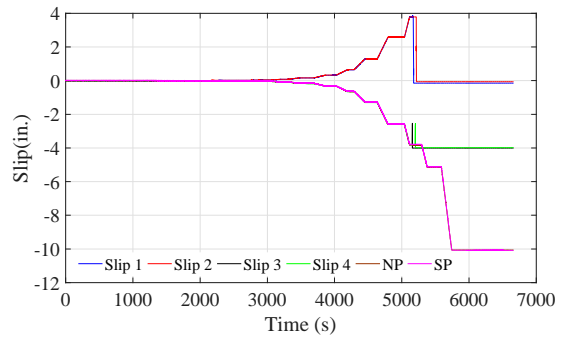
Actuator force variation



Actuator displacement variation

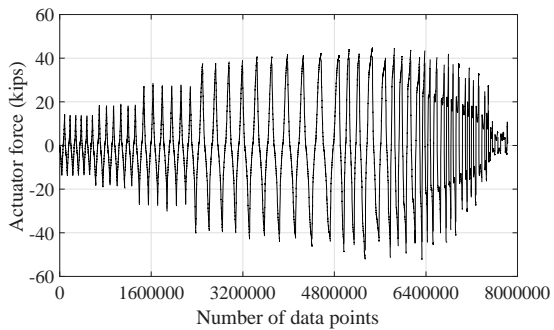


Actuator force vs. Actuator displacement

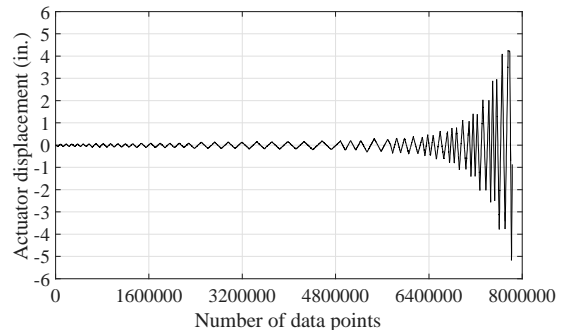


Slip vs. Time

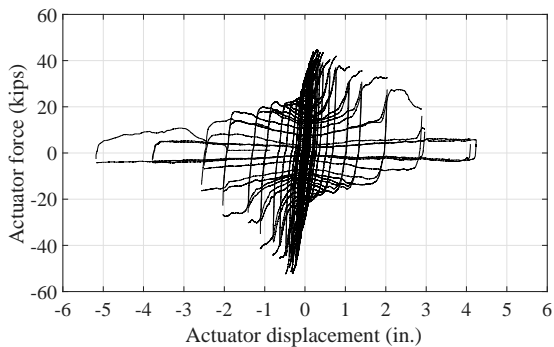
Test 9-M20-2C-RH-LM



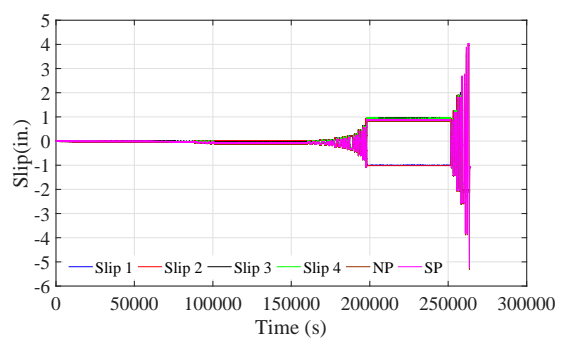
Actuator force variation



Actuator displacement variation



Actuator force vs. Actuator displacement



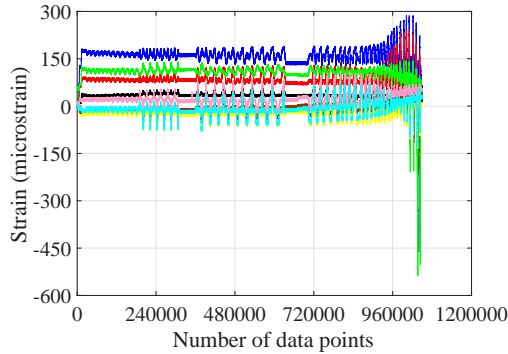
Slip vs. Time

Test 10-M20-2C-RH-LC

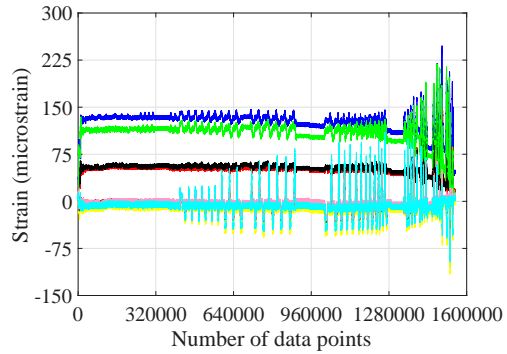
Figure E.2 Actuator force, actuator displacement and slip measurements

E.1.2.2 Beam strain gage

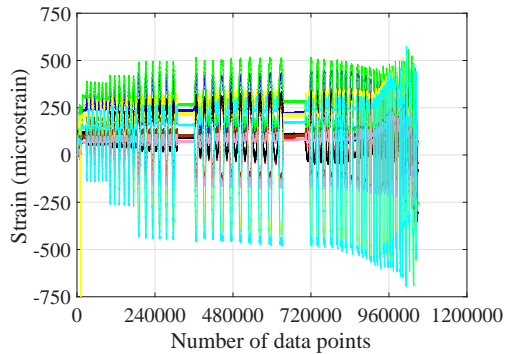
After pretensioning the bolts, the flange strains are generally larger than the web strains, and the outside strains on the flanges are larger than the inside strains, because those locations are closer to the clamps. The strains on the flanges are usually tensile (positive values). The readouts fluctuate while the cyclic shear force is applied. In Test 10-M20-2C-RH-LC, several gages behave abnormally, as indicated by the drift of the readings while the test is paused.



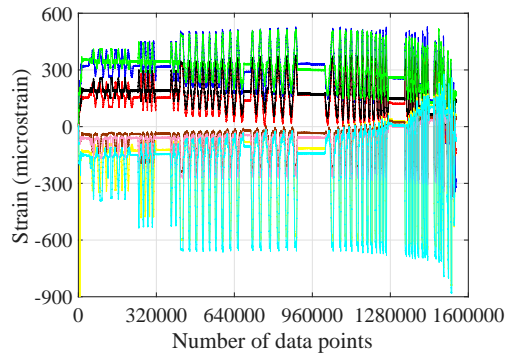
West section



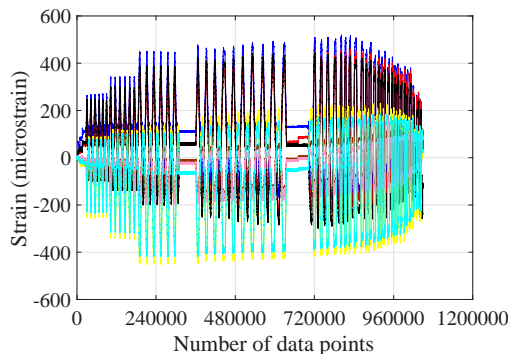
West section



Middle section

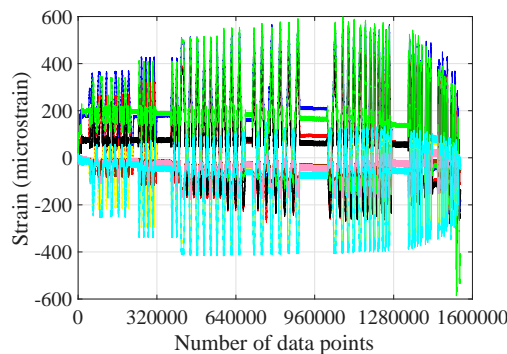


Middle section



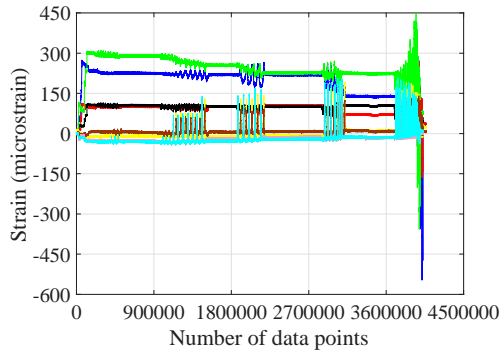
East section

Test 3-M24-2C-RL-LC

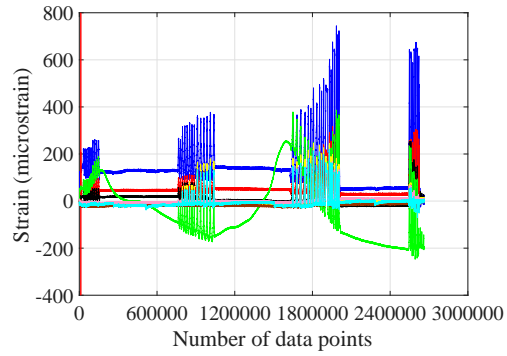


East section

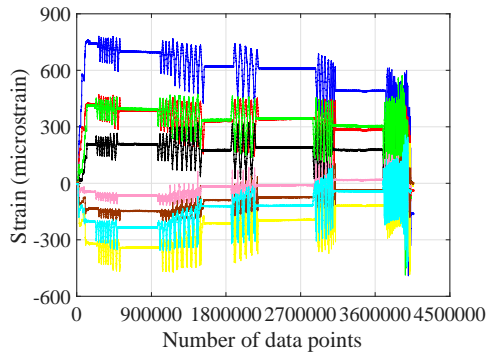
Test 5-M24-2C-RH-LC



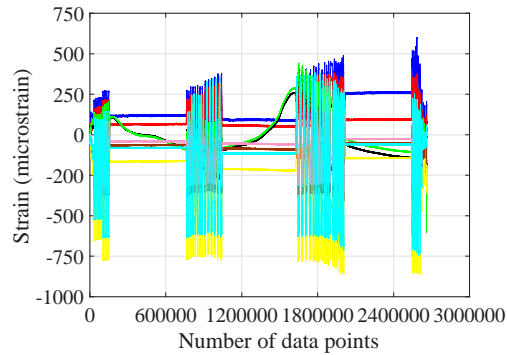
West section



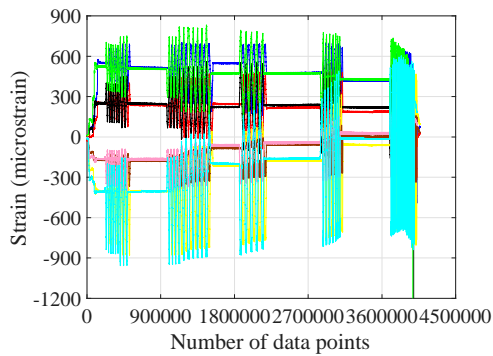
West section



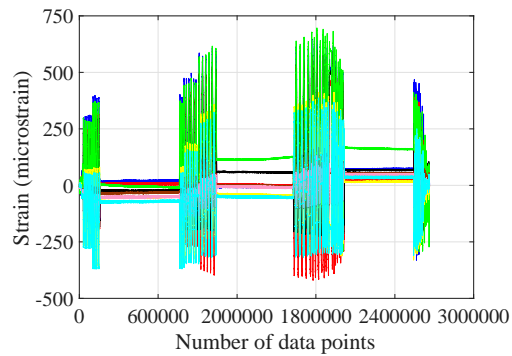
Middle west section



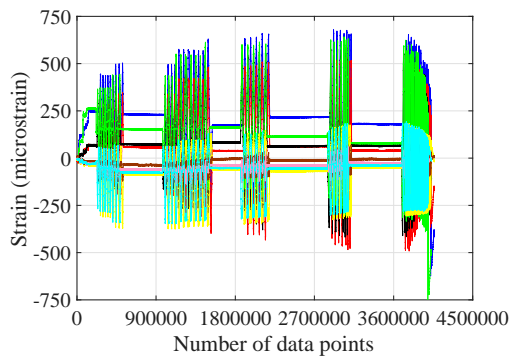
Middle section



Middle east section



East section



East section

Test 8-M24-3C-RH-LC

Test 10-M20-2C-RH-LC

Figure E.3 Beam strain gage readings

E.1.2.3 Bolt strain gage

It is noted that the measurements from the gages away from the steel section are commonly smaller than those from the gages close to the section. As the cyclic shear force is applied, fluctuation is observed in the strain measurements.

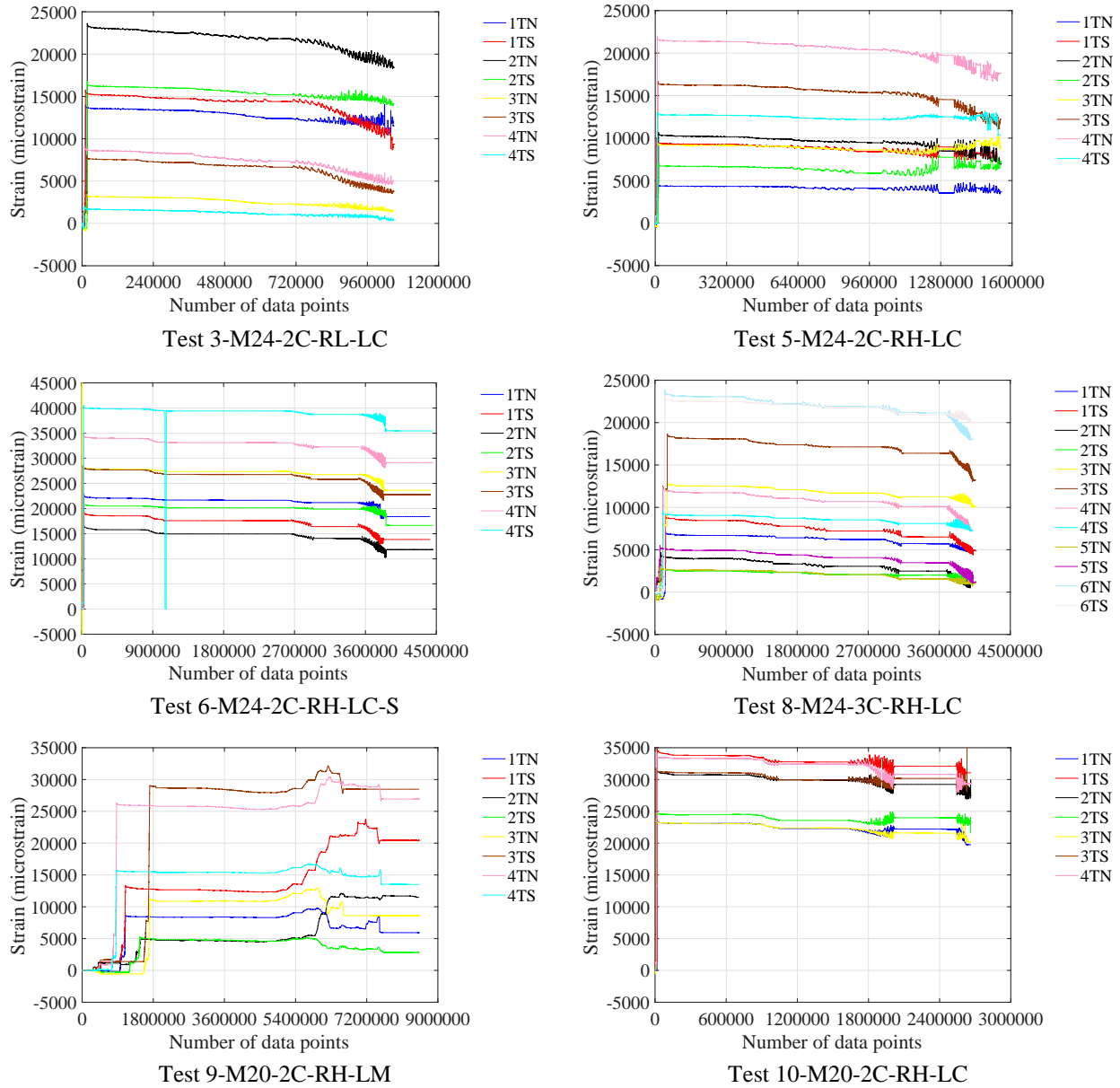
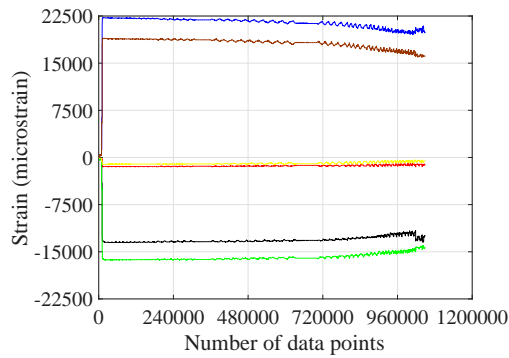


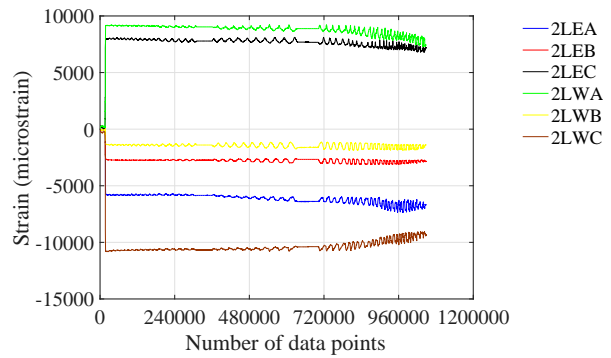
Figure E.4 Bolt strain gage readings

E.1.2.4 Channel lip strain gage

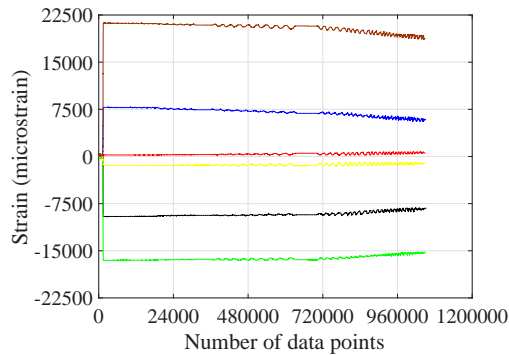
The readings from the rosette strain gages display a similar pattern as that observed from the bolt strain gages. The strains measured by the legs closer to the steel section are usually negative (compressive), while positive (tensile) strains are measured by the legs away from the steel section. Since the pretension force for the M20 bolt is smaller than that of the M24 bolt, the channel lip strains are smaller in the M20 bolt tests. Because of the different scales of the graphs, the variation of the strains due to the applied shear force seems to be tremendous in the M20 bolt tests.



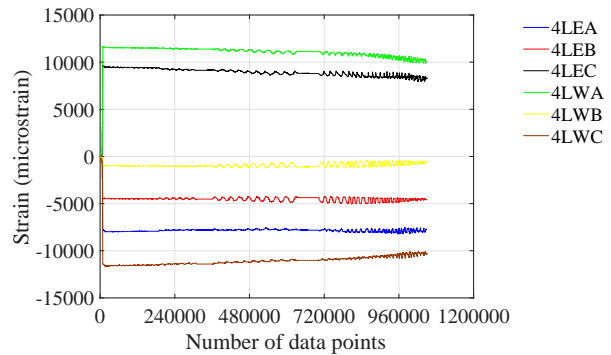
Channel 1



Channel 2

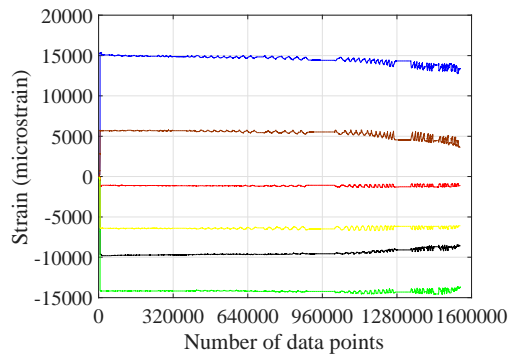


Channel 3

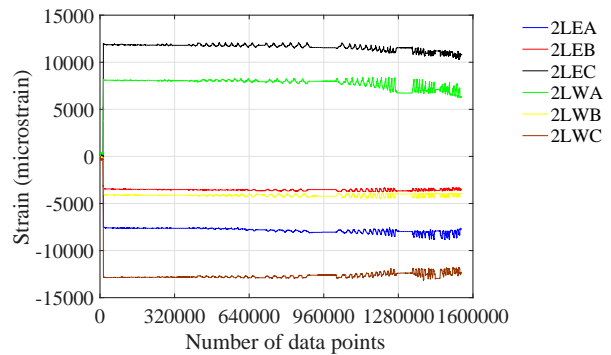


Channel 4

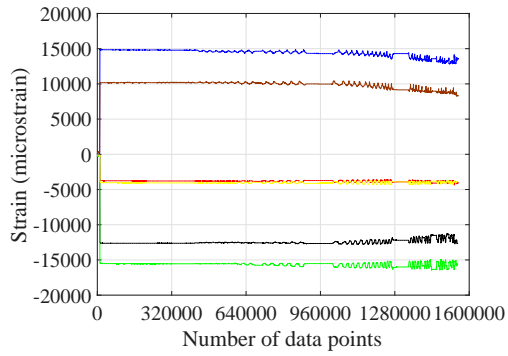
Test 3-M24-2C-RL-LC



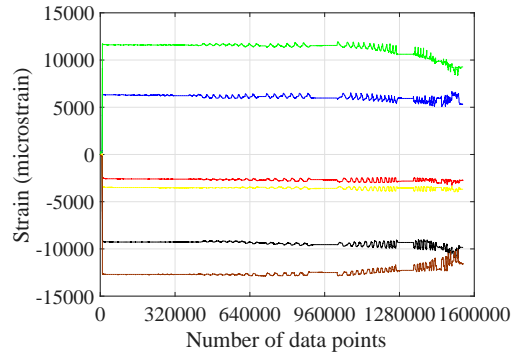
Channel 1



Channel 2

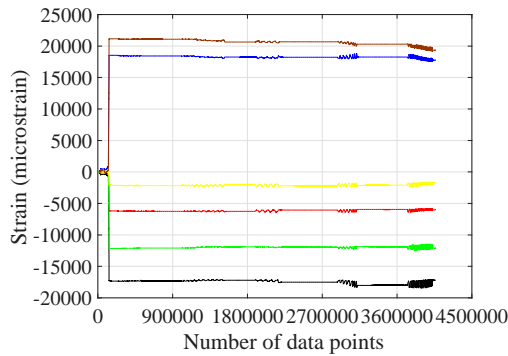


Channel 3

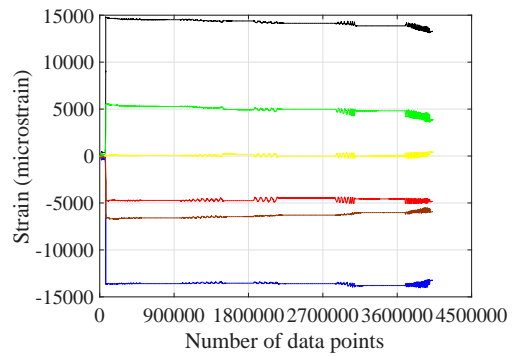


Channel 4

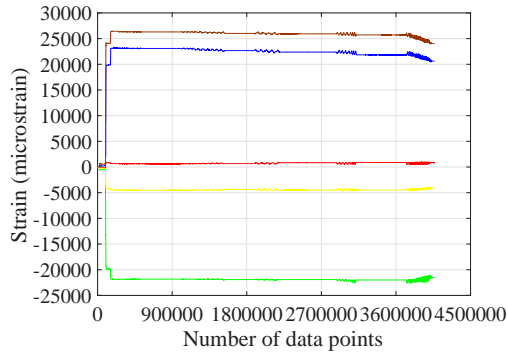
Test 5-M24-2C-RH-LC



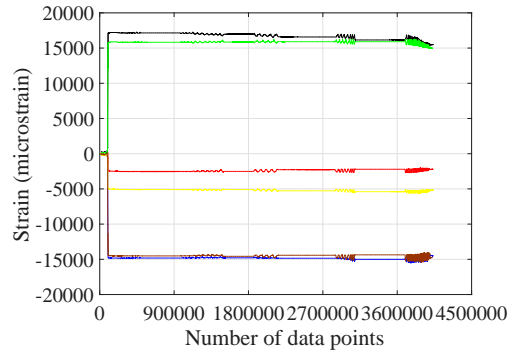
Channel 1



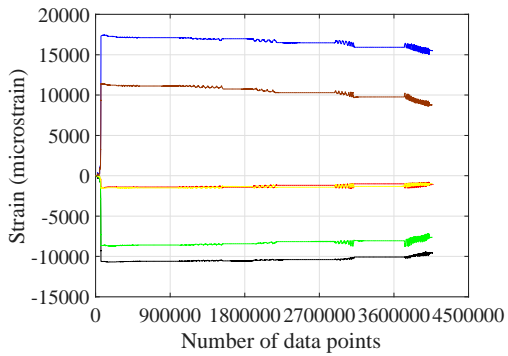
Channel 2



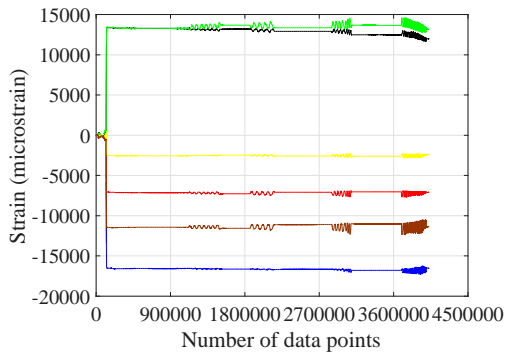
Channel 3



Channel 4

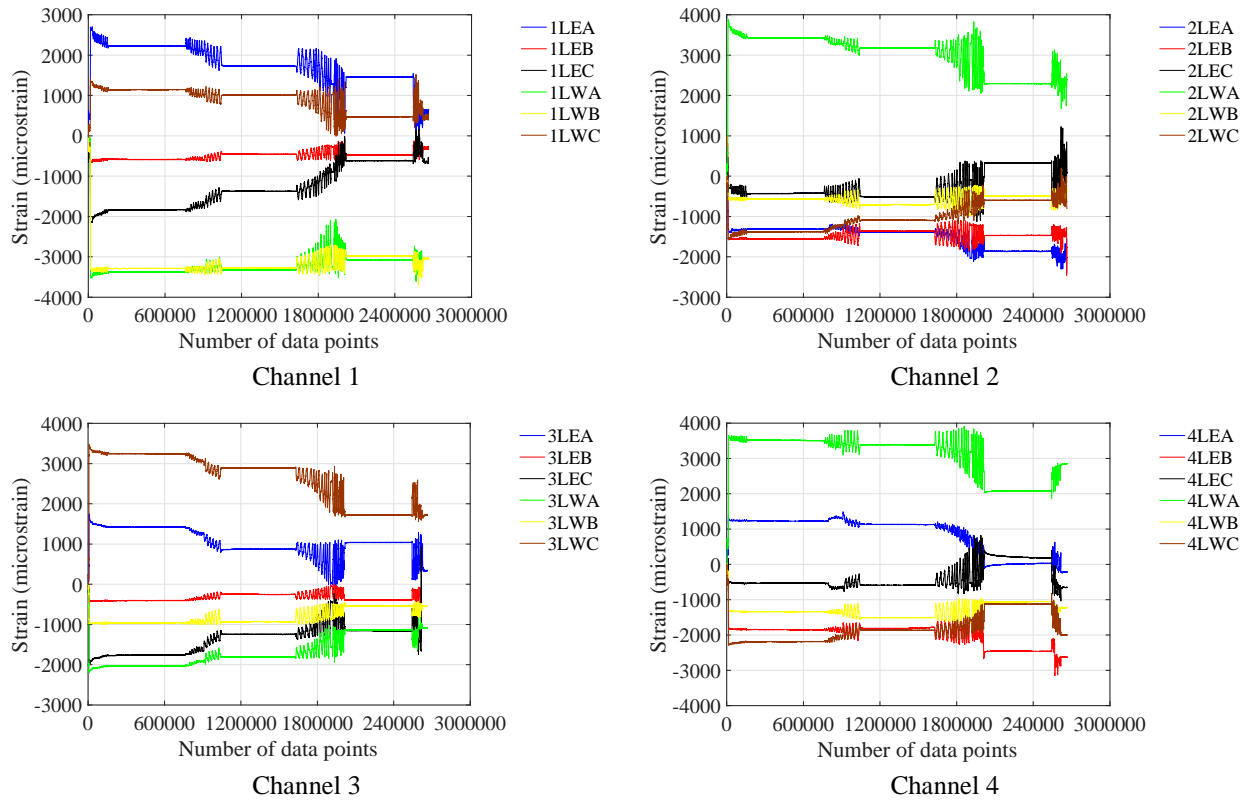


Channel 5



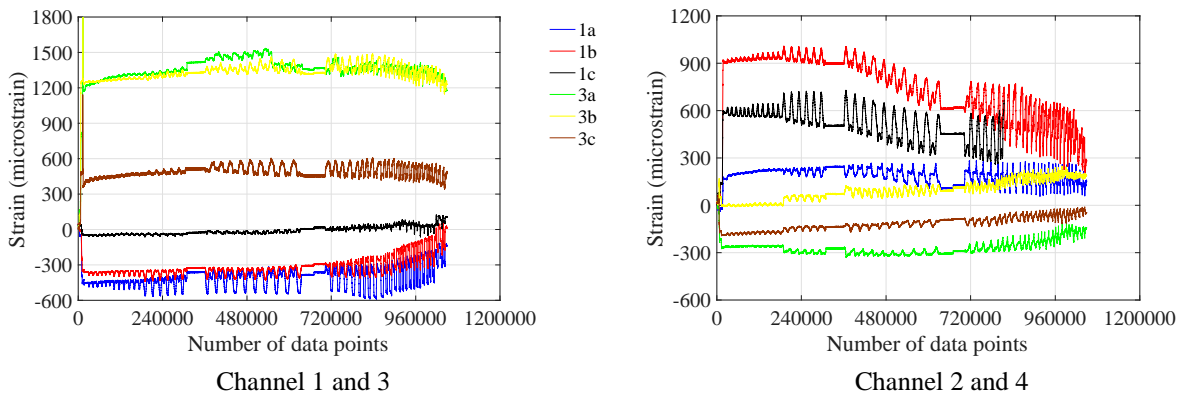
Channel 6

Test 8-M24-3C-RH-LC

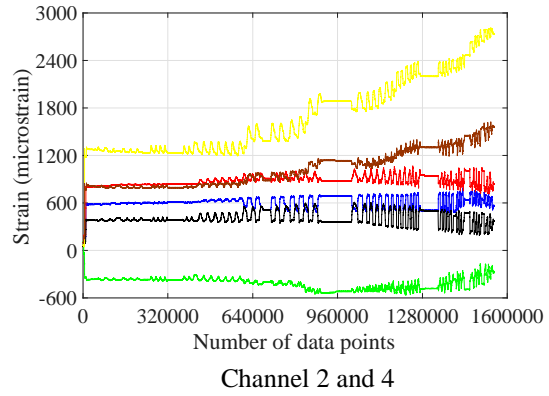
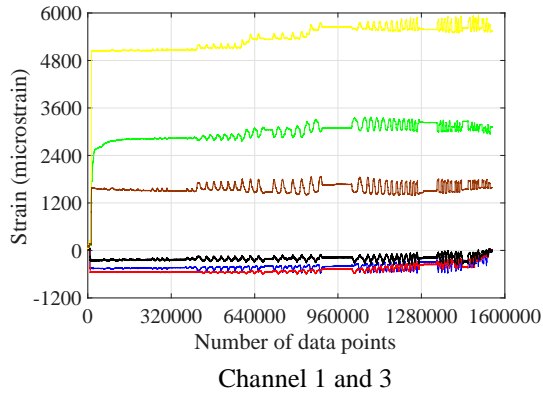


Test 10-M20-2C-RH-LC
Figure E.5 Channel lip strain gage readings

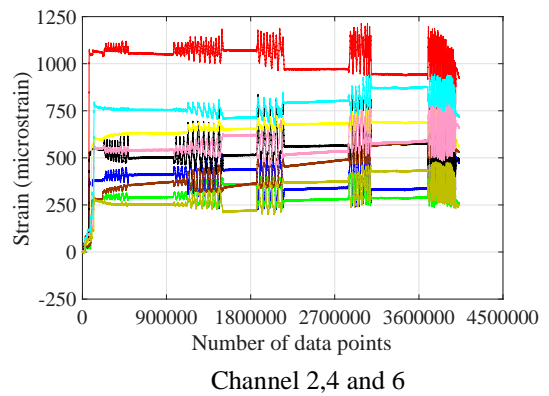
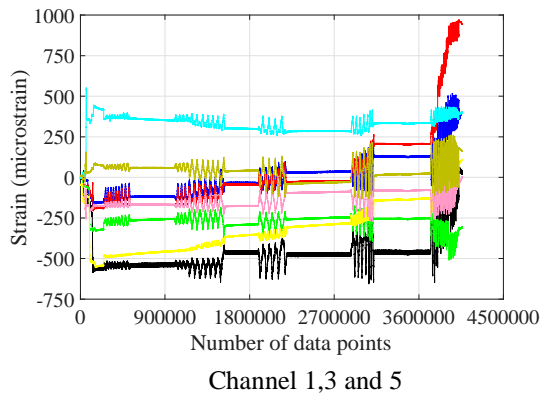
E.1.2.5 Channel anchor strain gage



Test 3-M24-2C-RL-LC



Test 5-M24-2C-RH-LC



Test 8-M24-3C-RH-LC

Figure E.6 Channel anchor strain gage readings

E.1.2.6 Reinforcement strain gage

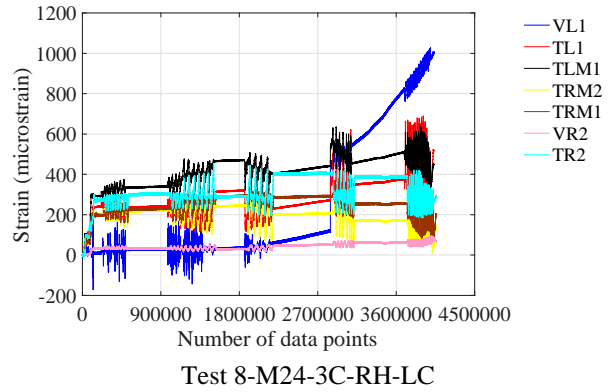
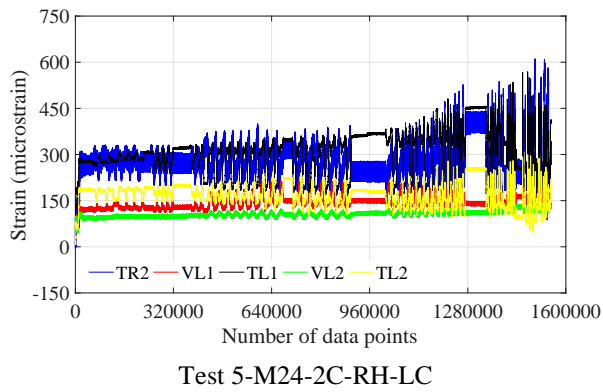


Figure E.7 Reinforcement strain gage readings

Appendix F. Mill Certifications

F.1 Pushout test

F.1.1 Steel frame

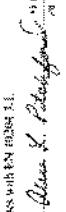
Page 13

CERTIFIED MATERIAL TEST REPORT																																													
<p>GERDAU US-ML-PETERSBURG 25801 HODDINGER WAY PETERSBURG, VA 23860 USA</p> <p>Customer Ship To: COPRA METALS CO 55 PENT HWY WASHINGTON DC 20007-2716 USA</p> <p>Customer Purchase Order Number: NF-40013</p>	<p>Grade: A572-50 A572-50</p> <p>Sheet Size: 48" X 100" X 250 X 80</p> <p>Heat Mark II: #01319007</p> <p>Customer Material No: 3116002488048</p> <p>Bill of Lading: 1150-0000000004</p> <p>Date: 06-01-2015</p>																																												
<p>Chemical Composition:</p> <table border="1" style="width: 100%; border-collapse: collapse;"> <tr> <td>C %</td> <td>0.23</td> <td>Mn %</td> <td>0.34</td> <td>P %</td> <td>0.013</td> <td>S %</td> <td>0.027</td> <td>Si %</td> <td>0.26</td> <td>Al %</td> <td>0.01</td> <td>Ni %</td> <td>0.12</td> <td>Cu %</td> <td>0.12</td> <td>Cr %</td> <td>0.11</td> <td>Mo %</td> <td>0.022</td> <td>Ca %</td> <td>0.014</td> <td>Co %</td> <td>0.001</td> <td>Nb %</td> <td>0.017</td> <td>As %</td> <td>0.005</td> </tr> </table>	C %	0.23	Mn %	0.34	P %	0.013	S %	0.027	Si %	0.26	Al %	0.01	Ni %	0.12	Cu %	0.12	Cr %	0.11	Mo %	0.022	Ca %	0.014	Co %	0.001	Nb %	0.017	As %	0.005	<p>Physical Properties:</p> <table border="1" style="width: 100%; border-collapse: collapse;"> <tr> <td>UTS</td> <td>74100</td> <td>Y.T. 0.2%</td> <td>64</td> </tr> <tr> <td>YS 0.01%</td> <td>55000</td> <td>Y.T. 0.01%</td> <td>40</td> </tr> <tr> <td>ELONG</td> <td>24.00</td> <td>ELONG</td> <td>20.00</td> </tr> <tr> <td>REDUCED</td> <td>50.00</td> <td>REDUCED</td> <td>40.00</td> </tr> </table>	UTS	74100	Y.T. 0.2%	64	YS 0.01%	55000	Y.T. 0.01%	40	ELONG	24.00	ELONG	20.00	REDUCED	50.00	REDUCED	40.00
C %	0.23	Mn %	0.34	P %	0.013	S %	0.027	Si %	0.26	Al %	0.01	Ni %	0.12	Cu %	0.12	Cr %	0.11	Mo %	0.022	Ca %	0.014	Co %	0.001	Nb %	0.017	As %	0.005																		
UTS	74100	Y.T. 0.2%	64																																										
YS 0.01%	55000	Y.T. 0.01%	40																																										
ELONG	24.00	ELONG	20.00																																										
REDUCED	50.00	REDUCED	40.00																																										
<p>Mechanical Properties:</p> <table border="1" style="width: 100%; border-collapse: collapse;"> <tr> <td>UTS</td> <td>74100</td> <td>Y.T. 0.2%</td> <td>64</td> </tr> <tr> <td>YS 0.01%</td> <td>55000</td> <td>Y.T. 0.01%</td> <td>40</td> </tr> <tr> <td>ELONG</td> <td>24.00</td> <td>ELONG</td> <td>20.00</td> </tr> <tr> <td>REDUCED</td> <td>50.00</td> <td>REDUCED</td> <td>40.00</td> </tr> </table>		UTS	74100	Y.T. 0.2%	64	YS 0.01%	55000	Y.T. 0.01%	40	ELONG	24.00	ELONG	20.00	REDUCED	50.00	REDUCED	40.00																												
UTS	74100	Y.T. 0.2%	64																																										
YS 0.01%	55000	Y.T. 0.01%	40																																										
ELONG	24.00	ELONG	20.00																																										
REDUCED	50.00	REDUCED	40.00																																										
<p>Comments:</p>																																													

Sheet No 709127
 Sheet Number 80113158

Customer Name
 CAPONE IRON CORPORATION

The above figures are certified chemical and physical test results as compared to the guarantee of the company. We certify that these figures conform with the applicable with specific requirements. This material, including the above, was produced and manufactured in the USA. © 2015 Gerdau Metals, Inc. 10/24/15


 Alan K. Peterson
 VP - QUALITY CONTROL
 25801 HODDINGER WAY
 PETERSBURG, VA 23860



US-ML-PETERSBURG
25801 HOFFMEIER WAY
PETERSBURG, VA 23803
USA

Heat Number
60113201

Shipment No
714430

CUSTOMER SHIP TO
INTEKA METALS CO
1 STURBILLS WAY
NEW BOSTON OH 45662
USA

CUSTOMER BILL TO
INTEKA METALS CO
1 STURBILLS WAY
NEW BOSTON OH 45662
USA

SALES ORDER
25962600040

GRADE
A992A572-50

SHAPE / SIZE
Wide Flange Beams 78 X 314 / 290 X 461

LENGTH
48'0"

WEIGHT
7,490 LB

HEAT / BATCH
60113201/03

CUSTOMER MATERIAL N°

DATE
06222015

BILL OF LADING
1330-000055439

CUSTOMER PURCHASE ORDER NUMBER
OH-491525

CHEMICAL COMPOSITION

	C	Mn	P	S	Si	Cr	Ni	Mo	Al	Other
%	0.28	0.95	0.012	0.025	0.22	0.37	0.12	0.06	0.029	0.018

CHEMICAL COMPOSITION
CEN: 0.29

MECHANICAL PROPERTIES

YS	UTS	YS	UTS	YF	EL	RA	AV
ksi	70000	78000	990	496	0.235	0.000	0.001
MPa	4830	53000	693	353	0.27%	0.000	0.001

MECHANICAL PROPERTIES

YS	UTS	YS	UTS	YF	EL	RA	AV
ksi	70000	78000	990	496	0.235	0.000	0.001
MPa	4830	53000	693	353	0.27%	0.000	0.001

MECHANICAL PROPERTIES

YS	UTS	YS	UTS	YF	EL	RA	AV
ksi	70000	78000	990	496	0.235	0.000	0.001
MPa	4830	53000	693	353	0.27%	0.000	0.001

COMMENTS / NOTES

The above figures are certified chemical and physical test records as contained in the permanent records of company. We certify that these data are correct and in compliance with specified requirements. This material, including the billets, was notified and manufactured in the USA. CMTR complies with EN 10204 3.1.

Maskey BISHAR YALAMANCHERI
QUALITY INSPECTOR

Wesley H. Atchford
QUALITY ASSURANCE MGR

Customer Name
CAPONE IRON CORPORATION

**Bescheinigung
über Werkstoffprüfungen**

Document on materials testing
Document de contrôle des matériaux

Datum 06.03.2014
Date

Blatt 2/2
Page

nach/according to/suivant

EN 10204-3.1

Mannstaedt GmbH, Postfach 1462, D-53858, Troisdorf
Halfen GmbH
Liebigstr. 14
40764 Langenfeld-Richrath

Allgemeine Daten / General Informations / Informations d'ordre General	
Zeugnis-Nr. Test Report No. Certificat-No.	01269108
Bestelltag Date of Order Date de cde	02.10.2012
Kundenauftrags-Nr. Our Order-No.	6001587
Ihre Bestell-Nr. Your Order-No.	
Reif/Usine-No.	
Gegenstand Object Objet	Warmprofile DIN EN 10025
Stahlsorte Steel grade Nuance d'acier	S235JRG2 (RST 37-2 ZN-AL) DIN EN 10025
Profil-Nr. Profile-No.	W 76.097.5
Kunden-id.Nr. Customer id.No. No. de référence	0280.180-00002
Zusatzinformationen / Additional Information / Informations complémentaires	
120045	Kaltgerichtet
124748	Kaltgerichtet

Die gelieferten Produkte sind frei von ionisierender Strahlung, die über die natürliche Strahlung hinausgeht.

The delivered products are free of ionized emission, which is above the natural emission.


Les produits livrés n'ont pas été exposés à des rayons ionisants dépassant le rayonnement naturel.

Bei Rückfragen wenden Sie sich bitte an / If you have any queries please contact / Pour tout renseignement complémentaire veuillez vous adresser à:

Peter Leye (p.leye@mannstaedt.de; Tel.: + 49(0)2241/84-2327) oder / or / ou Marco Vostell (m.vostell@mannstaedt.de; Tel.: + 49(0)2241/84-2324)

Der Werkssachverständige / The Work's Inspector / L'expert d'usine: Joachim Braun

Maschinell erstellter Beleg, ohne Unterschrift gültig. / This document has been issued electronically and is valid without signature. / Document valable sans signature.

Qualitätswesen Werk Langenfeld	
Zeugnis geprüft	
Datum: 25.03.14	Unterschrift: 
Norm:	<input checked="" type="checkbox"/> Erfüllt <input type="checkbox"/> nicht erfüllt

Halfen GmbH

Liebigstraße 14
D- 40764 Langenfeld
Telefon: +49 (0) 2173/970-0
Telefax: +49 (0) 2173/970-123
Internet: www.halfen.com
E-Mail: info@halfen.com

Abteilung
Qualitätswesen / Quality department
Telefon: +49 (0) 2173/970-743
E-Mail: qs-langefeld@halfen.de

Halfen GmbH * Postfach 1262 * D-40764 Langenfeld

Dr. Frank Häusler
Abt. Forschung und Entwicklung
Halfen GmbH

22.09.15 / si Seite 1

Abnahmeprüfzeugnis nach EN 10204-3.1 - No. 9580
Acceptance inspection certificate M / 3.1

Kunden-Bestell-Nr./Customer order No.: Versuche USA

Projekt-Kennung/Project Identification:

Liefergegenstand/Delivery Item

Loskennung/Lot-ID HS 72/48 M24x150mm GV 8.8

Loskennung/Lot-ID: 5300Lxxxxxx

Auftrags-Nr

Chemische Analyse/Chemical analysis:

4721 Schrauben / bolt - Norm: DIN ISO 8992, DIN EN ISO 898 T.1 - 36CrB4 - 1.7077

Charge Heat No.	C %	Si %	Mn %	P %	S %	Cr %	B %
255080	0,370	0,100	0,790	0,011	0,003	1,090	0,0030

Mechanische Eigenschaften/Mechanical properties:

4721 Schrauben / bolt - Norm: DIN ISO 8992, DIN EN ISO 898 T.1 - 36CrB4 - 1.7077

Charge Heat No.	Streckgrenze Yield strength Rp 0,2 MPa	Zugfestigkeit Tensile strength Rm MPa	Dehnung Elongation A %	Schichtdicke Coating µm	Härte Hardness HV
255080	>660N/mm ² 812	>830N/mm ² 908	>12 14,8	>12 18-22	255-335HV 294-302HV

Ausführung/ Conditions of delivery: galvanisch verzinkt / elektroplated coatings DIN EN ISO 4042

Das oben beschriebene Produkt ist konform mit den in der Bestellung festgelegten Anforderungen. Gleichzeitig wird bestätigt, dass die festgestellten Prüfergebnisse die Anforderungen aus der Bestellung erfüllen.

The products described above are conformal with the requirements specified in the order. In addition we confirm, that the test results fulfill the requirements stated in the order.

Halfen GmbH

Abnahmebeauftragter

The person responsible for material release

i.v. Michael Dörner

Das Zeugnis ist maschinell erstellt und trägt keine Unterschrift

This document has been computer generated and is valid without signature.

Halfen GmbH, AG Düsseldorf HRB 55272
USt-ID-Nr. DE 190725092, Steuer-Nr. 135/5732/1062
Geschäftsführung: Richard Wachter, Arjan J. Bakker
Commerzbank AG Langenfeld (BLZ 342 400 50), Konto Nr. 3 506 607
ING Bank N.V., Frankfurt (BLZ 500 210 00), Konto 0 010 141 778



Reg.-Nr.: 2499-CPR-0113070

Zertifikat -Nr. QS-281 HH

Das Qualitätsmanagementsystem der Halfen GmbH ist für die Standorte in Deutschland, Frankreich, Österreich, Polen, Schweiz, Niederlande und der Tschechischen Republik zertifiziert nach DIN EN ISO 9001:2008.



Northeastern University
 2 Evans St.
 APT R
 Woburn, MA 01801 4804

HALFEN USA
 PO Box 547, 8521 FM 1976
 Converse, Texas 78109
 USA
 Phone: (800) 423 9140
 Fax: (877) 874 7923
 Internet: www.halfenusa.com
 E-Mail: info@halfenusa.com

CONCRETE - Anchoring Systems
 FACADE - Fixing Systems
 FRAMING - Products and Systems

E-Mail: ahernandez@halfenusa.com

February 24, 2016

Acceptance Inspection Certificate M / 3.1

Customer PO No: kyle 01-14-16
Delivery Item: Halfen HS 72/48 M20x100 GV-S (8.8) – Bolts and Nuts
Project Name: Northeastern University
Order: S023259

Chemical Analysis:

<i>According to Standard: DIN ISO 8992, DIN EN ISO 898-1/-2</i>									
Charge Heat No:	C %	Si %	Mn %	P %	S %	Cr %	Mo %	B %	Ni %
245954	0.370	0.090	0.770	0.008	0.003	1.08	-	0.0026	-

Mechanical properties:

<i>According to Standard: DIN ISO 8992, DIN EN ISO 898-1/-2</i>					
Charge Heat No.	Yield Point (Rp) MPa	Tensile strength (Rm) MPa	Elongation (A) %	Hardness HV	Coating μ m
245954	818	905	15.6	289-302	18-22

The products described above are conformal with the requirements specified in the order. In addition we confirm that the test results fulfill the requirements specified in the order.

Halfen USA, Inc. 
 Alonso Hernandez- Operational Quality Manager

F.1.3 Lindapter clamps and washers



TRAKYA DÖKÜM
SANAYİ VE TİC.A.Ş.

25/12/2013

LOT-011201

QUALITY CONTROL DEPARTMENT LABORATORY REPORT

(Inspection certificate 3.1 acc. To standard EN 10204:2004)

FIRM : LINDAPTER

PART NO : 5017 H

PART NAME : M 20 TYPE AF SHORT TAIL (5017-H)

PATERN NO-PATERN PART NO:

REPORT NO : 11

CASTING DATE : 28.09.2013

SHIPPING AMOUNT (Pcs): 3,000

ORDER NUMBER : M 027085

SAFETY

SAMPLE

FIRST PRODUCTION

ACTUAL PRODUCTION

MODIFICATION

CHEMICAL COMPOSITION:

METARIAL : EN - GJS - 600.3

%	C	Si	Mn	S	P	Cr	Cu	Mg
SPECIFICATION								
INSP.RESULT	3,60 3,58	2,53 2,61	0,21 0,20	0,0026 0,0021	0,022 0,021	0,023 0,021	0,042 0,048	0,030 0,036

MECHANICAL PROPERTIES:

HB Ø 10/3000/15"

HB Ø 5/750/15"

	HARDNESS(BHN) SURFACE	HARDNESS(BHN) CORE	TEN.STRENGTH N/mm ²	YIELD STREN. N/mm ²	ELONGATION %		
SPECIFICATION	210 - 260		600 MIN.		3 MIN.		
INSP.RESULT	232-236		645.24		8.22		

MICROSTRUCTURE : (100X)

	GRAPHITE FORM	GRAPHITE DISTRIBUTION	NODULARITY PERCENT %	NOD.COUNT IN 20 Inch ²	MATRIX	CEMENTITE
SPECIFICATION	0A-4.7	HOMOGENEOUS	90%	150 MIN.	%60 MIN PEARLITE	NO
INSP.RESULT	0A-5.7	HOMOGENEOUS	100%	180-220	% 60 - 65 PEARLITE	NO

NOT:

- THE PARTS , WERE CONTROLLED BY VISUAL INSPECTION IN 100 %.

-" NO WELDING OR FILLER MATERIAL PERFORMED ON THIS MATERIAL "

LABORATORY
YAŞAR SOLAK

Prepared by software media.Approved.

CONTROL
ADNAN ÖZGÜR

Prepared by software media.Approved.

F01/FY-40.37

Record Retention: 5 years

LOT-009024
 LOT-009025 28-11-12

FAO A.1172010

H. Goodwin (Castings) Ltd
 Manufacturers of Engineering Castings and Assemblies

Lidget LLP T/A - Lindapter International

DECLARATION OF CONFORMANCE

Order Number	Description	Part Number	Delivery Note Number	Qty
M-026392	M20 Type AFW Washer	5020	17131	5753
M-026340	M12 Type W Deep Washer	4436	17017	3900
Cast Date 29/10/12 AS 440/12 A 425 N/mm2 - 8% Elongn B 403 N/mm2 - 8% C 401 N/mm2 - 8% D 403 N/mm2 - 8%				
Cast Date 30/10/12 AS 443/12 A 405 N/mm2 - 8% Elongn B 425 N/mm2 - 8% C 403 N/mm2 - 8% D 401 N/mm2 - 8%				
Cast Date 31/10/12 AS 446/12 A 423 N/mm2 - 8% Elongn B 402 N/mm2 - 8% C 403 N/mm2 - 8% D 420 N/mm2 - 8%				
Page 1 of 2				
Material Specification: WHM 400/3		Deviation Number:		
We hereby certify that the parts referred to comply with the requirements of the current drawing specification and contract order. We hereby certify that no welding has been performed or filler material used in the manufacture of the above component(s).				
Delivered to - Lidget LLP T/A - Lindapter International				
For and behalf of H Goodwin (castings) Ltd.				
Signed - <i>Les Elwell</i>				
Name - Les Elwell		Position - Metallurgist		
Date - 29/11/2012				

Registered Office: 155 Stafford Street, Walsall, WS2 8EY
 Telephone: 01922 633511 Fax: 01922 633515
 Registered in England: No. 4377806 VAT No. GB 792 4857 79

FAO A. TAYLOR

Lot 009024
Lot 009025

H. GOODWIN CASTINGS LTD

DATE 31/10/12

FURNACE 3

AS 446 12

TIME	STD ID	C	SI	Mn	S	P
	65514	2.00	1.92	469	0.90	1.96
Correction factor						
		-0.00	+0.09	-0.29	-0.14	-0.16

TIME	SAMPLE ID	Thermal Analysis						Spectro Analysis						WHITEHEART BASE						ADDITIONS
		CE	C	SI	Mn	S	P	C	SI	Mn	S	P	Cr	NI	AI	B	Mn/S			
6.57	B1	3.09	2.93	.80	.55	7192	.002	.020	.022	.005	.007	.47							1KSC	
	B1.4				.86	389	7192	.019	.022	.005	.007	.54								
	B3	3.32	3.11	.85	.77	420	7192	.016	.020	.017	.005	.008	.50							
	B3.4				.79	456	7192	.019	.020	.022	.005	.009	.50							

IDEAL	MIN	3.3	3.1	0.75	3.1	0.75	0.2	0.11	n/a	n/a	n/a	n/a	0.1	0.055	0.1	n/a	n/a	0.5
RANGE	MAX	3.56	3.3	0.85	3.3	0.85	0.4	0.23	0.1	0.005	0.02	0.6						



TRAKYA DÖKÜM
SANAYİ VE TİC.A.Ş.

25/12/2013
LOT-011195

**QUALITY CONTROL DEPARTMENT
LABORATORY REPORT**

(Inspection certificate 3.1 acc. To standard EN 10204:2004)

FIRM : LINDAPTER
PART NO : 5077 H
PART NAME : M 24 TYPE AF SHORT TAIL (5077-H)
PATTERN NO-PATTERN PART NO:

REPORT NO : 09
CASTING DATE : 14.12.2013
SHIPPING AMOUNT (Pcs): 500
ORDER NUMBER : M 027113

SAFETY SAMPLE FIRST PRODUCTION ACTUAL PRODUCTION MODIFICATION

CHEMICAL COMPOSITION:

METARIAL : EN - GJS - 600.3

%	C	Si	Mn	S	P	Cr	Cu	Mg
SPECIFICATION								
INSP.RESULT	3,59 3,59	2,53 2,59	0,22 0,22	0,0025 0,0025	0,032 0,033	0,022 0,021	0,082 0,075	0,030 0,036

MECHANICAL PROPERTIES: HB Ø 10/3000/15" HB Ø 5/750/15"

	HARDNESS(BNH) SURFACE	HARDNESS(BHN) CORE	TEN.STRENGTH N/mm ²	YIELD STREN. N/mm ²	ELONGATION %			
SPECIFICATION	210 - 260		600 MIN.		3 MIN.			
INSP.RESULT	236-239		634.56		8.2			

MICROSTRUCTURE : (100X)

	GRAPHITE FORM	GRAPHITE DISTRIBUTION	NODULARITY PERCENT %	NOD COUNT IN 20 inch ²	MATRIX	CEMENTITE	
SPECIFICATION	0A-4.7	HOMOGENEOUS	90%	150 MIN.	%60 MIN PEARLITE	NO	
INSP.RESULT	0A-5.7	HOMOGENEOUS	100%	180-220	% 60 - 65 PEARLITE	NO	

NOT : - THE PARTS , WERE CONTROLLED BY VISUAL INSPECTION IN 100 %.

- " NO WELDING OR FILLER MATERIAL PERFORMED ON THIS MATERIAL "

LABORATORY
YAŞAR SOLAK

Prepared by software media.Approved.

CONTROL
ADNAN ÖZGÜR

Prepared by software media.Approved.

F01/FY-40.37

Record Retention: 5 years



TRAKYA DÖKÜM
SANAYİ VE TİC.A.Ş.

31/01/2014
LOT-011457

QUALITY CONTROL DEPARTMENT
LABORATORY REPORT

(Inspection certificate 3.1 acc. To standard EN 10204:2004)

FIRM : LINDAPTER
PART NO : 5077 H
PART NAME : M 24 TYPE AF SHORT TAIL (5077-H)
PATTERN NO-PATTERN PART NO:

REPORT NO : 01
CASTING DATE : 11.01.2014
SHIPPING AMOUNT (Pcs): 2,000
ORDER NUMBER : M 027121

SAFETY SAMPLE FIRST PRODUCTION ACTUAL PRODUCTION MODIFICATION

CHEMICAL COMPOSITION:

METARIAL : EN - GJS - 600.3

%	C	Si	Mn	S	P	Cr	Cu	Mg
SPECIFICATION								
INSP.RESULT	3,60 3,62	2,54 2,57	0,25 0,28	0,0033 0,0026	0,038 0,041	0,017 0,017	0,022 0,023	0,029 0,031

MECHANICAL PROPERTIES:

HB Ø 10/3000/15" HB Ø 5/750/15"

	HARDNESS(BHN) SURFACE	HARDNESS(BHN) CORE	TEN STRENGTH N/mm ²	YIELD STREN. N/mm ²	ELONGATION %		
SPECIFICATION	210 - 260		600 MIN.		3 MIN.		
INSP.RESULT	223-227		632.46		10.92		

MICROSTRUCTURE : (100X)

	GRAPHITE FORM	GRAPHITE DISTRIBUTION	NODULARITY PERCENT %	NOD. COUNT IN 20 inch ²	MATRIX	CEMENTITE	
SPECIFICATION	OA-4.7	HOMOGENEOUS	90%	150 MIN.	%60 MIN PEARLITE	NO	
INSP.RESULT	OA-5.7	HOMOGENEOUS	100%	180-220	% 60 - 65 PEARLITE	NO	

NOT : - THE PARTS , WERE CONTROLLED BY VISUAL INSPECTION IN 100 %.

- " NO WELDING OR FILLER MATERIAL PERFORMED ON THIS MATERIAL "

LABORATORY
YAŞAR SOLAK

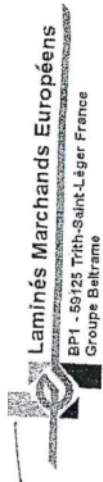
CONTROL
ADNAN ÖZGÜR

Prepared by software media.Approved.

Prepared by software media.Approved.

F01/FY-40.37

Record Retention: 5 years



42506

ABRAM PULMAN & SONS LTD
WALTON STREET
GB 0 HX6 1AN-SOWERBY BRIDGE

INSPECTION DOCUMENT N. 1108356
OFFICIAL REGULATION EN 10025-2
INSPECTION CERTIFICATE 3.1 - EN 10204
ENCLOSE CERTIFICATION **CE**

Steel from Electric Arc Furnace

AGENT ORDER N. 8056
CUSTOMER CODE PC-042596
CUSTOMER ORDER N. ABRAM PULMAN & SONS LTD
CONSIGNEE S275JH+AR
GRADE

LOADING NUMBER 2014.2309 INTERNAL ORDER 2014.1294

IT.	CAST	SECTION	DIMENSIONS (mm)	CE	LENGTH	CHEMICAL COMPOSITION (%)														
						C	Si	Mn	P	S	Cu	Cr	Ni	V	Mo	N	Ti	Al	Nb	Ceq
1	LM 89351	FLAT	30X6	0398	6,00	0,08	0,19	0,57	0,021	0,034	0,36	0,08	0,11	0,001	0,03	0,0116	0,0008	0,002	0,001	0,23
2	LM 88123	FLAT	30X10	0398	6,00	0,08	0,18	0,53	0,033	0,039	0,34	0,11	0,16	0,001	0,03	0,0068	0,0009	0,002	0,001	0,23
3	LM 89024	FLAT	40X5	0398	6,00	0,08	0,20	0,60	0,025	0,034	0,34	0,08	0,17	0,002	0,03	0,0088	0,0008	0,002	0,001	0,24
4	LM 89337	FLAT	40X5	0398	6,00	0,08	0,18	0,62	0,030	0,032	0,39	0,09	0,15	0,001	0,03	0,0085	0,0009	0,002	0,001	0,24
5	LM 88525	FLAT	50X5	0398	6,00	0,08	0,19	0,62	0,018	0,034	0,39	0,07	0,17	0,002	0,03	0,0110	0,0001	0,002	0,002	0,24
6	LM 87802	FLAT	50X10	0398	6,00	0,10	0,21	0,62	0,032	0,034	0,41	0,10	0,18	0,002	0,03	0,0098	0,0005	0,001	0,001	0,27
7	LM 88803	SQUARE	20	0398	6,00	0,07	0,20	0,62	0,024	0,033	0,32	0,10	0,15	0,001	0,03	0,0088	0,0001	0,001	0,001	0,23
8	LM 89215	ROUND	20	0398	6,00	0,09	0,19	0,58	0,019	0,034	0,39	0,08	0,17	0,003	0,03	0,0089	0,0005	0,001	0,001	0,25

LT. 011629

IT.	CAST ORIGIN	PRODUCT REGULATION	TEST NUM	Balls n.	WEIGHT Kg	TENSILE TEST		IMPACT TEST KV (J)	GRAIN
						ReL (MPa)	Rm (MPa)		
1	LM 89351 TRITH	EN 10058	489976	1	2355	294	429	33,4	
2	LM 88123 TRITH	EN 10058	446723	1	2331	298	426	33,0	
3	LM 89024 TRITH	EN 10058	478542	1	2307	300	436	34,0	
4	LM 89337 TRITH	EN 10058	489324	2	4736	304	439	34,0	
5	LM 88525 TRITH	EN 10058	461659	2	4663	303	439	34,0	
6	LM 87802 TRITH	EN 10058	461700	2	4864	305	441	33,8	
7	LM 88803 TRITH	EN 10058	466326	2	4864	306	438	32,2	
8	LM 89215 TRITH	EN 10060	472751	1	2165	298	429	33,0	
			484844	1	2172	298	429	32,5	

INSPECTOR TRITH DATE 6/02/2014
FACTORY TRITH
QUALITY CONTROL DEPT Florian Devisscher
QUALITY ASSURANCE DEPT Oriane Devallez



F.1.4 Reinforcement

NUCOR
NUCOR STEEL AUBURN, INC.

Mill Certification
4/24/2015

MTR #: 000040290
 25 Quarry Road
 AUBURN, NY 13021
 (315) 253-4561
 Fax: (315) 253-8441

Sold To: HARMAC REBAR & STEEL CORP
 SUB A H HARRIS & SONS INC
 STE 202
 433 S MAIN ST
 W HARTFORD, CT 06110
 (207) 935-3531
 Fax: (207) 935-3058

Ship To: HARMAC REBAR & STEEL CORP
 CORNSHOP ROAD
 FRYEBURG, ME 04037-0000
 (207) 935-3531
 Fax: (207) 935-3058

Customer P.O.	861447	Sales Order	313570.4
Product Group	Rebar	Part Number	900000134807065
Grade	ASTM A706/A706M-09b GR60 [420]	Lot #	AU1510043502
Size	13/#4 Rebar	Heat #	AU15100435
Product	13/#4 Rebar 40' A706 GR60 WELDABLE	B.L. Number	Y1-454226
Description	A706M WELDABLE	Load Number	Y1-200707
Customer Spec		Customer Part #	

I hereby certify that the material described herein has been manufactured in accordance with the specifications and standards listed above and that it satisfies those requirements.

Roll Date: 2/9/2015 Melt Date: 1/18/2015 Qty Shipped LBS: 5,050 Qty Shipped Pcs: 189

C	Mn	P	S	Si	Cu	Ni	Cr	Mo	V	Cb	CEA706
0.26%	1.10%	0.019%	0.039%	0.24%	0.33%	0.09%	0.14%	0.024%	0.0220%	0.001%	0.47%

CEA706: A706 CARBON EQUIVALENT

Yield 1: 67,400psi

Tensile 1: 90,100psi

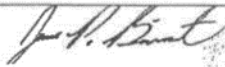
Elongation: 20.9% in 8"(% in 203.3mm)

Bend OK

Tensile/Yield: 1.34

Specification Comments:

ALL MANUFACTURING PROCESSES OF THE STEEL MATERIALS IN THIS PRODUCT, INCLUDING MELTING, HAVE OCCURRED WITHIN THE UNITED STATES. ALL PRODUCTS PRODUCED ARE WELD FREE. MERCURY, IN ANY FORM, HAS NOT BEEN USED IN THE PRODUCTION OR TESTING OF THIS MATERIAL.



Jim Biemat
 Division Metallurgist

CERTIFIED MATERIAL TEST REPORT



US-ML-SAYREVILLE
 NORTH CROSSMAN ROAD
 SAYREVILLE, NJ 08872
 USA

CUSTOMER SHIP TO HARMAC REBAR & STEEL CORP 301 HARTLE ST SAYREVILLE, NJ 08872-1790 USA		CUSTOMER BILL TO HARMAC REBAR & STEEL CORP 433 S MAIN ST STE 202 WEST HARTFORD, CT 06110-2812 USA		GRADE A706-60	SHAPE / SIZE Rebar / #3 (10MM)
SALES ORDER 1501854/000100		CUSTOMER MATERIAL N°		LENGTH 40'0"	WEIGHT 45,120 LB
BILL OF LADING 1331-0000026685		DATE 11/17/2014		SPECIFICATION / DATE or REVISION ASTM A706/A706M-14	

CUSTOMER PURCHASE ORDER NUMBER
851828

CHEMICAL COMPOSITION		YS		UTS		CEq	
C %	0.25	MPa	440	MPa	94818	%	0.019
Mn %	1.04	MPa	442	MPa	654	%	0.46
P %	0.014	Bend Test		UTS		G/L	
S %	0.034	OK		95364		Inch	
Si %	0.26	OK		658		mm	
Ca %	0.33						
Ni %	0.24						
Cu %	0.33						

MECHANICAL PROPERTIES		YS		UTS		G/L	
YS	63818	MPa	440	MPa	94818	Inch	8.000
PSI	64090	MPa	442	MPa	654	mm	200.0
Elong.	17.00	Bend Test		UTS		G/L	
	18.00	OK		95364		mm	
		OK		658			

MECHANICAL PROPERTIES		YS		UTS		G/L	
YS	63818	MPa	440	MPa	94818	Inch	8.000
PSI	64090	MPa	442	MPa	654	mm	200.0
Elong.	17.00	Bend Test		UTS		G/L	
	18.00	OK		95364		mm	
		OK		658			

GEOMETRIC CHARACTERISTICS		Dist Gap		Dist Spine	
% Light	2.10	mm	0.095	mm	0.256
	2.00	mm	0.095	mm	0.256


COMMENTS / NOTES

The above figures are certified chemical and physical test records as contained in the permanent records of company. We certify that these data are correct and in compliance with specified requirements. This material, including the billets, was melted and manufactured in the USA. CMTR complies with EN 10204 3.1.

Maskey
 BHASKAR YALAMANCHILI
 QUALITY DIRECTOR

Jose T. Homic
 JOSEPH T HOMIC
 QUALITY ASSURANCE MGR

F.1.5 Concrete



Benevento
CONCRETE CORP.
Wilmington • Georgetown

DISPATCH
978-658-5300

Remit to:
P.O. Box 459
Wilmington, MA 01887
Fax: (978) 658-9580

TICKET NUMBER 111709

SLUMP POURED 3-6 / WATER ADDED _____ GALS.

LINE	8:03	To Job	8:22	On Job	9:10	Placing	9:22	Plant	
PLANT	05/06/15	ORDER #	SC	TRUCK #	527	DRIVER	J. STARRA	LOAD SIZE	SLUMP
CUSTOMER #		SOLD TO	COD'S BSS / BAC			PO #	FRONT NORTHEASTE		
DELIVERY ADDRESS		141 BEDFORD ST			BURLINGT				
LOT #		USE	TO NORTHEASTERN UNIV.			DATE ON JOB			

INSTRUCTIONS:
TO BIG GARAGE DOOR
WAYNE WILL COLLECT

Benevento CONCRETE CORP.

Slump, cylinders = 6-8" Slump
All Tested

LOAD QUANTITY	CUMULATIVE QUANTITY	ORDERED QUANTITY	PRODUCT CODE	PRODUCT DESCRIPTION	UOM	UNIT PRICE	AMOUNT
2.00	2.00	2.00	6042240	6000 3/4 AE			

Water added on job at Customer's request +6 +2+2 gallons

Signature _____

We are not responsible for any deliveries over the curb line.

Signature _____

CAUTION: Contact between fresh concrete and skin surface or eyes will cause skin irritation or chemical burns. Wash exposed skin areas or eyes promptly with water.

NOTICE: Upon request Material Safety Data Sheets are available to all consumers and/or users.

Received By [Signature]

DEL. CHG.

SUB TOTAL

DIS.

TAX

TOTAL

PREVIOUS TOTAL

GRAND TOTAL

F.2 Beam test

F.2.1 Steel frame

Customer Name: CAPONE IRON CORPORATION
 Customer PO#: 14741 NORTHEASTERN
 Invoice No: 897664
 Shipper No: 879999
 Heat Number: B119214



CERTIFIED MILL TEST REPORT

Printed: 02/24/2016
 Produced: 02/24/2016

Ship to:
 Infra Metals-CT
 2 East Highway
 Wallingford, CT 06492-108
 Attn: Kevin Purcell
 Customer # 000198

Bill to:
 INFRA METALS CORPORATION (CT)
 55 Paint Highway
 Wallingford, CT 06492 US
 Attn: Kevin

2601 SWS BLDG (260) 824-3900 FAX
 Quality Steel 100% EAF Melted
 and Manufactured in the USA
 Recycled content: PC = 77.5%, PI = 19.4%
 ISO 9001:2008 and ISO Certified

GENERAL INFORMATION		SPECIFICATIONS		SHIPMENT DETAILS	
Product	Wide Flange Beam	Standards	Grade	Bundle / ASN #	ROL # 000199253 - 1201.00 lbs
Size	W14X26	ASTM A992M - 04	A992 (A992M)	16662227	36' 0" x NE-S06032
Heat Number	W 350 x 30	* ASTM A572/A572M - 11	A572 60/60/45	Count PO / Raw PO / Job	
Condition(s)	B316214	ASTM A572/A572M - 13a	A572 60/60/45		
	As-rolled	AASHTO M270M-2270 - 12	A572 60/60/45		
	Flux Coated	CSA S40 Z6-13	60W/200W		
	Flux Metal	ASTM A36/A36M - 14	A36 / A36M		
	HotWeld Repair				

CHEMICAL ANALYSIS (weight percent)

C	Mn	P	S	Si	Cu	Ni	Cr	Mo	Sn	V	Nb	Cl	Al	N	B	*C1	*C2	*C3	*PC	%	Analysis Type
0.09	1.08	0.02	0.02	0.25	0.05	0.05	0.07	0.08	0.017	0.008	0.002	0.001	0.0102	0.0003	0.0003	0.28	0.35	0.28	0.28	5.67	Heat

MECHANICAL TESTING

Test	Tensile (ksi)		Y / Y _{0.2}	% Elong	Temp	Charpy Impact Tester (available only when specified at time of order)	
	TS	TS _{0.2}				Absorbed Energy	R _{0.2} / J
1	55 / 261	60 / 476	80	24			
2	58 / 268	63 / 476	81	26			
3							
4							
5							
6							
7							
8							

Notes: *Standard Chemistry Values: Carbon 0.25%, Mn 1.00%, P 0.02%, S 0.02%, Si 0.25%, Cu 0.05%, Ni 0.05%, Cr 0.07%, Mo 0.08%, Sn 0.017%, V 0.008%, Nb 0.002%, Cl 0.001%, Al 0.0102%, N 0.0003%, B 0.0003%, *C1 0.28, *C2 0.35, *C3 0.28, *PC 5.67
 C1, C2, C3, PC, and PC_{0.2} are based on the chemical analysis of the steel. The values for C1, C2, C3, and PC are based on the chemical analysis of the steel. The values for PC_{0.2} are based on the chemical analysis of the steel.
 The Charpy impact test results are based on the Charpy impact test results of the steel. The Charpy impact test results are based on the Charpy impact test results of the steel.
 The Charpy impact test results are based on the Charpy impact test results of the steel. The Charpy impact test results are based on the Charpy impact test results of the steel.

ABB CERTIFICATION

Signed: _____
 I hereby certify that the contents of this report are accurate and correct. All tests and calculations performed by this mill test manufacturer are in accordance with the requirements of the national specifications and applicable purchaser designated requirements.

Signed: **Jeremy Cronkhite**
 Manager of Product Quality and Process Improvement

State of Indiana, County of Wabash sworn to and subscribed before me this _____ day of _____

Signed: _____ My commission expires: _____

F.2.2 Bolted connections



CMC STEEL SOUTH CAROLINA
310 New State Road
Cayce SC 29033-3704

CERTIFIED MILL TEST REPORT
For additional copies call
800-637-3227

We hereby certify that the test results presented here
are accurate and conform to the reported grade specification

Richard S. Ray
Richard S. Ray - CMC Steel SC.
Quality Assurance Manager

1SERIES-BPS

HEAT NO.: 2050587
SECTION: ROUND 5/8 x 20"0"
A36/52950
GRADE: ASTM A36-14/A529-05 Gr 50
ROLL DATE: 04/01/2016
MELT DATE: 03/27/2016

S O'Neal Steel Inc
L 744 41st St N
D Birmingham AL
T US 35222-1124
O 2055998000
2055998037

S O'Neal Steel
H 841 N Michigan Rd
I Shelbyville IN
P US 48176-9754
T 3174211200

Delivery#: 81770179
BOL#: 71588014
CUST PO#: 683355
CUST P/N: 834646
DLVRY LBS / HEAT: 10012,000 LB
DLVRY PCS / HEAT: 480 EA

Characteristic	Value	Characteristic	Value	Characteristic	Value
C	0.15%	Reduction of Area test 1	44%		
Mn	0.65%	Yield to tensile ratio test1	0.74		
P	0.011%	Yield Strength test 2	57.3ksi		
S	0.022%	Tensile Strength test 2	76.5ksi		
Si	0.22%	Elongation test 2	25%		
Cu	0.32%	Elongation Gage Lgth test 2	8IN		
Cr	0.16%	Reduction of Area test 2	51%		
Ni	0.19%	Yield to tensile ratio test2	0.75		
Mo	0.044%	C+(Mn)6	0.26%		
V	0.000%				
Cb	0.014%				
Sn	0.010%				
Al	0.000%				
Ti	0.002%				
N	0.0034%				
Carbon Eq A529	0.38%				
Yield Strength test 1	56.5ksi				
Tensile Strength test 1	76.0ksi				
Elongation test 1	26%				
Elongation Gage Lgth test 1	8IN				

REMARKS : HIS MATERIAL IS FULLY KILLED, 100% MELTED AND MANUFACTURED IN THE USA, WITH NO WELD REPAIR OR MERCURY CONTAMINATION IN THE PROCESS.

U.S. SO MEETS ASTM GRADE A36 REV.03A, A529 GR.50, A572-2015 GR.50, A709 GR.36, A709 GR.50, A992, AASHTO GRADE M270 GR.36, M270 GR.50, CSA G40.21-04 GRADE 44W, 0WASME SA-36 2008A ADDEND A.

F.2.3 Halfen channels and bolts

HALFEN USA Inc. *8521 FM Rd.1976* Converse, TX 78109* USA

Halfen USA
402 Gibbs Sprawl
Converse, TX 78109



HALFEN
YOUR BEST CONNECTIONS

HALFEN USA
8521 FM Road 1976
Converse, TX 78109
Phone: 1 800 423-9140
Fax: 1 888 277 1695
E-Mail: info@halfen.com
Quality department
ahernandez@halfenusa.com

06/10/16 / he / Page 1

inspection certificate EN 10204-3.1 - No. 11765

Customer order No.: 4996

Project Identification:

Delivery Item Anchor I 128/6x40 WB

Chemical analysis:

4705 weld-on anchor - Norm: EN 10025-2 / Halfen Group - S 235JR - 1.0038

Heat No.	C %	Si %	Mn %	P %	S %	Al %	Si+2*p %	Cu %	Cr %	Mo %	V %	Ni %	Cev %
6084126	0,080	0,030	0,390	0,013	0,009	0,022	0,063	0,120	0,050	0,020	0,000	0,080	0,170

Mechanical properties:

4705 weld-on anchor - Norm: EN 10025-2 / Halfen Group - S 235JR - 1.0038

Heat No.	Yield strength <i>Re</i> MPa	Tensile strength <i>Rm</i> MPa	Elongation <i>A</i> %
6084126	357	410	27,6

The products described above are in conformance with the requirements specified in the order

HALFEN USA

The person responsible for material release

Alonso Hernandez

This document has been computer generated and is valid without signature.

Halfen USA Inc.
Manager: Richard Wachter, Dr.Marcus Albrecht



Halfen GmbH

Liebigstraße 14
D- 40764 Langenfeld
Telefon: +49 (0) 2173/970-0
Telefax: +49 (0) 2173/970-123
Internet: www.halfen.com
E-Mail: info@halfen.com

Abteilung
Qualitätswesen / Quality department
Telefon: +49 (0) 2173/970-743
E-Mail: qs-langenfeld@halfen.de

Halfen GmbH * Postfach 1262 * D-40764 Langenfeld

Halfen USA
402 Gibbs Sprawl

78109 Converse, TX
UNITED STATES

04.01.16 / ba / Seite 1

Abnahmeprüfzeugnis nach EN 10204-3.1 - No. 10430
inspection certificate EN 10204-3.1

Kunden-Bestell-Nr./Customer order No.: PO 047 P007700-1
Projekt-Kennung/Project Identification:
Liefergegenstand/Delivery Item HM 72/48-WB-6070
Loskennung/Lot-ID 5300L6965244
Loskennung/Lot-ID: 5300L6965245 Pos. 21
Auftrags-Nr 5300S253926

Chemische Analyse/Chemical analysis:

4840 Warm-Schienen/hot-rolled channel - Norm: EN 10025-2 / Halfen Group - S 235JR - 1.0038

Charge Heat No.	C %	Si %	Mn %	P %	S %	Al %	Si+2*P %	Cu %	Cr %	Mo %	V %	Ni %	Cev %
6090296	0,070	0,030	0,360	0,010	0,007	0,022	0,055	0,140	0,040	0,010	0,000	0,070	0,150

Mechanische Eigenschaften/Mechanical properties:

4840 Warm-Schienen/hot-rolled channel - Norm: EN 10025-2 / Halfen Group - S 235JR - 1.0038

Charge Heat No.	Streckgrenze Yield strength		Zugfestigkeit Tensile strength		Dehnung Elongation A %
	Re MPa	Rm MPa	Rm MPa		
6090296	436		443		15,0

Das oben beschriebene Produkt ist konform mit den in der Bestellung festgelegten Anforderungen.
The products described above are conformal with the requirements specified in the order.



Halfen GmbH
Abnahmebeauftragter
inspection representative
i.v. Michael Dörner

Das Zeugnis ist maschinell erstellt und trägt keine Unterschrift.
This document has been computer generated and is valid without signature.

Halfen GmbH, AG Düsseldorf HRB 55272
USt-ID-Nr. DE 190725092, Steuern-Nr. 135/5732/1062
Geschäftsführung: Richard Wächter, Arjan J. Bakker
Commerzbank AG Langenfeld (BLZ 342 490 50), Konto-Nr. 3 905 607
ING Bank N.V., Frankfurt (BLZ 500 210 05), Konto 0 010 141 778



Reg.-Nr.: 2499-CPR-0113070 Zertifikat-Nr. QS-281 HH

Das Qualitätsmanagementsystem der Halfen GmbH ist für die Standorte in Deutschland, Frankreich, Österreich, Fides, Schweiz, Niederlande und der Tschechischen Republik zertifiziert nach DIN EN ISO 9001:2008.



Kostos Building/Northeastern
Univ.
141 S BEDFORD ST
BURLINGTON, MA 01803 5118

HALFEN USA
PO Box 547, 8521 FM 1976
Converse, Texas 78109
USA
Phone: (800) 423 9140
Fax: (877) 874 7923
Internet: www.halfenusa.com
E-Mail: info@halfenusa.com

CONCRETE - Anchoring Systems
FACADE - Fixing Systems
FRAMING - Products and Systems

E-Mail: ahernandez@halfenusa.com

July 12, 2016

Acceptance Inspection Certificate M / 3.1

Customer PO No: Jerome 02-18-16
Delivery Item: Halfen HS 72/48 M20x100 GV-S (8.8) – Bolts and Nuts
Project Name: Northeastern University
Order: S023808

Chemical Analysis:

According to Standard: DIN ISO 8992, DIN EN ISO 898-1/-2									
Charge Heat No:	C %	Si %	Mn %	P %	S %	Cr %	Mo %	B %	Ni %
153808	0.36	0.13	0.84	0.009	0.005	1.10	0.01	0.0018	0.05

Mechanical properties:


According to Standard: DIN ISO 8992, DIN EN ISO 898-1/-2					
Charge Heat No.	Yield Point (Rp) MPa	Tensile strength (Rm) MPa	Elongation (A) %	Hardness HV	Coating µm
153808	824	910	14.9	292-302	18-22

The products described above are conformal with the requirements specified in the order. In addition we confirm that the test results fulfill the requirements specified in the order.

Halfen USA, Inc.
Alonso Hernandez- Operational Quality Manager



F.2.4 Lindapter clamps and washers

	TRAKYA DÖKÜM SANAYİ VE TİC.A.Ş.	19/11/2015 LOT-014955							
QUALITY CONTROL DEPARTMENT									
LABORATORY REPORT									
(Inspection certificate 3.1 acc. To standard EN 10204:2004)									
FIRM : LINDAPTER PART NO : 5077 H PART NAME : M 24 TYPE AF SHORT TAIL (5077-H) PATERN NO-PATERN PART NO: COUNTRY OF ORIGIN: TURKEY	REPORT NO : 13 CASTING DATE : 07.11.2015 CASTING DATE CODE: - SHIPPING AMOUNT (Pcs): 500 ORDER NUMBER : M 028032								
<input type="checkbox"/> SAFETY <input type="checkbox"/> SAMPLE <input type="checkbox"/> FIRST PRODUCTION <input checked="" type="checkbox"/> ACTUAL PRODUCTION <input type="checkbox"/> MODIFICATION									
CHEMICAL COMPOSITION:									
METARIAL : EN - GJS - 600.3									
	%	C	Si	Mn	S	P	Cr	Cu	Mg
SPECIFICATION									
INSP.RESULT		3,60 3,61	2,55 2,57	0,22 0,29	0,0030 0,0015	0,010 0,036	0,016 0,017	0,019 0,019	0,029 0,031
MECHANICAL PROPERTIES:			<input type="checkbox"/> HB Ø 10/3000/15" <input checked="" type="checkbox"/> HB Ø 5/750/15"						
	HARDNESS(BHN) SURFACE	HARDNESS(BHN) CORE	TEN-STRENGTH N/mm ²	YIELD STREN. N/mm ²	ELONGATION %				
SPECIFICATION	210 - 260		600 MIN.		3 MIN.				
INSP.RESULT	222-230		705.06		12				
MICROSTRUCTURE : (100X)									
	GRAPHITE FORM	GRAPHITE DISTRIBUTION	NODULARITY PERCENT %	NOD.COUNT IN 20 inch ²	MATRIX	CEMENTITE			
SPECIFICATION	0A-4.7	HOMOGENEOUS	90%	150 MIN.	%60 MIN PEARLITE	NO			
INSP.RESULT	0A-5.7	HOMOGENEOUS	100%	180-220	% 60 - 65 PEARLITE	NO			
NOT :									
- THE PARTS , WERE CONTROLLED BY VISUAL INSPECTION IN 100 %.									
- " NO WELDING OR FILLER MATERIAL PERFORMED ON THIS MATERIAL "									
LABORATORY					CONTROL				
ADEM BAŞAKÇI					YAŞAR SOLAK				
Prepared by software media.Approved.					Prepared by software media.Approved.				
F01/FY-40.37					Record Retention: 5 years				



TRAKYA DÖKÜM
SANAYİ VE TİC.A.Ş.

30/09/2015
LOT-014623

QUALITY CONTROL DEPARTMENT
LABORATORY REPORT

(Inspection certificate 3.1 acc. To standard EN 10204:2004)

FIRM : LINDAPTER
PART NO : 5077 H
PART NAME : M 24 TYPE AF SHORT TAIL (5077-H)
PATERN NO-PATERN PART NO:
COUNTRY OF ORIGIN: TURKEY

REPORT NO : 10
CASTING DATE : 05.09.2015
CASTING DATE CODE:
SHIPPING AMOUNT (Pcs): 500
ORDER NUMBER : M 027957

SAFETY SAMPLE FIRST PRODUCTION ACTUAL PRODUCTION MODIFICATION

CHEMICAL COMPOSITION:
METARIAL : EN - GJS - 600.3

%	C	Si	Mn	S	P	Cr	Cu	Mg
SPECIFICATION								
INSP.RESULT	3,62	2,58	0,24	0,0028	0,031	0,016	0,046	0,028

MECHANICAL PROPERTIES: HB Ø 10/3000/15" HB Ø 5/750/15"

	HARDNESS(BHN) SURFACE	HARDNESS(BHN) CORE	TEN.STRENGTH N/mm ²	YIELD STREN. N/mm ²	ELONGATION %		
SPECIFICATION	210 - 260		600 MIN.		3 MIN.		
INSP.RESULT	223-229		705.06		12		

MICROSTRUCTURE : (100X)

	GRAPHITE FORM	GRAPHITE DISTRIBUTION	NODULARITY PERCENT %	NOD.COUNT IN 20 inch ²	MATRIX	CEMENTITE	
SPECIFICATION	OA-4.7	HOMOGENEOUS	90%	150 MIN.	%60 MIN PEARLITE	NO	
INSP.RESULT	OA-5.7	HOMOGENEOUS	100%	180-220	% 60 - 65 PEARLITE	NO	

NOT : - THE PARTS , WERE CONTROLLED BY VISUAL INSPECTION IN 100 %.

- " NO WELDING OR FILLER MATERIAL PERFORMED ON THIS MATERIAL "

LABORATORY
ADEM BAŞAKÇI

Prepared by software media.Approved.

CONTROL
YAŞAR SOLAK

Prepared by software media.Approved.

F01/FY-40.37

Record Retention: 5 years



TRAKYA DÖKÜM
SANAYİ VE TİC.A.Ş.

30/09/2015
LOT-014636

QUALITY CONTROL DEPARTMENT
LABORATORY REPORT

(Inspection certificate 3.1 acc. To standard EN 10204:2004)

FIRM : LINDAPTER
PART NO : 5017 H
PART NAME : M 20 TYPE AF SHORT TAIL (5017-H)
PATERN NO-PATERN PART NO:

REPORT NO : 08
CASTING DATE : 25.07.2015
CASTING DATE CODE :
SHIPPING AMOUNT (Pcs): 1,000
ORDER NUMBER : M 027884

SAFETY SAMPLE FIRST PRODUCTION ACTUAL PRODUCTION MODIFICATION

CHEMICAL COMPOSITION:
METARIAL : EN - GJS - 600.3

%	C	Si	Mn	S	P	Cr	Cu	Mg
SPECIFICATION								
INSP.RESULT	3,60 3,61	2,60 2,59	0,26 0,27	0,0023 0,0017	0,034 0,033	0,017 0,016	0,022 0,020	0,030 0,030

MECHANICAL PROPERTIES: HB Ø 10/3000/15" HB Ø 5/750/15"

	HARDNESS(BNH) SURFACE	HARDNESS(BHN) CORE	TEN.STRENGTH N/mm ²	YIELD STREN. N/mm ²	ELONGATION %			
SPECIFICATION	210 - 260		600 MIN.		3 MIN.			
INSP.RESULT	220-226		687.84		8.8			

MICROSTRUCTURE : (100X)

	GRAPHITE FORM	GRAPHITE DISTRIBUTION	NODULARITY PERCENT %	NOD.COUNT IN 20 inch ²	MATRIX	CEMENTITE	
SPECIFICATION	OA-4.7	HOMOGENEOUS	90%	150 MIN.	%60 MIN PEARLITE	NO	
INSP.RESULT	OA-5.7	HOMOGENEOUS	100%	180-220	% 60 - 65 PEARLITE	NO	

NOT: - THE PARTS , WERE CONTROLLED BY VISUAL INSPECTION IN 100 %.
- " NO WELDING OR FILLER MATERIAL PERFORMED ON THIS MATERIAL "

LABORATORY
ADEM BAŞAKÇI

Prepared by software media.Approved.

CONTROL
YAŞAR SOLAK

Prepared by software media.Approved.

F01/FY-40.37

Record Retention: 5 years

Lot: 015128

B-027303

8-1-16

3.1 Material Test Certificate

Quality : S275JR, C, Pickled, MEDIUM/NORMAL OILING, Skelpressed Milden Steels Ltd

Thickness:	5.00	Net Weight:	16.240	Width:	1253.0
Internal Diameter:	762	Specification Name:	SSD19025-2:2004	Specification Grade:	S275JR+AR
Edge Condition:	MILL EDGE	Branding:	Yes	Linear Metrage:	386

Mechanical Details

Rockwell D Result	493	Yield Stress	355
Tensile Stress	493	Elongation 50mm	27

Chemical Analysis

C	0.1480	Si	0.0080	Mn	0.0050	P	0.0030	S	0.0100	Cu	0.0020	Mg	0.0010
N	0.0020	Al	0.0470	As	0.0010	B	0.0002	Co	0.0060	Cr	0.0010	Ni	0.0007
Nb	0.0010	Ti	0.0020	Sn	0.0020	Th	0.0010	V	0.0020	W		Zn	
Al ₂ O ₃	0.0430	Ca		Co ₂		H		Pb		P ₂ O ₅		MnO	

AFW20-GRN 27222

WATERHOUSE PRESSINGS MANUFACTURING LTD WP21

Precision Pressing for Industry
 SNAYGILL IND ESTATE, SKIPTON, NORTH YORKSHIRE BD23 2QR
 Telephone : Skipton (01756-794577/8) Fax : (01756-701481)

611 014827 13.11.15 Certificate of Conformance

E-mail : paul@waterhousepressings.co.uk ----- WEBSITE : http://www.waterhousepressings.co.uk

CHARACTERISTIC	Upper tol	Lower tol	1st sample	2nd sample	3rd sample	High-Ok-Lo
Hole	26.00	minimum	26.49	26.48	26.50	OK
Thickness	10.50	10.00	10.10	10.10	10.12	OK
Stamp						
Visual Deep						OK
Burrs minimal						OK

Batch quantity	2,057	3 Samples		visual	1 stillage		Compiled by W.P.M Ltd
----------------	-------	-----------	--	--------	------------	--	--------------------------

SPEC NO	10539	CUSTOMER	Lindapter International
ORDER NOs	B-027445	CUSTOMER NO	N/A
PART NUMBER	AFW24U	ISSUE LEVEL	2
INSPECTION Lvl	ZERO DEFECT	DRAWING NUMBER	LSTD - 2791

FAULTS FOUND	DEVIATIONS & REASON	AS DISCUSSED

CONCESSION NUMBER	GIVEN BY
REF NUMBER	

INSPECTION CARRIED OUT BY : PAUL WATERHOUSE	
DATE: 13.11.15	APPROVED BY : PAUL WATERHOUSE

Made in UK _____

CELSA STEEL UK
 OFFICES: Build, 59, Castle Works, East Moors Road
 CF24 5NN Cardiff (United Kingdom)



INSPECTION CERTIFICATE
BS-EN 10204-2004, Type 3.1

Standard
 BS-EN 10025-2:2004

CUSTOMER

Destination:

Delivery number: 25942570
 Order number : 11564932
 Your order : 1001723

Lot: 014827

PAGE 2

AT0244

MATERIAL	CAST	C	MC	ST	S	P	Cr	Ni	Cu	No	V	CE	Reh	Re	A	T	Ren1	Ren2	Ren3	Reh
		Y	Y	Y	Y	Y	Y	Y	Y	Y	Y	Y	NPA	NPA	%	*C	Y	Y	Y	Y
Hot rolled structural steel products																				
S 275 JR -AR 50X12 6m	CM094195	0.10	0.57	0.15	0.034	0.026	0.100	0.010	0.12	0.019	0.000	0.248	322	454	36.9					
S 275 JR -AR 50X12 6m	CM094194	0.12	0.53	0.15	0.029	0.023	0.089	0.011	0.16	0.43	0.025	0.271	313	486	42.7					
S 275 JR -AR 50X12 6m	CM094194	0.12	0.53	0.15	0.029	0.023	0.089	0.011	0.16	0.43	0.025	0.271	342	483	42.7					
S 275 JR -AR 50X12 6m	CM094194	0.12	0.53	0.15	0.029	0.023	0.089	0.011	0.16	0.43	0.025	0.271	342	478	42.1					
S 275 JR -AR 50X12 6m	CM094195	0.09	0.51	0.16	0.028	0.020	0.096	0.011	0.16	0.44	0.022	0.239	341	484	42.1					
S 275 JR -AR 50X12 6m	CM094195	0.09	0.51	0.16	0.028	0.020	0.096	0.011	0.16	0.44	0.022	0.239	335	482	40.7					
													356	482	40.7					

The materials has been evaluated and radiation is within national limits
 Product suitable for galvanizing: 0.14e-Si<0.25 & P<0.035.

Steel making process -
 Electric arc

Certified that the material detailed hereon meets the
 requirements of the specified standard.
 Cardiff, 17.09.2014

Stuart Thomas
 Stuart Thomas
 Quality Manager

F.2.5 Reinforcement



US-ML-SAYREVILLE
 NORTH CROSSMAN ROAD
 SAYREVILLE, NJ 08872
 USA

CUSTOMER SHIP TO
 MACFARLANE STEEL
 103 CORNSHOP RD
 FRYEBURG, ME 04037
 USA

CUSTOMER BILL TO
 HARMAC REBAR & STEEL CORP
 433 S MAIN ST STE 202
 WEST HARTFORD, CT 06110-2812
 USA

SALES ORDER
 3129698000010

CUSTOMER MATERIAL N°

GRADE
 60 (420)

SHAPE / SIZE
 Rebar / #3 (10MM)

WEIGHT
 45.120 LB

HEAT/BATCH
 6110536602

CUSTOMER PURCHASE ORDER NUMBER
 897477

BILL OF LADING
 1331-0000041206

DATE
 12/11/2015

SPECIFICATION / DATE or REVISION
 ASTM A615/A615M-15

CHEMICAL COMPOSITION	C	Mn	P	S	Si	Cr	Ni	Mo	Sp	N	CEq
%	%	%	%	%	%	%	%	%	%	%	%
	0.47	0.68	0.014	0.043	0.22	0.28	0.12	0.08	0.025	0.011	0.018
											0.50

MECHANICAL PROPERTIES	YS	UTS	EL	GA	GA	GA
MPa	MPa	%	Inch	Inch	Inch	mm
75346	107636	521	14.50	0.078	0.252	200.0
76433	111273	527	14.50	0.078	0.252	200.0

MECHANICAL PROPERTIES	Bend Test
Elong.	OK
14.50	OK

GEOMETRIC CHARACTERISTICS	Def/Inch	Def/Inch	Def/Inch
3.10	0.078	0.078	0.252
1.50	0.020	0.078	0.252

COMMENTS / NOTES

The above figures are certified chemical and physical test records as contained in the permanent records of company. We certify that these data are correct and in compliance with specified requirements. This material, including the labels, was melted and manufactured in the USA. CMTR complies with EN 10204 3.1.

Maskey BHASKAR VALAMANCHILI QUALITY DIRECTOR

Joseph T. Romig JOSEPH T ROMIG QUALITY ASSURANCE MGR.

Welcome BROCKIE.GERRY@AHHARRIS.COM

03/15/16 [Nucor Announces Guidance For Its First Quarter Earnings](#)

[Click here](#) to complete Nucor's online credit application

HOME | SIGN OUT

	PRODUCTS	MY ACCOUNT	REPORTS	ANNOUNCEMENTS	Safety First NO ONE GETS HURT ON OUR SHIFT TODAY.
--	----------	------------	---------	---------------	--

MILL CERTIFICATION DETAILS

Cart: 1
CONTINUE SHOPPING

[<< Return To Search](#)

PDF VERSION	EMAIL REPORT
-------------	--------------

[Request Original Mill Certificate](#)

Purchase Order #: 901011
 Customer: HARMAC REBAR & STEEL CORP - OSSIPEE
 Bill of Lading : 468204
 Certified By : Jim Biernat
 Lot #: AU1510692101
 Grade: ASTM A615/A615M-14 GR 60[420] AASHTO M31-07
 Melt Date : 11/24/2015
 Qty Shipped LBS: 59745
 Comments:

Heat #: AU15106921
 Customer Part #:
 Length: 40'0"
 Date: 11/24/2015
 Tag #: AU1511136961
 Size : # 4(13) RS
 Division : NSAU-Auburn, NY
 Qty Shipped PCS : 2236
 Roll Date : 11/25/2015

Chemical Properties -Wt.%

C	Mn	Si	S	P	Cu	Cr	Ni	Mo
0.39	1.02	0.22	0.066	0.026	0.36	0.22	0.15	0.039
V	Nb							
0.0020	0.001							

Physical Properties

	Imperial-psi
Tensile:	96800
Yield:	66500
Elongation (in 8 inches):	15.5
Elongation (in 2 inches):	
Bend Test:	OK

Carbon Equiv:

I hereby certify that the material described herein has been manufactured in accordance with the specification and standards listed above and that it satisfies those requirements. All melting and manufacturing process were performed in the United States of America unless otherwise noted on the mill test report.

Jim P. Biernat
 Chief Metallurgist

HOME | LOCATIONS | PRIVACY POLICY | TERMS & CONDITIONS | CAREERS | FAQ | SIGN OUT

© 2014 Nucor Corporation

NUCOR
NUCOR STEEL CONNECTICUT, INC.

Mill Certification
4/4/2016

MTR #: W1-179556
 35 Toelles Road
 WALLINGFORD, CT 06492
 (203) 265-0615
 Fax: (203) 284-8125

Sold To: HARMAC REBAR & STEEL CORP
 CORP CENTER W
 433 S MAIN ST
 STE 202
 W HARTFORD, CT 06110
 (207) 935-3531

Ship To: HARMAC REBAR-REBAR
 CORNSHOP ROAD
 FRYEBURG, ME 04037
 (207) 935-3531

Customer P.O.	907606	Sales Order	233429.2
Product Group	Rebar	Part Number	95013276CT46000
Grade	ASTM A615-16 / A706-16 & AASHTO M 31-15 Gr 60	Lot #	WL1690001840
Size	#4 Rebar (Coil)	Heat #	JK16100307
Product	#4 Rebar A615/A706 GR60 625X420	B.L. Number	W1-477579
Description	A615/A706 GR60 (CT2)	Load Number	W1-179556
Customer Spec		Customer Part #	

I hereby certify that the material described herein has been manufactured in accordance with the specifications and standards listed above and that it satisfies those requirements.
Melt Date: 1/22/2016

C	Mn	P	S	Si	Cu	Ni	Cr	Mo	V	Cb	Sn
0.26% CEA706 0.47%	1.15%	0.030%	0.035%	0.24%	0.28%	0.09%	0.14%	0.020%	0.0420%	0.002%	0.012%

CEA706: A706 CARBON EQUIVALENT

Roll Date: 3/24/2016

Yield 1: 67,100psi

Bend OK

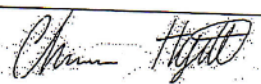
Tensile 1: 98,850psi

Tensile/Yield: 1.47

Elongation: 16.3% in 8" (% in 203.3mm)

Specification Comments:

1. Except where noted, all manufacturing processes including melting were performed in the USA.
2. No mercury, mercury compounds or mercury containing devices came into contact with this product.
3. Weld repair was not performed on this material.
4. Hexavalent Chromium, Radium or Alpha Source materials in in any form were not used in the production or testing of this material



Charlie Hyatt
 Division Metallurgist

F.2.6 Concrete

Pour 1

Truck 400	Driver 97	User user	Disp 8462	Ticket Num 97376	Ticket ID 6	11:40 Date 11:37 6/24/16	
Load Size 6.50	Mix Code CY 5040230	5000 3/4 MRWR	Seq D	Load ID 104821			
Material	Design Qty	Required	Batched	% Var	% Moisture	Actual	Wat
88 STONE	510 lb	3440 lb	3440 lb	0.01%	3.76% A	125 lb	
24 STONE	1190 lb	7807 lb	7760 lb	-0.61%	0.94% A	72 lb	
SAND STATE	1220 lb	8267 lb	8280 lb	0.16%	4.25% A	337 lb	
CEMENT	705.0 lb	4582.5 lb	4590.0 lb	0.16%			
WATER	279 lb	1169 lb	1162 lb	-0.63%		1162 lb	
GLEN7620	21.20 oz	137.80 oz	138.00 oz	0.15%			
MICRO AIR	1.80 oz	11.70 oz	11.40 oz	-2.56%			

Actual Load	25241 lb	Design W/C	0.396	Water/Cement	0.395	T	Design	1813.5 lb	Actual	1695.9 lb	To Add	117.6 lb
Slump	5.00 in	Water in Truck	0.0 lb	Adjust Water	0.0 lb / Load	Trim Water	-16.0 lb /	Manual	11.37 18	CY		

Benevento CONCRETE CORP.
Wilmington • Georgetown

DISPATCH
978-658-5300

Remit to:
P.O. Box 459
Wilmington, MA 01887
Fax: (978) 658-9580

TICKET NUMBER 8462

SLUMP POURED _____ / WATER ADDED _____ GALS.

Load 11:37 To Job 1149 On Job _____ Houring _____ Fresh Pour/TTD _____ At Plant _____

PLANT DATE 06/24/16 ORDER # 1308 TRUCK # 400 DRIVER SCHEMILLIN, LOAD SIZE 6.5 SLUMP 5.0

SUBSTONETS SOLD TO NORTHEASTERN

DELIVERY ADDRESS 141 S. BEDFORD ST. CITY/TOWN BURLINGTON

DESCRIPTION UNKNOWN JOB USE MISC DUE ON JOB _____

INSTRUCTIONS PAID CC

LAST TRUCK ON JOB: Benevento CONCRETE CORP.

Title Water -16.00

LOAD QUANTITY	CUMULATIVE QUANTITY	ORDERED QUANTITY	PRODUCT CODE	PRODUCT DESCRIPTION	UOM	UNIT PRICE	AMOUNT
6.50	6.50	6.50	5040230	5000 3/4 MRWR		98.00	637

Water added on job at Customer's request _____ gallons

Signature _____

We are not responsible for any deliveries over the curb line.

Signature _____

CAUTION: Contact between fresh concrete and skin surface or eyes will cause skin irritation or chemical burns. Wash exposed skin areas or eyes promptly with water.

NOTICE: Upon request Material Safety Data Sheets are available to all consumers and/or users.

Received By _____

DEL. CHG.	
SUB TOTAL	1637.00
DIS.	
TAX	
TOTAL	1637.00
PREVIOUS TOTAL	
GRAND TOTAL	1637.00

Pour 2

Truck 601 Driver 310 User user Disp Ticket Num 9918 Ticket ID 98710 Date 9:33 7/20/16
 Load Size 6.50 CY Mix Code 5042232 5000 3/4 MRWR 15% FLY AS Seq D Load ID 106274

Material	Design Qty	Required	Batched	% Var	% Moisture	Actual	Wat
3/8 STONE	510 lb	3447 lb	3440 lb	-0.19%	3.97% A	131 lb	
3/4 STONE	1190 lb	7812 lb	7740 lb	-0.92%	0.99% A	76 lb	
SAND STATE	1200 lb	8196 lb	8200 lb	0.05%	5.08% A	396 lb	
CEMENT	600.0 lb	3900.0 lb	3900.0 lb	0.00%			
FLY ASH	105.0 lb	682.5 lb	690.0 lb	+ 1.10%			
WATER	275 lb	1047 lb	1018 lb	-2.75%		1018 lb	
MICRO AIR	1.50 oz	9.75 oz	9.60 oz	-1.54%			
GLEN7620	21.20 oz	137.80 oz	136.00 oz	-1.31%			

Actual Load 24997 lb Slump: 5.00 in Num Batches: 1 Design W/C: 0.390 Water/Cement: 0.0 lb Adjust Water: 0.0 lb / Load Design 1787.5 lb Actual 1621.7 lb Manual 9:33:55 To Add: 165.8 lb
 Water in Truck: 0.0 lb Trim Water: -20.0 lb / CY

Benevento CONCRETE CORP.

Wilmington • Georgetown

DISPATCH 978-658-5300

Remit to:
 P.O. Box 459
 Wilmington, MA 01887
 Fax: (978) 658-9580

SLUMP POURED 5 / WATER ADDED 6 GALS. TICKET NUMBER 9918

Load	To Job	On Job	Pouring	Finish Pour/RTG	At Plant		
	9:54	10:22	10:27	11:37			
PLANT	DATE	ORDER #	TRUCK #	DRIVER	LOAD SIZE	SLUMP	
006	07/20/16	JOB	601	SOLANO, ST	6.5	5.0	
CUSTOMER #	SOLD TO		PO #				
000	NORTHEASTERN UNIV						
DELIVERY ADDRESS			CITY/TOWN				
141 SOUTH BEDFORD ST.			BURLINGTON				
DESCRIPTION		USE		DUE ON JOB			
UNKNOWN JOB		MISC					
INSTRUCTIONS							
PAID CONORTHEASTERN CAMPUS							
LAST TRUCK ON JOB:							
Trim Water -20.00 lbs/y							
LOAD QUANTITY	CUMULATIVE QUANTITY	ORDERED QUANTITY	PRODUCT CODE	PRODUCT DESCRIPTION	UOM	UNIT PRICE	AMOUNT
6.50	6.50	6.50	5042232	5000 3/4 MRWR 15% FLY AS		96.00	637
DEL. CHG.							
SUB TOTAL	\$637.00						
DIS.							
TAX	\$39.81						
TOTAL	\$676.81						
PREVIOUS TOTAL							
GRAND TOTAL	\$676.81						

Pour 3

Truck 403	Driver 214	User user	Disp Ticket Num 10935	Ticket ID 16 99631	8:36 Date 8:32 8/5/16
Load Size 6.50 CY	Mix Code 5042232	5000 3/4 MRWR 15% FLY AS	Seq D	Load ID 107293	

Material	Design Qty	Required	Batched	% Var	% Moisture	Actual	Wat
3/8 STONE	510 lb	3411 lb	3380 lb	-0.91%	2.89% A	95 lb	
3/4 STONE	1190 lb	7800 lb	7780 lb	-0.25%	0.84% M	65 lb	
SAND STATE	1200 lb	8238 lb	8240 lb	0.02%	5.62% A	439 lb	
CEMENT	600.0 lb	3900.0 lb	3905.0 lb	0.13%			
FLY ASH	105.0 lb	662.5 lb	675.0 lb	< -1.10%			
WATER	275 lb	1026 lb	1023 lb	-0.30%		1023 lb	
MICRO AIR	1.70 oz	11.05 oz	11.10 oz	0.45%			
GLEN7620	21.20 oz	137.80 oz	137.00 oz	-0.58%			

Actual load	25012 lb	Design W/C:	0.390	Water/Cement:	0.390 T	Design	1787.5 lb	Actual	1621.2 lb	To Add:	166.3 lb
Slump:	5.00 in	Water in Truck:	0.0 lb	Adjust Water:	0.0 lb / Load	Trim Water:	-24.0 lb /	CY	Note: Manual feed occurred		

Benevento
CONCRETE CORP.
Wilmington • Georgetown

DISPATCH
978-658-5300

Remit to:
P.O. Box 459
Wilmington, MA 01887
Fax: (978) 658-9580

TICKET NUMBER 10935

SLUMP POURED _____ / WATER ADDED _____ GALS.

Plant: 0130 To Job: 654 On Job: _____ Paving: _____ Finish Pour/RTG: _____ At Plant: _____

PLANT	DATE	ORDER #	TRUCK #	DRIVER	LOAD SIZE	SLUMP
00E	08/05/16	JOB	403	LESPEANCE	6.5	5.0

CUSTOMER # _____ SOLD TO _____ CITY/TOWN _____ PUBLIC _____

ELIVERY ADDRESS: 141 SOUTH BEDFORD ST. BURLINGTON

DESCRIPTION: PUBLIC USE: OUTSIDE FL DUE ON JOB _____

INSTRUCTIONS: PAID CC

LAST TRUCK ON JOB: Benevento Concrete Corp.

Trim Water: -24.00 lbs

LOAD QUANTITY	CUMULATIVE QUANTITY	ORDERED QUANTITY	PRODUCT CODE	PRODUCT DESCRIPTION	UOM	UNIT PRICE	AMOUNT
6.50	6.50	6.50	5042232	5000 3/4 MRWR 15% FLY AS		96.00	637

Water added on job at Customer's request _____ gallons

Signature _____

We are not responsible for any deliveries over the curb line.

Signature _____

CAUTION: Contact between fresh concrete and skin surface or eyes will cause skin irritation or chemical burns. Wash exposed skin areas or eyes promptly with water.

DEL. CHG.	
SUB TOTAL	\$637.00
DIS.	
TAX	
TOTAL	\$637.00
PREVIOUS TOTAL	

Appendix G. Interpretation of Strain Gage Data

Using procedures provided in this appendix, useful quantities are extracted from raw data displayed in Appendix E. The plots of pushout tests are discussed in Chapter 5.

G.1 Pushout tests

The strategies for handling abnormal strain gage data are as follows:

- (1) Drifts are commonly seen in the strain gage measurements in the cyclic tests that last for days, and they are eliminated by subtracting the differences between the readings after pausing the test on the previous day and the readings before resuming the test on the next day for the subsequent data.
- (2) In Test 5-M24-2C-RH-LC, a tiny portion of the data is lost due to the crash of the DAQ system. After reviewing the existing data, it is believed that the offset in the gage readings before and after the crash is insignificant. Since the missing data belongs to one of the cycles at the first load-control level, the effect of those data on interpreting the results is less important and therefore no change is made to the raw data.
- (3) A few gages open up or display erratic readings. These gages are not included in the plots in Appendix E. When these gages are essential for calculations, a substitute is found which potentially has the same measurement. For example, when Gage EFSO is dead in Test 3-M24-2C-RL-LC, Gage EFNO is utilized along with other gages on the south side to estimate the axial force at the east section. However, a reasonable substitute does not exist for Gage 3c in Test 8. Useful quantities, such as tensile stress and shear stress, are not computed for this anchor.
- (4) Overshoot is occasionally seen in the strain gage measurements. The readings, however, become normal afterwards. For those gages, the raw data with overshoot is used for calculations. As a result, the processed data also shows overshoot which should be disregarded.
- (5) After strain gage calibration, several gages still exhibit readings as large as 100 microstrains. The whole measurements from those gages are offset such that the readings start from zero.
- (6) Erratic readings from bolt strain gages are minimally manipulated, because the material is nonlinear and the calculated stresses are dependent on the history of the deformations. The pretension of bolt 3 in Test 6-M24-2C-RH-LC-S is calculated using the south strain gage data only. The sharp drop shown in the south strain gage attached on bolt 4 is processed by removing that segment. When estimating the tension of bolt 4 in Test 10-M20-2C-RH-LC, only the north strain gage data is used.

G.1.1 Load distribution among the clamps

In order to calculate the axial force at a cross section, three assumptions are made: (1) plane sections remain plane; (2) stresses are uniform along the flange and web thickness; (3) since the axial force mainly flows through the flange, the contribution from the top plates welded on the web is neglected. The process is shown below:

Contribution from the web:

$$\Phi_N = \frac{3(\varepsilon_5 - \varepsilon_6)}{d - b_f} \quad (\text{G.1})$$

$$\Phi_S = \frac{3(\varepsilon_7 - \varepsilon_8)}{d - b_f} \quad (\text{G.2})$$

$$\varepsilon_{tN} = \varepsilon_5 + \Phi_N \frac{d - b_f}{3} \quad (\text{G.3})$$

$$\varepsilon_{tS} = \varepsilon_7 + \Phi_S \frac{d - b_f}{3} \quad (\text{G.4})$$

$$\varepsilon_{bN} = \varepsilon_6 - \Phi_N \left(b_f + \frac{d - b_f}{3} \right) \quad (\text{G.5})$$

$$\varepsilon_{bS} = \varepsilon_8 - \Phi_S \left(b_f + \frac{d - b_f}{3} \right) \quad (\text{G.6})$$

$$P_w = \frac{(\varepsilon_{tN} + \varepsilon_{tS} + \varepsilon_{bN} + \varepsilon_{bS})}{4} E d t_w \quad (\text{G.7})$$

Contribution from the flange:

$$P_f = \frac{(\varepsilon_1 + \varepsilon_2 + \varepsilon_3 + \varepsilon_4)}{4} E (b_f - t_w) t_f \quad (\text{G.8})$$

Figure G.1 shows the definition of the notations. The axial force variation at different cross sections for different specimens is plotted in Figure G.2.

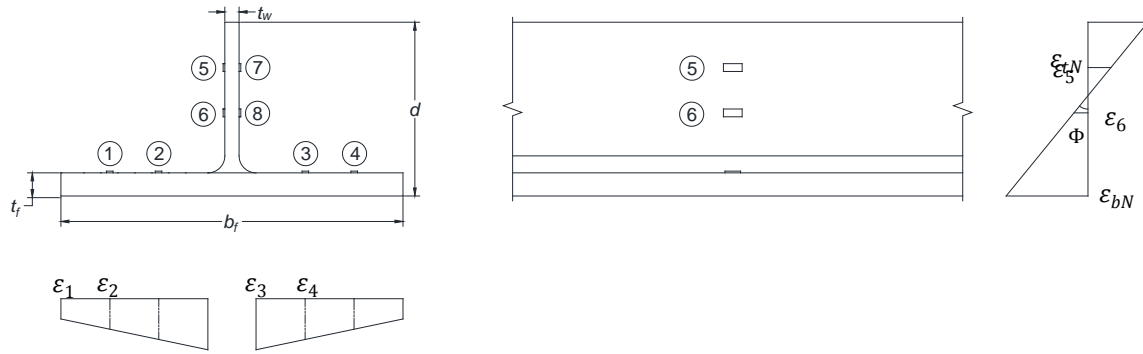
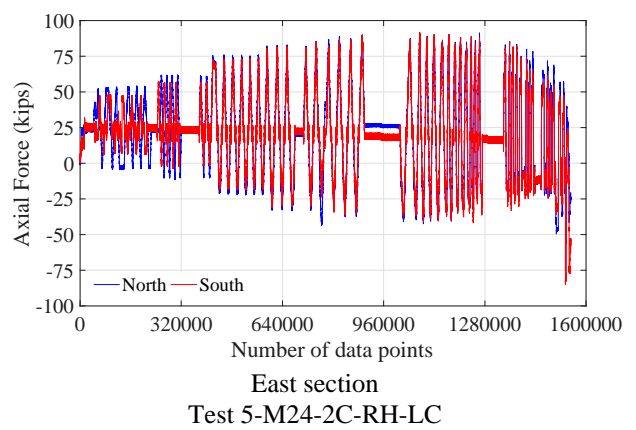
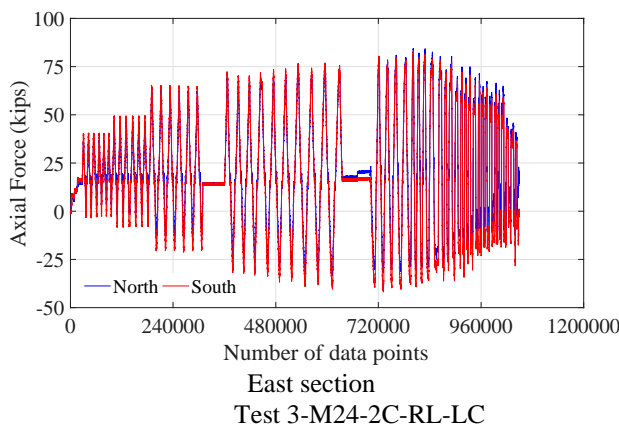
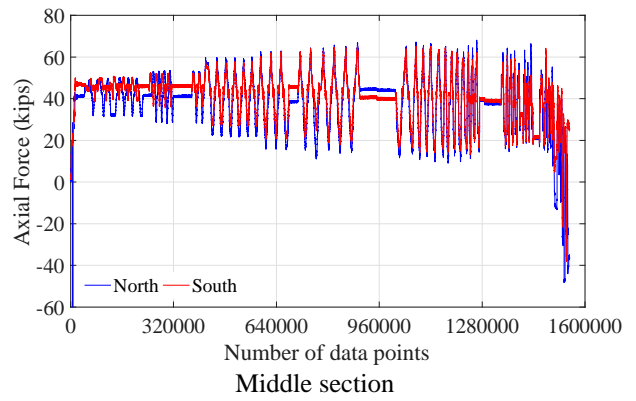
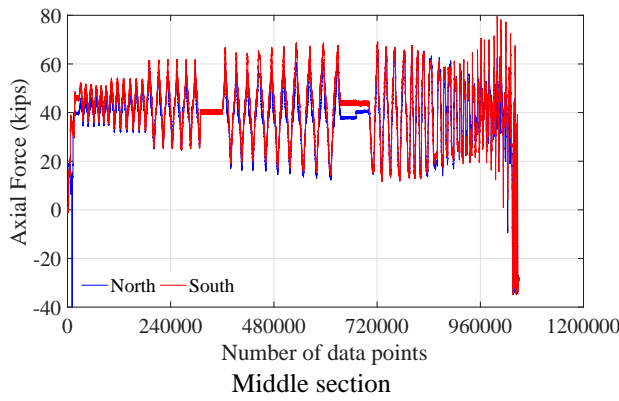
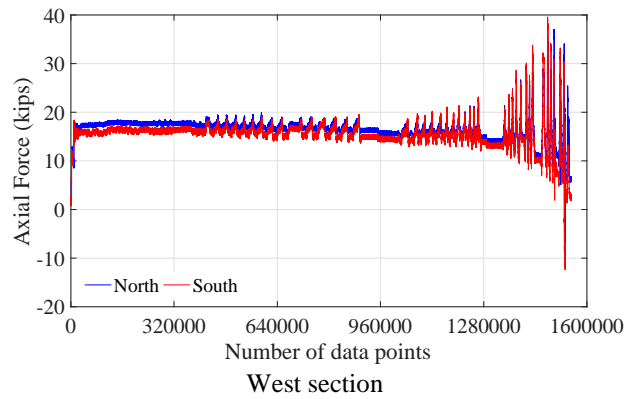
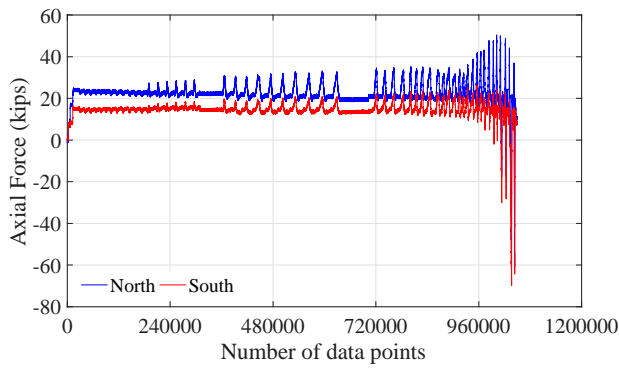
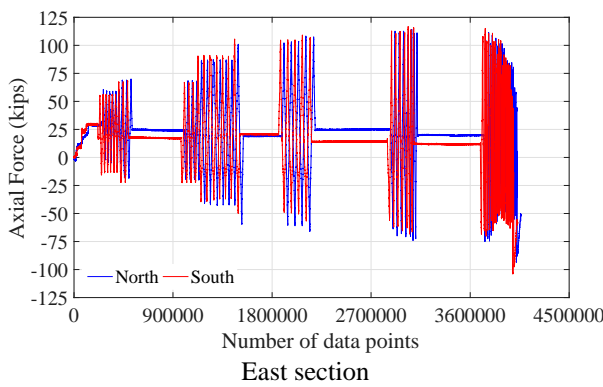
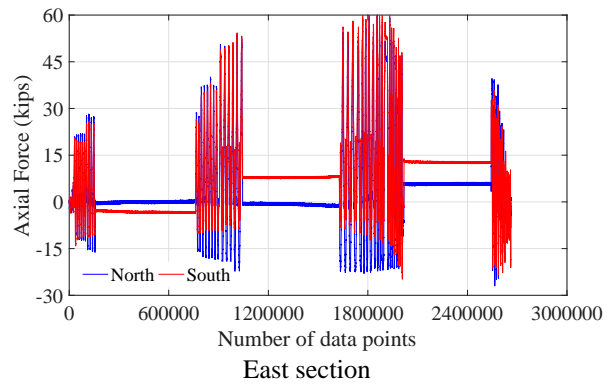
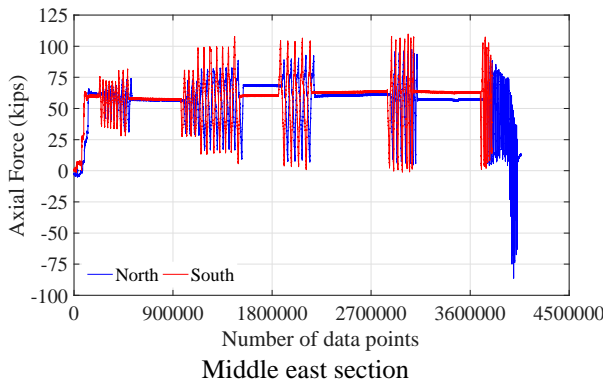
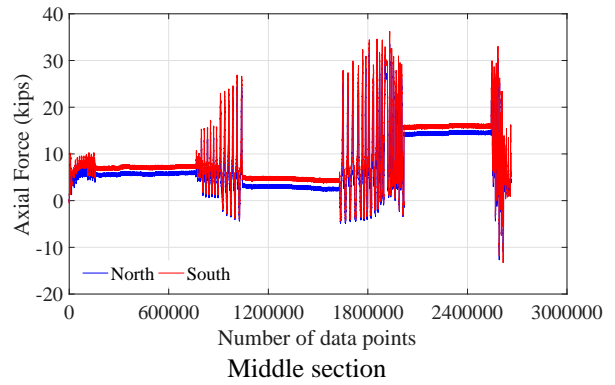
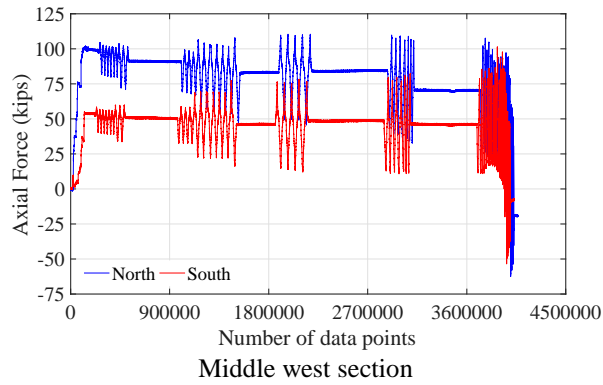
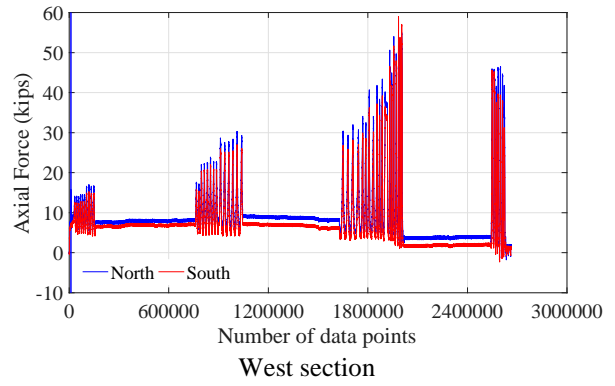
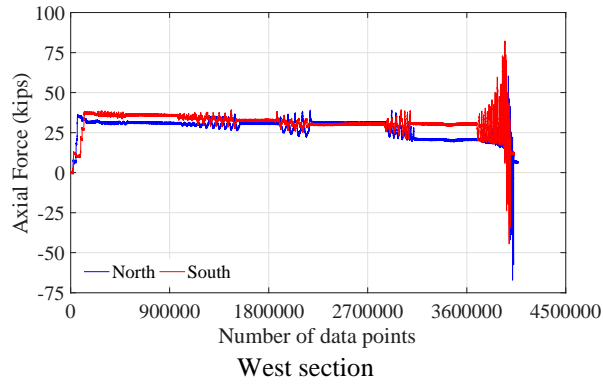


Figure G.1 Strain gage locations and numbering at a section





Test 8-M24-3C-RH-LC

Test 10-M20-2C-RH-LC

Note: positive value represents tensile force; negative value represents compressive force.

Figure G.2 Axial force variation

G.1.2 Bolt pretention force variation

In Chaboche model without isotropic hardening, the nonlinear kinematic strain hardening rule determines how the yield surface is translated in the stress space following the backstresses. The hardening law for each backstress is

$$d\alpha_k = \frac{C_k}{\sigma^0} (\sigma - \alpha_k) d\varepsilon_{eq}^{pl} - \gamma_k \alpha_k d\varepsilon_{eq}^{pl} \quad (G.9)$$

Where C_k is the initial kinematic hardening modulus; γ_k is the rate at which the kinematic hardening modulus decreases with increasing plastic strain. Both are independent parameters and can be calibrated with test data. σ^0 is the size of the yield surface; ε_{eq}^{pl} is the equivalent plastic strain. The overall backstress is calculated as:

$$\alpha = \sum_{k=1}^N \alpha_k \quad (G.10)$$

Where N is the number of backstresses.

The analysis is conducted in Abaqus/Standard with a single three-dimensional, linear, reduced integration solid element, see Figure G.3.

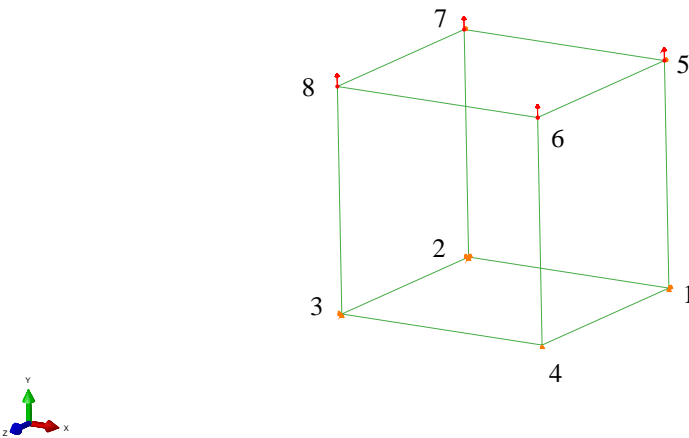


Figure G.3 Stress analysis model

Material properties assigned to the element include elastic modulus and Poisson's ratio, which are 30900 ksi and 0.3, respectively. The kinematic hardening behavior of the material is defined

by specifying half-cycle data. In Abaqus, the input stress and strain are true stress and true plastic strain. However, the stress and strain obtained from the material testing are nominal stress and nominal strain, which are calculated based on the undeformed configuration of the coupons. The relationship between the two types of strain and stress values is shown below.

Assume the original length and the unreduced cross-sectional area of the material coupon are l_o and A_o , respectively. After certain load or displacement is applied, the current length and area of the coupon become l and A .

The incremental true strain is defined as:

$$d\varepsilon_{true} = \frac{dl}{l} \quad (G.11)$$

The total true strain is the integral of Equation (G.12)

$$\varepsilon_{true} = \int_{l_o}^l \frac{dl}{l} = \ln\left(\frac{l}{l_o}\right) \quad (G.12)$$

The true stress can be written as:

$$\sigma_{true} = \frac{P}{A_o} \quad (G.13)$$

The nominal strain and stress are calculated as:

$$\varepsilon_{nom} = \frac{l - l_o}{l_o} \quad (G.14)$$

$$\sigma_{nom} = \frac{P}{A} \quad (G.15)$$

Since the plastic deformation of the material is incompressible, if the elastic deformation is assumed to be incompressible, the material volume is constant

$$l_o A_o = l A \quad (G.16)$$

By combining all equations above, the conversion from nominal stress and strain to true stress and strain can be expressed as:

$$\epsilon_{true} = \ln(1 + \epsilon_{nom}) \quad (G.17)$$

$$\sigma_{true} = \sigma_{nom}(1 + \epsilon_{nom}) \quad (G.18)$$

The true plastic strain is thus calculated as

$$\epsilon_{true}^{pl} = \epsilon_{true} - \sigma_{true}/E \quad (G.19)$$

The input yield stress and plastic strain values provided in Table G.5 are based on the stress-strain relationship that is the average of the four tested stress-strain curves, see Figure G.4. Three backstresses are defined to adequately characterize the variation of the strain hardening modulus. Nodes 1, 2, 5, and 7 are restrained from moving in the Z direction, while the bottom nodes are fixed in the Y direction, and nodes 2 and 3 are prevented from translating in the X direction. The strain measurements are used as the displacement assigned to the top nodes.

Table G.5 Bolt true stress and true plastic strain

True stress (ksi)	True plastic strain
106.27	0.00000
113.93	0.00031
119.24	0.00212
122.69	0.00598
125.23	0.00985
127.45	0.01372
129.87	0.01756
130.89	0.01948
134.37	0.02715
135.30	0.02906
136.68	0.03287
137.91	0.03668
138.99	0.04048

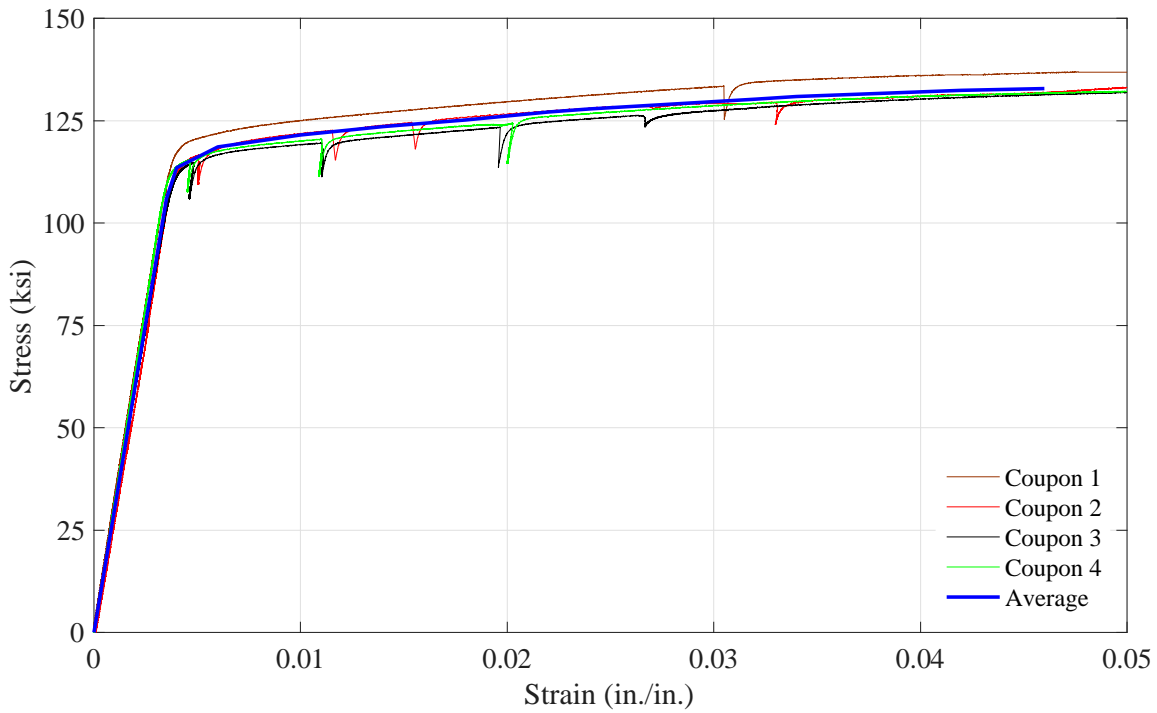
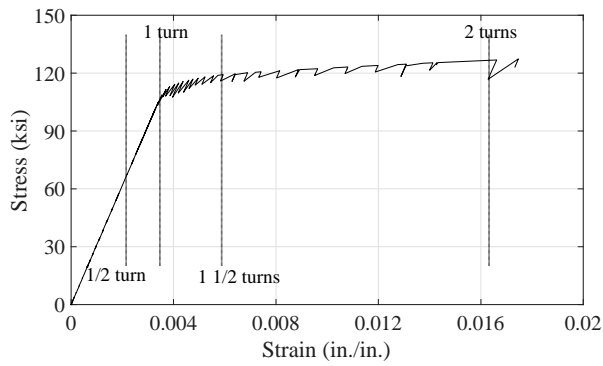
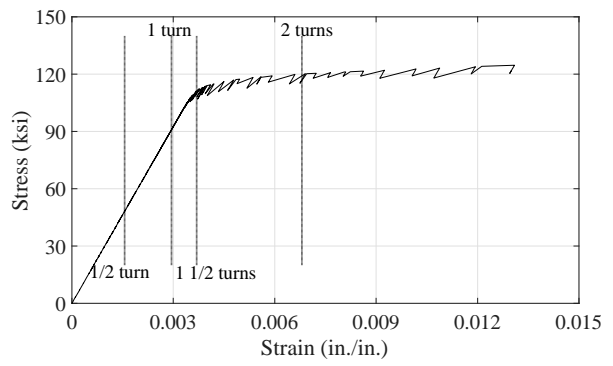


Figure G.4 Bolt stress strain curves

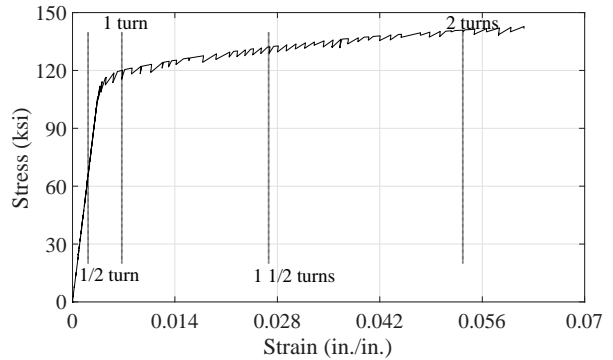
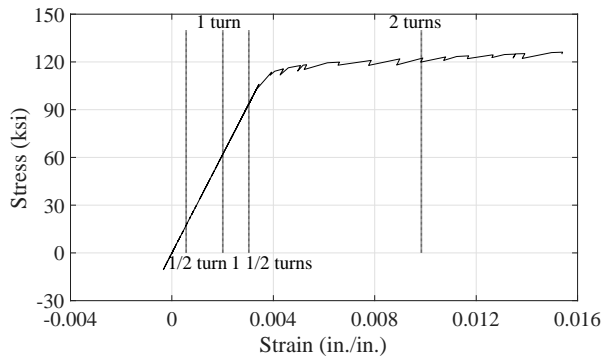
G.1.2.1 Pretension test



M24 bolt test 1



M24 bolt test 2



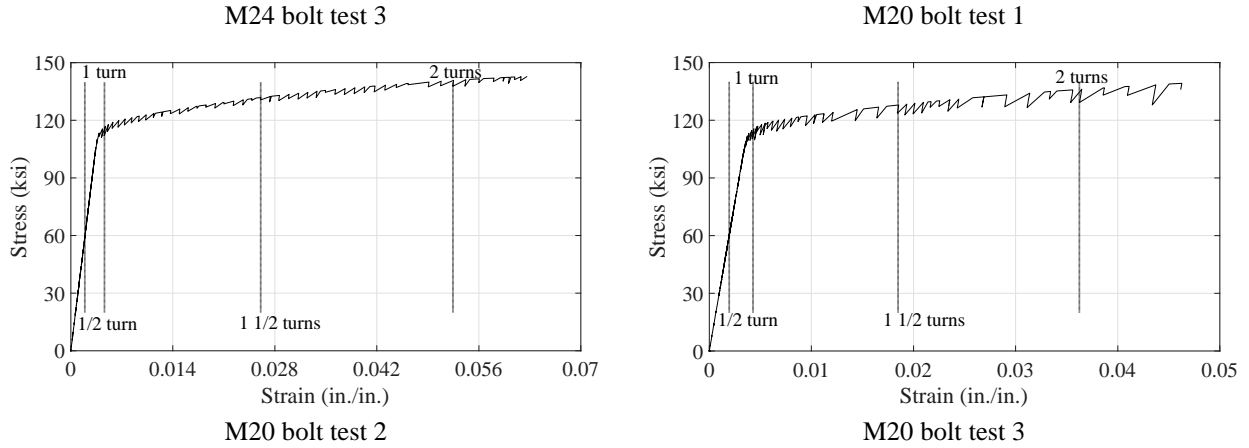
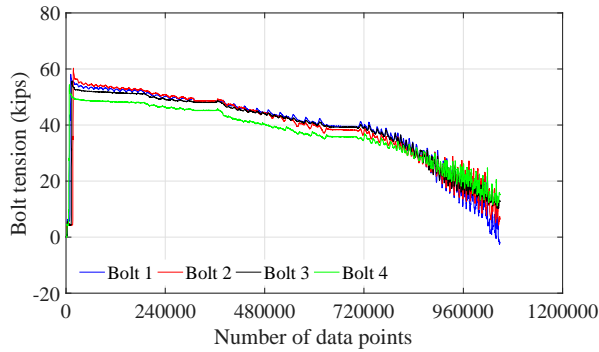
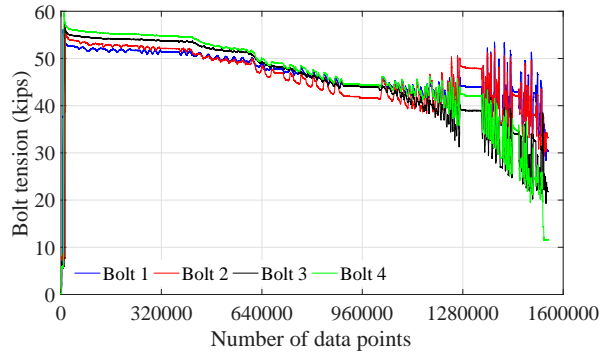


Figure G.5 Bolt material cyclic stress-strain curve

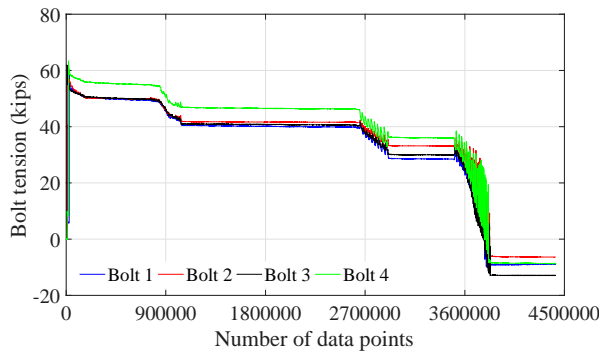
G.1.2.2 Pushout test



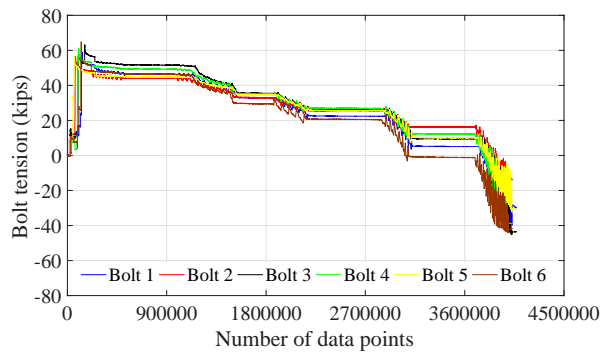
Test 3-M24-2C-RL-LC



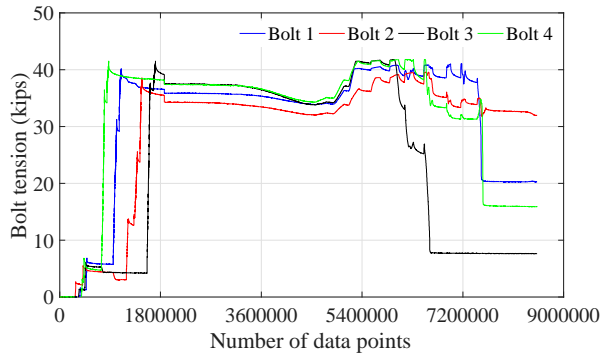
Test 5-M24-2C-RH-LC



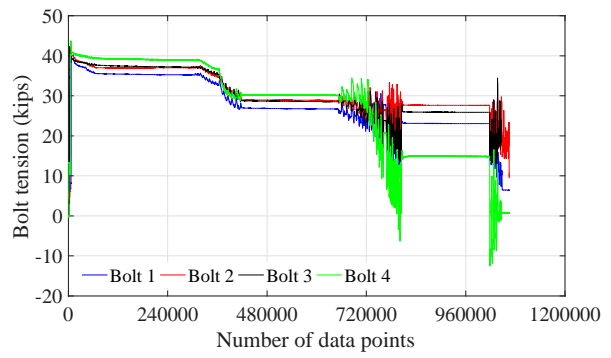
Test 6-M24-2C-RH-LC-S



Test 8-M24-3C-RH-LC

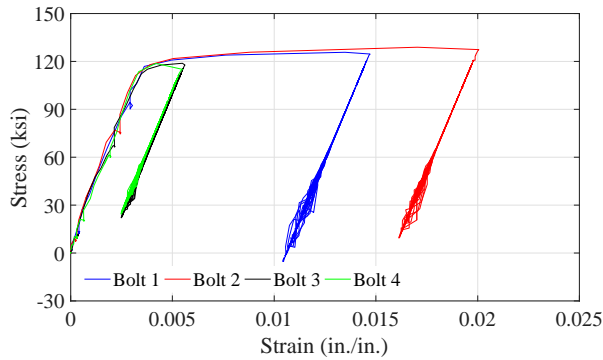


Test 9-M20-2C-RH-LM

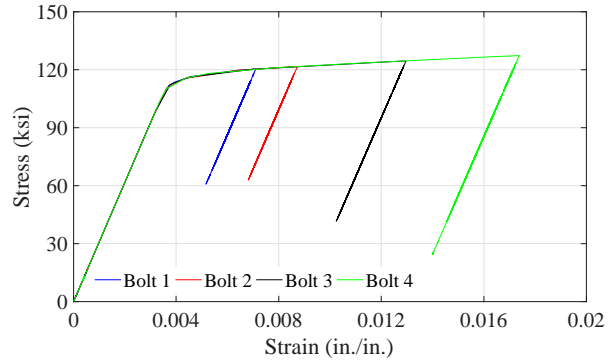


Test 10-M20-2C-RH-LC

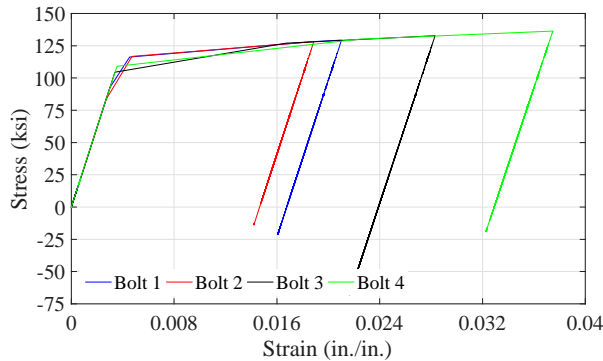
Figure G.6 Bolt axial force variation



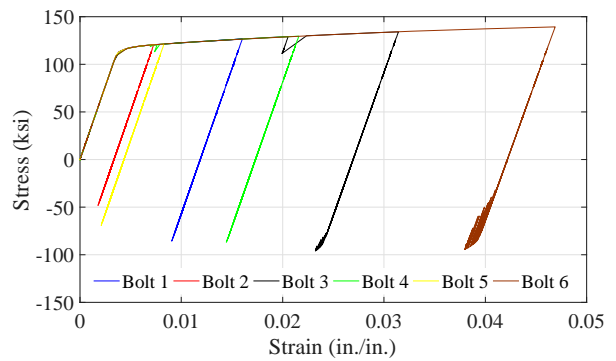
Test 3-M24-2C-RL-LC



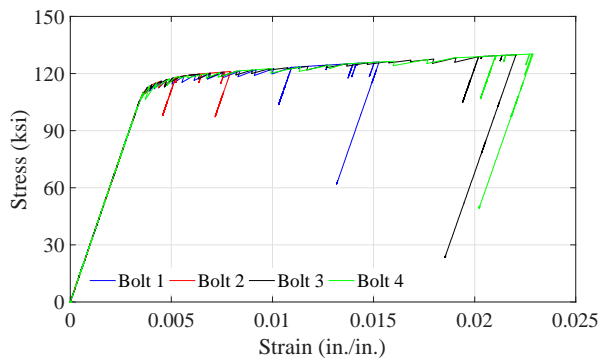
Test 5-M24-2C-RH-LC



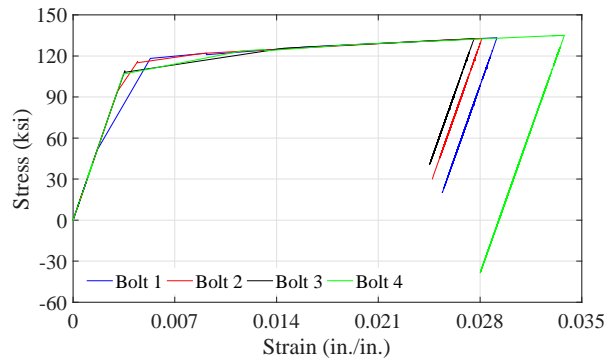
Test 6-M24-2C-RH-LC-S



Test 8-M24-3C-RH-LC



Test 9-M20-2C-RH-LM



Test 10-M20-2C-RH-LC

Figure G.7 Bolt material cyclic behavior

G.1.3 Forces acting on the channel anchors

Two-dimensional strain transformation is shown in Figure G.8. The orientation of the three legs in a rosette strain gage attached on the channel anchor is shown in Figure G.9 . A coordinate system is also defined for the transformed strains. Given the 3 strain measurements from a rosette strain gage, the axial and shear strain can be calculated using the following equations.

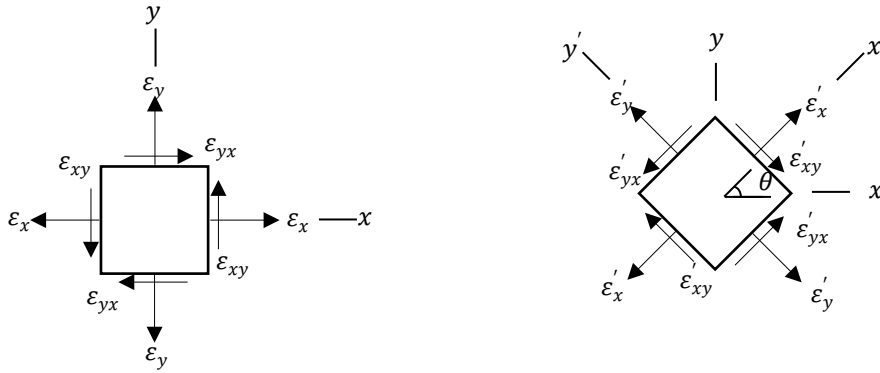


Figure G.8 Strain transformation between different coordinates

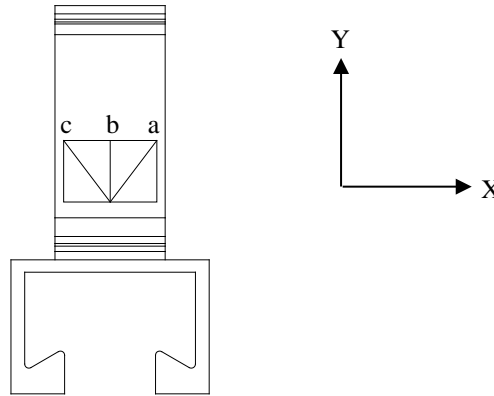


Figure G.9 Gage orientation and new coordinate system

$$\varepsilon'_x = \varepsilon_x \cos^2 \theta + \varepsilon_y \sin^2 \theta + \gamma_{xy} \sin \theta \cos \theta \quad (\text{G.20})$$

$$\varepsilon_a = \varepsilon_x \cos^2 \frac{\pi}{4} + \varepsilon_y \sin^2 \frac{\pi}{4} + \gamma_{xy} \sin \frac{\pi}{4} \cos \frac{\pi}{4} = \frac{1}{2} (\varepsilon_x + \varepsilon_y + \gamma_{xy}) \quad (\text{G.21})$$

$$\varepsilon_b = \varepsilon_x \cos^2 \frac{\pi}{2} + \varepsilon_y \sin^2 \frac{\pi}{2} + \gamma_{xy} \sin \frac{\pi}{2} \cos \frac{\pi}{2} = \varepsilon_y \quad (\text{G.22})$$

$$\varepsilon_c = \varepsilon_x \cos^2 \frac{3\pi}{4} + \varepsilon_y \sin^2 \frac{3\pi}{4} + \gamma_{xy} \sin \frac{3\pi}{4} \cos \frac{3\pi}{4} = \frac{1}{2} (\varepsilon_x + \varepsilon_y - \gamma_{xy}) \quad (\text{G.23})$$

$$\varepsilon_x = \varepsilon_a + \varepsilon_c - \varepsilon_b \quad (\text{G.24})$$

$$\varepsilon_y = \varepsilon_b \quad (\text{G.25})$$

$$\gamma_{xy} = \varepsilon_a - \varepsilon_c \quad (\text{G.26})$$

Where

$\varepsilon_a, \varepsilon_b, \varepsilon_c$ = strain measurements from the rosette strain gages

$\varepsilon_x, \varepsilon_y, \varepsilon_{xy}$ = strain components with respect to the defined coordinate system

The stress-strain relationship for elastic elements in a two-dimensional plane stress state is provided in Equations (G.27) through (G.30). The Von Mises yield criterion in Equation (G.31) is utilized to ascertain that the anchors are elastic.

$$\begin{pmatrix} \sigma_x \\ \sigma_y \\ \tau_{xy} \end{pmatrix} = \frac{E}{1-\nu^2} \begin{pmatrix} 1 & \nu & 0 \\ \nu & 1 & 0 \\ 0 & 0 & (1-\nu)/2 \end{pmatrix} \begin{pmatrix} \varepsilon_x \\ \varepsilon_y \\ \gamma_{xy} \end{pmatrix} \quad (\text{G.27})$$

$$\sigma_x = \frac{E}{1-\nu^2} (\varepsilon_x + \nu\varepsilon_y) \quad (\text{G.28})$$

$$\sigma_y = \frac{E}{1-\nu^2} (\varepsilon_y + \nu\varepsilon_x) \quad (\text{G.29})$$

$$\tau_{xy} = G\gamma_{xy} \quad (\text{G.30})$$

$$\sigma_{VM} = \sqrt{\sigma_x^2 + \sigma_y^2 - \sigma_x\sigma_y + 3\tau_{xy}^2} \quad (\text{G.31})$$

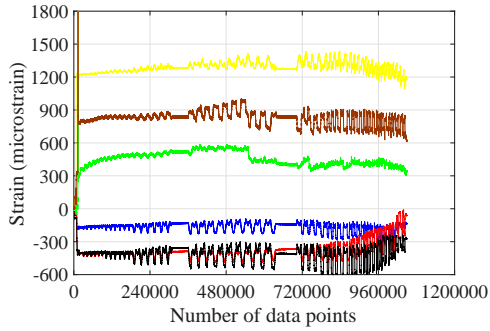
Where

E = modulus of elasticity

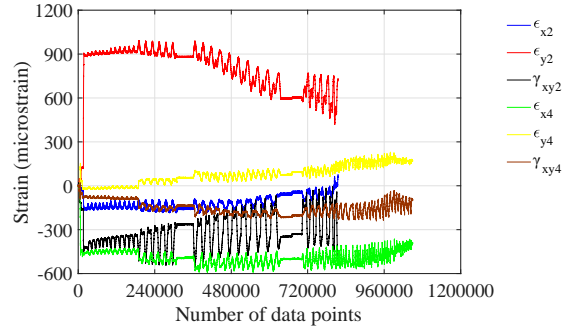
G = shear modulus

ν = poisson's ratio

When the material is inelastic, such as anchors 3 and 4 in Test 5-M24-2C-RH-LC, the strains are converted into stresses using the single element model shown in Figure G.3. To prevent rigid body motion of the element, the same boundary conditions described in Section G.1.2 are defined. The transformed axial strain in the y direction (i.e., σ_y) is assigned to the top nodes, while the transformed axial strain in the x direction (i.e., σ_x) and shear strain (i.e., τ_{xy}) are applied to nodes 1 and 4 and nodes 7 and 8, respectively. The displacement of nodes 5 and 6 is the summation of σ_x and τ_{xy} . The material stress-strain relationship given in Table 5.7, which is obtained from tensile coupon testing, is employed for the anchors. The variations of the anchor strain and stress of the anchors are plotted in Figure G.10.

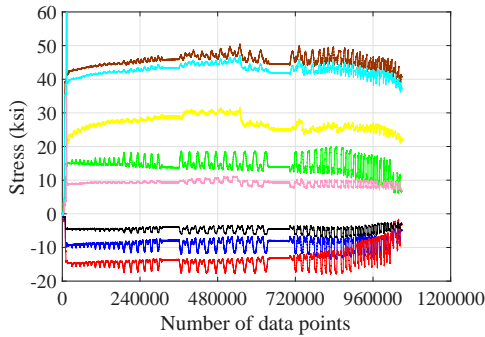


Anchors 1 and 3

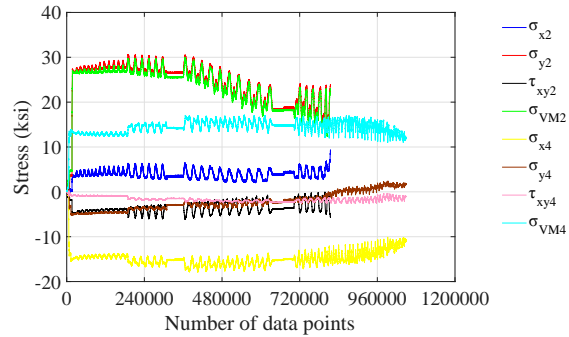


Anchors 2 and 4

Strain components



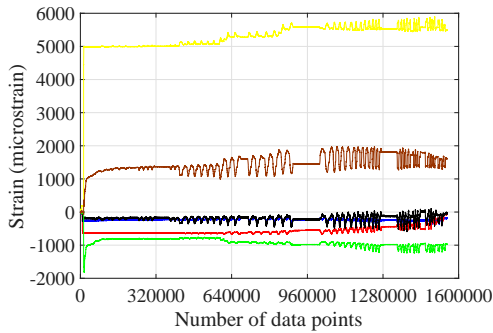
Anchors 1 and 3



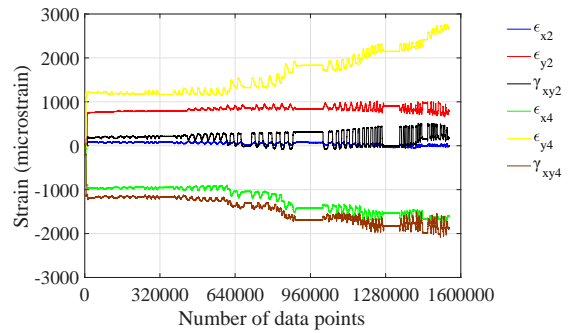
Anchors 2 and 4

Stress components

Test 3-M24-2C-RL-LC

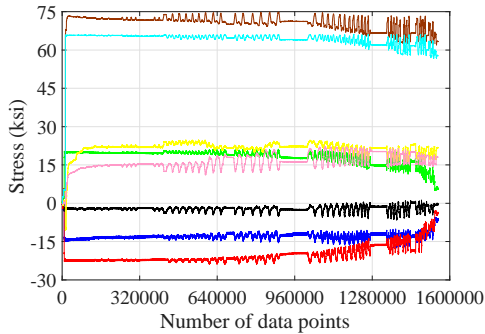


Anchors 1 and 3

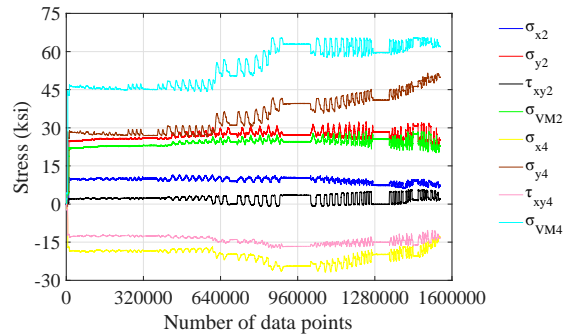


Anchors 2 and 4

Strain components



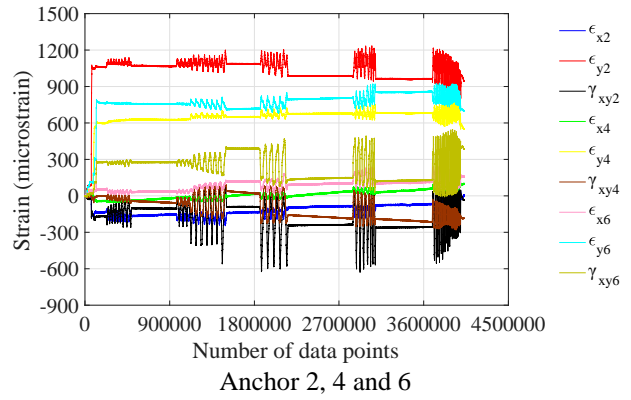
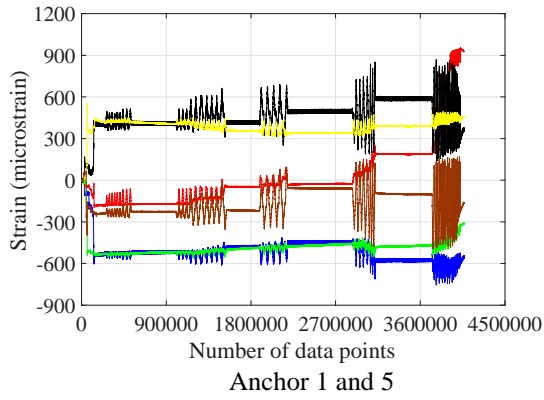
Anchors 1 and 3



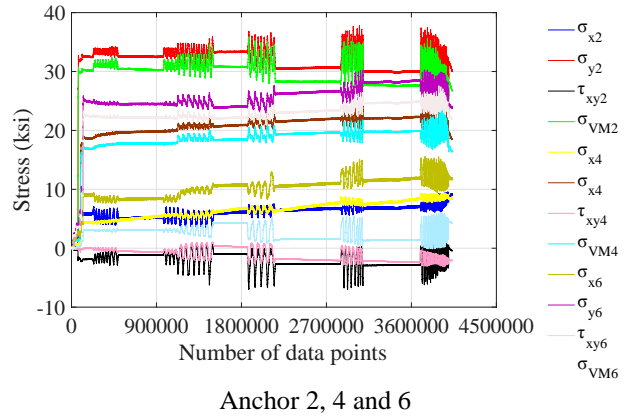
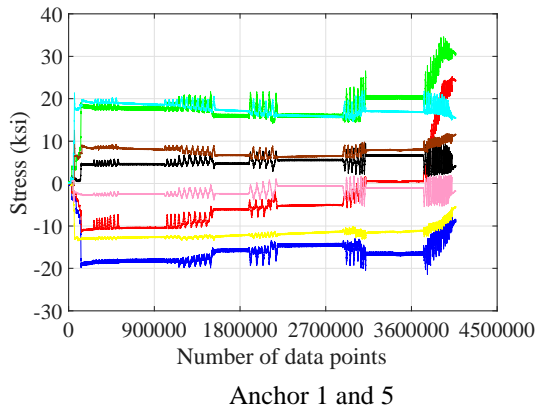
Anchors 2 and 4

Stress components

Test 5-M24-2C-RH-LC



Strain components



Stress components

Test 8-M24-3C-RH-LC

Figure G.10 Anchor strain and stress variation

Appendix H. Beam Test Specimen Design

H.1 Lifting points on the concrete planks

The lifting inserts are placed at the two outer fifth points of the plank so that the maximum bending moment induced by handling is minimized. It is expected that the most critical handling for these planks is to pull the specimens from the formwork. Two sections are deemed to be the worst: (1) the section where the maximum moment occurs; (2) the section with cutouts and embedded PVC pipe. The tensile stress is conservatively calculated with the maximum moment and the section with the smallest moment of inertia.

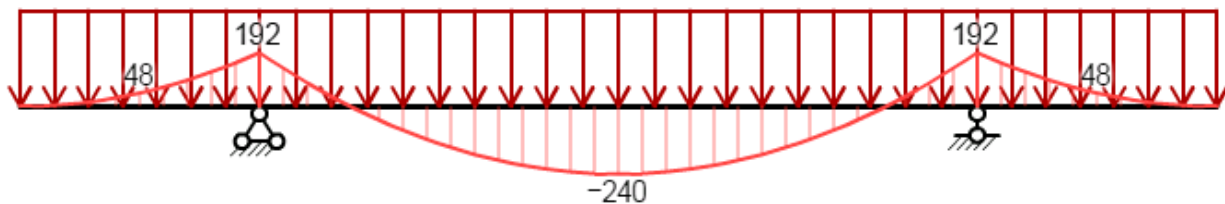


Figure H.1 Moment diagram of a concrete plank under gravity loading (units: lb-ft)

Calculation:

Maximum moment in the panel:

$$M_{pos} = \frac{1}{40} q l^2 = \frac{1}{40} \rho b h l^2 = \frac{1}{40} \times 150 \times \frac{6}{12} \times 2 \times 8^2 = 240 \text{ lb-ft}$$

Section moment of inertia without considering the cast-in channels, the:

$$I = 285.7 \text{ in}^4$$

Tensile Stress in the panel:

$$f_t = \frac{M_{pos}}{I} c = \frac{240 \times 12 \times 3.27}{285.7} = 32.96 \text{ psi}$$

According to Table 5.3 in Chapter 5, concrete reaches a compressive strength of at least 3,500 psi when the specimens are lifted, and the modulus of rupture of concrete:

$$f_r = 7.5 \lambda \sqrt{f'_c} = 7.5 \times \sqrt{3500} = 444 \text{ psi}$$

A multiplier is employed to account for form suction and impact. Conservatively, 1.7 is selected from Table 8.3.1 in PCI Design Handbook (2010). Meanwhile, a safety factor of 1.5 is recommended for the modulus of rupture.

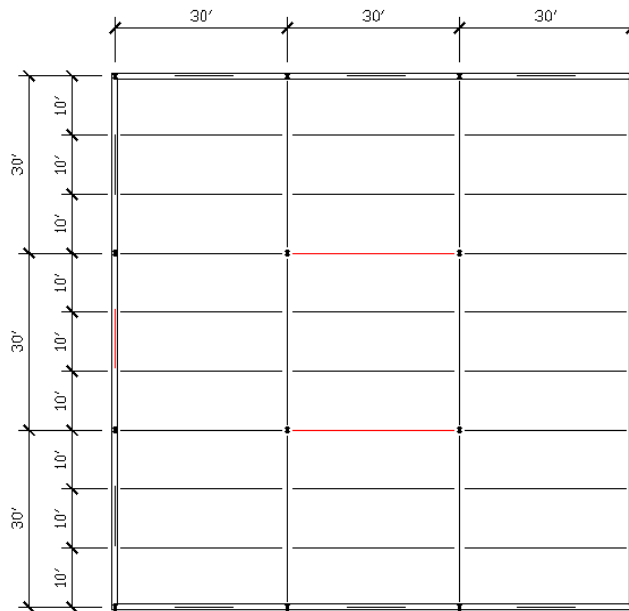
With multiplier, tensile stress = $1.7 \times 32.96 = 56 \text{ psi}$

With safety factor, modulus of fracture = $444/1.5 = 296 \gg 56 \text{ psi}$

The above calculation shows that the selected lifting points are effective.

H.2 Selection of threaded rods

The selection of the threaded rods is based on the in-plane diaphragm force calculated in accordance with ASCE 7-10 using the prototype structure shown in Figure H.2. Low gravity loading is employed to represent office occupancy, which is a uniform load of 92.5 psf dead load (32 psf for roof) and 80 psf live load. High gravity loading corresponds to storage warehouse, which is designed for a uniform load of 92.5 psf dead load (32 psf for roof) and 250 psf live load. The weights of the partitions and walls, which are 20 psf and 15 psf equivalent, are also taken into account for seismic force calculation. The building is presumed to be located in Los Angeles. The site is classified as site D. Special concentrically braced frames (SCBF) are chosen as the LFRS systems.



Note: The red lines show the lateral force-resisting system

Figure H.2 Prototype structure floor plan

Diaphragm force calculation as per ASCE 7-10

According to ASCE 7-10 Section 12.10.1.1, the diaphragm should be designed for inertial forces determined as the maximum of (1) and (2).

- (1) The design seismic force from the structural analysis of LFRS. This is commonly taken as the force from the Equivalent Lateral Force Procedure, where

$$F_x = C_{vx}W \quad (\text{H.1})$$

$$C_{vx} = \frac{w_x h_x^k}{\sum_{i=1}^n w_i h_i^k} \quad (\text{H.2})$$

- (2) The diaphragm design force F_{px} , where

$$F_{px} = \frac{\sum_{i=x}^n F_i}{\sum_{i=x}^n w_i} w_{px} \quad (\text{H.3})$$

but not less than

$$F_{px,min} = 0.2S_{DS}I_e w_{px} \quad (\text{H.4})$$

and not need exceed

$$F_{px,min} = 0.2S_{DS}I_e w_{px} \quad (\text{H.5})$$

Low gravity:

Diaphragm force obtained based on Approach 1:

According to Table 12.6-1 in ASCE 7-10, Equivalent Lateral Force (ELF) procedure is permitted to be used for the building.

Period of the building:

$$T_a = C_t h_n^x = 0.02 \times 117^{0.75} = 0.71 \text{ s}$$

Seismic response coefficient:

$$\begin{aligned} C_s &= \frac{S_{DS}}{\left(\frac{R}{I_e}\right)} = \frac{2S_{MS}}{3\left(\frac{R}{I_e}\right)} = \frac{2F_a S_S}{3\left(\frac{R}{I_e}\right)} = \frac{2 \times 1.0 \times 2.0}{3 \times \frac{6}{1.0}} = 0.222 \\ &\leq \frac{S_{D1}}{T\left(\frac{R}{I_e}\right)} = \frac{2F_v S_1}{3T\left(\frac{R}{I_e}\right)} = \frac{2 \times 1.5 \times 0.75}{3 \times 0.71 \times \frac{6}{1.0}} = 0.176 \end{aligned}$$

$$C_s \geq 0.044S_{DS}I_e = 0.044 \times 1.33 \times 1.0 = 0.059 \geq 0.01$$

$$C_s = 0.176$$

Weight of the building:

$$W = 294 + 1032 \times 8 = 8550 \text{ kips}$$

Base shear:

$$F_x = C_{vx}V = 0.176 \times 8550 = 1505 \text{ kips}$$

Vertical force distribution:

Level	w_x (kips)	h_x (ft.)	h_x^k	$w_x h_x^k$	C_{vx}	F_x (kips)
Roof	294	117	188	55380	0.070	105.222
9	1032	104	165	170772	0.216	324.468
8	1032	91	143	147443	0.186	280.143
7	1032	78	121	124447	0.157	236.450
6	1032	65	99	101832	0.129	193.481
5	1032	52	77	79668	0.101	151.369
4	1032	39	56	58056	0.073	110.308
3	1032	26	36	37166	0.047	70.616
2	1032	13	17	17339	0.022	32.944
			Total	792103	1	1505

Diaphragm force obtained based on Approach 2:

Level	w_x (kips)	$\sum_{i=x}^n w_i$ (kips)	F_i (kips)	$\sum_{i=x}^n F_i$ (kips)	F_{px} (kips)
Roof	294	294	105.222	105.222	105.222
9	1032	1326	324.468	429.69	334.419
8	1032	2358	280.143	709.833	310.665
7	1032	3390	236.450	946.283	288.072
6	1032	4422	193.481	1139.764	265.996
5	1032	5454	151.369	1291.133	244.307
4	1032	6486	110.308	1401.441	222.986
3	1032	7518	70.616	1472.057	202.070
2	1032	8550	32.944	1505.001	181.656

Minimum diaphragm design force:

$$F_{px,min} = 0.2S_{DS}I_e w_{px} = 0.2 \times 1.33 \times 1.0 \times 1032 = 274.51 \text{ kips}$$

Maximum diaphragm design force:

$$F_{px,min} = 0.4S_{DS}I_eW_{px} = 0.4 \times 1.33 \times 1.0 \times 1032 = 549.02 \text{ kips}$$

The diaphragm design force is 334.42 kips in both directions, and the equivalent uniform loading is 3.72 kips/ft.

When the lateral force-resisting system is at the exterior of the structure, as shown in Figure H., the maximum shear demand occurs. The largest required shear flow between planks is 1860 lbs/ft.

The design of a composite diaphragm commonly assumes that the bending of the diaphragm is resisted by the steel chords, and the diaphragm has to be designed for the shear demand (Sabelli et al. 2011). In the deconstructable system, the shear is resisted by the friction between the adjacent planks, and then resisted by the steel rods provided that the friction is overcome and the steel rods start to bear against the concrete.

The shear friction analogy can be adapted to select the threaded rods, and a shear friction coefficient of 0.6 given in Section 11.6.4.3 of ACI 318-11 may be valid. However, a frictional coefficient of 1.0 is assumed when designing the threaded rods in the composite beam tests. The higher frictional coefficient leads to smaller rods with less pretensioning forces which makes the assembly of the test specimens easier. More importantly, in real practice, an interlocking mechanism can be achieved with intermittent tongue and groove joints, or the concrete surfaces can be purposely roughened. A higher coefficient of friction can thus be justified. In addition, the behavior of the composite beam under gravity loading is not believed to be strongly affected by the normal force between the planks.

Based on the above assumptions, Grade A36, 5/8 in. threaded rods are selected. The normal force between the planks is taken as the lower value determined from the limit states of tensile yielding and tensile rupture:

Stress area:

$$= 0.785\left(D - \frac{0.9743}{n}\right)^2 = 0.785 \times \left(0.625 - \frac{0.9743}{11}\right)^2 = 0.226 \text{ in.}^2$$

Where

D = nominal bolt diameter

n = number of threads per inch

Tensile yielding:

$$\phi_t P_n = \phi_t F_y A_g = 0.9 \times 36 \times 0.226 = 7.32 \text{ kips}$$

Tensile rupture:

$$\phi_t P_n = \phi_t F_u A_e = 0.75 \times 58 \times 0.226 = 9.83 \text{ kips}$$

The available shear flow between the planks = $7320/4 = 1830 \approx 1860 \text{ lbs/ft}$

Appendix I. Moment of inertia

When the design of a composite beam is controlled by deflection, a reasonable evaluation of the moment of inertia of the composite section is necessary. In the AISC 360 commentary, several types of moment of inertia are provided. When a composite section behaves elastically, an equivalent moment of inertia, I_{equiv} , is used which is the moment of inertia of the transformed section for a fully composite section. For a partially composite section, it is interpolated between the moment of inertia of the steel section and the moment of inertia of the fully composite section. Research by Leon et al. (1993), however, indicates that the deflection of a composite beam under serviceability cannot be estimated accurately with I_{equiv} ; thus, an effective moment of inertia, I_{eff} , is recommended which is taken as $0.75 I_{equiv}$. A lower bound moment of inertia, I_{LB} , is also suggested which neglects the stiffness contribution of the concrete in the tensile zone. Seemingly, the deflection is overestimated when I_{LB} is employed. However, it is demonstrated in Leon et al. (1993) that I_{LB} gives a good estimate of the initial stiffness of a composite beam.

- Equivalent moment of inertia

The location of the elastic neutral axis is measured from the bottom surface of the steel section and computed using Equation (I.1). It can be found that the cast-in channels and the supplementary reinforcements placed around the middle anchors are ignored in the calculation.

$$y_{ENA} = \frac{\frac{tb_{eff}}{n} \left(d + \frac{t}{2} \right) + A_s \frac{d}{2} + N_{tb} \frac{1}{4} \pi d_{tb}^2 (d + D_{tb}) + N_{bb} \frac{1}{4} \pi d_{bb}^2 (d + D_{bb})}{\frac{tb_{eff}}{n} + A_s + N_{tb} \frac{1}{4} \pi d_{tb}^2 + N_{bb} \frac{1}{4} \pi d_{bb}^2} \quad (I.1)$$

Where

b_{eff} = effective width of the concrete slab (in.), which could be calculated based on the concrete strain measurements

d = nominal height of the steel section (in.)

d_{bb} = nominal bottom transverse bar diameter (in.) = 0.375 in.

d_{tb} = nominal top transverse bar diameter (in.) = 0.375 in.

f'_c = concrete compressive strength (psi), which could be obtained from compressive cylinder testing

n = modulus ratio = E_s/E_c

t = nominal thickness of the concrete slab (in.) = 6 in.

A_s = nominal area of the steel section (in².)

D_{bb} = nominal distance between the bottom bars and the top surface of the steel section (in.) = 2.19 in.

D_{tb} = nominal distance between the top bars and the top surface of the steel section (in.) = 5.19 in.

E_s = elastic modulus of steel (psi), which could be determined from the tensile coupon testing

E_c = elastic modulus of concrete (psi) = $57000\sqrt{f'_c}$

N_{bb} = number of bottom transverse bars = 5

N_{tb} = number of top transverse bars = 21

The transformed moment of inertia of a fully composite section is then given in Equation (I.2).

$$I_{tr} = I_s + A_s \left(y_{ENA} - \frac{d}{2} \right)^2 + \frac{1}{12n} b_{eff} t^3 + \frac{t b_{eff}}{n} \left(d + \frac{t}{2} - y_{ENA} \right)^2 + N_{tb} \frac{1}{4} \pi d_{tb}^2 (d + D_{tb} - y_{ENA})^2 + N_{bb} \frac{1}{4} \pi d_{bb}^2 (d + D_{bb} - y_{ENA})^2 \quad (I.2)$$

Where

I_s = nominal moment of inertia for the structural steel section (in⁴.)

When the section is partially composite, the equivalent moment of inertia could be approximated by

$$I_{equiv} = I_s + \sqrt{\left(\frac{\sum Q_n}{C_f} \right)} (I_{tr} - I_s) \quad (I.3)$$

Where

$\sum Q_n$ = strength of steel anchors between the point of maximum positive moment and the point of zero moment to either side (kips)

C_f = compressive force in concrete slab for fully composite beam; smaller of $A_s F_y$ and $0.85 f'_c A_c$ (kips)

A_c = area of concrete slab within the effective width (in².)

- Lower bound moment of inertia

The equations for the elastic neutral axis and moment of inertia are given in Equations (C-I3-1) and (C-I3-2) in the AISC 360 commentary.

$$Y_{ENA} = \frac{A_s d_3 + \frac{\sum Q_n}{F_y} (2d_3 + d_1)}{A_s + \frac{\sum Q_n}{F_y}} \quad (I.4)$$

$$I_{LB} = I_s + A_s (Y_{ENA} - d_3)^2 + \frac{\sum Q_n}{F_y} (2d_3 + d_1 - Y_{ENA})^2$$

Where

d_1 = distance from the compressive force in the concrete to the top surface of the steel section (in.)

d_3 = distance from the resultant steel tensile force for full section tension yield to the top surface of the steel section (in.) = $d/2$

All the parameters used in these equations are given in Table I.1.

Table I.1 Equivalent moment of inertia parameters

Parameters	Nominal			
	Specimen 1	Specimen 2	Specimen 3	Specimen 4
f'_c (psi)	5,000	5,000	5,000	5,000
f_y (psi)	50,000	50,000	50,000	50,000
E_s (psi)	29×10^6	29×10^6	29×10^6	29×10^6
E_c (psi)	4.03×10^6	4.03×10^6	4.03×10^6	4.03×10^6
n	7.20	7.20	7.20	7.20
b_{eff} (in.)	90	90	90	90
A_s (in ² .)	11.2	11.2	7.69	7.69
d (in.)	14.1	14.1	13.9	13.9
y_{ENA} (in.)	15.89	15.89	16.06	16.06
Y_{ENA} (in.)	13.26	11.57	13.21	11.18
I_s (in ⁴ .)	385	385	245	245
I_{tr} (in ⁴ .)	1622	1622	1183	1183
$\sum Q_n$ (kips)	663	309.4	602.8	191.8
C_f (kips)	560	560	384.5	384.5
A_c (in ² .)	540	540	540	540
I_{equiv}	1622	1305	1183	907
I_{LB}	1250	1029	848	660
I_{LB}/I_{equiv}	0.77	0.79	0.72	0.73